ACTA TECHNICA

ACADEMIAE SCIENTIARUM HUNGARICAE

REDIGIT: M. MAJOR

TOMUS 82
FASCICULI 1–2

AKADÉMIAI KIADÓ, BUDAPEST 1976

ACTA TECHNICA

Az *Acta Technica* angol, francia, német és orosz nyelven közöl értekezéseket a műszaki tudományok köréből.

Az *Acta Technica* változó terjedelmű füzetekben jelenik meg, több füzet alkot egy kötetet.

A közlésre szánt kéziratok a következő címre küldendők:

Acta Technica
1051 Budapest, Münnich Ferenc u. 7.

Ugyanerre a címre küldendő minden szerkesztőségi és kiadóhivatali levelezés.

Megrendelhető a belföld számára az „Akadémiai Kiadó"-nál (1363 Budapest Pf. 24. Bankszámla 215 11448), a külföld számára pedig a „Kultúra" Könyv- és Hírlap Külkereskedelmi Vállalatnál (1389 Budapest 62, P.O.B. 149 Bankszámla: 218 10990) vagy annak külföldi képviseleteinél és bizományosainál.

Die *Acta Technica* veröffentlichen Abhandlungen aus dem Bereiche der technischen Wissenschaften in deutscher, englischer, französischer und russischer Sprache.

Die *Acta Technica* erscheinen in Heften wechselnden Umfanges. Vier Hefte bilden einen Band.

Die zur Veröffentlichung bestimmten Manuskripte sind an folgende Adresse zu senden:

Acta Technica
1051 Budapest,
Münnich Ferenc u. 7.
Ungarn

An die gleiche Anschrift ist auch jede für die Schriftleitung und den Verlag bestimmte Korrespondenz zu richten. Abonnementspreis pro Band: $ 32.00

Bestellbar bei dem Buch- und Zeitungs-Außenhandels-Unternehmen »Kultúra« (1389 Budapest 62, P.O.B. 149 Bankkonto Nr. 218 10990) oder bei seinen Auslandsvertretungen und Kommissionären.

ACTA TECHNICA

TOMUS. 82

INDEX

BUCHBESPRECHUNG — BOOK REVIEW

ACTA TECHNICA

ACADEMIAE SCIENTIARUM HUNGARICAE

REDIGIT: M. MAJOR

TOMUS 82

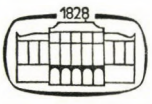

AKADÉMIAI KIADÓ, BUDAPEST 1976

Acta Technica Academiae Scientiarum Hungaricae, Tomus 82 (1—2), pp. 1—7 (1976)

CORRUGATED CONICAL SHELLS

E. BÖLCSKEI*
CORR. MEMBER OF THE HUNG. AC. OF SCI.

(Manuscript received September 10, 1974)

Corrugated conical shells having a vertical axis, a circular ground plane and free boundary are analysed in a cylindrical system of co-ordinates. The investigated shells are subject to uniform vertical loads, and supported by radial ribs. Formulae are given for the determination of the reduced stress resultants. Their distribution is illustrated for two practical cases.

1. Differential equation of membrane shells written in cylindrical co-ordinates

Internal forces in the usual types of membrane shells subject to distributed vertical loads are generally determined by means of the Pucher differential equation written in orthogonal co-ordinates. There are, however, some special shell surfaces easier to solve — with less mathematical difficulties — by transforming this differential equation into cylindrical co-ordinates.

Differential equation of membrane shells subject to distributed vertical loads written in cylindrical co-ordinates takes the form:

$$\frac{1}{r}(F_r z_r)_r + \frac{1}{r^2}(F_{rr} z_{\varphi\varphi} + F_{\varphi\varphi} z_{rr}) - 2\left(\frac{1}{r}F_\varphi\right)_r \left(\frac{1}{r} z_\varphi\right)_r + p = 0,$$

$F(r, \varphi)$, $z(r, \varphi)$ and $p(r, \varphi)$ being the stress function, the shape function and the reduced load function, respectively, written in cylindrical co-ordinates. Here and throughout this study, subscripts indicate partial differentiation with respect to the corresponding variable.

Reduced stress resultants are obtained from expressions:

$$n_\varphi = F_{rr},$$

$$n_r = \frac{1}{r}F_r + \frac{1}{r^2}F_{\varphi\varphi},$$

$$n_{r\varphi} = -\left(\frac{1}{r}F_\varphi\right)_r.$$

*Prof. Dr. E. Bölcskei, Muskotály u. 37., H-1118 Budapest, Hungary.

2. Equation of a corrugated conical shell written in cylindrical co-ordinates

A so-called *corrugated conical shell* is a free-edged surface (Fig. 1) expressed as:

$$z = c\,r\,\sin\alpha\varphi + h\,r, \qquad \alpha = 1,2,3,\ldots,\ n$$

any of its cylindrical sections giving a sine curve, if expanded.
Derivatives are:

$$z_r = c\sin\alpha\varphi + h\,,$$

$$z_{rr} = 0\,,$$

$$z_\varphi = c\alpha r\cos\alpha\varphi\,.$$

$$z_{\varphi\varphi} = -c\alpha^2 r\sin\alpha\varphi\,,$$

$$z_{r\varphi} = c\alpha\cos\alpha\varphi\,.$$

This surface has inflection lines at $\alpha\varphi = 0, \pi, \ldots, n\,\pi$. Therefore, it is advisable to take such a surface where the absolute value of the sine curve can be reckoned with. This surface, shown axonometrically in Fig. 2, is described as:

$$z = cr\,|\sin\alpha\varphi\,| + hr\,.$$

Of course, ribs are to be applied along the troughs to be supported.

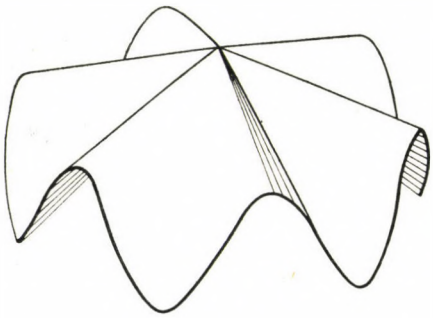

Fig. 1

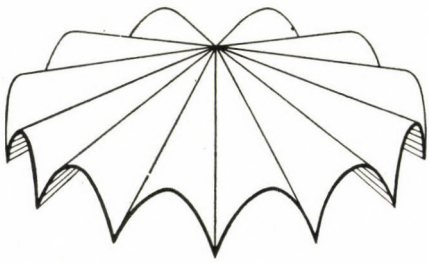

Fig. 2

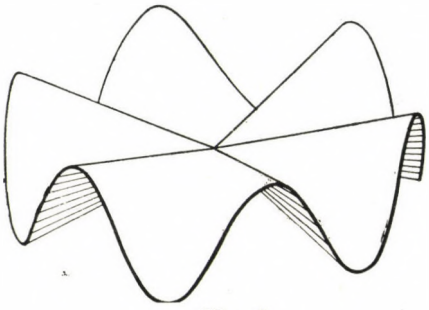

Fig. 3

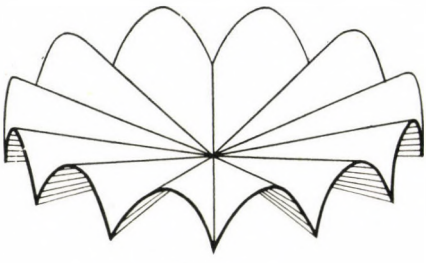

Fig. 4

A special case is that with a constant $h = 0$, where the cone vertex is in the ground plane. Such a surface is shown in Fig. 3 and the case where z is replaced by its absolute value, in Fig. 4.

3. Analysis of the state of stresses

Be the reduced shell load p = constant. Substituting the earlier defined partial derivatives into the differential equation of membrane shells, written in cylindrical co-ordinates, and so arranging the results, the relation

$$\frac{1}{r} F_{rr} [c(1 - \alpha^2) \sin \alpha\varphi + h] = - p$$

is obtained, valid for the sector $0 \leqq \alpha\varphi \leqq n$. Hence,

$$F_{rr} = - \frac{pr}{c(1 - \alpha^2) \sin \alpha\varphi + h} = - \frac{pr}{\beta \sin \alpha\varphi + h}$$

and twice integrating gives the stress function:

$$F_r = - \frac{1}{2} \frac{pr^2}{\beta \sin \alpha\varphi + h} + K_1(\varphi),$$

$$F = - \frac{1}{6} \frac{pr^3}{\beta \sin \alpha\varphi + h} + rK_1(\varphi) + K_2(\varphi).$$

Hence:

$$F_\varphi = \frac{1}{6} \frac{pr^3 \beta\alpha \cos \alpha\varphi}{(\beta \sin \alpha\varphi + h)^2} + r(K_1)_\varphi + (K_2)_\varphi,$$

$$F_{\varphi\varphi} = - \frac{pr^3 \beta\alpha^2}{6} \frac{\beta(1 + \cos^2 \alpha\varphi) + h \sin \alpha\varphi}{(\beta \sin \alpha\varphi + h)^3} + r(K_1)_{\varphi\varphi} + (K_2)_{\varphi\varphi},$$

$$F_{r\varphi} = \frac{pr^2 \beta\alpha}{2} \cdot \frac{\cos \alpha\varphi}{(\beta \sin \alpha\varphi + h)^2} + (K_1)_\varphi$$

where

$$\beta = c(1 - \alpha^2).$$

Knowing the stress function, the derivatives permit to calculate the reduced stress resultants:

$$n_\varphi = - \frac{pr}{\beta \sin \alpha\varphi + h}$$

$$n_r = - \frac{pr}{2(\beta \sin \alpha\varphi + h)} \left[1 + \frac{\beta\alpha^2}{3} \frac{\beta(1 + \cos^2 \alpha\varphi) + h \sin \alpha\varphi}{(\beta \sin \alpha\varphi + h)^2} \right] +$$

$$+ \frac{1}{r} [K_1 + (K_1)_{\varphi\varphi}] + \frac{1}{r^2} (K_2)_{\varphi\varphi},$$

$$n_{r\varphi} = -\frac{1}{3}\, pr\,\beta\alpha\,\frac{\cos\alpha\varphi}{(\beta\sin\alpha\varphi + h)^2} + \frac{1}{r^2}\,(K_2)_\varphi .$$

4. Boundary conditions

No force is known to be an outlet along the boundary $r = R$, thus,

$$n_{r\varphi} = 0,$$

$$n_r = 0.$$

From these conditions the unknown constants can be determined, namely, from the first condition

$$n_{r\varphi} = -\frac{1}{1}\, pR\,\beta\alpha\,\frac{\cos\alpha\varphi}{(\beta\sin\alpha\varphi + h)^2} + \frac{1}{R^2}\,(K_2)_\varphi = 0\,,$$

hence,

$$(K_2)_\varphi = \frac{1}{3}\, pR^3\,\beta\alpha\,\frac{\cos\alpha\varphi}{(\beta\sin\alpha\varphi + h)^2}$$

is obtained and from the second one:

$$n_r = -\frac{1}{2}\,\frac{pR}{(\beta\sin\alpha\varphi + h)}\left[1 + \frac{\beta\alpha^2}{3}\,\frac{\beta(1+\cos^2\alpha\varphi) + h\sin\alpha\beta}{(\beta\sin\alpha\varphi + h)^2}\right] +$$

$$+ \frac{1}{R}\left[K_1 + (K_1)_{\varphi\varphi}\right] + \frac{1}{R^2}\,(K_2)_{\varphi\varphi} = 0\,.$$

Expression $(K_2)_\varphi$ already being known from the foregoing, thus

$$(K_2)_{\varphi\varphi} = -\frac{1}{3}\, pR^3\,\beta\alpha\,\frac{\beta(1+\cos^2\alpha\varphi) + h\sin\alpha\varphi}{(\beta\sin\alpha\varphi + h)^3}\,,$$

hence

$$n_r = -\frac{pR}{2\,(\beta\sin\alpha\varphi + h)} - \frac{pR\,\beta\alpha^2}{2} \times$$

$$\times\,\frac{\beta(1+\cos^2\alpha\varphi) + h\sin\alpha\varphi}{(\beta\sin\alpha\varphi + h)^3} + \frac{1}{R}\,\left[K_1 + (K_1)_{\varphi\varphi}\right] = 0$$

and as a conclusion:

$$K_1 + (K_1)_{\varphi\varphi} = \frac{pR^2}{2(\beta\sin\alpha\varphi + h)^3}\left\{(\beta\sin\alpha\varphi + h)^2 + \right.$$

$$\left. + \beta\alpha^2\left[\beta\,(1+\cos^2\alpha\varphi) + h\sin\alpha\varphi\right]\right\}.$$

Thus, the boundary conditions led to a differential equation of the second order, one particular solution being:

$$K_1 = \frac{pR^2}{2\,(\beta \sin \alpha\varphi + h)}\,.$$

Namely:

$$(K_1)_\varphi = -\frac{pR^2\,\beta\alpha}{2}\,\frac{\cos \alpha\varphi}{(\beta \sin \alpha\varphi + h)^2}\,,$$

$$(K_1)_{\varphi\varphi} = \frac{pR^2\,\beta\alpha^2}{2}\,.\,\frac{\beta\,(1 + \cos^2 \alpha\varphi) + h \sin \alpha\varphi}{(\beta \sin \alpha\varphi + h)^3}\,.$$

The substitution of these values into the differential equation yields an identity. Thus, the reduced stress resultants sought for are:

$$n_\varphi = -\frac{pr}{\beta \sin \alpha\varphi + h}\,,$$

$$n_{r\varphi} = \frac{1}{3}\,pr\;\beta\alpha\,\frac{\cos \alpha\varphi}{(\beta \sin \alpha\varphi + h)^2}\left(\frac{R^3}{r^3} - 1\right),$$

$$n_r = \frac{pr}{2(\beta \sin \alpha\varphi + h)}\left[\left(\frac{R^2}{r^2} - 1\right) + \right.$$

$$\left. + \frac{1}{3}\,\beta\alpha^2\,\frac{\beta(1 + \cos^2 \alpha\varphi) + h \sin \alpha\varphi}{(\beta \sin \alpha\varphi + h)^2}\left(3\,\frac{R^2}{r^2} - 2\,\frac{R^3}{r^3} - 1\right)\right].$$

5. Examples

To show the application of the above investigations, two examples are presented.

As a first example the structure to be seen in Fig. 2 is discussed, where $h > 0$. Its internal stresses are shown in Figs 5 and Fig. 6. Stresses are seen to be finite throughout, except at the cone vertex, where the reduced radial and tangential stress resultants are infinite.

As another example, the same surface is presented for $h = 0$. Fig. 6 shows all three reduced stress resultants, along the supported edges to be infinite. Thus, such structures can only be built if flexural reinforcement is applied in areas where the reduced stress resultants are infinite.

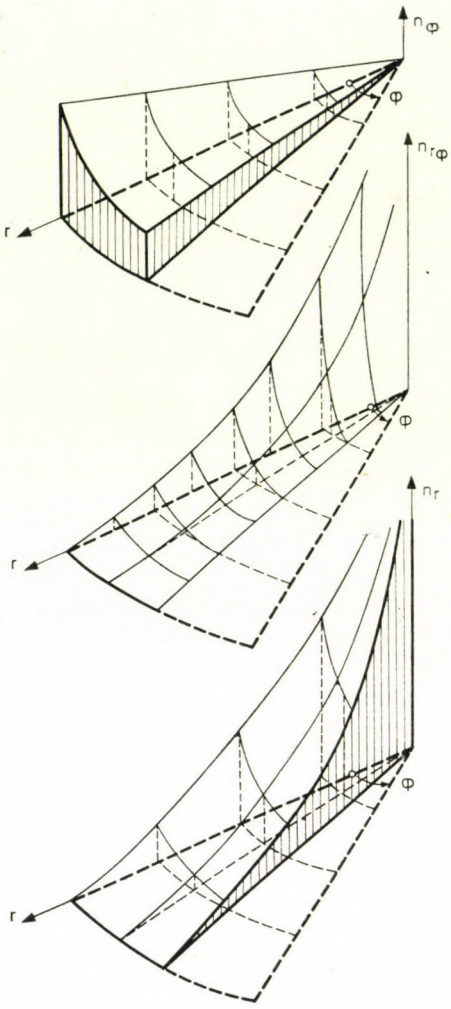

Fig. 5

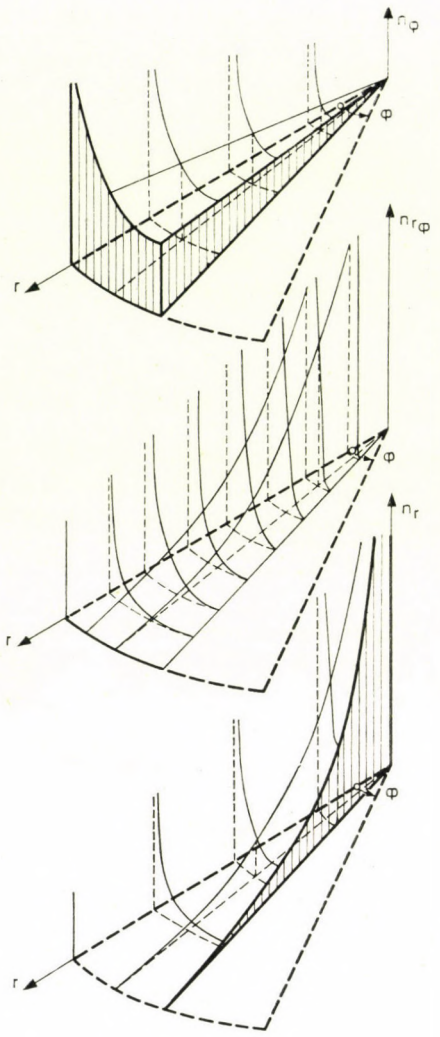

Fig. 6

REFERENCES

1. MENYHÁRD, I.: Theory of Shell Structures I—II.* Mérnöki Továbbképző Intézet, 1943/44, 1—32, 197—236
2. BÖLCSKEI, E.—OROSZ, Á.: Reinforced Concrete Structures II. Theory of Shell Structures.* Tankönyvkiadó, Budapest 1965
3. CSONKA, P.: Differential Equation of Membrane Shells Written in a Cylindrical System of Co-ordinates.* *Mélyépítéstudományi Szemle* (1974), 241—243

*In Hungarian

Wellenkegelschalen. Wellenkegelschalen mit lotrechter Achse, Kreisgrundriß und freiem Rand werden in einem zylinderischen Koordinatensystem analysiert. Die untersuchten Schalen sind durch gleichverteilte Vertikallast beansprucht und durch radiale Rippen versteift. Für die Bestimmung der reduzierten Spannungsresultanten sind Formeln angegeben. Die Spannungsverteilung wird an zwei praktischen Beispielen gezeigt.

Конусообразные гофрированные оболочки. Работа занимается исследованием конусообразных гофрированных оболочек круглого плана с вертикальной осью и со свободным краем в системе цилиндрических координат. Свободно вращающиеся оболочки работают под нагрузкой совместно распределяющихся вертикальных усилий и опираются на радиальные реборды. В данной работе приводятся формулы для расчета редуцированных секущих усилий и их распределение иллюстрируется двумя практическими примерами.

Acta Technica Academiae Scientiarum Hungaricae, Tomus 82 (1—2), pp. 9—13 (1976)

SOME RECIPROCAL PROPERTIES OF STRESS COMPONENTS

J. BARTA*
DOCTOR OF TECHN. SCI.

[Manuscript received December 15, 1974]

Two of the reciprocal properties presented here, are purely mathematical properties referring not only to stress components, but also to all vector components. The further reciprocal properties shown here are, in the last analysis, physical properties, because they are derived from the well-known equality $p_{ab} = p_{ba}$ which is a consequence of the dynamical equilibrium.

The aim of the present paper is to prove that stress components possess reciprocal properties II—VI. The reciprocal property I is well-known in the Analysis of Stresses (see for ex. [1]) and will be used here to prove II, III and VI.

Ler Q be a point of the continuum, Fig. 1. Let the surface elements A, B, C, pass through the point Q. We denote the normals of A, B, C by a, b, c, the stress vectors acting on A, B, C by $\mathbf{p}_a$, $\mathbf{p}_b$, $\mathbf{p}_c$. The stress components

$$p_{aab},\quad p_{abb},\quad p_{abc},\quad \ldots,\quad p_{cba} \tag{1}$$

are defined as follows: p_{bac} (for example) signifies the component of $\mathbf{p}_b$ in direction a when the cutting plane is orthogonal to c. Stress components p_{bac} and p_{bcc} can be seen in Fig. 2, so that the normals a and c lie in the drawing plane, but the normal b and the stress vector $\mathbf{p}_b$ do not generally lie there; the cutting plane is indicated by a dotted line. The stress componente have the unit kg/cm².

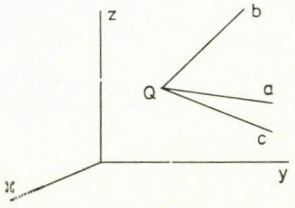

Fig. 1

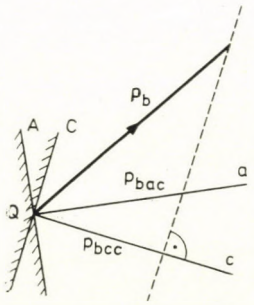

Fig. 2

*Prof. Dr. Ing. J. BARTA, József körút 35. H-1085 Budapest, Hungary.

As usual, two sorts of continua will be distinguished, namely, classical continuum and Cosserat continuum. In the classical continuum, only ordinary stresses and forces are present. In the Cosserat continuum, in addition to the ordinary stresses and forces, also couple stresses (or couple stresses with volume moments) are present. The notion "Cosserat continuum" includes the notion "classical continuum" as a special case. Thus, all ascertainments referring to Cosserat continuum refer also to classical continuum, but the reverse does not generally hold. We denote the couple stress vector acting on A, B, C by $\mathbf{m}_a$, $\mathbf{m}_b$, $\mathbf{m}_c$. The couple stress components are scalar quantitites, having the unit kp/cm, and will be denoted in the present paper by

$$m_{aab}, \quad m_{abb}, \; m_{abc}, \; \ldots, \quad m_{cba} \tag{2}$$

defined in the very same manner as (1).

Most authors denote the stress components by

$$\sigma_x, \; \sigma_y, \; \sigma_z, \; \tau_{yz}, \; \tau_{zy}, \; \tau_{zx}, \; \tau_{xz}, \; \tau_{xy}, \; \tau_{yx} \tag{3}$$

where the directions x, y, z are orthogonal to one another, and write

$$\begin{array}{lll} \sigma_x & \text{instead of} & p_{xxx} \\ \tau_{yz} & \text{instead of} & p_{yzz} \\ p_{ab} & \text{instead of} & p_{abb} \\ p_{ba} & \text{instead of} & p_{baa} \\ p_{bc} & \text{instead of} & p_{bcc} \\ \ldots\ldots\ldots\ldots\ldots & & \end{array} \tag{4}$$

In the classical continuum, the relations $\tau_{yz} = \tau_{zy}$, $\tau_{zx} = \tau_{xz}$, $\tau_{xy} = \tau_{yx}$ hold, but in Cosserat continuum, they do not generally hold.

We shall consider the following reciprocal properties of the stress components:

I. If a and b are two directions, then at any point of the classical continuum, the equation $p_{abb} = p_{baa}$ holds.

II. If a and b are two directions, then at any point of the classical continum, the equation $p_{aab} = p_{bba}$ holds.

III. If a, b, c are three directions, then at any point of the classical continuum, the equation $p_{abc}\, p_{bca}\, p_{cab} = p_{acb}\, p_{bac}\, p_{cba}$ holds.

IV. If a, b, c are three directions, then at any point of the Cosserat continuum, the equation $p_{aba}\, p_{bcb}\, p_{cac} = p_{aca}\, p_{bab}\, p_{cbc}$ holds.

V. If a, b, c are three directions, then at any point of the Cosserat continuum, the equation $m_{aba}\, m_{bcb}\, m_{cac} = m_{aca}\, m_{bab}\, m_{cbc}$ holds.

VI. If the directions a, b, c form an equiangular tripod (Fig. 3), then at any point of the classical continuum, the equations $p_{abc} = p_{cba}$, $p_{bca} = p_{acb}$, $p_{cab} = p_{bac}$ hold.

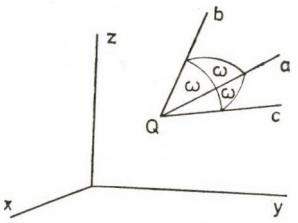

Fig. 3

With the notations (4), one writes (for example) in I

$$p_{ab} = p_{ba} \quad \text{instead of} \quad p_{abb} = p_{baa}.$$

The proof of II can be carried out in the following manner. It is to be seen from Fig. 2 that the equation $p_{bcc} = p_{bac} \cos(c, a)$ holds. By writing a instead of b, and b instead of c, the equation

$$p_{abb} = p_{aab} \cos(b, a) \tag{5}$$

arises. Analogously, also the equation

$$p_{baa} = p_{bba} \cos(a, b) \tag{6}$$

is to be found. Inserting (5) and (6) into I, and taking into account the equality $\cos(b, a) = \cos(a, b)$, II is obtained.

The proof of III can be carried out as follows. **a b c** are the unit vectors of the normals a, b, c. As usual in Vector Calculus, **ac** signifies the scalar product of **a** and **c**. From Fig. 2 and relation $\mathbf{ac} = \cos(a, c)$, the equation

$$p_{bac} = \frac{\mathbf{p}_b \mathbf{c}}{\mathbf{ac}} \tag{7}$$

follows. According to I, the equation $p_{bcc} = p_{cbb}$ is valid. This reads, in vector notation,

$$\mathbf{p}_b \mathbf{c} = \mathbf{p}_c \mathbf{b}. \tag{8}$$

Introducing (8) into (7),

$$p_{bac} = \frac{\mathbf{p}_c \mathbf{b}}{\mathbf{ac}} = \frac{\mathbf{p}_c \mathbf{b}}{\mathbf{ca}} = \frac{\mathbf{ab}}{\mathbf{ca}} \cdot \frac{\mathbf{p}_c \mathbf{b}}{\mathbf{ab}} = \frac{\mathbf{ab}}{\mathbf{ca}} p_{cab}$$

is obtained. Thus the equation

$$\frac{\mathbf{ab}}{\mathbf{ca}} p_{cab} = p_{bac} \tag{9}$$

is valid. Similarly, also the equations

$$\frac{\mathbf{bc}}{\mathbf{ab}} p_{abc} = p_{cba}, \qquad \frac{\mathbf{ca}}{\mathbf{bc}} p_{bca} = p_{acb} \tag{10-11}$$

hold. By multiplying the left sides and also the right sides of equations (9), (10), (11), III is arrived at.

The proof of IV can be carried out in the following way. After replacing b by a, a by b, c by a, (7) takes the form

$$p_{aba} = \frac{\mathbf{p}_a \mathbf{a}}{\mathbf{ba}} = \frac{\mathbf{ca}}{\mathbf{ba}} \cdot \frac{\mathbf{p}_a \mathbf{a}}{\mathbf{ca}} = \frac{\mathbf{ca}}{\mathbf{ba}} p_{aca} .$$

This shows that the equation

$$p_{aba} = \frac{\mathbf{ca}}{\mathbf{ba}} p_{aca} \tag{12}$$

is valid. A similar way leads to equations

$$p_{bcb} = \frac{\mathbf{ab}}{\mathbf{cb}} p_{bab}, \qquad p_{cac} = \frac{\mathbf{bc}}{\mathbf{ac}} p_{cbc} . \tag{13-14}$$

If the left sides, and also the right sides of equations (12), (13), (14) are multiplied, and the equalities $\mathbf{ab} = \mathbf{ba}$, $\mathbf{bc} = \mathbf{cb}$, $\mathbf{ca} = \mathbf{ac}$ are taken into account, then IV arises.

The proof of V the is following. We consider the fact that IV expresses only a property of vectors, regardless of the physical meaning of the vectors, and its proof happened without direct or indirect employment of I. Also $\mathbf{m}_a$, $\mathbf{m}_b$, $\mathbf{m}_c$ are vectors, and their physical meaning does not play a role in V. Thus, the validity of V immediately follows from IV.

The proof of VI can be carried out in the following way. We take into account that the directions a, b, c now form an equiangular tripod. Hence, the relation $\mathbf{bc} = \mathbf{cb} = \mathbf{ca} = \mathbf{ac} = \mathbf{ab} = \mathbf{ba}$ subsists. Therefore, equations (9), (10), (11) express VI.

R e m a r k s: Reciprocal properties IV and V are purely mathematical properties, because not only the stress components but also all vector components possess these properties. — Reciprocal properties I, II, III, VI are physical properties, because they were derived from the dynamical equilibrium of the continuum. — If the directions a, b, c are perpendicular to each other, then I yields the equations $p_{yzz} = p_{zyy}$, $p_{zxx} = p_{xzz}$, $p_{xyy} = p_{yxx}$ which in the most books will be written in the form $\tau_{yz} = \tau_{zx}$, $\tau_{zx} = \tau_{xz}$, $\tau_{xy} = \tau_{yx}$, however, II, III, IV, V, VI yield only the uninteresting equation $\infty = \infty$.

REFERENCE

1. SOKOLNIKOFF, I. S.: Mathematical Theory of Elasticity. First edition 1946 § 16, or second edition 1956 § 16.

Über einige Reziprozitätseigenschaften der Spannungskomponenten. Es werden einige Reziprozitätseigenschaften der Spannungskomponenten mitgeteilt. Zwei von diesen sind reine mathematische Eigenschaften, denn sie beziehen sich nicht nur auf Spannungskomponenten, sondern auch auf allerlei Vektorkomponenten. Die übrigen sind physikalische Eigenschaften, denn sie gründen sich auf die Gleichung $p_{ab} = p_{ba}$, also auf das dynamische Gleichgewicht.

Некоторые обратные свойства составляющих напряжений. Из числа перечисленных в данной работе обратных свойств два свойства являются чисто математическими, так как они касаются не только составляющих напряжений, но и любых векторных составляющих. Однако, остальные же можно считать в качестве физических свойств, так как их вывод основывается на равенстве $P_{ab} = P_{ab}$, а это равенство является следствием динамического равновесия.

Acta Technica Academiae Scientiarum Hungaricae, Tomus 82 (1—2), pp. 15—29 (1976)

DESIGN OF STAR-SHELLS SUBJECTED TO FULL LOAD

P. CSONKA*
DOCTOR OF TECHN. SC.

[Manuscipt received October 1, 1975]

The paper deals with paraboloid shells of revolution subjected to an axisymmetrically distributed full load (dead load and snow load applied simultaneously) acting in vertical direction. The form of the base over which the shell in question is constructed, is a regular polygon-like configuration with concave curved sides, a so-called *star-polygon*. The treated shell — the so-called *star-shell* — is bordered by an edge beam supported along its whole length by a wall, wherefore, the cross-section of the edge beam is only subjected to a centric normal force, the so-called *string force*. By using a convenient calculation method the shape of the starpolygon is so designed that the stress resultants, generated in the shell, can be calculated with the aid of closed formulae. A numeric example proves the suggested method as being expedient.

1. Introduction

By the term *star-polygon* a regular polygon-like planar configuration is understood having concave curved sides; a paraboloid shell of revolution constructed over a star-polygonal base, is called a *star-shell* (Fig. 1). In connection

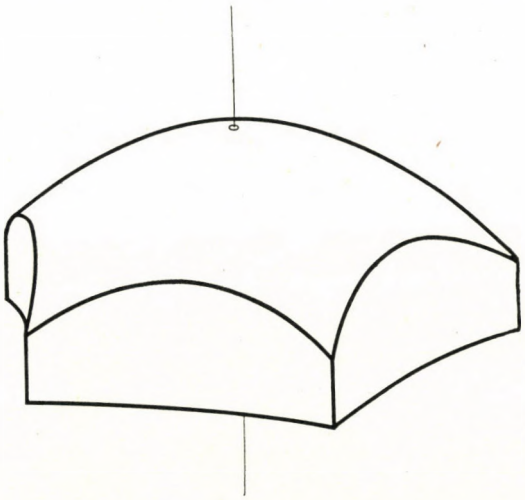

Fig. 1. Five-sided star-shell

*Prof. Dr. P. Csonka, Bartók B. u. 31. H-1114 Budapest, Hungary.

with this latter it is assumed that the shell is bordered by an edge beam supported along its whole length by a wall. In the cross-sections of these edge beams only centric normal forces — *string forces* — are generated [5].

Axisymmetrically distributed vertical forces are assumed as being applied on the shell (dead load and a simultaneously acting snow load).

The investigations are performed by using the customary assumptions of the membrane theory. The bending and torsional forces generated by the diverse deformations of the shell and edge beam are neglected.

Depending on the load system to be taken into account, the shape of the star polygon will be designed so that the stress resultants induced in the shell wall by this load system (or load systems proportional to it) can be calculated with the aid of closed formulae.

A particular simple type of star-shells, i.e., the problem of star-shells design for a load system *uniformly distributed* on the base surface, was already treated in two previous papers by the author [3, 4]. In the present paper a more general problem, that of star-shells loaded by axisymmetrically distributed system of vertical forces (dead load and snow load applied at the same time), is discussed.

2. The shape function

The investigations will be carried out in a cylindrical system of co-ordinates $0(r, \varphi, z)$ represented in Fig. 2. The origin 0 of this system of co-ordinates is at the vertex of the middle surface of the shell, the axis z coincides with the axis of revolution of the paraboloid shell. The positive leg of axis z is directed downwards from the origin, and the polar plane $\varphi = 0$ halves one of the sides of the base figure.

The radius of the circle circumscribed around the star-polygon is denoted by R, that of the inscribed circle by r_0 ,and the altitude of the shell by h.

The co-ordinates of the corners of the star polygon having n sides are as follows:

$$r = R, \quad \varphi = \frac{\pi}{n}, \frac{3\pi}{n}, \frac{5\pi}{n}, \ldots, \frac{(2n-1)\pi}{n}.$$

In the system of co-ordinates $0(r, \varphi, z)$ the shape of the star-shell is characterized by the equation of its middle surface:

$$z = \frac{h}{R^2} r^2.$$

This equation is called the *shape function* of the shell.

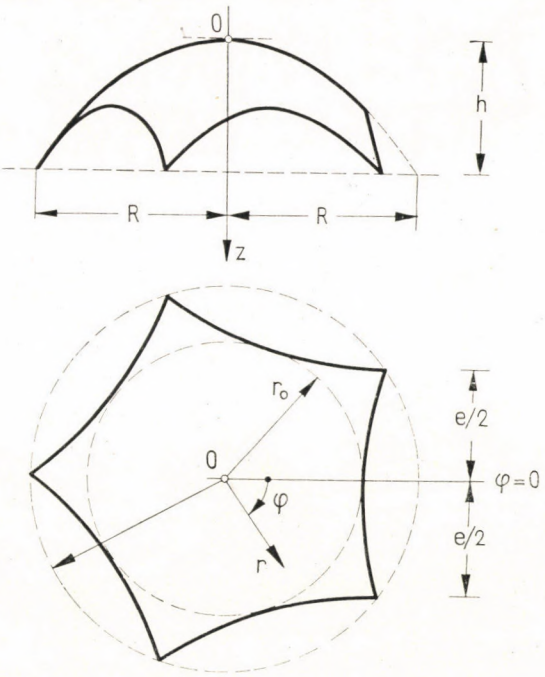

Fig. 2. Cylindrical system of co-ordinates $0\ (r, \varphi, z)$

3. The load function

The load to which the shell is subjected, is characterized by its specific value related to the unit area of the *base surface*, the so-called *reduced load*. The function

$$\bar{p} = \bar{p}(r)$$

expressing the reduced load-value is called *load function*.

Two types of load functions are dealt with hereafter.

3.1 The exact load function

This is the term for the load function expressing the total value to which the shell wall is subjected: the dead load of the shell wall of constant thickness and the load, uniformly distributed on the basic surface. Be the specific weight of the shell wall related to the unit area of the *middle surface*

$$p_0 = \text{const.},$$

and the specific value of the snow load related to the unit area of the *base surface*

$$p_s = \text{const.}$$

In this case the exact load function may be expressed by the formula

$$\bar{p} = p_0 \sqrt{1 + \left(\frac{dz}{dr}\right)^2} + p_s = p_0 \sqrt{1 + \frac{4\,h^2\,r^2}{R^4}} + p_s. \tag{2}$$

By introducing the simplifying notation

$$a \equiv \frac{R^2}{2h}, \tag{3}$$

formula (2) may be reduced to the form

$$\bar{p} = \frac{p_0}{a} \sqrt{a^2 + r^2} + p_s. \tag{4}$$

3.2. The approximate load function

This is the name of that load function, where the total load to which the shell is subjected (dead load and snow load applied simultaneously) is approached by a polynome having the form

$$\bar{p} = A_0 + A_1 \frac{r^2}{R^2} + A_2 \frac{r^4}{R^4} + \ldots + A_k \frac{r^{2k}}{R^{2k}}. \tag{5}$$

A load function of similar construction may also be applied as an approximation in lieu of the "exact" load function described in paragraph 3.1. In these cases, as an approximate polynome, the expression

$$\bar{p}^* = (p_0 + p_s) + \frac{9}{5} p_0 \gamma \frac{r^2}{R^2} - \frac{2}{3} p_0 \gamma^2 \frac{r^4}{R^4} \tag{5*}$$

may be used, where

$$\gamma = \frac{h^2}{R^2}.$$

4. The stress function

The stress function $F = F(r, \varphi)$ of shells of revolution subjected to uniformly distributed vertical forces $\bar{p} = \bar{p}(r, \varphi)$ has, in general [3], to satisfy the following differential rquation:

$$\frac{\partial^2 F}{\partial r^2} \cdot \frac{1}{r} \cdot \frac{dz}{dr} + \frac{1}{r} \cdot \frac{\partial F}{\partial r} \cdot \frac{d^2 z}{dr^2} + \frac{1}{r^2} \cdot \frac{\partial^2 F}{\partial \varphi^2} \cdot \frac{d^2 z}{dr^2} + \bar{p} = 0.$$

In case of a paraboloid shell of revolution the relations

$$\frac{dz}{dr} = \frac{2h}{R^2}\, r = \frac{r}{a}, \quad \frac{d^2 z}{dr^2} = \frac{2h}{R^2} = \frac{1}{a}$$

are valid and so the differential equation to be satisfied by the stress function will be simplified as follows:

$$\frac{\partial^2 F}{\partial r^2} + \frac{1}{r} \cdot \frac{\partial F}{\partial r} + \frac{1}{r^2} \cdot \frac{\partial^2 F}{\partial \varphi^2} + a\,\bar{p} = 0. \tag{6}$$

Hereafter, a finite solution to the above differential equation is to be sought for which satisfies on the one hand the condition

$$F = 0 \tag{7}$$

along the edge line of the shell, and on the other hand

$$\frac{\partial F}{\partial r} = 0 \tag{8}$$

at the corners of the shell.

The boundary condition (7) might be prescribec to every shell whose edge beam is continuously supported [5], while the restriction (8) is justified by the fact that the points $r = R$ of the edge line of the star-polygon must be so-called *double points*. A further condition of the existence of the double points, i.e., that at the points $r = R$, at least one of the second derivatives of F should differ from zero, is fulfilled in this case, because at the points $r = R$ the load value is $\bar{p} \neq 0$.

4.1. Case of the exact load function

In case of the "exact" load function (4), the differential equation (6) will take the following form:

$$\frac{\partial^2 F}{\partial r^2} + \frac{1}{r} \cdot \frac{\partial F}{\partial r} + \frac{1}{r^2} \cdot \frac{\partial^2 F}{\partial \varphi^2} + p_0 \sqrt{a^2 + r^2} + p_s a = 0. \tag{9}$$

The function F satisfying the differential equation (9) will be composed of two parts: from the axisymmetrical solution of the form

$$F_i = F_i(r)$$

of the *inhomogeneous* differential equation, and from the solution of the form

$$F_h = C_n r^n \cos n\,\varphi, \qquad C_n = \text{const.}$$

of the *homogeneous* differential equation. Accordingly we have

$$F = F_i + F_h = F_i + C_n\, r^n \cos\, n\,\varphi. \tag{10}$$

First the function F_i should be determined. An axisymmetrical case being at issue, the following ordinary differential equation, instead of the partial differential equation (9), may be used:

$$\frac{d^2 F_i}{dr^2} + \frac{1}{r} \cdot \frac{dF_i}{dr} + p_0 \sqrt{a^2 + r^2} + p_s a = 0.$$

This second-order differential equation is transformed by the substitution

$$\frac{dF_i}{dr} = U(r) \tag{11}$$

into the first-order differential equation

$$\frac{dU}{dr} + \frac{1}{r} dU + p_0 \sqrt{a^2 + r^2} + p_s a = 0,$$

whose general solution is

$$U = -\frac{p_0}{3}\left[\frac{\sqrt{(a^2 + r^2)^3}}{r} + \frac{C_0}{r}\right] - p_s \frac{a r}{2}.$$

Consequently,

$$\frac{dF_i}{dr} = -\frac{p_0}{3}\left[\frac{\sqrt{(a^2 + r^2)^3}}{r} + \frac{C_0}{r}\right] - p_s \frac{a r}{2},$$

and hence, after integration

$$F_i = -\frac{p_0}{3}\left[\frac{4a^2 + r^2}{3}\sqrt{a^2 + r^2} - a^3 \ln\left(a + \sqrt{a^2 + r^2}\right) + a^3 \ln r + C_0 \ln r\right] - p_s \frac{a r^2}{4} + C_1. \tag{12}$$

The above expression can only be finite, if

$$C_0 = -a^3.$$

With this replacement, formula (12) of function F_i becomes:

$$F_i = -\frac{p_0}{3}\left[\frac{4a^2 + r^2}{3}\sqrt{a^2 + r^2} - a^3 \ln\left(a + \sqrt{a^2 + r^2}\right)\right] - p_s \frac{a r^2}{4} + C_1. \tag{13}$$

The function F_i, i.e., the first part of function F being familiar, function F itself can be produced by completing this part of the function with the expression $C_n r^n \cos n\varphi$.

Accordingly

$$F = -\frac{p_0}{3}\left[\frac{4a^2 + r^2}{3}\sqrt{a^2 + r^2} - a^3 \ln\left(a + \sqrt{a^2 + r^2}\right)\right] - p_s \frac{a r^2}{4} + C_1 + C_n r^n \cos n\varphi. \tag{14}$$

The indefinite constants C_1 and C_n entering the above formula should and could be determined by taking the *boundary conditions* (7) and (8) into account.

First, let us put down condition (8), i.e., the requirement that at point

$r = R$, $\varphi = \pi/n$, the derivative of function F with respect to r could disappear:

$$-\frac{p_0}{3}\left[\frac{2a^2R + R^3}{\sqrt{a^2+R^2}} - \frac{a^3R}{\left(a+\sqrt{a^2+R^2}\right)\sqrt{a^2+R^2}}\right] - \\ - p_s\frac{aR}{2} - C_n nR^{n-1} = 0\,.$$

Hence,

$$C_n = -\frac{p_0}{3}\left(a + \frac{a^2+R^2}{a+\sqrt{a^2+R^2}}\right)\frac{1}{nR^{n-2}} - p_s\frac{a}{2nR^{n-2}}\,. \tag{14a}$$

Substitution of this value into formula (14) yields

$$F = -\frac{p_0}{3}\left[\frac{4a^2+r^2}{3}\sqrt{a^2+R^2} - a^3\ln\left(a+\sqrt{a^2+r^2}\right) + \right. \\ \left. + \left(a + \frac{a^2+R^2}{a+\sqrt{a^2+R^2}}\right)\frac{r^n\cos n\varphi}{nR^{n-2}}\right] - p_s a\left(\frac{r^2}{4} + \frac{r^n\cos n\varphi}{2nR^{n-2}}\right) + C_1. \tag{15}$$

Afterwards, the only thing to be done is to satisfy condition (7), i.e., to make sure that all along the edge line of the star-shell the value of function F should be equal to zero. This requirement should, in the first line, be written only in respect to the corner point $r = R$, $\varphi = \pi/n$:

$$-\frac{p_0}{3}\left[\frac{4a^2+R^2}{3}\sqrt{a^2+R^2} - a^3\ln\left(a+\sqrt{a^2+R^2}\right) - \right. \\ \left. - \left(a + \frac{a^2+R^2}{a+\sqrt{a^2+R^2}}\right)\frac{R^2}{n}\right] - p_s a\left(\frac{R^2}{4} - \frac{R^2}{2n}\right) + C_1 = 0.$$

Expressing C_1 from this equation and replacing it into formula (15), the following expression is obtained as stress function:

$$F = -\frac{p_0}{3}\left[\frac{4a^2+r^2}{3}\sqrt{a^2+r^2} - \frac{4a^2+R^2}{3}\sqrt{a^2+R^2} - \right. \\ - a^3\ln\frac{a+\sqrt{a^2+r^2}}{a+\sqrt{a^2+R^2}} + \left(a + \frac{a^2+R^2}{a+\sqrt{a^2+R^2}}\right)\left.\frac{R^n - r^n\cos n\varphi}{nR^{n-2}}\right] + \\ + p_s a\left(\frac{R^2-r^2}{4} - \frac{R^n + r^n\cos n\varphi}{2nR^{n-2}}\right). \tag{16}$$

However, condition (7) should be satisfied all along the length of the edge line, and not only at the corners. Therefore, the outline of the base figure cannot be assumed arbitrarily; it should be so drawn that along the line in

question, F should be equal to zero everywhere, i.e., the following condition should be satisfied all along the length of this line:

$$-\frac{p_0}{3}\left[\frac{4a^2+r^2}{3}\sqrt{a^2+r^2}-\frac{4a^2+R^2}{3}\sqrt{a^2+R^2}-\right.$$

$$-a^3\ln\frac{a+\sqrt{a^2+r^2}}{a+\sqrt{a^2+R^2}}+\left(a+\frac{a^2+R^2}{a+\sqrt{a^2+R^2}}\right)\frac{R^n-r^n\cos n\varphi}{nR^{n-2}}\Bigg]+$$

$$+p_s a\left(\frac{R^2-r^2}{4}-\frac{R^n+r^n\cos n\varphi}{2n\,R^{n-2}}\right)=0\,. \tag{17}$$

Formula (16) is that of the stress function of the star-shell designed for the "exact" load, and formula (17) is the equation of the edge line of the star-polygon, i.e., of the base figure of the shell.

4.2. Case of the approximate load function

If the load applied to the shell is expressed by polynom (5), then for the stress function of the shell the formula

$$F=\frac{R^4}{8h}\left[\frac{A_0}{1}\left(1-\frac{r^2}{R^2}\right)+\frac{A_1}{4}\left(1-\frac{r^4}{R^4}\right)+\ldots+\frac{A_k}{(k+1)^2}\left(1-\frac{r^{2k+2}}{R^{2k+2}}\right)-\right.$$

$$\left.-\frac{2}{n}\left(\frac{A_0}{1}+\frac{A_1}{2}+\ldots+\frac{A_k}{k+1}\right)\left(1+\frac{r^n}{R^n}\right)\cos n\varphi\right], \tag{18}$$

and for the edge line of the star-shell the formula

$$\frac{A_0}{1}\left(1-\frac{r^2}{R^2}\right)+\frac{A_1}{4}\left(1-\frac{r^4}{R^4}\right)+\ldots+\frac{A_k}{(k+1)^2}\left(1-\frac{r^{2k+2}}{R^{2k+2}}\right)-$$

$$-\frac{2}{n}\left(\frac{A_0}{1}+\frac{A_1}{2}+\ldots+\frac{A_k}{k+1}\right)\left(1+\frac{r^n}{R^n}\cos n\varphi\right)=0 \tag{19}$$

are obtained.

Should the load to which the shell is subjected be taken into account by the approximate formula (5*) instead of the exact formula (4), so

$$\begin{aligned} A_0&=p_0+p_s,\\ A_1&=\frac{9}{5}p_0\gamma\,,\\ A_2&=-\frac{2}{3}p_0\gamma^2\,,\\ A_3&=A_4=\ldots=A_k=0. \end{aligned} \tag{20}$$

In this case, the formula of the approximate stress function will be

$$F^* = \frac{R^4}{8h}\left[(p_0+p_s)\left(1-\frac{r^2}{R^2}\right)+\frac{9}{20}p_0\,\gamma\left(1-\frac{r^4}{R^4}\right)-\frac{2}{27}p_0\,\gamma^2\left(1-\frac{r^6}{R^6}\right)-\right.$$

$$\left.-\frac{2}{n}\left(p_0+p_s+\frac{9}{10}p_0\,\gamma-\frac{2}{9}p_0\,\gamma^2\right)\left(1+\frac{r^n}{R^n}\cos\,n\varphi\right)\right], \qquad (18^*)$$

and the equation of the edge line of the star-polygon is

$$(p_0+p_s)\left(1-\frac{r^2}{R^2}\right)+\frac{9}{20}p_0\gamma\left(1-\frac{r^4}{R^4}\right)-\frac{2}{27}p_0\,\gamma^2\left(1-\frac{r^6}{R^6}\right)-$$

$$-\frac{2}{n}\left(p_0+p_s+\frac{9}{10}p_0\,\gamma-\frac{2}{9}p_0\,\gamma^2\right)\left(1+\frac{r^n}{R^n}\cos\,n\varphi\right)=0. \qquad (19^*)$$

In the above formulae

$$\gamma=\frac{h^2}{R^2}\,.$$

5. Stress resultants

The reduced stress results of the star-shell can be calculated with the aid of the following well-known formulae [2]:

$$\bar{N}_r=\frac{1}{r}\cdot\frac{\partial F}{\partial r}+\frac{1}{r^2}\cdot\frac{\partial^2 F}{\partial\varphi^2},$$

$$\bar{N}_{r\varphi}=\frac{1}{r^2}\cdot\frac{\partial F}{\partial\varphi}-\frac{1}{r}\cdot\frac{\partial^2 F}{\partial r\cdot\partial\varphi}, \qquad (21)$$

$$\bar{N}_\varphi=\frac{\partial^2 F}{\partial r^2}\,.$$

The positive sense of these stress resultants is shown in Fig. 3.

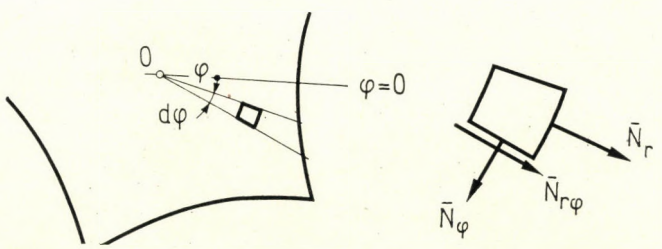

Fig. 3. Reduced stress resultants $\bar{N}_r$, $\bar{N}_{r\varphi}$, $\bar{N}_\varphi$

5.1. *Case of the exact load function*

When formulae (21) are applied to the exact function F given by equation (16), then, for the reduced stress resultants the following formulae are obtained:

$$\bar{N}_r = -\frac{p_0}{3}\frac{\sqrt{(a^2+r^2)^3}-a^3}{r^2} - p_s\frac{a}{2} - C_n n(n-1)r^{n-2}\cos n\varphi,$$

$$\bar{N}_{r\varphi} = C_n n\,(n-1)r^{n-2}\sin n\varphi, \tag{22}$$

$$\bar{N}_\varphi = -\frac{p_0}{3}\frac{(2r^2-a^2)\sqrt{a^2+r^2}+a^3}{r^2} - p_s\frac{a}{2} + C_n n(n-1)r^{n-2}\cos n\varphi.$$

In the above formulae, the meaning of C_n is as given by (14a).

5.2. *Case of the approximate load function*

Applying formulae (21) to the approximate stress function (18), the following formulae are obtained for the reduced stress resultants:

$$\bar{N}_r = -\frac{R^2}{4h}\left[A_0 + \frac{A_1}{2}\cdot\frac{r^2}{R^2} + \frac{A_2}{3}\cdot\frac{r^4}{R^4} + \ldots + \frac{A_k}{k+1}\cdot\frac{r^{2k}}{R^{2k}} - \right.$$
$$\left. - \left(A_0 + \frac{A_1}{2} + \frac{A_2}{3} + \ldots + \frac{A_k}{k+1}\right)\frac{(n-1)\,r^{n-2}}{R^{n-2}}\cos n\varphi\right],$$
$$\bar{N}_{r\varphi} = -\frac{R^2}{4h}\left(A_0 + \frac{A_1}{2} + \frac{A_2}{3} + \ldots + \frac{A_k}{k+1}\right)\frac{(n-1)r^{n-2}}{R^{n-2}}\sin n\varphi, \tag{23}$$
$$\bar{N}_\varphi = -\frac{R^2}{4h}\left[A_0 + \frac{3A_1}{2}\cdot\frac{r^2}{R^2} + \frac{5A_2}{3}\cdot\frac{r^4}{R^4} + \ldots + \frac{(2k+1)\,A_k}{k+1}\cdot\frac{r^{2k}}{R^{2k}} + \right.$$
$$\left. + \left(A_0 + \frac{A_1}{2} + \frac{A_2}{3} + \ldots + \frac{A_k}{k+1}\right)\frac{(n-1)r^{n-2}}{R^{n-2}}\cos n\varphi\right].$$

Should the total load to which the shell is subjected, be taken into account by the approximate polynome (5*), so the formulae of the reduced stress resultants will take the forms:

$$\bar{N}_r^* = -\frac{R^2}{4h}\left\{\left(1+\frac{9}{10}\gamma\frac{r^2}{R^2} - \frac{2}{9}\gamma^2\frac{r^4}{R^4}\right)p_0 + p_s - \right.$$
$$\left. - \left[\left(1+\frac{9}{10}\gamma - \frac{2}{9}\gamma^2\right)p_0 + p_s\right](n-1)\frac{r^{n-2}}{R^{n-2}}\cos n\varphi\right\},$$

$$\bar{N}^*_{r\varphi} = -\frac{R^2}{4h}\left[\left(1+\frac{9}{10}\gamma-\frac{2}{9}\gamma^2\right)p_0 + p_s\right](n-1)\frac{r^{n-2}}{R^{n-2}}\sin n\varphi,$$

$$\bar{N}^*_{\varphi} = -\frac{R^2}{4h}\left\{\left(1+\frac{9}{5}\gamma\frac{r^2}{R^2}-\frac{5}{3}\gamma^2\frac{r^4}{R^4}\right)p_0 + p_s + \right.$$

$$\left. + \left[\left(1+\frac{9}{10}\gamma-\frac{2}{9}\gamma^2\right)p_0 + p_s\right](n-1)\frac{r^{n-2}}{R^{n-2}}\cos n\varphi\right\}. \qquad (23^*)$$

6. The string force

In the edge beam of the star-shell only axial forces — string forces — are induced. The value of these forces is, at the corners of the edge beam equal to zero, their maximum value being generated in the cross-sections $\varphi = 0$, $2\pi/n$, $4\pi/n$, ... $(2n-2)\pi/n$.

In the following, the cross-section $\varphi < \pi/n$ will be called cross-section I and that of $\varphi = \pi/n$ cross-section II, and the forces belonging to them are designated by superscripts I and II, respectively.

The horizontal component $\bar{H}^{\mathrm{I}}$ of the string force H^{I} arising at any cross-section I of the edge beam, can be determined by analysing the conditions of the equalibrium of the shell sector *0 I II*, cut out of the shell according to Fig. 4. On the side *0 II* of this shell sector, only forces $\bar{N}^{\mathrm{II}}_{\varphi}$ are acting, and on the cross-section *0 II* of the edge beam the string force is equal to zero. Thus, $\bar{H}^{\mathrm{I}}$ can easily be defined.

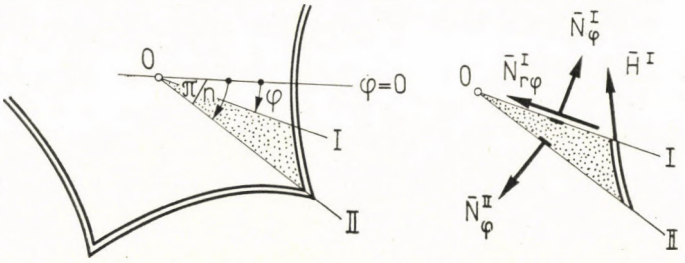

Fig. 4. Sector of shell cut out for the investigation of equilibrium

7. Numerical example

Let us apply the process of calculation described above to the axisymmetrical paraboloid shell of revolution having a constant thickness, constructed above a star-polygon having $n = 5$ sides, depicted in Fig. 5.

The geometrical data of the shell to be calculated are as follows:

$$R = 20{,}0 \text{ m}; \qquad h = 14{,}0 \text{ m}.$$

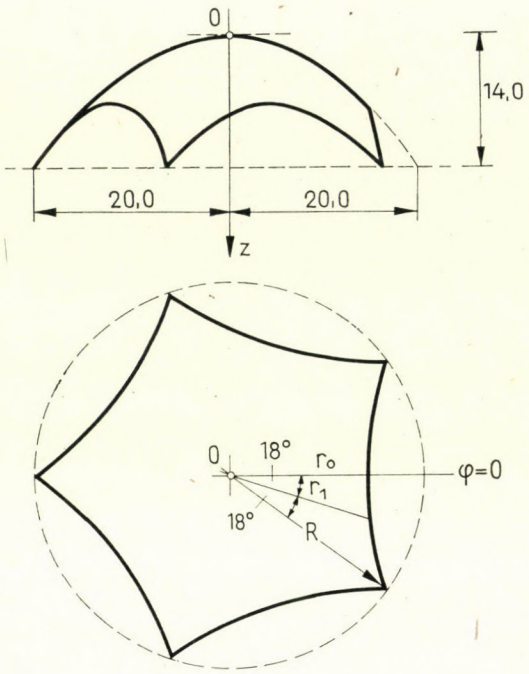

Fig. 5. Numerical example

The loads are: dead weight of an intensity of

$$p_0 = 200 \text{ kp/m}^2$$

and snow load applied at the same time

$$p_s = 80 \text{ kp/m}^2.$$

In case of the problem in hand

$$\gamma = \frac{h^2}{R^2} = \frac{14.0^2}{20.0^2} = 0{,}49,$$

and hence, the "exact" load function according to formula (2) is

$$\bar{p} = 200 \sqrt{1 + 4\gamma^2 \frac{r^2}{R^2}} + 80 = 200 \sqrt{1 + 1{,}96 \frac{r^2}{R^2}} + 80,$$

and the approximate load function according to formula (5*)

$$\bar{p}^* = 280 + \frac{9}{5} 200 \cdot 0{,}49 \frac{r^2}{R^2} - \frac{2}{3} 200 \cdot 0{,}49^2 \frac{r^4}{R^4} = 280 + 176{,}4 \frac{r^2}{R^2} - 32{,}013 \frac{r^4}{R^4}.$$

The exact load value $\bar{p}$ and the approximate one $\bar{p}^*$, as well as the relative value of the error, due to the application of the approximate load function instead of the exact one, are indicated in Table I. As is to be seen, the greatest divergence between the two load values is only 0,003 times of the exact load value, i. e., it is quite negligible. The error being quite

Table I

Relative value of the error when using the approximate load values $\overline{p}^*$ instead of the exact values $\overline{p}$

r/R	$\overline{p}$ kp/m²	$\overline{p}^*$ kp/m²	$(\overline{p}^* - \overline{p})/\overline{p}$
0	280,0	280,0	0,00
0,1	282,0	281,8	−0,001
0,2	287,7	287,0	−0,002
0,3	296,9	295,6	−0,004
0,4	309,2	307,4	−0,006
0,5	324·1	322,1	−0,006
0,6	341,2	339,4	−0,005
0,7	360,0	358,7	−0,003
0,8	380,3	379,8	−0,001
0,9	401,7	401,9	+0,000
1,0	424,1	424,4	+0,001

insignificant, it is always permitted to use the approximate load function (5*) instead of the exact one (4).

In case of the approximate load function, the stress function of the star-shell will, according to formula (18*), be as follows:

$$F^* = \frac{20^4}{8 \cdot 14{,}0}(200 + 80)\left(1 - \frac{r^2}{R^2}\right) + \frac{9}{20}200 \cdot 0{,}49\left(1 - \frac{r^4}{R^4}\right) -$$

$$- \frac{2}{27}200 \cdot 0{,}49^2\left(1 - \frac{r^6}{R^6}\right) - \frac{2}{5}\left(200 + 80 + \frac{9}{10}200 \cdot 0{,}49 -\right.$$

$$\left. - \frac{2}{9}200 \cdot 0{,}49^2\right)\left(1 + \frac{r^5}{R^5}\cos\ 5\varphi\right),$$

and the equation of the edge line of the star-polygon, according to formula (19*):

$$280\left(1 - \frac{r^2}{R^2}\right) + 44{,}1\left(1 - \frac{r^4}{R^4}\right) - 3{,}55\dot{7}0\dot{3}\left(1 - \frac{r^6}{R^6}\right) -$$

$$- 143{,}011\dot{5}\left(1 + \frac{r^5}{R^5}\cos 5\varphi\right) = 0.$$

Knowing the equation of the edge line of the star-polygon, the radius r_0 of the circle inscribed in it, may be obtained from the equation:

$$280\left(1 - \frac{r_0^2}{R^2}\right) + 44{,}1\left(1 - \frac{r_0^4}{R^4}\right) - 3{,}55\dot{7}0\dot{3}\left(1 - \frac{r_0^6}{R^6}\right) -$$

$$- 143{,}011\dot{5}\left(1 + \frac{r_0^5}{R^5}\right) = 0$$

and the radius vector r_1 associated to the polar angle $\varphi = \pi/10 = 18°$, may be determined with the aid of the equation

$$280\left(1 - \frac{r_1^2}{R^2}\right) + 44{,}1\left(1 - \frac{r_1^4}{R^4}\right) - 3{,}55\dot{7}0\dot{3}\left(1 - \frac{r_1^6}{R^6}\right) - 143{,}011\dot{5} = 0.$$

The results of the calculation are:

$$\frac{r_0}{R} = 0{,}7097, \quad \text{thus} \quad r_0 = 14{,}194 \text{ m},$$

$$\frac{r_1}{R} = 0{,}7636, \quad \text{thus} \quad r_1 = 15{,}272 \text{ m}.$$

In possession of these values, the edge line of the star-polygon may easily be drawn.*

The reduced stress resultants induced in the shell wall can be calculated according to formula (23*). Their values given in kp/m are:

$$\overline{N}_r^* = -2000 - 630\frac{r^2}{R^2} + 76{,}2\dot{}\frac{r^4}{R^4} + 1430{,}115\dot{}\frac{r^3}{R^3}\cos 5\varphi,$$

$$\overline{N}_{r\varphi}^* = -1430{,}115\dot{}\frac{r^3}{R^3}\sin 5\varphi\,,$$

$$\overline{N}_\varphi^* = -2000 - 189\,0\frac{r^2}{R^2} + 381{,}1\dot{}\frac{r^4}{R^4} - 1430{,}115\dot{}\frac{r^3}{R^3}\cos 5\varphi.$$

The distribution of the stress resultants N_x^* and N_y^* along the cross-section $y = 0$ is represented in *Fig.* 6.

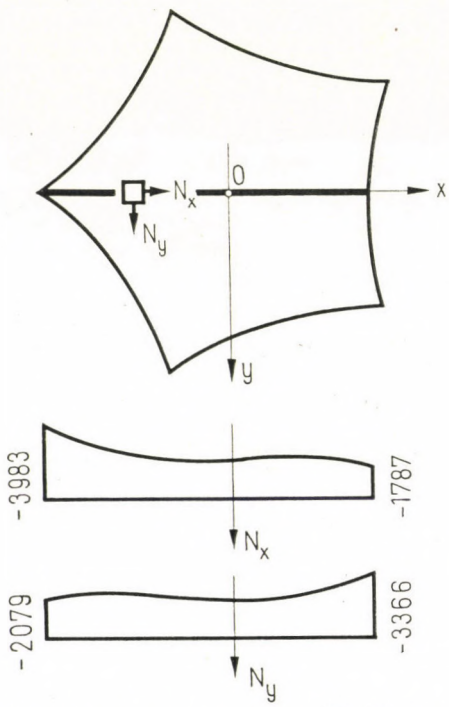

Fig. 6. Distribution of the reduced stress resultants $\overline{N_x}$, $\overline{N_y}$ along the cross-section $y = 0$

* If the sides of the star-polygon would be replaced by circular arcs of a radius $\varrho = 35{,}792$ m, passing through the points $r = 14{,}194$, $\varphi = 0$ and $r = 20{,}0$, $\varphi = \pm 36°$, then the length of the radius vector of the edge line at the point $\varphi = \pm 18°$ would be 15,252 m, instead of the exact value 15,272 m. Thus, the divergence between the two values is not greater than 2 cm.

The diagram of the N_y-forces shown in *Fig.* 6. also allows to easely determine the maximum string force, generated in the edge beam of the star-shell. This force is, namely, by simple reasons of equilibrium, equal to the surface of the diagram in question. Its value can be determined with the aid of formula

$$S_{max} = \int_{14,194}^{-20,0} \left(-2000 - 630 \frac{r^2}{R^2} + 76{,}2 \frac{r^4}{R^4} + 1430{,}115 \frac{r^3}{R^3} \right) dr.$$

Performing the calculation for the maximum string force, the value

$$S_{max} = 78356 \text{ kp}$$

is arrived at.

REFERENCES

1. MENYHÁRD, I.: Theory of Shell Structures — Part II.* *Publications of the Institute of Postgraduate Training for Civil Engineers.* **19** (1943), No. 48, p. 25
2. GIRKMANN, K.: Flächentragwerke. Einführung in die Elastostatik der Scheiben, Platten, Schalen und Faltwerke. Springer Verlag, Wien 1956. V. Aufl. p. 26
3. CSONKA, P.: Paraboloid Shells of Revolution on Star Polygon Base.* *Műszaki Tudomány*, **42** (1970), 243—256
4. CSONKA, P.: Axisymmetrically Loaded Paraboloid Shells of Revolution on Star-polygon Base.* *Műszaki Tudomány* **44** (1971), 149—165
5. CSONKA, P.: Membrane Shells with Edge Beam Supported by a Wall. *Acta Technica Hung.* **71** (1971), 149—159

Berechnung von Sternschalen für Totalbelastung. Der Aufsatz befaßt sich mit der Berechnung von Drehparaboloidschalen belastet durch eine drehsymmetrisch verteilte vertikale Totallast (Eigengewicht und Schneelast). Die Grundrißfigur der behandelten Schalen ist ein regelmäßiges vieleckähnliches Gebilde mit nach innen gebogenen Seiten, die als *Sternvieleck* bezeichnet wird. Das Randglied der in Rede stehenden Schalen — *der Sternschalen* — ist in seiner ganzen Länge durch Mauerwerk gestützt, darum können in den Querschnitten des Randgliedes ausschließlich Normalkräfte, sogenannte *Seilkräfte* zustande kommen. Die Form der Sternschale selber ist mit Hilfe eines entsprechenden Rechenverfahrens so bestimmt, daß ihre Schnittkräfte mit geschlossenen Formeln berechnet werden können. Die Zweckmäßigkeit der vorgeschlagenen Berechnungsmethode wird anhand eines Zahlenbeispieles bewiesen.

Проектирование звездных оболочек для тотальных нагрузок. Работа занимается проектированием оболочек в виде параболоида вращения, к которым приложена центрально симметричная распределяющаяся тотальная нагрузка (при одновременно действующих нагрузках от собственного веса и веса снега). Форма основания рассматриваемых оболочек имеет правильную форму в виде т. н. звездного многоугольника. Краевая балка рассматриваемых оболочек, то есть т. н. звездных оболочек по всей своей длине имет стеновую опору, вследствие чего на разрез балок действует только центральное усилие — веревочное усилие. Форма самого звездного многоугольника определена с таким расчетом, чтобы силы натяжения оболочки можно было бы рассчитывать с помощью замкнутых формул. Простота предложенного метода расчета подтверждается числовым примером.

*In Hungarian.

Acta Technica Academiae Scientiarum Hungaricae, Tomus 82 (1–2), pp. 31–46 (1976)

BERECHNUNG FORMORTHOTROPER FLÄCHENTRAGWERKE

R. BAREŠ*
KANDIDAT DER TECHN. WISSENSCHAFTEN

[Manuskript eingegangen am 27. Januar 1975]

Es wird eine Methode zur Berechnung formorthotroper Flächentragwerke vorgeführt, die neben der Biegungs- und Torsionsteifigkeiten auch den Einfluß der Kontraktionsfähigkeit der Konstruktion berücksichtigt. Durch die angegebene Methode kann der mühsame Teil der Berechnung und die Arbeit des Statikers auf ein Mindestmaß beschränkt werden.

Analog zur Materialorthotropie bei Platten werden heute formorthotrope Flächentragwerke bereits laufend mit ausreichender Genauigkeit analysiert, die schon vielmals nachgewiesen wurde [4, 12]. Die meisten Methoden sind jedoch entweder übermäßig mühevoll, oder sie beruhen auf einigen nicht völlig berechtigten Voraussetzungen. Der Autor legt eine Methode der Berechnung formorthotroper Flächentragwerke eines einfachen Brückentyps vor, die neben den Biegungs- und Torsionssteifigkeiten auch den Einfluß der Kontraktionsfähigkeit der Konstruktion in Rechnung stellt; die Methode ist so gestaltet, daß der mühsame Berechnungsteil tabelliert und die Arbeit des Statikers auf ein Mindestmaß beschränkt werden kann. Die Hubersche Gleichung wird nach der Methode der dimensionslosen Beiwerte gelöst, deren Vorteilhaftigkeit schon früher, z. B. in [1, 5, 10, 11] nachgewiesen wurde.

Die Formorthotropie der Platte entsteht entweder durch ihre verschiedene Bewehrung oder Vorspannung in zwei orthogonalen Richtungen oder durch ihre Verbindung mit Balken, sei es in der Längsrichtung, Querrichtung oder in beiden Richtungen, eventuell durch die Verhinderung oder absichtliche Reduktion der Übertragung einiger Kräfte in der Querrichtung (der zusammengesetzten Konstruktion). Die materialorthotrope Platte ist der erste Grenzfall, im zweitem Grenzfall wird die Konstruktion nur durch zwei Systeme von Balken (Längsträger und Querträger) gebildet. Gemäß der relativen Wichtigkeit der einzelnen Elemente (der Platte, prismatische Elemente) und der Anordnung der Konstruktion ändert sich stark der Einfluß der Torsion und der Querkontraktion auf den inneren Spannungszustand.

* Richard Bareš, Institut für theoretische und angewandte Mechanik der Tschechoslowakischen Akademie der Wissenschaften, Prag, ČSSR.

Das Verhalten einer allgemeinen formorthotropen Flächenkonstruktion gemäß Bild. 1 wird durch die für eine *äquivalente Platte* formulierte Hubersche Gleichung beschrieben

$$\varrho_L \frac{\partial^4 w}{\partial x^4} + 2H \frac{\partial^4 w}{\partial x^2 \partial y^2} + \varrho_Q \frac{\partial^4 w}{\partial y^4} = p(x, y). \tag{1}$$

Unter den Einheitsbiegungssteifigkeiten ϱ_L und ϱ_Q versteht man die Biegungssteifigkeiten der wirklichen Konstruktion in der Längs- und Querrichtung,

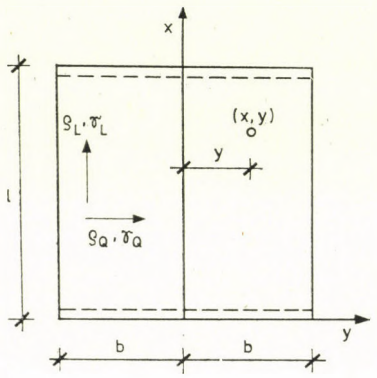

Bild 1

bezogen auf die Schwerpunktsachse des Querschnittes auf die Einheit der Breite bzw. Länge. Das mittlere Glied $2H$ hat die Bedeutung

$$2H = (\varrho_L \nu_Q + \varrho_Q \nu_L) + (\gamma_L + \gamma_Q). \tag{2}$$

Unter den Einheitstorsionssteifigkeiten γ_L und γ_Q versteht man die Torsionssteifigkeiten der wirklichen Konstruktion in der Längs- und Querrichtung, bezogen auf die Einheit der Breite, bzw. Länge. Die Beiwerte ν_L und ν_Q sind nicht Poissonsche Beiwerte in präzisem Sinn, sondern sie bezeichnen den Einfluß der Spannung $\sigma_y(\sigma_x)$ auf die Verformung $\varepsilon_x(\varepsilon_y)$ und umgekehrt, keineswegs den durch die Anisotropie des Materials, sondern den durch die Orthotropie der Konstruktion verursachten Einfluß [4]. Sie beeinflussen in gewissem Sinn alle Steifigkeiten (ϱ_L, ϱ_Q, γ_L, γ_Q). Durch die Unterbrechung der Kontinuität des Querschnittes in einen Horizontalebenen der formorthotropen Konstruktion wird die Querübertragung der Verformungen unmöglich gemacht, und dadurch werden sich die Werte ν_L, ν_Q immer von denjenigen unterscheiden, die dem Material, aus dem die Konstruktion hergestellt wurde, entsprechen.*

*Die Bestimmung der Steifigkeit eines formorthotropen Flächentragwerkes bei konsequenter derartiger Berücksichtigung des Einflusses der Querkontraktion, daß sie der Wirklichkeit entspricht, ist nicht einfach; diese wurde in [2] behandelt.

Die Innenkräfte M_L, M_Q, M_T, Q_L, Q_Q, $\bar{Q}_T$ sind durch die bekannten Ausdrücke [7] gegeben, in denen die Indizes L, Q die Indizes x, y zur Unterscheidung der Formorthotropie von der Materialorthotropie ersetzen.

Man kann sämtliche Querschnitts- und Materialeigenschaften der Konstruktion durch folgende drei dimensionslose Parameter vollkommen charakterisieren:

I. Die verhältnismäßige Querbiegsamkeit der Konstruktion gibt, gemäß [6], der dimensionslose Parameter

$$\vartheta = \frac{b}{l} \sqrt[4]{\frac{\varrho_L}{\varrho_Q}}$$

an, der *Parameter der Querversteifung heißt.* Je größer ϑ ist, um so nachgiebiger ist die Querversteifung. Ihre Größe kann sich im Bereich von $0 \leq \vartheta \leq \infty$ bewegen.

II. Die verhältnismäßige Torsionssteifigkeit der Konstruktion gibt, gemäß [10], der dimensionslose Parameter

$$\alpha = \frac{\gamma'_L + \gamma'_Q}{2\sqrt{\varrho'_L \cdot \varrho'_Q}}$$

an, *der Torsionssteifigkeits-Parameter* heißt. Seine Größe kann Werte im Bereich von $0 \leq \alpha \leq 1$ erreichen. Einen höheren Wert von α als den Wert 1, der einer vollen orthotropen (oder isotropen) Platte angehört, kann man sich nicht vorstellen.[1]

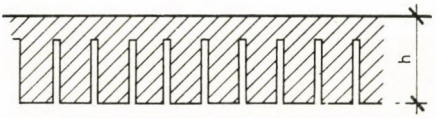

Bild 2

[1]Man kann sich nämlich jede, durch Balken versteifte Konstruktion des Plattentyps reversibel als eine Platte vorstellen, deren Dicke dem höchsten Querschnitt der Konstruktion gleicht, von der der Teil der Masse zwischen den Balken ausgenommen ist. Es ist einleuchtend, daß die Torsionssteifigkeit einer derartigen geschwächten Platte kleiner sein muß als die einer vollen Platte. Trotzdem zwingen einige Autoren [4, 9] irrtümlich der dritten von den möglichen Rechnungslösungen der charakteristischen Gleichung der 4. Stufe, d. h. für den Fall, wo $H^2 > \varrho_L \varrho_Q$ (oder $\alpha > 1$), einen physikalischen Sinn auf. Jedoch der einzige, der bestrebt war, die Existenz einer Konstruktion dieses Typs nachzuweisen, und dessen Ergebnisse auch die übrigen Autoren übernahmen, war, soweit dem Autor bekannt ist, GEDIZLI [3]. Seine Berechnung für eine Konstruktion, die von einer Platte mit engen Ausschnitten gemäß Bild 2 gebildet wird, war jedoch ungenau, da er bei der Berechnung der Biegungssteifigkeit nur den gedrückten Querschnittsteil (nach den Bauvorschriften), bei der Berechnung der Torsionssteifigkeit den ganzen Querschnitt gemäß der Elastizitätstheorie berücksichtigte. Bei richtiger Berechnung gemäß der Elastizitätstheorie, für die die Methode abgeleitet ist, geht allerdings $\alpha \leq 1$ auch in diesem Fall hervor.

Mit dem Index Q sind hier die unter der Voraussetzung, daß der Querkontraktionsbeiwert des Konstruktionsmaterials einen Nullwert hat, berechneten Steifigkeiten bezeichnet. Bei einer äquivalenten Platte ist also

$$\gamma_L = \frac{\gamma'_L}{1+\eta}\,;\ \gamma_Q = \frac{\gamma'_Q}{1+\eta}\,;\ \varrho_L = \frac{\varrho'_L}{1-\eta^2}\,;\ \varrho_Q = \frac{\varrho'_Q}{1-\eta^2}\,,$$

so daß man gleichfalls setzen kann

$$\alpha = \frac{\gamma_L + \gamma_Q}{2(1-\eta)\sqrt{\varrho_L\,\varrho_Q}}\,. \tag{4b}$$

III. Wenn man die aus dem reziproken Bettischen Theorem [3] hervorgehende Symmetrie der Einheitssteifigkeiten einführt

$$\nu_L\,\varrho_Q = \nu_Q\,\varrho_L\,, \tag{5}$$

dann drückt die verhältnismäßige Widerstandsfähigkeit der Konstruktion gegen Querkontraktion der dimensionslose Parameter

$$\eta = \nu_L \sqrt{\frac{\varrho_Q}{\varrho_L}} \tag{6}$$

aus, der *Kontraktionsfähigkeitsparameter* heißt. Seine Größe kann sich im Bereich von $0 \leq \eta \leq 0{,}5$ bewegen.

Durch Einsetzung der vorhergehenden Beziehungen in (2) und durch Zurichtung erhalten wir, daß

$$2H = 2\sqrt{\varrho_L\,\varrho_Q}\,[\eta+\alpha(1-\eta)] = 2\varepsilon\sqrt{\varrho_L\,\varrho_Q} \tag{7}$$

wo ε *Parameter des Mittelgliedes der Huberschen Gleichung* benannt ist, und er ist

$$\varepsilon = [\eta + \alpha(1-\eta)] = [\alpha + \eta(1-\alpha)]. \tag{8}$$

Ebenso wie der Parameter α kann auch ε aus gleichen Gründen nur im Bereich von $0 \leq \varepsilon \leq 1$ sein. Aus der oben angeführten Darlegung ersieht man, daß bei $\eta \neq 0$ der relative Wert des Mittelgliedes der Huberschen Gleichung im Bereich

$$\eta \leq \frac{2H}{2\sqrt{\varrho_L\,\varrho_Q}} \leq 1$$

bleibt.

Die Lösung der Grundgleichung der Platte finden wir als Summe der Lösung der homogenen Gleichung ${}^2w$ nach M. LÉVY, in der Form

$${}^2w = \sum_{m=1}^{\infty} y_{(y)m}\ \sin\frac{m\pi x}{l} \tag{9}$$

und der partikularen Lösung ^1w für eine endlos breite Platte (Gurt) d. h.

$$w = {}^1w + {}^2w; \tag{10a}$$

unter folgenden Voraussetzungen:

—Die Belastung ist sinusförmig in der Richtung der Hauptträger verteilt, d. h. die Belastung ist definiert als

$$p_x = \sum_m p_m \sin \frac{m\pi x}{l}; \tag{11}$$

wo p_m die Amplitude des m-ten Gliedes der Belastungsentfaltung in der Form einer einfachen Fourierschen Reihe bedeutet, also die Größe der Belastung in $x = 2$ (Bild. 3);

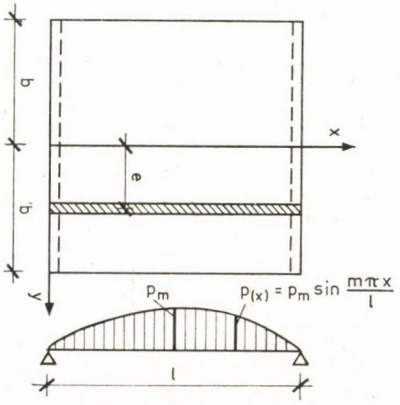

Bild 3

— die Randbedingungen an den freien Rändern sind, wenn man die Kirchhofsche Vereinfachung [7] für den Ersatz der Randtorsionsmomente durch zusätzliche Schubkräfte verwendet

$$\begin{aligned} M_Q &\to \left(\frac{\partial^2 w}{\partial y^2} + \eta \sqrt{\frac{\varrho_L}{\varrho_Q}} \frac{\partial^2 w}{\partial x^2} \right)_{y=\pm b} = 0 \\ \bar{Q}_Q &\to \left[\frac{\partial^3 w}{\partial y^3} + \sqrt{\frac{\varrho_L}{\varrho_Q}} \left(\eta + 2\alpha(1-\eta)\right) \frac{\partial^3 w}{\partial x^2 \partial y} \right]_{y=\pm b} = 0 ; \end{aligned} \tag{12}$$

— die Randbedingungen an den zwei anderen, frei aufliegenden Seiten sind

$$w_{(x=0;l)} = 0, \quad \left(\frac{\partial^2 w}{\partial x^2} \right)_{(x=0,l)} = 0 . \tag{13}$$

Die Funktion Y_m der homogenen Lösung ebenso wie die in [11] angeführte partikulare Lösung gelten auch hier, wenn ε gegen α ausgetauscht wird. Für die

vollständige Lösung wird ein zu [11] analoger Vorgang verwendet. Aus den Bedingungen an den freien Rändern werden vier Gleichungen für die Bestimmung der Integrationskonstanten A, B, C, D gewonnen:

$$e^{mnb}\{[(\varepsilon-\eta)A_m+\sqrt{1-\varepsilon^2}\,\bar{B}_m]\cos mtb+[-\sqrt{1-\varepsilon^2}\,A_m+(\varepsilon-\eta)\bar{B}_m]\ \ldots$$
$$\ldots\sin mtb\}+e^{-mnb}\{[(\varepsilon-\eta)C_m-\sqrt{1-\varepsilon^2}\,\bar{D}_m]\cos mtb+[\sqrt{1-\varepsilon^2}\,C_m+$$
$$+(\varepsilon-\eta)\bar{D}_m]\sin mtb\}+C_m^*e^{-mn|b-e|}\left[(1-\eta)\sqrt{\frac{1+\varepsilon}{1-\varepsilon}}\sin mt|b-e|-\right.$$
$$\left.-(1-\eta)\cos mt|b-e|\right]=0,$$

$$e^{-mnb}\{[(\varepsilon-\eta)A_m+\sqrt{1-\varepsilon^2}\,\bar{B}_m]\cos mtb+[\sqrt{1-\varepsilon^2}\,A_m-(\varepsilon-\eta)\bar{B}_m]\ldots$$
$$\ldots\sin mtb\}+e^{mnb}\{[(\varepsilon-\eta)C_m-\sqrt{1-\varepsilon^2}\,\bar{D}_m]\cos mtb-[\sqrt{1-\varepsilon^2}\,C_m+$$
$$+(\varepsilon-\eta)\bar{D}_m]\sin mtb\}+C_m^*e^{-mn(b+e)}\left[(1-\eta)\sqrt{\frac{1+\varepsilon}{1-\varepsilon}}\sin mt(b+e)-\right.$$
$$\left.-(1+\eta)\cos mt(b+e)\right]=0, \tag{14}$$

$$e^{mnb}\left\{\left[(-1+\eta)\sqrt{\frac{1+\varepsilon}{1-\varepsilon}}A_m+(1+\eta)\bar{B}_m\right]\cos mtb+\left[-(1+\eta)A_m+\right.\right.$$
$$\left.\left.+(-1+\eta)\sqrt{\frac{1+\varepsilon}{1-\varepsilon}}\bar{B}_m\right]\sin mtb\right\}+e^{-mnb}\left\{\left[(1-\eta)\sqrt{\frac{1+\varepsilon}{1-\varepsilon}}C_m+\right.\right.$$
$$\left.\left.+(1+\eta)\bar{D}_m\right]\cos mtb+\left[-(1+\eta)C_m+(1-\eta)\sqrt{\frac{1+\varepsilon}{1-\varepsilon}}\bar{D}_m\right]\sin mtb\right\}+$$
$$+\frac{2}{1-\varepsilon}C_m^*e^{-mn|b-e|}\left[(\varepsilon-\eta)\sin mt|b-e|+\sqrt{1-\varepsilon^2}\cos mt|b-e|\right]=0,$$

$$e^{mnb}\left\{\left[(1-\eta)\sqrt{\frac{1+\varepsilon}{1-\varepsilon}}C_m+(1+\eta)\bar{D}_m\right]\cos mtb+[(1+\eta)C_m-(1-\eta)\ldots\right.$$
$$\left.\ldots\sqrt{\frac{1+\varepsilon}{1-\varepsilon}}\bar{D}_m\right]\sin\ mtb\ \Big]+e^{-mnb}\left\{\left[-(1-\eta)\sqrt{\frac{1+\varepsilon}{1-\varepsilon}}A_m+(1+\eta)\bar{B}_m\right]\ldots\right.$$
$$\left.\ldots\cos mtb+\left[(1-\eta)A_m+(1-\eta)\sqrt{\frac{1+\varepsilon}{1-\varepsilon}}\bar{B}_m\right]\sin mtb\right\}-\frac{2}{1-\varepsilon}C_m^*\ldots$$
$$\ldots e^{-mn(b+e)}\left[(\varepsilon-\eta)\sin mt(b+e)+\sqrt{1-\varepsilon^2}\cos mt(b+e)\right]=0,$$

$$n=\frac{\pi\vartheta}{b}\sqrt{\frac{1+\varepsilon}{2}};$$

$$t=\frac{\pi\vartheta}{b}\sqrt{\frac{1-\varepsilon}{2}}.$$

Durch die Lösung folgt

$$A_m = \frac{C_m^*}{2\,V_1\,V_2}\,(U + W) = C_m^*\,A'_m,$$

$$B_m = -\frac{C_m^*}{2\,V_1\,V_2}\,(X + Y) = C_m^*\,B'_m,$$

$$C_m = \frac{C_m}{2\,V_1\,V_2}\,(W - U) = C_m^*\,C'_m,$$

$$D_m = -\frac{C_m^*}{2\,V_1\,V_2}\,(X - Y) = C_m^* D'_m\,,$$

wo sukzessive

$$U = V_1(Qn_4 - Tn_8),$$

$$W = V_2(Rn_2 - Sn_6),$$

$$X = V_2(Rn_1 + Sn_5),$$

$$Y = V_1(Q_{n3} + T_{n7})$$

$$n_1 n_6 + n_2 n_5 = V_1,$$

$$n_3 n_8 + n_4 n_7 = V_2,$$

$$Q = \frac{G - H}{C_m^*},$$

$$R = \frac{G + H}{C_m^*},$$

$$S = \frac{E + F}{C_m^*},$$

$$T = \frac{E - F}{C_m^*}, \qquad (16)$$

$$n_1 = K(\varepsilon - \eta) - \gamma(\sqrt{1 - \varepsilon^2}), \qquad n_5 = L(1 - \eta)a + I(1 + \eta),$$

$$n_2 = K\sqrt{2(1+\varepsilon)} + \gamma\,\frac{\varepsilon - \eta}{\sqrt{\frac{1 - \varepsilon}{2}}}, \quad n_6 = L\,\frac{1 + \eta}{\sqrt{\frac{1 - \varepsilon}{2}}} - I\,\frac{(1 - \eta)a}{\sqrt{\frac{1 - \varepsilon}{2}}},$$

$$n_3 = L(\varepsilon - \eta) - \sqrt{1 - \varepsilon^2}\,I \qquad n_7 = K(1 - \eta)a + \gamma(1 + \eta),$$

$$n_4 = L(\sqrt{2(1+\varepsilon)} + I\,\frac{\varepsilon - \eta}{\sqrt{1 - \varepsilon}}, \quad n_8 = K\,\frac{1 + \eta}{\sqrt{\frac{1 - \varepsilon}{2}}} - \gamma\,\frac{(1 - \eta)a}{\sqrt{\frac{1 - \varepsilon}{2}}},$$

$$E = C_m^*\,e^{-mn'(\pi-\psi)}[(1 - \eta)\,a \sin mt'(\pi - \psi) - (1 + \eta)\cos mt'(\pi - \psi)],$$

$$F = C_m^*\,e^{-mn'(\pi+\psi)}\,[(1 - \eta)a \sin mt'(\pi+\psi) - (1+\eta)\cos mt'(\pi+\psi))],$$

$$G = 2C_m^*\,e^{-mn'(\pi-\varphi)}\left[\frac{\varepsilon - \eta}{1 - \varepsilon}\sin mt'(\pi - \psi) + a\cos mt'(\pi - \psi)\right],$$

$$H = 2C_m^*\,e^{-mn'(\pi+\psi)}\left[\frac{\varepsilon - \eta}{1 - \varepsilon}\sin mt'(\pi + \psi) + a\cos mt'(\pi + \psi)\right],$$

$$a = \sqrt{\frac{1+\varepsilon}{1-\varepsilon}}; \quad \varphi = \frac{\pi y}{b}; \quad \psi = \frac{\pi e}{b}; \tag{16a}$$

$$n' = \vartheta \sqrt{\frac{1+\varepsilon}{2}}; \; t' = \vartheta \sqrt{\frac{1-\varepsilon}{2}},$$

$$K = (e^{mn'\pi} + e^{-mn'\pi}) \cos mn'\pi, \quad n(b+e) = n'(\pi+\psi),$$

$$L = (e^{mn'\pi} - e^{-mn'\pi}) \cos mn'\pi, \quad t(b+e) = t'(\pi+\psi),$$

$$I = (e^{mn'\pi} + e^{-mn'\pi}) \sin mn'\pi, \quad n|b-e| = n'(\psi-\pi),$$

$$J = (e^{mn'\pi} - e^{-mn'\pi}) \sin mn'\pi, \quad t|b-e| = t'(\pi-\psi).$$

Die Gleichung (10a) für die Durchbiegung der untersuchten Konstruktion können wir wie folgt schreiben:

$$w(x, y) = \sum_m \frac{p_m l^4}{2bm^4\pi^3 \varrho_L} K(y)_m \sin \frac{m\pi x}{l}, \tag{10b}$$

wo

$$K(y)_m = \frac{m\vartheta}{\sqrt{2(1+\varepsilon)}} \{[A'_m M_{\varphi m} + \bar{B}'_m N_{\varphi m}][C'_m O_{\varphi m} + \bar{D}'_m P_{\varphi m}] + \\ + [O_{|\varphi-\psi|m} + a P_{|\varphi-\psi|m}]\}$$

der *erste dimensionslose Beiwert* ist, der von φ, ψ, ϑ, α und η abhängt. Für ihn gilt, daß

$$K_{\varphi,\psi} = K_{\psi,\varphi};$$

und

$$\frac{1}{2b} \int_{-b}^{+b} \frac{\pi K_{ei(y)} \, dy}{(1 + K^{\circ}_{ei})} = 1,$$

wenn K^0 den Wert des dimensionslosen Beiwertes für eine harmonische, auf die Breite gleichmäßig verteilte Belastung bedeutet. Die Werte M, N, O, P sind

$$M_{\varphi m} = e^{mn'\varphi} \cos mt'\varphi,$$

$$N_{\varphi m} = e^{mn'\varphi} \sin mt'\varphi, \quad O_{|\varphi-\psi|m} = e^{-mn'|\varphi-\psi|} \cos mt'|\varphi-\psi|,$$

$$O_{\varphi m} = e^{-mn'\varphi} \cos mt'\varphi,$$

$$P_{\varphi m} = e^{-mn'\psi} \sin mt'\varphi, \quad P_{|\varphi-\psi|m} = e^{-mn'|\varphi-\psi|} \sin mt'|\varphi-\psi|.$$

Für die Biegungsmomente in den Hauptträgern (in der Richtung X) gilt, daß

$$M_L = \sum_m \frac{p_m l^2}{2b\pi m^2} \{K(y)_m + \eta_l \mu(y)_m\} \sin \frac{m\pi x}{l}, \tag{20}$$

wo der *zweite dimensionslose Beiwert*, der von φ, ψ, ϑ, α und η abhängig ist,

folgenden Wert hat:

$$\mu(y)_m = -\frac{m\vartheta}{\sqrt{2(1+\varepsilon)}}\Big[\varepsilon(A'_m M_{\varphi m} + \bar{B}'_m N_{\varphi m}) + \sqrt{1-\varepsilon^2}\,(-A'_m N_{\varphi m} + \\ + \bar{B}'_m M_{\varphi m}) + \varepsilon(C'_m O_{\varphi m} + \bar{D}'_m P_{\varphi m}) + \sqrt{1-\varepsilon^2}\,(C'_m P_{\varphi m} - \\ - \bar{D}'_m O_{\varphi m}) + \sqrt{\frac{1+\varepsilon}{1-\varepsilon}}\,P_{|\varphi-\psi|m} - O_{|\varphi-\psi|m}\Big]. \tag{21}$$

Für die Biegunsmomente in den Querträgern (in der Richtung Y) ist

$$M_Q = \sum_m \frac{p_m l}{2\vartheta^2\, m^2\,\pi}\,[\eta\, K(y)_m + \mu(y_m)]\,\sin\frac{m\pi x}{l}\,. \tag{22}$$

Die Torsionsmomente sind gegeben durch den Unterschied

$$(M_{LQ} - M_{QL}) = \sum_m \alpha(1-\eta)\,\frac{p_m l}{2\pi m}\,[\tau(y)_m]\,\cos\frac{m\pi x}{l}\,, \tag{23}$$

wo der *dritte dimensionslose Beiwert*, der von φ, ψ, ϑ, α und η abhängt, folgenden Wert hat:

$$\tau(y)_m = [A'_m M_{\varphi m} + \bar{B}'_m N_{\varphi m}] + \sqrt{\frac{1-\varepsilon}{1+\varepsilon}}\,[-A'_m N_{\varphi m} + \\ + \bar{B}'_m M_{\psi m}] - [C'_m O_{\psi m} + \bar{D}'_m P_{\psi m}] + \sqrt{\frac{1-\varepsilon}{1+\varepsilon}}\,\times \\ \times\,[-C'_m P_{\psi m} + \bar{D}'_m O_{\psi m}] \mp \frac{2}{\sqrt{1-\varepsilon^2}}\,P_{|\varphi-\psi|m}\,. \tag{24}$$

Das Vorzeichen des letzten Gliedes ist unterschiedlich gemäß der gegenseitigen Beziehung von φ und ψ. Für $\psi > \varphi$ gilt das Pluszeichen, für $\psi < \varphi$ das Minuszeichen. Die Torsionsmomente für die Richtung X der äquivalenten Platte sind

$$M_{LQ} = \frac{\gamma_L}{\gamma_L + \gamma_Q}\,(M_{LQ} - M_{QL}) \tag{25a}$$

und ähnlich für die Richtung Y

$$M_{QL} = \frac{\gamma_Q}{\gamma_L + \gamma_Q}\,(M_{LQ} - M_{QL})\,. \tag{25b}$$

Die Schubkräfte in den Hauptträgern (in der Richtung X)

$$Q_L = \sum_m \frac{p_m l}{2bm}\left\{K(y)_m + \left(\frac{\gamma_Q}{\sqrt{\varrho_L\,\varrho_Q}} + \eta\right)\mu(y)_m\right\}\cos\frac{m\pi x}{l} \tag{26}$$

und für die Reaktion gilt ähnlich

$$\bar{Q}_L = \sum_m \frac{p_m l}{2bm} \{K(y)_m + (2\varepsilon - \eta)\, \mu(y)_m\} \cos \frac{m\pi x}{l} . \tag{27}$$

Die Schubkräfte in den Querträgern (in der Richtung Y) sind

$$Q_Q = \sum_m p_m \left\{K(y)_m + \frac{1}{4}\left(\eta + \frac{\gamma_L}{\sqrt{\varrho_L \varrho_Q}}\right) \tau(y)_m\right\} \sin \frac{m\pi x}{l} , \tag{28}$$

wo der *vierte dimensionslose Beiwert*, der wieder von φ, ψ, ϑ, α und η abhängig ist, folgenden Wert hat:

$$K(y)_m = -\frac{1}{4}\left[(2\varepsilon - 1)\,(A'_m\, M_{\varphi m} + \bar{B}'_m\, N_{\varphi m}) - (2\varepsilon + 1)\sqrt{\frac{1-\varepsilon}{1+\varepsilon}}\,(A'_m\, N_{\varphi m} - \right.$$

$$- \bar{B}'_m\, M_{\varphi m}) - (2\varepsilon - 1)\,(C'_m\, O_{\varphi m} + \bar{D}'_m\, P_{\varphi m}) - (2\varepsilon + 1)\sqrt{\frac{1-\varepsilon}{1+\varepsilon}} \times$$

$$\left. \times\, (C'_m\, P_{\varphi m} - \bar{D}'_m\, O_{\varphi m}) \pm \left(\frac{2\varepsilon}{\sqrt{1-\varepsilon^2}}\, P_{|\varphi - \psi| m} - 2\, O_{|\varphi - \psi| m}\right)\right] . \tag{29}$$

Sobald die dimensionslosen Beiwerte berechnet sind, ist die weitere Berechnung äußerst einfach, nur auf einige algebraische Operationen beschränkt. Immerhin wird der praktische Vorgang nur dank folgenden zwei Tatsachen ermöglicht:

A. Für eine allgemeine, in die Fouriersche Reihe in der Richtung X entwickelte Linienlast muß man gewöhnlich mit mehr Gliedern der Reihe als mit einem einzigen rechnen, besonders für einige statische Größen (Momente, Schubkräfte, Reaktionen). Die Tabellierung der dimensionslosen Beiwerte χ würde allerdings in Anbetracht des übermäßigen Umfanges ihre praktische Bedeutung verlieren, sobald man die Werte der Beiwerte für mehr Glieder der Reihe zahlenmäßig festlegen müßte. Glücklicherweise zeigte es sich bei detaillierter Analyse der Gleichungen, daß das m-te Glied der Reihe, das der Verteilung der Belastung

$$p(x) = \sum p_m \sin \frac{m\pi x}{l}$$

entspricht dem ersten Glied der Reihe eines Systems mit m-fach nachgiebigeter Querversteifung, d. h. mit dem Biegungssteifigkeitsparameter $m\ \vartheta$, gleich

[1] An den Rändern gilt allerdings mit Rücksicht auf die Kirchhofsche Vereinfachung

$$\bar{Q}_Q = \sum_m p_m \left[\frac{1}{4}(2\varepsilon - \eta)\, \tau(y)_m + K(y)_m\right] \sin \frac{m\pi x}{l} . \tag{28a}$$

ist. Das bedeutet mit anderen Worten, daß die Querversteifung für die Belastung

$$p(x)_m = p_m \sin \frac{m\pi x}{l}$$

zu einer m-fach biegsameren wird als für die Belastung

$$p(x)_1 = p_1 \sin \frac{\pi x}{l} .$$

Diese Erkennntnis ist außerordentlich wichtig, denn sie ermöglicht, die dimensionslosen Beiwerte χ nur für das erste Glied der Reihe, d.h. $m = 1$, zu tabellieren, sie jedoch für ein beliebiges Glied der Entwicklung zu verwenden. Die Beiwerte $\chi(y)_1, \chi(y)_2, \chi(y)_3 \ldots\ldots \chi(y)_m$ für die Belastungen

$$p_1 \sin \frac{x\pi}{l}, \quad p_2 \sin \frac{2\pi x}{l}, \quad p_3 \sin \frac{3\pi x}{l} \ldots p_m \sin \frac{m\pi x}{l}$$

werden aus den Tabellen der Werte $\chi(y)_1$, fortschreitend für ϑ, 2ϑ, $3\vartheta \ldots m\vartheta$ gewonnen.

B. Die dimensionslosen Beiwerte χ sind (außer φ und ψ) Funktionen der dimensionslosen Parameter ϑ, α, η, die in ihren vorher angeführten Grenzen beliebige Werte erlangen können. Das würde natürlich auch wegen des untragbaren Umfanges eine Tabellierung der Beiwerte χ unmöglich machen: es wäre unbedingt nötig, jeden Beiwert χ in jedem System φ und ψ für alle Kombinationen der drei Parameter ϑ, α, η mit angemessen detaillierter Teilung zu tabellieren. Die praktische Verwendbarkeit der Methode ermöglichte der Umstand, daß die Änderung der dimensionslosen Beiwerte mit α bzw. η in den Grenzen ihrer Extreme durch eine kontinuierliche, meist monotone und leicht ausdrückbare Interpolationsfunktion gegeben ist. Es zeigte sich, daß man in allen Fällen, ohne eine Verringerung der Genauigkeit der Methode erwägen zu müssen, zwischen des Grenzwerten (Grundwerten) der Parameter $\alpha = 0$, $\alpha = 1$ und $\eta = 0$, $\eta = 0{,}25$ interpolieren kann, und daß man einheitliche parabolische Interpolationen gemäß der Formel

$$\chi_k = \chi_{\min} + (\chi_{\max} - \chi_{\min})\, F(k) \tag{30}$$

verwenden kann. Dadurch wird die Tabellierung der dimensionslosen Beiwerte auf ein annehmbares Maß reduziert: im praktisch verwendbaren Umfang des ersten Parameters ϑ von 0,05 bis 5,0 muß man die Beiwerte nur für die zwei Grenzwerte des zweiten Parameters $\alpha = 0$ und $\alpha = 1$ sowie die zwei Grenzwerte des dritten Parameters $\eta = 0$ und $\eta = 0{,}25$ tabellieren.

Gemäß dem Charakter des Verlaufes der dimensionslosen Beiwerte in Abhängigkeit von α und η erwies es sich ferner als vorteilhafter, für alle dimensionslosen Beiwerte $\chi = f(\alpha, \eta)$ die Interpolation vorerst gemäß η

(sukzessive für $\alpha = 0$ und für $\alpha = 1$) auszuführen. Das bedeutet, daß mit Hilfe der Grundfunktionen $X_{0;0}$, $X_{0;25}$, $X_{1;0,25}$ die Funktionen $X_{0;\eta}$ und $X_{1;\eta}$ gefunden werden. Erst danach wird die übriggebliebene Interpolation zwischen diesen zwei Funktionen gemäß α ausgeführt, d. h. es wird die gesuchte Funktion $X_{\alpha;\eta}$ gefunden. Der Wert $F(k)$ ist für verschiedene dimensionslose Beiwerte mäßig unterschiedlich und er ist außer α bzw. η auch von ϑ, φ und ψ abhängig; dieser Wert muß daher für jeden dimensionslosen Beiwert gesondert bestimmt werden.

Die Interpolationsfunktionen wurden durch eine detaillierte Analyse der berechneten Werte der Beiwerte für verschiedene ϑ, $\alpha = 0$, $\alpha = 0{,}25$; $\alpha = 0{,}5$, $\alpha = 0{,}75$, $\alpha = 1{,}0$ und $\eta = 0$; $\eta = 0{,}075$; $\eta = 0{,}15$; $\eta = 0{,}20$; $\eta = 0{,}25$ und für das Netz von 49 Punkten in Abhängigkeit von φ und ψ bestimmt. Es wurde darauf geachtet, daß der reduzierte Fehler zwischen dem richtigen und dem interpolierten Wert nirgends größer war als 2,5%; die Reduktion des Fehlers wurde für jeden Parameter ϑ im Verhältnis des größten absoluten Wertes des Beiwertes $X_{\max}$ zum ermittelten Wert des Beiwerts X ausgeführt. In Tafel I sind die derart gewonnenen Werte der Interpolationsfunktion $F(k)$ angeführt.

Im Spezialfall, wo die harmonische Belastung $p(x)$ auf die Breite 2b gleichmäßig aufgeteilt ist, d. h.

$$p^0_{(x)} = p^0_m \sin \frac{m\pi x}{l} = \frac{p(x)}{2b},$$

ist die Berechnung der Integrationen der Einflußflächen der einzelnen Innenkräfte mühsam und ungenau. Durch ein gleichartiges Verfahren kann man jedoch analoge Beziehungen für die einzelnen Innenkräfte bei gleichmäßig verteilter Belastung direkt, wie im folgenden gezeigt wird, erhalten.

Die Durchbiegungsfunktion ist

$$w^\circ(x, y)_m = \frac{l^4 p^0_m}{\varrho_L \pi^4 m^4} \left\{1 + \eta \left[A^{0\prime}_m(M_{\varphi m} + O_{\varphi m}) - \bar{B}^{0\prime}_m(N_{\varphi m} - P_{\varphi m})\right]\right\} \sin \frac{m\pi x}{l}, \tag{31}$$

wo das erste Glied die Dimension der gesuchten Größe hat und wo $K^0(y)_m$ der erste Beiwert aus einer weiteren Doppelreihe dimensionsloser Beiwerte, von φ, ϑ, α und η abhängig ist und den Wert

$$K^0(y)_m = \eta[A^{0\prime}_m(M_{\varphi m} + O_{\varphi m}) - \bar{B}^{0\prime}_m(N_{\varphi m} - P_{\varphi m})] \tag{32}$$

hat, wo

$$\begin{aligned} A^0_m &= C^0_m = \frac{C^{**}_m n_6}{Z} = C^{**}_m A^{0\prime}_m = C^{**}_m C^{0\prime}_m, \\ B^0_m &= -D^0_m = -\frac{C^{**}_m n_5}{Z} = -C^{**}_m B^{0\prime}_m = C^{**}_m D^{0\prime}_m, \end{aligned} \tag{33}$$

Tafel I

Wert der Interpolationsfunktion $F(k)$

Beiwert	ϑ	Interpolationsgemäß $\alpha=0$	Interpolationsgemäß $\alpha=1$	ϑ	Interpolationsgemäß α	
K	0,05 ↕ 5,0	4η	4η	0,05 ↕ 0,40	$\alpha(-0{,}06+0{,}90\,\vartheta)$	
				0,45 ↕ 5,0	$\sqrt{\alpha}$	
μ	0,05 ↕ 5,0	4η	4η	0,05 ↕ 0,40	$\varphi\cdot\psi \gtrless 0$: $\alpha(-0{,}012+0{,}72\vartheta)$	$\varphi\cdot\psi \quad 0$: $\alpha(1{,}07-1{,}21\,\vartheta)$
				0,45 ↕ 5,0	$\sqrt{\alpha}$	
τ	0,05 ↕ 5,0	4η	4η	0,05 ↕ 0,40	$\psi=0$: $\alpha(0{,}075-1{,}42\,\vartheta)$	$\psi\neq 0$: $\alpha(-0{,}055+0{,}88\vartheta)$
				0,45 ↕ 5,0	$\sqrt{\alpha}$	
χ	0,05 ↕ 5,0	4η	4η	0,05 ↕ 0,4	$\alpha(-0{,}045+0{,}70\,\vartheta)$	
				0,45 ↕ 5,0	$\sqrt{\alpha}$	

und weiter

$$Z = n_1 n_6 + n_2 n_5, \tag{34}$$

$$C_m^{**} = \frac{l^4 p_m^0}{\varrho_L \pi^4 m^4}\,\eta\,. \tag{35}$$

n_1, n_2, n_5, n_6 und M, N, O, P sind durch die Beziehungen (16) und (19) gegeben.

Das Längsbiegungsmoment ist

$$M_L^0 = \sum_m \frac{p_m^0 l^2}{\pi^2 m^2}\left[1 + K^0(y)_m - \eta\mu^0(y)_m\right]\sin\frac{m\pi x}{l}, \tag{37}$$

wo

$$\mu^0(y)_m = \eta\left\{\varepsilon(A_m^{0\prime} M_{\varphi m} - \bar{B}_m^{0\prime} N_{\varphi m}) - \sqrt{1-\varepsilon^2}\,(A_m^{0\prime} N_{\varphi m} + \bar{B}_m^{0\prime} M_{\varphi m}) + \right.$$
$$\left. + \varepsilon\,(-A_m^{0\prime} O_{\varphi m} + \bar{B}_m^{0\prime} P_{\varphi m}) - \sqrt{1-\varepsilon^2}\,(A_m^{0\prime} P_{\varphi m} + \bar{B}_m^{0\prime} O_{\varphi m})\right\}, \tag{38}$$

das Querbiegungsmoment

$$M_Q^0 = \sum_m \frac{p_m^0 b^2}{\vartheta^2 \pi^2 m^2}\,[\eta - \mu^0(y)_m + \eta\, K^0(y)_m] \sin\frac{m\pi x}{l}, \tag{39}$$

der Unterschied der Torsionsmomente

$$(M_{LQ} - M_{QL})^0 = \sum_m \frac{2p_m^0}{\pi^2 m^2}\,\frac{lb}{\vartheta}\,(\alpha - \eta)\,[\tau^0(y)_m] \cos\frac{m\pi x}{l}, \tag{40}$$

wo

$$\tau^0(y)_m = \eta\sqrt{\frac{1+\varepsilon}{2}}\,[A_m^{0\prime} M_{\varphi m} - \bar{B}_m^{0\prime} N_{\varphi m}] - \sqrt{\frac{1-\varepsilon}{1+\varepsilon}}\,(A_m^{0\prime} N_{\varphi m} +$$
$$+ \bar{B}_m^{0\prime} M_{\varphi m}) + (A_m^{0\prime} O_{\varphi m} - \bar{B}_m^{0\prime} P_{\varphi m}) + \sqrt{\frac{1-\varepsilon}{1+\varepsilon}}\,(A_m^{0\prime} P_{\varphi m} + \bar{B}_m^{0\prime} O_{\varphi m})], \tag{41}$$

die Längsschubkraft

$$Q_L^0 = \sum_m \frac{lp_m^0}{\pi m}\left\{1 + K^0(y)_m - \frac{\gamma_L\,\eta + (2\varepsilon - \eta)\gamma_Q}{\varrho_L + \varrho_Q}\,\mu^0(y)_m\right\} \cos\frac{m\pi x}{l}, \tag{42}$$

die Reaktion

$$\bar{Q}_L^0 = \sum_m \frac{lp_m^0}{\pi m}\{1 + K^0(y)_m - (2\varepsilon - \eta)\mu^0(y)_m\} \cos\frac{m\pi x}{l} \tag{43}$$

und schließlich die Querschubkraft

$$Q_Q = \sum_m \frac{p_m^0 b}{\pi m \vartheta}\left\{\left[\eta + \frac{\gamma_L}{\sqrt{\varrho_L \varrho_Q}}\right]\tau^0(y)_m - \chi^0\,(y)_m\right\}, \tag{44}$$

wo

$$\varkappa^0(y)_m = \eta\sqrt{\frac{1+\varepsilon}{2}}\left[-(1-2\varepsilon)(A_m^{0\prime} M_{\varphi m} - \bar{B}_m^{0\prime} N_{\varphi m}) - \right.$$
$$- (1+2\varepsilon)\sqrt{\frac{1-\varepsilon}{1+\varepsilon}}\ldots(A_m^{0\prime} N_{\varphi m} + \bar{B}_m^{0\prime} M_{\varphi m}) -$$
$$- (1-2\varepsilon)\,(A_m^{0\prime} O_{\varphi m} - \bar{B}_m^{0\prime} P_{\varphi m}) + (1+2\varepsilon) \times$$
$$\left. \times \sqrt{\frac{1-\varepsilon}{1+\varepsilon}}\,(A_m^{0\prime} P_{\varphi m} + \bar{B}_m^{0\prime} O_{\varphi m})\right].$$

Auch für diese Belastung kann man ein analoges Tabellierungs- und Interpolationsverfahren anwenden. Die Interpolation wird gemäß der gleichen Beziehung (30) ausgeführt, und die Interpolationsfunktionen $F(k)$ sind in der weiteren Tafel II angeführt.

Tafel II

Wert der Interpolationsfunktion $F(k)$

Beiwert	ϑ	Interpolation gemäß η		ϑ	Interpolation gemäß α
		$\alpha = 0$	$\alpha = 1$		
K_0	0,05 ↕ 0,50	$4\eta^{\exp(0{,}65-0{,}82\,\vartheta)}$	$4\eta^{\exp(0{,}62-0{,}45\vartheta)}$	0,05 ↕ 0,50	$\alpha^{(1{,}06-1{,}14\,\vartheta)}$
	0,55 ↕ 5,0	$(4\,\eta)^{5/4}$	$(4\,\eta)^{4/3}$	0,55 ↕ 5,0	$\sqrt{\alpha}$
μ_0	0,05 ↕ 0,50	$(4\,\eta)$	$(4\,\eta)$	0,05 ↕ 0,50	$\alpha^{(1-\vartheta)}$
	0,55 ↕ 5,0	$(4\,\eta)^{5/4}$	$(4\,\eta)$	0,55 ↕ 5,0	$\sqrt{\alpha}$
τ°	0,05 ↕ 5,0	$(4\,\eta)$	$(4\,\eta)$	0,05 ↕ 0,50	$\alpha^{(1{,}05-1{,}11\,\vartheta)}$
				5,0 ↕ 0,55	$\sqrt{\alpha}$
$\varkappa^\circ$	0,05 ↕ 0,50	$\varphi \neq \pi$ | $\varphi = \pi$ $4\eta^{\exp(0{,}74-0{,}17\,\vartheta)}$	$(4\,\eta)$	0,05 ↕ 0,50	$\alpha^{(1{,}02-0{,}73\,\vartheta)}$
	0,55 ↕ 5,0	$(4\,\eta)$ | $(4\,\eta)^2$		0,55 ↕ 5,0	$\sqrt{\alpha}$

[1] An den Rändern gilt die Gleichung

$$\bar{Q}^0_Q = \sum_m \frac{p^0_m\, b}{m\pi\vartheta}\left\{[2\varepsilon - \eta)\ \tau^0(y)_m - \varkappa^0\ (y)_m\right\} \sin\frac{m\pi x}{l}. \qquad (44a)$$

SCHRIFTTUM

1. BAREŠ, R.—MASSONNET, Ch.: Le calcul des grillages de poutres et dalles orthotropes selon la méthodique Guyon—Massonnet—Bareš, Dunod, Paris 1956
2. BAREŠ, R.: Bestimmung der Biege- und Torsionssteifigkeit von Flächentragwerken unter Berücksichtigung der Querkontraktion. *VDI—Z.* **116**, 834—839
3. GEDIZLI, H. S.: Bending of Rectangular Anisotropic Slabs, Supported Free at Two Sides and Loaded Normal to the Middle Plane, *Mémoires AICP*, **11** (1951)
4. GIRKMANN, K.: Flächentragwerke, 5[e] éd., Wien 1959
5. GUYON, Y.: Calcul des ponts-dalles. Ann. des Ponts et Chaussées de France 119, 1949, pp. 555—589, 683—718
6. GUYON, Y.: Calcul des ponts larges à poutres multiples solidarisées par des entretoises. *Ann. des Ponts et Chaussées de France* (1946) 553—612
7. HUBER, M. T.: Über die genaue Berechnung einer orthotropen Platte. *Bauingenieur* **7** (1925), 878
8. KIRCHHOFF, G. J.: *Math.* (Grelle) **40** (1850), 51
9. KOLÁŘ, Vl.: Vybrané stati z teorie stavebních konstrukcí SNTL, Praha 1969
10. LEONHARDT, F.: Die vereinfachte Berechnung zweiseitig gelagerter Trägerroste, *Bautechnik* (1938), 535
11. MASSONNET, Ch.: Méthode de calcul des ponts à poutres multiples tenant compte de leur résistance à la torsion, *Mémoires A.I.P.C.* **10** (1950), 147—182
12. TIMOSHENKO, S.: Theory of Plates and Shells, New York 1940

Analysis of Structurally Orthotropic Plane Structures. Paper describes an analysis of structurally orthotropic plane systems. It takes into calculation not only the bending and torsional stiffness of the structure but also its contraction ability. Application of the derived method reduces the lengthy and most tiring part of the calculation, as well as the structural engineer's work to the minimum.

Расчет по форме ортотропных повеких конструкций. В работе для расчета тоских конструкций ортотропных по форме описывается такая методика, которая кромежесткости конструкции в отношении изгиба и кручения учитывает также контракционные способности данной конструкции. Благодаря описанной методики расчета часть расчетов требующая много энергии и в том месте работа статика становтся минимальными.

Acta Technica Academiae Scientiarum Hungaricae, Tomus 82 (1—2), pp. 47—52 (1976)

NONSTEADY TEMPERATURE FIELD IN THE ROTATING ANODE OF AN X-RAY TUBE

U. GAMER*

[Manuscript received March 6, 1974]

Using the temperature distribution due to an instantaneous point source, the temperature field in an infinite disk caused by a heat source moving along a circle is calculated. For constant output and constant circular frequency the mean value of the temperature over the circumference is received in closed form by application of the Laplace transformation and short time expansion. The numerical results are represented graphically.

1. Introduction

The life time of the anode of an X-ray tube may be limited by several causes. All of them are connected with the high temperatures occurring in the anode. Evaporation of the material takes place. In tubes operated on A. C. overheating results in inverse emission [1]. Thermal stresses may cause failure. To reduce the maximum temperature, rotating anodes are sometimes used. Elastic–plastic thermal stresses in the rotating anode of high-power X-ray tubes and the condition for shakedown were investigated by [2]. To calculate the thermal stresses, the knowledge of the temperature field is essential. To numerically evaluate the formula for the temperature given there a computer is needed since it involves twofold infinite summation. A simpler formula which gives the temperature in terms of tabulated functions is derived in the following.

2. Statement of the problem and solution

The anode is considered an unbounded thin disk heated by a point source of constant output moving along the circle $r = a$ with constant circular frequency ω (Fig. 1). Since loads of short duration are considered only, the temperature field in the infinite disk applies also as a good approximation of the finite disk as is shown below. Differences of temperature in z-direction and dissipation of heat by radiation are neglected.

*Dr. U. GAMER, I. Institut für Mechanik der Technischen Hochschule Wien, Österreich.

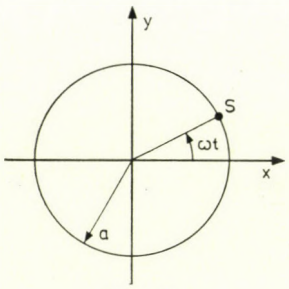

Fig. 1

Using the method of point sources, the problem can be solved exactly. Under the conditions stated, heat flow occurs in the x, y-plane only, and the temperature at point x, y as a function of time t caused by the release of the amount of heat Q per unit length in z-direction at x', y' and time t' is

$$T(x, y, t) = \frac{Q}{4\pi\lambda(t - t')} \exp\left(-\frac{(x - x')^2 + (y - y')^2}{4k(t - t')}\right). \tag{1}$$

Here λ means the thermal conductivity and k the thermometric conductivity.

The source of constant output W per unit length is supposed to start at $t = 0$ at the point $x = a$, $y = 0$. This does not imply a loss of generality but fixes the coordinate system and the time scale. It moves according to

$$x = a \cos \omega t,$$

$$y = a \sin \omega t.$$

Replacing the Cartesian co-ordinates by cylindrical coordinates

$$re^{i\varphi} = x + iy$$

end integrating over t', there follows

$$T(r, \varphi, t) = \frac{W}{4\pi\lambda} \int_0^t \exp\left(-\frac{r^2 + a^2 - 2ar\cos(\varphi - \omega t')}{4k(t - t')}\right) \frac{dt'}{t - t'}. \tag{2}$$

The temperature at a fixed point oscillates about a monotonously increasing level. The amplitude becomes the smaller the faster the anode runs. The mean value of the temperature over the circumference is by integration [3]

$$T(r, t) = \frac{1}{2\pi} \int_0^{2\pi} T(r, \varphi, t)\, d\varphi =$$

$$= \frac{W}{4\pi\lambda} \int_0^t \exp\left(-\frac{r^2 + a^2}{4k(t - t')}\right) I_0\left(\frac{ar}{2k(t - t')}\right) \frac{\mathrm{d}t'}{t - t'} \tag{3}$$

where I_0 represents the modified Bessel function of the first kind. It is not expressible in terms of tabulated functions [4]. The numerical evaluation of this integral is not easy. Since the load is applied for short times only, a closed form solution of the equation of heat conduction is derived by application of the Laplace transformation and short-time approximation.

3. Mean value of the temperature over the circumference for short times

The infinite disk is separated into two regions $r \leq a$ and $r \geq a$ free of sources. Heat is supplied at the boundary $r = a$. The temperature is governed by the equation of heat conduction

$$\frac{\partial^2 T}{\partial r^2} + \frac{1}{r}\frac{\partial T}{\partial r} - \frac{1}{k}\frac{\partial T}{\partial t} = 0 \tag{4}$$

and the boundary conditions

$$\left.\begin{aligned} T_1 &= T_2, \\ 2\pi a\lambda\left(\frac{\partial T_1}{\partial r} - \frac{\partial T_2}{\partial r}\right) &= WU(t) \end{aligned}\right\} r = a. \tag{5}$$

The subscripts 1 and 2 designate the inner and outer region, respectively. $U(t)$ is the Heaviside unit-step function.

Taking Laplace transforms, (4) and (5) read

$$\frac{d^2T^*}{dr^2} + \frac{1}{r}\frac{dT^*}{dr} - \frac{s}{k} = 0\,, \tag{6}$$

$$\left.\begin{aligned} T^*_1 &= T^*_2, \\ 2\pi a\lambda\left(\frac{dT_1^*}{dr} - \frac{dT_2^*}{dr}\right) &= \frac{W}{s} \end{aligned}\right\} r = a. \tag{7}$$

$T^*(r, s)$ means the Laplace transform of $T(r, t)$. The two solutions of (6) are the modified Bessel functions of order zero $I_0(qr)$ and $K_0(qr)$ with $q = \sqrt{s/k}$. Since bounded the transformed temperature is represented in the inner region by

$$T_1^* = AI_0(qr)$$

and in the outer region by

$$T_2^* = BK_0(qr).$$

A and B are determinzd from the boundary conditions

$$I_0(qa)A - K_0(qa)B = 0,$$

$$I_1(qa)\,A + K_1(qa)\,B = \frac{W}{2\pi a\lambda qs}\,,$$

and thereform

$$T_1^* = \frac{W}{2\pi a\lambda qs} \frac{K_0(qa)}{I_0(qa)\, K_1(qa) + K_0(qa)\, I_1(qa)} I_0(qr) \,, \tag{8}$$

$$T_2^* = \frac{W}{2\pi a\lambda qs} \frac{I_0(qa)}{I_0(qa)\, K_1(qa) + K_0(qa)\, I_1(qa)} K_0(qr) \,. \tag{9}$$

The denominator becomes ([5], p. 375)

$$I_0(qa)\, K_1(qa) + K_0(qa)\, I_1(qa) = \frac{1}{qa} \,.$$

Expansion of the modified Bessel function of zero order for large values of the argument $|z|$ yields ([5], p. 377/378)

$$I_0(z) = \frac{e^z}{\sqrt{2\pi z}} \left[1 + \frac{1}{8z} + \frac{9}{128\, z^2} + \ldots\right],$$

$$K_0(z) = \sqrt{\frac{\pi}{2z}}\, e^{-z} \left[1 - \frac{1}{8z} + \frac{9}{128 z^2} + \ldots\right].$$

With the first three terms of these series, T_1^*, in a form suitable for inverse transformation, reads

$$T_1^* = \frac{W}{4\pi\lambda \sqrt{ar}}\, e^{-(a-r)q} \left[\frac{k^{1/2}}{s^{2/2}} + \frac{1}{8}\left(\frac{1}{r} - \frac{1}{a}\right)\frac{k}{s^2} + \right.$$
$$\left. + \frac{1}{128}\left(\frac{9}{r^2} - \frac{2}{ar} + \frac{9}{a^2}\right)\frac{k^{3/2}}{s^{5/2}}\right].$$

A similar expression is obtained for T_2^*.

Using pair No. 11 of the table of Laplace transforms in [4], p. 494, and the recurrence formula for the repeated integrals of the error function ([4], p. 484) one arrives, after tedious but straightforward calculation, at

$$T_1 = \frac{W}{4\pi\lambda} \frac{1}{\sqrt{\varrho}} \left\{-(1-\varrho)\left[1 + \frac{1}{768}(9 - 50\varrho + 9\varrho^2)\left(\frac{1}{\varrho} - 1\right)^2 + \right.\right.$$
$$+ \frac{9}{128}\left(\frac{1}{\varrho} - 1\right)^2 \tau\left]\left(1 - \operatorname{erf}\frac{1-\varrho}{2\sqrt{\tau}}\right) + \left[2 + \frac{1}{384}(9 - 50\varrho + 9\varrho^2) \times\right.\right.$$
$$\left.\left. \times \left(\frac{1}{\varrho} - 1\right)^2 + \frac{1}{96}\left(-9\,\frac{2}{\varrho} + \frac{9}{\varrho^2}\right)\tau\right]\sqrt{\frac{\tau}{\pi}} \exp\left(-\frac{1-\varrho}{4\tau}\right)^2\right\}, \tag{10}$$

$$T_2 = \frac{W}{4\pi\lambda} \frac{1}{\sqrt{\varrho}} \left\{-(\varrho - 1)\left[1 + \frac{1}{768}\left(9 - \frac{50}{\varrho} + \frac{9}{\varrho^2}\right)(\varrho - 1)^2 + \right.\right.$$
$$+ \frac{9}{128}\left(1 - \frac{1}{\varrho}\right)^2 \tau\left]\left(1 - \operatorname{erf}\frac{\varrho - 1}{2\sqrt{\tau}}\right) + \left[2 + \frac{1}{384}\left(9 - \frac{50}{\varrho} + \frac{9}{\varrho^2}\right) \times\right.\right.$$
$$\left.\left. \times (\varrho - 1)^2 + \frac{1}{96}\left(9 - \frac{2}{\varrho} + \frac{9}{\varrho^2}\right)\tau\right]\sqrt{\frac{\tau}{\pi}} \exp\left(-\frac{\varrho - 1)^2}{4\tau}\right)\right\}. \tag{11}$$

The temperature is expressed as a function of the nondimensional radius $\varrho = r/a$ and the nondimensional time $\tau = tk/a^2$. A table of the error function erf x can be found e.g. in [5]. Fig. 2 shows the nondimensional temperature $T\,4\,\pi\lambda/W$ in the region $0{,}6 \leq \varrho \leq 1{,}35$ for different times up to $\tau = 0{,}02$.

It should be noted that (10) cannot be used for small values of ϱ but it is of sufficient accuracy in calculating the temperature in the neighbourhood of the source. Within the range $0{,}6 \leq \varrho \leq 1$ there is very good agreement between the temperature calculated from (10) and that calculated according to (8.4) in [2] involving twofold infinite summation.

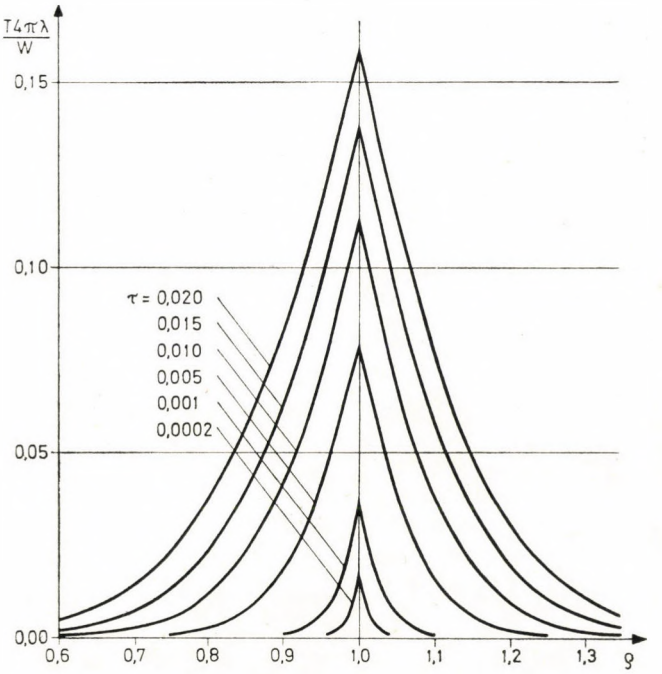

Fig. 2

Still open is the question whether the unbounded disk is a reasonable approximation for the finite disk. If dissipation by radiation is neglected, there should be no heat flow through the cylindrical surface since the anode is surrounded by vacuum. With the help of (11) numerical calculation shows that for $\tau = 0{,}02$ only 0,8 per cent of the total heat supplied pass the radius $\varrho = 1{,}5$. Therefore (10) and (11) are valid for finite diks, too.

The removal of the heat source is equivalent to the superposition of a second source of output $-W$, and thus, the temperature field during cooling of the disk can easily be calculated.

REFERENCES

1. OOSTERKAMP, W. J.: The Heat Dissipation in the Anode of an X-ray Tube, *Philips Res. Rep.* **3** (1948), 49—59 and 161—173
2. GAMER, U.: Ein radialsymmetrischer Wärmespannungszustand in der ideal-plastischen Scheibe, *Ingenieur-Archiv* **36** (1967), 174—191
3. GRÖBNER, W.—HOFREITER, N.: Integraltafel, Zweiter Teil. Springer, Wien 1950
4. CARSLAW, H. S.—JAEGER, J. C.: Conduction of Heat in Solids. Oxford University Press, London 1959
5. ABRAMOWITZ, M.—STEGUN, I. A.: Handbook of Mathematical Functions. Dover, New York 1965

Das instationäre Temperaturfeld in der rotierenden Anode einer Röntgenröhre. Unter der Verwendung der Temperaturverteilung zufolge einer instantanen punktförmigen Wärmequelle wird das Temperaturfeld in einer unendlich ausgedehnten Scheibe bei Erwärmung durch eine sich längs eines Kreises bewegende Wärmequelle angegeben. Für konstante Leistung und konstante Winkelgeschwindigkeit folgt die geschlossene Lösung des Mittelwerts der Temperatur über den Umfang, die durch Laplace-Transformation und Kurzzeitentwicklung gewonnen wird. Das Ergebnis ist in einem Schaubild dargestellt.

Нестационарное температурное поле во вращающемся аноде некоторой рентгеновской трубки. В отношении применения распределения температуры для некоторого нестационарного точкообразного источника тепла дается температурное поле в некотором бесконечном диске при нагреве от некоторого источника тепла, двигающегося вдоль некоторого круга. Для константной мощности и для константной угловой скорости получается решение замкнутой формы для среднего значения температуры для объема, которое решение получается с помощью преобразования Лапласа и кратковременного разложения.

Acta Technica Academiae Scientiarum Hungaricae, Tomus 82 (1—2), pp. 53—59 (1976)

ON THE RELATIONSHIP BETWEEN DIFFERENT APPROXIMATING METHODS

P. SCHARLE*

[Manuscript received January 28, 1974]

The paper deals with some common properties of several well-known approximating methods. It separates the concepts of the approximating principle and approximating technique. Attempts are made to construct a general treatment for relating the approximating principles used in the numerical investigations of a wide class of nonlinear continuum problems. It is possible to recognise a very expressive connection between the different methods as the least squares, weighted residuals, direct approximation and variational ones.

1. The concept of error vectors

Let us consider the problem of having a general operator equation such as

$$N(\mathbf{u}) = \mathbf{f} \tag{1}$$

where N may be a linear or nonlinear operator. Here $\mathbf{u}$ is a generalized vector containing scalar-function elements; the domain of definition for these functions will be the cartesian product of the three-dimensional euclidean space B with the boundary ∂B and the time interval $(-\infty, \infty)$. It is understood that (1) is to be satisfied in B. On ∂B, for the sake of simplicity, we assume to have homogeneous boundary conditions. Assuming that an exact solution $\mathbf{u}_0$ exists (in B, on ∂B) at least locally. In other words we presuppose the existence and the uniqueness of $\mathbf{u}_0$ — for the case of nonlinear N this uniqueness is local. In what follows we only consider the problem of finding an approximating solution, which is an element in the U-space, U being the domain of N. Let $\mathbf{f} \in V$, V being the range of N, then we can call the V-space the image of U, U and V are real Banach spaces. We shall assume that N is regular in the sense that there is a one-to-one correspondence between the elements of U and V.

Our aim is to find a "good" approximation for $\mathbf{u}_0$. We propose that

$$\mathbf{u} = c_i \mathbf{u}_i = \sum_{j=1}^{n} c_j \mathbf{u}_j \tag{2}*$$

*Dr. P. SCHARLE, Péterfy S. u. 44. II. 1. H-1076 Budapest, Hungary.
*Summation convention on repeated indices is applied in the sequel.

where $\mathbf{u}_i \in U$ are a set of linearly independent elements. The union of these elements determines a subspace U_n in U, c_i are undetermined parameters. In the U-space $\mathbf{u}_0$ and $\mathbf{u}$ can be considered as vectors and likewise $\mathbf{f}$ in the V-space ($\mathbf{f}$ is the image of $\mathbf{u}_0$). Now we have for the image of $\mathbf{u}$

$$N(\mathbf{u}) = N(c_i\mathbf{u}_i).$$

In this manner, we can interpret two kinds of error vectors (see Fig.; ÖDMAN[2])

$$\mathbf{g} = \mathbf{u}_0 - c_i\mathbf{u}_i \tag{3}$$

and

$$\mathbf{h} = \mathbf{f} - N(c_i\mathbf{u}_i). \tag{4}$$

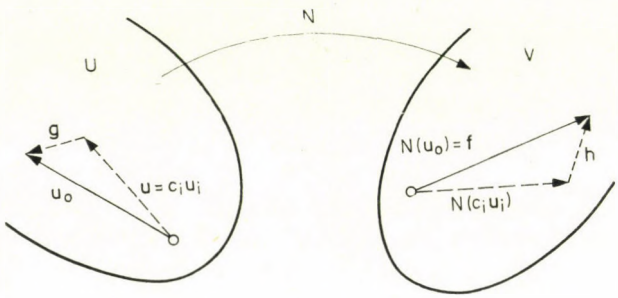

Fig. 1

Naturally, $\mathbf{g}$ and $\mathbf{h}$ are not independent. For instance, if N were linear,

$$\mathbf{h} = N(\mathbf{g}).$$

The *first* step for constructing an approximating solution is to define that we consider the approximation as "good" if some measure of $\mathbf{g}$ and/or $\mathbf{h}$ is rather small. There are several possibilities in choosing this measure (e.g. a type of norm, a vector, etc.). In what follows we will accept that this measure is a scalar, without discussing any of the other possibilities. In this case we have two alternatives; we can require either

a) the length of the chosen error-vector, which is the projection of the vector on itself, shall be a minimum, or that

b) some projections of the error vector should be zero — in other words the vector must be orthogonal to some subspace.

To define the length and orthogonality conditions we shall use the concept of a scalar-product. This product is defined as a bilinear functional in its arguments and indicated by

$$\langle \mathbf{a}, \mathbf{b} \rangle$$

where $\mathbf{a}$, $\mathbf{b}$ are the arguments, not necessarily defined in the same function-space (TONTI [3]). This bilinear functional puts U and V into duality.

If the number of the linearly independent $\mathbf{u}_i$ vectors is large enough, we can expect that the chosen measure of the error, e. g.

a) the length of the error vector or

b) the non-vanishing components of the error vector will become negligible small.

The *second* step is the selection of the error vectors. We can consider only **g** or only **h**, or simultaneously both of them. Clearly, the two steps are not totally independent, moreover in some cases the a) and b) alternatives are equivalent (in accordance with the projection-theorem in Hilbert-spaces). However, we will not discuss these questions in this paper.

2. The approximating principles

It seems to be appropriate to separate the ideas of the approximating principle and the approximating technique. An approximating principle needs to have a definition of error and a measure of it, according to the above definitions. On the other hand, it is usually important to find a rather wide U_n subspace of the $\mathbf{u}_i$ approximating vectors. The approximating techniques of finite differences, finite elements or the Kantorovich, for instance, because of the discretization involved allow for a wider subspace, independent of the approximating principles applied. We can call an approximating method the coupling of some approximating principle and some approximating technique. However, in what follows, we will only be concerned with the approximating principles defined in the above sense.

Generally, we can separate six type of these principles:

2.1. Consider the error-vector **g** and the minimum-condition

$$\langle \mathbf{g}, \mathbf{g} \rangle = \min. \tag{5}$$

This condition is not useable as we cannot eliminate from it the unknown $\mathbf{u}_0$.

2.2. Consider the error-vector **g** as orthogonal with respect to a set of linearly independent functions (ψ_ν) constituting some space

$$\langle \mathbf{g}, \psi_\nu \rangle = 0, \qquad \nu = 1, 2, \ldots, n. \tag{6}$$

Expanding (6) we find

$$\langle \mathbf{u}_0 - \mathbf{u}, \psi_\nu \rangle = \langle \mathbf{u}_0, \psi_\nu \rangle - \langle c_i \mathbf{u}_i, \psi_\nu \rangle = 0. \tag{7}$$

This equation again contains the $\mathbf{u}_0$ solution, but now we can choose ψ_ν as a set of images of an arbitrary $\varphi_\nu \in U$ set, so that

$$\psi_\nu = N(\varphi_\nu). \tag{8}$$

Now, from (7) we obtain

$$\langle \mathbf{u}_0,\ N(\varphi_\nu)\rangle = \langle c_i\,\mathbf{u}_i,\ N(\varphi_\nu)\rangle. \tag{9}$$

If the N operator is symmetric* in the sense

$$\langle \mathbf{p},\ N(\mathbf{q})\rangle = \langle \mathbf{q},\ N(\mathbf{p})\rangle \tag{10}$$

where $\mathbf{p}, \mathbf{q} \in U$ (TONTI [3], ODEN [4] etc.), then from equation (9) can be written

$$\langle c_i\mathbf{u}_i,\ N(\varphi_\nu)\rangle = \langle \varphi_\nu,\ N(\mathbf{u}_0)\rangle. \tag{11}$$

This equation is the general form of the so-called *direct* approximation method (TOTTENHAM [5]).

2.3. Consider **h** error with the minimum-condition:

$$\langle \mathbf{h},\ \mathbf{h}\rangle = \text{min!} \tag{12}$$

By expanding (12) we obtain

$$\langle N(\mathbf{u}_0),\ N(\mathbf{u}_0)\rangle - \langle N(\mathbf{u}_0),\ N(c_i\,\mathbf{u}_i)\rangle - \langle N(c_i\,\mathbf{u}_i),\ N(\mathbf{u}_0)\rangle + \\ + \langle N(c_i\mathbf{u}_i),\ N(c_i\mathbf{u}_i)\rangle = \text{min}\,! \tag{13}$$

The necessary condition for the minimum is

$$\frac{\partial}{\partial c_\nu}\langle \mathbf{h},\ \mathbf{h}\rangle = 0 \tag{14}$$

which gives

$$-\left\langle N(\mathbf{u}_0), \frac{\partial}{\partial c_\nu} N(c_i\,\mathbf{u}_i)\right\rangle - \left\langle \frac{\partial}{\partial c_\nu} N(c_i\,\mathbf{u}_i),\ N(\mathbf{u}_0)\right\rangle + \\ + \left\langle \frac{\partial}{\partial c_\nu} N(c_i\,\mathbf{u}_i),\ N(c_i\,\mathbf{u}_i)\right\rangle + \left\langle N(c_i\,\mathbf{u}_i), \frac{\partial}{\partial c_\nu} N(c_i\,\mathbf{u}_i)\right\rangle = 0. \tag{15}$$

This expression is the most general form of the *least squares* approximation method.

2.4. Consider the **h** error-vector with the orthogonality condition:

$$\langle \mathbf{h},\ \mathbf{m}_\nu\rangle = 0 \tag{16}$$

where $\mathbf{m}_\nu$ is an arbitrary system of linearly independent vectors. Equation (16) can be written

$$\langle N(c_{i-i}),\ \mathbf{m}_\nu\rangle = \langle N(\mathbf{u}_0),\ \mathbf{m}_\nu\rangle. \tag{17}$$

This is the general form of the *weighted residual* method.

2.5. Consider simultaneously **g** and **h** with the minimum-condition:

$$\langle \mathbf{g},\ \mathbf{h}\rangle = \text{min}\,! \tag{18}$$

*Here we take the advantages of the homogeneous boundary conditions. The inhomogeneous case is more involved but can be accommodated in a similar manner (see ODEN [4]).

Expanding (18) we obtain

$$\langle \mathbf{u}_0, N(\mathbf{u}_0)\rangle - \langle c_i\mathbf{u}_i, N(\mathbf{u}_0)\rangle - \langle \mathbf{u}_0, N(c_i\mathbf{u}_i)\rangle + \langle c_i\mathbf{u}_i, N(c_i\mathbf{u}_i)\rangle = \min ! \quad (19)$$

Minimizing (19) with respect to c_ν the first term on the left-hand side disappears and the others become

$$\begin{aligned}\langle \mathbf{u}_\nu, N(\mathbf{u}_0)\rangle - \langle \mathbf{u}_\nu, N(c_i\,\mathbf{u}_i)\rangle + \left\langle \mathbf{u}_0, \frac{\partial}{\partial c_\nu} N(c_i\,\mathbf{u}_i)\right\rangle - \\ - \left\langle c_i\,\mathbf{u}_i, \frac{\partial}{\partial c_\nu} N(c_i\,\mathbf{u}_i)\right\rangle = 0,\end{aligned} \quad (20)$$

or, in a more conscise form,

$$\langle \mathbf{u}_\nu, \mathbf{h}\rangle + \left\langle \mathbf{g}, \frac{\partial}{\partial c_\nu} N(c_i\,\mathbf{u}_i)\right\rangle = 0 \quad (21)$$

where the second term of the left-hand side contains the unknown solution. If the first Gateaux-derivative (see, for example VAINBERG [9]) of the operator N is symmetric in the sense defined by (10), $\mathbf{u}_0$ can be eliminated and (21) furnishes a usable equation for c_i. Thus, we have obtained the general expression of the so-called *variational* formulation.

2.6. Consider $\mathbf{g}$ and $\mathbf{h}$ with the orthogonality-condition:

$$\langle \mathbf{g}, \mathbf{h}\rangle = 0. \quad (22)$$

Analogously to (5) the left-hand side is now fully symmetric in $\mathbf{u}_0$, even if $\langle\ ,\ N(\ )\rangle$ is not symmetric and (22) does not provide a new approximating principle. Nevertheless, it is well worth noticing that (22) is fulfilled and the two error-vectors are orthogonal in the sense of (21), as they are expressed in a unique biorthogonal system, but in two complementary subspaces of that one.

3. Some consequences and remarks

3.1. Clarly, each of the above principles can be restricted, in accordance with the actual structure of the N operator. For example, if N was linear and symmetric, from (9) we obtain the "auxiliary solution method" referred by TOTTENHAM [1]; from (15) we arrive to the familiar expression of the least squares method:

$$\langle c_i\, N(\mathbf{u}_i) - N(\mathbf{u}_0),\ N(\mathbf{u}_\nu)\rangle = 0$$

and from (19) we obtain (leaving the first term out as we know we shall derive the expression) the MIKHLIN [6]-problem

$$\langle N(c_i\mathbf{u}_i) - 2N(\mathbf{u}_0),\ c_i\mathbf{u}_i\rangle = \min !$$

The possibilities provided by (17) are discussed in great length by FINLAYSON [7].

3.2. Each of the principles has advantages and disadvantages. For example, the direct approximation furnishes linear equation for c_i, the least squares principle provides symmetric coefficient-matrix, and so on. Our choice among the principles may be governed by our possibilities of finding an appropriately wide U_n subspace and, in this context, is also influenced by the applied techniques. In general, however, if n is rather large, there is no preferred approximating principle (CRANDALL [10]). The extensive analysis of this question is beyond the scope of this paper.

3.3. The power of the Galerkin-method is due to the possibility of choosing for the $\mathbf{u}_i$ functions the eigenfunctions of the N operator. When this happens, each of the approximating principles becomes more simple (for example, we arrive at the direct method used by MIKHLIN [8], relating to (11)), and each of them can be considered as a modification of the other.

For the variational method, both of the error-vectors are controlled and for this reason it provides a very rigorous solution. However, the requirement of the symmetry of the Gateaux-derivative is a severe restriction in comparison with the other principles. Moreover, the condition of the meaningful existence of (18) requires further analysis. We may assume — mostly intuitively and with certain optimism — that if our governing equations are independent and the state-fields are able to describe the interactions of the considered physical problem, N will be, at least locally, linear and there will exist a variational principle.

3.4. For time-dependent problems, $<, >$ represents the Gurtin-convolution product (see [3], for example). As to the regularity of N, intuitively we can expect it to be equivalent with the principle for the conservation of the energy (and matter). If there were zero-eigenvalues for N, it may mean that we have left out some of the interactions connected with the investigated physical problem.

3.5. It is worth remarking that in (21) the idea of the complementary variational principles is implied.

3.6. The intention of this paper was to relate the different approximating principles presented in the literature. This work may give rise to some statements which can be considered as work-hypotheses and still require a more rigorous analysis. We hope it will help to further interest in the existing topic of computing methods.

Acknowledgements

The ideas summarized in the paper are based on the investigations stimulated by Professor J. SZABÓ to whom the author feels himself deeply indebted. An early version was written in the form of an internal report [11]; the author is very grateful to Professor H. TOTTENHAM and Dr. C. A. BREBBIA for having discussed the material and for their help in correcting some of the original errors.

REFERENCES

1. Variational Methods in Engineering (Edited by C. A. Brebbia and H. Tottenham) — *Proceedings of an International Conference.* Southampton 1973
2. ÖDMAN, S. T. A.: Studies of Boundary Value Problems — Swedish Cement and Concrete Research Institut, Stockholm 1953
3. TONTI, E.: A Systematic Approach to the Search for Variational Principles — see Ref. 1
4. ODEN, J. T.: Variational Principles in Nonlinear Continuum Mechanics — see Ref. 1
5. TOTTENHAM, H.: A Direct Numerical Method for the Solution of Field Problems — *Int. Jnl. for Num. Meth. in Eng.*, 1970, 117—131
6. MIKHLIN, S. G.: The Problem of the Minimum of a Quadratic Functional, Holden-Day, 1965
7. FINLAYSON, B. A.: The Method of Weighted Residuals and Variational Principles — Academic Press, 1972
8. MIKHLIN, S. G.: Variational Methods in Mathematical Physics, Pergamon, 1964
9. VAINBERG, M. M.: Variational Methods for the Study of Nonlinear Operators, Holden Day, 1964
10. CRANDALL, S. H.: Engineering Analysis, McGraw Hill, 1956
11. SCHARLE, P.: On the Relationship between Different Approximating Methods (Internal Report at the Civil Engineering Department, University of Southampton — Manuscript) Southampton, 1973

Einige Fragen des zwischen den Annäherungsmethoden bestehenden Zusammenhangs. Gewisse gemeinsame Eigenschaften einiger wohlbekannten Näherungsmethoden werden behandelt. Die Begriffe des Näherungsprinzips und der Näherungstechnik werden abgesondert. Die Systematisierung der bei der Untersuchung von nichtlinearen Kontinuumproblemen gebrauchten Näherungsprinzipien wird versucht. Ein sehr ausdruckvoller Zusammenhang ist erkennbar zwischen den Methoden der kleinsten Quadrate, der gewogenen Restbeträge und der direkten Näherung, sowie dem Variationsverfahren.

Некоторые вопросы связи, существующей между приближенными методами. Данная работа занимается определенными общими свойствами нескольких хорошо известных методов. Производится разделение принципа приближения и тесники приближения. Сделана попытка систематизации принципов приближения, использованных во время числового анализа нелинейных контиуумных задач. Можно установить очень ярко выраженную зависимость между методами наименьших квадратов, взвешанных остатков и непосредственного приближения.

Acta Technica Academiae Scientiarum Hungaricae, Tomus 82 (1—2), pp. 61—67 (1976)

AN INFINITE VISCOELASTIC THICK PLATE CONTAINING AN EXTERNAL CRACK

SATYANARAYAN MANDAL*

[Manuscript received: July 12, 1974]

This paper is concerned with the stress fields in an infinite viscoelastic thick plate containing an external crack due to the application of normal pressure to its faces. The crack is taken to lie in the central plane of the plate normal to the axis of symmetry and occupies the region outside the circle. It is assumed that the two faces of the crack are loaded exactly the same way and the viscoelastic layer is in a rigid casing. Hankel transforms of the displacement vector are introduced. Mixed boundary conditions lead to dual integral equations. These equations are then reduced to Fredholm integral equation of the second kind. This type of equation is solved by an iterative process for large values of thickness of the plate. The stress intensity factor has been calculated.

1. Introduction

For axisymmetric stress distribution to the plane of the crack, solutions have been given by SNEDDON [1]. LOWENGRUB [2] has dealt with the stress field in the vicinity of a crack in a thick plate. DHAWAN [3] has derived the stress distribution for an infinite elastic thick plate containing an external crack due to the application of normal pressure to its faces.

This paper concerns the distribution of stress in an infinite thick viscoelastic plate containing an external crack due to the application of normal pressure to its faces. The medium of the plate is viscoelastic and of the special linear type, its thickness being 2h. It is assumed that there is symmetry about the Z- axis and the external crack lies in the central plane of the plate normal to this axis. The crack occupies the region outside the circle of radius unity whose centre lies on the axis of symmetry.

The boundary surfaces of the plate are constrained by two rigid walls, *vide* [4], which permit no normal displacement. Further, the contact between the viscoelastic layer and its rigid casing is frictionless so that the shearing stress on the surfaces $z = \pm h$ of the plate is equal to zero.

Physical quantities of maximum interst appear to be the normal component of the stress tensor and the normal component of the displacement vector

*SATYANARAYAN MANDAL, Hatuganj M.N.K. High School, P. O. Hatuganj, Dt. 24-Parganas, West Bengal.

for their usefulness in computing the stress intensity factor and the crack energy.

By introducing Hankel transforms of the displacement components, the partial differential equations of equilibrium are reduced to ordinary differential equations. On applying mixed boundary conditions, the pair of dual integral equations are obtained. These equations are, thereafter, reduced to Fredholm integral equation of the second kind. For particular types of loading this equation is solvable by the technique employed by DHAWAN [3] for small values of 1/h. The stress intensity factor has been calculated.

2. Formulation of the problem

Let us choose cylindrical co-ordinates (γ, s, z) and the axis of symmetry to the Z- axis. For a symmetrical deformation of the viscoelastic plate this displacement vector **U** may be taken to have components (u, s, w), whereas the only nonvanishing components of the stress tensor are $\sigma_{r,}$, $\sigma_{\theta\theta}$, σ_{zz}, σ_{rz}.

In this paper the distribution of stress is considered in an infinite viscoelastic plate of finite thickness 2h. The crack is taken to lie on the line $z = 0$, $1 \leq r < \infty$, $(-h \leq Z \leq h)$. It is assumed that the two faces of the crack are loaded exactly the same way and it is convenient to convert the problem to a mixed boundary value problem for $0 \leq Z \leq h$

The equations of equilibirium are given by

$$\begin{aligned} &\frac{\partial \sigma_{rr}}{\partial \gamma} + \frac{\partial \sigma_{rz}}{\partial z} + \frac{\sigma_{rr} - \sigma_{\theta\theta}}{\gamma} = 0, \\ &\frac{\partial \sigma_{rz}}{\partial r} + \frac{\partial \sigma_{zz}}{\partial z} + \frac{\sigma_{rz}}{r} = 0. \end{aligned} \tag{1}$$

The stress-strain relation for homogeneous viscoelastic medium of the special linear type is taken as

$$\left(1 + a_1 \frac{\partial}{\partial t}\right) \sigma_{ij} = 2k_1 \left(1 + b_1 \frac{\partial}{\partial t}\right) e_{ij} \tag{2}$$

where σ_{ij} and e_{ij} respectively are the stress tensor and the strain tensor, whereas a_1, b_1, k_1 are material constants.

The boundary conditions are taken as on $z = 0$:

$$w = 0, \qquad 0 \leq r \leq 1 \tag{3.1}$$

$$\sigma_{rz} = 0, \qquad r \leq 0 \tag{3.2}$$

$$\sigma_{zz} = -p(r)e^{-\omega t}, \; 1 \leq \gamma < \infty, \; t \geq 0, \; \dot{w} > 0 \tag{3.3}$$

on $z = h$:

$$w = 0, \qquad r \leq 0 \tag{3.4}$$

$$\sigma_{rz} = 0, \qquad r \leq 0 \tag{3.5}$$

3. Method of solution

From Eq. (2) we obtain

$$\begin{aligned}
&\left(1 + a_1 \frac{\partial}{\partial t}\right) \sigma_{rr} = 2k_1 \left(1 + b_1 \frac{\partial}{\partial t}\right) e_{rr} = 2k_1 \left(1 + b_1 \frac{\partial}{\partial t}\right) \frac{\partial u}{\partial r}, \\
&\left(1 + a_1 \frac{\partial}{\partial t}\right) \sigma_{\theta\theta} = 2k_1 \left(1 + b_1 \frac{\partial}{\partial t}\right) e_{\theta\theta} = 2k_1 \left(1 + b_1 \frac{\partial}{\partial t}\right) \frac{u}{r}, \\
&\left(1 + a_1 \frac{\partial}{\partial t}\right) \sigma_{zz} = 2k_1 \left(1 + b_1 \frac{\partial}{\partial t}\right) e_{zz} = 2k_1 \left(1 + b_1 \frac{\partial}{\partial t}\right) \frac{\partial w}{\partial z}, \\
&\left(1 + a_1 \frac{\partial}{\partial t}\right) \sigma_{rz} = 2k_1 \left(1 + b_1 \frac{\partial}{\partial t}\right) e_{rz} = k_1 \left(1 + b_1 \frac{\partial}{\partial t}\right) \left(\frac{\partial w}{\partial r} + \frac{\partial u}{\partial z}\right).
\end{aligned} \tag{4}$$

Eq. (1) and (4) give

$$2k_1 \left(1 + b_1 \frac{\partial}{\partial t}\right) \left(\frac{\partial^2 u}{\partial \gamma^2} + \frac{1}{2} \frac{\partial^2 w}{\partial \gamma \partial z} + \frac{1}{2} \frac{\partial^2 u}{\partial z^2} + \frac{1}{\gamma} \frac{\partial u}{\partial \gamma} - \frac{U}{\gamma^2}\right) = 0,$$

$$2k_1 \left(1 + b_1 \frac{\partial}{\partial t}\right) \left(\frac{1}{2} \frac{\partial^2 \omega}{\partial \gamma^2} + \frac{1}{2} \frac{\partial^2 U}{\partial \gamma \partial z} + \frac{\partial^2 \omega}{\partial z^2} + \frac{1}{2\gamma} \frac{\partial \omega}{\partial \gamma} + \frac{1}{2\gamma} \frac{\partial U}{\partial z}\right) = 0. \tag{5}$$

Let us choose

$$\begin{aligned}
u(r, z, t) &= u_1(r, z) e^{-\omega t}, \\
w(r, z, t) &= w_1(r, z) e^{-\omega t}.
\end{aligned} \tag{6}$$

Using Eqs (6) we get from Eq. (5)

$$2\left(\frac{\partial^2 u_1}{\partial \gamma^2} + \frac{1}{\gamma} \frac{\partial u_1}{\partial \gamma} - \frac{u_1}{\gamma^2}\right) + \frac{\partial^2 u_1}{\partial z^2} + \frac{\partial^2 w_1}{\partial \gamma \partial z} = 0, \tag{7}$$

$$\left(\frac{\partial^2 w_1}{\partial r^2} + \frac{1}{r} \frac{\partial w_1}{\partial r}\right) + 2 \frac{\partial^2 w_1}{\partial z^2} + \frac{\partial}{\partial z}\left(\frac{\partial u_1}{\partial r} + \frac{u_1}{r}\right) = 0. \tag{8}$$

We introduce the first-order Hankel transform of the radial component of the displacement vector by the equation

$$\bar{u}_1(\xi, z) = \int_0^\infty r u_1(r, z)\, J_1(\xi r)\, dr \tag{9}$$

and the zero-order Hankel transform of the z component of the displacement vector by the equation

$$\overline{w}_1(\xi, z) = \int_0^\infty r w_1(r, z)\, J_0(\xi r)\, dr). \tag{10}$$

Multiplying both sides of Eq. (7) by r, $J_1(\xi r)$, integrating with respect to γ from 0 to ∞ and making use of the well-known properties of Hankel transform, we obtain

$$(D^2 - 2\,\xi^2)\overline{u}_1 - \xi\, D\, \overline{w}_1 = 0 \tag{11}$$

where

$$D = \frac{d}{dz}\,.$$

Again, if we multiply both sides of Eq. (8) by $r\, J_0(\xi r)$ and integrate from $r = 0$ to $r = \infty$, we get

$$(2\, D^2 - \xi^2)\overline{w}_1 + \xi\, D\, \overline{u}_1 = 0. \tag{12}$$

Eliminating $\overline{u}_1$ and $\overline{w}_1$ in turn from Eqs (11) and (12)

$$(D^2 - \xi^2)^2 \overline{u}_1 = 0, \tag{13}$$

$$(D^2 - \xi^2)^2 \overline{w}_1 = 0. \tag{14}$$

The solution of Eq. (14) may be taken as

$$\overline{w}_1 = (A + Bz)\cosh \xi z + (c + Dz)\sinh \xi z \tag{15}$$

where A, B, C, D are functions of ξ.

Using Eqs (12) and (15) we have

$$D\overline{u}_1 = -[(A + Bz)\,\xi \cosh \xi z + (c + Dz)\,\xi \sinh \xi z + 4B \sinh \xi z + 4\, D \cosh \xi z]. \tag{16}$$

Substituting expressions for u and ω into the last equation of Eqs (4), applying first-order Hankel transform, we have

$$\left(1 + a_1 \frac{\partial}{\partial t}\right) \sigma_{rz} = k_1 (1 - b_1 \omega)\, e^{-\omega t}\, [D\overline{u}_1 - \xi\, \overline{w}_1]. \tag{17}$$

On using Eqs (15) and (16) into Eq. (17), boundary condition (3.2) gives

$$\xi\, A = -2\, D. \tag{18}$$

Also boundary conditions (3.4) and (3.5) give respectively

$$(A + Bh)\cosh \xi h + (c + D\, h)\sinh \xi h = 0, \tag{19}$$

$$D = -B \tanh \xi h. \tag{20}$$

On using Eqs (18), (19) and (20), boundary conditions (3.1) and (3.3) give dual integral equations

$$\int_0^\infty \Phi(\xi)\, J_0(\xi\, r)\, d\, \xi = 0, \quad 0 < r < 1. \tag{21}$$

$$\int_0^\infty \xi\, \Phi\,(\xi)[1 - H(\xi\, h)]\, J_0(\xi r)\, d\, \xi = f(r), \qquad r > 1, \tag{22}$$

where

$$\xi\, A(\xi) = \Phi(\xi) \tag{23}$$

$$H(\xi h) = 1 - \frac{\xi h + \sinh\, \xi h \cosh \xi h}{\sinh^2 \xi h}, \tag{24}$$

$$f(r) = \frac{(1 - a_1\omega)\, p(r)}{k_1(1 - b_1\omega)}. \tag{25}$$

Let the solution be assumed as

$$\Phi(\xi) = \int_1^\infty \psi(x)\ \cos\ \xi\, x\, dx \tag{26}$$

where

$$\lim_{x \to \infty} \psi(x) = 0 \tag{27}$$

Now the Eq. (21) is satisfied identically for any function $\psi(x)$, which are continuous together with their first derivatives in the closed interval $(1, \infty)$,

where $$\int_0^\infty J_0\,(\xi\gamma) \cos\, \xi\alpha\, d\xi = \begin{cases} 0 & , \quad 0 < r < \alpha\,, \\ (r^2 - \alpha^2)^{1/2}\,, & \quad r > \alpha\,. \end{cases} \tag{28}$$

Substituting the value of $\Phi(\xi)$ from Eq. (26) into Eq. (22), we find [3]

$$\int_r^\infty \frac{dx}{\sqrt{x^2 - r^2}} \left[\psi'\,(x) - \frac{1}{\pi h}\int_1^\infty \psi'(y)\, [G'(x + y) + G'(x - y)]\, dy = -f(r), r > 1, \right. \tag{29}$$

where

$$\int_0^\infty r_0\,(\xi r) \sin\, \xi\beta\, d\xi = \begin{cases} 0 & , \quad \beta < r\,, \\ (\beta^2 - r^2)^{-1/2}\,, & \quad \beta > r\,, \end{cases} \tag{30}$$

$$J_0(\xi r) = \frac{2}{\pi} \int_r^\infty \frac{\sin\, \xi y\, dy}{\sqrt{y^2 - r^2}}, \tag{31}$$

$$G(u) = \int_0^\infty H(w_1) \cos\, \frac{u\, w_1}{h}\, d\omega\,, \tag{32}$$

Eq. (29)on inversion gives

$$\psi'(x) - \frac{1}{\pi h}\int_1^\infty \psi(y)[G'(x+y) + G'(x-y)]\,dy = \\ = \frac{2}{\pi}\frac{d}{dx}\int_x^\infty \frac{r f(r)\,dr}{\sqrt{r^2 - x^2}}, \quad 1 < x < \infty. \tag{33}$$

Since $p(r)$ is continuous differentiable in $(1, \infty)$, we integrate Eq. (33) and on using Eq. (27), we obtain Fredholm integral equation of the second kind

$$\psi(x) - \frac{1}{\pi h}\int_1^\infty \psi(y)K(x, y)\,dy = \frac{2}{\pi}\int_x^\infty \frac{rf(r)\,d\gamma}{\sqrt{r^2 - x^2}}, \; 1 < x < \infty, \tag{34}$$

where

$$K(x, y) = G(x+y) + G(x-y) = 2\int_0^\infty H(w_1)\cos\frac{w_1 x}{h}\cos\frac{w_1 y}{h}\,dw. \tag{35}$$

Now

$$[w]_{z=0} = e^{-\omega t}[w_1]_{z=0} = e^{-\omega t}\int_1^\infty \frac{\psi(x)\,dx}{\sqrt{r^2 - x^2}}, \quad r > 1 \tag{36}$$

where $\psi(x)$ satisfies Eq. (34).
Let us assume

$$\sigma_{zz}(r,\ z,\ t) = \sigma(r,\ z)e^{-\omega t}. \tag{37}$$

Using the third equation in Eqs (4) and (37)

$$\sigma_{zz}(r, o, t) = \frac{2k_1(1 - b_1 w)\,e^{-\omega t}}{(1 - a_1 w)}\left[\frac{\psi(1)}{\sqrt{1 - r^2}} + \int_1^\infty \frac{\psi'(x)\,dx}{\sqrt{x^2 - r^2}} - F(r)\right], \tag{38}$$

$$0 < r < 1$$

where

$$F(\gamma) = \frac{1}{\pi h}\int_r^\infty \frac{dx}{\sqrt{x^2 - r^2}}\int_1^\infty \psi(y)[G'(y+x) + G'(y-x]\,dy \tag{39}$$

Eq. (34) is solved in [3] for particular types of loading. Stress intensity factor is given by

$$N = \lim_{r \to 1-}\sqrt{1 - r}\;\sigma_{zz}(r, o, t) = \frac{\sqrt{2}k_1(1 - b_1 w)\,e^{-wt}\psi(1)}{(1 - a_1 w)}. \tag{40}$$

Acknowledgements

The author expresses his sincere gratitude to Dr. S. K. SARKAR, Jadavpur University, for his guidance in the preparation of this paper.

REFERENCES

1. SNEDDON, I. N.: The Distribution of Stress in the Neighbourhood of a Crack in an Elastic Solid, *Proc. Roy. Soc.*, **A187** (1946), 229
2. LOWENGRUB, M.: Stress in the Vicinity of a Crack in a Thick Plate, *Quart. Appl. Math.* **19** (1962), 119
3. DHAWAN, G. K.: The Distribution of Stress in the Vicinity of an External Crack in an Infinite Elastic Thick Plate, *Acta Mechanica* **16** (1973), 255
4. SRIVASTAV, R. P.—LEE, D.: Axisymmetric External Crack Problems for Media with Cylindrical Cavities, *Int. J. Engng. Sci.* **10** (1972) 219

Eine unendliche viskoelastische dicke Platte mit einem äußeren Sprung. Gegenstand der Arbeit sind die Spannungsfelder in einer unendlichen, dicken, viskoelastischen Platte, die einen äußeren Sprung enthält, der durch die Anwendung von Normaldruck auf ihre Oberflächen verursacht wurde. Angenommen wird, daß der Sprung in der Mittenebene der Platte normal zu der Symmetrieachse liegt und den Bereich außerhalb des Einheitskreises einnimmt. Angenommen wird ferner, daß die zwei Oberflächen des Sprunges in genau der gleichen Weise belastet werden und daß die viskoelastische Schicht sich in einem starren Gehäuse befindet. Für den Verschiebungsvektor werden Hankel-Transformierte eingeführt. Gemischte Grenzbedingungen führen zu doppelten Integralgleichungen. Die Gleichungen werden dann auf eine Fredholm'sche Integralgleichung zweiter Art reduziert. Diese Typen von Gleichungen können für große Werte der Plattendicke durch Iteration gelöst werden. Der Spannungsintensitätsfaktor wurde berechnet.

Бесконечный вязкоэластичный толстый лист с внешней трещиной. Предметом данной работы является поле напряжений в бесконечном вязкоэластичном толстом листе с внешней трещиной, в случае которого трещина происходит от вертикального услия, действующего на поверхность листа. На основе предположения трещина располагается препендикулярно к оси симметрии в нейтральной плоскости листа и трещина занимает область вне единичного круга. Предположим, что обе поверхности трещины нагружены точно таким же образом и что вязкоэластичный слой находится в жесткой оболочке. Автор вводит преобразование Ганкеля вектора сдвига. Смешанные предельные условия приводят к сдвоенным интегральным уравнениям, затем эти уравнения приводит к интегральному уравнению Фредгома второго рода. Уравнения такого типа в случае листов с очень большими размерами по толщине могут быть решены с помощью итерационного метода. Автором вычислены факторы интенсивности напряжений.

Acta Technica Academiae Scientiarum Hungaricae, Tomus 82 (1—2), pp. 69—85 (1976)

ALGORITHM FOR AUTOMATIC TRIPLET DESIGN

KALLÓ, P.*

[Manuscript received November 20, 1974]

After summing up the experiences collected through the application of the automatic design methods of optical systems known so far, an algorithm entirely new in its starting point and initial stages, suitable for the optimized automatic (and traditional) design of classical triplet-type objectives is decribed. The paper explains in detail the definition of the notion of performance-determinant parameters, the derivation of the basic triplet equations, and the relations of glass material selection; the well-known methods of bending and fine correction are covered only as much as needed. The important advantage of the new algorithm easy to program for a computer and providing for a number of optimization possibilities is that it requires as a starting point for automatic (and traditional) triplet design nothing but the knowledge of the relative aperture and field angle given in advance, and the data of the adaptable glass types, and that it is suitable for multilateral generalization (other optical system types containing cemented lenses as well, finite object distance, etc).

1. Introduction

Classic triplets [1] have about 80 years of traditions by now, while the application of computers in optical design can look back to a past of about 25 years. Nevertheless, the triplet theory, that is, the theory of the most thoroughly studied optical system cannot be considered as settled [3] in spite of certain opposite opinions [2], nor have been all the problems solved in the scope of automatic triplet design [4]. The present paper attempts to render much more exact fundamentals to the triplet theory than those known so far [3] by making the algorithmos expressing new correlations advantageously adaptable for both automatic and traditional [5] design efforts.

2. The present state of the automation of optical design [6]

Experiences collected through the application of automatic optical system design may be summarized as follows [7], [8]:

2.1 For the automatic design of optical systems of an optical type no adequate method could be elaborated so far.

*Dr. P. KALLÓ, Kapy u. 26/B, 1025 Budapest, Hungary.

2.2 For the automatic design of optical systems of a given type meeting the specified requirements with a fair approximation, already more or less suitable methods are known, but these may actually be considered as computerized alternatives of the relations of traditional design techniques as they do not contain new algorithms (special processes).

2.3 The success of the (traditional and) automatic optical system design methods depends decisively on the starting point.

2.4 With respect to the requirements set to image production, the multivariable function or functions describing the behaviour of the optical system has or have, respectively, several minima. One does not known, however, of the minimum determined from a given starting point by means of a given method which of all the possible minima it is, whether it is one of the "minimum minima" or not.

2.5 It is due among others, to the uncertainties under 2.3 and 2.4 that there is such a multitude of merit functions and mathematical methods of special techniques, suitable only for fine correction, that may be made good use of for the automatic design of given type optical systems. It is no exaggeration if we state that in this field the labyrinth of mathematical methods and symbols are often suffered, unfortunately, by the physical contents and objectives of the essential features of optical design.

Delineating in detail the target of the present paper as specified in its title, hereafter in the determination of the automatic design algorithm of triplet-type objectives corrected to a distant object ($s_1 = \infty$), mainly the elimination of the uncertainties under 2.3, 2.4, and 2.5, and the ensurance of the possibility of generalization (2.1) will be endeavoured. An algorithm suggested for automatic triplet design must be of such a character that, by means of the program making use thereof, and with the relative aperture, field angle, and available glass assortment data given, the computer should be able to select and calculate the structural characteristics of the corrected system (radii, air spaces, thickness values, glass type features) without any human intervention, whatsoever.

3. Introduction of the definitions of performance-determinant parameters

The majority of difficulties in (traditional and) automatic optical design work can be attributed to, and are concentrated in, the selection of a correct starting point (2.3).

This is why considering the initial data as performance-determinant parameters seems to be entirely justified. By using the symbols interpreted according to Fig. 1, the performance-determinant parameters of the triplet may be divided into two categories easy to distinguish. The extermal performance-

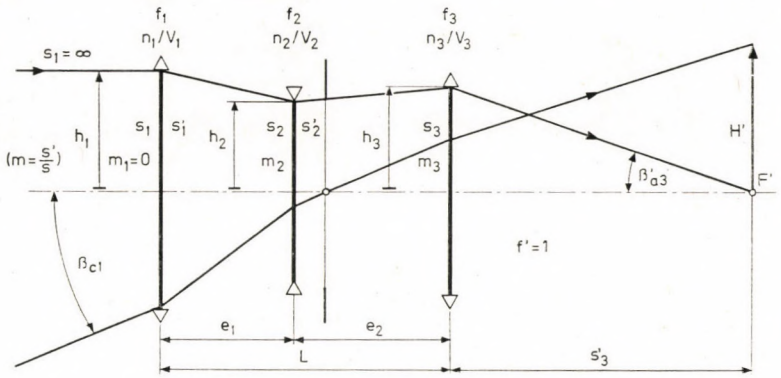

Fig. 1. Symbols

determinant parameters are the s_3' image distance and the L overall length (system characteristics), related to the triplet as a whole. The internal performance-determinant parametes, on the other hand, are the f_1, f_2, f_3 focal distances of the triplet components, and the e_1, e_2 air spaces between them.

The advantage of an approach based on the performance-determinant parameters is that, thereby, the difficulties of the initial optical design stage can be readily overcome, as the relations involved can be treated in two steps:

3.1 First, the relation of the $1 : \Phi_R$ relative aperture and $2\beta_{c1}$ field angle (specification requirements), decided upon in advance, to the external performance-determinant parameters is defined;

3.2 Then the regularity or regularities concerning the external and internal performance determinant parameters are established.

4. Relations between the specification requirements of the triplet and the external performance-determinant parameters

Since literature supplies the conjugate specification data and structural characteristics of a number of corrected triplets, the relations between the specification requirements and the external performance-determinant parameters can be successfully approximated empirically.

A total of 15 triplets obtained from the sources listed in Table I have been studied. First, the thin system of the individual triplets was determined then, with the corresponding characteristics correctly arranged, the relations were graphically plotted (Fig. 2). The graphs do not contain the scatter of the individual data exhibited by the thin systems of all the 15 triplets, as this would have made Fig. 2 far much crowded for a clear survey. The conjugate s_3' image distance and L overall length data, as represented by the graphs, deviate

Table I

Serial No	Source	Designer
1	Brit. Pat. 155 640	H. W. LEE
2	USA Pat. 2,503,751	W. LITTEN
3	USA Pat. 2,731,884	T. BRENDEL
4	USA Pat. 2,818,777	L. HUDSON
5	E. P. 364 994	R. RICHTER
6	USA Pat. 1,987,878	A. W. TRONNIER
7	USA Pat. 2,720,816	I. C. SANDBACK
8	*Rozpravy VED*	M. MALÝ
9	USA Pat. 2,270,234	A. WARMISHAM
10	*JOSA* (1960), 3	J. MEIRON
11	USA Pat. 2,298,090	A. WARMISHAM
12	*Kép- és Hangtechn.* (1970), 1	P. KALLÓ

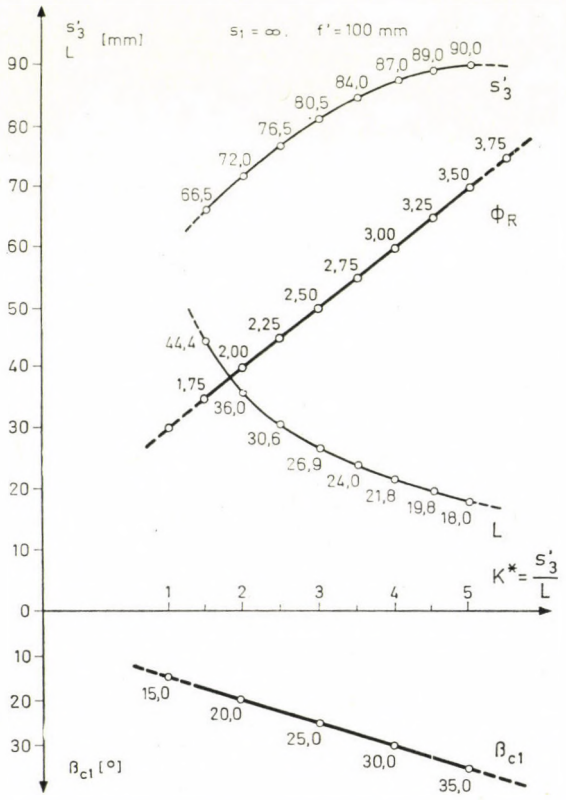

Fig. 2. Correlations between the specification data and the external performance-determinant parameters

from the corresponding data of the 15 triplets tested only by maximum 10 per cent. In the determination of the external performance-determinant parameter values, this accuracy satisfies the practical requirements, with the further advantage of making the correlations easy to review graphically.

The graphs of Fig. 2 reflecting the correlations between the specification requirements and the external performance-determinant parameters reveal that the graph of the Φ_R reciprocal relative aperture and the β_{c1} half field angle, illustrated in the function of s_3'/L, is a straight line. The graphs are used as follows: first, it will have to be determined whether the values of the $1 : \Phi_R$ relative aperture and the β_{c1} half field angle, given as requirements, can be satisfied by a triplet-type objective, or not, that is, the β_{c1} half field angle value must be located, with fair approximation, at the same ordinate where the Φ_R reciprocal relative aperture value can be found. If the β_{c1} half field angle value exceeds that permitted by the graph, then the requirements set cannot be satisfied by a triplet, whereas, if it is smaller, then the triplet is not sufficiently utilized (or, for example, a limitation of rays much more favourable than usual is endevoured), and it is quite possible that the requirements might be satisfied with a system much simpler than a triplet. Finally, the s_3' image distance and L overall length data pertaining to the Φ_R reciprocal relative aperture value are read off along the ordinate associated with the given Φ_R value, by means of the corresponging curve.

5. Correlations of the external and internal performance-determinant parameters of a triplet. The basic triplet equation

The image distance s_3' and the overall length L, that is, the external performance-determinant parameters corresponding to the specification requirements, have been determined graphically as described under 4. When deriving the correlations between the external and internal performance-determinant parameters, by using the symbols of Fig. 1 ($f' = 1$, $s_1 = \infty$), the procedure starts from the following conditional equations:

$$L = e_1 + e_2 \qquad \longrightarrow \quad e_2 = L - e_1 \tag{1}$$

$$\frac{h_1}{h_2} = \frac{f_1 - e_1}{f_1} \qquad \longrightarrow \quad h_2 = \frac{h_1 (f_1 - e_1)}{f_1} \tag{2}$$

$$f_1 m_2 m_3 = 1 \qquad \longrightarrow \quad m_2 = \frac{1}{f_1 m_3} \tag{3}$$

$$m_2 = \frac{\dfrac{s_3'}{m_3} + L - e_1}{f_1 - e_1} \tag{4}$$

$$m_3 + \frac{s_3'}{f_3} = 1 \qquad \longrightarrow \qquad m_3 = \frac{f_3 - s_3'}{f_3} \tag{5}$$

$$\frac{1}{m_2} = 1 + \frac{f_1 - e_1}{f_2} \qquad \longrightarrow \qquad e_1 = f_1 + f_2 - \frac{f_2}{m_2} \tag{6}$$

The above (1)—(6) equation system contains the following 8 unknowns, if s_3', L and Φ_R (h_1) are given:

$$\begin{array}{ccccc} f_1 & & f_2 & & f_3 \\ & e_1 & & e_2 & \\ & & m_2 & & m_3 \\ & & h_2 & & \end{array} \tag{7}$$

because, if the size of the Φ_R reciprocal relative aperture is known, the value of h_3 will be

$$h_3 = s_3' h_1. \tag{8}$$

Substituting the value of m_3 from equation (5) to (3), and the m_2 value thus obtained into (6), equations

$$m_2 = \frac{f_3}{f_1(f_3 - s_3')}, \tag{9}$$

and

$$e_1 = f_1 + f_2 - \frac{f_1 f_2 (f_3 - s_3')}{f_3} \tag{10}$$

will be arrived at.

Since the left side of equations (4) and (9) is identical, their right-hand sides must be equal. Thus, substituting the expression of e_1 from equation (10), and the m_3 value from (5), the following equation is obtained:

$$\frac{f_3}{f_1(f_3 - s_3')} = \frac{\dfrac{s_3' f_3}{f_3 - s_3'} + L - f_1 - f_2 + \dfrac{f_1 f_2 (f_3 - s_3')}{f_3}}{f_1 - f_1 - f_2 + \dfrac{f_1 f_2 (f_3 - s_3')}{f_3}}, \tag{11}$$

where the last two members of the numerator and denominator are identical and, therefore, it may be written as

$$\frac{f_3}{f_1(f_3 - s_3')} = \frac{\dfrac{(L - f_1)(f_3 - s_3') + s_3' f_3}{f_3 - s_3'}}{\dfrac{f_2[-f_3 + f_1(f_3 - s_3')]}{f_3}} + 1. \tag{12}$$

Rearranging

$$\frac{f_2[f_3 - f_1(f_3 - s_3')]}{f_1} = \frac{f_3[(L - f_1)(f_3 - s_3') + s_3' f_3]}{f_1(f_3 - s_3') - f_3}. \tag{13}$$

Finally, expressing the f_2 value from equation (13), the basic triplet equation is obtained:

$$f_2 = -\frac{f_1 f_3 [(L - f_1)(f_3 - s_3') + s_3' f_3]}{[f_1 (f_3 - s_3') - f_3]^2} \tag{14}$$

With respect to the simplicity of this basic equation, and since all the possible values of the f_1, f_2, f_3 focal distances of the components are within a relatively narrow range, the f_2 focal distance values of the negative lens can be determined after the correct selection of the adequate spacings of f_1 and f_3, and the optimum alternatives can be readily selected; determination of the air spaces and, with the relative aperture given, that of the entrance height of the aperture ray will cause no difficulties, whatsoever, by making use of equations (10), (1), (2) and (8).

6. Selection of the aperture stop position, and considerations on the tolerances of form-independent image production errors

As a result of the determination of the fundamental correlations between the performance-determinant parameters (Fig. 2, basic equation (14)), and starting from the (Φ_R, $2\beta_{c1}$) specification requirements given in advance, it is possible to determine the thin triplets characterized by the most favourable (e.g. of the maximum absolute value) focal distance triple f_1, f_2, f_3, whose e_1, e_2 air spaces and h_1, h_2, h_3 aperture ray entrance heights are known. These data are sufficient for the expression of the longitudinal chromatism and the Petzval curvature, as some of the form-independent image production defects, or, more precisely, for the expression of their third-order approximative equations, but in the case of a transversal chromatism the position of the aperture stop must also be known. As for selecting the latter, the following considerations should be taken into account.

It is well known that, among the third-order image production errors, transversal chromatism, astigmatism, and distortion depend on the aperture stop position. In the case of an aperture stop in the central range of the overall length, the central coma will not depend in practice on the position of the aperture stop. If the requirements set to distortion are not overstrict, then the correction of distortion will be potentially provided for by an aperture stop in the neighbourhood of the middle point of the overall length, in which case generally no astigmatism problems will be encountered, either, so the transversal chromatism will have to be compensated for with respect to this very point of aperture stop.

Thus the thin triplets available as described above can be selected, with respect to the air spaces e_1, e_2, according to the satisfaction of the following

preconditions:

$$|e_1-e_2| < 0.06\,f', \quad \text{or} \quad \sim 0.1\,f' > |e_1-e_2| > 0.06\,f', \tag{15}$$

where f' is the resultant focal distance of the thin triplet. The thin triplets of an air space size satisfying the first inequality are suitable for such objectives wherein no variable dia aperture stop is to be included (in this case the aperture stop will be represented by the mounting of the central lens). Triplets, on the other hand, of an air space size conforming to the second inequality may be used as starting points for objectives to which variable diameter aperture stop, too, must be added. Here the aperture stop is positioned within the larger air space, immediately next to the middle lens.

Finally, it will have to be noted here that hence, when correcting form and aperture stop position-dependent image production errors (above all astigmatism), occasionally the aperture stop position has to be modified, but not to such an extent, whereby the previous correction of the transversal chromatism could be significantly affected.

In the next step, taking the realistic requirements that may be set to the triplets as a basis, we have summarized in Table II the β'_{a3} exit aperture angles and H' image heights pertaining to the different $1 : \Phi_R$ relative apertures, and determined the corresponding T_1, T_2, T_3 optical tolerances in the case of a transversal and longitudinal chromatism, respectively, and when a Petzval curvature is encountered.

It is well known that, in the case of relative aperture and field angle (image height) requirements as shown in Table II, the triplets, due to their relative simplicity, cannot ensure that the third-order residual image production errors should not exceed significantly the values specified by the relevant tolerances. On the basis, therefore, of the data presented in Table II, the fol-

Table II

Serial No	Φ_R	β'_{a3}, °	H'_3, mm	β'_{c3}, °	Tolerance values, mm		
					$T_1 = \frac{f\lambda}{2H'_3 \sin \beta'_{a3}}$	$T_2 = \frac{\lambda}{\sin^2 \beta'_{a3}}$	$T_3 = \frac{0{,}025}{\sin \beta'_{a3}}$
1	1,75	16,0	22,1	12,5	0,00452	0,00728	0,0910
2	2,00	14,1	26,7	15,0	0,00425	0,00933	0,103
3	2,25	12,6	31,5	17,5	0,00402	0,0116	0,115
4	2,50	11,3	36,3	20,0	0,00388	0,0143	0,128
5	2,75	10,3	41,3	22,5	0,00377	0,0172	0,140
6	3,00	9,50	46,5	25,0	0,00356	0,0202	0,152
7	3,25	8,80	51,8	27,5	0,00347	0,0235	0,163
8	3,50	8,20	57,7	30,0	0,00337	0,0273	0,176

lowing optical tolerances are selected rather arbitrarily for all the triplets that may be reckoned with here, when $f' = 100$ mm:

$$T_1 = 4.10^{-3} \quad T_2 = 5T_1 \quad T_3 = 50T_1 \quad [\text{mm}]. \tag{16}$$

7. Determination of the conjugate refractivities and Abbe indices of glass types providing for the optimum compensation of the form-independent third-order image production errors

Sinee the numerical values of the image production tolerances are taken into account with $\pm$ signs, it will suffice to express the third-order equations only for the absolute values of the form-independent image production errors which, in the sequence of Petzval curvature, longitudinal and transversal chromatism, are as follows [9]:

$$\frac{1}{2} H_3'^2 \left[\frac{1}{f_1 n_1} + \frac{1}{f_2 n_2} + \frac{1}{f_3 n_3} \right] = p \cdot 50\, T_1, \tag{17}$$

$$\frac{s_3'^2}{a_3^2} \left[\frac{a_1^2}{f_1 V_1} + \frac{a_2^2}{f_2 V_2} + \frac{a_3^2}{f_3 V_3} \right] = p \cdot 5\, T_1, \tag{18}$$

$$H_3' \left[\frac{a_1 b_1}{f_1 V_1} + \frac{a_2 b_2}{f_2 V_2} + \frac{a_3 b_3}{f_3 V_3} \right] = p\, T_1, \tag{19}$$

where the symbols not used so far should be interpreted as follows:

p is a proportionality factor indicating that, due to the limitations of the glass type assortment, the form-independent image production residual defects approximate only, but do not reach the ideal values specified by the tolerances (in practice, therefore, the numerical value of p is always more than unit),

a_1, a_2, a_3 coefficients, related to the three lenses, represent the quotients of the incident height of aperture ray and the half diameter of the aperture stop,

b_1, b_2, b_3 are aperture stop coefficients, representing the quotient of the incident height of the central ray and the tangent of the angle included by the central ray passing through the centre of the aperture stop, and the optical axis [9].

Now, let us divide the conditional equations (17), (18), and (19) by the coefficients at their left-hand side, and introduce the following symbols:

$$c_1 = \frac{2 \cdot 50\, T_1}{H_3'^2}, \quad c_2 = \frac{5\, T_1 a_3^2}{s_3'^2}, \quad c_3 = \frac{T_1}{H_3'}. \tag{20}$$

If these are then substituted into the conditional equations (17), (18), and (19), then the equations expressed below will be obtained:

$$\frac{1}{f_1 n_1} + \frac{1}{f_2 n_2} + \frac{1}{f_3 n_3} = c_1 p, \tag{21}$$

$$\frac{a_1}{V_1 f_1} + \frac{a_2}{V_2 f_2} + \frac{a_3}{V_3 f_3} = c_2 p, \tag{22}$$

$$\frac{a_1 b_1}{V_1 f_1} + \frac{a_2 b_2}{V_2 f_2} + \frac{a_3 b_3}{V_3 f_3} = c_3 p \,. \tag{23}$$

Now let us deal only with (22) and (23) of the three above equations in order to determine the correlations between the Abbe numbers. Let us express the value of $a_1/(V_1 f_1)$ from both of them:

$$\frac{a_1}{V_1 f_1} = c_2 p - \frac{a_2}{V_2 f_2} - \frac{a_3}{V_3 f_3} \,, \tag{24}$$

$$\frac{a_1}{V_1 f_1} = \frac{c_3 p}{b_1} - \frac{a_2 b_2}{V_2 f_2 b_1} - \frac{a_3 b_3}{V_3 f_3 b_1} \,. \tag{25}$$

From the equality of the left-hand side of equations (24) and (25) the same of their right sides follows, that is

$$c_2 p - \frac{a_2}{V_2 f_2} - \frac{a_3}{V_3 f_3} = \frac{c_3 p}{b_1} - \frac{a_2 b_2}{V_2 f_2 b_1} - \frac{a_3 b_3}{V_3 f_3 b_1} \,. \tag{26}$$

Let us, furthermore, express V_3 in the function of V_2, preferably in the following way:

$$-\frac{a_3}{V_3 f_3} + \frac{a_3 b_3}{V_3 f_3 b_1} = \left(\frac{c_3}{b_1} - c_2\right) p + \frac{a_2}{V_2 f_2} - \frac{a_2 b_2}{V_2 f_2 b_1} \tag{27}$$

$$\frac{1}{V_3}\left[\frac{a_3 b_3}{f_3 b_1} - \frac{a_3}{f_3}\right] = \frac{1}{V_2}\left[-\frac{a_2 b_2}{f_2 b_1} + \frac{a_2}{f_2}\right] + p\left(\frac{c_3}{b_1} - c_2\right) \tag{28}$$

$$\frac{1}{V_3} = \frac{1}{V_2}\left[\frac{a_2 f_3 (b_1 - b_2)}{a_3 f_2 (b_3 - b_1)}\right] + \left[\frac{f_3 (c_3 - c_2 b_1)}{a_3 (b_3 - b_1)}\right] p \,. \tag{29}$$

Finally, if similarly to equations (24) and (25), $a_3/(V_3 f_3)$ is expressed instead of $a_1/(V_1 f_1)$, and the corresponding derivation (26)—(28) is performed, the equation

$$\frac{1}{V_1} = \frac{1}{V_2}\left[\frac{a_2 f_1 (b_3 - b_2)}{a_1 f_2 (b_1 - b_3)}\right] + \left[\frac{f_1 (c_3 - c_2 b_3)}{a_1 (b_1 - b_3)}\right] p \tag{30}$$

will be obtained.

Algorithms (29) and (30), together with conditional equation (21), can be used for the determination of the conjugate Abbe indices and refractivities of the glass types providing, with good approximation, for the compensation of the form-independent image production errors of triplets as described below.

The conjugate Abbe index and refractivity data of the available glass type assortment is assumed to be known. By means of algorithms (29) and (30) the V_1 and V_3 values can be readly generated in the function of V_2, that is, we

shall obtain the V_1, V_2, V_3 Abbe index triples compensating for the color aberrations with a good approximation which, however, must be reviewed whether the available assortment contains, or not, a glass type of that Abbe number which approximates to a satisfactory extent the calculated V_1 and V_3 Abbe indices. Then, substituting successively the refractivities pertaining to a reasonably narrow range of the V_1, V_2, V_3 Abbe numbers (for example $\Delta V = \pm 3$) into equation (21), the possibly best approximation of the value of $c_1 p$ is attempted. If in the case of the optimum alternative the p value calculated from (21) is much higher than that used in algorithms (29) and (30), the entire procedure should be repeated with a new p value sufficiently exceeding the original one, in order to approximate the "equal strength" deviation of each of the three form-independent image production errors from the corresponding tolerance (successive approximation).

Finally, it should be noted that the method described above might be used even if, for example, due to some special requirements, certain form-independent image production errors ought to be preferred against some others. Let us explain this through an actual case. When designing a large relative aperture and small-field angle triplet, correction of the longitudinal chromatism may be of a primary importance as against transversal chromatism or Petzval curvature. In the determination, therefore, of the constants (20) the value of c_2 is left unchanged while that of c_1 and c_3, respectively, is increased. The value of the new constants marked by asterisk, much more suitable for the purpose, may be as follows on the basis, of course, of (20):

$$c_1^* = 5c_1, \quad c_2^* = c_2, \quad c_3^* = 2c_1. \tag{31}$$

8. Compensation of the form-dependent image production errors

If the requirements set to distortion are not overstrict (1 . . . 3 per cent) then, when selecting the aperture stop position, the compensation of the distortion will be completed by the satisfaction of the form-independent conditions of distortion while compensating, and together with, the other form-dependent image production errors. Bending of the thin system is best performed by making use of the Coddington—Taylor equations [9]. Here, without going into minor details, only a structural explanation will be rendered. The quantities in the third-order image defect equation of spherical aberration, central coma, and astigmatism, respectively, are summarized in Table III.

The symbols of Table III, not used so far, mean:
ϱ is the aperture stop radius,
π_i indicates the position coefficient of the components, and
σ_i represents the form factor of the components involved.

Table III

Image production defect of the thin triplet \ function	n_i	f_i	π_i	a_i	b_i	h_1	ϱ	s'_3	H'_3	σ_i
Spherical aberration, $\Delta S'$	x	x	x	x			x	x		x
Central coma, $\Delta K'_c$	x	x	x			x		x		x
Astigmatism, $\Delta A'$	x	x	x	x	x				x	x

NOTE: 1. $i = 1, 2, 3$.

2. The image production errors depend on the quantities marked by x.

It is well known that the spherical aberration and astigmatism of the individual lenses are second degree, whereas the central coma a linear function of the form factor [9]. The individual image creation defects of the thin system of the triplet as a whole can be determined by summing up the homogeneous image production errors of the individual components. The task now is to determine the form factor triad at which.

(1) the joint value of the three form-dependent image production defects of the triplet equals zero, or

(2) the spherical aberration, minimum and central coma, and astigmatism of the triplet equal zero.

Since we have three equations with three unknowns, the σ_1, σ_2, σ_3 form factor values can be readily determined (if the distortion value is not sufficiently low, successive approximation must be used because the equation of distortion, too, has to be taken into account). The solution of this problem is facilitated by the experience collected through calculation practices according to which, in the case of triplets, we have $+0{,}5 < \sigma_1 < +2{,}5$ and $+0{,}5 > \sigma_2$, that is, $\sigma_3 > -1{,}5$. If the second one of the two above cases is actually existing, that is, $\Delta S' = \Delta S'_{\min}$ and $\Delta K'_c = 0$, $\Delta A' = 0$ (where $\Delta S'$ is the spherical aberration, $\Delta K's$ the central coma, and $\Delta A'$ the astigmatism), then, if $\Delta S'_{\min} \geq$ ≥ 5 mm, the triplet cannot be corrected (this alternative must be rejected), whereas if $\Delta S'_{\min} < 5$ mm, then the $\Delta S'_{\min}$ value must be reduced at least to $1 \div 2$ mm by increasing the refractivity of the second lens (at an almost unchanged Abbe index). If this is feasible, the system can most likely be corrected, but if not, then this version does not deserve further consideration ($f' = 100$ mm).

9. Fine correction

With the form factors σ_1, σ_2, and σ_3 as calculated in the previous chapter known, the frontal curvature radii of the triplet's three components are determined. The d_1, d_2, and d_3 thicknesses of the three lenses, in the function of the

$1 : \Phi_R$ relative aperture, are presented in Table IV. (It will be noted here that the lens thickness values in Table IV have been given with a certain safety, perhaps greater than necessary, but these offer a better starting point for fine

Table IV

Lens thickness, mm \ Relative aperture $1 : \Phi_R$	1:1,75	1:2,00	1:2,25	1:2,50	1:2,75	1:3,00	1:3,25	1:3,50
d_1		10,0		8,0			6,0	
d_2		4,0		3,0			2,0	
d_3		8,0		7,0			6,0	

(The resultant focal distance of the triplet: $f' = 100$ mm)

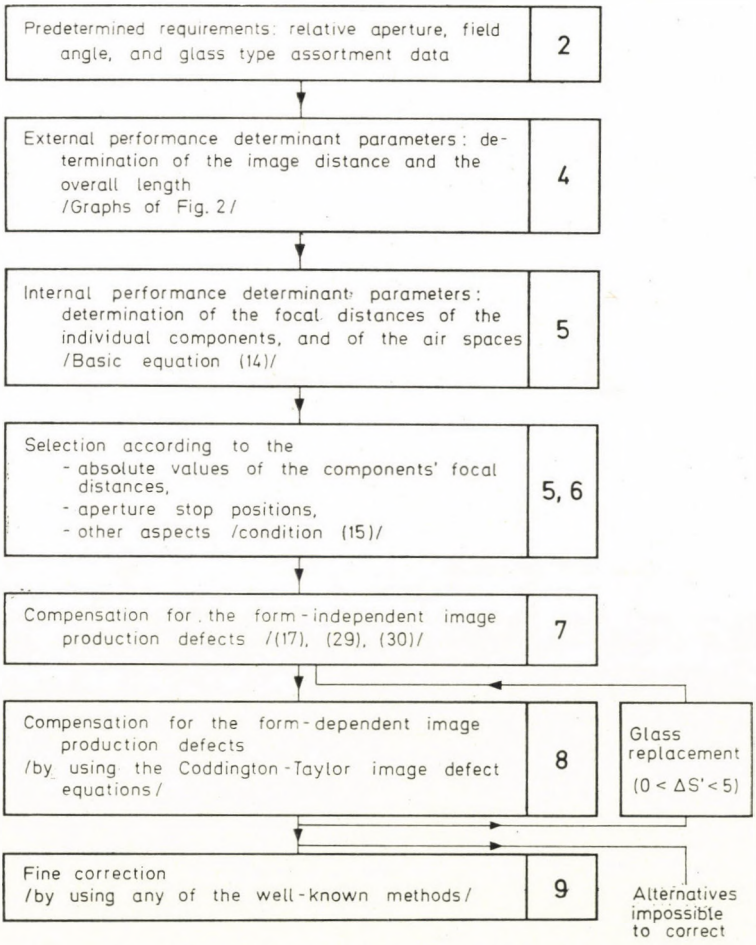

Fig. 3. Block diagram of automatic triplet design

correction). The second curvature radii of the three lenses are determined by starting from the assumption of unchanged f_1, f_2, and f_3 focal distances. Finally, the e_1 and e_2 air spaces as well as the aperture stop position are modified with respect to the principal plane positions of the thick lenses. The form-dependent residual image formation defects of a thick triplet appropriately characterized by each of its parameters will not exceed 1 or 2 per cent of the resultant focal distance, or 1 to 3 per cent thereof in the case of distortion.

The leftover triplet corrections will not be discussed in detail here since the last, that is, fine correction stage of optical design may be considered as the most successfully mechanized and automated area of optical calculations. So it will suffice to refer to the relevant literature [10], [11], and the further references therein. In addition, this is particularly justified by the fact that previously we have endeavoured to determine the alternatives that might be considered as optima because of their performance-determinant parameters.

For the sake of an easier survey, our train of thoughts as a summary of the present paper is illustrated by the block diagram in Fig. 3, completed with the corresponding Chapter numbers. Finally, the algorithm described above will be verified by [3], and the triplets designed with a traditional method (without a computer aid, [12]), meeting even extreme specification requirements and characterized by the data of Table V as well as the characteristic diagrams of Fig. 4. The new algorithm described in detail above, and summarized in the block diagram of Fig. 3 enables the preparation of a program for the realiza-

Table V

Lens	Radius of curvature, r, mm	Thickness d, mm	Air space e, mm	Refractivity n_e	Abbe index V_e
Triplet, $f' = 100$; 1 : 1,9; $2\times20°$					
I	+ 48,57 +217,1	9,62	15,00	1,79219	50,24
II	−111,6 + 37,51	12,22	10,10	1,62118	30,67
III	+ 82,72 − 96,18	5,77		1,79219	50,24
Triplet, $f' = 100$; 1 : 3,2 $2\times30°$					
I	+ 62,69 +800,1	7,84	8,59	1,88580	40,77
II	− 62,69 + 64,21	5,81	8,72	1,62118	30,67
III	∞ − 57,76	5,56		1,88580	40,77

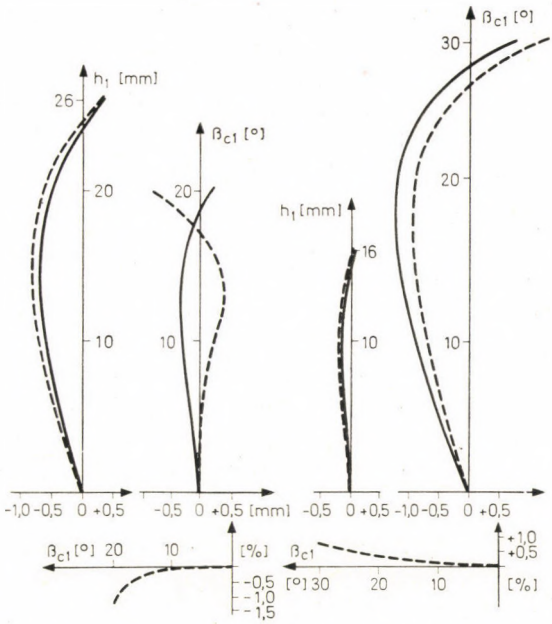

Fig. 4. Characteristic diagrams of the triplets described by the data of Table V

tion of automatic triplet design. Due to our field of interest, objectives, and possibilities, the actual composition of the program is not one of our targets, as we intend to carry on further investigations similar to the present work instead, like referred to under 10,1. etc.

10. Conclusions

The advantages of the new method described above can be summarized as follows, with references to those under 2. in brackets:

10.1 Due to its starting conditions and character, the new method is suitable for generalization in both the stricter and wider sense, respectively, of the term (2.1).

The algorithm described here is suitable for the automatic design of classical triplets but, by introducing the notion of equivalent simplet, and with a minimum of supplementation, it can also be used in the case of triplet modifications (e.g. Petzval, Tessar, Heliar, etc., types). There seems to be a realistic possibility for generalization from object distance aspects as well, since we are convinced that, unlike in the case of a distant object ($s_1 = \infty$) as assumed so far, there is a basic equation existing which can be readily determined, even if we start from a finite object distance, that would generate the performance-determinant parameters of all the possible triplets, and that might resemble

the one used at present (14), although of a much more sophisticated structure. Finally, if we start from the fact that any objective system can be reduced to a "triplet" consisting of three fundamental groups, it follows that the new method is suitable for total generalization as well.

10.2 The new method is based on algorithms given in both graphic and algebraic forms, advantageously adaptable for classical design tasks and, at the same time, excellently programmable for computer use (2.2), see (14), (29), (30), and Fig. 2.

10.3 The new method provides for the determination of the optimum initial data (2.3) by defining the correlations (Fig. 2 and (14)) between the basic specification data (relative aperture, field angle) and the performance-determinant parameters (image distance, overall length, focal distances, and air spaces). This way the residual values of the image production defects of a triplet obtained as a result of automatic (or classical) design will be some of the most favorable minima (2.4) a priori, at that, exactly because of the very start proper.

10.4 Development of the new method started from the fundamental correlations between optical design and geometrical optics (2.5), as such. As another essential feature, contrarily to the hitherto solutions, the new method is absolutely correct and precise in its objectives and algorithms both at the very beginning of the design work and in the course of delineating the performance-determinant initiation. The order of subsequent approximations will continuously decrease with the progress of problem solving (third order: glass type selection and thin system bending, first order: linear fine correction).

10.5. As a last advantage of the new method, it permits the systematic examination of all the feasible starting alternatives. The resultant safety is further increased by the objective possibility that in the case of automatic design, due to the very small number of data requiring any comments, even a low-storage capacity computer might run as much as ten alternatives parallelly by steps, that is, simultaneously.

Ever since, the computers appeared on the scene, the optical design methods and means did not create "uniform strength" systems. The computers accelerated the performance of numerical calculations by orders of magnitude, and the design time of optical systems diminished to some fractions of the original [7]. To eliminate this contradiction manifesting itself in an increasingly marked manner, and to follow the road towards some still better solutions of automatic optical system design, we must endeavour to create new effective algorithms suitable for multilateral generalization.

Acknowledgements

Thanks are due to Mr. Gábor LACK for the elegant algebraic derivations and for his unselfish contributions to the mathematical solution of the problems encountered.

REFERENCES

1. Taylor, H. D.: Lens. United States Patent Office, No. 568, **052** (1896), 1—11
2. Litten, W. et al.: Photographic Objectives of the Cooke Triplet Type. United States Patent Office, No. 2, 503, **751** (1950), 1—8
3. Kalló, P.: Critical Summary of the Design Methods of Form-Independent Thin Triplet Systems. *Acta Techn. Hung.* **73** (1974), 133—142
4. Volkmann, H.: Neue Dimensionen der photographischen Technologie. *Umschau* **72** (1972), 449—455
5. Kalló, P.: Some Fundamental Relations in the Design of Optical Systems. *Optica Applicata* **4** (1974), 3—7
6. Kalló, P.: The Present Situation of Optical Design Automation. *Kép- és Hangtechn.* **20** (1974), 69—70 (In Hungarian)
7. Sliusarev, G. G.: Metody rascheta opticheskikh sistem. 2. izd. Izdatel'stvo "Mashinostroenie", Leningrad 1969
8. Volosov, D. S.: Fotografitcheskaia optika. 1. izd. Izdatel'stvo "Iskusstvo", Moskow 1971
9. Emsley, H. H.: Aberration of Thin Lenses. 1. Ed. Constable and Company LTD, London 1956
10. Jamieson, T. H.: Optimization Techniques in Lens Design. 1. Ed. Adam Hilger, London 1971
11. Fialovszky, L.: Application of a differential method and compensating calculation for the fine correction of optical systems. *MTA Műsz. Tud. Oszt. Közl.*, **34** (1964), 410—434 (in Hungarian)
12. Kalló, P.: Triplet Type Objective Lens. Hungarian Patent Office, No. 3260 (1974), 1—5.

Ein Algorithmus für den automatischen Entwurf von Triplets. — Die bei der Anwendung der bisher bekannten automatischen Berechnungsverfahren für optische Systeme gemachten Erfahrungen werden zusammenfassend ausgewertet. Für den optimierten, automatischen (und traditionellen) Entwurf der klassischen Tripletobjektive wird ein in seinem Ausgangspunkt und Anfangsabschnitt vollkommen neuer Algorithmus vorgestellt. Die Arbeit behandelt eingehend die Definition des Begriffes »leistungsbestimmende Parameter«, die Ableitung der Grundgleichung für Triplets und die Zusammenhänge bei der Auswahl des Glaswerkstoffes; auf die bekannten Methoden der Durchbiegung und der Feinkorrektur wird nur im allernotwendigsten Ausmaß eingegangen. Die Bedeutung des neuen, gut programmierbaren und zahlreiche Optimierungsmöglichkeiten bietenden Algorithmus liegt darin, daß zur automatischen (und traditionellen) Berechnung der Triplets als Ausgang nur die voraus angegebene relative Öffnung, der Objektwinkel sowie die Angaben der verwendeten Gläser nötig sind und daß er in mehreren Richtungen (andere Typen von — auch geklebte Linsen enthaltenden — optischen Systemen, endliche Objektweite, usw.) verallgemeinert werden kann.

Алгоритм для автоматического проектирования триплета. После обобщающей оценки опыта, накопленного во время применения известных до сих пор методов автоматического проектирования оптических систем, дается описание алгоритма, который в исходной и начальной частях является совершенно новым и который пригоден для оптимизированного автоматического (и обычного) проектирования классических объективов триплетного типа. В работе детально рассматриваются определение понятий параметров, детерминирующих мощность, вывод основных уравнений триплетов и зависимости выбора стекольного материала; с известными методами изгибов и точной коррекции занимается автор только сжато, в самой необходимой степени. Значение нового алгоритма, имеющего форму, хорошо программируемую для ЭВМ, и обеспечивающего ряд возможностей оптимизации, состоит в том, что для начала автоматического (и обычного) проектирования триплетов требует только данные по предварительно заданным — относительное отверстие, угол зрения, а также данные по используемым сортам стекол, и подходит для обобщения в различных направлениях (оптические системы иного типа, содержащие также склееные линзы, конечное расстояние до предмета и т. д.).

Acta Technica Academiae Scientiarum Hungaricae, Tomus 82 (1—2), pp. 87—97 (1976)

GENERALIZATION OF PHYSICAL NETWORKS

LINEAR GEOMETRIC NETWORKS

Zs. GÁSPÁR*

[Manuscript received April 18, 1974]

Equations of the physical network (physical graph) defined as the generalization of bar systems directly yield relationships between bar systems in small displacement and linear electric circuits as special cases.

1. Introduction

Relationships for a linear physical network are generalized for small displacements of spatial bar systems.

Displacement values of the ends of bars — possibly of variable stiffness and curved axis — joining at nodal points need not be equal. The connection may be such that some of the displacement components are identical alone. The structure is assumed

— to be subject to loads at nodes alone;

— to suffer nodal displacements not greater than allowing the required accuracy to be obtained from relationships of the first-order theory;

— to have all bars under the validity of the Bernoulli—Navier hypothesis and the de Saint-Venant assumption.

All bars have their statical, pyhsical and compatibilty equations, united in knowledge of the structure topology, and equilibrium equations are also written for the nodes.

Relationships for the linear geometric network are written in item 2 using terminology of physical networks rather than of the bar system.

Item 3 presents adaptation of general relationships for bar systems or to structures consisting of bars of constant stiffness and straight axis, as solved in particulars in [1].

Item 4 demonstrates how equations of linear electrical networks result from general relationships.

Zs. GÁSPÁR, Kapy út 40/b, 1025 Budapest, Hungary

2. Linear geometrical networks

Mathematical models have been established for stationary and linear physical networks consisting of bipole branches where:

a) several intensive quantities result in extensive quantities;

b) nodal connection of branch edges may also be a partial one;

c) a preferential co-ordinate system may be specified for each branch.

2.1 *Theoretical considerations*

Let us construct a graph from m oriented bipole branches and n nodes. To any starting and end point of each branch, d independent intensive quantities belong. Let these be contained by vectors $\mathbf{i}_{bj}$ and $\mathbf{i}_{ej}$ at branch j. Discontinuity of intensive quantities may be specified at branch ends, denoted by $\mathbf{i}_{\Delta 0j}$ at branch j.

Because of the inhomogeneity of intensive quantities, at branch ends d independent extensive quantities ($\mathbf{e}_{ej}$) are induced, defined by the material law (physical equation). Using the branch balance equation, vector $\mathbf{e}_{ej}$ yields extensive quantities $\mathbf{e}_{bj}$ belonging to the starting point.

There is no absolute coincidence between vectors of intensive quantities belonging to branch ends joining one node. If among intensive quantities belonging to branches joining at node k there are d_k independent ones, then these are united in vector $\mathbf{i}_{pk}$ of size d_k. Graph branch connections are characterized by indicating the specified element ratios of vectors $\mathbf{i}_{pk}$ to $\mathbf{i}_{bj}$ and $\mathbf{i}_{ej}$. Any intensive nodal quantity may be specified as zero, then no corresponding intensive element will be involved in vector $\mathbf{i}_{pk}$.

Also extensive quantities are transferred to the node like the intensive ones. Extensive quantities transferred from all the joining branches and vectors $\mathbf{e}_{pk}$ containing the source of extensive quantities specified for that node have to meet the nodal balance equation.

If the vector of extensive quantities belonging to the branch ends can be subjected to orthogonal transformation, differing for each branch as a rule, granting the vector elements a preferential meaning, then also these transformations will be performed.

2.2 *Relationships*

Vectors assigned to starting and end points of branches should contain always the same independent quantities, in the same order. Nodal vectors differ by size, hence it is only required that the corresponding elements of $\mathbf{i}_{pk}$ and $\mathbf{e}_{pk}$ assigned to the same node should be mutually complementary.

Let us introduce notations:

$$d_p = \sum_{k=1}^{n} d_k ,$$

$$d_g = m \,.\, d,$$

$$\mathbf{i}_{gj} = \begin{bmatrix} \mathbf{i}_{bj} \\ \mathbf{i}_{ej} \end{bmatrix}; \quad \mathbf{e}_{gj} = \begin{bmatrix} \mathbf{e}_{bj} \\ \mathbf{e}_{ej} \end{bmatrix}.$$

In these vectors and the subsequently introduced ones, corresponding hypervectors referring to the entire structure will be marked by omitting subscripts j and k.

Branch-to-node correlations will be given by matrix **T** of size $2\ d_g \times d_p$

$$\mathbf{i}_g = \mathbf{T}\,\mathbf{i}_p \tag{1}$$

where

$$T_{ij} = \begin{cases} i_{gi}/i_{pi}, & \text{if this is a specified ratio;} \\ 0 & \text{otherwise.} \end{cases}$$

(T_{ij} being the j-th element in the i-th row of matrix **T**; vector subsripts i and j refer to the i-th or j-th scalar.)

In the general case, the vectors $\mathbf{i}_{bj}$ belonging to the starting point of the j-th branch can be reduced to the end point by means of a so-called transfer matrix $\mathbf{B}_j$. Intensive quantities belonging to the end points differ by:

$$\mathbf{i}_{\Delta sj} = -\mathbf{B}_j\,\mathbf{i}_{bj} + \mathbf{i}_{ej}.$$

For the entire network

$$\mathbf{i}_{\Delta s} = \mathbf{B}\mathbf{i}_g = \mathbf{B}\mathbf{T}\mathbf{i}_p \tag{2}$$

where

$$\underset{(d_g \times 2\,d_g)}{\mathbf{B}} = \begin{array}{|cc|cc|cc|} \multicolumn{2}{|c|}{-\mathbf{B}_1} & \mathbf{E} & & & \\ \hline & & \multicolumn{2}{c|}{-\mathbf{B}_2} & \mathbf{E} & \\ \hline & & & & \ddots & \\ \hline & & & & \multicolumn{2}{c|}{-\mathbf{B}_m} \\ & & & & \multicolumn{2}{c|}{\mathbf{E}} \\ \hline \end{array}$$

E being a unit matrix, and the blocks without notation are zero.

Vector $\mathbf{i}_{\Delta s}$ was specified to contain discontinuity $\mathbf{i}_{\Delta 0}$, extensive quantities being their difference:

$$\mathbf{i}_\Delta = \mathbf{i}_{\Delta s} - \mathbf{i}_{\Delta 0} = \mathbf{B}\mathbf{T}\mathbf{i}_p - \mathbf{i}_{\Delta 0}. \tag{3}$$

According to the Onsager relationship (the constitution law), extensive quantities developing in the j-th branch can be calculated as:

$$\mathbf{e}_{ej} = \mathbf{K}_j\ \mathbf{i}_{\Delta j} = \mathbf{F}_j^{-1}\ \mathbf{i}_{\Delta j}.$$

Matrices $\mathbf{F}_j$ and $\mathbf{K}_j$ can be composed into a hyperdiagonal each (**F** and **K**), to yield:

$$\mathbf{e}_e = \mathbf{K}\,\mathbf{i}_\Delta = \mathbf{K}\,(\mathbf{B}\mathbf{T}\mathbf{i}_p - \mathbf{i}_{\Delta 0}). \tag{4}$$

Be the matrix reducing the end-point extensive quantities ($\mathbf{e}_{ej}$) to the starting point temporarily denoted by $\mathbf{X}$. The result of the scalar product $\mathbf{i}^*_{\Delta sj}\,\mathbf{e}_{ej}$ does not change if both vectors are reduced to the starting point of the branch:

$$\mathbf{i}^*_{\Delta sj}\,\mathbf{e}_{ej} = (\mathbf{B}_j^{-1}\mathbf{i}_{\Delta sj})^*\ (\mathbf{X}\mathbf{e}_{ej}) = \mathbf{i}^*_{\Delta sj}\,\mathbf{B}_j^{*-1}\ \mathbf{X}\mathbf{e}_{ej},$$

hence

$$\mathbf{B}_j^{*-1}\,\mathbf{X} = \mathbf{E},$$

that is,

$$\mathbf{X} = \mathbf{B}_j^*.$$

Since the branches were not permitted to contain the source of the extensive quantities, they have as balance equation:

$$\mathbf{e}_{bj} + \mathbf{B}_j^*\ \mathbf{e}_{ej} = \mathbf{0}.$$

Hence

$$\mathbf{e}_g = \mathbf{B}^*\mathbf{e}_e = \mathbf{B}^*\ \mathbf{K}(\mathbf{B}\mathbf{T}\mathbf{i}_p - \mathbf{i}_{\Delta 0}). \tag{5}$$

Intensive quantities at branch ends and in nodes are related by (1). The corresponding extensive quantities are related by $-\mathbf{T}^*$. According to the nodal balance equation, sources of extensive quantities transferred from branches and of those prescribed for the nodes add up to zero:

$$-\mathbf{T}^*\mathbf{e}_g + \mathbf{e}_p = \mathbf{0},$$

hence, nodal extensive and intensive quantities are related as:

$$\mathbf{e}_p = \mathbf{T}^*\,\mathbf{B}^*\,\mathbf{K}\,(\mathbf{B}\mathbf{T}\mathbf{i}_p - \mathbf{i}_{\Delta 0}). \tag{6}$$

For given sources of intensive and extensive quantities $\mathbf{i}_{\Delta 0}$ and $\mathbf{e}_p$, the nodal intensive quantities $\mathbf{i}_p$ and branch-end extensive quantities e_e can be expressed as:

$$\mathbf{i}_p = (\mathbf{T}^*\mathbf{B}^*\ \mathbf{K}\mathbf{B}\mathbf{T})^{-1}\ (\mathbf{e}_p + \mathbf{T}^*\mathbf{B}^*\ \mathbf{K}\mathbf{i}_{\Delta 0}), \tag{7}$$

$$\mathbf{e}_e = \mathbf{K}\ (\mathbf{B}\mathbf{T}\mathbf{i}_p - \mathbf{i}_{\Delta 0}). \tag{8}$$

Relationships between known and unknown quantities can be included in a hypermatrix equation:

$$\begin{bmatrix} \mathbf{0} & -\mathbf{T}^*\mathbf{B}^* \\ -\mathbf{B}\mathbf{T} & \mathbf{F} \end{bmatrix} \begin{bmatrix} \mathbf{i}_p \\ \mathbf{e}_e \end{bmatrix} + \begin{bmatrix} \mathbf{e}_p \\ \mathbf{i}_{\Delta 0} \end{bmatrix} = \mathbf{0}. \tag{9}$$

If an orthogonal transformation $\mathbf{R}_j$ can be given for each branch, that applied to vectors $\mathbf{e}_{ej}$ and $\mathbf{i}_{\Delta 0}$ makes their elements preferential, then matrices $\mathbf{R}_j$ will be included in hyperdiagonal $\mathbf{R}$, the new quantities will be marked by

superscript Ξ and (9) can be replaced by

$$\begin{bmatrix} \mathbf{0} & -\mathbf{T}^*\mathbf{B}^*\mathbf{R}^* \\ -\mathbf{RBT} & \mathbf{F}^{\Xi} \end{bmatrix} \begin{bmatrix} \mathbf{i}_p \\ \mathbf{e}_e^{\Xi} \end{bmatrix} + \begin{bmatrix} \mathbf{e}_p \\ \mathbf{i}_{\Delta}{}_0^{\Xi} \end{bmatrix} = \mathbf{0} \,. \tag{10}$$

An advisable mode of solving (10) is by depending on the structure of the coefficient matrix, outside, however, the scope of this paper.

Network theory symbols have been complied in Table I.

Table I

Symbol	Definition
m	number of branches
n	number of nodes
d	number of independent extensive or intensive branch end quantities
k	k-th node
j	j-th branch
g	branch
p	point
b	starting point
e	end point
Δ	difference
o	initial value
$\mathbf{i}$	intensive quantity
$\mathbf{e}$	extensive quantity
$\mathbf{T}$	branch-to-node relation matrix
$\mathbf{B}_j$	transfer matrix
$\mathbf{B}$	matrix for branch orientation and branch end junction
$\mathbf{R}$	orthogonal matrix to transform into the preferential co-ordinate system pertaining to the branches
$\mathbf{K}$	conduction matrix
$\mathbf{F}$	$\mathbf{K}^{-1}$

3. Application for bar systems in small displacement

Interrelation between relationships of linear geometry networks and those obtained by the first-order theory for spatial systems of straight-axed bars with constant stiffness [1] will be expounded, taking also changes due to curved axis and/or variable stiffness into consideration.

3.1 *Mutually corresponding notations*

Bar system data will be given in an orthogonal, so-called global co-ordinate system $X(x, y, z)$. Intensive quantities are displacements, extensive quantities are generalized forces. In [1], displacements along, and rotations about the co-ordinate axes were chosen as independent intesive quantities. Accordingly, independent extensive quantities are axial forces and moment vectors. Thus, for general spatial bar systems: $d = 6$.

Sources of nodal extensive quantities are loads, and for bars corresponding to branches, the internal forces. Bars are granted so-called local co-ordinate systems Ξ (ξ being the bar axis, η and ζ the principal directions of inertia), where each bar force component has its name (normal force, the two shear forces, torque, the two bending moments). Orthogonal transformation $\mathbf{R}_j$ corresponds to matrix $\mathbf{T}_{jk}$.

The constitutional law involves flexibility and stiffness matrices **F** and **K**. For a straight-axed bar of constant stiffness:

$$\mathbf{F}_j = \begin{bmatrix} \frac{l}{EA} & & & & & & & & & & & \\ & \frac{l^3}{3EJ_\zeta} & & & & & & & & & \frac{l^2}{2EJ_\zeta} & \\ & & \frac{l^3}{3EJ_\eta} & & & & & & -\frac{l^2}{3EJ_\eta} & & & \\ & & & \frac{l}{GJ_\xi} & & & & & & & & \\ & & -\frac{l^2}{2EJ_\eta} & & & & & \frac{l}{EJ_\eta} & & & & \\ & \frac{l^2}{2EJ_\zeta} & & & & & & & & & \frac{l}{EJ_\zeta} & \end{bmatrix}_j$$

A bar of varying stiffness or curved axis will be approximated by a polygon containing intervals of straight lengths and constant stiffness. This polygon is considered as clamped at its starting point, and displacement of the cantilever and due to unit forces parallel to the axes of a co-ordinate system belonging to its end point ($P_{je\xi}$, $P_{je\eta}$, $P_{je\zeta}$, $M_{je\xi}$, $M_{je\eta}$, $M_{je\zeta}$) will be determined. The μ-th component of the displacement due to the ν-th unit force referred to the end-point co-ordinate system yields the μ-th element of the ν-th column of matrix $\mathbf{F}_j$ ($\mu, \nu = 1, 2, \ldots, 6$). The calculation is rather easy because of the peculiar advantages of the cantilever. Transfer matrix $\mathbf{B}_{jk}$ in [1] lends itself for transforming vectors in the local co-ordinate system,

here $\mathbf{B}_j$ is valid in the global co-ordinate system:

$$\mathbf{B}_j = \begin{bmatrix} 1 & & & & & z_e - z_b & y_b - y_e \\ & 1 & & z_b - z_e & & & x_e - x_b \\ & & 1 & y_e - y_b & x_b - x_e & & \\ & & & 1 & & & \\ & & & & 1 & & \\ & & & & & 1 & \end{bmatrix}_j$$

with e.g. z_{bj} standing for the co-ordinate z of the starting point of the j-th bar.

The counterpart of matrix **T** is the connecting matrix **P** (p. 87 in [1]). Product $-\mathbf{RB}$ is identical with the geometry matrix of the still unconnected structure. The triple product $-\mathbf{RBT}$ is identical with the geometry matrix of the connected structure, omitting columns corresponding to boundaries. Correspondence between symbols in item [2] and in [1] are shown in Table II.

Table II

Network theory	Bar system	
d	6	
$\mathbf{i}_p$	**u**	nodal displacements
$\mathbf{e}_p$	**q**	nodal loads
$\mathbf{i}_e$		bar end displacements
$\mathbf{e}_e^{\Xi}$	**s**	internal forces
$\mathbf{i}_\Delta\, s$	$\Delta\,\mathbf{u}$	relative bar end displacements
$\mathbf{i}_\Delta\, o$	**t**	initial strains
$\mathbf{i}_\Delta$		relative bar end displacements from bar deformation
$\mathbf{B}_j$	$\sim\mathbf{B}_{jk}$	transfer matrix (in another co-ordinate system)
$\mathbf{R}_j$	$\mathbf{T}_{jk}$	rotation matrix
$\mathbf{F}^{\Xi}$	**F**	flexibility matrix
$\mathbf{K}^{\Xi}$	$\mathbf{F}^{-1}$	stiffness matrix
T	**P**	connecting matrix
$-\mathbf{RB}$	$\mathbf{G}_r$	geometry matrix of the unconnected structure
$-\mathbf{RBT}$	**G**	geometry matrix

3.2 *Deviations from the bar system theory*

Some minor differences between relationships of the general network theory and the bar system theory [1] are the following:

a) As mentioned in 3.1, transfer matrices $\mathbf{B}_j$ and $\mathbf{B}_{jk}$ belong to different

co-ordinate systems. This modification is advantageous for the calculation of structures with some curved bars [4].

b) The network theory left the displacements defined by constraint conditions inconsidered. Thereby the analysis of the effect of support movements (requiring application of kinematic loads) and the calculation of reactions (requiring addition of stresses in bar ends joining at a fixed node) are far from self-intended.

c) Displacement other than along the co-ordinate axes may be required to be equal or zero. This will be exemplified on a simple beam for sake of simplicity (Fig. 1):

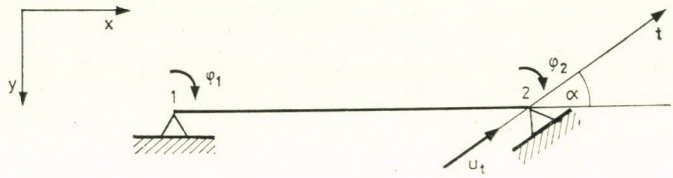

Fig. 1

For the beam on two supports, sketched in Fig. 1:

$$\mathbf{i}_{p1} = [\varphi_1]\,; \qquad \mathbf{i}_{p2} = \begin{bmatrix} u_t \\ \varphi_2 \end{bmatrix}.$$

According to (1), bar ends and nodes are related as:

$$\begin{bmatrix} u_{bx} \\ u_{by} \\ \varphi_b \\ u_{ex} \\ u_{ey} \\ \varphi_e \end{bmatrix} = \begin{bmatrix} 0 & 0 & 0 \\ 0 & 0 & 0 \\ 1 & 0 & 0 \\ 0 & \cos\alpha & 0 \\ 0 & -\sin\alpha & 0 \\ 0 & 0 & 1 \end{bmatrix} \begin{bmatrix} \varphi_1 \\ u_t \\ \varphi_2 \end{bmatrix}.$$

3.3 *Remarks*

a) The denoted matrix multiplications need not always be performed on full matrices, thus for instance **R*B*KBR** will be a hyperdiagonal one, which may be computed block-wise.

b) In structure where — as a frequent case — bar ends joining the node else than rigidly are not subject to loads corresponding to the lifted constraint, neither are stiffly connected bar nodes hinged (Fig. 2), the stiffness matrix **T*R*B*KBRT** of the entire structure can be constructed by compilation. Thereby also the equation systems decrease (by omitting e. g. the rotation of the hinged bar end) and advantage may be taken from the fact that the stiffness matrix is a symmetric band matrix.

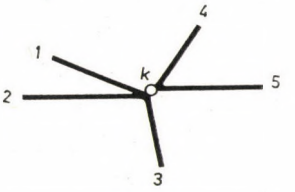

Fig. 2

c) Structure relationships may be arrived at by induction as Singer, D. did it ([2, 3]). In generalizing, however, linear electric circuit relationships, one must remind that for bar systems:

— beside topology, also structural geometry is of interst;

— intensive and extensive variables are vectors rather than scalars;

— extensive quantities vary along branches hence they can only be assigned to given points of the branch to be unambiguous;

— branch end connections are more general, and may also mean the identity of certain components;

— variables may be interpreted both in local and in global co-ordinate systems.

One must be careful in applying the inductive method since, leaving some differences out of consideration or generalizing erroneously leads to wrong results.

4. Application for linear electric circuits

For electric circuits constructed from branches with known impedances, branches may be specified to contain voltage sources and nodes current sources. It is aimed at determining nodal voltages referred to basic points, and branch current intensities. At a difference from [2], current sources have been assumed at nodes as some other authors do ([5], [6]).

In electric circuits also intensive and extensive quantities of branches, (voltages referred to basic points, and current intensities, resp.) are scalars, thus, $d = 1$. Intensive quantities are equal on all branch ends joining a node, hence $d_k = 1$, and matrix $\mathbf{T}$ cannot have other elements but 0 and 1.

The circuit has no preferential co-ordinate system for each branch, hence $\mathbf{R} = \mathbf{E}$, and (10) may be replaced by (9).

The current intensities at starting and end points of branches differ only by sign, hence $\mathbf{B}_j = \mathbf{B}_j^* = 1$. Matrix $\mathbf{B}$ reflects only the graph orientation (with elements: 0,1, -1). Correspondence between notations in item 2 and [2] are seen in Table III.

With these symbol changes, first matrix equation in (9) becomes:

$$\mathbf{A}^* \mathbf{i} + \mathbf{1}' = \mathbf{0},$$

Table III

Network theory	Electric network	
d	1	
d_k	1	
$-i_{pk}$	e'	Nodal voltage referred to the basic point
e_{pk}	I'	nodal current sources
$i_{\Delta sj}$	e	voltage difference between two branch ends
$-i_{\Delta 0j}$	E	specified voltage source
$i_{\Delta j}$	V	$e + E$
e_{ej}	i	current intensity
$\mathbf{B}_j$	1	transfer
R		unit matrix
−BT	**A**	branch node matrix
F	**Z**	primitive impedance matrix
K	**Y**	primitive admittance matrix

i.e. Kirchhoff's first theorem for a network loaded by nodal current sources; the second matrix equation in (9) is:

$$-\mathbf{A}\,\mathbf{e}' + \mathbf{Z}\,\mathbf{i} - \mathbf{E} = 0$$

conceivable as a different formulation of Kirchhoff's second theorem (difference between voltage drops at resistors and voltage sources equals the difference of scalars assigned to the joining nodes for each branch, hence it is zero for each loop).

REFERENCES

1. SZABÓ, J.—ROLLER, B.: Theory and Analysis of Bar Systems.* Műszaki Könyvkiadó Budapest 1971, pp. 266
2. SINGER, D.: Network Theory of Bar Structures *Acta Techn. Hung.* **73** (1972), 217—235
3. SINGER, D.: Generalization of Physical Networks and Systems Theory of Technology Processes. Thesis,* Budapest 1973
4. GÁSPÁR, Zs.: Analysis of Large Displacements in Bar Systems Using Different Models.* *Építés-Építészettudomány* **4** (1973), 345—356
5. MACNEAL, R. H.: Electric Circuit Analogies for Elastic Structures. John. Wiley and Sons, Inc., New York—London 1962
6. ПУХОВ, Г. Е.: Электрическое моделирование стрежневых и тонкостенных конструкций. Изд. Академии наук Украинской ССР. Киев 1960

*In Hungarian

Eine Verallgemeinerung physikalischer Netze (lineargeometrischer Netze). Gleichungen des physikalischen Netzes definiert als Verallgemeinerung der Stabwerke (physikalischer Graph) ergeben unmittelbar die Zusammenhänge zwischen Stabnetzen mit kleinen Verrückungen und linearen elektrischen Netzen als Sonderfall.

Одно обобщение физических сетей. Уравнения физической сети (физический граф), определенные в качестве обобщения стержневых конструкций, в качестве специального случая непосредственно дают зависимости стержневых конструкций, претерпевающих небольшие сдвиги, и линейных электрических сетей.

Acta Technica Academiae Scientiarum Hungaricae, Tomus 82 (1—2), pp. 99—119 (1976)

CONSOLIDATION AROUND SAND DRAINS IN NON-DARCIAN SOILS

R. J. KRIZEK*—H. A. ELNAGGAR**—A. S. AZZOUZ***

[Manuscript received May 22, 1973]

The effect of non-Darcian flow on the consolidation behavior of clay soils is evaluated for conditions of radial drainage only and combined radial and vertical drainage. This is accomplished by postulating a reasonably general four-parameter velocity-gradient relationship, which by proper choice of parameters is capable of characterizing much of the published experimental data on the flow of water through clay soils, and combining this relationship with the other standard assumptions of classical consolidation theory to develop a nonlinear parabolic partial differential equation, which is solved by use of finite difference procedures. Several typical solutions show that the time rate of consolidation for soils which exhibit non-Darcian flow characteristics is substantially less than that predicted by classical consolidation theory. Although a numerical solution to the two-dimensional flow problem was easily obtained by an explicit finite difference scheme, restrictive stability criteria rendered such solutions expensive.

Symbols

The following symbols are used in this paper:

a	Empirical coefficient
d	$r_e - r_w$
H	Thickness of single-drained clay layer
i	Hydraulic gradient
i_t	Apparent threshold gradient
k	Coefficient of permeability
k_m	Minimum permeability
k_u	Ultimate permeability
k_{u0}	Value of k_u at top of clay layer
k_{ur}	Value of k_u in radial direction
k_{uz}	Value of k_u in vertical direction
m	Modulus of volume change of the soil matrix
m_0	Value of m at top of a clay layer
r	Radial coordinate axis
r_e	Radius of influence of sand drain
r_w	Radius of sand drain
S	d/H
T_r	Time factor in the radial direction
T_z	Time factor in the vertical direction
t	Time
u	Excess pore water pressure

*Raymond J. KRIZEK, Professor of Civil Engineering. The Technological Institute, Northwestern University, Evanston, Illinois

**Hameed A. ELNAGGAR, Assistant Professor of Civil Engineering, University of Pittsburgh, Pittsburgh, Pennsylvania

***Amr S. AZZOUZ, Research Assistant in Civil Engineering, Massachusetts Institute of Technology, Cambridge, Massachusetts

v Discharge velocity
W Dimensionless excess pore water
z Vertical coordinate axis
α Coefficient expressing permeability variation with depth
β Coefficient expressing compressibility variation with depth
γ_w Unit weight of water
ζ Dimensionless depth
Θ Empirical coefficient
λ $\sqrt{k_{ur}/k_{uz}}$
μ_r Threshold gradient parameter in radial direction
μ_z Threshold gradient parameter in vertical direction
ϱ Dimensionless radial distance
ϱ_e Dimensionless radius of influence of sand drain
ϱ_w Dimensionless radius of sand drain
$\Delta\sigma$ Increment of load intensity applied at the surface
φ Variable coefficient

1. Introduction

The existence of non-Darcian flow can serve to explain (though not uniquely) many of the discrepancies that are often observed between field measurements and theoretical predictions of time rates of settlement in a clay stratum. Whether or not Darcy's law be used to characterize the flow of water through clays has been subject to much debate among soil engineers and soil scientists (KING, 1898; MILLER and LOW, 1963; OLSEN, 1965; KRAFT and YAAKOBI, 1966; MITCHELL and YOUNGER, 1967; and others). In general, most researchers agree that deviations from Darcian flow probably exist under low hydraulic gradients, but these deviations can be detected only if extremely sensitive measuring equipment and careful laboratory procedures are employed. Although some investigators support the concept of a threshold gradients, others claim that it does not exist, and the potential errors associated with experimental measurements are sufficiently large to render either argument inconclusive. Presented herein is an evaluation of the effect of non-Darcian flow (where Darcian flow is a special case) on the time rate of vertical consolidation due to radial drainage only or combined radial and vertical drainage in a sand drain installation.

2. Brief background

Extensive studies of sand drain performance have been reported by RENDULIC (1935, 1936), BARRON (1948), RICHART (1957), MORAN, PROCTOR, MUESER, and RUTLEDGE (1958), and HANSBO (1960), but all of these investigators have employed the assumption of Darcian flow. In this comprehensive review of sand drain theories, RICHART (1957) showed that time-dependent variations in void ratio did not significantly affect the consolidation-time response for vertical consolidation due to vertical drainage; accordingly, he

did not introduce any modifications to the assumptions of classical consolidation theory. However, SCHIFFMAN (1958) considered the sand drain problem in which the permeability of the soil varies with time and therefore void ratio. Much of the discussion presented in the report by MORAN, PROCTOR, MUESER, and RUTLEDGE (1958) deals with the effect of boundary conditions (such as smear at the well face) on the performance of sand drains. Although many researchers have considered the influence of various deviations from the assumptions of classical consolidation theory of the rate of vertical consolidation due to vertical drainage, virtually nothing can be found in the literature on the role of non-Darcian flow in the performance of sand drain installations.

3. Proposed flow relation

In many cases the flow of water through a clay soil may be conveniently characterized by the empirical relationship (ELNAGGAR, KARADI, and KRIZEK, 1971)

$$v = k_u \left[i - (1 - a) i_t \left\{ 1 - \exp\left(- \frac{\Theta_i}{i_t} \right) \right\} \right] \tag{1}$$

where v is the discharge velocity, i is the hydraulic gradient, and k_u, i_t, a and Θ are constants for a given soil. The initial slope, which may also be defined as the "minimum permeability", k_m ,is given by

$$k_m = \left. \frac{\mathrm{d}v}{\mathrm{d}i} \right|_{i=0} = k_u \left[1 - (1 - a)\Theta \right], \tag{2}$$

and the equation of the asymptote may be written as

$$v = k_u (i - i_t), \tag{3}$$

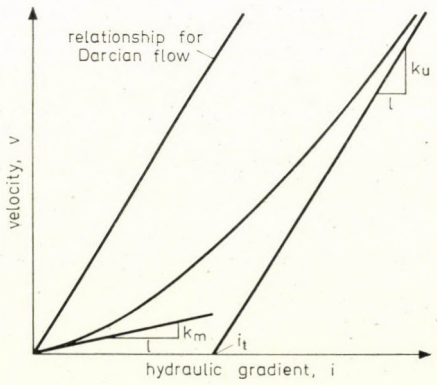

Fig. 1. Velocity-gradient relationship for proposed flow equation

where k_u is the maximum or "ultimate permeability" and i_t is the "apparent threshold gradient"; these parameters are illustrated in Fig. 1. Equation (1) reduces to Darcy's law if i_t equals zero or if a equals unity.

4. Field equation

If a clay stratum of uniform thickness is fully penetrated by sand drains spaced in a triangular pattern, the zone of influence for each drain is hexagonal; however, these hexagons may be approximated by circles with a diameter that is slightly larger than the spacing of the drains. Thus, the consolidating domain is axially symmetric, and the inner and outer boundaries are cylindrical with radii r_w and r_e, respectively. Except for the flow relation, the one-dimensional consolidation equation derived herein incorporates the standard assumptions of classical consolidation theory (TERZAGHI, 1923); hence, we may write

$$\frac{1}{r}\frac{\partial}{\partial r}(rv_r) + \frac{1}{r}\frac{\partial v_\Theta}{\partial \Theta} + \frac{\partial v_z}{\partial z} = m\frac{u\partial}{\partial t} \tag{4}$$

where v_r, v_Θ, and v_z are the velocity components in the x, y, and z directions, respectively, m is the modulus of volume change of the soil matrix, i is time, and u is the excess pore water pressure. For the axially symmetric case Eq. (4) reduces to

$$\frac{1}{r}\frac{\partial}{\partial r}(rv_r) + \frac{\partial v_z}{\partial z} = m\frac{\partial u}{\partial t}\,. \tag{5}$$

If the non-Darcian velocity-gradient relationships in the vertical and radial directions are given by

$$v_z = k_{uz}\left[i_z - (1-a)i_t\left\{1 - \exp\left(-\frac{\Theta i_z}{i_t}\right)\right\}\right], \tag{6a}$$

$$v_r = k_{ur}\left[i_r - (1-a)i_t\left\{1 - \exp\left(-\frac{\Theta i_r}{i_t}\right)\right\}\right] \tag{6b}$$

where

$$i_z = \frac{1}{\gamma_w}\frac{\partial u}{\partial z}, \tag{7a}$$

$$i_r = \frac{1}{\gamma_w}\frac{\partial u}{\partial r}, \tag{7b}$$

and if the vertical permeability and compressibility are assumed to vary with

depth according to

$$k_{uz} = k_{uo}\left(1 + \alpha \frac{z}{H}\right) \tag{8a}$$

and

$$m = m_o\left(1 + \beta \frac{z}{H}\right), \tag{8b}$$

where k_{u0} and m_0 denote the vertical permeability and compressibility, respectively, at the top of the clay layer and α and β are two parameters which characterize the respective variations with depth, the governing consolidation equation may be written as

$$\begin{aligned}\frac{m_0\gamma_w}{k_{u0}}\frac{\partial u}{\partial t} = {} & \frac{\gamma^2}{1+\beta\, z/H}\left[1 - (1-a)\,\Theta\,\exp\left(\frac{-\Theta}{i_t\gamma_w}\frac{\partial u}{\partial r}\right)\right]\frac{\partial^2 u}{\partial r^2} + \\ & + \frac{\lambda^2}{r(1+\beta\, z/H)}\left[\frac{\partial u}{\partial r} - (1-a)i_t\gamma_w\left\{1 - \exp\left(\frac{-\Theta}{i_t\gamma_w}\frac{\partial u}{\partial r}\right)\right\}\right] + \\ & + \frac{1+\alpha\, z/H}{(1+\beta\, z/H)}\left[1 - (1-a)\Theta\,\exp\left(\frac{-\Theta}{i_t\gamma_w}\frac{\partial u}{\partial z}\right)\right]\frac{\partial^2 u}{\partial z^2} + \\ & + \frac{\alpha}{H(1+\beta\, z/H)}\left[\frac{\partial u}{\partial z} - (1-a)i_t\gamma_w\left\{1 - \exp\left(\frac{-\Theta}{i_t\gamma_w}\frac{\partial u}{\partial z}\right)\right\}\right]\end{aligned} \tag{9}$$

where i_t is the same in both the vertical and radial directions and

$$\lambda^2 = \frac{k_{ur}}{k_{uz}}\,. \tag{10}$$

If both the permeability and compressibility are assumed to be constant thoroughout the clay layer, Eq. (9) reduces to

$$\begin{aligned}\frac{m\gamma_w}{k_{uz}}\frac{\partial u}{\partial t} = {} & \lambda^2\left[1 - (1-a)\Theta\exp\left(-\frac{\Theta}{i_t\gamma_w}\frac{\partial u}{\partial r}\right)\right]\frac{\partial^2 u}{\partial r^2} + \\ & + \frac{\lambda^2}{r}\left[\frac{\partial u}{\partial r} - (1-a)i_t\gamma_w\left\{1 - \exp\left(\frac{-\Theta}{i_t\gamma_w}\frac{\partial u}{\partial r}\right)\right\}\right] + \\ & + \left[1 - (1-a)\Theta\exp\left(-\frac{\Theta}{i_t\gamma_w}\frac{\partial u}{\partial z}\right)\right]\frac{\partial^2 u}{\partial z^2}\,,\end{aligned} \tag{11}$$

which, for radial flow only, becomes

$$\begin{aligned}\frac{m\gamma_w}{k_{ur}}\frac{\partial u}{\partial t} = {} & \left[1 - (1-a)\Theta\exp\left(-\frac{\Theta}{i_t\gamma_w}\frac{\partial u}{\partial r}\right)\right]\frac{\partial^2 u}{\partial r^2} + \\ & + \frac{1}{r}\left[\frac{\partial u}{\partial r} - (1-a)i_t\gamma_w\left\{1 - \exp\left(\frac{-\Theta}{i_t\gamma_w}\frac{\partial u}{\partial r}\right)\right\}\right].\end{aligned} \tag{12}$$

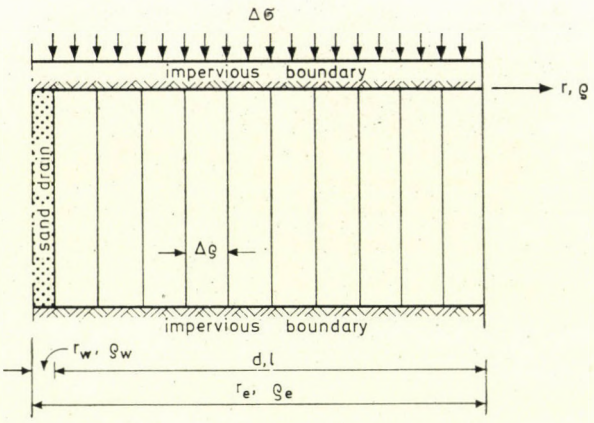

(a) Radial drainage only

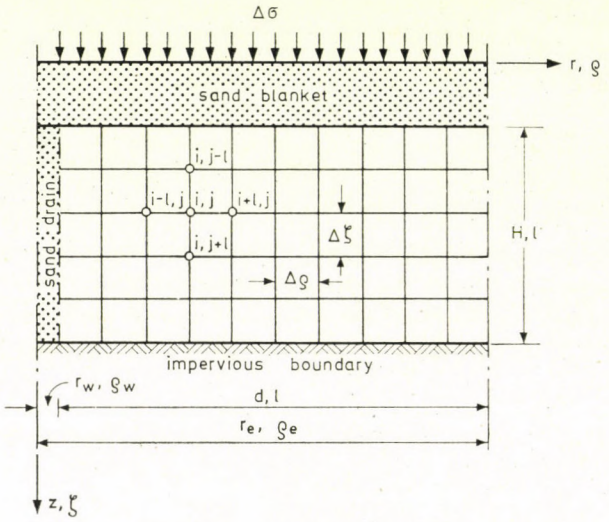

(b) Combined radial and vertical drainage

Fig. 2. **Boundary configuration and discretization for problems considered**

If we define the dimensionless variables (Fig. 2)

$$W = \frac{u}{\Delta\sigma}, \tag{13a}$$

$$\varrho = \frac{r}{r_e - r_w} = \frac{r}{d}, \tag{13b}$$

$$\zeta = \frac{z}{H}, \tag{13c}$$

$$S = \frac{d}{H}, \tag{13d}$$

$$T_r = \frac{k_{ur} t}{m \gamma_w d^2}, \tag{13e}$$

$$T_z = \frac{k_{uz} t}{m \gamma_w H^2}, \tag{13f}$$

$$\mu_r = \frac{d \gamma_w}{\Delta\sigma} i_t, \tag{13g}$$

and

$$\mu_z = \frac{H \gamma_w}{\Delta\sigma} i_t \tag{13h}$$

where $d = r_e - r_w$ and $\Delta\sigma$ is the increment of load intensity applied at the surface, Eqs (11) and (12) become

$$\frac{\partial W}{\partial T_z} = \frac{\gamma^2}{S^2}\left[1 - (1-a)\Theta \exp\left(-\frac{\Theta}{\mu_z S}\frac{\partial W}{\partial \varrho}\right)\right]\frac{\partial^2 W}{\partial \varrho^2} +$$

$$+ \frac{\lambda^2}{S^2}\frac{1}{\varrho}\left[\frac{\partial W}{\partial \varrho} - (1-a)\mu_z S\left\{1 - \exp\left(-\frac{\Theta}{\mu_z S}\frac{\partial W}{\partial \varrho}\right)\right\}\right] +$$

$$+ \left[1 - (1-a)\Theta \exp\left(-\frac{\Theta}{\mu_z}\frac{\partial W}{\partial \zeta}\right)\right]\frac{\partial^2 W}{\partial \zeta^2} \tag{14}$$

and

$$\frac{\partial W}{\partial T_r} = \left[1 - (1-a)\Theta \exp\left(-\frac{\Theta}{\mu_r}\frac{\partial W}{\partial \varrho}\right)\right]\frac{\partial^2 W}{\partial \varrho^2} +$$

$$+ \frac{1}{\varrho}\left[\frac{\partial W}{\partial \varrho} - (1-a)\mu_r\left\{1 - \exp\left(\frac{-\Theta}{\mu_r}\frac{\partial W}{\partial \varrho}\right)\right\}\right]. \tag{15}$$

In Eqs (14) and (15) μ_z and μ_r may be termed "thresehold gradient" parameters, and they reflect essentially the effect of the apparent threshold gradient i_t relative to the magnitude of the load increment $\Delta\sigma$ under which the clay stratum is being consolidated. When these "threshold gradient" parameters vanish (that is, $i_t = 0$), Eqs (14) and (15) reduce to the field equations of classical consolidation theory.

5. Vertical consolidation due to radial flow only

The boundary conditions for the problem of vertical consolidation due to radial flow have been expressed in two different ways (BARRON, 1948); the first is called the "free strain" case and corresponds to a situation of uniform surface loading under which the soil is free to settle as the pore water pressure dissipates, whereas the second is termed "equal strain" and corresponds to the situation wherein vertical strains in the consolidating soil mass are everywhere equal. In actuality, however, an intermediate condition is most probable. For linear problems BARRON (1948) and RICHART (1957) presented results which indicated that the difference between the "free strain" and "equal strain" solutions is small, and they preferred the "equal strain" approach for reasons of simplicity. However, since "free strain" is more representative of actual field conditions, this case was chosen for the analysis herein (Fig. 2a).

5.1. *Boundary and Initial Conditions*

Accordingly, the boundary conditions for a signle sand drain are

$$W(\varrho_w, T_r) = 0 \tag{16a}$$

and

$$\frac{\partial W}{\partial \varrho}(\varrho_e, T_r) = 0\,. \tag{16b}$$

Since the initial pore water pressure is assumed to be uniform throughout the soil mass and equal to the instantaneously applied load $\Delta\sigma$,the initial condition may be expressed in dimensionless form as

$$W(\varrho, 0) = 1, \quad \varrho_w \leq \varrho \leq \varrho_e\,, \tag{16c}$$

5.2. *Numerical Solution*

Equation (15), subject to the boundary and initial conditions given by Eqs (16), may be expressed explicitly by the finite difference equation

$$W_{i,j+1} W_{i,j} + R_r \varphi_{i,j}\, \delta^2(W_i)_{,j} + \frac{\Delta T_r}{2\Delta\varrho} \cdot \frac{1}{\varrho_i}\, \delta(W_i)_j + \frac{\Delta T_r}{\varrho_i} E_i\,, \tag{17}$$

$$i = 1,2, \ldots N, \text{ and } j = 0,1,2, \ldots$$

where

$$\varphi = 1 - (1-a)\,\Theta \exp\left(\frac{-\Theta}{\mu_r}\,\frac{\partial W}{\partial \varrho}\right), \tag{18a}$$

$$E = -(1-a)\mu_r \left\{1 - \exp\left(\frac{-\Theta}{\mu_r} \frac{W\partial}{\partial \varrho}\right)\right., \tag{18b}$$

and

$$R_r = \frac{\Delta T_r}{(\Delta \varrho)^2}. \tag{18c}$$

If the domain $(p_w \leq p \leq p_e)$ is divided into N equal subintervals, each of length Δp equal to $1/N$, we may write

$$\varrho_i = \varrho_w + i\Delta\varrho. \tag{19}$$

As verified by experience, the stability criterion for the numerical solution to this problem is

$$R_r \leq \frac{1}{2\varphi_i}, \tag{20}$$

since the coefficient $1/\varrho$ of the lower-order term in Eq. (15) will always be positive.

5.3. *Results*

As can be seen from Figs 3a and 3b, the ratio n of the effective radius r_e to the radius of the drain well r_w exerts a considerable influence on the time rate of consolidation, whether the flow is Darcian ($\mu_r = 0$) or non-Darcian ($\mu_r = 5$; $a = 0{,}50$). Figs 3c and 3d show the average percent consolidation as a function of time for various values of μ_r and for a equal to 0,01 (almost zero) and 0,50. As noted, the process of consolidation becomes considerably slower as μ_r increases; for example, Fig. 3c shows that, at a time factor of 0,8, over 60 percent consolidation is predicted by classical theory ($\mu_r = 0$), but only 30 percent is perdicted when μ_r equals 5. A comparison of Figs 3c and 3d also indicates that the rate of consolidation decreases as the parameter a decreases; since $a = 1$ corresponds to the case of classical consolidation, three values of a (0,01, 0,50, and 1,00) are actually represented on these figures. The distribution of excess pore water pressure over the radius of influence of a sand drain is given as function of time in Figs 4a and 4b for μ_r equal to 0 and 5, respectively, where n was assumed to be 10; it is apparent that the existence of non-Darcian significantly impedes the dissipation of excess pore water pressure. The effect of non-Darcian flow is illustrated in Figs 5a and 5b, where the excess pore water pressures at one-half d are shown. The delay in the pore pressure dissipation may be readily seen, especially at large times; in other words, the excess pore pressure dissipates faster during the early stages of consolidation than toward the end.

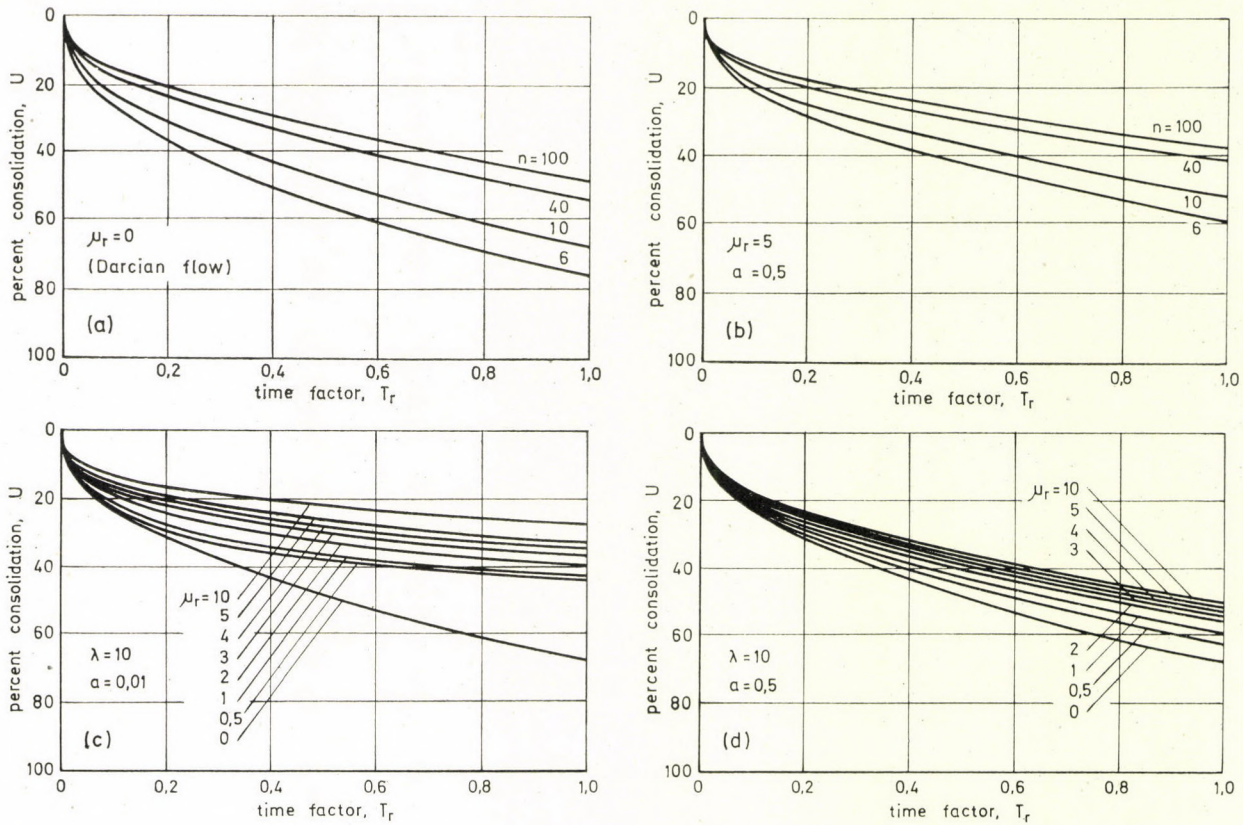

Fig. 3. Percent consolidation versus time factor for radial flow only

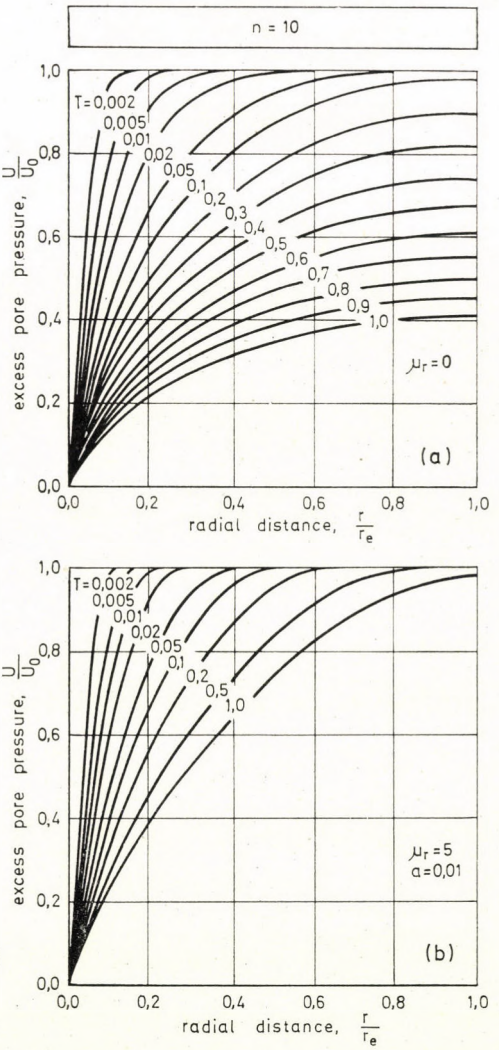

Fig. 4. Radial distribution of excess pore pressure for radial flow only

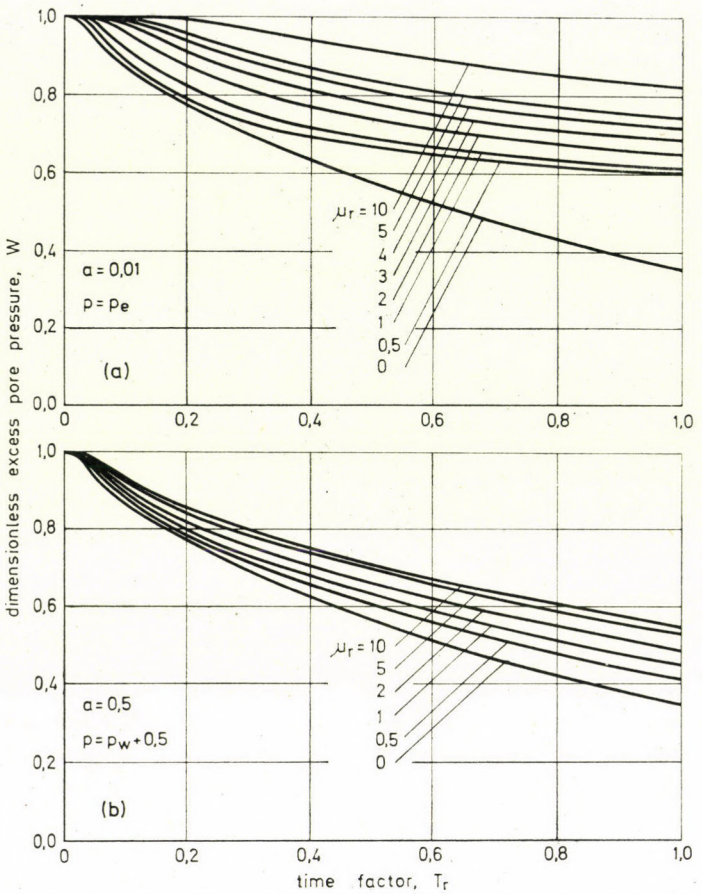

Fig. 5. Excess pressure versus time factor for radial flow only

6. Vertical consolidation due to vertical and radial flow

Consider now the case in which vertical flow toward a sand blanket is combined with radial flow towards a sand drain; the governing differential equation of consolidation for this situation is given by Eq. (14), and the most general solution presented herein is for the case where the flow of water in both the vertical and radial directions is assumed to be non-Darcian with different values for the vertical and horizontal permeabilities (Fig. 2b).

6.1. *Boundary and Initial Conditions*

The boundary conditions for this problem are

$$W(\varrho u, \zeta, T_z) = 0, \tag{21a}$$

$$W(\varrho, 0, T_z) = 0, \tag{21b}$$

$$\frac{\partial W}{\partial \varrho}(\varrho_e, \zeta, T_z) = 0, \tag{21c}$$

$$\frac{\partial W}{\partial \zeta}(\varrho, 1, T_z) = 0. \tag{21d}$$

and the initial condition is

$$W(p, \zeta, 0) = 1, \tag{21e}$$

for $\varrho_w \leq \varrho \leq \varrho_e$ and $0 \leq \zeta \leq 1$.

6.2. *Finite Difference Formulation*

The finite difference technique is used to solve the two-dimensional partial differential equation given by Eq. (14). After the spatial domain $(\varrho - \zeta)$ is replaced by a rectangular or square grid, the ϱ-dimension is divided into M equal intervals of length $\Delta\varrho$ and the ζ-dimension is divided into N equal intervals of length $\Delta\zeta$. The coordinates of the nodal points in the (ϱ, ζ)-plane are $(\varrho_i, \zeta_j) = (i\,\Delta\varrho, j\,\Delta\zeta)$ for $i = 0, 1, 2, \ldots M$ and $j = 0, 1, 2, \ldots N$. The time dimension forms a third ordinate such that the time-spatial nodal points have the coordinates $(\varrho_i, \zeta_j, T_k) = (i\,\Delta\varrho,\ j\,\Delta\zeta,\ k\Delta T_z)$ for $k = 0, 1, 2, \ldots$, where the time axis is perpendicular to the plane of Fig. 2b and the nodal points are situated at various time increments ΔT_z.

In order to simplify the presentation of the equations for the finite difference solution, when the values of the variable $W(\varrho, \zeta, T_z)$ at time T_z are known, this variable will be called $Y(\varrho, \zeta)$ otherwise, it will be referred to as W. Thus, the explicit finite difference scheme for Eq. (14) takes the form

$$\begin{aligned} W_{i,j} = Y_{i,j} &+ \frac{\Delta T_z}{(\Delta\varrho)^2}\,\frac{\lambda^2}{S^2}\,\varphi^r_{i,j}\,\delta^2(Y_i)_{,j} + \\ &+ \frac{\Delta T_z}{(\Delta\zeta)^2}\,\varphi^z_{i,j}\,\delta^2(Y_j)_{,i} + \\ &+ \frac{\Delta T_z}{2\Delta\varrho}\,\frac{\lambda^2}{S^2}\,\frac{1}{\varrho_i}\,\delta(Y_i)_{,j} + \\ &+ \Delta T_z\,\frac{\lambda^2}{S^2}\,\frac{1}{\varrho_i}\,E^r_{i,j}, \end{aligned} \tag{22}$$

where

$$\varphi^r_{i,j} = 1 - (1-a)\Theta \exp\left(\frac{-\Theta}{2\mu_z S \Delta\varrho}\,\delta(Y_i)_{,j}\right), \tag{23a}$$

$$\varphi^z_{i,j} = 1 - (1-a)\Theta \exp\left(\frac{-\Theta}{2\mu_z \Delta\zeta}\,\delta(Y_{j,i}\right), \tag{23b}$$

and

$$E^r_{i,j} = (1-a)\mu_z S\left\{1 - \exp\left(\frac{-\Theta}{2\mu_z S\Delta\varrho}\,\delta(Y_i)_{,j}\right)\right\}. \tag{23c}$$

6.3. *Stability Condition*

The explicit finite difference representation given by Eq. (22) appears to be simple, but, in fact, it is very complicated from a computational point of view. This is due to the increased number of unknown nodal points and, more importantly, the stability requirements, which are given by

$$\frac{\Delta T_z}{(\Delta\varrho)^2}\,\frac{\lambda^2}{S^2}\,\varphi^r_{i,j} + \frac{\Delta T_z}{(\Delta\zeta)^2}\,\varphi^z_{i,j} \leq \frac{1}{2}, \tag{24}$$

for all values of i and j. The use of $R_z = \Delta T_z/(\Delta\zeta)^2$ allows the stability condition to be expressed as

$$R_z \leq \frac{1}{2\left[\dfrac{M}{N}\,\dfrac{\lambda^2}{S^2}\,\varphi^r_{i,j} + \varphi^z_{i,j}\right]} \tag{25}$$

and the explicit method, with ΔT_z, $\Delta\varrho$, and $\Delta\zeta$ satisfying Eq. (25), was used to obtain the solutions presented herein. The consolidation domain (ϱ, ζ) was replaced by a grid with the same number of subdivisions in both directions; hence, M is equal to N. The intervals of $\Delta\varrho$ and $\Delta\zeta$ were taken equal to 0,10, and ΔT_z was chosen such that the stability condition specified by Eq. (25) was satisfied.

6.4. *Results*

Shown in Fig. 6 is the average percent consolidation versus the time factor for λ and S both rqual to unity, n equal to ten, a equal to 0,01, and various values for the threshold gradient parameter μ_z. Comparisons with the classical consolidation case ($\mu_z = 0$) indicate that non-Darcian flow exerts a significant effect on the consolidation rate. The excess pore water pressure at midpoint between drains is given in Fig. 7a as a function of depth and the factor; alternatively, Fig. 7b shows the excess pore water pressure along the impervious bottom of the clay stratum as a function of time and radial distance. In order

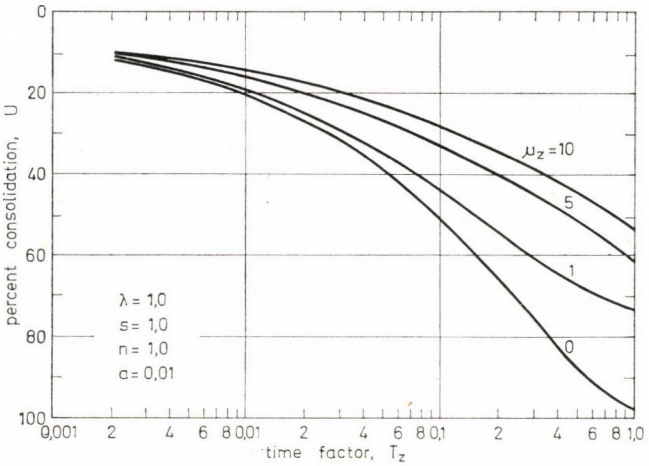

Fig. 6. **Percent consolidation versus time factor for radial and vertical flow**

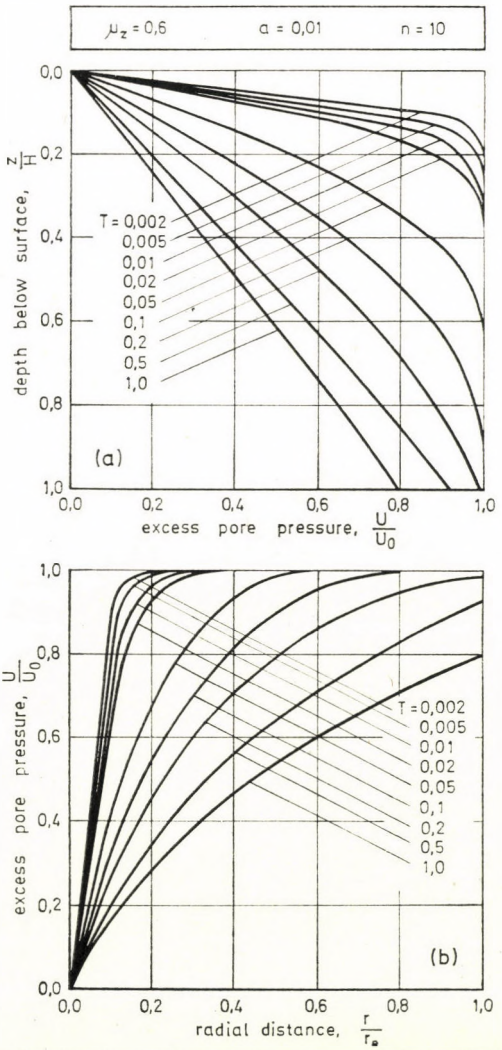

Fig. 7. **Various distributions of excess pore pressure for radial and vertical flow**

to better illustrate the effect of non-Darcian flow on the time rate at which the excess pore water pressure dissipates, the response is given at two spatial points, (ϱ_z, 1) Fig. 8a and ($\varrho_w + 0{,}5$, 0,5) in Fig. 8b. Once again, the drastic

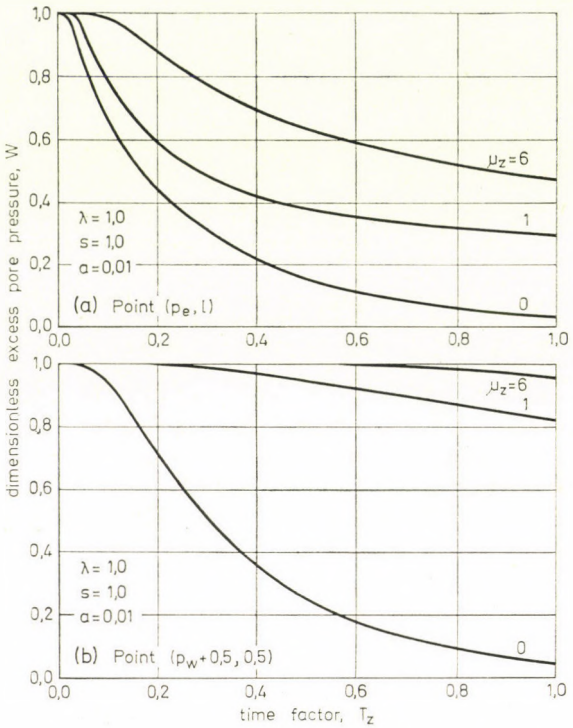

Fig. 8. Excess pore pressure versus time factor for radial and vertical flow

effect of the threshold gradient parameter is observed. The distribution of excess pore water pressure in a typical (ϱ, ζ)-plane at T_z equal to 0,50 is shown isometrically in Fig. 9a, 9b, and 9c for μ_z equal to 0, 0,6, and 1,0, respectively, and the values of W for these plots are summarized in Table I.

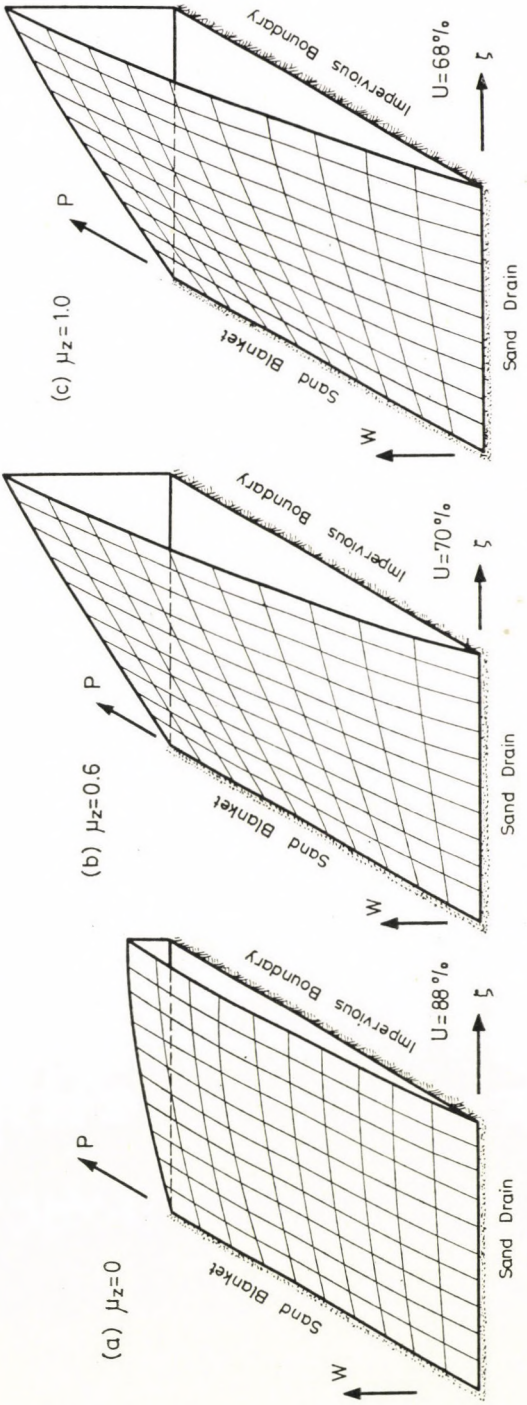

Fig. 9. Typical qualitative distributions of excess pore pressure

Table I

Dimensionless excess pore water pressures as a function of radial distance and depth
($T = 0.50$, $a = 0.01$, and $n = 10$)

ζ	Dimensionless excess pore water pressures for														
	0,10			0,20			0,30			0,40			0,50		
	0,00	0,60	1,00	0,00	0,60	1,00	0,00	0,60	1,00	0,00	0,60	1,00	0,00	0,60	1,00
0,10	0,01	0,02	0,02	0,02	0,04	0,04	0,03	0,05	0,06	0,03	0,06	0,07	0,03	0,07	0,08
0,20	0,03	0,04	0,05	0,04	0,07	0,08	0,05	0,10	0,11	0,06	0,12	0,14	0,07	0,14	0,16
0,30	0,04	0,06	0,07	0,06	0,11	0,12	0,08	0,15	0,17	0,09	0,18	0,20	0,10	0,21	0,23
0,40	0,05	0,08	0,09	0,08	0,15	01,6	0,10	0,20	0,22	0,11	0,24	0,27	0,12	0,28	0,30
0,50	0,06	0,10	0,11	0,09	0,18	0,20	0,12	0,24	0,27	0,14	0,30	0,32	0,15	0,34	0,37
0,60	0,07	0,13	0,13	0,11	0,22	0,24	0,13	0,29	0,31	0,15	0,35	0,38	0,17	0,40	0,44
0,70	0,07	0,15	0,15	0,12	0,25	0,27	0,15	0,33	0,36	0,17	0,40	0,43	0,19	0,46	0,50
0,80	0,08	0,16	0,17	0,12	0,28	0,30	0,16	0,38	0,40	0,18	0,46	0,48	0,20	0,52	0,56
0,90	0,08	0,18	0,19	0,13	0,31	0,33	0,16	0,42	0,44	0,19	0,50	0,53	0,21	0,58	0,61
1,00	0,08	0,20	0,20	0,13	0,34	0,35	0,17	0,46	0,47	0,19	0,55	0,57	0,21	0,64	0,66

ζ	Different values of ϱ (frist row) and μ_2 (second row)														
	0,60			0,70			0,80			0,90			1,00		
	0,00	0,60	1,00	0,00	0,60	1,00	0,00	0,50	1,00	0,00	0,60	1,00	0,00	0,60	1,00
0,10	0,04	0,08	0,09	0,04	0,08	0,09	0,04	0,09	0,10	0,04	0,10	0,10	0,04	0,10	0,11
0,20	0,07	0,16	0,17	0,07	0,17	0,19	0,07	0,18	0,20	0,08	0,19	0,21	0,08	0,20	0,21
0,30	0,10	0,23	0,26	0,11	0,25	0,28	0,11	0,27	0,29	0,11	0,28	0,31	0,11	0,30	0,32
0,40	0,13	0,31	0,34	0,14	0,33	0,36	0,14	0,36	0,39	0,14	0,38	0,40	0,15	0,39	0,42
0,50	0,16	0,38	0,41	0,17	0,41	0,45	0,17	0,44	0,47	0,17	0,47	0,50	0,18	0,49	0,52
0,60	0,18	0,45	0,49	0,19	0,49	0,53	0,20	0,52	0,56	0,20	0,55	0,59	0,20	0,58	0,61
0,70	0,20	0,52	0,55	0,21	0,56	0,60	0,22	0,60	0,64	0,22	0,64	0,67	0,22	0,67	0,70
0,80	0,21	0,58	0,62	0,22	0,64	0,67	0,23	0,68	0,71	0,23	0,72	0,75	0,24	0,76	0,78
0,90	0,22	0,65	0,68	0,23	0,71	0,74	0,24	0,76	0,79	0,24	0,80	0,83	0,24	0,84	0,87
1,00	0,22	0,71	0,73	0,24	0,77	0,80	0,24	0,83	0,85	0,25	0,88	0,90	0,25	0,93	0,94

7. Ultimate settlements

If k_m were equal to zero, the velocity-gradient relationship illustrated in Fig. 1 could be expressed as

$$\begin{aligned} v &= 0, \qquad i \leq i_t, \\ v &= k_u(i - i_t), \qquad i > i_t \end{aligned} \tag{26}$$

and all excess pore water pressures associated with a gradient less than it would be unable to dissipate, thereby reducing the ultimate settlement determined by means of classical consolidation theory. One such case of undissipated or "residual" excess pore water pressures in a Norwegian clay deposit hundreds of years old was reported by BJERRUM (1970). However, regardless of whether or not a threshold gradient does actually exist in a clay soil, the numerical procedures employed in this study do not admit the singularity that would develop if Eq. (26) were incorporated into Eq. (5). Consequently, use of the "smooth" velocity-gradient relationship given by Eq. (1) implies that all excess pore water pressures will fully dissipate at sufficient large times, and the ultimate settlements predicted by this modified theory will be equal to those calculated from classical theory.

8. Conclusions

Based on the non-Darcian flow relationship proposed herein and the associated modified theory of consolidation applied to sand drain installations, the following conclusions can be advanced:

1. The rate of consolidation due to radial drainage only, as well as combined radial and vertical drainage, may be substantially delayed in soils which exhibit non-Darcian flow characteristics, thereby providing one feasible explanation for the discrepancies that are often observed between the actual field performance of a sand drain installation and the theoretical estimates that are deduced from classical consolidation theory.

2. The spacing of the sand drains and the ratio of the effective radius to the radius of the drain well exerts a considerable influence on the time rate of consolidation, whether the flow is Darcian or non-Darcian.

3. The consolidation process is considerably accelerated by the combined use of vertical and radial drainage, as opposed to radial drainage only, but the influence of non-Darcian flow is strong in both cases.

REFERENCES

1. BARRON, R. A.: Consolidation of Fine-grained Soils by Drain Wells, *Transactions of American Society of Civil Engineers* **113** (1948), 718—754
2. BJERRUM, L.: Personal Communication (1970)
3. ELNAGGAR, H. A.—KARADI, G. M.—KRIZEK, R. J.: Non-Darcian Flow in Clay Soils, *Proceedings of the Symposium on the Measurement and Control of Flow in Science and Industry*, Instrument Society of America, Pittsburgh, Pennsylvania (1971), 53—61
4. HANSBO, S.: Consolidation of Clay with Special Reference to Influence of Vertical Sand Drains. *Proceedings of the Swedish Geotechnical Institute* (1960), Number 18, Stockholm, Sweden
5. KING, F. H.: Principles and Conditions of the Movement of Ground Water, *Nineteenth Annual Report*, United States Geological Survey (1898), Part 2, 59—294
6. KRAFT, R.—YAAKOBI, D.: Some Remarks on Non-Darcy Flow, *Journal of Hydrology* **4** (1966), 171—181
7. MILLER, R. J.—LOW, P. F.: Threshold Gradient for Water Flow in Clay Systems, *Proceedings of the Soil Science Society of America* **27** (1963), 605—699
8. MITCHELL, J. K.—YOUNGER, J. S.: Abnormalities in Hydraulic Flow through Fine-grained Soils, *American Society for Testing and Materials*, Special publication **417** (1967), 106—139
9. MORAN—PROCTOR—MUESER—RUTLEDGE (1958): Study of Deep Soil Stabilization by Vertical Sand Drains, *Report submitted to the Bureau of Yards and Docks* (1958), Department of the Navy, Washington, D. C.
10. OLSEN, H. W.: Deviations from Darcy's Law in Saturated Clays, *Proceedings of the Soil Science Society of America* **29** (1965), No. 2, 135—140
11. RENDULIC, L.: Der hydrodynamische Spannungsausgleich in zentral entwässerten Tonzylindern, *Wasserwirtsch. u. Technik* **2** (1935), 250—253
12. RENDULIC, L.: Porenziffer und Porenwasserdruck in Tonen, *Der Bauingenieur* **17** (1936), 559—564
13. RICHART, F. E., JR.: A Review of the Theories for Sand Drains, *Journal of the Soil Mechanics and Foundations Division*, American Society of Civil Engineers **83** (1957), No. SM3, Proceedings paper 1301, 1301—1338
14. SCHIFFMAN, R. L.: Consolidation of Soil under Time-dependent Loadings and Variable Permeability, *Proceedings of the Highway Research Board*, **37** (1957), 584—617
15. TERZAGHI, K.: Die Berechnung der Durchlässigkeitsziffer des Tones aus dem Verlauf der hydrodynamischen Spannungserscheinungen, *Akademie der Wissenschaften in Wien, Sitzungsberichte*, Mathematische Naturwissenschaftliche Klasse, Part IIa, Volume $\mathbf{132}$ (1928), No. 3/4, 125—138.

Befestigung von Böden die dem Darcyschen Strömungsgesetz nicht folgen, im Bereich der Sandsickerdrainage. Der Einfluß der nichtdarcyschen Strömung auf den Befestigungsvorgang der tonigen Böden wird ermittelt, teils für den Fall von radialen, teils von kombinierten radialen und vertikalen Sickerdrainen. Dies geschieht durch Ansetzung einer vernünftigerweise allgemeinen, vierparametrigen Abhängigkeit für den Geschwindigkeitsgradient des Ablaufs der Befestigung, die im Fall von richtig ausgewählten Parametern geeignet ist zur Charakterisierung von zahlreichen empirischen, d. h., Versuchsergebnissen über die Strömung des Wassers durch tonige Böden und durch Kombination dieser Abhängigkeit mit anderen allgemeinen Voraussetzungen der klassichen Bodenbefestigungstheorie zur Entwicklung einer nichtlinearen partialen Differentialgleichung, die durch Anwendung des Verfahrens von endlichen Differenzen gelöst werden kann. Mehrere Lösungstype beweisen, daß die Geschwindigkeit des Befestigungsvorgangs in Böden, wo die Wasserströmung nichtdarcysche Eigenschaften aufweist, erheblich kleiner sind, als der mit Hilfe der klassischen Befestigungstheorie ermittelte Wert. Dessen ungeachtet, daß die Aufgabe der Zweidimensionsströmung mit Hilfe einer expliziten Formel der endlichen Differenzen leicht gelöst werden kann, einige Beschränkungskriterien der Stabilität machen derartige Lösungen kostspielig.

Упрочнение грунта вокруг песчаных фильтров в грунтах, не удовлетворяющих закону Дарси. Определение воздействия на процесс упрочнения глинистых грунтов движения потока не в соответствии с законом Дарси в случае исключительно только радиальной системы фильтрации, а также в случае совместного радиального и вертикального

систем фильтрации. Это определение производится при принятии за основу такой целесообразно общей четырехпараметричной зависимости градиента скорости, которая при правильном выборе параметров пригодна для характеристики большой части сообщенных результатов, касающихся движения потока воды в глинистых грунтах, и при совместном использовании этой зависимости и прочими обычными предположениями обычной теории упрочения для вывода некоторого нелинейного параболического парциального дифференциального уравнения, который последний можно решить с помощью применения метода конечных разностей. Ряд типичных решений показывает, что протекание упрочнения во времени в отношении таких грунтов, в случае которых можно установить свойства движения потока, не удовлетворяющих закону Дарси, имеет значительно меньшую скорость, чем которую можно определить на основе обычной теории упрочнения. Несмотря на то, что двумерная задача движения потока может быть решена числовым методом легко при применении некоторой эксплицитной формулы конечных разностей, все-таки строгие условия устойчивости такое решение делают слишком дорогим.

Acta Technica Academiae Scientiarum Hungaricae, Tomus 82 (1—2), pp. 121—168 (1976)

EXPERIMENTAL INVESTIGATION OF THE LIFE OF SEMICONDUCTOR DEVICES, III.

BULK BREAKDOWN MECHANISMS AND TRANSISTOR LIFE TESTS IN SWITCHING OPERATION

Á. P. KEMÉNY*

[Manuscript received October 15, 1973]

The generally used methods of prolonged d.c. operating life tests of transistors, which provoke mainly the thermally activated surface degradation phenomena, give little information on the deterioration in switching operation. A method is proposed where the transistors are loaded as common base inverters in switching operation with fixed 50 Hz or higher repetition frequency, at exactly controlled and determined swithing- on and -off transient energy. This method permits the economical examination of large samples and is useful mainly as a *screen* test for the quick selection of individuals with hidden structural defects. Such tests supported by microphotographs of failed samples seem to be in accordance with the analytical results of a bulk degradation process treated here and emphasize the necessity of a flawless geometrical structure of such devices.

1. Introduction

Transistor life expectancy in switching service is an important area especially in the development of digital circuits, e.g. second generation computers or solid-state telephone centrals where transistors are used in big lots. Though the method of life testing of transitors employed in analog circuits were well-known [1—10, 17] and widely used (utilizing the continuous or interrupted d.c. electrical stress), they do not give really useful information of the failure rate of a transistor type used in switching service. Surely, the failure rates gained in a d.c. electrically loaded operation or simply in a thermal stress are too loosely related to the degradation in switching operation mode, although some correlation undoubtedly exists.

Obviously, the best solution would be the life testing conducted in switching operation. However, some obstacles arise there as may be summarized in the followings.

In the d.c. electrical stress the results gained at a given collector dissipation (i.e. junction temperature) and at a given collector reverse voltage, may be converted into failure rates valid at a different junction temperature (dissipation) or at a different collector voltage, aided by a relatively simple Arrhenius-

Dr. Á. P. KEMÉNY, Rajk L. u. 48, H-1136 Budapest, Hungary

type formulae, well-known in the practice and describing the relationship among the failure rate, the junction temperature and the collector voltage [1—9, 17]. This relationship is well-established by numerous experimental data and it is proved that degradation in analog (e.g. in d.c.) electrical operation is related to surface phenomena activated by the elevated temperature and by the reverse voltage of the collector diode [1—10, 17]. Hence, life tests executed in analogous (d.c.) operation may be standardized: it is sufficient to make the experiments at a given single — usually high — temperature and voltage level and all failure rates in differring conditions may be reduced to the one gained from the standardized unique test [8, 9, 10, 17].

The situation is quite different with the switching service life testing because an almost infinite variety of stress conditions may be imagined since degradation is influenced by repetition frequency, duration of turnover transients (rise and fall time), further by the applied collector voltage and collector current stress levels, let alone the ambient temperature and collector circuitry (resistive or inductive load). One can conclude that standardization of switching service life tests seems to be a hopeless aim. This statement is confirmed by the fact that recently no interrelation is known among failure rate and the previous parameters and the experiments presented in this article proved to still be insufficient to draw a well-estiblished numerical relationship between failure rate and stress parameters, obviously because the number of tests conducted and of the tested transistors, were too few. The work dealt with here is meant to be the first step.

To overcome the problem of "standardization", one may suggest always to make the tests in the circuit where the transistors are used, under normal or forced operational conditions. If a transistor type is used in a great number of identical or nearly identical digital circuits, e.g. in a computer, this seems to be an adequate solution and the life tests may be conducted by the equipment manufacturer as well as by the transistor manufacturer. This is the situation especially at highly complex IC-s where operation mode (supply voltage, temperature etc.) is standardized.

But what can the transistor manufacturer do if a given type is specified for a wide variety of applications generally used in switching service? Naturally, circuit-development engineers need some general data of reliability if making a choice among various makes or types. Hence, some form of "standardization" in switching service life-testing seems inescapable.

A relatively simple but still efficient method is suggested here where the tested transistors are operating on a common base inverter circuit with resistive load, since most pulse circuits may be originated from the plain transistor inverter. For the sake of simplicity, a repetition frequency equal to the 50 Hz mains frequency was chosen at the low switching-rate types (e.g. alloyed ones) and 5 kHz for high-speed (mesa or planar) types.

Comparative test results had shown that at normal or low pulse current stress levels the degradation processes were indistinguishable from the processes occurring in a d.c. electrical stress. However, by high stress levels, usually beyond data-sheat limit values of $I_{C\,max}$, truly volumetric degradation causes were beginning to play the leading role, obviously originating from structural irregularities in geometry or material constants. Thus, the pulsed life testing method presented here finds its use mainly as an accelerated *screen-testing* method to sort out transistors inherently poor in life expectancy, due to structural faults. Nevertheless, it was proved that some puzzling failures, occurring in the switching service still within data-sheet limits and unexplainable by d.c. parameter measurements as well as by life tests conducted in d.c. electrical or in elevated-temperature storage stress, may find their explanation in inherent structural failures. These failures leading to the occurrence of hot-spots-formation and hence punch-through in the transistor bulk, may fully develop in the test method given here in the followings. Surface phenomena, on the other hand, have no significant importance on switching service degradation.

2. Basic degradation causes

Information gained from experiments which will be dealt with later,had shown that in switching circuits the average dissipation (and hence the average junction temperature) plays but a minor role in the degradation or deterioration of the transistors. This picture is in contrast with the one ruling degradation processes in analog or d.c. service where junction temperature is of main importance. Maximum collector ($\cong$ emitter) current and maximum collector voltage have, on the other hand, a very important but indirect influence. The main cause of deterioration, as was proved, is the occurrence of "hot spots" i. e. elevated-temperature- zones in some minute volumes along the junction, due to the very high transient energy peaks during the transition [turning-over from the saturated (switched-on) state to the cutoff (switched-off) condition or vice versa]. A calculus of these turnover transient energies will be presented later, in Section 6.

Since Ge or Si semiconductor materials have rather good heat conductive properties, the temperature gradient along the junction is practically zero at a continuous (i.e. at d.c.) electrical load in the d.c. electrical life testing. The situation is quite different at the switching service life test, where a brief but large energy peak occurs at the turnover.

As will be explained in the subsequent paper in this series [22], the temperature increase due to the turnover transient lies in the order of some tenth °C . . . some °C considering a fair plane-parallel structure with even current distribution along the collector (and emitter) junction, in spite of the huge turn-

over power, because the heat source — actually the collector depletion layer — is excellently cooled by its surroundings in the semiconductor wafer. What counts here, is the energy of the turnover transient divided by the thermal capacity of the wafer's volume section heated up by the transient and, on the one hand, this thermal capacity is rather large; and the heated-up volume section extends on both sides of the laminar collector junction as the square root of time, on the other, which means that the longer a turnover transient, the worse will be the cooling properties of the wafer. At the brief turn-on and turn-off times of a usual transistor, however, the cooling properties of the wafer for a brief transient thermal thrust remain excellent and this explains the amazingly low temperature jumps in a perfect structure.

This advantageous picture, however, is spoiled by the fact that a junction is scarcely perfectly plane-parallel and free from resistivity inhomogeneities, hence a current concentration takes place preferently at the loci of these irregulaties where enormous current density (approximating still 10^4 A cm^{-2}) comes into existence causing the formation of hot spots and leading to a punch-through between collector and emitter or a breakdown between base and collector. Thus, the peak instantaneous power amplitude and the duration of turn-over transient play the main role in switching service degradation.

Let us imagine the situation during and after the turn-over from the saturated state to the cut-off state. If there is a geometrical irregularity of the collector-base junction where the base layer width is narrower than in the remaining junction area, i. e. the junction barrier has a curvature showing toward the base, the current density pattern will be uneven and the emitter current will be concentrated into this tiny area of irregularity, causing an overheating in a minute volume in the very vicinity of the junction, within the base region. The same situation occurs when instead of a geometrical curvature, a speck of low-resistivity material is embedded in the high-resistivity base structure, near to the junction. The overheating is still significant in the saturated (switched-on) state but will be tremendous during the turn-over transient within an arising hot-spot, if the collector current level is high enough. After the turn-over, the transistor gets in cut-off state and the V_{CB} reverse collector voltage appears on the junction, causing the reverse current I_{CBO} to flow. Since the reverse current is exponentially proportional to the junction temperature, the reverse current will be highly increased in the zone of inhomogeneity, causing the reverse power dissipation (during cutoff) to rise significantly, hence heating the device further in the hot-spot region. In other words, the formation of hot spots and the increased reverse current flowing through them counteracts cutoff and leads inescapably to a cumulative thermal-electrical feedback process, or thermal runaway and, consequently, the temperature may reach the melting point of the semiconductor material within the minute volume of the hot spot, and hence, alloying goes further

toward the emitter junction : the highly doped collector zone advances toward the emitter, and the base zone width will become gradually narrower. The gradual advance of the highly doped collector zone will terminate in a complete short at the instant when the barrier of the collector depletion layer reaches the emitter junction barrier, that is the V_{pt} punch-through voltage of the transistor, after a gradual decrease, reaches and falls short of the applied collector voltage.

The failure process described above [11, 12] creates a pinhole-like narrow channel in the base consisting of the highly doped material of the collector. This is the unambigous situation if the base layer consists of a lightly doped (high-resistivity) material, e.g. in the case of an alloyed transistor structure (see Insets 1 and 2). If the structure is reversed, as in the case of a planar or mesa transistor where the collector zone is made of a high-resistivity material, the advance of the low-resistivity base zone toward the collector takes place. If the collector zone is a relatively narrow epitaxial layer of high-resistivity material and a low-resistivity collector contact zone follows, the situation will be the same as dealt with earlier but in the reverse direction: the advance of the low-resistivity material through the collector zone (toward the collector contact zone) will stop if the remainder of the epitaxial collector zone width will be equal to the collector depletion layer width at the given V_{CB} collector voltage. After this event, the width of the depletion layer will gradually become narrower and finally the breakdown of the collector diode takes place: a short between base and collector, also in the form of a narrow pinhole-like molten and recrystallized channel through the epitaxial layer (see Inset 4 in the Appendix).

If the planar or mesa structure is not an epitaxial one, the thermal runaway process will terminate — usually at relatively higher current levels, or later — in a complete melting-through of the structure, i.e. in a complete short, within a narrow channel [12].

Thus, the volumetric degradation previously described causes a new scale of catastrophic failures, which in turn causes the punch-through of the transistor structure, not known in d.c. electrical life tests [10, 11, 12]. The unique degradation-type failure which may occur due to the above volumetric causes, is the significant decrease of the V_{pt} punch-through voltage, when the base layer is made of a high-resistivity material (alloyed transistor). This phenomenon precedes the complete punch-through by a short time and hence, there is little probability to catch a specimen by V_{pt} measurement, where the punch-through voltage was decreased to some volts from some hundred volts. In the other case, if epitaxial planar or mesa types are tested, the gradual decrease of the epitaxial collector zone width will lead to the occurrence of a sensible decrease of the BV_{CBO} volumetric breakdown voltage, which latter may easily be measured by pulsed methods [13, 14].

To explain the events of the decrease of the punch-through voltage, and the occurrence of complete punch-through or breakdown numerically, the well-known relationship the V_{CB} collector voltage, the field strength E_M and the depletion layer width X should be introduced:

$$E_M = \left(\frac{2qN_1}{\varepsilon_r \varepsilon_0} \cdot V_{CB} \right)^{1/2} = \frac{qN_1 X}{\varepsilon_r \varepsilon_0} = \frac{X}{\mu \varrho \varepsilon_r \varepsilon_0} \tag{1}$$

where:

E_M = maximum field strength within the depletion layer at the metallurgical junction, in V/cm; q = charge of electron, that is $-1{,}6 \times 10^{-19}$ Asec; N_1 = the net impurity concentration in the lightly doped layer in cm^{-3}; ε_r = the relative dielectric constant of the semiconductor material (16,5 for germanium and 12 for silicon); ε_0 = the dielectric permittivity of the void space, that is $8{,}86 \times 10^{-14}$ Asec/Vcm; μ = majority carrier mobility in cm^2/Vsec in the lighter doped side; ϱ = resistivity of the lightly doped side in Ohm cm; X = width of the depletion layer in cm.

If a breakdown of the collector diode takes place (e.g. at an epitaxial planar or mesa structure) then $V_{CB} = BV_{CBO}$ and $E_M = E_{MB}$, further $X = X_B$, thus

$$X_B = \left(\frac{2\varepsilon_r \varepsilon_0}{qN_1} BV_{CBO} \right)^{1/2} = \sqrt{2 \varepsilon_r \varepsilon_0 \mu \varrho \, BV_{CBO}} \tag{2}$$

will be the critical width of the remaining collector zone in an epitaxial planar or mesa structure, when a gradual narrowing of this zone takes place due to hot-spot formation and the base-collector barrier advances toward the low-resistivity collector contact during the switching service operation. Obviously, when the BV_{CBO} voltage gradually decreases and finally reaches the applied V_{CB} voltage, the breakdown and the destruction of the transistor takes place (provided that collector current is not limited by R_C to a safe low V_{CC}/R_C value).

In the case of an alloyed transistor where the highly doped collector zone penetrates through the base zone during the switching service stress in the narrow cross section of an occurring hot spot, the critical base layer width (equal to the critical depletion layer width) will be at complete punch-through, using equation (1):

$$W_{B\,\mathrm{min}} = X_{\mathrm{crit}} = \left(\frac{2\varepsilon_r \varepsilon_0}{qN_1} V_{pt} \right)^{1/2} \tag{3}$$

where $V_{CB} = V_{pt}$, the critical punch-through voltage will be then equal to the applied collector voltage. During the actual life test measurements, especially by power transitor types having a large collector junction area and just before complete punch-through, a rate of $W_{B\,\mathrm{average}}/W_{B\,\mathrm{min}} \geq 10$ could be identified on specimens having an excessively inhomogeneous structure. The electrical measurement of $W_{B\,\mathrm{average}}$, the mean base width of the "sound" portion may be accomplished by alpha-cutoff-frequency measurement [11],

while the actual "minimum" base width of the defective portion can be computed on the basis of equation (3) by punch-through voltage measurement, if $V_{pt} < BV_{CBO}$.

3. Peak temperature during commutation

Let us deal with the problem of the peak temperature jump during commutation which is of paramount importance. To attack this sophisticated thermodynamical problem, a lot of neglections or approximations must be considered, as was the situation in ref. [22], i. e., the following paper of this series where an analysis and some numerical examples are presented.

First of all, the question arises whether or not the heat generated during the huge turnover transient causes a serious warming-up of the device. This depends primarily on the thermal capacity of the heated-up volume in the semiconductor bulk, till the heat-flow reaches out at the end of the the turnover transient. It is surprising on first consideration, how large this "inner" thermal capacity actually is which plays a role at the brief process of turnover, contrary to the customary concept, and in spite of the fact that this volume section along the laminar heat source, i. e. the collector junction, is actually rather small. In fact, the boundaries of elevated temperature due to the high turnover transient energy hardly leave the thin collector depletion layer during the commutation, since the velocity of heat conduction is surprisingly low also in solids, e. g. conductors or semiconductors with good heat-conductive properties. Speaking the language of solid-state physics, the highest propagation velocity of a disturbance in a solid is the velocity of sound due to phonon-to-phonon interactions in the crystal lattice, that is, some 10^3 m/sec in metals, since this kind of disturbance of the crystal lattice is "oriented". However, the propagation velocity of heat conduction (as well as electrical conduction) is less by orders of magnitude, lying in the order of some (or split) m/sec, since the vibration of metal atoms in the crystal lattice is a random movement (a stochastic process). Moreover, the heat propagation velocity is not a constant as the sound propagation velocity but is proportional to the thermal gradient [19—21] which means that during the advancement of heat conduction, after a brief thermal thrust, this thermal gradient will be gradually less and less as the heated-up volume section extends and, consequently, the thermal conduction velocity will also be gradually slower. In other words, *the thermal propagation velocity is inversely proportional to the square root of time*, i. e., the switchover transient duration, as may be proved by the solution of the thermal conductivity differential equation [19—22]. No wonder then that the heat cannot spread widely in the semiconductor bulk during the brief switchover transient of some nanosec to some μsec duration and the bounds of elevated temperature remain well within, or but inconsiderably exceed, the depletion layer width, the latter mounting up to some μm at a usual voltage V_{CC} lying in some 10 V order of magnitude. Despite this tiny volume (approx. the product of X and junction area A), its thermal capacity is rather high and so the temperature jump is rather small. For a quick survey of conditions, three examples are given in Table 1 regarding a minute TTL—IC totem-pole (output circuit) transistor, a medium-power silicon planar transistor BSY 34 and a bulky germanium alloyed power transistor ASZ 18, the computation methods for the determination of the heated-up volume being presented in ref. [22].

The estimation of peak temperature jump due to the commutation transient energy goes ahead with the afore mentioned assumptions quite simply: it would be the turnover energy divided by the product of the volume of collector depletion layer [more accurately, the afore mentioned volume $V_{\vartheta(i)}(t = t_{\text{off}})$ in which the elevated temperature occurs till the end of the transient] and the specific density and specific heat of the semiconductor material in question, as is shown in Table 1 and in the analysis and numerical examples of ref. [22].

The following conclusions may be drawn from the numerical examples in Table 1:

(i) At the very low switching power rates of a digital IC, i.e. at some V and some mA levels, the turnover energy is also very low, leading to *turnover temperature jumps only in the* $10^{-4} \div 10^{-2}$ °C *order of magnitude* assuming a

Table I

Thermal relations during switching-off of some typical transistors

Transistor type	TTL IC (totem-pole) (e. g. SN 7400 N)	BSY 34 npn epitaxial planar silicon, medium-power	ASZ 18 pnp alloyed germanium low-speed, high power
Junction area, A_{nom}	$1{,}2\times10^{-3}$ mm^2	0,25 mm^2	5 mm^2
Supply voltage, V_{CC}	5 V	40 V	−30 V
Peak switching power, $P_{dt\,max}$, cf. Eq. (12)	20 mW	5 W	45 W
Switching-off time, t_{off}	5 *n*sec	0,5 μsec	35 μsec
Total switching-off energy, L_{off}, cf. Eq. (9)	~0,1 *n*Wsec	0,475 μWsec	1,67 mWsec
Heated-up volume section, $V_{\vartheta(i)}(t=t_{off})$ during switch-off, till $t = t_{off}$*	$\sim2\times10^{-6}$ mm^3	2×10^{-3} mm^3	0,66 mm^3
Thermal capacity of $V_{\vartheta(i)}$ volume section $C_{\vartheta(i)}(t=t_{off}) = \gamma c_\vartheta V_{\vartheta(i)}(t=_{off})$**	~3,5 nWsec/°C	3,5 μWsec/°C	1,08 mWsec/°C
Max. temperature jump during turnover $\Delta\hat{T}_{m(off)}=L_{off}/C_{\vartheta(i)}(t=t_{off})$***	~0,029 °C	0,135 °C	1,46 °C

*See ref. [22].

**γ stands for specific density: 2,3 g cm^{-3} for silicon and 5,3 g cm^{-3} for germanium; c_ϑ denotes specific heat: 0,735 Wsec g^{-1} °C^{-1} for silicon and 0,31 Wsec g^{-1} °C^{-1} for germanium.

***Assuming an even current distribution without appreciable current concentration.

fair structure. Consequently, *at digital IC-s the effect of transient turnover energy plays but a negligible role*, and shorts occuring there during switching or d.c. operation, though advancing by "hot-spot" mechanisms too, are caused by other phenomena, e.g. slow spurious diffusion of the dopant or contacting metal through "pinholes" in the thermally grown SiO_2 layer due to photolithography failures [23], see Insets 6 and 7.

(ii) *The peak temperature jumps are low or quite negligible (some tenth of a* °C*) at low-power devices assuming a structure of perfect or near-perfect geometry and homogeneity*; whilst

(iii) *At power types with a fair structure, the temperature rise due to the turnover transient might be significant* (some °C) which *can be described, contrary to a larger junction area, to the fact that the advantages of the good "static" (d.c.) cooling of the case get lost totally at the very brief turnover duration and what really counts here, is the many times higher turnover power of some ten V and some A switching level*, quickly heating the depletion layer having here a volume not essentially larger (e.g. only by a factor of 5 to 50) than in a low- or medium-power device. This is the reason that the power transistors are more likely prone to switching service deterioration, the larger junction area and thus a higher probability of structural defects here play only a secondary role.

Such mild overheating as occurs at geometrically perfect and homogeneous structures spreading evenly in the whole volume of the collector depletion layer, cause but little harm. The really dangerous case is if there is a strong tendency for current-flow concentration, due to a structural imperfection. Then the energy of turnover transient concentrates in a considerably less volume, causing there a temperature jump inversely proportional to the real volume involved in current flow (so in heat generation), *as compared to the whole volume of depletion layer.* A concentration ratio of 10^3, or even more, can be considered as not a too rare event, hence, the temperature may rise to some 100 °C or greater by a thermal runaway process, leading to a melting-through of the semiconductor material in the "hot-spot's channel" and finally, to total destruction.

4. Volumetric failure mechanisms due to bonding and contacting

At high-current levels the voltage drops across the "lead-in" spreading resistances of the transistor will be considerably increased, so V_{EB} due to r_E; $V_{CB\text{sat}}$ due to r_C; finally, both voltages due to $r_{BB'}$ base spreading resistance. Thus, in turned-on (saturated) state the instantaneous power loss

$$I_{Ep}^2[r_E + (r_{BB'}/h_{FE})]$$

on the emitter side, while

$$I_{Cp}^2[r_C + (r_{BB'}/h_{FE})]$$

on the collector side will be significant if the lead-in resistances increase during the operation due to contacting degradation. At planar and mesa types the increase of r_C collector-side contact resistance is rare since this contact consists of the soldering-on of the wafer onto the header with gold. All the more important are the failures of the base and emitter contacts due to the well-known "plague" of these thermo-compression Au—Al bonds (see Insets 3 and 5), i.e. the occurrence of Au Al_2, AuAl, Au_2 Al, Au_5Al_2, and Au_4Al intermetallic compounds which are still good conductors but mechanically brittle and full of voids due to volume changes and so structurally weak [9, 10]. The situation due to such contact-plague failures is still more serious at pulsed life tests while the plague process is temperature-activated and so an uneven current distribution at the bonding, especially at the high current level of the emitter contact, leads to a further source of "hot-spot" formation and to the rapid development of a cumulative plague process until the contact will be completely broken. This is another family of "volumetrically originated" failures where instead of the average temperature, the temperature of the "hot spot", thus indirectly, again the current level plays the first role.

The main difference as compared to other "volumetric" failure mechanisms is at such "contact-plague hot-spot" degradation processes that the t_p duration of the switched-on (saturated) state (i.e., the pulse duration) and so the $t_p f_r$ duty cycle are no longer unimportant since the thermal energy developing the contact failures is directly proportional to t_p, and so is the average power proportional to the product $t_p f_r$. Consequently, the executed testing equipments are provided with a pulse duration control where t_p pulse duration can be varied in a ratio of 1 : 4 and, moreover, these equipments which will be dealt with later have been constructed in two different versions, namely, one for low-speed alloyed transistors where t_p ranges between 150 ÷ 500 μsec and another for high-speed planar types exhibiting a 1,5 ÷ 5 μsec pulse duration range. In the Appendix some life test results are shown applying both kinds of transistors and especially of the experiment (*f*) where a planar epitaxial transistor type exhibiting serious technological imperfections, e.g. plague-afflicted bonding, was tested and a surprisingly high portion failed because of broken emitter (see Table V) if the tested lot of 480 pcs was subjected to a low-frequency, high switchover-energy testing alternative using $t_p = 200$ μsec: 136 of 480 failed in this manner, obviously (at least partly) due to the afore mentioned "contact-plague hot-spot" volumetric degradation (see also the emitter contacts badly afflicted by intermetallic formation in Inset 5, especially SEM pictures *b*, *c*, and *d* where the bonds were completely detached). Contrary to this, if the high-frequency, low switchower-energy test alternative with $t_p = 5$ μsec had been made use of, in another lot of 480 transistors taken from the same batch only 1 failed for broken emitter.

Another family of volumetric failures frequently occurring in the minute transistor structures on monolithic ICs [23] due to pinhole-caused shorts, is shown in Insets 6 and 7.

5. Basic principles of the test method

Since the energy of turn-over transients is of the greatest importance by switching service life tests, both magnitude and duration of these transients must be held so constant and reproducible during the test, while the repetition is held automatically constant at 50 Hz mains frequency for the low-frequency alloyed types or higher (e.g. 5 kHz) for high-frequency types.

One may suggest, too, that varying the duration of the turnover transients (naturally with exact reproducibility) seems to be a convenient means for the alteration of the transient energies. This idea was put into practice by the executed life testing apparatus.

The turn-on and turn-off states are not identical in all respects from the degradation point of view, though theoretically both transient energies are the

same if rise time and fall time are equal. As was stated in the Section 2, the situation is more critical at the turning-off transition since then a high reverse voltage V_{CB} appears and larger-than-normal reverse current flows through the "hot spots" leading to local thermo-electrical feedback and finally to the punch-through or breakdown of the device.

If current density, reverse voltage, further the duration and the repetition frequency of the turn-off transients are all sufficiently high, this degradation process will be accelerating rapidly on devices having a poor structure, as is described in Section 2.

In the applied test method, therefore, the amount of turn-off transient energy, i.e. the duration of this transition, was chosen to be much greater than the duration of the turn-on transient. On the other hand, this energy must be held exactly constant during test and be made variable between wide limits and with fair reproducibility.

If turn-off (as well the turn-on) time was made much longer artificially than the spontaneous switching-off time (and switching-on time) of the tested transistors in the given inverter test circuit, the aim is acquired. This condition can only be accomplished in a common base circuit configuration where the transistor's spontaneous switching-on and -off times are much shorter than in a common emitter circuit.* The relatively long turn-over transient times are compelled to the tested transistors by the emitter current pulse generator. Thus, the common base configuration was chosen despite a much higher pulse generator output current demand. By this method the interference caused by the spread of spontaneous switching times of the tested transistors in the circuit, are avoided.

Fig. 1 shows the basic schematic test circuit and the wave form of pulse which drives the tested transistors into the saturated (turned-on) condition. A heavy-duty transistorized pulse generator in series with the individual R_E emitter resistors acts as an emitter current generator. The collector circuit containing individual collector resistors R_C and a common, high-current, V_{CB} supply.

The repetition frequency of the driving pulse equals the 50 Hz mains frequency for a simple outfit of the pulse generator. The pulse wid this continuously adjustable between 150 and 500 microseconds. The turn-on time is held at a constant 10 microseconds value, whilst the more important turn-off time is adjustable between 10 and 100 microseconds in 24 fixed and calibrated steps. This setup was used for low-switching-rate, alloyed Ge transistors. — Another construction served for the testing of high-speed planar and mesa types with an adequately higher repetition rate of 5 kHz, a fall time adjustable between 0,1 and 1 μsec, a fixed rise time of 0,1 μsec and with a pulse duration variable between 1,5 and 5 μsec.

*Actually, by a factor of approx. $1 + h_{fe}$.

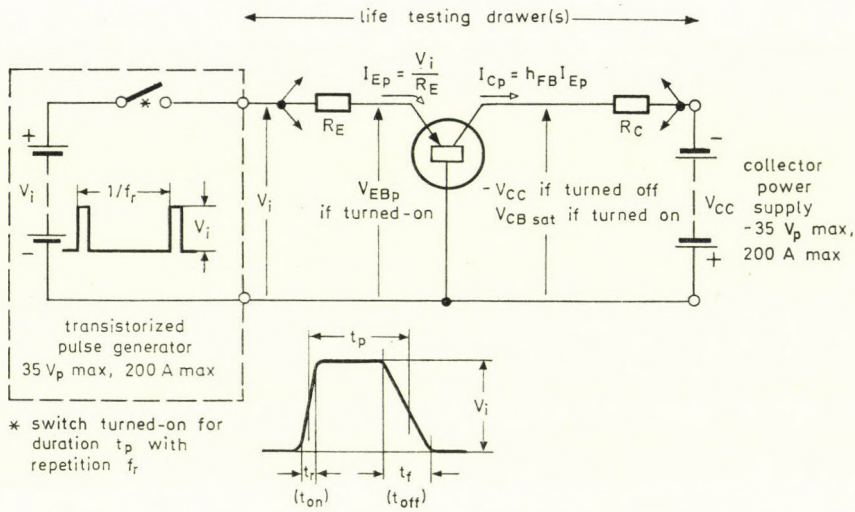

Fig. 1. Basic schematic circuit of the suggested switching-mode life testing equipment and characteristic voltage (and current) wave forms of the emitter current pulse generator. The testing of a p-n-p type transistor is depicted here. For n-p-n transistors, all polarities should be reversed

6. Calculus of the transient power and energy during commutation

The quasi-stationary dissipated power in the saturated (turned-on) state $(V_{CB\,sat} + V_{EBp})I_{Cp}$, averaged to the full period time is, using here the approximation $I_{Ep} \simeq I_{Cp}$, see Eq. (6), with h_{FB} current amplification factor not considerably less than unity:

$$\overline{P_{on}} = t_p f_r (V_{CB\,sat} + V_{EBp}) I_{Cp}\,, \tag{4}$$

since in the saturated state both voltages $V_{CB\,sat}$ and V_{EBp} on the collector and emitter junctions are forward-directed and being in the same order of magnitude (0,3 ÷ 1,5 V), thus both causing significant power loss.

Similarly, in the cut-off (turned-off) state the averaged quasi-stationary dissipated power will be

$$\overline{P_{off}} = f_r V_{CC} \int_0^{2\pi} I_{CBO}(t)\, \mathrm{d}(\omega t) \cong V_{CC}\, I_{CBO}\,, \tag{5}$$

by the latter assuming that I_{CBO} reverse current is constant in time, and the device is not in a thermal runaway condition, further that the $t_p f_r$ duty cycle is low, i.e. $t_p f_r \ll 1$, otherwise Eq. (5) should be multiplied by $(1 - t_p f_r)$. Here t_p is the duration of the current pulse (i.e. the duration of the turned-on time), f_r the repetition frequency, $V_{CB\,sat}$ is the saturation voltage of the turned-on transistor (up to about 1,5 V), V_{CC} is the collector supply voltage and, finally,

I_{Cp} is the collector current amplitude in a saturation state, and may be computed as

$$I_{Cp} \cong h_{FB}\, I_{Ep} \cong [h_{FE}/(1 + h_{FE})]\, I_{Ep} \tag{6}$$

and $I_{Ep} = V_i/R_E$

where V_i is the output voltage amplitude of the pulse generator (here it is usually 25 volts).

The value of the collector resistor R_C cannot be assumed to be independent, since

$$R_C = \frac{(1 + h_{FE})\, V_{CC}}{h_{FE}\, I_{Ep}} \tag{7}$$

and at the very high emitter current of the life test, h_{FE} is not yet markedly greater than unity, thus

$$h_{FB} = h_{FE}/(1 + h_{FE})$$

is significantly less than unity (e.g. about 0,8 to 0,95).

In this wise one may draw the conclusion that both quasi-stationary losses $\overline{P_{on}}$ in saturated state, and $\overline{P_{off}}$ in cut-off state are negligible in comparison to the turnover transient power losses, since in Eq. (4) in the saturated state $V_{CB\,sat}$ is very low, though the full current I_{Cp}, is flowing, while in the cutoff state I_{CBO} is very low (at least compared to I_{Cp}), though V_{CC} supply voltage is usually high. To prove this, let us calculate the turnover transient energies and powers, using the exponential approximation of switchover-transient currents and voltages.

The amount of transient energy at each turning-off commutation, integrating the product of the exponential voltage and current vs. time functions displayed in Fig. 2, between the normalized time boundaries 0 and t/τ_0 and multiplied by τ_0, will be:

$$L_{off}(t/\tau_0) = \tau_0 \int_0^{t/\tau_0} I_C\left(\frac{t}{\tau_0}\right) V_{CB}\left(\frac{t}{\tau_0}\right) d\left(\frac{t}{\tau_0}\right) =$$

$$= \frac{\tau_0\, V_{CC}^2}{R_C} \int_0^{t/\tau_0} \left\langle \exp - \frac{t}{\tau_0}\left(1 - \exp - \frac{t}{\tau_0}\right)\right\rangle d\frac{t}{\tau_0}\,;$$

and after the integration

$$L_{off}(t/\tau_0) = \frac{\tau_0\, V_{CC}^2}{2\, R_C}\left[1 + \exp\left(-\frac{2t}{\tau_0}\right) - 2\exp\left(-\frac{t}{\tau_0}\right)\right]. \tag{8}$$

Obviously, the energy of the turn-on transient has the same form except that the τ_i turn-on time constant must be substituted instead of τ_0 turn-

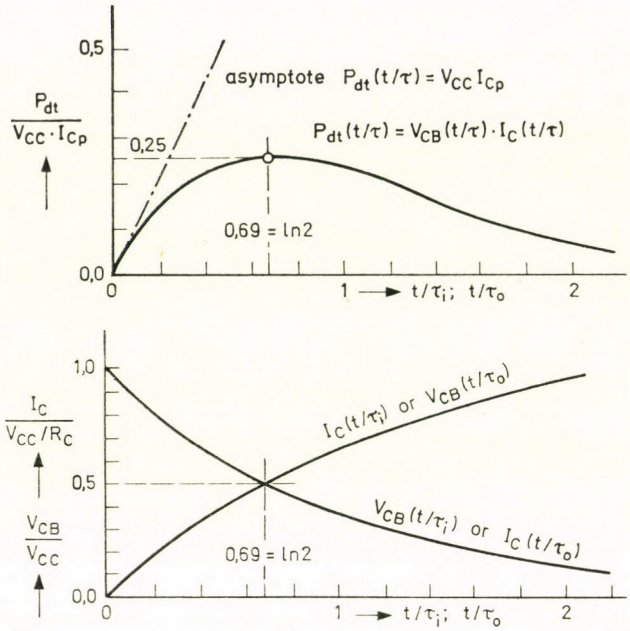

Fig. 2. Characteristic time functions of the turn-over transients. Time is normalized in t/τ_i and t/τ_0 terms. Lower diagram: exponential rise or fall of collector current (I_C) and collector voltage (V_{CB}) in $I_C R_C/V_{CC}$ and V_{CB}/V_{CC} normalized terms. The peak transient power appears when both current and voltage are at the half of their quasi-stationary final amplitudes at the normalized time instant of $t/\tau \cong 0{,}69 \cong \ln 2$. Upper diagram: the time function of the instantaneous power, $P_{dt}(t/\tau)$

off time constant. The expression (8) will than give at $t = \infty$ (or, more practically, with $t \gg \tau_0$)

$$L_{\text{off}} = \tau_0 V_{CC}^2/2\, R_C = \tau_0 V_{CC}\, I_{Cp}/2 \tag{9}$$

for one single turn-off commutation process, which can be in turn *a tremendous amount of energy*, especially at high switching power levels.

The instantaneous power of the turn-off transient may be gained as the product of instantaneous $I_C(t/\tau_0)$ and $V_{CB}(t/\tau_0)$ exponential time functions of Fig. 2, as

$$P_{dt\,\text{off}}(t/\tau_0) = \frac{V_{CC}^2}{R_C}\left\langle \exp\left(-\frac{t}{\tau_0}\right)\left[1 - \exp\left(-\frac{t}{\tau_0}\right)\right]\right\rangle = \\ = \frac{V_{CC}^2}{R_C}\left[\exp\left(-t/\tau_0\right) - \exp\left(-2t/\tau_0\right)\right]. \tag{10}$$

Differentiating this time function by t, the maximum value of $P_{dt\,\text{off}}$ will be where $\mathrm{d}P_{dt\,\text{off}}/\mathrm{d}t = 0$, hence

$$dP_{dt\,\text{off}}/dt = \frac{V_{CC}^2}{\tau_0 R_C}\left[-1 + 2\exp\left(-\frac{t}{\tau_0}\right)\right] = 0,$$

thus $2 \exp(-t/\tau_0) = 1$, and $P_{dt\,\mathrm{off}}$ has the maximum when

$$t/\tau_0 = \ln 2 \cong 0{,}6931$$

as can be seen in the upper diagram of Fig. 2 and further, in the instant $I_C(t) = I_{Cp}/2$ and $V_{CB}(t) = V_{CC}/2$. In other words, at the instant of the transient power peak both the collector current and the collector voltage are exactly at the half of their quasi-stationary maximal amplitudes.

Thus, substituting $\exp(-t/\tau_0) = 0{,}5$ into the function (10), the maximum value of the instantaneous power at each turnover (turn-on as well as turn-off) will be

$$P_{dt\,\max} = V_{CC}^2/4R_C = V_{CC}\, I_{Cp}/4, \tag{12}$$

which is a really considerable power peak if switching levels are high and for which the switching-service degradation can be blamed if this transient power peak concentrates in one or more of the minute volumes of "hot spots". This power surge occurs twice in every switching cycle: once at switching-on and once at switching-off.

Finally, the power of the turn-off transient, when averaged for the full $1/f_r$ period time, is equal to the whole energy of the transient in equation (9), multiplying it by f_r:

$$\overline{P_{dt\,\mathrm{off}}} = L_{\mathrm{off}} f_r = \tau_0 f_r\, V_{\mathrm{CC}}^2/2\, R_{\mathrm{C}} = \tau_0 f_r V_{\mathrm{CC}}\, I_{\mathrm{Cp}}/2. \tag{13}$$

It may be seen, comparing this result to $\overline{P_{\mathrm{on}}}$ in equation (4) and to $\overline{P_{\mathrm{off}}}$ in equation (5), that these quasi-stationary dissipated powers $\overline{P_{\mathrm{on}}}$ and $\overline{P_{\mathrm{off}}}$ can be in most cases (i.e. if switching power level is high) neglected, since $V_{CC} \gg V_{CB\,\mathrm{sat}}$ and $I_{Cp} \gg I_{CBO}$, though t_p pulse duration is larger (but only about with one or some orders of magnitude) than τ_0 turn-off time constant.

In Fig. 2 the lower diagram shows the exponential voltage and current time functions for both the turn-on and turn-off transients with the justifiable neglections $V_{CB\ \mathrm{sat}} \ll V_{CC}$ and $I_{CBO} \ll I_{Cp}$, both in normalized terms of V_{CB}/V_{CC} and $I_C R_C/V_{CC}$, in the dependence of time also normalized as t/τ_i or t/τ_0. These functions are e.g. for the turning-off

$$V_{CB}(t) = V_{CC} \exp(-t/\tau_0) \text{ and } I_C(t) = (V_{CC}/R_C)\,[1 - \exp(-t/\tau_0).$$

Since these functions are symmetrical in respect to $I_C R_C/V_{CC} = 0{,}5$ or $V_{CB}/V_{CC} = 0{,}5$ and also for the independent variables $t/\tau_i = \ln 2$ or $t/\tau_0 = \ln 2$ and in the previous equations always the product of current and voltage time functions are utilized, it may be seen that the end results in equations (9), (11), (12) and (13) are obviously valid for the turn-on transient too, only τ_i turn-on time constant should be written instead of τ_0, and naturally, L_{on}, $P_{dt\,\mathrm{on}}$ and $\overline{P_{dt\,\mathrm{on}}}$ should be meant.

Finally, let us seek for a numerical example choosing a low power, universal-use silicon epitaxial planar transistor* where $I_{Cp} = V_{CC}/R_C = 0{,}25$ A; $V_{CC} = -32\ V = V_{CB\,max}$, hence $R_C = 125$ Ohms. If $\tau_0 = 100\ \mu$sec is compelled by the pulse generator adjusted this way, the transient energy of one single turn-off transient will be, using equation (9)

$$L_{off} = \tau_0\, V_{CC}^2/2\, R_C = 10^{-4} \times 32^2/2{,}5 \times 10^2 = 4 \times 10^{-4}\ \text{W sec},$$

and this nearly one half mWsec is indeed a very large energy, taking the minute volume of some cubic microns of a hot spot into consideration.

The surge amplitude of the transient power, using equation (12), will be

$$P_{dt\,max} = V_{CC}^2/4\, R_C = 32^2/5 \times 10^2 = 2\ W$$

also many times exceeding the maximum d. c. power dissipation of 125 ÷ 250 mW of these given transistor types.

On the other hand, let us compute the quasi-stationary averaged power losses in the same type. With $V_{CB\,sat} = 1\ V = V_{EBp}$ and $I_{CBO} = 30\ \mu$A, $t_p = 250\ \mu$sec and $f_r = 50$ Hz. Eq. (4) gives at $I_{Cp} = 0{,}25$ A current level $\overline{P_{on}} = 6{,}2 \times 10^{-3}$ W and Eq. (5) gives $\overline{P_{off}} = 10^{-3}$ W.

Comparing these results to the averaged power originating from the turn-over transients and utilizing Eq. (13) with $\tau_i = 10\ \mu$sec and $\tau_0 = 100\ \mu$sec, this gives for both switching-on and -off transients together $\overline{P_{dt}} = 22 \times 10^{-3}$ W which latter in turn is higher by two orders of magnitude as compared to $\overline{P_{off}}$ and by half an order of magnitude as compared to $\overline{P_{on}}$. Thus, the latter quasi-stationary power losses cannot be neglected if there is a considerably high $V_{CB\,sat}$ or V_{EBp} voltage drop across the junctions due to serious contacting failures, e. g. contact plague;* and also if V_{CC} is relatively low, lying in the order of $V_{CB\,sat}$ (as is the situation e.g. at digital IC-s).

7. Some ideas on test principles

The question may arise here whether this concept of exactly equal switching-on or -off times from transistor to transistor, compelled to the tested specimens by an external pulse generator, is the right method of life testing. On the other hand, there is the life-test method where the given transistor type operates in a typical common emitter inverter circuit, e.g. in the test circuit given in the data-sheet of the type, and one makes use of a driving pulse generator having turn-over time durations much shorter than the transistor itself. This second method has, of course, some advantages as follows. Surely,

*E. g. npn types BC 108, BC 109, BC 172, BC 173, BC 238, BC 239, BCY 58, 2N 2368 and 2369; further pnp types BC 252, BC 253, BC 262, BC 308, BC 309, BCY78 and 2N 212 as well as alloyed Ge pnp types OC 72 and AC 125.

*Contact plague as a main failure cause, leading to an enhanced contact resistance and later to a complete open circuit, emerges at high temperatures after a prolonged operation at wire bonded contact systems of gold and aluminium (i. e., thermocompression bonds of Si and Ge, planar and mesa, technologies, thus also at monolithic ICs) by Au_mAl_n intermetallic formation, containing voids in an ever growing extent. This process has a characteristic activation energy of 1 eV.

the switching-on and-off times t_{on} and t_{off} have a significant spread by a given transistor type. A sample with large turnover times will certainly be subjected to a higher stress since the amount of transient turn-over energy is proportional to the switching-on and -off time in the given test circuit, cf. Eq. (9). Hence, a larger turn-over time will represent a larger proneness to more rapid degradation and deterioration. Putting the idea of this second test method into operation, individual differences in a spontaneous turnover time of the tested transistors are influencing the degradation processes and hence, long-run life tests conducted with this method will furnish results most exactly related to real inverter service, but, unfortunately, only in one single typical inverter circuit, thus far from any "standardization".

Another advantage of this testing concept is the use of a more simple driver pulse generator with significantly lower output power. However, the inability of this method to make significantly accelerated tests may be considered as a disadvantage, since turn-over times are determined by the tested transistor itself and only elevated collector current and collector voltage levels as well as repetition frequency and ambient temperature may be counted in for acceleration parameters but within very restricted limits.

The most adequate means for acceleration, the increasing of repetition frequency is hindered by the finite switching-on and -off times of the tested transistor. Rising of the V_{CC} supply voltage is obviously limited by the breakdown of the collector diode and, on the other hand, the increasing of I_{Cp} will lead to an enormous fall of h_{FE}, thus to an excessive driving power demand, not significantly less than in the common base circuit. Finally, as was previously stated, the elevated ambient temperature does not act as a main volumetric failure cause.

Let us deal with the method of compelling the turn-over transient times equally on the tested transistors and using a driving pulse generator with turn-over time durations much in excess of the spontaneous common base turn-over times of the tested transistors itself, i.e. the method chosen here. If one wishes to seek for the relationship between degradation (the failure rate) and transient turnover energy, this method seems to be more adequate, since the exact amount of turnover energy may always be computed with ease, contrary to the previous method where, due to the spread of individual turnover times of the tested transistors, this is impossible. On the other hand, acceleration of the test may easily be accomplished by the artificial elongation of the turn-off transient time, with really fair reproducibility.

Finally, though this method is not intended for giving characteristic failure rates of a given transistor type in switching service, the method seems to be an excellent means for sorting out samples with an inherently poor structure, i.e. as a good "screening" method and nevertheless as a quick comparison test for different batches or makes.

The method also tends to an easy "standardization" as a life test independent of circuit parameters and circuit characters, since all instantaneous peak and average powers as well peak transition energies may easily be computed and settled.

One can say that the proposed test method seems to incline toward excessive acceleration of degradation processes, since the artifically elongated turn-off transient time represents a too high stress on the tested transistors. Surely, the fall time adjustable between 10 and 100 μ sec is several times in excess of the spontaneous turn-over times of some tenth of a microsecond by a low-speed, alloyed transistor in c.b. circuit and this is the situation also with the $0{,}1 \div 1\,\mu$sec fall times compared to the c. b. turn-over times of high-speed, mesa or planar types which latter lie in the order of some nanoseconds. However, these turn-over times are much longer in c. e. circuit if no reverse bias is applied in the cut-off state onto the base circuit (for the quick removal of stored charges in the base region).

The employded artificial elongation of the turn-off time in one version of the executed life testing equipment, ranging from 10 to 100 μ sec, seems adequate for low-speed switching service transistors (e.g. alloyed ones), both for low-power and power types, although it is surely too long for high-speed switching types with thin base structures. The experiments, presented here later, were made predominantly on low-or medium-speed alloyed Ge types, but the concept was put into operation also with several times smaller turn-over times, according to high-speed planar transistor types too, as it was with the 5 kHz repetition frequency, $0{,}1 \div 1$ μ sec fall time version, cited earlier.

Obviously, the two different life test methods mentioned here, find their particular use for different aims and are not intended to replace each other.

8. Circuitry of the pulsed life-testing apparatus

The version for testing the low-speed alloyed transistors is dealt with here. The pulse generator (Fig. 3) uses a big storage capacitor C_S which is fully charged by the rectified a. c. mains voltage through a high-current transformer Trl, a silicon power rectifier diode D_{ch} and a low-valued charging resistor R_{ch}. The switching element is a transistor emitter-follower cascade (EFC), apt for the reliable switching of 200 A pulse current. This EFC switch (shown in the Fig. 3 within dashed lines) contains 4 stages, employing thoroughly cheap, alloyed Ge, low-speed power transistors.

The EFC is driven by a solid-state gate pulse generator shown at the bottom of Fig. 3. This generator serves gate pulses negative in respect to the common ground with mains frequency repetition and pulse durations adjustable between 150 and 500 μsec. The operation of the generator is similar to the one described in another work of the author [15]. The phase shifter R_p, C_p is necessary since it allows that the instant of the output pulse will coincide with the peak of the mains voltage, i. e. when the storage capacitor C_S is fully charged. Omitting the phase shifter, the instant of the output pulse would be around the zero transition of the a. c. mains voltage, since the driving pulse generator operates in such a manner, that the gate pulse front coincides with the zero-transition of the 50 Hz input voltage led to the base of the first stage T_1. Adjusting the optimal phase lag of 90 deg. by the potentiometer R_p, has the advantage that the charge of the output pulse only partly originates from the charge stored in C_S, the other half of it is gained directly from the high-current transformer secondary,

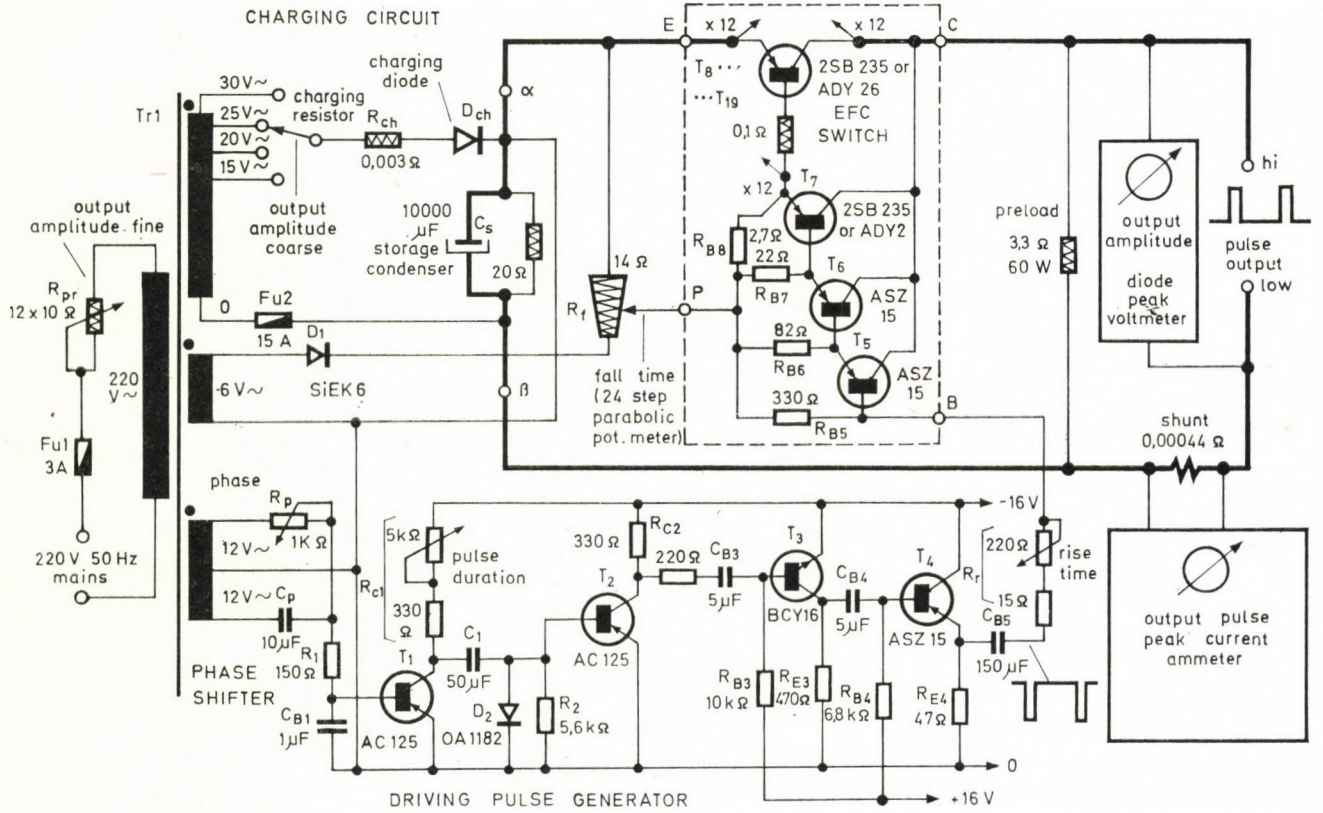

Fig. 3. Simplified circuit diagram of the 200 A, 25 V_p, transistorized pulse generator. The d. c. power supplies, the protection circuits and the "quadrupling" of some important components in Moore—Shannon-quad-type hammocks (for achieving very high reliability through redundancy techniques) are not shown. The "low-frequency" ($f_r = 50$ Hz) version is depicted here

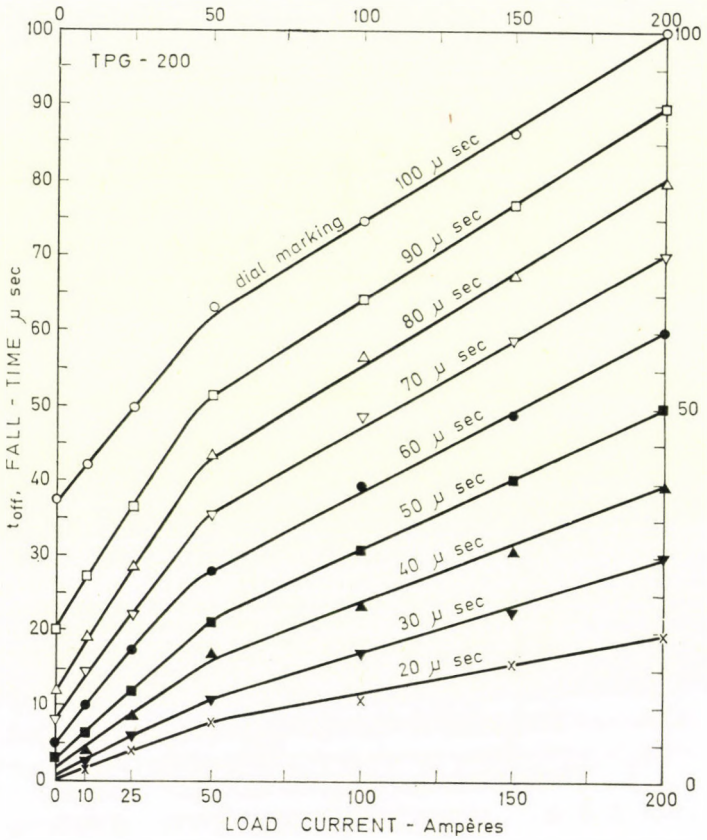

Fig. 4. Dependence of the fall time on the load current at the executed pulse generator TPG-200 (the 50 Hz version)

without the risk of severe ringing (attenuated oscillation) after the turning-on and turning-off of the EFC, due to the stray inductance of the transformer and circuit. However, the transformer's stray inductance, the C_S storage capacitor and the full series resistive component of the charging circuit (including the low-valued 0.03 Ohm extra resistor) is forming a circuit a bit beyond the aperiodic boundary condition. By this means it was achieved that a much smaller storage capacitor of 10 000 μF value reached out without perceptible ringing. The negative-going output-gate-pulse is led to the base input-point of the EFC through a C_{B5}, 150 μF coupling capacitor and the variable R_r series resistor, the latter serving as the control of output pulse rise time.

The fall time may be controlled by the variable amount of reverse bias applied on the bases of the EFC transistors. The fall time will be the longest when this reverse bias is zero, i. e. the slider of the 24-step potentiometer R_f (point P of the EFC) is connected to the common emitter point (E) of the EFC. The reverse voltage is connected to each base of the EFC stages by the R_{B5}. . .R_{B8} "draw-out" resistors. The operation of the fall-time control lies in the fact that the charge stored in the base zone of the turned-on EFC transistors and originating from the pulse current, can disappear after the turning-off only in a finite time. If there is no reverse bias applied, the disappearance of the stored charge occurs only by recombination, and the latter is a relatively slow process since the base zone is rather wide in alloyed types. When a reverse voltage is applied through a fairly low-valued resistor to the base, the stored charges are drawn-out the more rapidly, the higher the reverse voltage i. e. the larger the "drawing-out current" is. This is accomplished here by utilizing the potentiometer R_f, the latter having

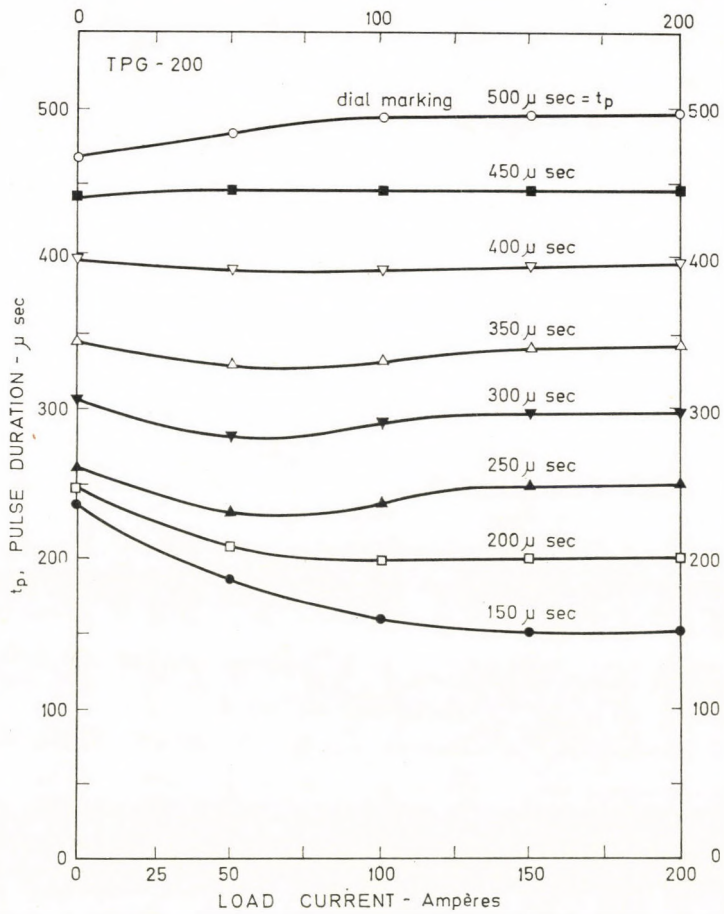

Fig. 5. Dependence of the pulse duration on the load current at the executed pulse generator TPG-200 (50 Hz version)

24 fixed steps in a near-parabolic manner and so allowing a nearly linear characteristics of fall time increment pro step.

Surely, this simple method for the control of fall time has the disadvantage that the fall time is dependent on load current. This can be surmounted in a manner, where fall time is calibrated at full load and the dependence of fall time vs. load may be displayed on the front panel of the pulse generator in tabulated form, or using a diagram similar to Fig. 4, where, as is shown, the fall time depends nearly linearly on load current between full load and one quarter of it. The pulse duration also depends on the load current but to a considerably less extent. The situation is depicted in Fig. 5. It may be assumed that this dependence is not significant between full load and 1/4 of the full load, thus it seems unnecessary to use a correction diagram, since small variations in pulse length have no effect on degradation because the dissipation of the saturated (turned-on) transistor can usually be neglected in comparison to the turn-over transient power losses.

The output pulse peak current meter is a diode voltmeter with a transistorized linear pulse amplifier preceding it. The current is measured by utilizing a low-resistance shunt in the output circuit. This shunt has a value of 0,00044 Ohm, and is made from numerous short bars of manganine resistance wire, parallel-connected between heavy copper bars and having very low inductance. The voltage drop on the shunt is very low in this way, that is, approx.

0,1 V. The output amplitude may be adjusted between 12,5 and 27,5 V limits, using the tappings of the high-current transformer secondary as a rough control and the R_{pr} variable resistor in the same transformer's primary (with 12 steps) as fine control or by the use of a toroidal (variac) transformer in the primary.

It is very important that the probability of EFC short-circuit and hence, the risk of overloading the tested transistors should be very low. For achieving this aim, derating of the used components as well as redundancy techniques have been used. For example, the storage capacitor C_S, the charging diode D_{ch}, further the diode D_1 are employed as Moore—Shannon "hammocks" containing four identical components. Parallel redundancy was used at the last stage of the EFC and at R_{Bs}. Calculation and live test for the m.t.b.f. (mean time between failures) showed that this value fairly exceeds 5×10^4 test hours of undisturbed use. Five pieces of this pulse generator are in operation for more than five years and only 3 failures were registered (all in the last year) for a net operation time of about $5 \times 3 \times 10^4$ hours (in all three cases a transistor was shorted in the EFC last stage). The gate pulse generator has non-redundant circuitry. Since a capacitor (C_{B5}) is applied between the gate pulse generator output and the EFC input, the EFC remains in cutoff (turn-off) state when the gate generator ceases to give driving pulse output.

Fig. 6 shows the shape of the output pulse voltage, varying the load current and the fall time, while in Fig. 7 the oscillograms of the pulse front are depicted, varying the load current and rise time.

The collector power supply has the same charging—storage capacitor circuitry as the one used in the pulse generator, with the obvious exception that here is no EFC and the related gate pulse generator. Naturally, the polarities of the charging diode D_{ch} and the electrolytic storage capacitor are reversed, and in this way the supply gives negative collector voltage (in respect to the ground) when a p-n-p type is tested. The output points in this case are the ones marked by alpha and beta in Fig. 3.

The V_{CC} voltage may be adjusted between 12,5 and 32 volts in the same way (transformer secondary tappings and series variable resistor in the primary) as in the pulse generator. Here the meters are, of course, moving coil types, one for the indication of the d. c. collector voltage, the other serving as average output current meter. The voltmeter may be switched over to measuring the peak V_{EBp} voltage between emitter and base, when the tested transistors are turned-on (i. e. the pulse generator just gives a pulse), aiding a diode peak meter circuit with 2,5 V range.

The primary of the mains transformer is connected to the primary of the pulse generator's mains transformer in such a manner that in the instant of the pulse (that is when the a. c. secondary voltage in the pulser is at the positive peak and D_{ch} is conducting) the a. c. secondary voltage in the collector power supply should be at its opposite (negative) peak value and, hence, the charging diode D_{ch} should be conducting at this instant, too. Thus, the charge of the collector current pulse is gained here, too, only partly from the storage capacitor, with the other part originating directly from the transformer secondary. Though this method has the advantage of using storage capacitors having only about one third capacitance as it would be otherwise necessary, the uneven, pulse-like load toward the mains and also the constraint to use larger transformers with larger secondary copper cross section may be regarded as disadvantages.

Both the pulse generator and collector power supply are fixed and permanent units in the whole apparatus. The life-testing drawers, containing the R_E emitter and R_C collector resistors per testing place, are connected to them by heavy copper bars, since pulse current amplitudes up to 200 A or more are flowing there and the stray inductance of these interconnections must be held at minimum, counteracting the elongation of the rise time or preventing "overshoot" after the turning-on.

One set of a pulse generator and collector supply can serve one or more life-testing drawers, up to a total pulse current consumption of 200 A depending on the type (i. e. power) of the tested transistors. Eight types of such life-testing drawers were developed, namely, 5 types for fixed collector peak currents between 0,05 and 1,2 A, each with 160 test positions for the life-testing of small-to-medium power transistors, and three further types serving for the life-testing of power types (e. g. in TO-3 case) with built-in heat sinks for the cooling of the tested transistors, for peak collector currents ranging from 3 to 15 A and for 30 or 12 test sites each, respectively. The R_E and R_C resistors are of fixed and equal value. For a given I_{Cp} current these fixed resistance values determine the necessary V_{CC} and V_i voltages. The collector current amplitude value may be so adjusted in a relatively wide range by the simultaneous adjustment of both V_i and V_{CC} voltages, depending on the chosen amount of I_{Cp}/I_{Ep} ratio, or in other words. on the chosen h_{FB} (or h_{FE}) value held at the test, cf. Eq. (7).

For the measurement of V_{EBp} during the life test, the emitter point of each tested tran-

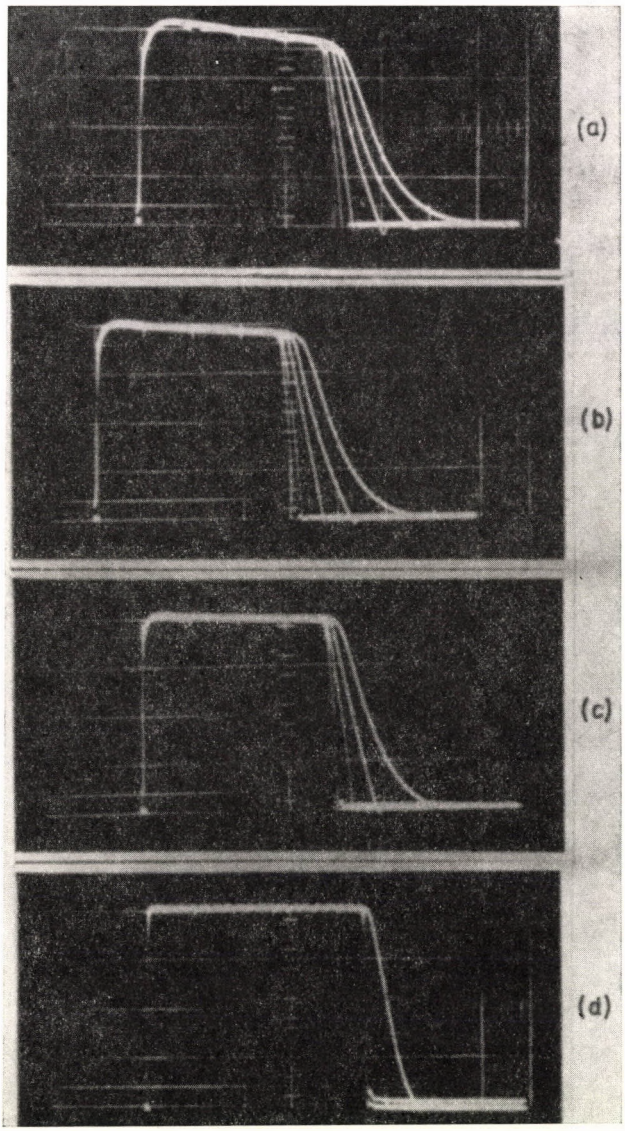

Fig. 6. Oscillograms of the output voltage pulse at various load current levels at the 200 A, 50 Hz pulser version. Nominal pulse duration is 200 μsec. Fall time control is adjusted to t_{off} = 20, 30, 50, 70 and 100 μsec nominal (scale) values. Time base is 50 μsec/div.

(a) 200 A load, t_{off} = 20, 30, 50, 70 and 100 μsec
(b) 100 A load, t_{off} = 11, 17, 32, 49 and 75 μsec
(c) 50 A load, t_{off} = 8, 11, 21, 36 and 64 μsec
(d) zero load, t_{off} = 2, 2,5, 3, 8 and 38 μsec

The variation of fall time due to load current change may be studied. At zero load a minute amount of ringing occurs. Pulse top fall increases with rising load current. The oscillograms were made by multiple exposure. (Vertical scale is 5 V/div.)

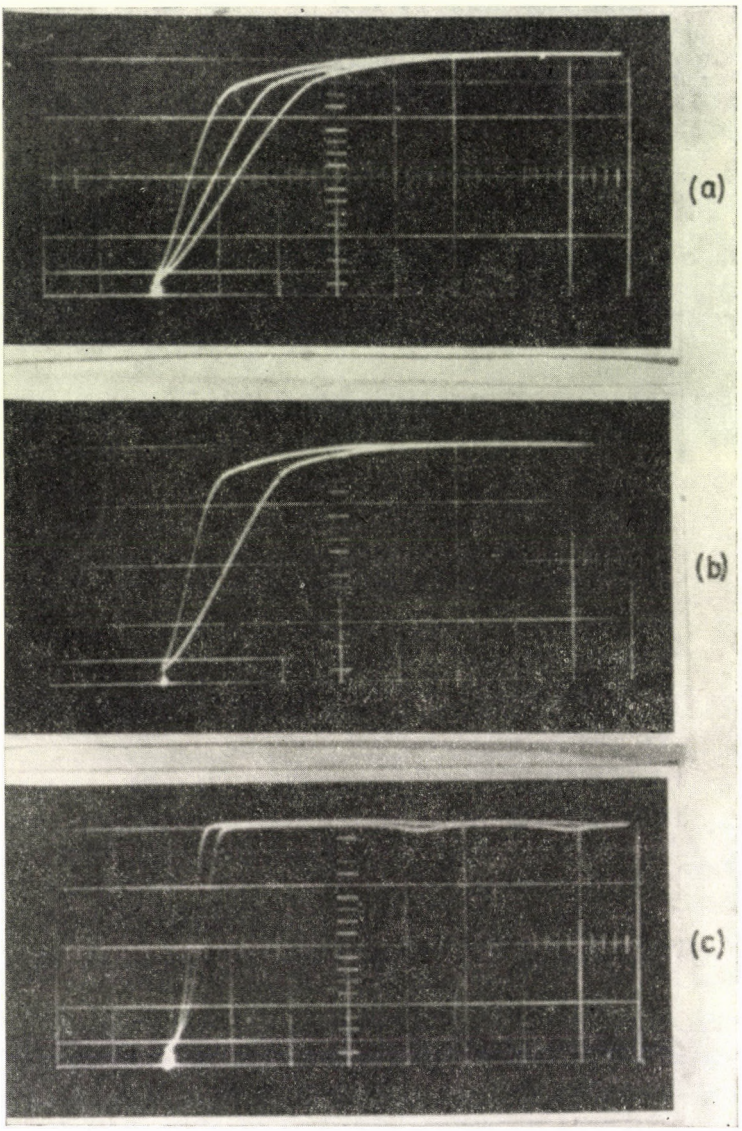

Fig. 7. Oscillograms of the pulse front at various load current levels. Pulse duration is 200 μsec Vertical scale is 5 V/div., horizontal scale is 5 μsec/div.

(a) 200 A load; $t_{on\ min} = 5\ \mu$sec; $t_{on} = 8\ \mu$sec; $t_{on\ max} = 12{,}5\ \mu$sec
(b) 100 A load; $t_{on\ min} = 5\ \mu$sec; $t_{on\ max} = 10\ \mu$sec
(c) zero load; $t_{on\ min} = 2\ \mu$sec; $t_{on\ max} = 3{,}5\ \mu$sec

sistor may be connected to the V_{EBp} diode peak meter (on the collector supply) in sequence, utilizing multi-pole switches. This measurement also serves for the quick determination of catastrophic failures of the tested specimens. If V_{EBp} is zero, the transistor in question is short-circuited between emitter and base. If the indicated voltage equals the V_i pulse amplitude

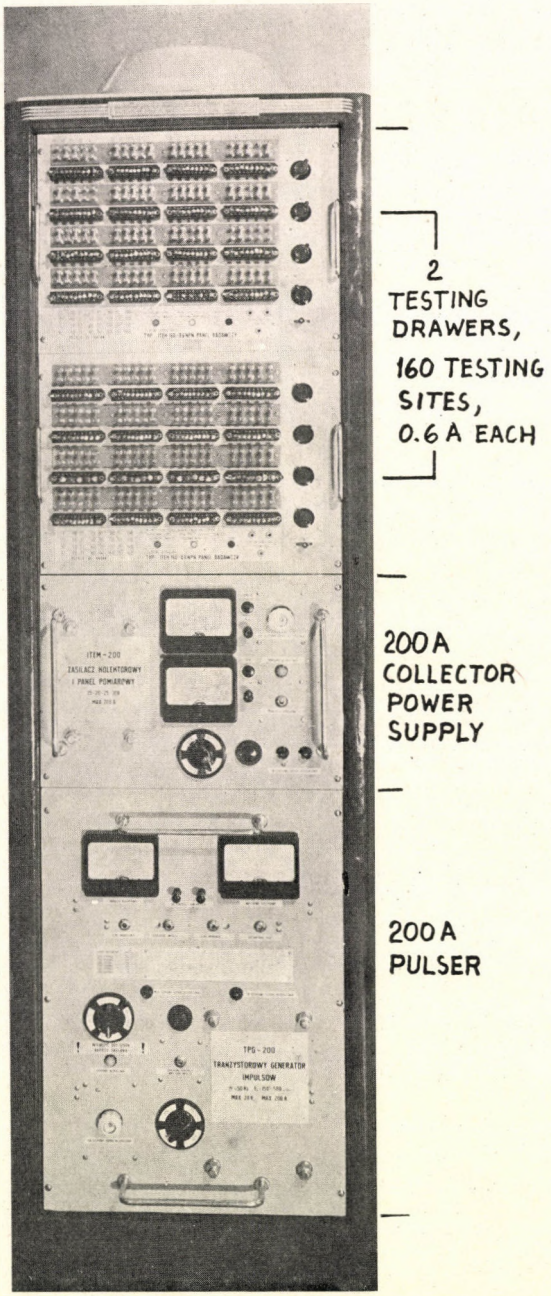

Fig. 8. Photograph of a pulsed-operation life tester accommodating 320 medium-power npn planar transistors of 0,6 A collector current pulse amplitude for each (50 Hz version)

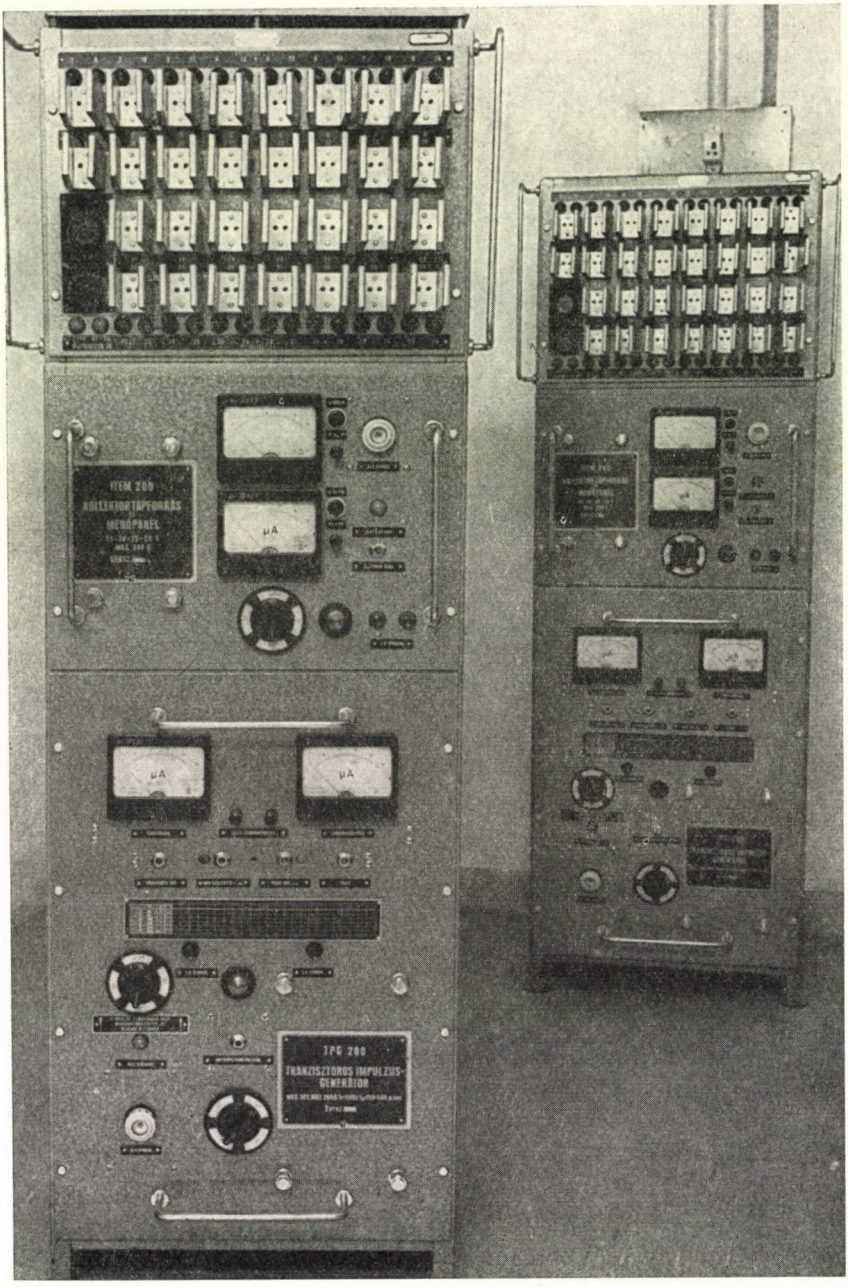

Fig. 9. Photograph of a pulsed operation life tester for 30 pnp power transistors of 6 A peak collector current. The outfit serves for types having TO-3 cases. Details on the front panels of all units may be clearly seen (50 Hz version)

(around 20 ÷ 30 V), the emitter diode is broken. A range between 0,2 and 2 V represents here an "operating" (sound) device. Using simple sensor circuits for the above standing voltage limits (aiding Schmitt-trigger or similar solid-state circuits), the three conditions are indicated by signal lamps. The collector points of all the tested transistors are similarly led to the V_{CC} moving coil meter, using the same multi-position switches. If there is a collector-base or collector-emitter short, the indication of the meter will be zero and this fact may be used for the indication of collector short-circuit by a signal lamp. Bringing out the emitter and collector points through the multi-position switches to two pairs of binding posts, this gives the possibility of an individual wave-form checking by an oscillo-synchroscope and hence for the measurement of $V_{CB\,sat}$ saturation voltage by the scope.

When a collector diode short-circuit occurs in one or more tested transistors, this leads to the overload of the R_C resistance as well as of the collector supply. To prevent this, fuses are placed in series with the R_C collector resistor. At the life test drawers of 1 A peak collector current or in excess of it, this can easily be made by individual fuses per testing position. At the lower-current types, group fuses are joining twin or quintuple test positions. In the latter case, special low-resistance fuses must be used. In the 0,05 A and 0,1 A drawers, no fuses are amployed at all.

When an EFC short occurs in the pulse generator, this is harmless for the tested transistors (which become in a saturated condition for a short time) but both pulse generator and collector supply would hardly be overloaded, let alone the R_E and R_C resistors. If this occurs the fuse Fu2 in the charging circuit blows. Since a similar fuse is placed in the charging circuit also in the collector supply, both units and also the R_E and R_C resistors are fully protected against overload.

Fig. 8 shows the photograph of a life tester unit having 2 drawers for 0,6 A peak collector current per testing position, for a total of 320 n-p-n test sites. In Fig. 9 a similar pulsed life tester is shown but for the accommodation of 30 p-n-p power transistors, in the TO-3 case in one single life-testing drawer at the top.

Separate types serve for pnp or for npn types. For testing npn types, the base (B) and emitter (E) terminals of the EFC in Fig. 3 must be reversed and the polarity of both charging diodes D_{ch} and also both storage capacitors C_S in the pulser and in the collector supply must be reversed.

The other version for testing the high-speed switching transistors differs in several ways in construction of the pulser only, though using the same principles. Instead of the 50 Hz phase shifter a 5 kHz astable multivibrator drives a gate pulse generator with short switching times and with a pulse duration variable between 1 and 5 μsec. The EFC here contains fast-switching planar transistors, e. g. 25 pcs of a rather expensive 10 A, 50 V, 50 nanosec power type in the last stage.

A more detailed description of the circuits and the operation of them is described elsewhere [16].

9. Some test results and their interpretations

All life tests in this section, as follows, were made on alloyed Ge, low-speed pnp transistors. The results of three typical experiments are described here, executed by the test method suggested in this article. — Comparative screen test experiments made on other alloyed transistors as well as medium-power, medium-speed silicon planar transistors are presented in the Appendix.

Another non-accelerated experiment, conducted on a medium-speed, micro-alloyed pnp Ge type at collector current stress levels within data-sheet limits, has shown no added informations beyond the usual d. c. electrical life test results and hence is not interpreted here.

Really, the experiments mentioned above and approximating 12 million device-hr in total, have been made as parallel step-stress tests where the collector current level was doubled in each step. These relatively large steps are reasonable since the R_E and R_C resistors are fixed (and identical) in the life-

testing drawers and if all voltage levels remain unaltered in the subsequent steps, the doubling, quadrupling etc. of the pulse current levels may easily be accomplished by connecting parallel 2, 4, 8 etc. test positions. By this rude method some informations could be gained on the relationship between failure rate and pulse current level.

Experiment (a):

A medium-power, low-speed, germanium pnp alloyed type (similar to OC 72) was tested having the following characteristic data: $V_{CB\,max} = -32$ V; $V_{EB\,max} = -10$ V; $I_{C\,max} = 0{,}25$ A; $I_{B\,max} = 0{,}125$ A; $T_{j\,max} = 75$ °C; $R_T \leq 0{,}4$ °C/mW without any heat radiator, in free (resting) air environment at room temperature (25 °C).

Normal and accelerated tests were made in the "low-frequency, high turnover energy" (50 Hz) version in three parallel groups taken from the same manufacturing batch. The normal (non-accelerated) test conditions correspond to the ones described as a numerical example, at the end of Section 6. Acceleration was made simply by doubling and quadrupling the I_{Cp} collector pulse current level.

The test conditions and test results are summarized in Table II. $I_{C\max}$ is there the collector peak current data-sheet limit, L_{on} is the energy of the turn-on transient and L_{off} is the same for the turn-off commutation, aiding equation (9) with the τ_i and τ_0 turn-over times given in the table and used in the experiment. The value of $h_{FB} = I_{Cp}/I_{Ep} = 0{,}9$ was held by the properly chosen ratio of voltages $V_{CB}/V_i = h_{FB}$ (if $R_C = R_E$), cf. Appendix A. 2. The value of the power peak of both commutations is 2 W as the numerical examples show at the end of Section 6. The cumulative failure rate was computed as

$$\bar{\lambda} = k_{tot}/N_0\, t_{tot},$$

where N_0 is the initial number of tested specimens and
k_{tot} the total number of failures during the t_{tot} total test time.

In the Tables k_d denotes the number of degradation-type failures while k_c the catastrophic ones, further $\lambda_{min}/\bar{\lambda}$ is the lower relative confidence limit and $\lambda_{max}/\bar{\lambda}$ the upper relative confidence limit.

The two last bars of Table II represent seriously accelerated tests. At the most accelerated experiment (a3) with $I_{Cp}/I_{C\,max} = 4$, the single failure caused by volumetric degradation, V_{pt} too low, occurred after the first 100 hours and all other failures, except two I_{CBO} failures, within the first 1000 hours. At the $I_{Cp}/I_{C\max} = 2$ experiment (a2) the single failure occurred between 200 and 500 hours. Finally, at the non-accelerated test (a1) one failure appeared before 500 hours and the other after 3000 hours.

In Table II the $P_{dt\,max}$ transient peak power computed on the basis of Eq. (12), as well as the average power losses $\overline{P_{dt\,on}}$ and $\overline{P_{dt\,off}}$ computed from equation (13), finally the averaged quasi-stationary losses $\overline{P_{on}}$ and $\overline{P_{off}}$ calculated by Eq. (4) and (5), are shown. All the four latter average power dissipations are summed up in the row $\overline{P_{d\,tot}}$ cf. equation (14) later, and contribute in the heating of the transistor, leading to a junction temperature rise $\Delta T_j = \overline{P_{d\,tot}}\, R_T$ also indicated in the middle row of Table II. Adding ΔT_j to the 25 °C ambient test temperature, one can conclude that the $T_{j\,av}$ junction temperature occurring in this way rises significantly due to the previous average power losses, especially at the (a3) experiment where $T_{j\,av}$ approximates the $T_{j\,max}$ data-sheet limit value. Consequently, the average junction temperature rise also contributes in degradation at the highly accelerated experiments (a2) and (a3), causing "surface-type" (degradation) failures nearly as much as the high-current-level-originated "volumetric" ("catastrophic") failures e. g. shorts due to the turn-over transients and hot-spot's formation. This way the "surface-originated" and "volumetric" failures cannot be separated unambigously. However, by raising the current level the volumetric failures are prevailing more and more.

In the last row of Table 2 the estimate of peak temperature rise during switch-off is also shown, based on the method given in the next paper of this series [22].

Experiment (b):

Since at the non-accelerated stress level ($I_{Cp}/I_{C\,max} = 1$) test conditions of the experiment (a1) very few failures occurred to gain a satisfactory statistical confidence, a prolonged

Table II

Test results of experiment (a):

Medium-power, low-speed, alloyed Ge, pnp transistor (OC 1072).
Test conditions: $t_p = 250\ \mu$sec; $\tau_i = 10\ \mu$sec; $\tau_0 = 100\ \mu$sec; $f_r = 50$ Hz; $V_i = 35$ V; $V_{CC} = -32$ V; $T_a = 25 \pm 3$ °C; test time 3000 hr

Experiment code	(a1)	(a2)	(a3)
I_{Cp} (A)	0,25	0,5	1,0
$I_{Cp}/I_{C\max}$	1	2	4
$R_C = R_E$ (Ω)	125	62,5	31,25
L_{on} (mWsec)	0,04	0,08	0,16
L_{off} (mWsec)	0,4	0,8	1,6
$P_{dt\max}$ (W)	2	4	8
$\overline{P_{dt\,on}}$ (mW)	2	4	8
$\overline{P_{dt\,off}}$ (mW)	20	40	80
$\overline{P_{on}}$ (mW)	6,25	12,5	25
$\overline{P_{off}}$ (mW)	~1	~1	~1
$\overline{P_{d\,tot}}$ (mW)	29,25	57,5	114
ΔT_j (°C)	12	23	45,5
$T_{j\,av} = T_a + \Delta T_j$ (°C)	37	48	70,5
N_0, initial lot (pcs)	320	80	40
k_{tot}, failed (pcs)	2	2	12
k_c, catastrophic (pcs) failure cause:	—	1 C—E short	7 C—E short
k_d, degradation (pcs) failure causes:	2 excess I_{CBO}	1 excess I_{CBO}	5 I_{CBO} (2pcs) BV_{CBO} (2pcs) V_{pt} (1pc)
$\bar{\lambda}$, approx., (1/hr)	$2{,}1\times10^{-6}$	$8{,}3\times10^{-6}$	1×10^{-4}
$\lambda_{\min}/\bar{\lambda}$ *	0,18	0,18	0,58
$\lambda_{\max}/\bar{\lambda}$ *	3,15	3,15	1,63
$\Delta\hat{T}_m$, approx. (°C) **	1,43	2,86	5,72

*At 90%, bilateral, confidence level.

**Minimum estimate of peak temperature jump along the junction due to the transient jurn-off energy, assuming $\varrho_n = 2$ ohm·cm base resistivity and $A = 3{,}85\times10^{-3}$ cm² nominal tunction area and perfect structure with even current distribution; cf. ref. [22], Eq. (28) there.

experiment was conducted with a large initial lot on the same type and in the same conditions as was in experiment (a1). A total number of 480 transistors were tested for 10 000 hours with $I_{Cp} = 0{,}25$ A $= I_{C\,\max}$, where only nine failures resulted as a total. In details, one transistor was found to be C—E short-circuited between 2000 and 3000 hr, seven transistors failed by excess I_{CBO} reverse current and another one by too low a h_{FE}. Most of the failures occurred in the first 2000 hr. This result gives a total cumulative failure rate of $1{,}87\times10^{-6}$/hr with relative confidence limits of $\lambda_{\max}/\bar{\lambda} = 1{,}9$ and $\lambda_{\min}/\bar{\lambda} = 0{,}63$, both at 90%, two-sided confidence level. Thus, this experiment does not serve any significant new information in comparison to the d. c. operational electrical stress experiment made on the same transistor type [9, 10, 17] at $P_{d\,\max} = 128$ mW and $V_{CB\,\max} = -32$ V data-sheet limit stress levels, where the total failure rate was approx. $1{,}5\times10^{-5}$/hr for a 12 000 hr experiment on a lot of 720 transistors. The relative distribution of failure causes were nearly the same at this d. c. electrical test and by experiment (b): the main failure cause was excessive I_{CBO}, over 60% in proportion, and only one sample has shown catastrophic failure (C—E short), probably originating from volumetric degradation by experiment (b), while 2 catastrophic failures occurred altogether (only 1 shorted transistor) in the d. c. electrical test. These facts suggest the idea that the switching operation life test conducted at relatively low, e. g. normal (not heavily accelerated) stress levels, causes but an insignificant effect on volumetric degradation and surface degradation mechanisms dominate. This is the situation at least by alloyed types, e. g. with all the previously described experiments except (a3), where the $I_{Cp}/I_{C\,\max} = 4$ stress level ratio seems to be sufficiently high to develop latent proneness to volumetric degradation.

Supporting the previous idea, let us compute the average junction temperature rise caused by all of the transient and quasi-stationary losses in the transistor. The overall loss will be the sum of the average power losses in Eqs (4), (5) and (13) and the same as Eq. (13) but with τ_i instead of τ_0. Hence

$$\overline{P_{d\,\mathrm{tot}}} = \overline{P_{\mathrm{on}}} + \overline{P_{\mathrm{off}}} + \overline{P_{dt\,\mathrm{on}}} + \overline{P_{dt\,\mathrm{off}}}. \tag{14}$$

Calculating Eq. (14) with the test conditions of experiment (a1), that is, with the values of the numerical example given at the end of Section 6: $\tau_i = 10\ \mu\mathrm{sec} \simeq t_{\mathrm{on}}/2$; $\tau_0 = 100\ \mu\mathrm{sec} \simeq t_{\mathrm{off}}/2$; $t_p = 250\ \mu$sec; $I_{Cp} = 0{,}25$ A; $V_{CC} = -32$ V, further with $V_{EBp} = 1$ V and $V_{CB\,\mathrm{sat}} = 1$ V and finally, with $I_{CBO} = 30\ \mu$A data-sheet limit values, the results are $\overline{P_{dt\,\mathrm{off}}} = 20$ mW, $\overline{P_{dt\,\mathrm{on}}} = 2$ mW, $\overline{P_{\mathrm{on}}} = 6{,}2$ mW and $\overline{P_{\mathrm{off}}} \cong 1$ mW.

Thus, with $\overline{P_{d\,\mathrm{tot}}} \cong 29$ mW, the average junction temperature rise above the $T_a = 25$ °C ambient temperature by the experiments, with $R_T = 0{,}4$ °C/mW thermal resistance of the given type, will maximally be $\Delta T_j = R_T P_{d\,\mathrm{tot}} = 0{,}4\times29 \cong 12$ °C. Hence, the average junction temperature will be equal to, or less than, $T_{j\,\mathrm{av}} = 25 + 12 = 37$ °C.

In the next step let us estimate the failure rate of the type at this low temperature from the failure rate gained by the d. c. electrical life test at $P_{d\,\max}$ as it was referred to in the first paper of this series [17] and, where the junction temperature was near to $T_{j\,\max} = 75$ °C, say at $T_j = 70$ °C. The related literature [1—9, 17] gives an activation energy of $qV_a/k = 12\,000$ °K (i. e., round 1 eV) for temperature-activated surface degradation mechanisms, which corresponds approximately to a doubling of the failure rate for each 8 °C temperature rise. Since the failure rate of $1{,}5\times10^{-5}$ hr. gained at 70 °C, must be divided by approx. 16 (corresponding to a 33 °C temperature difference of the pulsed and the d. c. electrical life test experiments), the estimate of the failure rate of a pure d. c. electrical stress at 37 °C temperature will be $1{,}5\times10^{-5}/16 \cong 1\times10^{-6}$/hr. Hence, one can conclude that the result of the experiment (b): $\bar{\lambda} = 1.87\times10^{-6}$/hr is fairly close to the previous estimate.

This way the former assumption that a pulsed life test made at non-accelerated current stress levels does not develop significantly the volumetric failure mechanisms related to structure failures, is supported and it is suggested to conduct "screening" type life tests at elevated collector current levels well beyond data-sheet limits, at least by alloyed types.

Experiment (c):

Small lots of a typical low-speed alloyed germanium p-n-p power transistor were life-tested for 3000 hours in the pulsed circuit of Fig. 1 and 3.

The tested OC 26 type having a TO-3 casing has the following typical and limiting data: $V_{CB\,max} = -40$ V; $I_{C\,max} = 3{,}4$ A; $T_{j\,max} = 90$ °C; $R_{T(j-c)} \leq 2$ °C/W between junction and case. Test conditions are shown in Table III. For calculating the $\overline{P_{d\,tot}}$ average dissipated power, the mean values of $V_{CB\,sat} = 0{,}7$ V and $V_{EBp} = 0{,}7$ V too, further the $I_{CBO} \leq$ ≤ 1 mA (at $T_a = 25$ °C and $V_{CB} = -32$ V) were used.

Since the transistors are mounted in the test equipment on cooling fins having a thermal resistance of about $R_{T(cf)} = 16 \div 18$ °C/W, the junction temperature rise is:

$$\Delta T_{j\,av} = (R_{T(j-c)} + R_{T(cf)}) \cdot \overline{P_{d\,to\,1}}$$

These values, added to the $T_a = 25$ °C ambient temperature, are also shown in Table III.

All that was concluded at the end of description of experiment (a), applies also here. However, the shift toward a "volumetric" failure prevalence with rising current level seems here more emphasized. As can be seen in Table III, the junction temperature rise is not too significant, yet at the highest stress level of the experiment (c3), and thus average junction temperature plays but the second role in degradation. (However, the effect of average power losses on degradation cannot be fully neglected here either.) Contrary to this, collector current stress level acts as the main cause of volumetric degradation. At the highest stress level of the experiment (c3), all failures except one (high I_{CBO}) are assumed as being of volumetric origin, e. g. also the 2 degradation-type failures of too low V_{pt}. Also the proportion of catastrophic-type failures increases here more rapidly with a rising I_{Cp} level than it does by low-power transistors, cf. Table II (e.g. the 8 C—E shorted transistors in the experiment with the highest stress level). Hence, one can risk the statement that failures of volumetric origin are more likely occurring at power transistors due to the several times higher turnover energy concentrating at a not essentially larger volume. — Unfortunately, the number of tested transistors proved to be too few at the lower stress levels and hence statistical confidence of the results are there too low. However, one can also risk the statement that the volumetric failure mechanisms are "masked" here as well by surface processes at relatively low stress levels.

In the last row of both Tables II and III, the peak temperature jumps $\Delta \hat{T}_m$ during the turn-off transient are given, based on the estimation presented in Section 3 and ref. [22], assuming a perfect structure without any current concentration. As can be seen, these temperature jumps of $1{,}4 \div 5{,}75$ °C are harmless even at the highest current levels despite the elongated turn-off time. However, if a considerable current concentration takes place as a consequence of structural imperfections and thermo-electrical feedback process, huge temperatures may occur since $\Delta \hat{T}_m$ is proportional, besides L_{off}, also to the reciprocal of the thermal capacity of the volume involved in current conduction and which is heated up during the turnover transient. If the actual conducting junction area is decreased by a given factor due to hot-spot formation, the temperature jump $\Delta \hat{T}_m$ will be increased by the same amount, e.g. at a current concentration diminishing the actual conducting area by a factor of 100, the

Table III

Test results of experiment (c):

Low-speed, alloyed Ge, pnp power transistor (OC 26).
Test conditions: $t_p = 250\ \mu$sec; $\tau_i = 10\ \mu$sec; $\tau_0 = 100\ \mu$sec; $f_r = 50$ Hz; $V_i = 35$ V; $V_{CC} = -32$ V; $T_a = 25 \pm 3$ °C; transistors mounted on $R_{T(c-f)} \cong 18$ °C/W heat sink; test time 3000 hr

Experiment code	(c1)	(c2)	(c3)
I_{Cp} (A)	3,0	6,0	12,0
$I_{Cp}/I_{C\max}$	0,855	1,715	3,43
$R_C = R_E$ (Ω)	10,5	5,25	2,625
L_{on} (mWsec)	0,49	0,98	1,96
L_{off} (mWsec)	4,9	9,8	19,6
$P_{dt\ \max}$ (W)	24,5	49,0	98,0
$\overline{P_{dton}}$ (W)	0,0245	0,049	0,196
$\overline{P_{dtoff}}$ (W)	0,245	0,49	1,96
$\overline{P_{on}}$ (W)	0,0625	0,125	0,250
$\overline{P_{off}}$ (W)	~0,032	~0,032	~0,032
$\overline{P_{d\ tot}}$ (W)	0,364	0,696	2,44
ΔT_j (°C)	7,3	14,0	48,8
$T_{j\ av} = \Delta T_j + T_a$ (°C)	32,3	39,0	73,8
N_0, initial lot (pcs)	120	60	30
k_{tot}, failed (pcs)	1	2	11
k_c, catastrophic (pcs) failure cause:	—	1 C—E short	8 C—E short
k_d, degradation (pcs) failure cause:s	1 excess I_{CBO}	1 excess I_{CBO}	3 excess I_{CBO} (1pc) low V_{pt} (2pcs)
$\bar{\lambda}$, approx. (1/hr)	$2{,}78\times10^{-6}$	$1{,}11\times10^{-5}$	$1{,}22\times10^{-4}$
$\lambda_{min}/\bar{\lambda}$*	~0,065	0,18	0,56
$\lambda_{max}/\bar{\lambda}$*	~4,74	3,15	1,65
$\Delta\hat{T}_m$, approx. (°C)**	1,36	2,72	5,45

*At 90% bilateral confidence level.

**Minimum estimate of peak temperature jump during turn-off, at even current distribution and perfect structure, see ref. [22], eq. (28); with $\varrho_n = 3$ ohm·cm base resistivity and $A_{nom} = 5\times10^{-2}$ cm² junction area.

peak temperature rise will be the hundredfold of those given in Tables I and II, i.e. amounting to 140 ÷ 570 °C which in turn lead to rapid or quite instantaneous deterioration.

It is also interesting that the values of $\Delta \hat{T}'_m$ differ but negligibly from each other in the interrelated test pairs (a1)—(c1); (a2)—(c2) and (a3)—(c3), i.e. if comparing the values with the same relative collector current level $I_{Cp}/I_{C\,max}$. However, this is not surprising considering the fact that current density as well as specific turnover energy density are nearly equal at both the tested medium-power and power types (since the junction areas are proportional to $I_{C\,max}$), and furthermore, V_{CC} and switching times are identical at both experiments (a) and (c).

Experiment (d):

This was in fact a repetition of experiment (c) on enlarged lots of the same OC 26 power transistor but originating from another manufacturing batch, with the obvious aim of collecting more information on failure behaviour. Only the (c1) and (c3) experiment have been repeated, i. e. the ones with the lowest and highest collector current stress level. Test conditions were exactly the same as in experiments (c1) and (c3).

In experiment (d1), 180 pcs were submitted at $I_{Cp}/I_{C\,max} = 0{,}855$ (i. e. $I_{Cp} = 3$ A) to a 3000 hr test, yielding in total only a single I_{CBO} failure and a failure rate of $1{,}85 \times 10^{-6}$/hr. This single failure can hardly be attributed to the turnover stress i. e. to a volumetric origin, thus the test was ineffective.

In experiment (d3) an initial lot of $N_0 = 120$ pcs was also submitted to a 3000 hr test but with the highest $I_{Cp} = 12$ A stress level. 51 transistors failed here, yielding a cumulative failure rate of $1{,}42 \times 10^{-4}$/hr, a bit higher than in experiment (c3) though the difference is not considerable. Most of the failures (38 pcs) occurred in the first 500 hr. Emitter-collector shorts prevailed: 39 pcs (i. e. 76,5% of all failures), the rest being 2 broken emitters (obviously due to a preceding C—E short), a collector-base short and 3 pcs too low V_{pt}; further 4 pcs failed by excess I_{CBO}, one by too low BV_{CBO} and one by too low h_{FE}. Hence, the ratio of failures suspected of volumetric origin (including all shorts, the broken ones and also the V_{pt} failures) of all failures was here $45/51 = 0{,}89$ while the similar ratio was 0,91 — nearly the same — at experiment (c3). Contrary to these results of power transistors, this ratio was $8/12 = 0{,}67$, i. e. considerably lower at the experiment (a3) which latter was also conducted at the highest $I_{Cp}/I_{C\,max} = 4$ stress level. These results seem to support the idea that the higher ratio of transient turnover energy to depletion-layer volume at power transistors (i. e. the many times higher current levels and the loss of all advantages of better cooling of the wafer in the swift turnover process there) can be blamed for the fact that power transistors are more likely to fail in switching service than low-power ones do.

A comparative test of the same OC 26 power transistor type, where no elongated turnover times have been compelled to the transistors, is given in the Appendix 1. For comparison, the failure rate of this power transistor type was about 3×10^{-5}/hr in a d. c. electrical life test at $P_{d\,max}$ (i. e. near to $T_{j\,max}$) and $V_{CB\,max}$ conditions.

To make a rough estimate for the relationship between degradation and pulse current stress, the total failure rate is plotted against the normalized $I_{Cp}/I_{C\,max}$ current stress level in Fig. 10, where the results of the previous life test experiments, as well as the planar types dealt with in the Appendix, are utilized. Although there are too few points for risking an unambigous statement, it seems that the logarithm of the failure rate versus the I_{Cp} pulse current rate gives a linear relationship. However, the slope of the real relationship is supposedly much steeper than in the Fig. 10, since there all failures are included in

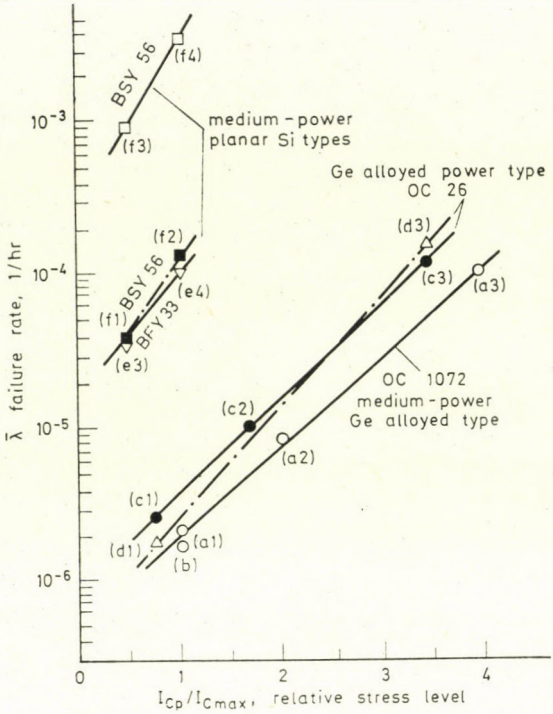

Fig. 10. Relation between failure rate and $I_{Cp}/I_{C\,max}$ relative current stress level by the experiments (a), (b), (c), (d), (e) and (f). The upper 3 straight lines represent npn planar silicon types while the 3 lower ones p-n-p, alloyed transistors. The logarithm of failure rate seems to be proportional to the I_{Cp} stress level, with only minor differences in slope

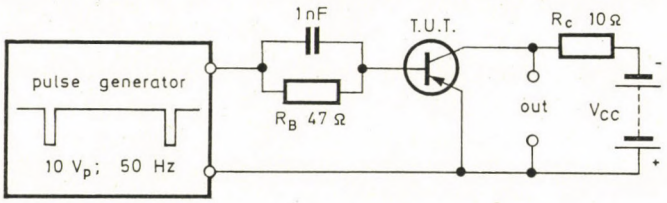

Fig. 11. Test circuit for the life testing of an alloyed p-n-p power transistor (OC 26) in c. e. pulsed operation (inverter service) where the spontaneous switching time durations of the transistor determine the turn-over transient energies. This is the data-sheet circuit for the determination of switching times

the computation of failure rate and hence the usual surface-degradation mechanisms "mask" the effect of the pure volumetric degradation at least at relatively low stress levels. On the other hand, the number of failures of presumably volumetric origin are too few in the executed experiments, especially at low I_{Cp}, to make an attempt for a proper extrapolation.

Test results of medium-power silicon planar transitors are presented in Appendix 2.

10. Conclusions

An electrical life test method was suggested here to obtain the dependence of the failure rate on stress parameters of transistors in switching-operation, where it is presumed that degradation is caused mainly by volumetric processes. The method makes use of a common base inverter test circuit where the rise and fall times are artificially elongated by a transistorized pulse generator and these turn-over transient times exceed several times the spontaneous turn-over times of the tested transistors.

The causes of switching-operation degradation have been elucidated and the computation of transient energies and powers was given. The conclusion was drawn that the huge amount of turnover transient energy can be blamed primarily for volumetric degradation, leading at properly high switching power levels to the formation of hot spots due to uneven current distribution (caused but only by structural imperfections) and finally to the destruction of the transistor by collector-emitter (alloyed types) or collector-base (epitaxial mesa or planar types) short-circuit or to a too low punch-through voltage. It was, or will also be [22] demonstrated that junction temperature rather closely follows the transient power-time function during commutation at the beginning portion of temperature vs. time function, since the collector depletion layer where the heat is generated and from which the thermal energy of the commutation transient can hardly spread further during the brief transient (because heat conduction is a very slow process), exhibits a rather low thermal resistance and a rather high thermal capacity. Although this transient temperature does not cause any harm in a transistor with a fair structure (where it amounts to some tenth ... some °C), excessive temperature and thermal gradient may arise in the inherently uneven transistor structure at the beginning of the very brief turn-over time where these thermal processes may be assumed as nearly adiabatic and the turnover energy concentrates in the minute volume of the occurring hot-spot, instead of spreading evenly through the whole collector depletion layer. Quasi-stationary power dissipation in both the saturated and the cut-off state, on the other hand, may be neglected as compared to the power losses originated from the turn-over transients, at least if the collector supply voltage is high ($V_{CC} \gg V_{CB\,\mathrm{sat}}$). Hence, the average junction temperature has not a prime effect on volumetric degradation. Instead of, the pulse current level and the duration of turn-over transients are playing the leading role.

The circuitry of the pulsed service-life-testing equipment was given.

The life test experiments, conducted on low-speed alloyed germanium and medium-speed silicon planar transistor types and which utilized a parallel step-stress methodology varying the pulse current level, supported the previous hypotheses of volumetric degradation mechanisms. Though the experi-

ments presented here seem to be insufficient in number and also in tested transistor lots (obviously due to economic considerations), some conclusions may still be drawn (valid at least for alloyed transistors) which are summarized as follows:

(i) Life tests conducted in such a manner that the collector pulse current stress level (as well as the V_{CB} collector voltage) remain well within the data-sheet limit values, do not serve any further information about switching-operation life expectancy and volumetric degradation processes than a usual pure d.c. electrical stress does, contrary to the fact that the "compelled" turn-over transient time durations are $10 \div 100$ times longer than the spontaneous turn-over times of the transistor itself. In such test conditions failures are mainly surface-degradation-originated and surface degradation processes tend to conceal the volumetric processes.

(ii) If the collector pulse current level is much beyond the data-sheet limit value, the test method will be effective to develop real volumetric degradation processes and hence the suggested method seems to be useful primarily as a screen-test for sorting out samples inherently poor in structure and prone to later deterioration in switching operation mode. Such an accelerated screen test of some hundred hours seems to be adequate. Acceleration factors ranging to $I_{Cp}/I_{C\,\max} = 4$, may be assumed as non-destructive for transistors of rather good structure (i.e. tend to accelerate already existing failure mechanisms instead of developing new ones), at least by alloyed transistor types. The same is true but with $I_{Cp}/I_{C\,\max} = 1 \div 2$ for mesa or planar devices with more delicate structure.

(iii) At high current stress levels, failure types of characteristically volumetric origin occurred in an exponentially increasing manner by raising the collector current level, mainly as C—E shorts and in few occasions as a heavily decreased punch-through voltage. Contrary to this, at stress levels ranging up to $I_{Cp}/I_{C\,\max} = 4$, the proportion of typical surface degradation failures (e.g. excessive I_{CBO} or too low h_{FE}) did not show such an excessively increasing tendency, obviously because the raising of the collector current level increased the junction temperature, but only moderately.

(iv) Having turn-over times held constant, the failure rate seems to be exponentially proportional to the collector pulse current level, at least until $I_{Cp}/I_{C\,\max} = 4$ at alloyed types and until $I_{Cp} = I_{C\,\max}$ at the less rugged planar types.

(v) Power transistor types (having several times larger junction area) seem to be more subject to volumetric degradation processes, e.g. to collector-emitter punch-through or C—B short, than low-power types with small junction diameter/base width ratio, obviously also because by the power transistors the probability of a structural imperfection is larger due to the larger junction area; but the main cause is here the many $(10 \div 100)$ times higher

current, i.e. switching power level, consequently also the $10 \div 100$ times higher transient peak power of the commutation which concentrates here in a depletion layer volume not essentially larger than in low-power devices — at least not larger proportionally with the switching power. Hence, the *density* of the commutation transient energy is considerably greater in power transistors and so the transient temperature crest will be several times higher than in low-power devices despite the better *stationary* cooling of the wafer here, which latter advantage gets totally lost, since the thermal commutation energy can hardly leave the bounds of the depletion layer during the brief turnover time, so the better cooling (lower thermal resistance) remains ineffective here.

The final aim of such life test experiments is udoubtedly to find a rate process formula similar to the "Arrheniusian" or Eyring one used at d.c. electrical, and thermal storage, life tests, which describes the relation between failure rate and stress parameters as $I_{Cp}/I_{C\ \max}$ normalized pulse current level, turnover transient energy (or turnover transient time durations) as main agents, furthe as collector supply voltage and junction temperature, as degradation cause agents of secondary importance. However, the life test experiments presented here have been too few for achieving this final aim. Such experiments, where only the amount of turn-over energy would be varied and all other parameters held constant, have been considered to be carried out later, though an attempt is also made here dealing with planar transistors. The sole statement could be made that the logarithm of the failure rate seems to be proportional to the collector pulse current amplitude but the slope of this relationship could not be determined due to the "masking" effect of surface degradation processes at lower current stress levels on the one hand, and the current level steps have been chosen too roughly for making a proper extrapolation, on the other. These relationships are supposedly different to less or more extent with transistor technologies strongly differing from the alloyed and planar techniques. In the beginning step here only the alloyed technology was dealt within details in this respect, with some results of planar types added. It will be a future work to make sufficient experiments for the establishment of a really useful rate process formula.

Acknowledgements

The author is indebted to Professor I. P. VALKÓ, Ph. D., formerly leader of our laboratory and to Mr. M. KOCSIS, Hd. of Dept. of HIKI, for aiding and criticising this work and for the microsections presented; further he wishes to express his best thanks to Mr. J. SZÉCSEI who contributed valuably in the analysis given in Section 3; further to Mr. G. KALMÁR and Mr. L. NAGY of Tungsram Works Ltd, Budapest for the permission, and to Mr. V. STEFÁNIAY of Res. Inst. for Metallurgy, Budapest, for the preparation, of SEM micrographs. Finally, the author thanks the publication permission to Mr. A. KOMPORDAY, Manager in Chief and Mr. F. BRÁDA, Hd. of Section, all of Institute HIKI.

REFERENCES

1. REICH, B.: An Empirical Study of the Degradation of Alloy Transistor Characteristics with Operating Temperature; *Semicond. Prod.* **1** (1958) Jan.
2. ROBERTS, F. F.—HENDERSON, J. C.—HASTIE, R. A.: An Accelerated Ageing Experiment on Germanium p-n-p Alloy Type Transistors; *Proc. Inst. Electrical Eng*'s, **106** (1959), Part B, Suppl. No. 17, p. 958
3. WILSON, H. R.: Degradation Mechanisms in Germanium P-N-P Alloy Transistors; *Semicond. Prod.* **5,** (1962), Part 1; N° 6, p. 25, Part 2; N° 7, p. 18
4. PECK, D. S.: Semiconductor Reliability Predictions from Life Distribution Data; in "Semiconductor Reliability" edited by J. E. Shwop and H. J. Sullivan, Engineering Publ's, Elizabeth, N. J., U.S.A., 1962
5. MILLER, L. E.—MACKINTOSH, I. M.: Reliability of Silicon Transistors and Diodes, see [4]
6. ZIERDT, C. H., Jr.: Comparison of Operating Life Tests and Storage Tests; see [4]
7. COLE, W. P.—ZUCKERMANN, B.: Comparison of Field Experience with Accelerated Life Test on Precision Etched Electrochemical Transistors, see [4]
8. KEMÉNY, A.: Optimaler Arbeitspunkt der Transistoren beim Zuverlässigkeitstest durch elektrische Dauerlast; *Tungsram Techn. Mitt.*, Nr. 16, (1967) Ste 705
9. KEMÉNY, A. P.: Experiments Concerning the Life Testing of Transistors, I: Operating and Storage Life Testing of Transistors for the Determination of Temperature and Voltage Dependence of the Failure Mechanisms; *Microelectronics and Reliability*, **10** (1971), 169—194
10. KEMÉNY, A.: Reliability of Semiconductor Devices (in Hungarian), published by the *Advanced Eng. Course of the Budapest Tech. University*, Book No 4649, Budapest 1968
11. KOCSIS, M.: Zusammenhang zwischen inhomogener Basisdicke und Zerstörung des legierten Transistors; *Tungsram Techn. Mitt.* Nr. 8 (1963), Ste 317
12. KOCSIS, M.: Electrical Test Methods of Bulk Structure Failures in Semiconductor Devices; *Symp. on Test Methods of Semicond. Devices*, Budapest, Apr. 25—28, 1967, Preprint, Vol. 1
13. KEMÉNY, A. P.: Effect of Structural Irregularities on Avalanche Breakdown in p-n Step Junctions; *Acta Techn. Acad. Sci. Hung.* **61** (1968), 101—136
14. KEMÉNY, A.: Messung der Durchbruchsspannung von Flächentransistoren; *Tungsram Techn. Mitt.* Nr. 21, (1969) Ste 907, Dez.
15. KEMÉNY, A. P.: Life Testing of Semiconductor Power Rectifiers with Energy Sparing Synthetic Circuits; *Microelectronics and Reliability*, **8** (1969), 121—133
16. KEMÉNY, A. P.: Developmental Problems of an Extra High Current Transistorized Pulse Generator Having Extreme Reliability, *Research Reports of the Ind'l Res. Inst. for Electronics HIKI*, Electronic Lab., Dec. 1964. No xii (in Hungarian), also to be published
17. KEMÉNY, A. P.: Experimental Investigations of the Life of Semiconductor Devices, I. Accelerated Life Tests of Transistors under Static Electrical Load and High Temperature Storage. *Acta Techn. Hung.*, **74** (1973), 85—142
18. KEMÉNY, A. P.: Experiments Concerning the Life Testing of Semiconductor Devices, II. Life Testing of Transistors in Switching Operation Mode. *Microelectronics and Reliability*, **10** (1971), 75—93
19. KITTEL, C.: Introduction to Solid State Physics; J. Wiley, New York 1961, Chapter 6
20. PEARS, J. H.: Chemical Engineer's Handbook (4th ed.); McGraw-Hill, N. Y., Chapter "Thermal Conductivity"
21. DOOB, J. L.: Stochastic Processes; J. Wiley, New York and Chapman and Hall, London, 1954
22. KEMÉNY, A. P.: Experimental Investigations on the Life of Semiconductor Devices, IV. Role of Peak Temperature Caused by Turnover Transients in the Volumetric Deterioration of Switching Transistors and Logical Integrated Circuits, *Acta Techn. Hung.*, under press
23. KEMÉNY, A. P.: Life tests of TTL SSI Integrated Circuits, *Microelectronics and Reliability*, **13** (1974), 119—142

APPENDIX

A. 1. Comparative power transistor tests in c. e. circuit, without artificial elongation of switchover times

Experiment (c4)

A comparative life test experiment (c4) was made by the transistor factory on the same low-speed alloyed power transistors as described in Section 9, experiments (c), originating from the same batch, in the test circuit of Fig. 11, where the transistors operated as common-emitter inverters in a "typical" circuit and where switching times had not been elongated artificially.

The driving pulse generator was of very low output impedance and having rise and fall times falling short of 1 μsec, thus the base current turn-over times were several times shorter than the spontaneous turnover times of the collector current pulse. Test conditions have been: $V_{CC} = -32$ V; $R_C = 10\Omega$; thus $I_{Cp} = 3{,}2$ A, nearly the same as in experiment (c1), further a base current of approximately 0,2 A compelled by the base resistor. Repetition frequency was 50 Hz and base current pulse duration 200 μsec. Hence, the conditions of this experiment corresponded to the experiment (c1) in all respect with the only exception that no prolonged turn-over times had been compelled by the test circuit.

The characteristic switching time durations are in this operation: $t_{on} =$ max. 25 μsec, switching-on time and $t_{off} =$ max. 30 μsec, switching-off time, the latter is well below the 100 μsec turn-off time compelled in the experiment (c1).

A lot, a total of 400 transistors was tested for 5000 hours. The results of this experiment (c4) have shown no sign of significant volumetric degradation. Six failures occurred, out of which four with excess I_{CEO}, one with too low h_{FE} and one with C–E short-circuit; this last one may be assumed as being of suspectedly volumetric origin, and all the others obviously were developed by surface degradation. The total failure rate mounted up to 3×10^{-6}/hr, which is only insignificantly higher than the result of experiment (c1), despite the fact that the stress level was here a bit lower since turn-off transient was shorter.

Experiment (c5)

As a control test, the sound remainder of experiments (c3) and (d3), that is, the power transistor type OC 26, was repeatedly tested in the same c. e. circuit conditions as Fig. 11 and so in operating conditions identical with experiment (c4) but here for a subsequent 17 000 hr after the 3000 hr, 12 A current-level, elongated switching time screening of experiment (c3) or (d3). Thus, 19 pcs were involved as the sound remainder of experiment (c3) and 69 pcs in the same way from experiment (d3), i. e. 88 pcs total. It is not too surprising that only a single failure occurred (excess I_{CBO}) and no shorts at all, showing that the elongated turnover, enhanced current-level screening prior to this long duration test was very effective in sorting out specimens prone to volumetric degradation due to inherent structure unevenness. The single failure means a failure rate $\bar{\lambda} = 1/(88\times17\,000) \simeq 0{,}67\times10^{-6}$/hr which is nearly by an order of magnitude less than the result of the unscreened lot of experiment (c4). These figures show the potentialities of such screening tests dealt with in Tables II–V.

A. 2. Step-stress screen tests carried out on planar transistors

Two medium-power, medium-speed types were submitted to parallel-series step-stress experiments for rough and quick orientation of the potentialities of the method suggested in this paper for this most important technology.

One type tested was the BFY 33 npn silicon planar transistor (not an epitaxial one), having the maximum ratings of $V_{CBO} = 50$ V; $I_{C\,max} = 0{,}5$ A; $T_{j\,max} = 200$ °C; $R_T \leq 0{,}22$ °C/mW (between junction and still air environment); finally $V_{EBp} \leq 1{,}5$ V; $V_{CE\,sat} \leq 2{,}5$ V; $f_T \geq$ ≥ 80 MHz and $t_{off\,max} = 0{,}25$ μsec; all the four latter parameters referred to $I_C = 0{,}5$ A and $I_B = 0{,}05$ A.

The other type, BSY 56 is a similar but epitaxial planar transistor having the limit ratings of $V_{CBO} = 120$ V; $I_{C\,max} = 0{,}5$ A; $T_{j\,max} = 200$ °C; $R_T \leq 0{,}22$ °C/mW (between junction and resting ambient air); further $V_{EBp} \leq 1{,}5$ V; $V_{CE\,sat} \leq 1{,}4$ V; $f_T \geq 145$ MHz and $t_{off\,max} = 0{,}16$ μsec; all the four latter data corresponding to $I_C = 0{,}5$ A and $I_B = 0{,}05$ A. Hence, this type is a higher frequency (faster switch), higher-voltage construction than the BFY 33, though being identical with the latter in all other data. The particular sample tested

here originated from an early (1971) pilot-plant production exhibiting several serious technological imperfections, mainly a poor thermocompression bonding.

Experiments on both types were carried out in the c. b. test circuit of Fig. 1 in two groups corresponding to the "high-frequency" (5 kHz) and "low-frequency" (50 Hz) test circuit versions and, furthermore, in two subsequent current-level steps for each group. The first group of each type was so tested at $f_r = 5$ kHz and $t_p = 5$ μsec, i. e. a duty cycle of $t_p f_r = 0{,}025$ and compelling in the same time elongated switching times of $t_{on} = 0{,}2$ μsec and $t_{off} = 2$ μsec on the transistors, at $I_{Cp}/I_{C\,max} = 0{,}5$ and 1 current level steps. The second groups of both types were submitted to a test made at $f_r = 50$ Hz and $t_p = 200$ μsec (i. e. $t_p f_r = 0{,}01$), compelling $t_{on} = 20$ μsec and $t_{off} = 100$ μsec excessively elongated switchover times on the transistors, also at $I_{Cp}/I_{C\,max} = 0{,}5$ and 1 relative current levels. Test times were 168 hr (one week) uniformly for each step, with test conditions being identical for both types in the corresponding step. In all these tests, $V_{CC} = 22$ V and a ratio $I_{Cp}/I_{Bp} = 10 \cong h_{FE}$ were used. The latter criterion can be simply fulfilled by the properly chosen ratio of V_{CC}/V_i voltages (V_i is the pulse generator output amplitude) assuming $R_C = R_E$ (see Fig. 1) since, utilizing Eqs (6) and (7) and the relationship $I_{Ep} = (V_i - V_{EBp})/R_E \cong V_i/R_C$ (because usually $V_i \gg V_{EBp}$), one gets

$$h_{FB} = h_{FE}/(1 + h_{FE}) = V_{CC}/V_i$$

i. e., in our case a V_i exceeding V_{CC} by 10% has to be used to ensure $h_{FB} = 0{,}9$ or $h_{FE} = 10$.

Test results are given in Tables IV and V. The test conditions chosen are the same in both types (since both types have identical current and thermal ratings), slight differences being only in $\overline{P_{on}}$ and consequently, in $\overline{P_{d\,tot}}$ and ΔT_j, because the epitaxial BSY 56 type has a bit lower saturation voltage. The power loss $\overline{P_{off}}$ may be fully neglected since the I_{CBO} reverse current lies in the very low nanoampere range by planar silicon transistors. Moreover, the ΔT_j junction temperature rise is negligibly small in all tests, thus it has no considerable effect yet on surface degradation either.

By the test pairs made in the "high-frequency" and "low-frequency" testing equipment versions, the test conditions were selected in such a manner that there are considerable differences only in the transient turnover energies, i. e. L_{on} and L_{off}, where 50 ÷ 100 times higher energies occur at the "low frequency" (50 Hz repetition rate) test pairs as compared to the corresponding turnover energy levels of the "high-frequency" (5 kHz repetition) tests, since rise and fall times are longer in the 50 Hz version in the same amount. The *average* power dissipations $\overline{P_{dt\,on}}$ and $\overline{P_{dt\,off}}$, however, are equal or differ only slightly despite the turnover energies differing 50 ÷ 100 times from each other, because the repetition frequency is 100 times higher in the 5 kHz ("high-frequency") version and this compensates the effect of the turnover energies being 50 ÷ 100 times less there, cf. Eq. (13). Thus, the sole main difference between test conditions of experimental steps with identical I_{Cp} current levels and differing only in f_r, that is, the experiment pair of even codes or odd codes, lies in the 50 times higher L_{off} turn-off energy of the 50 Hz version which leads suspectedly to a many times higher rate of deterioration, especially to those failures that have a "volumetric" origin. Considering the results, this indeed is the situation if one compares the results of (e3) to the ones of (e1), or similarly, (e4) to (e2) etc.

Experiment (e)

As is shown in Table IV where the non-epitaxial type is dealt with, the failure rate is only slightly higher at the 50 ÷ 100 times higher turnover energies of the "low-frequency", 50 Hz, 50 μsec test pair (e3)–(e4) as compared to the results of the "high-frequency", 5 kHz, 1 μsec test pair (e1)–(e2). Moreover, in the "high-frequency, low turnover energy" test pair (e1)–(e2) no "volumetric" failures occurred at all and the single I_{CBO} failure at the test (e2) can be attributed to the mild junction temperature increase of 18 °C there, i. e. to a "surface"-originated cause. Hence, both steps (e1) and (e2) of the "*high-frequency, low turnover energy*" *test version may be judged as completely ineffective in developing inherent "volumetric" failures.* Contrary to this, the conditions of the "low-frequency, high turnover energy" test pair (e3)–(e4) turned out to be a bit coarse for the delicate structure of such a planar type: the predominant majority of failures were "broken emitter", i. e., the thin gold wire leading to the thermocompression bond evaporated suspiciously due to a previous short and one cannot be sure that all these failures, although not too high in number, (9 pcs in a lot of 960, total, and taking place during a week) originated by actually serious structure deficiencies and not by the excessively

Table IV

Results of the step-stress experiments (e)

Medium-speed, silicon planar npn transistor BFY 33.
Two parallel step-stress experiments each consisting of 2 subsequent current-level steps of 168 hr and containing initial lots of 480 pcs; in $T_a = 25 \pm 3$ °C resting air ambient, without any heat sink, $V_{CC} = 22$ V.

Experiment code	(e1)	(e2)	(e3)	(e4)
I_{Cp} (A)	0,25	0,5	0,25	0,5
$I_{Cp}/I_{C\,max}$	0,5	1,0	0,5	1,0
$R_C = R_E$ (Ω)	82,0	41,0	82,0	41,0
f_r (Hz)	5000	5000	50	50
t_p (μsec)	5,0	5,0	200	200
$t_{on}/2 \simeq \tau_i$ (μsec)	0,1	0,1	10	10
$t_{off}/2 \simeq \tau_0$ (μsec)	1,0	1,0	50	50
L_{on} (μWsec)	0,296	0,592	29,6	59,2
L_{off} (μWsec)	2,96	5,92	148,0	296,0
$P_{dt\,max}$ (W)	1,48	2,96	1,48	2,96
$\overline{P_{dt\,on}}$ (mW)	1,48	2,96	1,48	2,96
$\overline{P_{dt\,off}}$ (mW)	14,8	29,6	7,40	14,8
$\overline{P_{on}}$ (mW)	25,0	50,0	10,0	20,0
$\overline{P_{d\,tot}}$ (mW)	41,3	82,6	18,9	37,8
$\Delta T_j = P_{d\,tot} R_T$ (°C)	9,1	18,2	4,2	8,3
N_S, survived (pcs)	480	479	478	471
k_{tot}, failed (pcs)	—	1	2	7
k_c, catastrophic (pcs) failure causes:	—	—	1 E broken	4 E broken
k_d, degradation (pcs) failure causes:	—	1 excess I_{CBO}	1 excess I_{CBO}	3 2 pcs excess I_{CBO} 1 pc low h_{FE}
$\bar{\lambda}$, approx. (1/hr)	—	$1{,}24 \times 10^{-5}$	$2{,}48 \times 10^{-5}$	$8{,}75 \times 10^{-5}$
upper 60% confidence limit, (1/hr)	$1{,}18 \times 10^{-5}$	$2{,}57 \times 10^{-5}$	$3{,}92 \times 10^{-5}$	$1{,}05 \times 10^{-4}$
$\Delta \hat{T}_m$, during turn-off (°C) *	0,34	0,68	2,92	5,84

*Minimum estimate of turn-off transient temperature jump by even structure with $\varrho_n = 2$ ohm·cm collector resistivity and $A = 2{,}5 \times 10^{-3}$ cm^2 nominal (and actual) junction area; cf. Ref. [22], Eq. (27) there.

Table V

Results of the step-stress experiments (f)

Medium-speed; silicon epitaxial planar npn switching transistor BSY 56.
Two parallel step-stress experiments, each consisting of 2 subsequent current-level steps of 168 hr and containing initial lots of 480 pcs; in $T_a = 25 \pm 3$ °C resting air environment, without any heat sink; $V_{CC} = 22$ V.

Experiment code	(f1)	(f2)	(f3)	(f4)
I_{Cp} (A)	0,25	0,5	0,25	0,5
$I_{Cp}/I_{C\max}$	0,5	1,0	0,5	1,0
$R_C = R_E$ (Ω)	82,0	41,0	82,0	41,0
f_r (Hz)	5000	5000	50	50
t_p (μsec)	5,0	5,0	200	200
$t_{on}/2 \cong \tau_i$ (μsec)	0,1	0,1	10	10
$t_{off}/2 \cong \tau_0$ (μsec)	1,0	1,0	50	50
L_{on} (μWsec)	0,296	0,592	29,6	59,2
L_{off} (μWsec)	2,96	5,92	148,0	296,0
$P_{dt\,max}$ (W)	1,48	2,96	1,48	2,96
$\overline{P_{dt\,on}}$ (mW)	1,48	2,96	1,48	2,96
$\overline{P_{dt\,off}}$ (mW)	14,8	29,6	7,40	14,8
$\overline{P_{on}}$ (mW)	18,2	36,4	7,25	14,5
$\overline{P_{d\,tot}}$ (mV)	34,5	69,0	16,1	32,3
$\Delta T_j = P_{d\,tot} R_T$ (°C)	7,6	15,2	3,5	7,1
N_S, survived (pcs)	478	469	404	153
k_{tot}, failed (pcs)	2	9	76	251
k_c, catastrophic (pcs) failure causes:	—	3 1 pc, E broken 2 pcs, C—B short	47 21 pcs E broken 3 pcs, E—B short 7 pcs, C—E short 16 pcs, C—B short	200 115 pcs, E broken 63 pcs, E—B short 15 pcs, C—E short 7 pcs, C—B short
k_d, degradation (pcs) failure causes:	2 excess I_{CBO} excess I_{EBO} 1—1 pc	6 2 pcs, excess I_{CBO} 4 pcs, excess I_{EBO}	29 16 pcs, excess I_{CBO} 12 pcs, excess I_{EBO} 1 pc, low h_{FE}	51 32 pcs, excess I_{CBO} 17 pcs, excess I_{EBO} 2 pcs, low h_{FE}
$\bar{\lambda}$, approx. (1/hr)	$2{,}5 \times 10^{-5}$	$1{,}06 \times 10^{-4}$	$9{,}4 \times 10^{-4}$	$3{,}7 \times 10^{-3}$
Upper 60% confidence limit (1/hr)	$3{,}95 \times 10^{-5}$	$1{,}24 \times 10^{-4}$	$\sim 9{,}5 \times 10^{-4}$	$\sim 3{,}7 \times 10^{-3}$

For $\Delta \hat{T}_m$ see Table IV.

high turnover energy stress conditions. Beyond doubt, the failed transistors were presumably the ones having the worst structures. The tested type, however, can be considered as having a satisfactory quality.

Experiment (f)

Dealing with the epitaxial type (Table V), deterioration was significant also in the "high-frequency, low turnover energy" tests (f1)—(f2) but turned out to be truly disastrous at the "low-frequency, high turnover energy" test pair (f3)—(f4). No catastrophic failures occurred at the low-current-level test (f1) but 3 pcs failed by short or open-circuit at the maximum rated collector current-level test (f2), 2 of which has been C—B short. Beside these failures, surface-originated excess reverse current failures were dominating. — Discussing the results of the "low-frequency, high turnover energy" test pair (f3)—(f4), the failure pattern was reversed and failures of typically volumetric origin prevail there: in the overwhelming majority of cases the emitter (or base) leadout gold wire was broken in the form of a ball-shaped molten ending probably due to a previous short and solidified thereafter, near to the bonding. All these open-circuit failures as well as the C—E and C—B shorts are typical consequences of volumetric failures described in Section 2 and it is at least suspicious that the bonding failure mechanisms described in Section 4 have also had an important role in the excessively high number of such failures. For the C—B shorts are supposedly a direct consequence of the collector-base voltage breakdown described in Section 2, a pinhole-like molten and recrystallyzed channel within the collector epitaxial layer is expected to be found if making a microsection on a transistor failing in this manner. The lapping of the delicate structures, however, scarcely reveals such a failure since the probability to find the thin recrystallized channel in the bulk is very small (comparable to finding a needle in a haystack) and no "surface" marks exist which call attention to the presumed locus of bulk breakdown. Such a microsection where a channel rises from the ring-formed geometrical curvature of the collector junction beneath the emitter perimeter, i. e. an "emitter dip" rim and points toward the $n-n^+$ boundary of the epitaxial collector zone and the substrate and where this structure deficiency is presumed as the shorting channel, is shown in Inset 4. — It is surprising, however, that this particular C—B short failure occurred relatively rarely here, i. e., in only 25 cases among a total of 250 catastrophic failure events. A possible explanation for this is that the $V_{CC} = 22$ V reverse voltage applied in this test was many times lower than the $V_{CBO} = 120$ V data-sheet limit. The C—E shorts (22 pcs total), on the other hand, may also be attributed to hot-spot formation in, or near to, the emitter-base junction where current concentration is high (in fact, higher than in the collector junction) and turnover energies can also be significantly high, especially if V_{EBp} is excessively large. This latter phenomenon, or the local heating-up of the degradated emitter thermocompression bond (due to a Kirkendall-void formation, cf. Section 4 and Inset 5) may give the explanation for the amazingly high number of emitter-base shorts (68 pcs failed in this mode). — Anyway, the type tested here exhibited serious technological imperfections, also manifesting in an unusually high failure rate in simple storage and d. c. operating life test experiments and just this short-term pulsed screening method revealed the technological flaws in the pilot-plant production stage.

Experiment (g)

Finally, the results of a 168 hr screening of a medium-power, high-speed epitaxial planar transistor type BSX 59 are presented. A lot of 160 pcs originating from pilot-plant production was tested. Limit ratings and typical data are as follows: $V_{CBO} = 70$ V max, $V_{CEO} = 45$ V max, $I_{C\,max} = 1$ A, $T_{j\,max} = 200$ °C and $R_T \leq 0{,}22$ °C/mW; further $f_T \geq 250$ MHz, $t_{on} \leq 35$ nanosec and $t_{off} \leq 60$ nanosec, all three previous data valid at $I_C = 1$ A and $I_B = 0{,}1$ A. The test was made in the "low-frequency, high turnover energy" equipment version in the most adverse conditions, i. e. $f_r = 50$ Hz, $t_p = 500$ μsec, $t_{on} = 10$ μsec, $t_{off} = 100$ μsec, $V_{CC} = 25$ V, $h_{FB} = 0{,}9$, $R_C = R_E = 20{,}5$ ohms, $I_{Cp} = 1{,}2$ A, $T_a = 25 \pm 3$ °C (transistors applied without any heat sink), thus $P_{d\,max} = 25\ \text{V} \times 1{,}2\ \text{A}/4 = 7{,}5$ W; $L_{on} = t_{on}\, P_{d\,max} = 0{,}075$ mWsec; similarly but with t_{off}, the $L_{off} = 0{,}75$ mWsec. Despite these severe screening conditions only 8 transistors failed in a catastrophic mode, giving a cumulative failure rate of approx. 3×10^{-4}/hr, thus the type and its technology may be considered as acceptable. Failure causes were 6 C—E short, a single C—B short and a single broken emitter. The conclusion may be drawn from this experiment that a rather delicate high-speed epitaxial planar type can still withstand the enormously elongated switchover transients of 100 μsec duration and approx. 1 mWsec energy level if both technology and structure are adequate.

Summarizing the results of the above experiments it seems that the method of artificially elongated turnover transients as presented here is well applicable also in silicon planar transistors. Nevertheless, it has been proved that the volumetric failure mechanisms dealt with in Sections 2 and 4 are effectively developing in such stress conditions. For achieving the most characteristic results, however, the test conditions must be "matched" carefully to the particular type: for a medium-speed type $f_r = 1 \div 5$ kHz, $t_p = 3 \div 30$ μsec and $t_{off} = 1 \div 10$ μsec seems to be the optimum, whilst for a high-speed type with delicate structure and minute geometry the recommended test conditions are $f_r = 5 \div 20$ kHz, $t_p = 0{,}3 \div 3$ μsec and $t_{off} = 0{,}1 \div 1$ μsec. The compelled rise time t_{on} should always be chosen as the $1/10 \div 1/5$ of t_{off}. The "low-frequency, high turnover energy" version dealt with previously and having conditions of $f_r = 50$ Hz, $t_p = 150 \div 500$ μsec and $t_{off} = 10 \div 200$ μsec is adequate for testing low-speed (e. g. alloyed germanium) transistors but seems a bit rough for screening medium-speed types. Test times of some hundred hr and relative current levels of $I_{Cp}/I_{C\,max} = 1 \div 2$ are typical in planar transistors and fit the requirements of a screen-test developing "latent" structural imperfections. — On the other hand, repetition frequency can be assumed as a factor of secondary importance (since only the *average* power loss is proportional to it), the main agent being the turnover energy level, that is, the product of peak power (i. e. $0{,}25\ V_{CC}I_{Cp}$) and turnover duration.

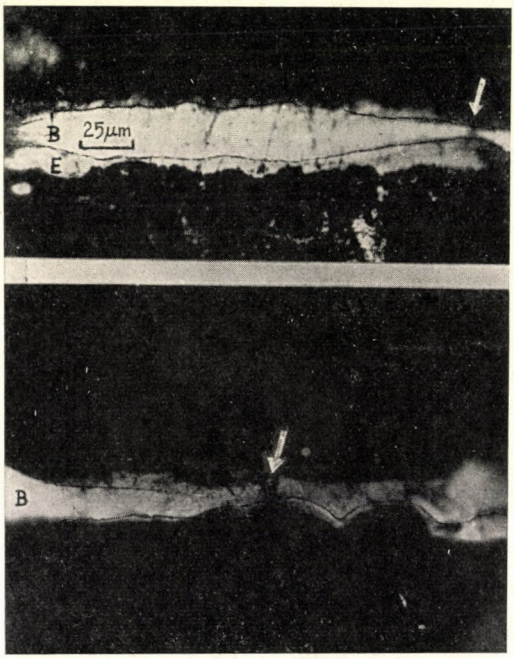

Inset 1 (to Section 2)

Microsections of excessively inhomogeneous, waved or indented junctions of a medium-power, low-speed, alloyed Ge pnp transistor type (OC 1076). The base layer appears in white, near the boundaries of which the metallurgical junctions appear as thin black lines and the lower being the emitter junction. Both specimens exhibited a punch-through voltage well below BV_{CBO}, before a complete punch-through (white arrows) occurred after a couple of hours in testing conditions identical with the ones in experiment (a3). (By courtesy of Mr. M. Kocsis, HIKI.)

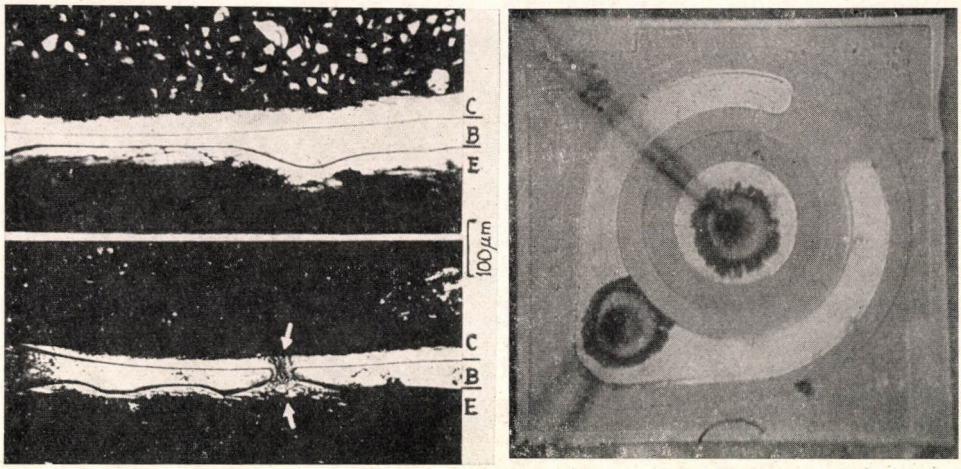

Inset 2 (to Section 2)

Microsections of alloyed Ge pnp, slow-speed, high-power transistors ASZ 18, showing up excessive inhomogeneity in base layer thickness (the latter appearing in bright white and the metallurgical junctions near to its bounds developing as thin black lines). The strongly waved emitter junction is the lower one. Due to mechanical strains by alloying, the junctions are badly warped. In the lower photograph the molten and recrystallized punch-through channel between collector and emitter can be clearly observed (white arrows). (By courtesy of Mr. M. Kocsis, HIKI.)

Inset 3 (to Section 4) (on the right)

Plague-afflicted Au—Al thermocompression bonds of a silicon planar transistor. (By courtesy of Tungsram Works Ltd, Budapest.)

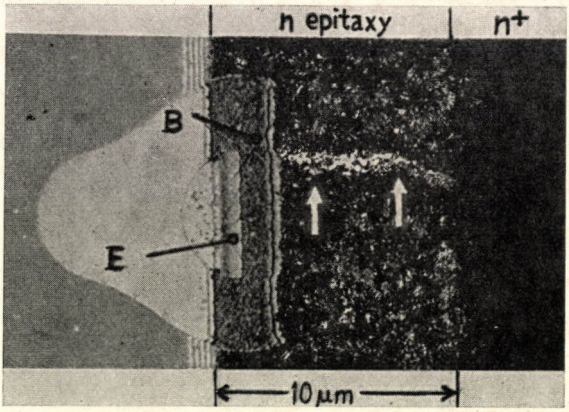

Inset 4 (to Appendix A. 2)

Microsection by angle lapping and staining of a medium-power, epitaxial, planar transistor revealing a breakdown channel (white arrows) between collector-base junction and n^+ substrate through the 8 μm thick collector epitaxial layer, rising from the "emitter dip" curvature of the C—B junction.

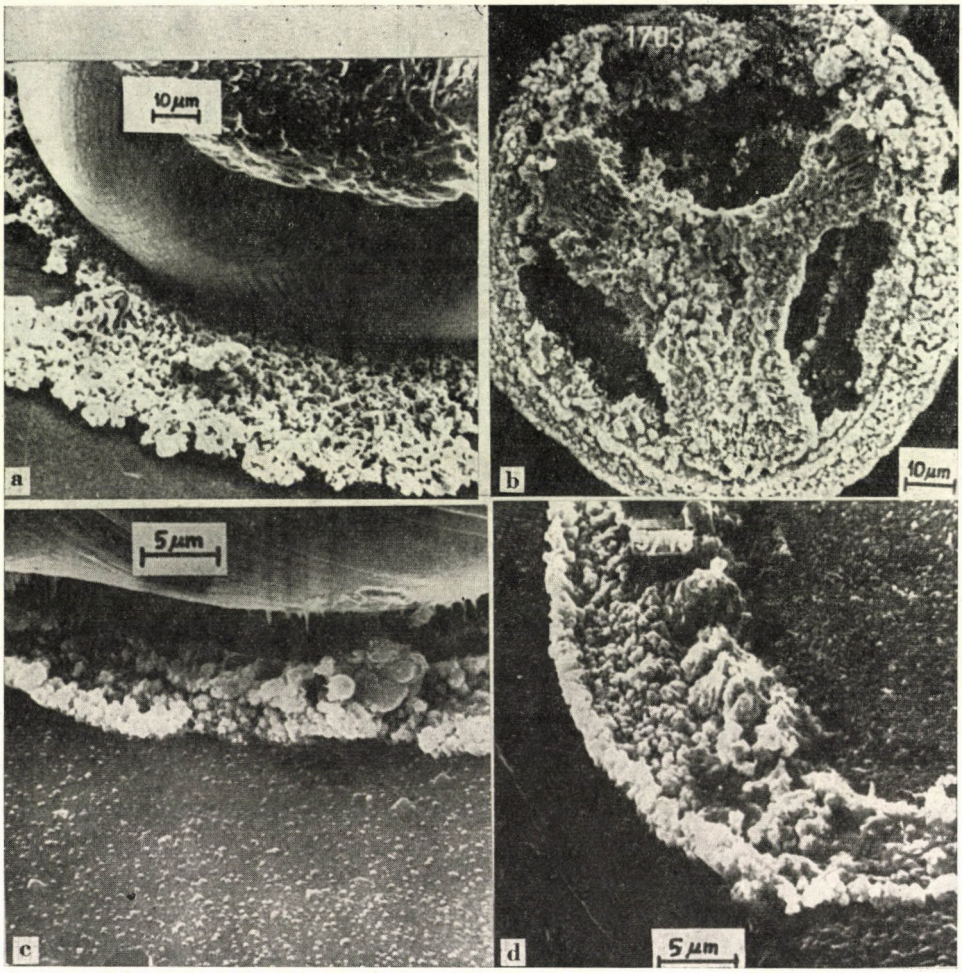

Inset 5 (to Appendix A. 2)

Au—Al nailhead thermocompression bonds at the emitter of a planar transistor, all badly afflicted by severe intermetallic formation (after exposure at 200 °C for 168 hr, followed by the screen test of experiment (*f*)). All micrographs were made with a usual, secondary electron mode, Scanning Electron Microscope (SEM).

(a) Characteristic plague compounds on the Al metallization around the gold ball. Contact resistance increased but the bond is still alive. (b) The aluminium side after complete and spontaneous separation of the gold ball, shows the bulky intermetallic products and voids left there. (c) A contiguous Kirkendall void has grown below the periphery of gold ball showing nondescript, coarse-grained intermetallics and "stalactite" features as well. (d) The aluminium side of picture (c) after almost spontaneous separation of the bond shows coarse grains, "huge" voids and "stalagmite" features of intermetallic on the periphery of bond, with a sharp boundary. (Courtesy of Mr. V. STEFÁNIAY of Res. Inst. for Metallurgy, Budapest and Mr. G. KALMÁR, Tungsram Works Ltd, Budapest.)

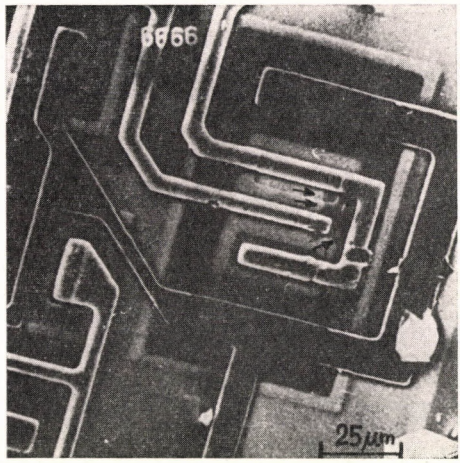

Inset 6 (to Section 4)

SEM micrograph of a typical volumetric failure of an IC transistor (an output transistor of a TL 7472 N master-slave J—K flipflop, after 6000 hr switching operation stress at 125 °C. The potential contrast technique reveals a latent collector-base short (arrows) as a dark spot on the otherwise light base zone, at the upper right corner of the U-shaped emitter metallized stripe. The collector stripe (bigger U) and the underlying collector zone appear as dark (because of being biased +5,25 V positive with respect to emitter and base, which appear as light areas). The scratch along the collector and emitter stripes (right center) proved to be harmless. The short was caused by a major pinhole above the fault site in the SiO_2 layer, through which a spurious boron diffusion (base dopant) advanced during operation at this "hot spot" and, after reaching the collector zone, made a complete short. (Courtesy of Mr. V. STEFÁNIAY and Mr. G. KALMÁR; Res. Inst. for Metallurgy and Tungsram Works, Ltd, Budapest, resp.)

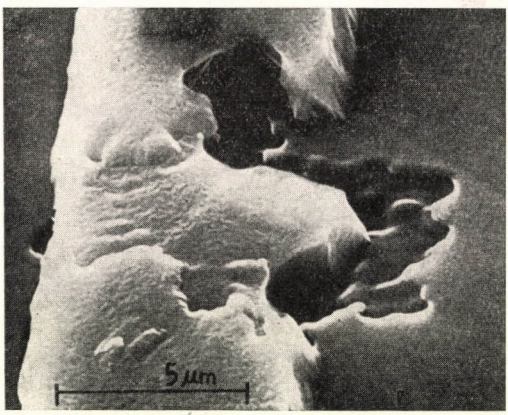

Inset 7 (to Section 4)

This interesting SEM micrograph reveals a "volumetric" short between the Al stripe on the top, and the underlying collector zone through a major pinhole in the oxide between them. The "hot spot" enhancing the migration of Al through the pinhole channel was originally started by the Joule heating of the constricted metal stripe above the failure site, due to the high current flowing through it, enhancing electromigration by the temperature gradient. The picture clearly shows the marks of the molten metal above the failure site, due to the short terminating this sequential failure of an analog IC. (Courtesy of Mr. V. STEFÁNIAY and Mr. G. KALMÁR; Res. Inst. for Metallurgy, and Tungsram Works Ltd, Budapest, resp.)

Experimentelle Untersuchung der Lebensdauer von Halbleiter-Bauelementen. — III. Räumliche Fehlermechanismen und Untersuchung der Lebensdauer von Transistoren in Schaltbetriebsart. Die bei Transistoren allgemein verwendeten statischen Dauerbelastungsmethoden, welche hauptsächlich thermisch aktivierte Oberflächendegradationserscheinungen hervorrufen, sind wenig informativ in Bezug auf das Zugrundegehen im Schaltbetrieb. Hier wird eine Methode vorgeschlagen, wo die Transistoren im Schaltbetrieb mit gemeinsamer Basis als Inverter mit fester Wiederholungsfrequenz von 50 Hz oder mehr belastet werden, bei genau festgelegter und regelbarer transienter Ein- und Ausschaltenergie, welche Methode die wirtschaftliche Untersuchung von großen Mustern ermöglicht und in erster Reihe als *Screening-Untersuchung* für die schnelle Auswahl von strukturell fehlerhaften Exemplaren von Nutzen ist.

Экспериментальное исследование срока службы полупроводниковых приборов, III. Механизмы объемных дефектов и испытание транзисторов на срок службы в переключательном режиме работы. Применяемые для транзисторов статические методы электрических испытаний продолжительной нагрузкой, которые вызывают в основном термически активированные поверхностные деградационные процессы, не дают достаточно информаций относительно порчи в переключательном режиме работы. Автор в данной работе предлагает такой метод, в случае которого на транзисторы в качестве работающих в переключательном режиме работы с общей базой инвертеров подается нагрузка фиксированной частоты в 50 Гц или более высокой частоты повторения при точно определенной и регулируемой переходной энергии включения и выключения; этот метод позволяет осуществить экономичное испытание больших серий образцов. Предлагаемый метод является полезным в первую очередь в качестве селективного метода для быстрого отделения образцов со скрытыми структурными дефектами. Такие испытания, подтвержденные микроснимками, смятыми с поврежденных полупроводниковых приборов, согласуются с результатами расмотренных здесь анализов объемных деграпапионных пропессов и обрашают внимание на необходимость бездефемтной геометрической структуры таких приборов.

Acta Technica Academiae Scientiarum Hungaricae, Tomus 82 (1—2), pp. 169—177 (1976)

POROSITY OF CEMENT STONE AS A FUNCTION OF THE WATER-CEMENT-RATIO

J. ROSTÁS*

[Manuscript received December 18, 1974]

Due to theoretical considerations the porosity and the solidity of the cement stone will be deduced as a function of water—cement-ratio and hydration degree. The results deduced for the various cases will be compared to experience, and good correspondence will be found.

1. Introduction

For the porosity of the cement stone as an important parameter for concrete, an empirical formula of approximating character is known so far [1].

Difference is made at the beginning, capillarity depending on the hydration degree and on gel porosities. Total porosity is considered as a sum of these two porosities. We will attempt to deduce the relation of porosity Φ, hydration degree $H(t)$ and water-cement-ratio v_c from the general theoretical manner.

2. Porosity if no change of volume is taken into consideration

The cement powder mixed with water starts a reaction with porous solid cement stone as a result of the hydrogen. The mass of non hydrated cement, at time moment t is marked by $M_c(t)$. At initial time $t = 0$: $M_c(0) = M_{c0}$ then, according to the definition, the hydration degree at moment t is:

$$H(t) = \frac{M_{co} - M_c(t)}{M_{co}} = 1 - \frac{M_c(t)}{M_{co}} . \tag{2.1}$$

The mass of the arisen hydrated product assumes the form $M_g(t)$ and the mass of non hydrated water $M_v(t)$ is marked as time moment t. According to the law of mass conservation:

$$M_{co} + M_{vo} = M_c(t) + M_v(t) + M_g(t). \tag{2.2}$$

* J. Rostás Üllői út 53/b, H-1091 Budapest, Hungary

Considering the water, the cement grains and the hydration products as a homogeneous medium:

$$M = \varrho V. \tag{2.3}$$

By using (2.3), (2.2) is equal to

$$\varrho_c V_{co} + \varrho_v V_{vo} = \varrho_c V_c(t) + \varrho_v V_v(t) + \varrho_g V_g(t). \tag{2.4}$$

In the mixture of cement and water hydration does not proceed to the full extent (due to different reasons), or even if the conditions of hydration are ensured for a long time. Therefore, in case

$$V_v(t) + V_c(t) + V_g(t) \geqq V_{co} + V_{vo} \tag{2.5}$$

which is always available (this will be proved later), following hydration of a duration of t, the total volume of the pores remaining in the solid cement stone will be equal to the remaining water that has not taken part in the hydration process

$$V_p = V_v(t). \tag{2.6}$$

Here, in the first approximation the water fixed at the surface is not taken into consideration, yet

$$V_p = \frac{1}{\varrho_v}\left\{\varrho_c\left(V_{co} - V_c(t)\right) + \varrho_v V_{vo} - \varrho_g V_g(t)\right\}. \tag{2.7}$$

Porosity Φ and water-cement-ratio v_c are defined in the following ways

$$\Phi = \frac{V_p}{V_{\ddot{o}}}, \tag{2.8}$$

$$v_c = \frac{M_{vo}}{M_{co}}. \tag{2.9}$$

Here it is assumed, during solidification time, that cement does not creep and expand:

$$V_{\ddot{o}} = V_{vo} + V_{co}. \tag{2.10}$$

By using (2.6), (2.7), (2.8), (2.9) and (2.10)

$$\Phi = \frac{1}{\varrho_v}\left[\frac{\varrho_c\left(V_{co} - V_c(t)\right) + \varrho_v V_{vo} - \varrho_g V_g(t)}{V_{co} + V_{vo}}\right]. \tag{2.11}$$

Instead of the volumes the masses and densities are written as:

$$\Phi = \varrho_c \frac{M_{co} - M_c(t) + M_{vo} - M_g(t)}{\varrho_v M_{co} + \varrho_c M_{co}}. \tag{2.12}$$

By using (2.9) and $\varrho_v = 1$, (2.12) is equal to

$$\Phi = \varrho_c \frac{1 - \dfrac{M_c(t)}{M_{co}} + v_c - \dfrac{M_g(t)}{M_{oo}}}{1 + \varrho_c v_c}. \tag{2.13}$$

It is assumed that the mass of the water M_v^* used for hydration is proportional to the mass of the hydrated cement

$$M_v^*(t) = K M_c^*(t) \tag{2.14}$$

where K is constant, a proportion factor. By using (2.1), (2.2) and (2.9)

$$\frac{M_g(t)}{M_{co}} = v_c + H(t) - \frac{M_v(t)}{M_{co}}. \tag{2.15}$$

Up to time moment t, the mass of the hydrated cement and water are as follows:

$$M_c^*(t) = M_{co} - M_c(t), \tag{2.16}$$

$$M_v^*(t) = M_{vo} - M_v(t). \tag{2.17}$$

By using (2.1), (2.9), (2.14), (2.16) and (2.17)

$$\frac{M_v(t)}{M_{co}} = v_c - K H(t). \tag{2.18}$$

With the aid of (2.1), (2.15) and (2.18), (2.13) is equal to

$$\Phi = \varrho_c \frac{v_c - K H(t)}{1 + \varrho_c v_c}. \tag{2.19}$$

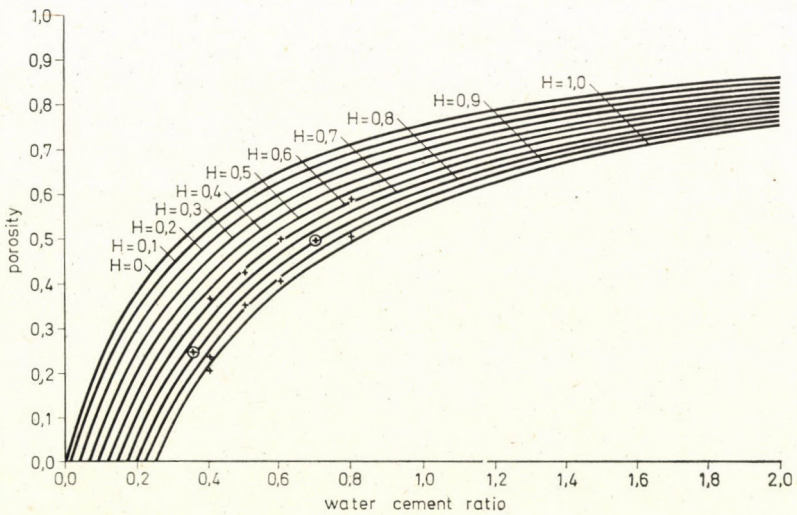

Fig. 1

According to the tables, this is equal to $2{,}95 \div 3{,}15$ gramm cm^{-3}. For the calculations $\varrho_c = 3{,}1$ has been used. According to CZERNIN [2] $K = 0{,}25$. Using this value at different degrees of hydration for porosity Φ as function of water-cement-ratio v_c the resulting host of curves is indicated in figure 1, illustration No. 1. The measuring results of POWERS [3] and FELDMAN [4] have been drawn up on the host of curves. Comparing the measured results with the theory, the following conclusions can be drawn. The theoretical curves closely follow the empirical values. Both authors succeded in keeping the hydration degree at the same level for different water-cement-ratio factors v_c.

3. Porosity, taking into consideration the change of volume

Eq. (2.19) was deduced on the assumption that there is no change of volume during solidification. If change of volume is permissible

$$V_{\ddot{o}} = V_v(t) + V_c(t) + V_g(t)\,, \tag{3.1}$$

then taking into consideration (2.7), (2.8), (2.9) and (3.1), porosity Φ is equal to

$$\Phi = \frac{\varrho_c\big(V_{co} - V_c(t)\big) + V_{vo} - \varrho_g V_g(t)}{V_v(t) + V_c(t) + V_g(t)}\,. \tag{3.2}$$

Expressing the volumes by masses and densities at $\varrho_v = 1$

$$\Phi = \varrho_c\varrho_g \frac{1 - \dfrac{M_c(t)}{M_{co}} + \dfrac{M_{vo}}{M_{co}} - \dfrac{M_g(t)}{M_{co}}}{\varrho_c\varrho_g \dfrac{M_v(t)}{M_{co}} + \varrho_c \dfrac{M_g(t)}{M_{co}} + \varrho_g \dfrac{M_c(t)}{M_{co}}}\,. \tag{3.3}$$

With the aid of (2.1), (2.9), (2.15) and (2.18), (3.3) is equal to

$$\Phi = \frac{\varrho_c\varrho_g\big[V_c - K\,H(t)\big]}{\varrho_c\varrho_g\big[v_c - K\,H(t)\big] + \varrho_c(1+K)\,H(t) + \varrho_g\big(1 - H(t)\big)}\,. \tag{3.4}$$

If it is represented as a function of v_c, the result will be similar to illustration No. 1.

As a matter of fact, the highest change of volume can take place at the highest hydration degree. Therefore, for the case of $H = 1$ the (2.19) and (3.4) are presented in illustration (see: illustration No. 2). From the illustration it is apparent that at the values $v_c < 1$ (for regular concrete) the deviation between the two formulas is not too significant. Up to the end of function (3.4) it remains under (2.19) throughout. This, at the same time bears evidence to our assumption under (2.5), as the deduction of (3.4) differs from (2.19) only in the fact, that here instead of $V_{c0} + V_{v0}$ we divide by $V_v(t) + V_c(t) + V_g(t)$.

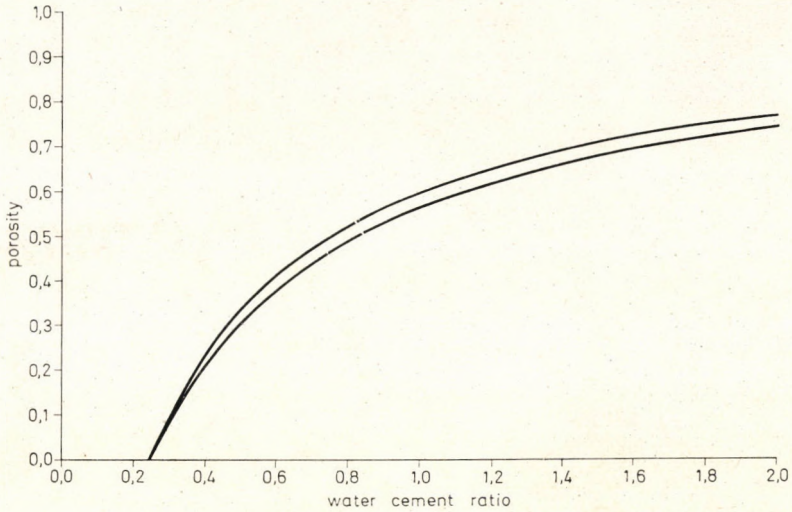

Fig. 2

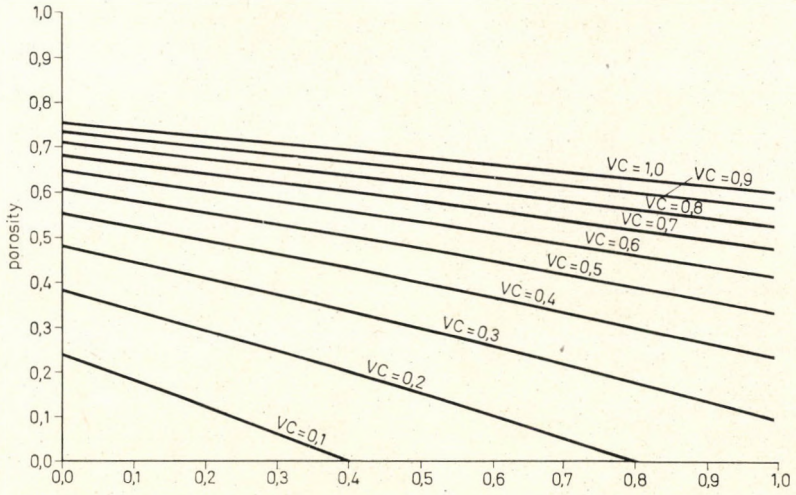

Fig. 3

4. The concept of the density factor, its dependence on water-cement-ratio V_t and hydration degree H(t)

For the cement stone, in a similar manner to the pore space, a dense volume V_t can also be defined in the following way

$$V_t = V_{\ddot{o}} - V_p \,. \tag{4.1}$$

By using (2.8) it will be

$$V_t = V_{\ddot{o}}(1 - \Phi) \,. \tag{4.2}$$

On the other hand, the density factor of the cement stone can be defined as a quotient of the dense volume and the total cement volume

$$\varphi_c = \frac{V_t}{V_{\ddot{o}}} . \tag{4.3}$$

By expressing this with the aid of (4.2) the result is

$$\varphi_c = 1 - \Phi . \tag{4.4}$$

According to (2.19), (4.4) φ_c is equal to

$$\varphi_c = \frac{1 + K\,H(t)}{1 + \varrho_c v_c} . \tag{4.5}$$

Then by using (3.4)

$$\varphi_c = \frac{\{(1 + K)\,\varrho_c - \varrho_g\}\,H(t) + \varrho_g}{\varrho_c\varrho_g\big(V_c - K\,H(t)\big) + \varrho_c(1 + K)\,H(t) - \varrho_g\big(1 - H(t)\big)} . \tag{4.6}$$

By taking (2.8), (2.9) and (4.2) into account the pore and the dense volumes are

$$V_p = M_{co}\big(v_c - K\,H(t)\big), \tag{4.7}$$

$$V_t = \frac{M_{co}}{\varrho_c}\big(1 + \varrho_c\,K\,H(t)\big) . \tag{4.8}$$

By using the porosity expression (3.4), V_p will be equal to (4.7) and at the same time V_t will be

$$V_t = \frac{M_{co}}{\varrho_c\varrho_g}\{[(1 + K)\,\varrho_c - \varrho_g]\,H(t) + \varrho_g\} . \tag{4.9}$$

5. Porosity of the cement stone taking the different mineral components into consideration

Taking into consideration that the cement consists of different minerals, marking the mass of the number i component by M_i^A, and the number r of the hydration products by M_r^g, the law of mass conservation can be written as follows

$$\sum_{i=1} M_i^A(t) + M_v(t) + \sum_{r=1} M_r^g(t) = \sum_{i=1} M_{io}^A + M_{vo} . \tag{5.1}$$

From this, expressing the $M_v(t)$ by the density and the volume and taking into consideration $\varrho_v = 1$, the pore volume is:

$$V_p = \sum_{i=1} M_{io}^A + M_{vo} - \sum_{i=1} M_i^A(t) - \sum_{r=1} M_r^g(t) . \tag{5.2}$$

We shall take into consideration only the case without change of volume, thus according to (2.10)

$$V_{\ddot{o}} = \sum_{i=1} \frac{M_{io}^A}{\varrho_i^A} + \frac{M_{vo}}{\varrho_v} . \tag{5.3}$$

By using (5.2) and (5.3) the porosity is:

$$\Phi = \frac{\sum_{i=1} M_{io}^A + M_{vo} - \sum_{i=1} M_i^A(t) - \sum_{r=1} M_r^g(t)}{\sum_{i=1} \frac{M_i^A}{\varrho_i^A} + \frac{M_{vv}}{\varrho_v}} . \tag{5.4}$$

Here, porosity is expressed only as a function of the individual mineral components. Then the water-cement-ratio is:

$$v_c = \frac{M_{vo}}{\sum_{i=1} M_{io}^A} = \frac{1}{\sum_{i=1} \frac{M_{io}^A}{M_{vo}}} . \tag{5.5}$$

Introducing the water-cement-ratio relative to the individual minerals, v_{ci} in the following manner is:

$$v_{ci} = \frac{M_{vo}}{M_{io}^A} . \tag{5.6}$$

By using (5.5) and (5.6) for the water-cement-ratios the result will be:

$$\frac{1}{v_c} = \sum_{i=1} \frac{1}{v_{ci}} . \tag{5.7}$$

In other words the water-cement-ratios relative to the individual minerals are added together in the same way, as are the resistences in parallel connection in electrotechniques.

By using (5.4) and (5.5) the porosity will be:

$$\Phi = \frac{M_v(t)}{M_{vo}} \frac{1}{\sum_{i=1} \frac{1}{\varrho_i^A} \frac{1}{v_{ci}} + 1} . \tag{5.8}$$

This porosity formula already contains also the dependence on the individual cement components. We transform its first factor by introducing the volume of the solid cement stone V_c^* in the following way:

$$\frac{M_v(t)}{M_{vo}} = \frac{\frac{M_v(t)}{V_c^*}}{\frac{M_{vo}}{V_c^*}} = \frac{\varrho_v(t)}{\varrho_{vo}} . \tag{5.9}$$

From (5.8) and (5.9)

$$\Phi = \varrho_v(t) \frac{1}{\sum_{i=1} \frac{\varrho_{vo}}{\varrho_i^A} \cdot \frac{1}{v_{ci}} + \varrho_{vo}} . \tag{5.10}$$

6. A method to measure porosity

The expression of porosity (5.10) involves the possibility of measuring porosity without destruction. When marking the second factor by a constant D^* it can be written in the following manner:

$$\Phi = \varrho_v(t)\, D^* . \tag{6.1}$$

D^* can be calculated from the preparation parameters or it must be determined by some other measuring procedure.

As dry cement stone provides electric insulation, it can be assumed that specific electric conductivity of the cement stone depends on the $\varrho_v(t)$ inherent in it, i.e. it is proportional to

$$\sigma(t) = \varrho_v(t)\, D^{**} \tag{6.2}$$

where D^{**} depends on the ratio of the ions dissolved in the water and on the degree of dissociation. This must also be determined by some measuring process. Assuming that D^* and D^{**} have already been determined, then taking these two constants together into a D constant, from (6.1) and (6.2)

$$\Phi = \sigma(t)\, D. \tag{6.3}$$

In this manner the measuring of porosity D^* and D^{**} specific resistence can be traced back. The way of determining D^* and D^{**} will be discussed on another occasion.

Acknowledgement

The author expresses his gratitude to Ervin Szűcs, Doctor of Technical Sciences and to János Újhelyi, Candidate of the Technical Sciences for their remarks and valuable suggestions relative to this work.

REFERENCES

1. Palotás—Kilián—Balázs: Betonszilárdítás (Concrete Hardening). Műszaki Könyvkiadó, Budapest 1968
2. W. Czernin: Zementchemie für Bauingenieure, Berlin 1960
3. T. C. Powers: *Proceedings* (1960), Vol. V. No. 2. p. 577
4. R. F. Feldmann: *Cement Technology*, January—February 1972

Porigkeit des Zementsteins in der Abhängigkeit des Wasser-Zement-Faktors. Aus theoretischen Erwägungen werden die Porigkeit und Dichte des erhärteten Zementsteins als Funktion des Wasser-Zement-Faktors und des Hydratationgrades abgeleitet. Die Gegenüberstellung der für die verschiedenen Fälle erhaltenen Ergebnisse den empirischen Werten ergab eine gute Übereinstimmung.

Пористость цементного камня в функции от водо-цементного фактора. Пористость затвердевшего цементного камня и его плотность выводятся в качестве функции водоцементного фактора V_c и степени гидратации $H(t)$ — на основе теоретических соображений. Результаты, полученные для различных случаев, сравниваются между собой и с практикой; при этом устанавливается удовлетворительное совпадение.

Acta Technica Academiae Scientiarum Hungaricae, Tomus 82 (1—2), pp. 179—196 (1976)

RESULTS OF SEMI-PILOT-MEASURINGS CONCERNING THE STEAM—AMMONIA HEAT-TRANSFORMATION IN BINARY POWER STATION SYSTEM

I. SZENTGYÖRGYI*—J. VARGA**—G. VERES***

[Manuscript received May 10, 1973]

At the beginning of the 1960's, when improving the air condenser system, Professor HELLER suggested the realization of the combined steam ammonia system. Later, in 1965, he published his recommendations concerning the structure of the suggested new system. Here he pointed out the dominant role of the heat exchanger dividing the partial cycles and also the difficulties concerning the realization were mentioned. It became evident, that experimental research was needed prior to realizing the dividing heat exchanger. Only the results of these experiments could show whether it is possible to build — at the necessary thermal conditions — a rational-dimension heat exchanger. In the course of the experimental work it was found possible to build a rational-dimension, steam—ammonia condenser boiler, which operates suitable even at the low, about 4 ÷ 6 °C temperature differences required from the thermal point.

Symbols

Δi	heat drop
i'	fluid enthalpy
i''	saturated vapour enthalpy
k	overall heat transfer coefficient
r	heat of evaporation
q	heat load
Δt	temperature difference
v'	fluid specific volume
v''	vapour specific volume
x	difference, steam-content, relative enthalpy $(i-i')/r$
F	surface
G	material flow
H	height of heat-exchanging tube
N	performance
Q	heat amount
S	entropy
T	temperature
V	volume
α	heat transfer coefficient
γ	specific weight
η	efficiency
λ	heat conductivity coefficient
μ	dynamic viscosity

*I. SZENTGYÖRGYI, Alpári Gy. u. 5. H-1051 Budapest, Hungary.
**J. VARGA, Toldi u. 11, 2330 Dunaharaszti, Hungary.
***G. VERES, Bogár u. 29/d. H-1022 Budapest, Hungary.

1. System Analysis

Together with the rapid growth in electric power requirements all over the world, and the development of ever greater, cooperating electric power systems, the tendency of development indicates the use of growing unit-performance turbo-generators, steam turbines and electric generators.

However, the volumetric conditions of the working medium flowing in the turbine pose a limit, over a certain value, to the growth in unit performance. Thus, first of all, it is the discharge cross section of the steam turbine that is such a limiting factor, as the blade length of the last stage, considering strength viewpoints, cannot be increased beyond a certain value.

Another major point, when establishing new, high-performance energetics units, is the maximum economy in cooling water, which requirement encourages the utilization of air-cooled, so-called "dry" cooling towers. Thus, the system to be evolved has to enable a rational consideration of the dry cooling tower solution.

The requirement noticed in the intensive industrialisation of very cold climates cannot be left out of consideration either, when bringing about new energetics units, namely, that these, serving the newly established industry and also the ample power supply of the inhabitants, have to operate in all circumstances without the danger of freezing. An added advantage, of course, is if the applied system is also in a position to utilize the potential thermodynamic capabilities of the surroundings.

For the striking solution of this group of problems Professor HELLER suggested the realization of a combined cycle where in the upper stage a steam cycle and in the lower one a "cold-vapour" cycle, as applied in cooling technology is the most suitable for an ammonia-cycle [1].

This combined cycle answers all the special requirements outlined above. As is to be seen from the T—S diagram characteristic of the cycle Fig. 1, in the upper temperature range the energy carrier is water while in the lower temperature range the working medium is NH_3. It is expedient to separate the two part-cycles from each other at a temperature where, on the one hand, the decisive amount of the heat fed to the NH_3 process can be taken into the system isothermally and, on the other, the structural elements of the part-cycle operating with water do not get under atmospheric pressure.

The schematic diagram in Fig. 2 gives information about the main equipment units of the system.

Between the upper and lower stage, as is also to be seen in Fig. 2, the energetics connection is provided by an intermediary heat exchanger which is practically a "cold" vapour boiler heated with condensing steam. The economy of the combined cycle is influenced in a major way by the characteristic features of this heat exchanger.

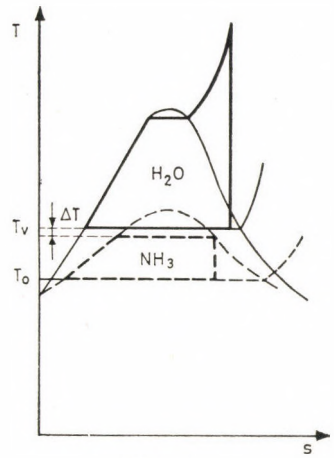

Fig. 1

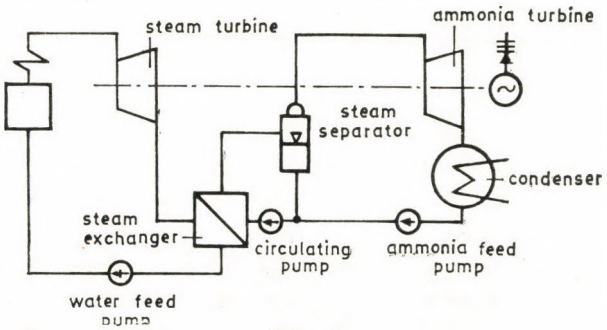

Fig. 2

On the basis of the system-technical and thermal investigations carried out with the suggested system in the past ten—twelve years, it was found that, expect for the heat exchanger of the combined system, all other system units can be realized. No special research and test is needed prior the their realization, the design work can be considered to be engineering task.

The same, however, cannot be stated about the heat exchanger. Already in the course of the initial investigation it became clear that this equipment-unit will cause the greatest difficulties when realizing the cycle. The construction of an experimental equipment was absolutely necessary with the aid of which, as for as possible, the processes evolving in the power station equipment could be simulated in the future.

In the course of experimental work some basic tests had to be carried out. Their results served as a kind of guarantee when designing the thermal and hydraulic dimensioning of the intermediary heat exchanger which, from the point of realization, is of great importance.

The heat transfer between the two media, as it is an isothermal one on both sides, will most probably be suitable. While, however, the condensation heat transfer of steam is a known process, there were no data available concerning that of ammonia. Though quite a number of measuring data were available concerning the boiling heat transfer of ammonia, these however, were measured in the low $1 \div 10$ at a pressure range usual in cooling technology and therefore the heat transfer coefficients were rather small [2, 3, 4, 5].

There are, of course, appropriate methods for calculating the boiling heat transfer coefficient, these methods, however, gave no unambiguosly identical results concerning ammonia (boiling heat transfer in this case is called the heat transfer process, when bubbles evolve from the fluid on the heating surface). Between the heat transfer coefficients calculated with the methods of ROHSENOW [6] and/or STEPHAN [2], the difference was, for example, nearly one order of magnitude.

The endeavour in the course of the experimental programme to determine the boiling heat transfer coefficient of ammonia and/or the achievable heat transfer coefficient in a steam—ammonia heat exchanger in a semi-pilot character equipment, at a realistic pressure was highly justified.

The primary objective of the experimental programme was to establish whether an exceptably dimensioned heat exchanger could be built in to the vapour—ammonia heat exchanger, at an optimal $4 \div 6$ °C temperature gap.

Let us now study, briefly, the considerations that justifield this small temperature gap, which posed a difficult task.

The heat flux in the heat exchanger could quite simply be calculated in such a way as to multiply the overall heat transfer coefficient with the surface and the temperature difference:

$$Q = kf \,.\, \Delta t.$$

The relationship between the surface and the temperature difference manifests itself in the fact that in case of a high temperature difference a small surface is needed, thus the heat exchanger would be cheap, while in case of a small temperature difference it would be costly. However, the relationship is not as simple as that. The temperature gap between the two media increases the thermal loss of the cycle. This loss is the smaller, the higher the dividing temperature is. The upper limit has to be below the critical temperature of ammonia (132,4 °C), while the lower limit has to be above the atmospheric boiling point of water (100 °C). Between such restricted temperature limits the optimal value is determined by the fact that the operation cost of the ammonia feed pump and the investment cost of the steam—ammonia heat exchanger is to be low. At such conditions the optimal dividing temperature is around 100 °C.

For the optimation of the heat exchanger temperature gap we have to know the size of this loss. This loss can be expressed with the aid of the con-

densation temperature (T_0 bottom temperature limit) and the entropy increase [7].

$$\Delta Q = T_0 \cdot \Delta S.$$

The entropy increase can be expressed with the heat flux in the heat exchanger Q, and the temperature prevailing on the two sides of the heat exchanger

$$\Delta S = Q\left(\frac{1}{T_a} - \frac{1}{T_v}\right) = Q\,\frac{\Delta t}{T_{v,a}^2}$$

where T_v is the condensation temperature of steam, T_a the evaporation temperature of ammonia in °K

$$T_{v,a} = (T_v \cdot T_a)^{0.5} \text{ and } T_v - T_a = \Delta t.$$

Substituting ΔS into expression ΔQ

$$\Delta Q = Q\,\frac{T_0}{T_{v,a}^2}\,\Delta t.$$

Let us express this loss related to the heat amount derived in the heat exchanger as

$$\frac{\Delta Q}{Q} = \frac{T_0}{T_{v,a}^2}\,\Delta t\ .$$

If, for instance $T_{v,a} = 380$ °K, $T_0 = 303$ °K, then

$$\frac{\Delta Q}{Q} = 0{,}002\ \Delta t\ .$$

Applying a temperature gap of $\Delta t = 5$ °C, the loss is 1 per cent of the heat derived in the heat exchanger.

A more accurate results also considering the quantitative relationship of steam and ammonia vapour and the expansion in the turbine, could be achieved if the equation expressing the efficiency of the combined system was applied to determine the loss of the temperature gap [8].

$$\eta = \frac{\Delta i_v + \varphi \Delta i_a}{\Delta i_v + \varphi\,(\Delta i_a + \Delta i_{k,a})}$$

where $\varphi = G_a/G_v$ is the quantitative ratio to be computed from the thermal balance of the heat exchanger, Δi_v is the steam heat drop, Δi_a is the ammonia vapour heat drop, determined from the expansion line where the losses have already been considered, $\Delta i_{k,a}$ is the heat dissipated in the amonia condenser.

If this efficiency is determined taking the temperature gap of the heat

exchanger into consideration and/or not considering it, the loss due to the temperature gap can be calculated from the $\Delta\eta$ difference of the two efficiencies.

$$\Delta N = \frac{N}{\eta}\,\Delta\eta$$

(efficiency here is the multiplication of the thermal efficiency and the turbine efficiency).

With the aid of this loss-calculation method, besides the quantitative relationship of the two media, also the character of the upper cycle is considered, as, for instance, in a high-pressure, superheated steam-cycle, Δi_v is much higher than in the saturated steam cycle of atomic power stations and, at the same time also the temperature gap loss will be different.

Knowing the temperature gap loss, the temperature gap can now be optimized. A possible method of optimation is to start from the fact that, despite the performance loss caused by the temperature gap of the heat exchanger, the performance of the power station has to remain unchanged. This can be achieved if this loss is already taken into consideration during the design work and a bigger power station is designed. A bigger power station, established with a surplus investment due to loss (the surplus investment burdens only certain installations of the power station) has to produce the performance loss caused by the heat stage with a surplus amount of fuel. Thus, when optimizing the temperature gap of the heat exchanger, the minimum of the yearly cost-ratio of the surplus investment (ΔC_a), the surplus fuel (ΔC_f) and the price of the heat exchanger (ΔC_h), viz. the solution of equation

$$\frac{\partial[\Delta C_a(\Delta t) + \Delta C_f(\Delta t) + \Delta C_h(\Delta t)]}{\partial(\Delta t)} = 0$$

is looked for [9]. The qualitative determination of such a cost minimum is shown in Fig. 3. In case of low temperature differences the surplus investment

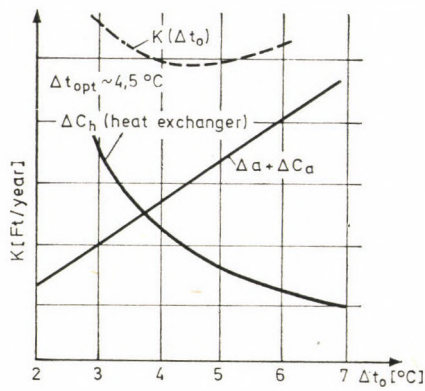

Fig. 3

and the fuel cost of the heat exchanger in a linear way, while the yearly cost of the heat exchanger in a hyperbolic way as regards the temperature gap. According to the power plant type (lignite-, coal-, oil heating or atomic power plant) the effect of the individual cost factors is not identical, thus an accurate value can be indicated only when precisely knowing the type of the power plant, power and heat exchanger price. However, from our hitherto investigations it can be established that the value of Δt_{opt} is between $4 \div 6$ °C.

This $4 \div 6$ °C temperature gap, however, is very small, lower than the usual value in heat exchangers or condensers. The question therefore crops up whether it is possible to establish a steam–ammonia heat exchanger with suitable dimensions, even at such a small temperature gap.

Investigating the heat transfer on both sides of the heat exchanger, it can be seen, concerning the condensing heat tansfer of steam that the small temperature gap provides no disadvantage, as the condensing heat transfer coefficient is highly suitable just in the case of low temperature differences.

The situation in case of the boiling heat exchange of the ammonia-side is the reverse, however, as in case of boiling the heat transfer coefficient changes by 2,3 powers of the temperature difference of the heating wall and the saturation temperature of the fluid, the so-called temperature difference of superheating. As the entire temperature difference of the heat exchanger may not exceed $4 \div 8$ °C, it was thought that no sufficiently high heat transfer coefficient could be achieved at the $2 \div 3$ °C temperature gap pertaining to the ammonia side.

2. Semi-pilot measurings

On basis of purely theoretical considerations no reassuring answer could be given to this question. We therefore decided to construct an equipment in the frame of the experimental program, with the aim of which an answer could be obtained concerning the heat transfer circumstances evolving int the flowing NH_3 tube, at boiling point. A major aspect was that, as far as possible, physical and geometrical conditions could be guaranteed in the experimental loop that could be realized in industrial circumstances in the future energetics installations.

The experimental installation was built in the laboratory of the Department of Energetics of the Technical University of Budapest, constructed by VEIKI, on basis of a commission by EGI. Former also undertook the measurings. The units of the installation, except for the instruments, were situated in the open air. The flow diagram of the test apparatus is to be seen in Fig. 4 [10, 11, 12].

The measuring section in the experimental measuring equipment was a 5 m long, having a 25 mm internal diameter tube, through which ammonia was

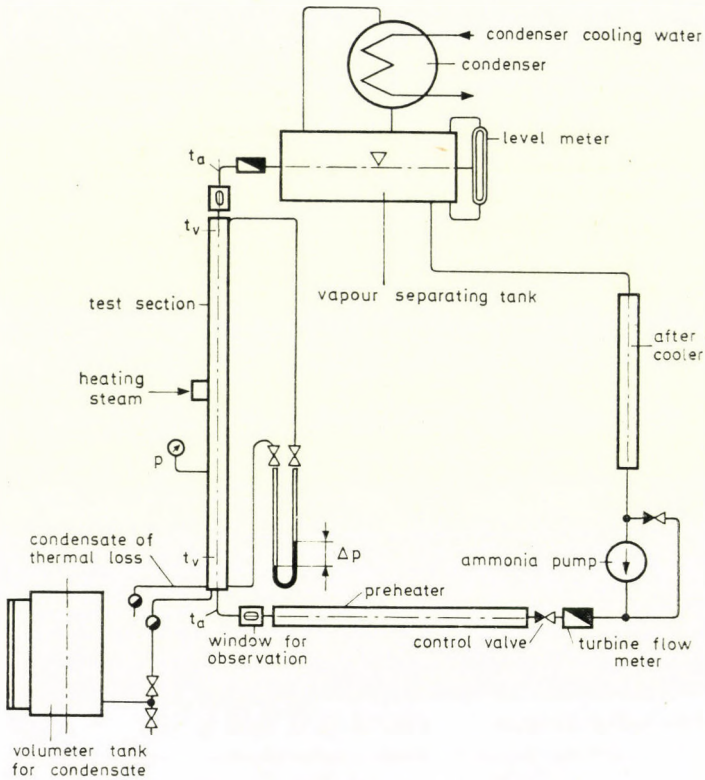

Fig. 4

coursed with the aid of a pump. The heating was realized by steam condensation on the external tube-wall. The pressure of the ammonia (70 at), the length and diameter of the tube guaranteed the realistic simulation of a small part (a pipe) of the combined system heat exchanger.

Part of the ammonia evaporated in the heat exchanger, the evolving vapour had to be condensed. A fluid-vapour two-phase mixture leaves the heat-exchanger, in front of the condenser the fluid is separated from the vapour by way of a vapour separator, wherefrom the separated fluid and the condensate is led to a pump, which keeps the flow up by interposing an after-cooler (to eliminate cavitation).

The density of the two-phase mixture evolving in the heat exchanger is lower than that of the fluid in the cold pipe section in front of the pump. Due to the difference in specific weight of the two pipe sections, a free flow may evolve in the heat exchanger. When starting the experiments we did not know whether the heat transfer coefficient of the ammonia side would be high enough, therefore also a circulating pump was built in. (A Rütchi product, glandless, Acid-Perfecta pump.)

The ammonia penetrates into the steam—ammonia heat exchanger, pre-heated by steam, which first warms to the saturation temperature in the heat exchanger and is then followed by the vapour formation. When designing the experimental apparatus, we endeavoured to produce both a few degrees sub-cooling (with the after-cooler) and a saturated temperature and (or relative enthalpy state higher than zero) with a pre-heater built at the inlet side of the section.

In the heat exchanger we measured the overall heat transfer coefficient and the boiling heat transfer coefficient on the ammonia side. For this purpose, the temperature of ammonia and the tube wall had to be measured with a high accuracy. Two kinds of sensors were applied for measuring the temperature, 100 ohm Pt. resistance thermometers and thermocoax crommel-alumel termo-couples. The temperature measured with the resistance thermometer were determined with a precision thermometer-bridge, while those measured with the aid of thermo-couples with a 16 measuring stage Kent-type compensograph. No problems were encountered in taking the steam and ammonia temperatures, the only thing that had to be guaranteed was to place the applied thermo-couples and resistance thermometers in a thermometer-case that do not conduct heat from the environment to the point of the measuring, and thus the temperature dominant at the measuring point was taken [13].

Greater care was needed when measuring the temperature of the tube-wall. A widely used method is to solder the thermo-couples to the external tube-wall. In our case, however, this method was not adequate as the heat transfer (condensation) on the tube-wall was very good and therefore, the thermo-couple soldered on to the surface — similar to a fin — would transfer heat to the surface. In this way, the thermo-couple would have measured a higher than real temperature. To avoid such an error, the thermo-couples were placed in a slot in the tube-wall, thus the thermo-couples did not protrude from the tube wall (Fig. 5.).

However, the termo-couple fastened to the tube wall measures a local temperature (which changed from one point to the other). The heat transfer coefficient on the other hand was computed from the temperature determined with the condensed vapour along the entire heat exchanger and thus suitable places had to be selected for measuring the wall temperature where the local heat transfer coefficient corresponded to the mean. This, seemingly complex method was needed because the vapour condensate on the heat transfer tube develops a precipitate film thickening towards the bottom, the heat resistance of which deteriorates the condensation heat transfer coefficient of vapour.

According to Nusselt's theory, the value of the local condensation heat transfer coefficient [14], is:

$$\alpha_x = \left[\frac{r \gamma^2 \lambda^3}{4 \mu X \Delta t} \right]^{1/4}$$

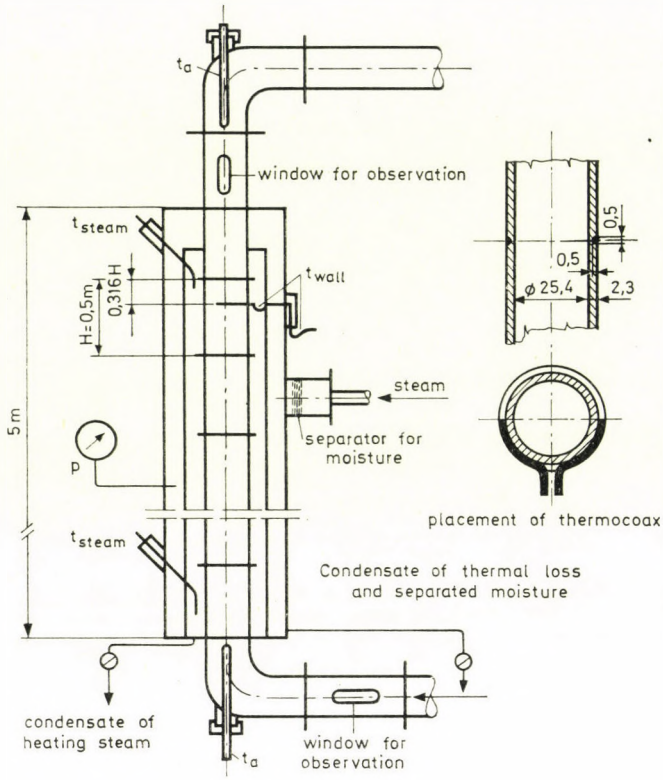

Fig. 5

the mean transfer coefficient, the one relating to an H tube-length is:

$$\alpha = \frac{1}{H}\int_0^H \alpha_x \, dx = \frac{4}{3}\left(\frac{r\,\gamma^2\,\lambda^3}{4\mu\,H\,\Delta t}\right)^{1/4}.$$

On the point in question $x = 0{,}316$ H, and with this condition

$$x = 0{,}316 \text{ H}.$$

A problem was encountered when measuring the mass flow of ammonia. After an unsucessful attempt to build-in a metering orifice, the reliable solution was achieved by applying turboquant turbine flow-meters.

The pressure of ammonia and steam was measured with Bourdon-tube manometers.

The basis for thermal calculations was the accurate measuring of the heat flow in the heat exchanger. For this purpose the most appropriate method was to determine the thermal balance on both sides of the heat exchanger, concerning the flowing material. On the condensation side the thermal balance

meant an accurate determination of the condensate

$$Q_1 = G_v r$$

measured in a volume meter. In the heat exchanger the steam does not only condensate on the heat transfer tube but, because of the heat loss, also along the external casing wall. Due to the inaccuracies in thermal loss calculation, an intermediary tube was placed around the heat transfer tube in the experimental equipment, which was split along a generatrix. This intermediary tube caused no resistance in the flow of steam, at the same time we were able to effictively separate the condensate of heat loss. The steam for heating was obtained from the steam-network of the Laboratory and, as here the steam was mostly moist, a moisture separator was built-in following the main steam valve.

The thermal balance on the ammonia side can be determined on basis of the relationship

$$Q_2 = G_a(i_2 - i_1)$$

where i_2 is the enthalpy of the outlet ammonia and i_1 that of the inlet ammonia. The inlet enthalpy can be determined in a unanimous way from the temperature of the ammonia, while for the outlet one we have to know the vapour content of ammonia, thus

$$i_2 = i' + x\,r.$$

The steam content can be best determined in the ammonia condenser (from the amount of the condensate). The method, however, is rather a complex one and, therefore, we rather measured the volume of the ammonia — ammonia vapour mixture in the outlet cross section of the heat exchanger and specified the vapour content from the ratio of the inlet and outlet volume (V_m/V')

$$V_m = [(1-x)v' + xv'']\ G$$

wherefrom

$$x = \left(\frac{V_m}{V'} - 1\right) \Big/ \left(\frac{v''}{v'} - 1\right).$$

The method could be applied as the circulating volumes at the inlet side of the test section (without vapour content) and after it (two-phase mixture) were measured with a high-accuracy turbine flow meter. The thermal balances calculated with the two methods coincided.

The test apparatus was dimensioned to 70 at, the assumed operational pressure. From the point of security several equipments, controlled by pressure-were installed, these guaranteed that the pressure in the loop should not exceed 90 at. As a safety valve a splitting disc operating at 90 at was built in, through which the ammonia — in case the disc broke — could get into an absorb-

ing tank, half filled with water (in the measuring carried out till the splitting disc was not necessary).

In the course of measurings we found that the commercial-quality ammonia, delivered in bottles, contained both water and oil as contaminants. As contaminants are disadvantageous both from the point of corrosion and heat transfer, a distiller was built into the system to purify the ammonia. This distiller was also suitable for pouring out the entire ammonia amount from the heat exchanger during operation and then purify it by distilling.

Windows were built into it to observe the purify of the ammonia in the system and the flow-circumstances developing in the heat exchanger.

The heat transfer coefficents computed from the data measured in the experimental heat exchanger are to be seen in Fig. 6 (because of measuring technical causes, greater than optimal, 2,5 mm-thickness steel tubes were built into the experimental heat exchanger and thus the temperature drop across the wall is higher than can be seen in Fig. 9, while the heat transfer coefficient was lower).

As not only the temperature of the two media but also that of the tube wall was measured, the temperature gap of the ammonia side could be calculated from the temperature of the tube wall and the ammonia

$$\Delta t_a = t_w - \Delta t_w - t_a,$$

and then also the heat transfer coefficient on the ammonia side

$$\alpha_a = \frac{q}{\Delta t_a}.$$

(The heat transfer coefficients on the ammonia side are shown in Fig. 7.)

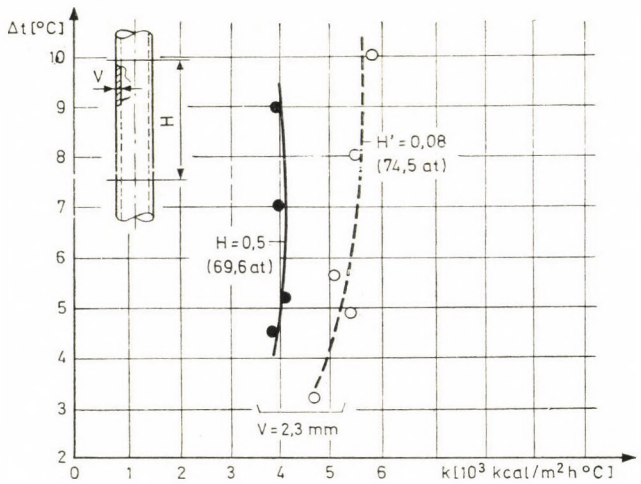

Fig. 6

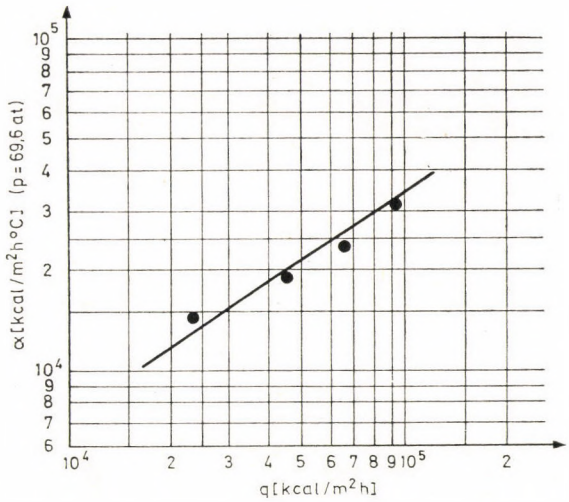

Fig. 7

The boiling-heat transfer of ammonia was measured in the experimental heat exchanger in conditions identical with a real situation. Sometimes the boiling heat transfer coefficient is also measured in a pool (pool boiling). In certain circumstances the results obtained in this way could also be applied concerning convective boiling (if the thermal load, at a given velocity and subcooling exceeds a limit value, we speak about a "developed" boiling and in such cases the boiling heat transfer coefficient is independent of the valocity).

3. Pool boiling measurements

In the laboratory of the Department of Chemical Machinery (T. U. of Budapest) the pool boiling heat transfer coefficient of ammonia was measured in the range of high pressure and thermal load. (This test was carried out together with L. VIMMER.) The dependence of the heat transfer coefficient on thermal load and pressure could be more accurately determined from measuring the data of pool boiling as in a semi-pilot plant, thus the heat transfer cricumstances of the ammonia side could also be investigated more profoundly.

At low pressure the heat transfer coefficients of pool boiling coincide, with a good approximation to the already mentioned measuring data available in literature and at high pressure with those measured in a semi-pilot experimental equipment. In this way a connection could be established between the high boiling-heat transfer coefficients indicated in literature as measured in a laboratory and a semipilot equipment.

In Fig. 8 the pool boiling-heat transfer coefficients in the function of heat load, at differente pressure, are clearly to be seen. The boiling-heat trans-

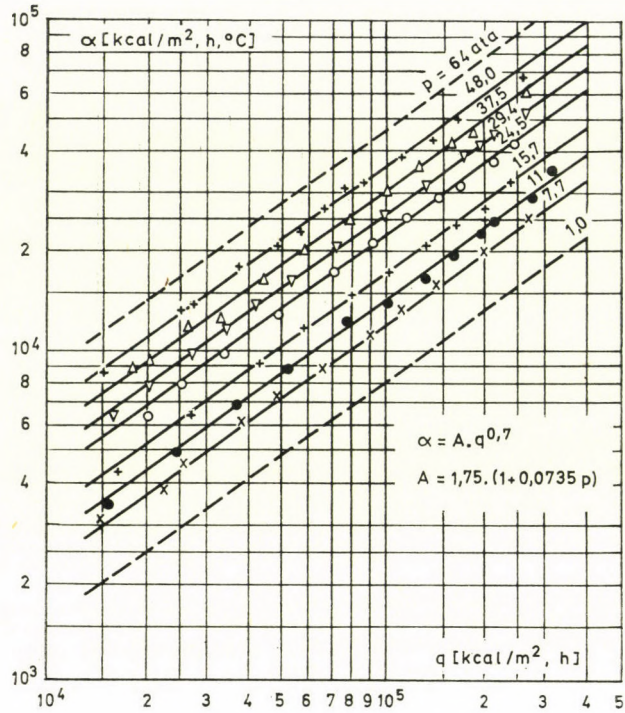

Fig. 8

fer coefficients of ammonia can be calculated — in the function of thermal load and/or temperature gap — with the following expressions: (15)

$$\alpha_a = A\, q^{0,7} = 1{,}75(1 + 0{,}0735\ \mathrm{p})\, q^{0,7},$$

$$\alpha_a = A' \Delta t^{2,3} = 7{,}6(1 + 0{,}0735\ \mathrm{p})^{3,7}\, \Delta t^{2,3}.$$

($p = 7 \div 50$ at pressure-range, valid only for ammonia).

4. Conclusions

From the theory of heat transfer it is known that the heat transfer coefficient can be effectively increased, if the heat transfer of the worse side is improved, while the heat transfer improvement of the "good" side but slightly changes the heat transfer coefficient.

However, in the course of our experiments we observed a seemingly paradox phenomenon, viz. that in the case in question the heat transfer conditions of the better side have to be improved to receive a higher heat transfer coefficient concerning the complete heat exchange. As a result of improving the

better side, we found that, regarding the complete temperature difference, the part of the better side is less, which, of course entails an increase in the temperature gap on the worse side. As is known, the boiling heat transfer coefficient can be increased only by a very high increase of the flow velocity (and this, of course, would not be economic because of the high power requirement of circulation) and, also a change in the surface roughness would bring about only a temporary improvement as, after a certein time, the surface roughness would be equalized. On the other hand, the boiling heat transfer coefficient can be improved in a major way by increasing the temperature difference between the heat-transmitting wall and the medium, as the boiling-heat transfer coefficient changes by a 2,3 exponent power of the temperature difference. In this way we achieved a decisive improvement of the worse side by improving the better one, a phenomenon indicating that with this seemingly paradox method we succeeded in a decisive way in improving the entire heat transfer coefficient.

However, as a result of the measurings that were carried out it was found that at a 70 at pressure, corresponding to the industrial one, the heat transfer coefficient of ammonia is very appropriate even at a less than 2 °C temperature gap on the ammonia side (it is about 20 000 kcal/m²h°C) and that this high heat transfer coefficient is already realized at a very low, 0,2 ÷ 0,3 m/s velocity. As has already been mentioned, the boiling-heat transfer coefficient of the ammonia side changes by a 2,3 power of the temperature gap, when increasing the same, the conclusion can be drawn that the ammonia side heat transfer coefficient is now better than the value to be achiebed in steam condensation, though this value is still better than those to be achieved in power plant condensers (due to the change in physical properties and because of a deficiency in condensing gases).

Not following the paradox consideration anymore longer but the usual method, viz. we aimed at improving the steam-side condensation, that of the worse one. Together with improving the steam condensation heat transfer we increased the heat transfer coefficient of the ammonia side too, something that would not have happened in the reverse case. In this way, however, the above mentioned paradox case is resolved, so, to improve the heat transfer, we followed the usual way, by taking steps on the worse side.

At the same time we improved the steam condensation coefficient by hindering a thickening of the condensate-film falling on the tube wall. Already during the first stage of measurings discs, serving to remove the falling condensate film, were placed at distances of $H = 0{,}5$ m, while we endeavoured to improve condensation, and together with it the heat transfer coefficient by increasing the number of these discs.

The phenomenon can be illustrated as follows: In case of a 110 °C steam and 105 °C ammonia, the temperature drop of the condensation, the ammonia-

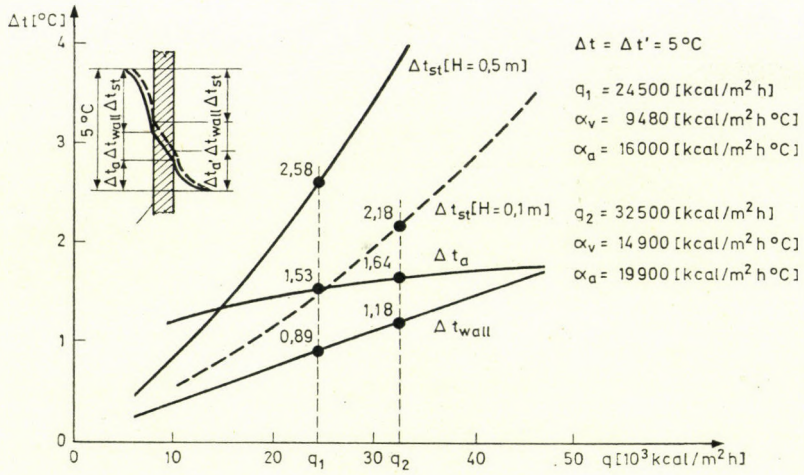

*Fig. 9**

side and the tube-wall were sketched in the function of the thermal load of the heat exchanger (Δt_{st}, Δt_a Δt_u). In the case of the curve to be seen in Fig. 9 the vapour condensation developed at a $H = 0{,}5$ m relative height tube (calculated value). As the condensation heat transfer coefficient changes according to the $-0{,}25$ exponent power of the temperature gap, while the ammonia boiling-heat transfer coefficient according to the 2,3 exponent power, the condensation heat transfer coefficient slightly worsens when increasing the thermal load, while the boiling heat transfer coefficient is ameliorated in a major way (accordingly, in the figure the temperature gap of condensation greatly increases in the function of thermal load, while the boiling heat transfer temperature gap changes but slightly).

The temperature gap of the heat exchanger is the sum total of the three partial temperature gaps and, according to the data of the figure, is 5 °C in case of a thermal load of $q = 24{,}500$ kcal/m²h ($k = 4900$ kcal/m²h°C). If we improve the condensation heat transfer (by increasing the number of condensate-removing discs placed at a distance of $H = 0{,}5$ m to a distance of $H' = 0{,}1$ m), the sum total of the three part-temperature gaps will be 5 °C at $q' = 32500$ cal/m²h ($k = 6500$ kcal/m²h°C). Expressed in a quantitative way, this means that the temperature gap on the condensation side decreases from 2,58 °C to 2,18 °C, at the same time the temperature gap of the ammonia side increased from 1,53 °C to 1,64 °C. Thus, a 57-per-cent improvement in the condensation heat transfer coefficient was accompanied by a 23-per-cent improvement in the ammonia side heat transfer. Accordingly, the overall heat transfer coefficient improved by 33-per-cent. The condensation heat

* Instead of Δt_v the correct value is Δt_{st}

transfer coefficient did not only improve as a result of decreasing the H height but also because the condensation temperature gap diminished too, and thus the improvement is

$$\frac{\alpha'_k}{\alpha_k} = \left(\frac{\Delta t}{\Delta t'}\right)^{1/4} \left(\frac{H}{H'}\right)^{1/4}.$$

It is a pity that, due to the high pressure and the agressive character of ammonia, no copper or aluminium tubes could be used — which have a low thermal resistance, — and that the thermal resistance of carbon steel tubes diminishes in a major way the value of the overall heat transfer coefficient.

The thickening of the steam condensate along the vertical heat transfer tube can be hindered with the aid of condensate-separating discs. Care has to be taken at the same time that the separated condensate does not go back to the neighbouring tube. Even in case of a suitable structural solution we have to reckon, however, with the fact that some of this condensate does penetrate into the neighbouring tubes and thus the heat transfer coefficient inprovement cannot be more than φ-times, where $\varphi < 1$.

The values of heat transfer coefficients obtained after increasing the number of the original $H = 0{,}5$ m-interval condensate-separating discs ($H' = 0{,}08$ m) are also shown in Fig. 6.

From the measuring results of semi-pilot steam ammonia heat exchangers it could be seen that in a combined power station heat exchanger a very intensive heat transmission takes place and thus, despite the optimal, though small ($4 \div 6$ °C) temperature gap, a high, $q = 10 \div 40.\ 10^3$ kcal/m^{2}h thermal load can be brought about.

Also on the basis of the above measuring results it could be observed that it is possible to construct a rational surface dimension heat exchanger, appropriate for our purposes, even with small temperature gaps. For a detailed and reliable designing — especially to be able to judge the hydromechanical behaviour, further experiment series are needed. In the course of this work we wish to determine mainly data concerning the heat transfer and hydromechanics of a two-phase medium with a relative enthalpy higher than zero.

Acknowledgements

To round off this paper we should like to express our thanks to the National Technical Development Committee and the Energy Economic Institute for the financial help that enabled our experiments to be carried out. Our thanks go also to Professor HELLER who initiated our research and followed up the results. But thanks are also due to all the colleagues who took part in the work.

REFERENCES

1. HELLER, L.: New Power Station System for Unit Capacities in the 1000 mW Order. *Acta Techn. Hung.* **50** (1965)
2. STEPHAN, K.: Berechnung des Wärmeüberganges an siedende Kältemittel. *Kältetechnik* **15** (1963)
3. CHAWLA, J. M.: Wärmeübergang und Druckabfall in waagerechten Rohren bei der Strömung von verdampfenden Kältemitteln. *VDI-Forschungsheft* **523** (1967)
4. FILATKIN, W.: Der Wärmeübergang beim Sieden wässriger Ammoniaklösungen. *Holodnaja Techn.* **34** (1957)
5. DANILOVA, G. N.: Heat Transfer to Boiling Refrigerants. Edited by S. S. Kutateladze: Problems of Heat Transfer and Hydraulics of Two-phase Media Pergamon Press, Oxford 1969
6. ROHSENOW, W. M.: Handbook of Heat Transfer. McGraw-Hill, 1973
7. SILBERRING, L.: Binärer Kreislauf für Kraftwerkblocke großer Leistung. *BWK* **21** (1969), 578/82
8. SLUSAREK, Z. M.: The Economic Feasibility of the Steam—Ammonia Power Cycle. Franklin Institute Research Laboratories, Philadelphia, Pennsylvania. P. B. 184—334 (1968)
9. SZENTGYÖRGYI, I.: Nagy egységteljesítményű erőművek kétközegű körfolyamattal (High Unit-Capacity Power Plants with Combined Cycles. In Hungarian) *Energia és Atomtechnika* (1972), 441—449
10. VARGA, J.: VEIKI-report 1969 (In Hungarian)
11. VARGA, J.: VEIKI-report 1970 (In Hungarian)
12. VARGA, J.: VEIKI-report 1971 (In Hungarian)
13. SZENTGYÖRGYI, I.—VARGA, J.—VERES, G.: Javaslat a vízgőz—ammonia hőcserélő továbbfejlesztésére (Suggestions for the Development of a Vapour—Ammonia Heat Exchanger. In Hungarian.) Not published
14. MIHEJEV, M. A.: A hőátadás gyakorlati számításának az alapjai (Basis for the Practical Calculation of Heat Transfer. In Hungarian.) Tankönyvkiadó, Budapest 1956
15. SZENTGYÖRGYI, I.: A vízgőz—ammonia hőcserélő néhány kérdése (Some Problems of Vapour Ammonia Heat Exchanger. In Hungarian.) Not published

Ergebnisse von halbbetriebsmäßigen Messungen im Zusammenhang mit der Wärmetransformation Wasserdampf—Ammoniak in Zweitstoffkraftwerken. — Anfang der sechziger Jahre schlug Prof. Heller im Zuge der Vervollkommnung des Luftkondensator-Systems vor, ein Wasserdampf—Ammoniak-Zweitstoffsystem zu verwenden; 1965 veröffentlichte er Vorschläge für den Aufbau des neuen Systems [1]. Hier wies er auf die entscheidende Bedeutung des die Teilvorgänge trennenden Wärmeaustauschers hin, sowie auf die Schwierigkeiten bei dessen Realisierung. Es wurde klar, daß vor der Verwirklichung des Trennwärmeaustauschers experimentelle Forschung benötigt wird. Nur die Durchführung der Versuche kann darauf Antwort geben, ob bei Einhaltung der notwendigen thermischen Bedingungen ein Wärmeaustauscher von rationellen Abmessungen gebaut werden kann. Im Verlauf der Versuchsarbeit konnte festgestellt werden, daß es möglich ist, einen solchen Wasserdampf—Ammoniak-Kondensator-Kessel zu bauen, der auch bei den thermisch erwünschten kleinen Temperaturdifferenzen von ca. 4—6 °C zufriedenstellend arbeitet.

Результаты полузаводских измерений в связи с термотрансформацией водяного пара — аммония двухсредной электростанции. В начале 60 годов профессор Хеллер при усовершенствовании системы воздушной конденсации предложил использование двухсредной комбинированной системы на базе водяного пара — аммония. После выполнения исследований в 1965 году профессор Хеллер опубликовал свои предложения, касающиеся построения предложенной им новой системы (1). В данной публикации он указал на решающим образом важную роль теплообменника, разделяющего частные циркуляционные процессы, и на затруднения, возникающие при решении такой системы. Стало ясным, что перед разработкой разделительного теплообменника необходимо провести экспериментально-исследовательскую работу. Только после завершения экспериментальных опытов можно получить ответ на вопрос, что возможно ли при необходимых термических условиях построить рациональный по размерам теплообменник.

Во время экспериментальных опытов установлено, что можно построить такой рациональный по своим размерам конденсаторный котел для водяного пара и аммония, который работает удовлетворительно даже в случае необходимой малой разности температур в прибл. 4—6° C.

Acta Technica Academiae Scientiarum Hungaricae, Tomus 82 (1—2), pp. 197—210 (1976)

EXAMINATION OF MIXING IN WATER STREAMS USING MASS FLUX CONSTANT CURVES

L. SOMLYÓDY*

[Manuscript received March 5, 1975]

The report deals with the mixing of a dissolved passive pollutant permanently released into a water stream. It assumes the velocity field as being known and makes use of the equation of turbulent diffusion, describing the said phenomenon by the introduction of depth-averaged values, in a co-ordinate system consisting of streamlines and equipotential lines normal to them. As in the case of streamlines, it defines the curves of mass flux constant which divide the original differential equation into two equations, more convenient to handle computationally. Furthermore, the report outlines certain characteristics of the curves, then deals with the computation of the distribution of the concentration, respectively, with the inverse case: the determination of the dispersion coefficients obtained by tracer measurements.

Symbols

x, y, z	Cartesian co-ordinates	[m]
s, b, z	Right-handed curvilinear orthogonal co-oordinate system; s being a streamline and b a co-ordinate normal to it	[m]
H_s, H_b	Lamé coefficients	
b_m	Co-ordinate of the mass flux constant curve	[m]
B	Width	[m]
h	Depth	[m]
v_s, v_b, v_z	Velocities in the directions of s, b, and z	[m s^{-1}]
c	Concentration	[kg m^{-3}]
D, D', D^*, $\tilde{\tilde{D}}^*$	Diffusion and dispersion coefficients	[m^2 s^{-1}]
q(b)	Distribution of the water discharge	[m^3 s^{-1}]
$\dot{m}$(b)	Distribution of the mass flux	[kg s^{-1}]
$\bar{a}$	Time-averaged value of (a)	
a'	The fluctuations of value (a)	
$\tilde{a}$	The depth integrated value of (a)	
a^*	The deviation of (a) from $\tilde{a}$	

Introduction

In case of a turbulent flow the mixing of a passive dissolved substance released into a water stream is described by the Reynolds equation of motion and by the equation of turbulent diffusion.

Although for the efficiency of water quality control the solution of this type of problem is indispensable, our knowledge in this field is still insufficient.

*Dr. L. SOMLYÓDY, Szamóca utca 6/b, H-1125 Budapest, Hungary.

One of the difficulties lies in the fact that not only are we unable as yet to compute correctly the distribution of the velocity in space but we cannot easily, for the time being, make on-site measurements either. Further facts which cause concern are the determination of the diffusion coefficients — of which we know very little — and the resolution of the equation of diffusion which, in a closed form, is at present only known for some special cases. As a consequence, research workers are compelled to seek solutions to certain part problems only.

Author in this report deals with the case of permanent mixing, assuming the velocity field as being known, and studying the phenomenon in a coordinate system consisting of a streamline and a trajectory normal to it (Chapter 1). It is assumed furthermore that release takes place without any differences in the density and in the velocity.

Author defines the mass flux constant curves (the lines along which the mass flux is constant) in Chapter 2. The so obtained equations are easy to handle numerically, in the determination of the distribution of concentration (Chapter 3), as well as in the determination of the dispersion coefficient (Chapter 4).

The method is applicable to optional water streams, within the limits set by the introduction of depth-integrated values.

1. The depth-averaged form of the governing equation of turbulent diffusion in a curvilinear co-ordinate system

The spatial distribution of a passive dissolved substance (pollutant) released permanently into a water stream, in the (s, b, z) right-hand curvilinear orthogonal co-ordinate system is given by the equation of turbulent diffusion

$$\frac{\partial}{\partial s}(H_b \bar{v}_s \bar{c}) + \frac{\partial}{\partial b}(H_s \bar{v}_b \bar{c}) + \frac{\partial}{\partial z}(H_s H_b \bar{v}_z \bar{c}) = \\ = \frac{\partial}{\partial s}(-H_b \overline{v_s' c'}) + \frac{\partial}{\partial b}(-H_s \overline{v_b' c'}) + \frac{\partial}{\partial z}(-H_s H_b \overline{v_z' c'}) \tag{1}$$

where the over-bars designate the average in time and the commend terms stand for the pulsations.

The system (s, b, z) will be more precisely defined later. For the time being, suffice it to state that s and b denote the "streamline" in the tangential plane of the free surface and the curvilinear coordinate normal to it, respectively, while z is the linear coordinate normal to the plane of s and b. H_s, H_b in the

equation are Lamé-coefficients [2]:

$$H_s = \sqrt{\left(\frac{\partial x}{\partial s}\right)^2 + \left(\frac{\partial y}{\partial s}\right)^2}, \quad H_b = \sqrt{\left(\frac{\partial x}{\partial b}\right)^2 + \left(\frac{\partial y}{\partial b}\right)^2},$$

while x and y in this case are Cartesian co-ordinates.

Eq. (1) can be resolved in knowing the boundary, the boundary conditions (along the boundaries the normal gradient of concentration is equal to zero), the velocity field and the correlations on the right-hand side. The latter are usually replaced by the coefficients of turbulent diffusion D_s, D_b, and D_z according to the Boussinesq hypothesis [3].

Experience has shown that the variations along z, following from the usual geometry of water streams (width $\gg$ depth) quickly decay [4]. This allows the simplification of the problem in such a manner that instead of the exact solution of (1) such solution is sought for which satisfies the equation along the depth, on an average.

Let us, accordingly, integrate the relationship (1) from the free surface to the bottom then, making use of the rule of Leibnitz, let us interchange the order of integration and differentiation [5]. Under such circumstances, in consideration of the conditions prevailing at the free surface and at the bottom (the normal gradient of the velocity and the concentration are equal to zero [4]), we have

$$\begin{aligned} \frac{\partial}{\partial s}\int_0^h H_b \bar{v}_s \bar{c}\,dz + \frac{\partial}{\partial b}\int_0^h H_s \bar{v}_b \bar{c}\,dz = \\ = \frac{\partial}{\partial s}\int_0^h - H_b \overline{v_s' c'}\,dz + \frac{\partial}{\partial b}\int_0^h - H_s \overline{v_b' c'}\,dz \end{aligned} \tag{2}$$

(in the time average of v and c the over-bars will hereinafter be omitted). Here

$$\partial H_s/\partial z = \partial H_b/\partial z = 0$$

and introducing the relations

$$c = \tilde{c} + c^*, \quad v_s = \tilde{v}_s + v^*, \quad v_b = \tilde{v}_b + v^*$$

(denoting with curved over-bar the depth-integrated values (2)), it assumes the following form:

$$\begin{aligned} \frac{\partial}{\partial s}(H_b h \tilde{v}_s \tilde{c}) + \frac{\partial}{\partial b}(H_s h \tilde{v}_b \tilde{c}) = \\ = \frac{\partial}{\partial s}\left[H_b \int_0^h (- \overline{v_s' c'} - v_s^* c^*)\,dz\right] + \\ + \frac{\partial}{\partial b}\left[H_s \int_0^h (- \overline{v_b' c'} - v_b^* c^*)\,dz\right]. \end{aligned} \tag{2a}$$

Let us now fix the directions s and b by dropping the second term on the left-hand side. This is fulfilled if the conditions

$$H_s h \tilde{v}_b = 0 \quad \text{and} \quad \frac{\partial}{\partial b}(H_s h \tilde{v}_b) = 0$$

are satisfied, which means that the direction s — under the continuity equation — (we assume that $\partial v/\partial t = 0$) must correspond to the tangential direction of the streamline. This is gained at the intersection of the free surface and the plane, obtained by the stra'ghtening of the stream surface arced along z [6].

Since, generally from field measurements, the velocity field in any given problem is known in advance, the (s, b) co-ordinate system may be chosen according to the method outlined above and can be simplified accordingly.

Let us now study the right-hand side of equation (2a) and introduce the following "Fickian" laws:

$$-\int_0^h (\overline{v_s' c'} + v_s^* c^*)\, dz = \frac{1}{H_s}(D_s + D_s')\frac{\partial \tilde{c}}{\partial s} h\,, \tag{3a}$$

$$-\int_0^h (\overline{v_b' c'} + v_b^* c^*)\, dz = \frac{1}{H_b} D_b \frac{\partial \tilde{c}}{\partial b} h - \widetilde{v_b^* c^*}\, h = \tag{3b}$$

$$= \frac{1}{H_b}(D_b + D_b')\frac{\partial \tilde{c}}{\partial b} h\,.$$

Thereby:

$$\frac{\partial}{\partial s}(H_b h \tilde{v}_s \tilde{c}) = \frac{\partial}{\partial s}\left[\frac{H_b}{H_s} h\,(D_s + D_s')\frac{\partial \tilde{c}}{\partial s}\right] + \tag{4}$$

$$+ \frac{\partial}{\partial b}\left[\frac{H_s}{H_b} h\,(D_b + D_b')\frac{\partial \tilde{c}}{\partial b}\right],$$

where

$D_s^* = D_s + D_s'$ designates the longitudinal, and
$D_b^* = D_b + D_b'$ the transversal coefficient of dispersion.

The first terms express the effect of turbulence, the second terms the deviation of the total convective effect from the average. D_s, and D_b are positive numbers and so is D_s^* according to TAYLOR and ELDER [7, 8]. D_b^*, however, depending on the secondary flows, the relative mass transport associated to them and on the character of the turbulent mass transfer, may also be negative. In such a case the introduction of the concept of transverse dispersion would be of no use and it is more reasonable to use the first line of the expression (3b). (A general method would be given only by the three-dimensional treatment which is at present beyond the range of our knowledge.)

D'_s, respectively D'_b disappears if

$$c^* = 0;$$
$$v_s^* = 0,\ v_b^* = 0;$$

or if the conditions

$$\int_0^h v_s^*\, c^*\, dz = 0,\ \int_0^h v_b^*\, c^*\, dz = 0$$

are met.

Due to these and to the order of magnitude of the derivative $\partial\, \tilde{c}/\partial\, s$, it is generally assumed that

$$\frac{\partial}{\partial s}\left[\frac{H_b}{H_s}\, h\, D_s^* \frac{\partial \tilde{c}}{\partial s}\right] \cong 0.$$

This assumption, except in the immediate surroundings of the pollutant source is fulfilled with a fair approximation (as proved by literature [4]).

It should be noted that the introduction of the concept of longitudinal dispersion is often unnecessary. If so then — neglecting the term with D_s (which is possible with a good approximation as verified by measurements on macro-turbulence in a straight open laboratory-size channel [6]) — (4) takes the following form:

$$\frac{\partial}{\partial s}(H_b h \widetilde{v_s \tilde{c}}) = \frac{\partial}{\partial b}\left[\frac{H_s}{H_b}\, h\, D_b^* \frac{\partial \tilde{c}}{\partial b}\right]. \tag{4a}$$

It deserves to be noted that D_s^* defined by the relation (3a) differs from the D_L longitudinal dispersion coefficient [9, 10] used in the one-dimensional method of writing.

The one-dimensional form and D_L may be derived by the integration of equation (4) in the direction of b, between the two banks of the water stream.

2. Mass flux constant lines

Once more, let us study the phenomenon of mixing in the previous coordinate system. Its b = const. lines, respectively, its surfaces normal to the (s, b) plane superposed thereon, are characterized by no water transport across these elements along z.

Lines or surfaces along which there is no mass transport may be interpreted in the same manner.

Fig. 1 shows the curves of the mass flux constant. To determine them, let us write down the time average of the mass fluxes across the planes normal to the water surface superposed upon the arced elements $d_s\ s$ and $d_b\ b_m$ which, according to the laws of conservation of matter, are equal to each other.

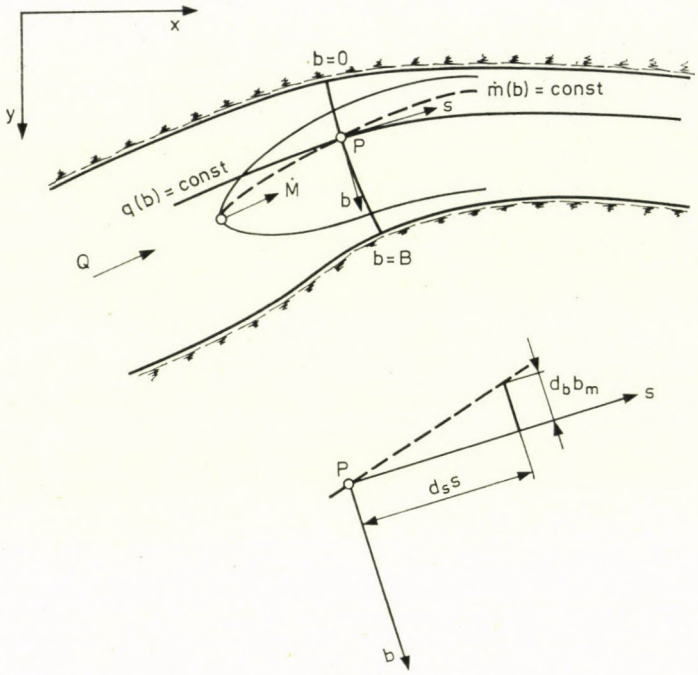

Fig. 1

With the customary designations

$$\int_0^h (v_b c + \overline{v_b' c'})\, dz\; H_s\, ds = \int_0^h \left[(v_s + v_s' + \frac{\partial (v_s + v_s')}{\partial s}\, ds\right] \times$$

$$\times \left[c + c' + \frac{\partial (c + c')}{\partial s}\, ds\right] dz \left[H_b + \frac{\partial H_b}{\partial s}\, ds\right] db_m.$$

After slight transformations, neglecting the quantities of second order and introducing depth-integrated values and the relationships (3a, b), we obtain

$$-\frac{H_s}{H_b}(D_b + D_b')\frac{\partial \tilde{c}}{\partial b}\, h\, ds = \left[\widetilde{v_s c} h H_b - \frac{H_b}{H_s} D_s \frac{\partial \tilde{c}}{\partial s}\, h\right] db_m =$$

$$= \left[\tilde{v}_s\, \tilde{c}\, h\, H_b - \frac{H_b}{H_s}(D_s + D_s')\frac{\partial \tilde{c}}{\partial s}\, h\right] db_m. \tag{6}$$

Hence, the equation of the mass flux constant curve (to be interpreted as time average) in the streamline — the equopotential line co-ordinate system will be

$$\frac{ds}{\left[\widetilde{v_s c} - \frac{1}{H_s} D_s \frac{\partial \tilde{c}}{\partial s}\right] h\, H_b} + \frac{db_m}{\frac{H_s}{H_b}(D_b + D_b')\frac{\partial \tilde{c}}{\partial b}\, h} = 0. \tag{7}$$

The expression is analogous with the differential equation of the streamlines in a two-dimensional flow.

For the tangent of the angle enclosed by the streamlines and the $\dot{m}(b) = \text{constant}$ curves (assuming that the denominator of the first term of (7) differs from zero), equation (7) yields the following relationship:

$$\frac{db_m}{ds} = -\frac{H_s}{H_b} \frac{(D_b + D'_b)\frac{\partial \tilde{c}}{\partial b}}{\widetilde{v_s c}\, H_b - \frac{H_b}{H_s} D_s \frac{\partial \tilde{c}}{\partial s}}, \tag{8}$$

or, with the first equality of (3b):

$$\frac{db_m}{ds} = -\frac{H_s}{H_b} \frac{D_b \frac{\partial \tilde{c}}{\partial b} - \widetilde{v_b^* c^*}\, H_b}{\widetilde{v_s c}\, H_b - \frac{H_b}{H_s} D_s \frac{\partial \tilde{c}}{\partial s}}. \tag{8a}$$

According to the foregoing, $\widetilde{v_s c}$ may be replaced by $\tilde{v}_s \tilde{c} - D_s/H_s \cdot \partial \tilde{c}/\partial s$; but the terms containing D_s and D'_s are mostly neglected.

To resolve a problem (8) in itself, this is not enough, since not only $\tilde{c}$ but also db_m/ds, is unknown.

According to the second equation, the variations of the mass flux along the stream-line are equal to the mass flux along the arced element db_m.

The equation can be derived as follows.

Let us take two trajectory elements at a distance $d_s s$ apart, and the $q(b) = \text{constant}$ streamline (Fig. 2), and a distribution of the mass flux which corresponds to Fig. 3.

The mass flux constant curve is characterised by $d\dot{m} = 0$.

This means that

$$d\dot{m} = \frac{\partial \dot{m}}{\partial s} ds + \frac{\partial \dot{m}}{\partial b} db_m = 0,$$

where the first term indicates the changes along line 1 and the second stands for the changes along line 2.

Hence

$$\frac{db_m}{ds} = -\frac{\partial \dot{m}/\partial s}{\partial \dot{m}/\partial b}. \tag{9}$$

The time-averaged mass flux is

$$\dot{m} = \int_0^b \widetilde{v_s c}\, h H_b\, db - \int_0^b \frac{H_b}{H_s} D_s \frac{\partial \tilde{c}}{\partial s} h\, db,$$

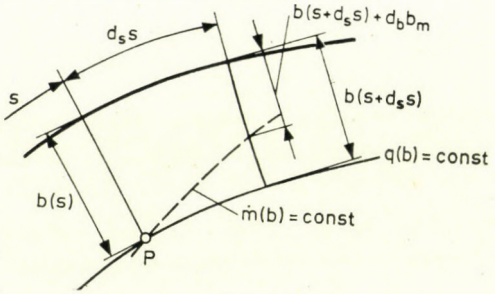

Fig. 2

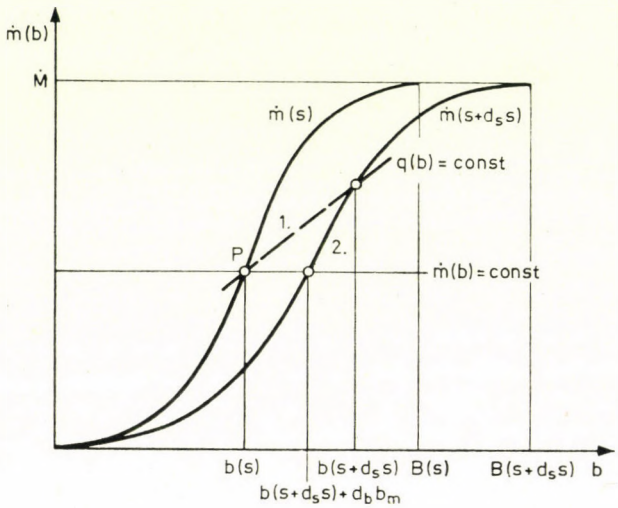

Fig. 3

and with it (9) takes the following form:

$$\frac{db_m}{ds} = -\frac{\dfrac{\partial}{\partial s}\int_0^b \widetilde{v_s ch H_b}\, db - \dfrac{\partial}{\partial s}\int_0^b \dfrac{H_b}{H_s} D_s \dfrac{\partial \tilde{c}}{\partial s}\, h\, db}{\widetilde{v_s ch H_b} - \dfrac{H_b}{H_s} D_s \dfrac{\partial \tilde{c}}{\partial s} h} \,. \tag{10}$$

The comparison of the relationship so obtained with (8) yields the original equation (4).

Accordingly, of the introduction of the mass flux constant curves the differential equation (4) is replaced by two equations. Their use, if a closed solution were sought for, would not allow simplification under all circumstances but their numerical application — as will be proved later — becomes considerably easier.

2.1. *Some characteristics of the derivative db_m/ds and the mass flux constant curve*

Setting out from equation (8) we assume that $(D_b + D_b') > 0$.

Since the boundary conditions at the points $b = 0$ and $b = B$ are

$$\left.\frac{\partial \tilde{c}}{\partial b}\right|_{b=0} = \left.\frac{\partial \tilde{c}}{\partial b}\right|_{b=B} = 0, \tag{11}$$

from which

$$\left.\frac{db_m}{ds}\right|_{b=0} = \left.\frac{db_m}{ds}\right|_{b=B} = 0 \tag{12}$$

all the more, since equation (8) is valid even for the flow of an ideal medium with which

$$\tilde{v}_s|_{b=0} \neq 0, \quad \tilde{v}_s|_{b=B} \neq 0,$$

and the denominator differs from zero — which means that (11) cannot be fulfilled in the general case, unless (12) holds true (see (8)). According to (12), the two banks are not only streamlines but also mass flux constant curves.

If, within the range, some of the cross-sections in point b are $\partial\tilde{c}/\partial b = 0$, this, too, is only possible then if $db_m/ds = 0$.

Introducing these points of successive cross-sections according to (8) and (9), the so obtained curve is not only a streamline but also a mass flux constant curve (with, naturally, every $\dot{m}(b) =$ constant curve passing through the point of release).

Since at $\partial\tilde{c}/\partial b = 0$ a maximum is concerned, the peak concentrations will be located along the above streamline (since in the opposite case the applicability of the second equation of (3b) becomes doubtful — see (4)).

From the above it follows that between the two banks of the water stream ($b = 0$, $b = B$) the function $db_m/ds = f(b)$ — unless it is zero at every point — must have an extreme value at least at one point of b. The extreme value (if there are several, then the one representing the highest absolute value) gives the tangent of the possibly greatest angle of spread in the cross section.

As complete mixing is approached, $\partial\tilde{c}/\partial\, b$, whereby $db_m/ds \to 0$, viz. the mass flux constant curves tend increasingly towards the streamlines.

A considerable advantage offered by the use of these curves is that they provide a picture also of the geometry of the mixing process.

3. Computing the distribution of concentration

In general, there is no closed solution to (8) and (10), although at a given value of s, in possession of $db_m/ds = f(b)$ and neglecting the longitudinal dispersion, $\tilde{c}(b)$ can be computed from (8). In this case, namely, the equation is reduced to an ordinary differential equation in which the variables can be separated.

The solution is

$$\tilde{c}(b) = \tilde{c}(b_1) \exp\left[-\int_{b_1}^{b} \frac{H_b^2}{H_s} \frac{\tilde{v}_s}{D_b^*} \frac{db_m}{ds} db' \right], \tag{13}$$

where $\tilde{c}(b_1)$ must be determined from the continuity condition:

$$\dot{M} = \tilde{c}(b_1) \int_0^B h\tilde{v}_s \exp\left[-\int_{b_1}^{b} \frac{H_b^2}{H_s} \frac{\tilde{v}_s}{D_b^*} \frac{db_m}{ds} db' \right] H_b \, db, \tag{14}$$

and it is rational to assume b_1 on the streamline passing through the point of release.

With the expressions (13) and (14) we have (15)

$$\tilde{c}(b) = \frac{\dot{M}}{\int_0^B h\tilde{v}_s \exp\left[-\int_{b_1}^{b} \frac{H_b^2}{H_s} \frac{\tilde{v}_s}{D_b^*} \frac{db_m}{ds} db' \right] H_b db} \times \\ \times \exp\left[-\int_{b_1}^{b} \frac{H_b^2}{H_s} \frac{\tilde{v}_s}{D_b^*} \frac{db_m}{ds} db' \right]. \tag{15}$$

This, provided that $H_b = H_s = 1$, $\tilde{v}_s$, h, $D_b^* =$ constant, $b^* = b - b_1$, $b^*(b = 0) \to -\infty$, $b^*(b = B) \to +\infty$, and

$$\to \frac{db_m}{ds} = \frac{b^*}{2(s - s_1)}, \tag{16}$$

(viz. the mass flux constant curves are parabolas with the axis s) will assume the form of

$$\tilde{c}(b) = \frac{\dot{M}}{2h\sqrt{\pi D_s^* \tilde{v}_s (s - s_1)}} \exp\left[-\frac{\tilde{v}_s}{4D_b^* \tilde{v}_s (s - s_1)} b^{*2} \right] \tag{15a}$$

corresponding to the well-known case of release from the point (s_1, b_1) into an infinitely large space.

Since thus solution is only rarely feasible, the following approximation may be applied.

Boundary, boundary conditions, the velocity distribution $\tilde{v}_s$ (and with it the streamlines, the equipotential curves, the coefficients H_s, and H_b and the transverse dispersion coefficients) are given (for simplicity's sake the longitudinal ones are neglected).

Also the $\dot{M}$ mass flux is known and the point and manner of release. As regards this latter, two cases can be distinguished for the purposes of computation.

First, it is assumed that along a finite length the concentration in one cross-section (at/or downstream from the point of release) is known. If so, then the distribution

$$db_m/ds(b)$$

can be computed from (8) and, replacing the curve $\dot{m}(b) = \text{constant}$ by its tangent (viz. using the differences), the points in the subsequent cross-section may be determined. Since between two adjacent mass flux constant lines the same mass is flowing, in possession of $\tilde{v}_s$, h both $\tilde{c}$ and the distribution in the new cross-section $\tilde{c}(b)$ can readily be determined.

Using this procedure over the entire region, the concentration field becomes obtainable.

In the second case release does not take place over a finite length, but point-like. Therefore, the concentration function will be singular and cause difficulties in the numerical solution. If this can be overcome and if a concentration distribution along a finite length near the source can be determined, then the process will be the same as described before.

There may exist an iterative method which, setting out from an approximation of the function $db_m/ds = f(s, b)$ is based on Eqs (8) and (10).

However, lacking the means to prove the convergency, it is reasonable to choose another method and assume that in the close vicinity of the point of release the spread is the result of random effects. In this case the distribution of concentration, unless the release takes place near the banks of the stream, will occur according to (15a). With pollutant sources on or close to the banks, solutions similar to (15a) — applying the principle of reflection — may be used [4, 11, 12].

This allows transition to finite length and the computation of the entire concentration field.

4. Determination of the dispersion coefficient from tracer measurements

Now, we wish to establich the coefficient defined by the known relationships (3a, b) in possession of the boundary, the velocities and the concentration field (the latter from tracer measurements).

From among these, the determination of the coefficient of the longitudinal dispersion, with the approximation $D_s^* \approx D_s'$ is only possible if the distributions $v_s(z), ;c(z)$ are also known. The computation on the basis of (3a) will cause no difficulty whatsoever.

Being interested primarily in D_b^*, for simplicity's sake let us assume that $D_s^* \cdot \partial \tilde{c}/\partial s \cong 0$. (This restriction, in the method to be described below, is unnecessary.)

From the measurement results first the distributions $\dot{m}(b)$ are computed, from which the curves $\dot{m}(b) = \text{const.}$ and the derivatives db_m/ds can be easily obtained (the latter possibly with equation (10)).

Assuming that $D_b^* > 0 (D_b > D_b')$; $\widetilde{v_s c}\ db_m/ds$ and the zero places of $\partial \tilde{c}/\partial b$ coincide (see (8)), further that here there exists a finite limit value of

$$\widetilde{v_s c}\,\frac{db_m}{ds}\Bigg/\frac{\partial \tilde{c}}{\partial b}\,.$$

D_b^* can be expressed as

$$D_b^*(s, b) = -\frac{H_b^2}{H_s}\,\frac{\dfrac{db_m}{ds}\,\widetilde{v_s c}}{\dfrac{\partial \tilde{c}}{\partial b}}\,, \tag{17}$$

and computed point by point.

In order to avoid the derivation of $\partial \tilde{c}/\partial b$ Taylor's polynom for D_b^* should be used and (17) should be rearranged.

As to whether it is worthwile to assume the dispersion coefficient as one varying in the flow field studied, we cannot say on the basis of the little information available to us at present.

On the one hand, most methods 'ab ovo' assuming that $D_b^*(s, b) = \text{constant}$ [except, for instance, HOLLEY (4) who computes $D_b^*(s)$by the "generalized change of moments" method, from the changes in longitudinal direction of the variance of the distributions $\dot{m}(b)$], on the other hand, we do not know to what degree errors in the measurements and evaluation effect the variations obtained as the result.

The definition of the function $D_b^*(s, b)$ in great detail is justified as a means to study better the transverse transport and the various effects it involves (see 3b), in particular, if it enables their separation. This, in fact, is feasible at certain points of the range being studied. Namely, as outlined in Chapter 2.1, if $D^* > 0$, the streamline passing through the point of release and the mass flux constant curve (on which also the concentration maxima are located), will coincide.

Let us now study a case in which this provision is not fulfilled. Obviously, in this case there is no reason to introduce D_b^*, so let us take equation (8a).

At some fixed s there are two characteristic points which meet the conditions

$$db_m/ds = 0, \quad \text{and} \quad \partial \tilde{c}/\partial b = 0, \quad \text{respectively.}$$

At b_1, according to the first

$$D_b(b_1)\frac{\partial \tilde{c}}{\partial b}(b_1) = \widetilde{v_b^* c^*}(b_1)\, H_b(b_1)\,, \tag{18}$$

the concentration peak not falling on the common line $q(b) = \text{const.}$ and $\dot{m}(b) = \text{const.}$

In the second case (with the foregoing approximations):

$$\widetilde{v_b^* c^*}(b_2) = \frac{H_b}{H_s}(b_2)\,\tilde{v}_s(b_2)\,\tilde{c}(b_2)\,\frac{db_m}{ds}(b_2), \tag{19}$$

viz. transverse transport, deviating from the turbulent, can be computed in point b_2. At some other b values this and also the separation of the two forms of mass transfer are feasible only with different assumptions and the consideration of (18) and (19).

This tends to show that (17) may be used to advantage in the computation of the variations of D_b^* within the cross-section, while (18) and (19) provide information about the transports of two different characters.

Nevertheless, we also need a relationship which helps define the average D_b^* for one cross-section.

It is rational to strive to obtain the correct mass flux computed with the average $(\widetilde{\widetilde{D}}_b^x)$ viz. transform (14) into

$$\dot{M} = \tilde{c}(b_1)\int_0^B h\tilde{v}_s \exp\left[-\frac{1}{\widetilde{\widetilde{D}}_b^*}\int_{b_1}^b \frac{H_b^2}{H_s}\,\tilde{v}_s\,\frac{db_m}{ds}\,db'\right] H_b\,db, \tag{14a}$$

which provides $\tilde{c}(b_1)$. From (14a) $\widetilde{\widetilde{D}}_b^*$ may be expressed using iteration.

Similarly, it is possible to prescribe the equality of the variance of the mass flux distribution or to fulfil a best fitting for $\tilde{c}$ (both between measured and computed values, using Eq. (13)).

REFERENCES

1. Fukuoka, S.—Sayre, W. W.: Longitudinal Dispersion in Sinuous Channels; *Journal of the Hydraulics Division, ASCE*, Vol. **99,** No. HY 1 (Jan, **1973)**
2. Farkas, M.: Speciális függvények (Special Functions); Műszaki Könyvkiadó, Budapest 1964
3. Hinze, J. O.: Turbulence; McGraw-Hill, London 1959
4. Holley, E. R.—Siemons, J.—Abraham, G.: Some Aspects of Analyzing Transverse Diffusion in Rivers; *Journal of Hydraulic Research*, **10** (1972), No 1
5. Bronstejn, J. N.—Szemengyejev, K. A.: Matematikai zsebkönyv (Mathematical Pocketbook) Műszaki Könyvkiadó, Budapest 1974.
6. Somlyódy, L.: Turbulens diffúzió és diszperzió elméleti kérdéseivel kapcsolatos laboratóriumi vizsgálatok (Laboratory Examinations of the Theory of Turbulent Diffusion and Dispersion) *VITUKI Report*, 1974
7. Taylor, G. J.: Dispersion of Soluble Matter in Solvent Flowing Slowly Through a Tube; *Proc. Royal Soc.* A. 212 (1953)

8. ELDER, J. W.: The Dispersion of Marked Fluid in Turbulent Shear Flow; *Journal of Fluid Mechanics*, **5** (1959)
9. STAROSOLSZKY, Ö.: Diffúzió és diszperzió a vízépítési hidraulikában (Diffusion and Dispersion in Hydraulic Engineering) *Műszaki Tudomány*, **43** (1970)
10. STAROSOLSZKY, Ö.: On the Interpretation of the Longitudinal Dispersion Coefficient; 15*th Congress of the IAHR*, Istambul 1973
11. SZEPESI, D.: Légszennyező anyagok turbulens diffúziójának meteorológiai feltételei Magyarországon (Meteorological Conditions for the Turbulent Diffusion of Air Pollutants in Hungary); *Országos Meteorológiai Intézet Hivatalos Kiadványai*, **32** (1967)
12. CZERNUSZENKO, W.: Mixing Process in Wide Open Channels; *Journal of Hydrology*, **19** (1973)

Untersuchung der Vermischung in Wasserläufen. — Gegenstand der Arbeit ist die Untersuchung der Vermischung einer in einen Wasserlauf permanent eingeleiteten passiven, gelösten Verschmutzung. Das Geschwindigkeitsfeld wird als bekannt vorausgesetzt und die turbulente Diffusionsgleichung wird unter Einführung der entlang der Tiefe integrierten Werte in einem aus Stromlinien und Niveaulinien bestehenden Koordinatensystem angewendet. Als Analogie der Stromlinien werden die Linien des konstanten Massenstroms definiert. Durch deren Verwendung zerfällt die ursprüngliche Differentialgleichung in zwei — bei der numerischen Lösung sehr einfach zu handhabende — Gleichungen. Einige Eigenheiten der obigen Kurven werden besprochen. Die Arbeit beschäftigt sich auch mit der Berechung der Konzentrationsverteilung bzw. mit der umgekehrten Aufgabe, der Bestimmung der Dispersionsfaktoren aus Farbenmessungen.

Исследование смешивания в водотоках. Работа занимается исследованием смешивания пассивного растворенного загразняющего вещества, поданного в некоторый водоток. Поле скоростей предполагается известным, и уравнение турбулентной диффузии, описывающее данное явление, путем введения интегральных средних вдоль вертикального разреза применяется в системе координат, состоящей из линий обтекания, перпендикулярных к последним линий уровня. В качестве аналогии линий тока дается определение тех кривых, по которым течение массы является постоянным. При их использовании первоначальное дифференциальное уравнение разлагается на два уравнения, которые с точки зрения числовых вычислений являются легкими в обращении. Излагаются некоторые характерные свойства упомянутых выше кривых, после чего рассматривается вычисление распределения концентрации, а также обратная задача, то есть определение коэффициентов дисперсии на основе данных измерений методом мечения.

Acta Technica Academiae Scientiarum Hungaricae, Tomus 82 (1—2), pp. 211—232 (1976)

A METHOD TO SOLVE SOME AXI-SYMMETRICAL PROBLEMS OF THE THEORY OF ELASTICITY

I. ECSEDI*

[Manuscript received August 6, 1973]

The paper deals with the solutions of axisymmetrical quasi-static problems of continua consisting of layers of infinite extension parallel to a given plane. It is assumed that each layer is homogeneous and isotropic, consisting of linearly elastic material having insignificant deformation.

Symbols

r, φ, z cylinder coordinates

$\vec{e}_r, \vec{e}_\varphi, \vec{e}_z$ unit vectors of a cylindrical system of coordinates r, φ, z

$\vec{t} = u(r, z)\,\vec{e}_r + w(r, z)\,\vec{e}_z$ displacement vector

γ_{rz} change of angle

$\varepsilon_r, \varepsilon_\varphi, \varepsilon_z$ specific elongations

$\sigma_r, \sigma_\varphi, \sigma_z$ normal stresses

τ_{rz} shear stress

$\mathbf{A}$ deformation tensor

$\mathbf{E}$ stress tensor

G shear elasticity modulus

ν Poisson's ratio

$\vec{q} = a(r, z)\,\vec{e}_r + b(r, z)\,\vec{e}_z$ intensity of system of forces distributed on volume

$v = \dfrac{\partial u}{\partial r} + \dfrac{u}{r}$, $P = \dfrac{\partial \tau_{rz}}{\partial r} + \dfrac{\tau_{rz}}{r}$ auxiliary values

$U = Gu$, $V = Gv$, $W = Gw$

$\hat{v} = \int_0^\infty v(r,z) r I_0(kr)\,dr$ zeroth-order Hankel transform of function $v = v(r, z)$ in variable r; zeroth-order Hankel transform is designated by the sign "Λ" over the symbol of the function

$I_0(r)$ zeroth-order Bessel function of the first kind

$I_1(r)$ first-order Bessel function of the first kind

$\hat{X}, \hat{B}, \hat{x}$ column vectors

$\mathbf{C}, \mathbf{K} = \lambda\mathbf{E} - \mathbf{C}$ fourth-order quadratic matrices

$\mathbf{E}$ fourth-order unit matrix

$\det \mathbf{K}$ determinant of matrix $\mathbf{K}$

$\mathbf{T}(k, z, \nu) = \mathbf{T}(k, z)$ transfer matrix related to vector $\hat{X}(k, 0)$

$\mathbf{L}(k, z, G, \nu) = \mathbf{L}(k, z)$ transfer matrix related to vector $\hat{x}(k, 0)$

$\mathbf{P}, \mathbf{Q}$ fourth-order permutation matrices; sign of layer "i" ($i = 1,2, \ldots, n-1, n$)

G_i, ν_i material constants of layer "i"

$\mathbf{L}_i = \mathbf{L}_i(k_i, z_i = h_i, G_i, \nu_i)$ transfer matrix with respect to layer "i"

$\mathbf{L} = \mathbf{L}_{m-1}\mathbf{L}_{m-2}, \ldots, \mathbf{L}_2\mathbf{L}_1 = \prod_{i=1}^{n} \mathbf{L}_i$ resulting transfer matrix of the elastic body consisting of n layers, with respect to vector $\hat{x}_1(k, 0)$

Other values and symbols are explained in the text.

*Dr. I. Ecsedi, H-3531 Miskolc, Vászonfehérítő u. 24, Hungary.

1. Introduction

The paper at hand is intended to present a method suitable for solving axisymmetrical peripheral value problems concerning the quasistatic continuum of infinite extension in the direction of the axes x, y; of isotropic, in each of its layers homogeneous linear elastic material, subjected to small deformations, represented in Fig. 1.1. The solution to the above problem, disregarding the axisymmetry, limited to one layer both to planar and space problems, is detailed by WLASSOV's and LEONTEV's book [1]. Here, the equations established with the aid of the method of initial functions worked out by WLASSOV are solved by means of the formal operator calculus. The analysis of axisymmetrical problems of a body of finite thickness built up in several layers, each layer consisting of an elastic material, is dealt with by NIKITIN and SAPIRO [4]. The basic principle of their method is the simultaneous determination of the integration constants entering the zeroth-order Hankel transform Love's stress functions. In the basic conception of the procedure, present-

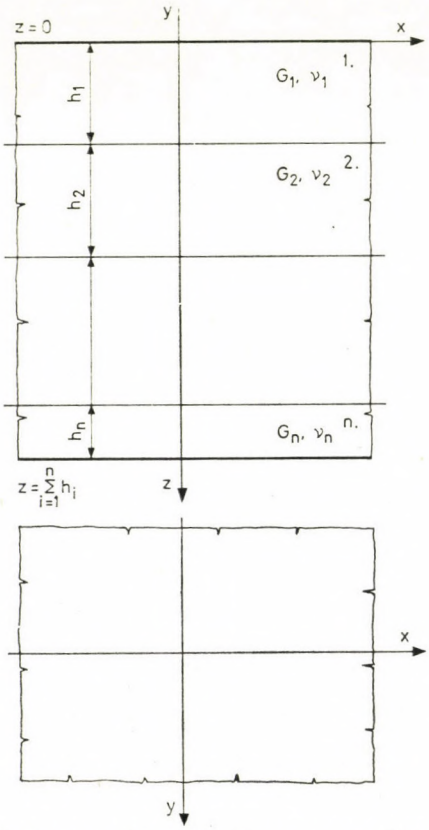

Fig. 1,1. Layered body in every layer of a homogeneous, linearly elastic material

ed in the paper, follows the method of "transfer matrix" worked out by Leon Y. BAHAR [2] for the analysis of a layered elastic medium in a state of planar deformation and planar stress state for solving the non-planar axisymmetrical problem described in the following.

2. Problem of axi-symmetrical boundary value of the theory of elasticity

First, the investigation of the axisymmetrical deformation of a body consisting of isotropic linearly elastic material having a thickness h, and of infinite extension of the axes x, y, represented in Fig. 2.1, is treated. It is known, as can be read in, for example, in [3], [8], that if the problem of the boundary value of the theory of elasticity, in connection with the above described body is axi-symmetrical then, in the cylindrical system of coordinates r, φ, z conveniently selecting the vector of displacement of a point P of the body in question will be

$$\vec{t} = u(r, z)\vec{e}_r + w(r, z)\vec{e}_z, \tag{2.1}$$

further, in the cylindrical system of co-ordinates r, φ, z the deformation and

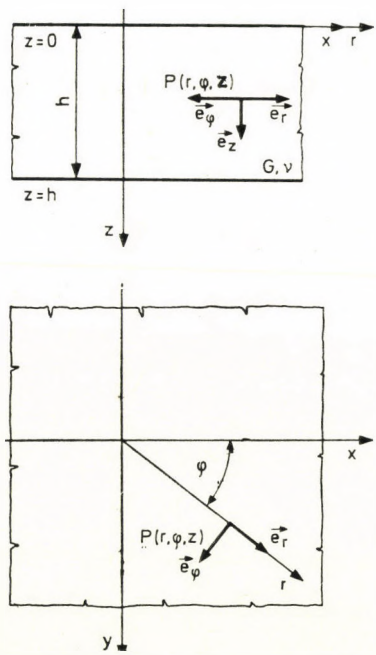

Fig. 2,1. Homogeneous elastic layer of thickness h

stress tensors at point P, respectively take the forms as follows:

$$\mathbf{A} = \begin{bmatrix} \varepsilon_r & 0 & \frac{1}{2}\gamma_{rz} \\ 0 & \varepsilon_\varphi & 0 \\ \frac{1}{2}\gamma_{zr} & 0 & \varepsilon_z \end{bmatrix}, \tag{2.2}$$

$$\mathbf{F} = \begin{bmatrix} \sigma_r & 0 & \tau_{rz} \\ 0 & \sigma_\varphi & 0 \\ \tau_{zr} & 0 & \sigma_z \end{bmatrix}. \tag{2.3}$$

Here, all of the scalar ordinates of **A** and **F** are only functions of r and z. In this case, the governing equations — geometric equations, Hooke's law, equilibrium equations — describing the behaviour of the homogeneous, isotropic, linearly elastic quasi-static body undergoing small deformations will be as follows:

— geometric equations connecting the elements of the vectors of displacement and deformation:

$$\varepsilon_r = \frac{\partial u}{\partial r}, \tag{2.4}$$

$$\varepsilon_\varphi = \frac{u}{r}, \tag{2.5}$$

$$\varepsilon_z = \frac{\partial w}{\partial z}, \tag{2.6}$$

$$\gamma_{rz} = \frac{\partial u}{\partial z} + \frac{\partial w}{\partial r}; \tag{2.7}$$

— Hooke's general law expressing the relation between the stress tensor and deformation tensor:

$$\sigma_r = \frac{2G}{1-2\nu}\left[(1-\nu)\,\varepsilon_r + \nu\,(\varepsilon_\varphi + \varepsilon_z)\right], \tag{2.8}$$

$$\sigma_\varphi = \frac{2G}{1-2\nu}\left[(1-\nu)\,\varepsilon_\varphi + \nu\,(\varepsilon_r + \varepsilon_z)\right], \tag{2.9}$$

$$\sigma_z = \frac{2G}{1-2\nu}\left[(1-\nu)\,\varepsilon_z + \nu\,(\varepsilon_r + \varepsilon_\varphi)\right], \tag{2.10}$$

$$\tau_{rz} = G\,\gamma_{rz}; \tag{2.11}$$

— the equations of mechanical equilibrium not identically satisfied:

$$\frac{\partial \sigma_r}{\partial r} + \frac{\partial \tau_{rz}}{\partial z} + \frac{\sigma_r - \sigma_\varphi}{r} + a = 0\,, \tag{2.12}$$

$$\frac{\partial \tau_{rz}}{\partial r} + \frac{\partial \sigma_z}{\partial z} + \frac{\tau_{rz}}{r} + b = 0\,. \tag{2.13}$$

In this latter equation $a = a(r, z)$ and $b = b(r, z)$ designate the scalar coordinates of the directions $\vec{e}_r$ and $\vec{e}_z$ of the specific load vector

$$\vec{q} = a(r, z)\,\vec{e}_r + b(r, z)\,\vec{e}_z. \tag{2.14}$$

σ_r, σ_φ, σ_z and τ_{rz} may directly be expressed by the coordinates u, w of the displacement vector

$$\sigma_r = \frac{2G}{1-2\nu}\left[(1-\nu)\frac{\partial u}{\partial r} + \nu\left(\frac{u}{r} + \frac{\partial w}{\partial z}\right)\right], \tag{2.15}$$

$$\sigma_\varphi = \frac{2G}{1-2\nu}\left[(1-\nu)\frac{u}{r} + \nu\left(\frac{\partial u}{\partial r} + \frac{\partial w}{\partial z}\right)\right], \tag{2.16}$$

$$\sigma_z = \frac{2G}{1-2\nu}\left[(1-\nu)\frac{\partial w}{\partial z} + \nu\left(\frac{\partial u}{\partial r} + \frac{u}{r}\right)\right], \tag{2.17}$$

$$\tau_{rz} = G\left(\frac{\partial u}{\partial z} + \frac{\partial w}{\partial r}\right). \tag{2.18}$$

Let us introduce the following notation and new variables:

$$U = Gu, \tag{2.19}$$

$$W = Gw, \tag{2.20}$$

$$\sigma_z = Z, \tag{2.21}$$

$$\tau_{rz} = R, \tag{2.22}$$

$$v = \frac{\partial U}{\partial r} + \frac{U}{r}, \tag{2.23}$$

$$V = Gv, \tag{2.24}$$

$$P = \frac{\partial R}{\partial r} + \frac{R}{r}\,. \tag{2.25}$$

The intention is to establish in the following a set of equations with the aid of which the variables U, W, V, Z, R, P from the "initial" values assumed in the plane $z = 0$, the values assumed in an arbitrary plane defined by the coordinate z $(0 \leq z \leq h)$, may directly be determined.

By virtue of Eq. (2.17) can be written

$$G\frac{\partial w}{\partial z}=\frac{1-2\nu}{2(1-\nu)}\sigma_z-\frac{\nu}{1-\nu}G\left(\frac{\partial u}{\partial r}+\frac{u}{r}\right). \tag{2.26}$$

By producing the difference between Eqs (2.15) and (2.16), the equation

$$\sigma_r-\sigma_\varphi=2G\left(\frac{\partial u}{\partial r}-\frac{u}{r}\right) \tag{2.27}$$

is obtained.

Substitution of Eq. (2.26) into Eq. (2.15) enables us to express σ_r also in the form

$$\sigma_r=\frac{2G}{1-\nu}\frac{\partial u}{\partial r}+\frac{2\nu G}{1-\nu}\frac{u}{r}-\frac{\nu}{1-\nu}\sigma_z. \tag{2.28}$$

Replacement of Eqs (2.27) and (2.28) into Eq. (2.12) and eliminating σ_r and σ_φ gives

$$\frac{\partial\tau_{rz}}{\partial z}=-\frac{2G}{1-\nu}\frac{\partial}{\partial r}\left(\frac{\partial u}{\partial r}+\frac{u}{r}\right)-\frac{\nu}{1-\nu}\frac{\partial\sigma_z}{\partial z}-a. \tag{2.29}$$

And from Eq. (2.13) it follows

$$\frac{\partial\sigma_z}{\partial z}=-\left(\frac{\partial\tau_{rz}}{\partial r}+\frac{\tau_{rz}}{r}\right)+b. \tag{2.30}$$

Eq. (2.18) may also be rearranged into the form

$$G\frac{\partial u}{\partial z}=-G\frac{\partial w}{\partial r}+\tau_{rz}. \tag{2.31}$$

From Eqs (2.31), (2.26), (2.30), (2.29), by making use of the new variables, defined by Eqs (2.19), (2.20), (2.21), (2.22), the following set of equations are obtained:

$$\frac{\partial U}{\partial z}=-\frac{\partial W}{\partial r}+R, \tag{2.32}$$

$$\frac{\partial W}{\partial z}=-\frac{\nu}{1-\nu}\left(\frac{\partial U}{\partial r}+\frac{U}{r}\right)+\frac{1-2\nu}{2(1-\nu)}-Z, \tag{2.33}$$

$$\frac{\partial Z}{\partial z}=-\left(\frac{\partial R}{\partial r}+\frac{R}{r}\right)-b, \tag{2.34}$$

$$\frac{\partial R}{\partial z}=-\frac{2}{1-\nu}\frac{\partial}{\partial r}\left(\frac{\partial U}{\partial r}+\frac{U}{r}\right)-\frac{\nu}{1-\nu}\frac{\partial Z}{\partial z}-a. \tag{2.35}$$

In case of an actual boundary value problem in the theory of elasticity, some of the combinations of the assumed values of the unknown variables (U, W, Z, R) assumed to be in the planes defined by $z=0$ and $z=h$, i. e., on

the limiting surfaces of the body investigated, are given. In other words, only the above variables will enter the boundary conditions.

By adding the paire of equations obtained from Eqs (2.32) and (2.35), by deriving with respect to r, and dividing with the variable r, then replacing the new variables defined by Eqs (2.23), (2.24) and (2.25) into the two new equations the following may be established:

$$\frac{\partial V}{\partial z} = -\left(\frac{\partial^2 W}{\partial r^2} + \frac{1}{r}\frac{\partial W}{\partial r}\right) + P, \tag{2.36}$$

$$\frac{\partial P}{\partial z} = -\frac{2}{1-\nu}\left(\frac{\partial^2 V}{\partial r^2} + \frac{1}{r}\frac{\partial V}{\partial r}\right) - \frac{\nu}{1-\nu}\left(\frac{\partial^2 Z}{\partial r^2} + \frac{1}{r}\frac{\partial Z}{\partial r}\right) - A. \tag{2.37}$$

Here, the notation

$$A = A(r, z) = \frac{\partial a}{\partial r} + \frac{a}{r}. \tag{2.38}$$

From Eqs (2.36), (2.33) and (2.37) the set of equations

$$\begin{aligned}
\frac{\partial V}{\partial z} &= -\left(\frac{\partial^2 W}{\partial r^2} + \frac{1}{r}\frac{\partial W}{\partial r}\right) + P, \\
\frac{\partial W}{\partial z} &= -\frac{\nu}{1-\nu} V + \frac{1-2\nu}{2(1-\nu)} Z, \\
\frac{\partial Z}{\partial z} &= -P - b, \\
\frac{\partial P}{\partial z} &= -\frac{2}{1-\nu}\left(\frac{\partial^2 V}{\partial r^2} + \frac{1}{r}\frac{\partial V}{\partial r}\right) - \\
&\quad -\frac{\nu}{1-\nu}\left(\frac{\partial^2 Z}{\partial r^2} + \frac{1}{r}\frac{\partial Z}{\partial r}\right) - A
\end{aligned} \tag{2.39}$$

will be built up, serving as a basis for further investigations.

For the solution to this set of partial differential equations, the method of integral transformation may be the most conveniently applied (see, for example [6], [7]).

3. Solution to the problem of the boundary values, making use of the Hankel transformation

By assuming the zeroth-order Hankel transform of the equations of the set of Eqs (2.39) "in the variable r", one arrives at the following set of ordinary

differential equations

$$\begin{aligned}
\frac{\partial \hat{V}}{\partial z} &= k^2 \hat{W} + \hat{P}\,, \\
\frac{\partial \hat{W}}{\partial z} &= -\frac{\nu}{1-\nu}\hat{V} + \frac{1-2\nu}{2(1-\nu)}\hat{Z}\,, \\
\frac{\partial \hat{Z}}{\partial z} &= -\hat{P} - \hat{b}\,, \\
\frac{\partial \hat{P}}{\partial z} &= \frac{2k^2}{1-\nu}\hat{V} + \frac{k^2\nu}{1-\nu}\hat{Z} - \hat{A}\,.
\end{aligned} \tag{3.1}$$

Here, $\hat{V}$, $\hat{W}$, $\hat{Z}$, $\hat{P}$, $\hat{b}$, $\hat{A}$ stand for the zeroth-order Hankel transform of the functions v, W, Z, P, b, A, respectively, with respect to the variable r, i.e., for example

$$\hat{V} = \hat{V}(k, z) = \int_0^\infty V(r, z)\, r\, I_0(kr)\, dr\,, \tag{3.2}$$

$$\hat{W} = \hat{W}(k, z) = \int_0^\infty W(r, z) r\, I_0(kr)\, dr\,, \tag{3.3}$$

$$(k > 0)$$

etc. By introducing the vectors

$$\hat{\mathbf{X}} = \hat{\mathbf{X}}(k, z) = \begin{bmatrix} \hat{V} \\ \hat{W} \\ \hat{Z} \\ \hat{P} \end{bmatrix}, \qquad \hat{\mathbf{B}} = \begin{bmatrix} O \\ O \\ -\hat{b} \\ \hat{A} \end{bmatrix}, \tag{3.4–3.5}$$

and the matrix

$$\mathbf{C} = \mathbf{C}(k) = \begin{bmatrix} 0 & k^2 & 0 & 1 \\ -\dfrac{\nu}{1-\nu} & 0 & \dfrac{1-2\nu}{2(1-\nu)} & 0 \\ 0 & 0 & 0 & -1 \\ \dfrac{2k^2}{1-\nu} & 0 & \dfrac{k^2}{1-\nu} & 0 \end{bmatrix} \tag{3.6}$$

the set of ordinary differential equations (3.1) may be concentrated into the following non-homogeneous, linear, first-order, vector differential equation of constant coefficient matrix

$$\frac{\partial \hat{\mathbf{X}}}{\partial z} = \mathbf{C}\hat{\mathbf{X}} + \hat{\mathbf{B}}\,. \tag{3.7}$$

The solution to the above differential equation is according to[5]:

$$\hat{X} = \hat{X}(k, z) = \exp(\mathbf{C}\, z)\, \hat{X}(k, 0) + \\ + \int_0^z \exp \mathbf{C}(z - \zeta)\, \hat{B}(k, \zeta)\, d\zeta\,. \tag{3.8}$$

As is known, (see [5]), the canonical resolution of the exponential matrix functions entering in the appearance (3.8) should be performed in different ways, depending on whether the roots of the minimum equation of the matrix $\mathbf{C}(k)$ are simple or multiple. In the problem in question the highest common divisor of the third-order minors of the characteristic matrix defined by the relation

$$\mathbf{K}(\lambda) = \lambda\, \mathbf{E} - \mathbf{C} \tag{3.9}$$

i.e., the elements of the matrix adj $(\lambda\, \mathbf{E} - \mathbf{C})$ built up from the foregoing minors, equals 1, therefore the matrix minimum equation

$$\det\ \mathbf{K}(\lambda) = \det\ (\lambda\, \mathbf{E} - \mathbf{C}) = 0 \tag{3.10}$$

of $\mathbf{C}$.

In the above equations $\mathbf{E}$ stands for the fourth-order unit matrix. Developing the expression (3.10) results in

$$\det \mathbf{K}(\lambda) = \begin{vmatrix} \lambda & k^2 & 0 & 1 \\ \dfrac{\nu}{1-\nu} & \lambda & -\dfrac{1-2\nu}{2(1-\nu)} & 0 \\ 0 & 0 & \lambda & 1 \\ \dfrac{2k^2}{1-\nu} & 0 & -\dfrac{\nu k^2}{1-\nu} & \lambda \end{vmatrix} = (\lambda^2 - k^2)^2,\ (k > 0)\,. \tag{3.11}$$

The roots of the above characteristic equation are

$$\lambda_1 = \lambda_2 = k, \quad \lambda_3 = \lambda_4 = -k, \ (k > 0). \tag{3.12}$$

The desired matrix functions may be established in the following form [5]:

$$\exp\ (\mathbf{C}z) = [\exp\ (kz)\, \mathbf{E} + z\ \exp\ kz\, (\mathbf{C} - k\mathbf{E})]\ H_{10}(\mathbf{C}) + \\ + [\exp\ (-kz)\, \mathbf{E} - z \exp\ (-kz)(\mathbf{C} + k\mathbf{E})]\ H_{20}(\mathbf{C}), \tag{3.13}$$

$$\exp\ [\mathbf{C}(z - \zeta)] = [\exp\ k(z - \zeta)\, \mathbf{E} + (z - \zeta) \exp\ k(z - \zeta)(\mathbf{C} - k\mathbf{E})]\, H_{10}\mathbf{C} + \\ + [\exp\ k(\zeta - z)\ \mathbf{E} + (\zeta - z) \exp\ k(\zeta - z)(\mathbf{C} + k\mathbf{E})]\ H_{20}(\mathbf{C}), \tag{3.14}$$

where $H_{10}(\lambda)$ and $H_{20}(\lambda)$ are the so-called Hermite polynomials satisfying the equations:

$$H_{10}(k) = H_{20}(-k) = 1, \tag{3.15}$$

$$H_{10}(-k) = H_{20}(k) = 0, \tag{3.16}$$

$$\left.\frac{dH_{10}(\lambda)}{d\lambda}\right|_{\lambda=\pm k} = \left.\frac{dH_{20}(\lambda)}{d\lambda}\right|_{\lambda=\pm k} = 0\,. \tag{3.17}$$

The explicit forms of the Hermite polynomials are:

$$H_{10}(\lambda) = \frac{1}{2k^2}\left(-\frac{1}{2k}\lambda + 1\right)(\lambda + k)^2\,, \tag{3.18}$$

$$H_{20}(\lambda) = \frac{1}{2k^2}\left(\frac{1}{2k}\lambda + 1\right)(\lambda - k)^2\,. \tag{3.19}$$

In consequence of the properties of the Hermite polynomials we have (see [5]):

$$H_{10}(\mathbf{C}) + H_{20}(\mathbf{C}) = \mathbf{E}. \tag{3.20}$$

By making use of the above equations we obtain the explicit form of the solution

$$\begin{aligned}
\hat{X} = \hat{X}(k, z) = \Bigg\{ & \frac{\exp kz}{4k^3}\Big[(-\mathbf{C}^2 + k\mathbf{C} + 2k^2\mathbf{E}) + z(-\mathbf{C}^3 + \\
& + 2k\,\mathbf{C}^2 + k^2\,\mathbf{C} - 2\,k^3\,\mathbf{E})\Big] + \frac{\exp(-kz)}{4k^3}\big[(\mathbf{C}^2 + k\mathbf{C} - \\
& - 2k^2\,\mathbf{E}) - z\,(\mathbf{C}^3 + 2k\,\mathbf{C}^2 - k^2\,\mathbf{C} - 2k^3\,\mathbf{E})\big]\Bigg\}\hat{X}\,(k, 0) + \\
& + \frac{1}{k^3}(-\mathbf{C}^2 + k\mathbf{C} + 2k^2\,\mathbf{E})\int_0^z \exp k(z - \zeta). \\
& ([0,0, \hat{b}(k, \zeta), \hat{A}(k, \zeta)]^T\,d\zeta + \frac{1}{k^3}(-\mathbf{C}^3 + 2k\,\mathbf{C}^2 + k^2\mathbf{C} - 2k^3\,\mathbf{E}) \times \\
& \times \int_0^z (z - \zeta)\exp k(z - \zeta)\,[0,0, \hat{b}(k, \zeta), \hat{A}(k, \zeta)]^T\,d\zeta + \\
& + \frac{1}{k^3}(\mathbf{C}^2 + k\,\mathbf{C} - 2k^2\,\mathbf{E})\int_0^z \exp k(\zeta - z) \\
& \times [0,0, \hat{b}(k, \zeta), \hat{A}(k, \zeta)]^T\,d\zeta + \frac{1}{k^3}\Big[\mathbf{C}^3 + 2k\,\mathbf{C}^2 - k^2\,\mathbf{C} - 2k^3\mathbf{E}) \times \\
& \times \int_0^z (\zeta - z)\exp k(\zeta - z). \\
& [0,0, \hat{b}(k, \zeta), \hat{A}(k, \zeta)]^T\,d\zeta,
\end{aligned} \tag{3.21}$$

where

$$[0,0, \hat{b}(k,\zeta), \hat{A}(k,\zeta)]^T = \begin{bmatrix} 0 \\ 0 \\ \hat{b}\,(k,\zeta) \\ \hat{A}(k,\zeta) \end{bmatrix}.$$

In the following, equations will be established with the aid of which the scalar coordinates of the displacement vectors $u = u(r, z)$, $w = w(r, z)$ and those of the stress tensor $\sigma_r = \sigma_r(r, z)$, $\sigma_\varphi = \sigma_\varphi(r, z)$, $\sigma_z = \sigma_z(r, z)$, $\tau_{rz} = \tau_{rz}(r, z)$ can be directly calculated from the coordinates of the vector $\hat{X}(k, z)$.

On the basis of the inversion formula relating to the zeroth-order Hankel transform this might be written as

$$w = w(r, z) = \frac{1}{G}\int_0^\infty \hat{W}(k, z)\, I_0(kr)\, k dk, \tag{3.22a}$$

$$w = w(r, z) = \int_0^\infty \hat{w}(k, z)\, I_0(kr) k dk, \tag{3.22b}$$

$$(0 \leq r < \infty, \qquad 0 \leq z \leq h).$$

From the equation

$$\frac{\partial u}{\partial r} + \frac{u}{r} = \frac{V}{G} = v \tag{3.23}$$

by making use of the inversion fromula of the zeroth-order Hankel transform and the equations

$$\frac{\partial u}{\partial r} + \frac{u}{r} = r\frac{\partial}{\partial r}(ur)\,, \tag{3.24}$$

$$\int_0^r \xi\, I_0(\xi\, k)\, d\xi = \frac{r}{k}\, I_1(k\, r)\,, \tag{3.25}$$

and by applying the rule of the partial integral, the following equation may be introduced

$$u = u(r, z) = \frac{1}{G}\int_0^\infty \hat{V}(k, z)\, I_1(kr)\, dk\,, \tag{3.26a}$$

$$u = u(r, z) = \int_0^\infty v(k,\ z)\ I_1(kr)\ \mathrm{d}k, \tag{3.26b}$$

$$(0 \leq r < \infty, \quad 0 \leq \geq \leq h).$$

By proceeding in a similar way, the following final formulae are given to σ_z and τ_{rz}

$$\sigma_z = \sigma_z(r,\ z) = \int_0^\infty \hat{Z}(k,\ z)\, I_0(kr)\, \mathrm{d}k, \tag{3.27}$$

$$\tau_{rz} = \tau_{rz}(r,\ z) = \int_0^\infty \hat{P}(k, z)\ I_1(kr)\ \mathrm{d}k, \tag{3.28}$$

$$(0 \leq r < \infty, \quad 0 \leq z \leq h).$$

For determining $\sigma_r = \sigma_r(r,z)$, it should set out from the equilibrium Eq. (2.12). Let us put this equation into the form

$$\frac{\partial}{\partial r}(r^2\sigma) = r_r(\sigma_r + \sigma_\varphi) - r^2\frac{\partial \tau_{rz}}{\partial z} - r^2 a\,. \tag{3.29}$$

Using the equation

$$\begin{aligned}(\sigma_r + \sigma_\varphi) &= \frac{2G}{1-2\nu}\left[\left(\frac{\partial u}{\partial r} + \frac{u}{r}\right) + 2\nu\frac{\partial w}{\partial z}\right] = \\ &= \frac{2G}{1-2\nu}\left(v + 2\nu\frac{\partial w}{\partial z}\right) = \\ &= \frac{2}{1-2\nu}\int_0^\infty\left[\hat{V}(k,z) + 2\nu\frac{\partial \hat{W}}{\partial z}\right]k\,I_0(k\,r)\,dk = \\ &= \frac{2G}{1-2\nu}\int_0^\infty\left[\hat{v}(k,z) + 2\nu\frac{\partial \hat{w}}{\partial z}\right]k\,I_0(k\,r)dk\,,\end{aligned} \tag{3.30}$$

the following equation may be written

$$\begin{aligned}\frac{\partial}{\partial r}(r^2\sigma_r) = \frac{2r}{1-2\nu}\int_0^\infty\left[\hat{V}(k,z) + 2\nu\frac{\partial \hat{W}}{\partial z}\right]k\,I_0(kr)\,dk - \\ - r^2\int_0^\infty\frac{\partial \hat{P}(k,z)}{\partial z}\,I_1(kr)\,dk - r^2\,a\,.\end{aligned} \tag{3.31}$$

From the above equation, by integration with respect to r and using the equations

$$\int_0^r \xi I_0(\xi\,k)\,d\xi = \frac{r}{k}\,I_1(kr)\,, \tag{3.32a}$$

$$\int_0^r \xi^2\,I_1(\xi\,k)\,d\xi = \frac{2r}{k^2}\,I_1(kr) - \frac{r^2}{k}\,I_0(kr)\,, \tag{3.32b}$$

the equation

$$\begin{aligned}(r^2\sigma_r) - (r^2\sigma_r)_{r=0} = \frac{2r}{1-2\nu}\int_0^\infty\left[\hat{V}(k,z) + 2\nu\frac{\partial \hat{W}(k,z)}{\partial z}\right]I_1(kr)\,dk - \\ - r\int_0^\infty\frac{\partial \hat{P}(k,z)}{\partial z}\left[2\frac{I_1(kr)}{k^2} - \frac{rI_0(kr)}{k}\right]dk - \int_0^r \xi^2\,a(\xi,z)\,d\xi\end{aligned} \tag{3.33}$$

might be deduced. In the following the investigations will be restricted only to stress distributions where

$$\lim_{r\to 0}(\sigma_r\,r^2) = 0. \tag{3.34}$$

With the restriction (3.34) in view, the final formula of σ_r will be

$$\sigma_r = \sigma_r(r, z) = \frac{2\nu}{(1-2\nu)\, r}\int_0^\infty \left[\hat{V}(k, z) + 2\nu \frac{\partial \hat{W}(k, z)}{\partial z}\right] I_1(kr)\, dk - \\ - \int_0^\infty \frac{\partial \hat{P}(k, z)}{\partial z}\left[\frac{2I_1(kr)}{rk^2} - \frac{I_0(kr)}{k}\right] dk - \frac{1}{r^2}\int_0^\infty \xi^2\, a(\xi, z)\, d\xi, \tag{3.35a}$$

$$\sigma_r = \sigma_r(r, z) = \frac{2G}{(1-2\nu)r}\int_0^\infty \left[\hat{v}(k, z) + 2\nu \frac{\partial \hat{w}(k, z)}{\partial z}\right] I_1(kr)\, dk - \\ - \int_0^\infty \frac{\partial \hat{P}(k, z)}{\partial z}\left[\frac{2\, I_1(kr)}{rk^2} - \frac{I_0(kr)}{k}\right] dk - \frac{1}{r^2}\int_0^r \xi^2\, a(\xi, z)\, d\xi, \tag{3.35b}$$

$$(0 \leq r < \infty, \quad 0 \leq z \leq h).$$

Determination of $\sigma_\varphi = \sigma_\varphi(r, z)$ may conveniently be carried out, starting out from equation

$$\sigma_\varphi = (\sigma_r + \sigma_\varphi) - \sigma_r. \tag{3.36}$$

Replacing (3.30) and (3.35) into (3.36), we obtain

$$\sigma_\varphi = \sigma_\varphi(r, z) = \frac{2}{1-2\,\nu}\int_0^\infty \left[\hat{V}(k, z) + 2\nu \frac{\partial \hat{W}}{\partial z}\right] k\, I_0(kr)\, dk - \\ - \frac{2}{(1-2\,\nu)r}\int_0^\infty \left[\hat{V}(k, z) + 2\nu \frac{\partial \hat{W}}{\partial z}\right] I_1(kr)\, dk + \\ + \int_0^\infty \frac{\partial \hat{P}(k, z)}{\partial z}\left[\frac{2\, I_1(kr)}{r^2k^2} - \frac{I_0(kr)}{k}\right] dk + \frac{1}{r^2}\int_0^r \xi^2\, a\,(r, \xi)\, d\xi, \tag{3.37a}$$

$$\sigma_\varphi = \sigma_\varphi(r, z) = \frac{2G}{1-2\nu}\int_0^\infty \left[\hat{v}(k, z) + 2\nu \frac{\partial \hat{w}(k, z)}{\partial z}\right] k\, I_0(kr)\, dk - \\ - \frac{2G}{(1-2\,\nu)r}\int_0^\infty \left[\hat{v}(k, z) + 2\nu \frac{\partial \hat{w}(k, z)}{\partial z}\right] I_1(kr)\, dk + \\ + \int_0^\infty \frac{\partial \hat{P}(k, z)}{\partial z}\left[\frac{2I_1(kr)}{k^2r^2} - \frac{I_0(kr)}{k}\right] dk + \frac{1}{r^2}\int_0^r \xi^2\, a(r, \xi)\, d\xi, \tag{3.37b}$$

$$(0 \leq r < \infty, \quad 0 \leq z \leq k).$$

Let it be:

$$\mathbf{T}(k, z, \nu) = \frac{\exp(kz)}{k^3}\left[/- \mathbf{C}^2 + k\,\mathbf{C} + 2k^2\mathbf{E}/ + \right. \\ + z(-\mathbf{C}^3 + 2k\,\mathbf{C}^2 + k^2\,\mathbf{C} - 2k^3\,\mathbf{E})] + \\ + \frac{\exp(-kz)}{k^3}[(\mathbf{C}^2 + k\,\mathbf{C} - 2k^2\,\mathbf{E}) - \\ \left. - z(\mathbf{C}^3 + 2k\,\mathbf{C}^2 - k^2\,\mathbf{C} - 2k^3\,\mathbf{E})\right]. \tag{3.38}$$

Hereafter, we assume that no system of forces distributed on the volume can be applied to the body investigated, i. e.,

$$\hat{B}(k, z) = [0, 0, \hat{b}(k, z), \hat{A}(k, z)]^T = 0. \tag{3.39}$$

In this case, Eq. (3.37) will be a homogeneous differential equation, and its general solution may be obtained as

$$\hat{X}(k, z) = \mathbf{T}(k, z, \nu)\hat{X}(k, o). \tag{3.40}$$

In connection with only one layer the dependence $\mathbf{T}(k, z, \nu)$ on ν is not particularly emphasized, i. e., we apply the simplifying designation

$$\mathbf{T}(k, z, \nu) = \mathbf{T}(k, z). \tag{3.41}$$

Since the matrix $\mathbf{T}(k, z)$ transforms the vector $\hat{X}(k, 0)$ into the vector $\hat{X}(k, z)$, therefore, $\mathbf{T}(k, z)$ is called transfer matrix of the vector $\hat{X}(k, z)$. The relationship between $\hat{X}(k, 0)$ and $\hat{X}(k, z)$ — by using the way of rep resentation adopted in the control technique — is schematically depicted in Fig. 3.1.

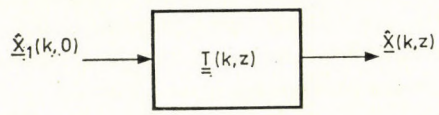

Fig. 3,1. Representation of the transfer matrix

On the basis of Eqs (3.22) (3.26), (3.28), (3.25), (3.37) and (3.39) it is easy to see that with the knowledge of vector $\hat{X}(k, 0)$, corresponding to the boundary conditions, all the variables of the boundary-value problem might be directly determined by an improper integral. For determining the vector $\hat{X}(k, 0)$ associated with the boundary conditions, let us write down by virtue of Eq. (3.40), the relationship between the vectors $\hat{X}(k, h)$ and $\hat{X}(k, 0)$

$$\hat{X}(k, h) = \mathbf{T}(k, h)\, \hat{X}\,(k, 0). \tag{3.42}$$

In general, in the above equation, in case of an actual boundary value problem of the theory of elasticity, two co-ordinates of each of the vectors $\hat{X}(k, h)$ and $\hat{X}(k, 0)$ are known. In order to determine the unknown co-ordinates of the vector $\hat{X}(k, 0)$, it is advisable to transpose and partition the coefficient matrix of the set of equations (3.42) according to the unknown vectors

$$\begin{bmatrix} \hat{Y}_{h,1} \\ \\ \hat{Y}_{h.2} \end{bmatrix} = \begin{bmatrix} S_{11} & S_{12} \\ \\ S_{21} & S_{22} \end{bmatrix} \begin{bmatrix} \hat{Y}_{0,1} \\ \\ \hat{Y}_{0,2} \end{bmatrix}. \tag{3.43}$$

Here

- $\hat{Y}_{h,1}$ vector in two dimensions uniting co-ordinates of the vector $\hat{X}(k, h)$ given directly or to be determined on the basis of the boundary conditions;
- $\hat{Y}_{h,2}$ column vector in two dimensions uniting unkown co-ordinates of vector $\hat{X}(k, h)$;
- $\hat{Y}_{0,1}$ column vector in two dimensions uniting co-ordinates of vector $\hat{X}(k, 0)$ given directly or to be determined from the boundary conditions;
- $\hat{Y}_{0,2}$ column vector in two dimensions uniting unknown co-ordinates of vector $\hat{X}(k, 0)$;

$$\mathbf{S} = \begin{bmatrix} \mathbf{S}_{11} & \mathbf{S}_{12} \\ \mathbf{S}_{21} & \mathbf{S}_{22} \end{bmatrix} = \mathbf{PT}(k, h)\,\mathbf{Q} \tag{3.44}$$

further, P and Q denote fourth-order permutation matrices, which satisfy Eqs (3,45) and (3,46):

$$\mathbf{P}\,\hat{X}(k, h) = \begin{bmatrix} \hat{Y}_{h,1} \\ \\ \hat{Y}_{h,2} \end{bmatrix}, \quad \hat{X}(k, o) = \mathbf{Q} \begin{bmatrix} \hat{Y}_{0,1} \\ \\ \hat{Y}_{0,2} \end{bmatrix}. \tag{3.45—3.46}$$

The blocks $\mathbf{S}_{ij}$ are two-by-two matrices. Application of the above resolution yields

$$\hat{Y}_{h,1} = \mathbf{S}_{11}\hat{Y}_{0,1} + \mathbf{S}_{12}\,\hat{Y}_{0,2} \tag{3.47}$$

i.e.,

$$\hat{Y}_{0,2} = \mathbf{S}_{12}^{-1}\,\hat{Y}_{h,1} - \mathbf{S}_{12}^{-1}\mathbf{S}_{11}\hat{Y}_{0,1} \tag{3.48}$$

provided that $\det \mathbf{S}_{12} \neq 0$. Replacement of (3.48) into (3.46) results for the vector $\hat{X}(k, 0)$ are given in the following:

$$\hat{X}(k, o) = \begin{bmatrix} \mathbf{E} & \mathbf{O} \\ -\mathbf{S}_{12}^{-1}\mathbf{S}_{11} & \mathbf{S}_{12} \end{bmatrix} \begin{bmatrix} \hat{Y}_{0,1} \\ \hat{Y}_{h,1} \end{bmatrix}. \tag{3.49}$$

In this equation **E** is a second-order unit matrix and **O** is a two-by-two zero matrix. Replacement of the vector $\hat{X}(k, 0)$ satisfying the boundary conditions into (3.39) gives $\hat{X}(k, z)$, wherefrom, by virtue of (3.26), (3.27), (3.28), (3.35) and (3.37) the displacement vector and stress pattern of the points of the investigated layer may be determined.

4. An example for the determination of the vector $\hat{X}(k,0)$

The body stiffly fixed at the face characterized by the coordinate $z = 0$, depicted in Fig. 4.1 is subjected on the plane of the co-ordinate $z = h$, to a distributed load of given intensity:

$$\sigma_r(r, h) = f(r) \tag{4.1}$$

$$\tau_{rz}(r, h) = 0. \tag{4.2}$$

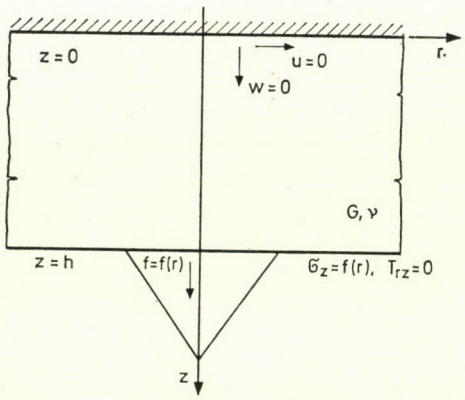

Fig. 4,1. Elastic layer of thickness h with axi-symmetrical boundary conditions

Apparently, the boundary condition at $z = 0$ is

$$u(r,\ 0) = 0, \tag{4.3}$$

$$w(r, 0) = 0. \tag{4.4}$$

From Eqs (4.3) and (4.4) it follows

$$U(r,\ 0) = 0, \tag{4.5}$$

$$V(r,\ 0) = 0, \tag{4.6}$$

$$V(r, o) = \frac{\partial U(r,o)}{\partial r} + \frac{U(r, o)}{r} = 0\,, \tag{4.7}$$

i.e., the first two co-ordinates of the vector $\hat{X}(k, 0)$ are equal to zero. Thus, taking Eqs (4.6), (4.7) into consideration, the vector $\hat{X}(k, 0)$, figuring in the problem in question, will be

$$\hat{X}(k, o) = \begin{bmatrix} \hat{Y}_{0,1} \\ \\ \hat{Y}_{0,2} \end{bmatrix} = \begin{bmatrix} 0 \\ 0 \\ \hat{Z}(k, o) \\ \hat{P}(k, o) \end{bmatrix}. \tag{4.8}$$

Taking the boundary conditions prescribed at the face $z = h$ into account, it can be written that

$$\hat{X}(k, h) = \begin{bmatrix} \hat{Y}_{h,1} \\ \\ \hat{Y}_{h,2} \end{bmatrix} = \begin{bmatrix} \hat{V}(k, h) \\ \hat{W}(k, h) \\ \hat{f}(k) \\ 0 \end{bmatrix}. \tag{4.9}$$

By virtue of Eqs (4.7) and (4.9) the fourth-order permutation matrix of **P** and **Q** can directly be written as:

$$\mathbf{Q} = \mathbf{E} = \begin{bmatrix} 1 & 0 & 0 & 0 \\ 0 & 1 & 0 & 0 \\ 0 & 0 & 1 & 0 \\ 0 & 0 & 0 & 1 \end{bmatrix}, \quad \mathbf{P} = \begin{bmatrix} 0 & 0 & 1 & 0 \\ 0 & 0 & 0 & 1 \\ 1 & 0 & 0 & 0 \\ 0 & 1 & 0 & 0 \end{bmatrix}. \tag{4.10—4.11}$$

By making use of the form:

$$\mathbf{T}(k, h) = \begin{bmatrix} \mathbf{T}_{11} & \mathbf{T}_{12} \\ \mathbf{T}_{21} & \mathbf{T}_{22} \end{bmatrix} \tag{4.12}$$

of the $\mathbf{T}(k, h)$ partitioned to two-by-two blocks, and by applying (3.44) we obtain

$$\mathbf{S} = \begin{bmatrix} \mathbf{S}_{11} & \mathbf{S}_{12} \\ \mathbf{S}_{21} & \mathbf{S}_{22} \end{bmatrix} = \begin{bmatrix} \mathbf{T}_{21} & \mathbf{T}_{22} \\ \mathbf{T}_{11} & \mathbf{T}_{12} \end{bmatrix}. \tag{4.13}$$

Finally, from Eqs (4.13) and (3.49) follows the result for $\hat{X}(k, 0)$

$$\hat{X}(k, o) = \frac{\hat{f}(k)}{t_{33}\, t_{44} - t_{34}\, t_{43}} \begin{bmatrix} 0 \\ 0 \\ -t_{44} \\ t_{43} \end{bmatrix}, \tag{4.14}$$

where

$$\mathbf{T}(k, h) = [t_{ij}], \; 1 \leq i, j \leq 4.$$

5. Axi-symmetrical boundary value problems of a layered body with isotropic layers of homogeneous linearly elastic material

The findings in connection with a one-layer body of homogeneous isotropic, linearly elastic material may be generalized to a layered body of finite thickness, consisting of linearly elastic material, homogeneous in each layer possessing axi-symetrical boundary conditions represented in Fig. 5.1.

The quantities related to the layers designated with i ($i = 1, 2, \ldots, n-1$). Thus, for example, parameters of the layer marked by i are:

- h_i thickness,
- ν_i Poisson's ratio of material,
- G_i shear elasticity modulus of material,
- $\vec{t}_i = u_i \vec{e}_i + w_i \vec{e}_{zi}$ = displacement vector of point P_i of layer in a cylindrical system of coordinates r_i, φ_i, z_i represented in Fig. 5,1,

etc.

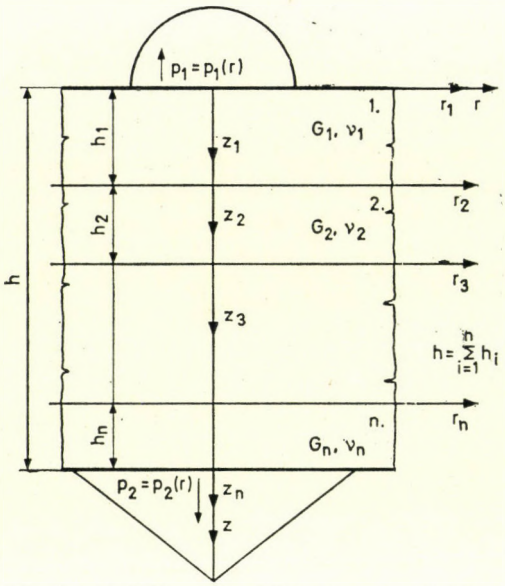

Fig. 5,1. Layered body of thickness h with axi-symmetrical boundary conditions

To each of the layers a cylindrical system of co-ordinates (r_i, φ_i, z_i) is connected (see Fig. 5.1) so that we have

$$\begin{aligned} r &= r_1 \\ \varphi &= \varphi_1 \\ z &= z_1 \end{aligned} \tag{5.1}$$

and

$$\begin{aligned} r_i &= r \\ \varphi_i &= \varphi \\ z_i &= z - h_1 + h_2 + \ldots + h_{i-1}), \\ (i &= 2, 3, \ldots \qquad n-1, n). \end{aligned} \tag{5.2}$$

The investigation also henceforward is restricted to the case where the vector of intensity $\vec{q}_i$ $(i = 1, 2, \ldots, n-1, n)$ of the volumetric system of forces is equal to zero. In connection with the layer i $(i = 1, 2, \ldots, n-1)$, by virtue of Eq. (3.40), it can be written with respect to the cylindrical system of co-ordinates r_i, φ_i, z_i:

$$\begin{aligned} \hat{X}_i(k, z_i) &= \mathbf{T}(k, z_i, \nu_i)\ \hat{X}(k, 0) \\ (0 &\leq z_i \leq h_i,\ k > 0). \end{aligned} \tag{5.3}$$

In the above equation k is not marked with i, because all the r_i s $(i = 1, 2, \ldots, n-1, n)$ are equal to each other and k is related to the integral transformation performed with respect to the variable r. It is advisable to change over

from the variable $\hat{X}_i(k, z)$ to another one which does not include the material constant G_i, but has the same properties as $\hat{X}_i(k, z)$. Let the new variable be:

$$\hat{X}_i(k, z_i) = \begin{bmatrix} \hat{V}_i(k, z_i) \\ \hat{W}_i(k, z_i) \\ \hat{Z}_i(k, z_i) \\ \hat{P}_i(k, z_i) \end{bmatrix}. \tag{5.4}$$

The relationship between $\hat{X}_i(k, z)$ and $\hat{x}_i(k, z_i)$ is expressed by the equations

$$\hat{X}_i(k, z_i) = \mathbf{G}_i \hat{x}_i(k, z_i), \tag{5.5}$$

$$\hat{x}_i(k, z_i) = \mathbf{\Gamma}_i \hat{X}_i(k, z_i), \tag{5.6}$$

$$\mathbf{G}_i \mathbf{\Gamma}_i = \mathbf{E} \tag{5.7}$$

where

$$\mathbf{G}_i = \begin{bmatrix} G_i & 0 & 0 & 0 \\ 0 & G_i & 0 & 0 \\ 0 & 0 & G_i & 0 \\ 0 & 0 & 0 & G_i \end{bmatrix}, \tag{5.8}$$

$$\mathbf{\Gamma}_i = \begin{bmatrix} \dfrac{1}{G_i} & 0 & 0 & 0 \\ 0 & \dfrac{1}{G_i} & 0 & 0 \\ 0 & 0 & \dfrac{1}{G_i} & 0 \\ 0 & 0 & 0 & \dfrac{1}{G_i} \end{bmatrix}, \tag{5.9}$$

and $\mathbf{E}$ is a fourth-order unit matrix.

Considering those mentioned in the foregoing, for the vector $\hat{x}(k, z_i)$ we obtain:

$$\hat{x}_i(k, z_i) = \mathbf{L}_i(k, z_i, \nu_i, G_i) x_i(k, o) \tag{5.10}$$

and the matrix $\mathbf{L}_i(k, z_i) = \mathbf{L}_i(k, z_i, \nu_i, G_i)$ describing its transformation

$$\mathbf{L}_i(k, z_i, \nu_i, G_i) = \mathbf{\Gamma}_i \mathbf{T}_i(k, z_i, \nu_i) G_i. \tag{5.11}$$

The issue of the chain-like interconnection of the layers — i.e. the fitting of the variables u, w, σ_z, τ_{rz} — is the following equation (see Fig. 5.2):

$$\hat{x}_i(k, h_i) = \hat{x}_{i+1}(k, 0), \tag{5.12}$$

$$(i = 1, 2, \ldots \quad n-1).$$

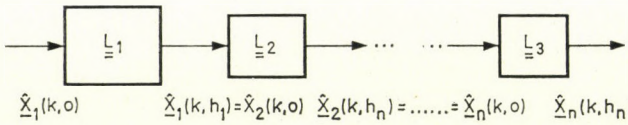

Fig. 5,2. Representation of the equation $\hat{x}_i(k, h_i) = \hat{x}_{i+1}(k, 0)$ $(i = 1,2, \ldots, n\text{-}1)$

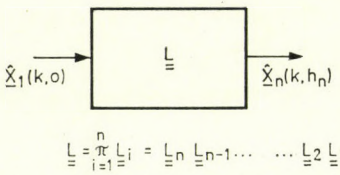

Fig. 5,3. Representation of the resultant transfer matrix

By making use of Eq. (5.12), the vector $\hat{x}_1(k, 0)$ may be brought into direct connection with the vector $\hat{x}_n(k, h_n)$ through the equation

$$\hat{x}_n(k, h_n) = \mathbf{L}\hat{x}_1(k, 0) \tag{5.13}$$

where $\mathbf{L} = \mathbf{L}(k, h_1, k_i, \ldots, k_i; \nu_1, \nu_2, \ldots, \nu_n; G_1, G_2 \ldots G_n)$ designates the resulting transfer matrix of the layer n which is to be established on the basis of the equation

$$\mathbf{L} = \mathbf{L}_n \mathbf{L}_{n-1} \ldots \mathbf{L}_2 \mathbf{L}_1 = \prod_{i=1}^{n} \mathbf{L}_i(k, h_i, \nu_i, G_i). \tag{5.14}$$

Here, the notation

$$\mathbf{L}_i = \mathbf{L}_i(k, h_i, \nu_i, G_i), \quad (i = 1, 2, \ldots n-1, n) \tag{5.15}$$

is introduced. The matrix $\mathbf{L}$ depends on the material constants of all of the media, globally characterizing the layered body. A possible demonstration of Eq. (5.13) is — by making use of a control-technique comparison — outlined in Fig. (5.3).

In case of a particular boundary-value problem as a first step, the resulting transfer matrix, therefore, the vector $x_1(k, 0)$ should be determined from the equation

$$\hat{x}_i(k, o) = \mathbf{Q}\begin{bmatrix} \mathbf{E} & \mathbf{O} \\ -\mathbf{S}_{12}^{-1}\mathbf{S}_{11} & \mathbf{S}_{12}^{-1} \end{bmatrix}\begin{bmatrix} \hat{y}_{0,1} \\ \hat{x}_{h,1} \end{bmatrix}. \tag{5.16}$$

In this equation
- $\mathbf{E}$ second-order unit matrix,
- $\mathbf{O}$ two-by-two zero matrix,
- $\hat{y}_{0,1}$ column vector built up from the two coordinates directly given or to be determined from the boundary conditions of the vector $\hat{x}_1(k, 0)$,
- $\hat{y}_{h,1}$ column vector containing the two coordinates directly given or to be determined from the boundary conditions of the vector $\hat{x}_n(k, h_n)$,
- $\mathbf{S}_{12}$ and $\mathbf{S}_{11}$ denote the blocks of the following two-by-two matrix.

$$\mathbf{S} = \begin{bmatrix} \mathbf{S}_{11} & \mathbf{S}_{12} \\ \mathbf{S}_{21} & \mathbf{S}_{22} \end{bmatrix} = \mathbf{PLQ}\,, \tag{5.17}$$

— here **P** and **Q** denote the fourth-order permutation matrices involving the equations

$$\mathbf{P}\hat{x}_n(k, h_n) = \begin{bmatrix} \hat{y}_{h,1} \\ \hat{y}_{h,2} \end{bmatrix}, \tag{5.18}$$

$$\hat{x}_1(k, o) = \mathbf{Q}\begin{bmatrix} \hat{y}_{0,1} \\ \hat{y}_{0,2} \end{bmatrix}, \tag{5.19}$$

where

— $\hat{y}_{h,2}$ two-dimensional column vector uniting unknown coordinates of the vector $\hat{x}_n(k, h_n)$.

— $\hat{y}_{0,2}$ two-dimensional column vector uniting unknown coordinates of the vector $\hat{x}_1(k, 0)$.

In the next step the vector $\hat{x}_i(k, 0)$ from the equation

$$\hat{x}_i(k, 0) = M_i\hat{x}_i(k, 0) \tag{5.20}$$

should be determined, where

$$\mathbf{M}_i = \mathbf{L}_{i-1}\mathbf{L}_{-2}\ldots\mathbf{L}_2\mathbf{L}_1 = \prod_{s=1}^{i-1} \tag{5.21}$$

is the resultant transfer matrix of the first $i-1$, $s = 1, 2, \ldots, i-1$ layers with respect to the vector $\hat{x}_1(k, 0)$. Knowing the value of $\hat{x}_i(k, 0)$, the vector $\hat{x}_i(k, z_i)$, $(0 \leq z_i \leq h_i,\ 0 < k)$, in the layer i, from Eq. (5.10) will be formed. From the co-ordinates $\hat{v}_i(k, z_i)$, $\hat{w}_i(k, z_i)$, $\hat{z}_i)$, $\hat{P}(k, z_i)$ of the vector $\hat{x}_i(k, z_i)$, from Eqs (3.22a), (3.26a), (3.27), (3.28), (3.35a), (3.37a) the scalar co-ordinates $u_i(r, z_i)$, $w_i(r, z_i)$and $\sigma_{z,i}(r, z_i)$, $\sigma_{\varphi,i}(r, z_i)$, $\sigma_{z,i}(r, z_i)$, $\tau_{r,z,i}(r, z_i)$ of the displacement vector and stress tensor, respectively, may be determined.

REFERENCES

1. Власов, В. З. и Леонтев, Н. Н.: Балки плиты и оболочки к упругостосювании, Государственное издательство Физико-Математической литературы Москва 1960
2. Bahar, Leon Y.: Transfer Matrix Approach to Layered Systems, *Journal of the Engineering Mechanics Division ASCE*, Vol. **98**, No. EM5, pp. 1159—1172
3. Лурье, А. И.: Теория упругости, Издательство наука, физико-математической литературы, Москва 1970
4. Никитин, В. С., Шапиро, Г. С.: Тространственные задачи теории упругости для многослойных сред, Вычислительный Цетр А. Н. СССР Москва 1970
5. Rózsa, P.: Linear Algebra and Applications. Műszaki Könyvkiadó, Budapest 1974 (In Hungarian)
6. Sneddon, Ian. N.: Elements of Partial Differential Equations. McGraw-Hill Book Company, Inc. New York—Toronto—London 1957
7. Sneddon, Jan. N.: Fourier Transforms, McGraw-Hill Book Company, Inc. New York—London—Toronto 1951
8. Timoshenko, S.—Goodier, I. N.: The Theory of Elasticity, McGraw-Hill Book Company, Inc. New York—Toronto—London 1951

Eine Lösungsmethode einiger Achsensymmetrieprobleme der Elastizitätslehre. Behandelt wird eine Lösungsmethode quadratischer Achsensymmetrieprobleme von mit einer gegebenen Ebene parallel unendlich ausgedehnten, kleinen Verformungen unterworfenen, in allen ihren Schichten aus homogenem, isotropischem und linearisch elastischem Material bestehenden Kontinua.

Один из методов решения некоторых центрально симметричных задач теории упругости. Данная работа занимается решением квазистатических центрально симметричных задач континуумов, претерпевших небольшую деформацию и имеющих параллельно с выделенной плоскостью бесконечные размеры, из послойно гомогенного, изотропного и линеарно упругого материала.

INDEX

M. HERPY

ANALOGE INTEGRIERTE SCHALTUNGEN

(Operationsverstärker und analoge Multiplizierer)

Die Technik der integrierten Analogschaltungen hat in den letzten Jahren eine stürmische Entwicklung genommen und dabei den Schaltungsentwurf auf eine völlig neue Stufe gehoben. Das vorliegende Buch beschäftigt sich mit diesem Themenkreis und spricht vor allem Schaltungsdesigner an, die nach selbständiger Entwurfsarbeit streben. Nach kurzer Darstellung der Herstellungsmethoden der integrierten Analogschaltungen werden zum besseren Verständnis ihrer Funktion die fundamentalen Stromkreise behandelt, auf denen die Mehrheit dieser Schaltungen aufbaut. Neben der Besprechung der typischen Vertreter der integrierten Operationsverstärker und analogen Multiplizierer nehmen die Analyse von zahlreichen Anwendungsschaltungen und die an einigen Beispielen demonstrierten Methoden des modernen Schaltungsentwurfs im Buch einen breiten Raum ein.

In deutscher Sprache · Etwa 450 Seiten · 17×25 cm · Ganzleinen

Eine Gemeinschaftsausgabe — vertrieben in den sozialistischen Ländern von KULTURA, Budapest, ISBN 963 05 0867 2, in allen anderen Ländern von A. M. HAKKERT, Amsterdam

AKADÉMIAI KIADÓ
Budapest

A. M. HAKKERT
Amsterdam

Printed in Hungary

A kiadásért felel az Akadémiai Kiadó igazgatója. Műszaki szerkesztő: Zacsik Annamária

A kézirat nyomdába érkezett: 1975. VIII. 28. — Terjedelem: 20,7 (A/5) ív, 76 ábra

76.2238 Akadémiai Nyomda, Budapest — Felelős vezető: Bernát György

Acta Techn. Hung. **82** (1976) pp. *1—7*

BÖLCSKEI, E.: *Corrugated Conical Shells*

Corrugated conical shells having a vertical axis, a circular ground plane and free boundary are analysed in a cylindrical system of co-ordinates. The investigated shells are subject to uniform vertical loads, and supported by radial ribs. Formulae are given for the determination of the reduced stress resultants. Their distribution is illustrated for two practical cases.

Acta Techn. Hung. **82** (1976) pp. *9—13*

BARTA, J.: *Some Reciprocal Properties of Stress Components*

Two of the reciprocal properties presented here, are purely mathematical properties referring not only to stress components, but also to all vector components. The further reciprocal properties showned here are in the last analysis, physical properties, because they are derived from the well known equality $p_{ab} = p_{ba}$ which is a consequence of the dynamical equilibrium.

Acta Techn. Hung. **82** (1976) pp. *15—29*

CSONKA, P.: *Design of Star-Shells Subjected to Full Load*

The paper deals with paraboloid shells of revolution subjected to an axisymmetrically distributed full load (dead load and snow load applied simultaneously) acting in vertical direction. The form of the base over which the shell in question is constructed, is a regular polygon-like configuration with concave curved sides, a so-called *star-polygon*. The treated shell — the so-called *star-shell* — is bordered by an edge beam supported along its whole length by a wall, wherefore, the cross-section of the edge beam is only subjected to a centric normal force, the so-called *string force*. By using a convenient calculation method the shape of the star-polygon is so designed that the stress resultants, generated in the shell, can be calculated with the aid of closed formulae. A numeric example proves the suggested method as being expedient.

Acta Techn. Hung. **82** (1976) pp. *31—46*

BAREŠ, R.: *Analysis of Structurally Orthotropic Plane Structures*

Paper describes a calculation method for formorthotropic plate-like structures. It takes into calculation not only the bending and torsional stiffness of the structure but also its contraction ability. Application of the above method reduces the lengthy ad most tiring part of the calculation, as well as the structural enginer's work to the minimum.

Acta Techn. Hung. **82** (1976) pp. *47—52*

GAMER, U.: *Nonsteady Temperature Field in the Rotating Anode of an X-ray Tube*

Using the temperature distribution due to an instantaneous point source, the temperatured field in an infinite disk caused by a heat source moving along a circle is calculated. For constant output and constant circular frequency the mean value of the temperature over the circumference is received in closed form by application of the Laplace transformation and short time expansion. The numerical results are represented graphically.

Acta Techn. Hung. **82** (1976) pp. *61—67*

MANDAL, S.: *An Infinite Viscoelastic Thick Plate Containing an External Crack*

This paper is concerned with the stress fields in an infinite viscoelastic thick plate containing an external crack due to the application of normal pressure to its faces. The crack is taken to lie in the central plane of the plate normal to the axis of symmetry and occupies the region outside the circle. It is assumed that the two faces of the crack are loaded exactly the same way and the viscoelastic layer is in a rigid casing. Hankel transforms of the displacement vector are introduced. Mixed boundary conditions lead to dual integral equations. These equations are then reduced to Fredholm integral equation of the second kind. This type of equation is solved by an iterative process for large values of thickness of the plate. The stress intensity factor has been calculated.

Acta Techn. Hung. **82** (1976) pp. *69—85*

KALLÓ, P.: *Algorithm for Automatic Triplet Design*

After summing up the experiences collected through the application of the automatic design methods of optical systems known so far, an algorithm entirely new in its starting point and initial stages, suitable for the optimized automatic (and traditional) design of classical triplet type objectives is decribed. The paper explains in detail the definition of the notion of performance determinant parameters, the derivation of the basic triplet equations, and the relations of glass material selection; the wellknown methods of bending and fine correction are covered only as much as needed. The important advantage of the new algorithm easy to program for a computer and providing for a number of optimization possibilities is that at requires as a starting point for automatic (and traditional) triplet design nothing but the knowledge of the relative aperture and field angle given in advance, and the data of the adaptable glass types, and that it is suitable for multilateral generalization (other optical system types containing cemented lenses as well, finite object distance, etc.).

Acta Techn. Hung. **82** (1976) pp. *87—97*

GÁSPÁR, ZS.: *Generalization of Physical Networks*

Equations of the physical network (physical graph) defined as the generalization of bar systems directly yield relationships between bar systems in small displacement and linear electric circuit as special cases.

Acta Techn. Hung. **82** (1976) pp. *99—119*

KRIZEK, R. J.—ELNAGGAR, H. A.—AZZOUZ, A. S.: *Consolidation Around Sand Drains in Non-Darcian Soils*

The effect of non-Darcian flow on the consolidation behavior of clay soils is evaluated for conditions of radial drainage only and combined radial and vertical drainage. This is accomplished by postulating a reasonably general four-parameter velocity-gradient relationship, which by proper choice of parameters is capable of characterizing much of the published experimental data on the flow of water through clay soils, and combining this relationship with the other standard assumptions of classical consolidation theory to develop a nonlinear parabolic partial differential equation, which is solved by use of finite difference procedures. Several typical solutions show that the time rate of consolidation for soils which exhibit non-Darcian flow characteristics is substantially less than that predicted by classical consolidation theory. Although a numerical solution to the two-dimensional flow problem was easily obtained by an explicit finite difference scheme, restrictive stability criteria rendered such solutions expensive.

Acta Techn. Hung. **82** (1976) pp. *121—168*

KEMÉNY, Á. P.: *Experimental Investigation of the Life of Semiconductor Devices* III.

The generally used methods of prolonged d. c. operating life tests of transistors, which provoke mainly the thermally activated surface degradation phenomena, give little information on the deterioration in switching operation. A method is proposed where the transistors are loaded as common base, inverters in switching operation with fixed S0 Hz or higher repetition frequency, at exactly controlled and determined swithing on and off transient energy. This method permits the economical examination of large samples and is useful mainly as a *screen* test for the quick selection of individuals with hidden structural defects. Such tests supported by microphotographs of failed sampler seem to be in accordance with the analytical results of a bulk degradation procers treated here and emphasize the necessity of a flawless geometrical structure of a such devices.

Acta Techn. Hung. **82** (1976) pp. *169—177*

ROSTÁS, J.: *Porosity of Cement Stone as a Function of the Water—Cement-Ratio*

Due to theoretical considerations the porosity and the solidity of the cement stone will be deduced as a function of water—cement-ratio and hydration degree. The results deduced for the various cases will be compared to experience, and good correspondence will be found.

Acta Techn. Hung. **82** (1976) pp. *179—196*

SZENTGYÖRGYI, I.—VARGA, J.—VERES, G.: *Results of Semi-Pilot-Measurings Concerning the Steem-Ammonia Heat-Transformation in Binary Power Station System*

At the beginning of the 1960's, when improving the air condenser system, Professor HELLER suggested the realization of the combined steam ammonia system. Later, in 1965, he published his recommendations concerning the structure of the suggested new system. Here he pointed out the dominant role of the heat exchanger dividing the partial cycles and also the difficulties concerning the realization were mentioned. It became evident, that experimental research was needed prior to realizing the dividing heat exchanger. Only the results of these experiments could show wheather it is possible to build — at the necessary thermal conditions — a rational dimension heat exchanger. In the course of the experimental work it was found possible to build a rational dimension, steam — ammonia condenser boiler, which operates suitable even at the low, about 4 — 6 °C temperature differences required from the thermal point.

Acta Techn. Hung. 82 (1976) pp. *197—210*

SOMLYÓDY, L.: *Examination of Mixing in Water Streams Using Mass Flux Constant Curves*

The report deals with the mixing of a dissolved passive pollutant permanently released into a water stream. It assumes the velocity field as being known and makes use of the equation of turbulent diffusion, describing the said phenomenon by the introduction of depth-averaged values, in a co-ordinate system consisting of streamlines and equipotential lines normal to them. As in the case of streamlines, it defines the curves of mass flux constant which divide the original differential equation into two equations, more convenient to handle computationally. Furthermore the report outlines certain characteristics of the curves, then deals with the computation of the distribution of the concentration, respectively, with the inverse case: the determination of the dispersion coefficients obtained by tracer measurements.

Acta Techn. Hung. 82 (1976) pp. *211—232*

ECSEDI, I.: *A Method to Solve Some Axi-Symmetrical Problems of the Theory of Elasticity*

The paper deals with the solutions of axi-symmetrical quasi-static problems of continua consisting of layers of infinite extension parallel to a given plane. It is assumed that each layer is homogeneous and isotropic, consisting of linearly elastic material having insignificant deformation.

Acta Techn. Hung. 82 (1976) pp. *53—59*

SCHARLE, P.: *On the Relationship between Different Approximating Methods.*

The paper deals with some common properties of several well-known approximatingmethods. It separates the concepts of the approximating principle and approximating technique. Attempts are made to construct a general treatment for relating the approximating principles used in the numerical investigations of a wide class of non-linear continuum problems. It is possible to recognise a very expressive connection between the different methods as the least squares, weighted residuals, direct approximation and variational ones.

The *Acta Technica* publish papers on technical subjects in English, French, German and Russian.

The *Acta Technica* appear in parts of varying size, making up one volume.

Manuscripts should be addressed to

Acta Technica
1051 Budapest
Münnich Ferenc u. 7.
Hungary

Correspondence with the editors and publishers should be sent to the same address.

The rate of subscription is $ 32.00 a volume. Orders may be placed with "Kultúra" Foreign Trade Company for Books and Newspapers (1389 Budapest 62, P.O.B. 149 Account No. 218 10990) or with representatives abroad.

Les *Acta Technica* paraissent en français, allemand, anglais et russe et publient des travaux du domaine des sciences techniques.

Les *Acta Technica* sont publiés sous forme de fascicules qui seront réunis en volumes.

On est prié d'envoyer les manuscrits destinés à la rédaction à l'adresse suivante:

Acta Technica
1051 Budapest
Münnich Ferenc u. 7.
Hongrie

Toute correspondance doit être envoyée à cette même adresse.

Le prix de l'abonnement est de $ 32.00 par volume.

On peut s'abonner à l'Entreprise pour le Commerce Extérieur de Livres et Journaux «Kultúra» (1389 Budapest 62, P.O.B. 149 compte courant No. 218 10990) ou à l'étranger chez tous les représentants ou dépositaires.

«*Acta Technica*» публикуют трактаты из области технических наук на русском, немецком, английском и французском языках.

«*Acta Technica*» выходят отдельными выпусками разного объема. Несколько выпусков составляют один том.

Предназначенные для публикации рукописи следует направлять по адресу:

Acta Technica
1051 Budapest
Münnich Ferenc u. 7.
Венгрия

По этому же адресу направлять всякую корреспонденцию для редакции и администрации.

Подписная цена — $ 32.00 за том. Заказы принимает предприятие по внешней торговле книг и газет «Kultúra» (1389 Budapest 62, P. O. B. 149 Текущий счет № 218 10990) или его заграничные представительства и уполномоченные.

Reviews of the Hungarian Academy of Sciences are obtainable at the following addresses:

AUSTRALIA

C. B. D. Library and Subscription Service
Box 4886, G. P. O.
Sydney N. S. W. 2001

Cosmor Bookshop
145 Acland St.
St. Kilda 3182

AUSTRIA

Globus
Höchstädtplatz 3
A—1200 Wien XX

BELGIUM

Office International de Librairie
30, Avenue Marnix
1050-Bruxelles

Du Monde Entier
162 Rue du Midi
1000—Bruxelles

BULGARIA

Hemus
Bulvar Ruszki 6
Sofia

KANADA

Pannonia Books
P. O. Box 1017
Postal Station "B"
Toronto, Ont. M5T 2T8

CHINA

C N P I C O R
Periodical Department
P. O. Box 50
Peking

CZECHOSLOVAKIA

Mad'arská Kultura
Národní třida 22
115 66 Praha

PNS Dovoz tisku
Vinohradská 46
Praha 2

PNS Dovoz tlače
Bratislava 2

DENMARK

Ejnar Munksgaard
Nörregade 6
DK—1165 Copenhagen K

FINLAND

Akateeminen Kirjakauppa
P. O. Box 128
SF—00101 Helsinki

FRANCE

Office International de Documentation et Librairie
48 Rue Gay Lussac
Paris 5

Librairie Lavoisier
11 Rue Lavoisier
Paris 8

Europeriodiques S. A.
31 Avenue de Versailles
78170 La Celle St. Cloud

GERMAN DEMOCRATIC REPUBLIC

Haus der Ungarischen Kultur
Karl-Liebknecht-Strasse 9
DDR—102 Beriin

Deutsche Post
Zeitungsvertriebsamt
Strasse der Pariser Kommüne 3—4
DDR—104 Berlin

GERMAN FEDERAL REPUBLIC

Kunst und Wissen
Erich Bieber
Postfach 46
7 Stuttgart S

GREAT BRITAIN

Blackwell's Periodicals
P. O. Box 40
Hythe Bridge Street
Oxford OX1 2EU

Collet's Holdings Ltd.
Denington Estate
London Road
Wellingborough Northants NN8 2QT

Bumpus Haldane and Maxwell Ltd.
5 Fitzroy Square
London W1P 5AH

Dawson and Sons Ltd.
Cannon House
Park Farm Road
Folkestone, Kent

HOLLAND

Swets and Zeitlinger
Heereweg 347b
Lisse

Martinus Nijhoff
Lange Voorhout 9
The Hague

INDIA

Hind Book House
66 Babar Road
New Delhi 1

India Book House
Subscription Agency
249 Dr. D. N. Road
Bombay 1

ITALY

Santo Vanasia
Via M. Macchi 71
20124 Milano

Libreria Commissionaria Sansoni
Via Lamarmora 45
50121 Firenze

JAPAN

Kinokuniya Book-Store Co. Ltd.
826 Tsunohazu 1-chome
Shinjuku-ku
Tokyo 160—91

Maruzen and Co. Ltd.
P. O. Box 5050
Tokyo International 100—31

Nauka Ltd.—Export Department
2—2 Kanda
Jinbocho
Chiyoda-ku
Tokyo 101

KOREA

Chulpanmul
Phenjan

NORWAY

Tanum-Cammermeyer
Karl Johansgatan 41—43
Oslo 1

POLAND

Węgierski Instytut Kultury
Marszalkowska 80
Warszawa

BKWZ Ruch
ul. Wronia 23
00—840 Warszawa

ROUMANIA

D. E. P.
Bucureşti

Romlibri
Str. Biserica Amzei 7
Bucureşti

SOVIET UNION

Sojuzpechatj — Import
Moscow
and the post offices in each town

Mezhdunarodnaya Kniga
Moscow G—200

SWEDEN

Almqvist and Wiksell
Gamla Brogatan 26
S—101 20 Stockholm

A. B. Nordiska Bokhandeln
Kunstgatan 4
101 10 Stockholm 1 Fack

SWITZERLAND

Karger Libri AG.
Arnold-Böcklin-Str. 25
4000 Basel 11

USA

F. W. Faxon Co. Inc.
15 Southwest Park
Westwood, Mass. 02090
Stechert-Hafner Inc.

Serials Fulfillment
P. O. Box 900
Riverside N. J. 08075

Fam Book Service
69 Fifth Avenue
New York N. Y. 10003

Maxwell Scientific International Inc.
Fairview Park
Elmsford N. Y. 10523
Read More Publications Inc.
140 Cedar Street
New York N. Y. 10006

VIETNAM

Xunhasaba
32, Hai Ba Trung
Hanoi

YUGOSLAVIA

Jugoslovenska Knjiga
Terazije 27
Beograd

Forum
Vojvode Mišića 1
21000 Novi Sad

ACTA TECHNICA

ACADEMIAE SCIENTIARUM HUNGARICAE

REDIGIT: M. MAJOR

TOMUS 82
FASCICULI 3–4

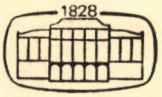

AKADÉMIAI KIADÓ, BUDAPEST 1976

ACTA TECHNICA

Az *Acta Technica* angol, francia, német és orosz nyelven közöl értekezéseket a műszaki tudományok köréből.

Az *Acta Technica* változó terjedelmű füzetekben jelenik meg, több füzet alkot egy kötetet.

A közlésre szánt kéziratok a következő címre küldendők:

Acta Technica
1051 Budapest, Münnich Ferenc u. 7.

Ugyanerre a címre küldendő minden szerkesztőségi és kiadóhivatali levelezés.

Megrendelhető a belföld számára az „Akadémiai Kiadó"-nál (1363 Budapest Pf. 24. Bankszámla 215 11448), a külföld számára pedig a „Kultúra" Könyv- és Hírlap Külkereskedelmi Vállalatnál (1389 Budapest 62, P.O.B. 149 Bankszámla: 218 10990) vagy annak külföldi képviseleteinél és bizományosainál.

Die *Acta Technica* veröffentlichen Abhandlungen aus dem Bereiche der technischen Wissenschaften in deutscher, englischer, französischer und russischer Sprache.

Die *Acta Technica* erscheinen in Heften wechselnden Umfanges. Vier Hefte bilden einen Band.

Die zur Veröffentlichung bestimmten Manuskripte sind an folgende Adresse zu senden:

Acta Technica
1051 Budapest,
Münnich Ferenc u. 7.
Ungarn

An die gleiche Anschrift ist auch jede für die Schriftleitung und den Verlag bestimmte Korrespondenz zu richten. Abonnementspreis pro Band: $ 32.00

Bestellbar bei dem Buch- und Zeitungs-Außenhandels-Unternehmen »Kultúra« (1389 Budapest 62, P.O.B. 149 Bankkonto Nr. 218 10990) oder bei seinen Auslandsvertretungen und Kommissionären.

Acta Technica Academiae Scientiarum Hungaricae, Tomus 82 (3–4), pp. 233–244 (1976)

MEMBRANE SHELLS WRITTEN IN CYLINDRICAL CO-ORDINATES

E. BÖLCSKEI*
CORRESP MEMBER OF THE HUNG. AC. OF SCI.

[Manuscript received 1 Nov. 1974]

Examples have been presented to show unambiguously that several types of shell structures lend themselves for treatment in cylindrical co-ordinates, rather than for shells of revolution alone. This statement is also valid for shells with intricate cyclic folds, or waves. For shells over sector — or ring sector — shaped ground-plans, also the boundary conditions can be relatively simply to be taken into consideration.

1. Introduction

In general orthogonal co-ordinate systems have been applied to investigate the state of stresses in membrane shells. These have been applied up to now to analyze the

barrel vault shells,
elliptical paraboloid shells,
hypar shells,
conoids,

the most commonly used types of shells in practice, while only equations describing the middle surfaces of shells of revolution, as well as differential equations describing their state of stresses, have been written in cylindrical co-ordinates.

In the present paper it will be pointed out that several practically feasible other shell forms, different from that of revolution, are rather simple to write in cylindrical co-ordinates. Again, the state of stresses analyzed in cylindrical co-ordinates often leads to differential equations which can be easily handled and solved.

In the following some shell surfaces will be presented, which are likely to be more simple to write in cylindrical, than in the usual Cartesian orthogonal co-ordinate system, such as:

helical shells,
corrugated conical shells,
waved shells,

* Prof. Dr. E. Bölcskei, Muskotály u. 37, 1118 Budapest, Hungary

cup-like shells,
polar-translation shells,
conoidal shells,
twisted shells,
calyx-shaped shells.

2. Helical shells

An ordinary *helical surface* is characterized by invariably horizontal sections parallel to the base plane (Fig. 1). It is expressed by:

$$z = c\varphi \, .$$

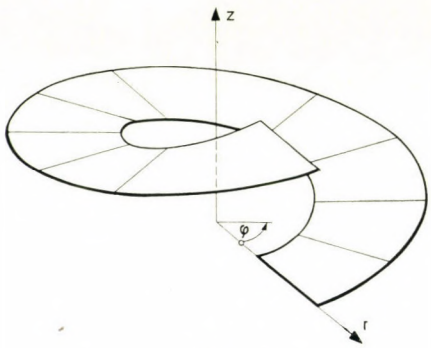

Fig. 1

The middle surface of the so-called *conical-helical* shells, expressed by

$$z = cr\varphi \, ,$$

is somewhat more complex. It has again straight generatrices, these, however, invariably pass through the origin of the co-ordinate system. Such a surface is shown in Fig. 2; a) being the first thread cut from the surface by a cylinder $r =$ constant, b) being its section cut by a plane parallel to the base plane at a height $z =$ constant.

Helical shells are of practical use, e.g. to support helical stairs, or as ramps in multistorey garages.

3. Corrugated conical shells

This shell type can be characterized in cylindrical co-ordinates by the general equation

$$z = cr \sin \alpha\varphi + hr$$

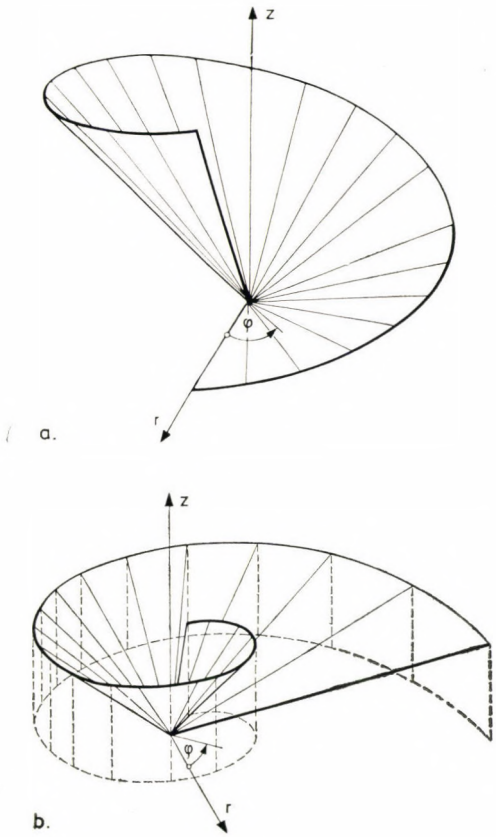

Fig. 2

where c, h, α are constants, α being the number of waves for a single revolution, numbering 6 in the examples of Fig. 3a.

If for practical reasons the valleys are to be replaced by ridges, then the absolute value of the quantity sin $\alpha\varphi$ has to be reckoned with. Fig. 3b shows an example of this type of shells. Its equation is:

$$z = cr \mid \sin \alpha\varphi \mid + hr .$$

A special case of this shell type is the c*ross-vault* with sine directrix. An example having a circular ground plan and a horizontal crown line is shown in Fig. 4.

Omitting the additive term, we obtain

$$z = cr \sin \alpha\varphi$$

or

$$z = cr \mid \sin \alpha\varphi \mid .$$

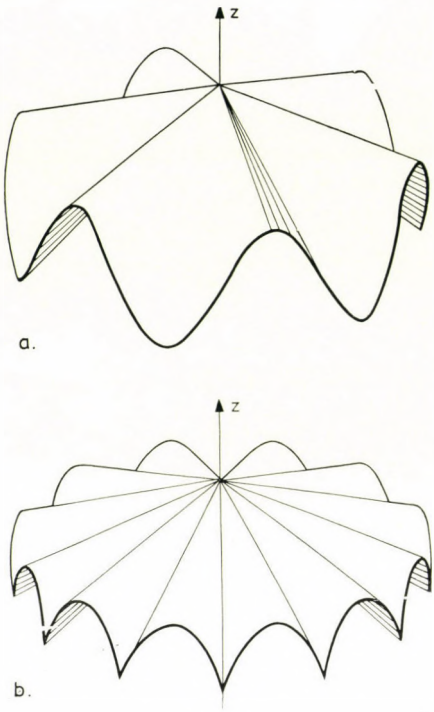

Fig. 3

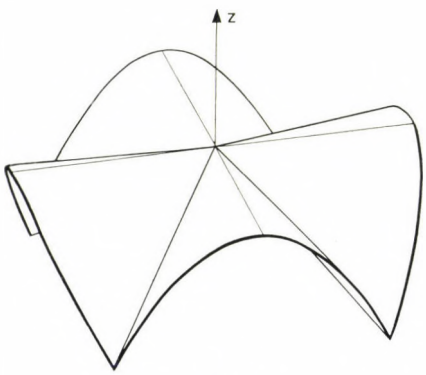

Fig. 4

In the latter case, valleys have again been transformed into ridges. Two varieties conform to the above equations are shown in Figs 5a and 5b.

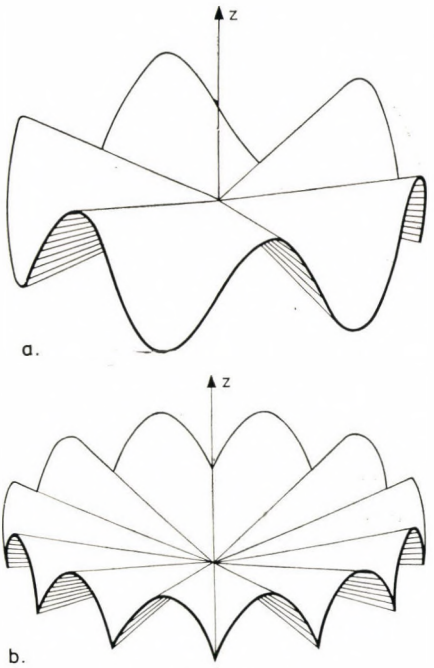

Fig. 5

4. Waved shells

A *waved shell* with an arbitrary directrix is described by the general equation

$$z = f(r) \sin \alpha\varphi$$

where function $f(r)$ can be chosen at will, such as:

$$f(r) = ce^r,\ c \cos hr,\ cr^2 \text{ etc.}$$

Accordingly, the shell can be termed a parabolic etc. one, with directrix e^r, cosh r or r^2 etc.

The so-called parabolic waved shell with directrix r^2 has a general equation of the form:

$$z = cr^2 \sin \alpha\varphi + hr^2.$$

Eliminating the valleys:

$$z = cr^2 \mid \sin \alpha\varphi \mid + hr^2,$$

as is shown in Fig. 6, with $\alpha = 3$ and $h < 0$.

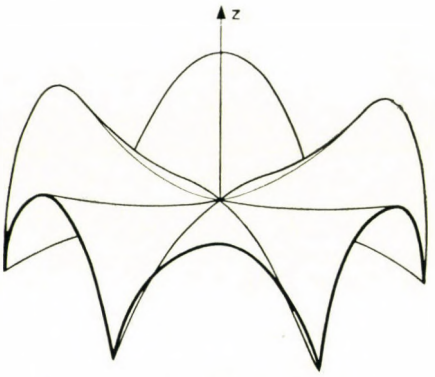

Fig. 6

Choosing the additive term as $h = 0$, and taking $\alpha = 6$, results in a parabolic waved shell (Fig. 7) expressed by:

$$z = cr^2 \sin \alpha\varphi \, .$$

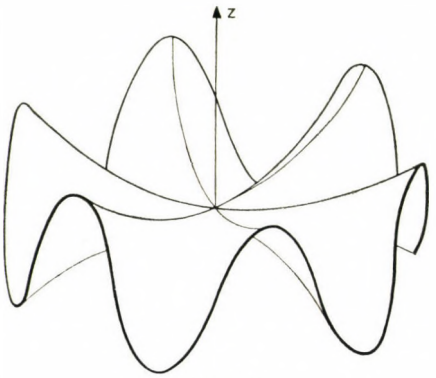

Fig. 7

5. Cup-like shells

Rather interesting, beautiful surfaces — *cup-like shells* — result from applying the periodic function used earlier as a multiplier — e.g. the sine function — as denominator, completed by an additive term β. For $\beta > 1$, the denominator is non-zero, hence, the fraction is never infinite.

The simplest form of cup-like shells that having a straight directrix, with the equation

$$z = \frac{cr}{\sin \alpha\varphi + \beta} \, ,$$

illustrated in Fig. 8.

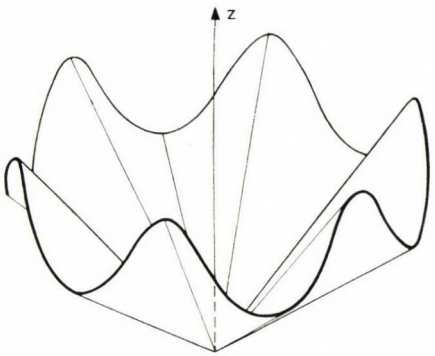

Fig. 8

The linear function can be replaced by any other function of the variable r, hence, the general equation of the so-called cup-like shell is of the form:

$$z = \frac{f(r)}{\sin \alpha\varphi + \beta} .$$

One of the simplest form of $f(r)$ is a parabola

$$f(r) = cr^2.$$

The corresponding parabolic cup-like shell (Fig. 9) is characterized by

$$z = \frac{cr^2}{\sin \alpha\varphi + \beta} .$$

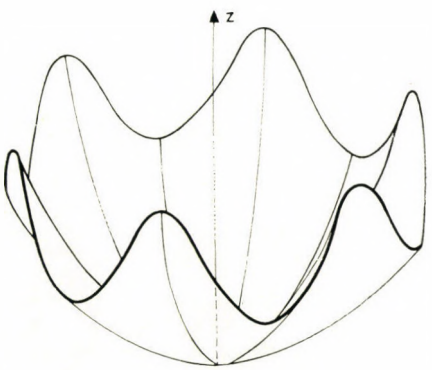

Fig. 9

6. Polar-translation shells

The middle surface of a *polar-translational shell* is obtained by turning a planar curve around a vertical axis and moving it at the same time up and down, so that it always touches a sinusoidal line drawn on a concentric cylinder surface. When the moving curve is a sinusoid then the equation of the shell's middle surface is

$$z = a \sin 2\pi \frac{r}{l} + b \sin \alpha\varphi .$$

A sector of this shell's middle surface cut out by two radial planes and a cylinder, is shown in Fig. 10. A part of a similar surface limited by two vertical planes passing through the axis and by two concentric cylinders (Fig. 11)

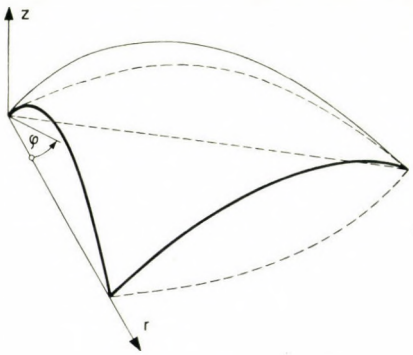

Fig. 10

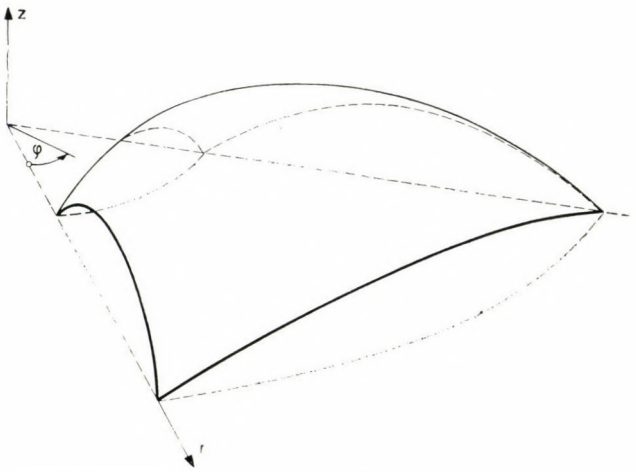

Fig. 11

is characterized by the equation:

$$z = a \sin 2\pi \frac{(r - r_0)}{l} + b \sin \alpha\varphi \,.$$

Surfaces confined by concentric circles and by straight radii are, in general, also easy to treat in cylindrical co-ordinates.

7. Conoidal shells

A *conoidal shell* with a radial straight directrix is shown in Fig. 12. Its equation is:

$$z = c(r - \mathrm{a})\ (\varphi^2 - \alpha^2) \,.$$

The *polar harmonic shell*, described by

$$z = c \cdot (r - a)^2\ (\varphi^2 - \alpha^2) \,,$$

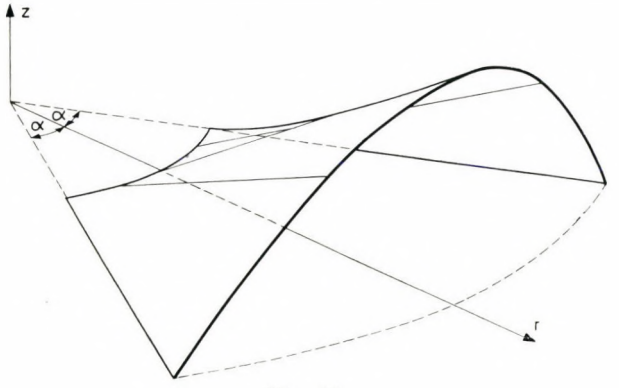

Fig. 12

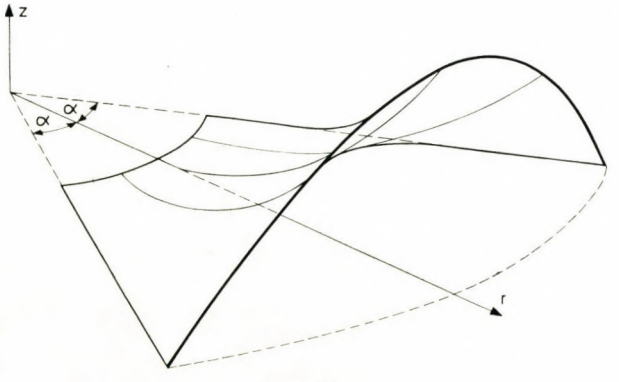

Fig. 13

is similar in character, except that here the radial sections are parabolae of the second-order instead of straight lines. Such a shell over a ground-plan confined by two radial straight lines and two concentric circles is shown in Fig. 13.

8. Twisted shells

A shape often encountered in Baroque architecture is the surface of a twisted column. The equation of its surface (Fig. 14) is easy to write in a polar system of co-ordinates as

$$r = a \sin (b\varphi - cz) ,$$

or, in the usual form:

$$z = \frac{1}{c}\left(b\varphi - \arcsin \frac{r}{a}\right) .$$

Considering in the former equation the absolute value of the sine term, i.e. taking

$$r = a \mid \sin (b\varphi - cz) \mid ,$$

another twisted surface is obtained (Fig. 15), differing from the former by featuring only convex sine half-waves.

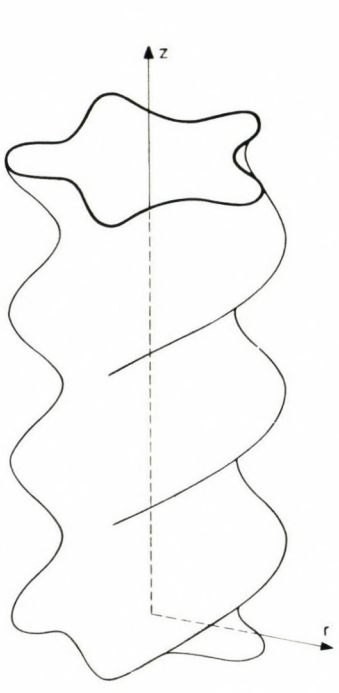

Fig. 14

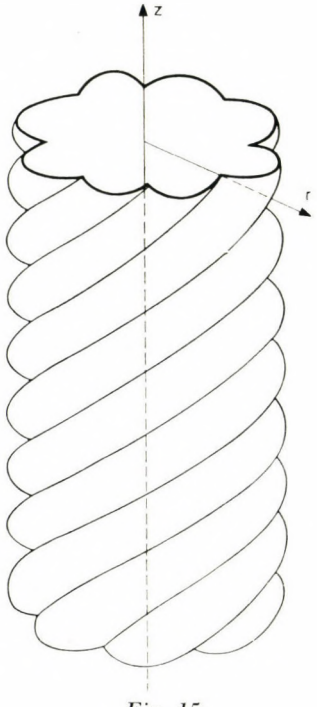

Fig. 15

9. Calyx-shaped shells

This expediency of the use of a polar co-ordinate system is pointed out by the polar translation shell having the equation

$$z = a \ln br + c \sin n\varphi .$$

Fig. 16 depicts axonometrically a part of this shell, limited by a concentric cylinder and also shows its sections cut out of the middle surface by planes $z/a = 1/2$, $z/a = 0$ and $z/a = -1/2$. This surface having a relatively simple equation, adapts itself to natural flower shapes.

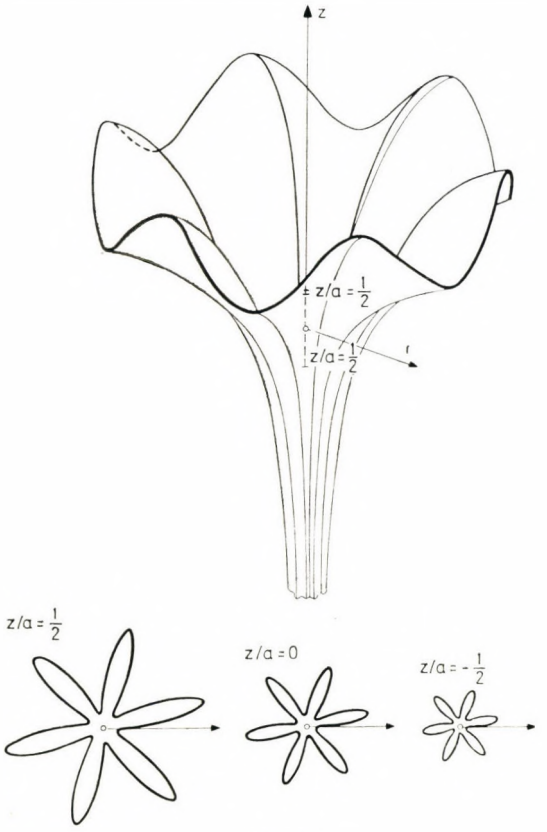

Fig. 16

Behandlung von Membranschalen in Zylinderkoordinaten. Beispiele sind vorgeführt, die eindeutig beweisen, daß sich eine Anzahl Schalenkonstruktionen für eine Behandlung in Zylinderkoordinaten eignen. Diese Behauptung beschränkt sich nicht auf Rotationsschalen, sondern gilt auch für verhältnismäßig verwickelte Schalenflächen mit periodischen Falten. Bei Kreissektor- oder Kreisringsektorschalen lassen sich auch die Randbedingungen ziemlich einfach beachten.

Мембранные оболочки в цилиндрических координатах. Приведенные примеры однозначно подтверждают, что оболочечные конструкции относительно сложной формы отлично подходят для рассмотрения их на основе цилиндрических координат. Данное определение касается не только оболочек в форме поверхности вращения, но оно действительно также для относительно сложных поверхностей оболочек, оформленных с периодически повторящимся гофрировванием. Окружные условия можно учитывать относительно просто в том случае, когда идет речь об оболочках с планом в виде сегмента круга или сегмента кольца, ограниченного на плане радиальными прямыми или же концентрическими кругами вокруг оси вращения.

Acta Technica Academiae Scientiarum Hungaricae, Tomus 82 (3—4), pp. 245—254 (1976)

PROCESS OF HYDRAULIC SOIL FAILURE

Á. KÉZDI*
MEMBER OF THE HUNG. AC. OF SCI.

[Manuscript received 7 March, 1975]

The quicksand condition which takes place under the influence of the water flow directed upwards within a sand mass, is commonly calculated on the basis that the soil structure forms a rigid skeleton. Laboratory tests showed that by increasing the value of the hydraulic gradient, partly the phenomenon of outwash, partly loosening or densification takes place, depending on whether the initial state was dense or loose, respectively. The full failure itself, just as the shear failure, is associated with the development of a critical void ratio. Attaining a hydraulic gradient determined on the basis of the assumption of a mentioned rigid skeleton, means the transition from the laminar flow of water into the turbulent one. In the course of the development of the quick condition, the permeability changes in another way than had been believed on the basis of the change in density; also this may be explained by the occurrence of turbulent flow.

If there is an upward directed vertical water flow in a sand mass bounded by a horizontal unloaded surface, and the water supply is sufficient to keep the value of the hydraulic gradient at a constant level then, within the sand layer, the pattern of the vertical stresses is as shown in Fig. 1 (see KÉZDI, 1974). The level of the ground water coincides with the soil surface, accordingly, on the surface, the piezometric head is equal to zero; but in the piezometer pipe arranged at a depth h, the water level must be above the soil surface by a value Δh in order to allow a vertical water flow to be directed upwards. If $\Delta h = 0$, the pattern of the neutral stresses develops according to the broken line $\overline{13}$; the total stresses are shown by the broken line $\overline{15}$. If a differential pressure $\Delta h \gamma_w$ is produced, the neutral stress at depth h increases by the value $\Delta u = \Delta h \gamma_w$, and since the total stress did not change, the effective stress had to decrease by the same amount. That is, at depth h:

$$\sigma_z = h\gamma_t - (h + \Delta h)\,\gamma_w\,. \tag{1}$$

By increasing the value of Δh and at the same time also that of the hydraulic gradient $i = \Delta h/h$ a condition will be attained where the value of the effective stress is equal to zero: $\bar{\sigma}_z = 0$. In this case, from Eq. (1) the associated so-called critical hydraulic gradient may be determined:

$$i_{\text{crit}} = \frac{\Delta h_{\text{crit}}}{h} = \frac{\gamma_t - \gamma_w}{\gamma_w} = \frac{\gamma_b}{\gamma_w}\,. \tag{2}$$

* Prof. Dr. Á. KÉZDI, 1012 Lógodi u. 9. Budapest, Hungary

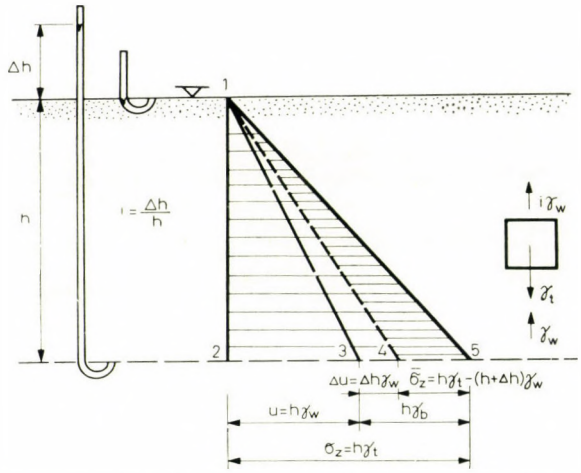

Fig. 1. Vertical stresses in a sand mass of infinite extension, due to its own weight

Here γ_b is the bulk density of the soil reduced by the uplift force, the so-called buoyant unit force weight. Since in this case only neutral stresses are acting in the sand mass, the shear strength of the sand is zero, and the sand grains are not supported either from above, nor from below, the mass behaves as a viscous liquid having a bulk density γ_b .

The simple considerations outlined above assume that the grains of the sand mass during the increase of the value of Δh up to Δh_{crit} constitute a skeleton; no change in the volume takes place and the strength rapidly, becomes zero almost in a moment. If this would be true, the value $i_{crit} = \gamma_b/\gamma_w$ would indeed precisely express its condition. However, this is not the case: on increasing Δh, in general, two processes are taking place: on the one hand from the mass some fine grains will be washed out, and on the other hand, grains become more inclined to move due to the reduction of the effective stress, and a displacement which implies volume change. This volume change may be both loosening and compaction. Both phenomena cause changes in the value of the void ratio and coefficient of permeability. Therefore, the process of the quick condition may be described only as a first approximation by the simple formula shown in Fig. 1 and by Eq. (1).

Let us first investigate the question of *washing out*. Let us assume that a grain having a diameter d during the increase of the value Δh is no longer supported at its sides and is only subjected to vertical forces. The velocity of the upward flow of water according to Darcy's law is:

$$v_w = \frac{v}{n} = k \frac{\Delta h}{h} \cdot \frac{1}{n} . \tag{3}$$

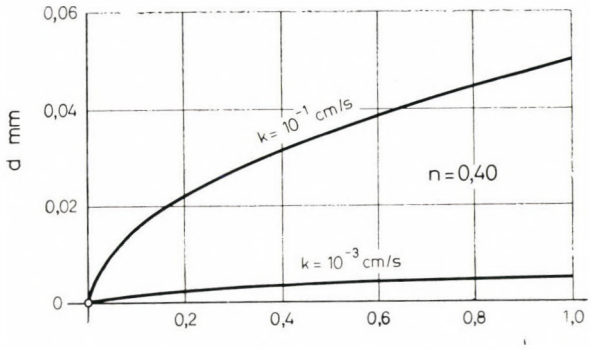

Fig. 2. Critical grain diameter with respect to outwash as a function of the hydraulic gradient

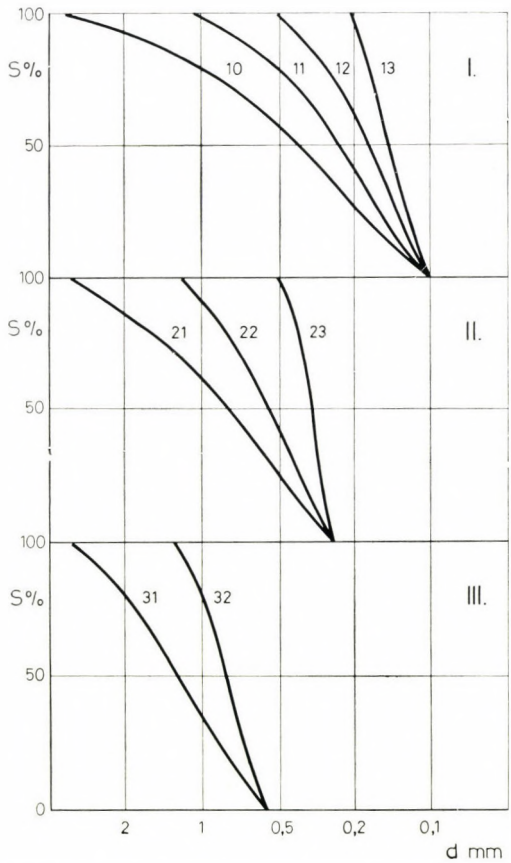

Fig. 3. Grain-size-distribution curves of soils used at tests

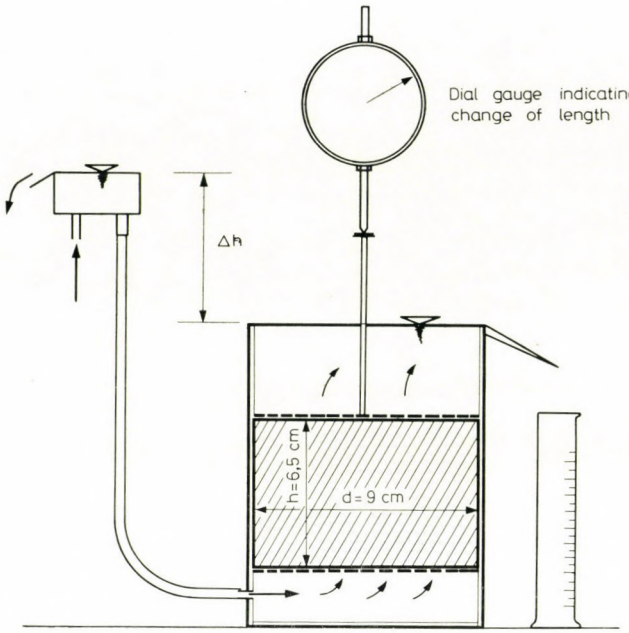

Fig. 4. Scheme of test set-up

If we assume spherical grains, the velocity of water flow directed upwards at which the grain attains the state of suspension, may be calculated from Stoke's law as follows:

$$v_w = \frac{\gamma_s - \gamma_w}{18\,\eta}\, d^2 \tag{4}$$

where η is the viscosity of the liquid and d is the diameter of the spherical grain. If the velocity of the water flow reaches this value, also the lower support of the grain will be discontinued and the grain goes into a suspending movement. If the hydraulic gradient i is given, so the diameter of the grain going into the state of suspension, may be calculated by equating the right-hand sides of Eqs (3) and (4):

$$d_{\text{crit}} = \sqrt{\frac{18\,\eta}{\gamma_s - \gamma_w} \cdot \frac{ki}{n}} = C \sqrt{\frac{k}{n}} \sqrt{i}\,. \tag{5}$$

The values of d_{crit} under average conditions at several values of k are plotted as functions of i in Fig. 2. Grains of smaller diameters may be washed out of the mass if their free displacement is possible.

The volume change due to the increase of the value $\Delta h/h$ has been experimentally investigated. In the following some characteristic test results are presented.

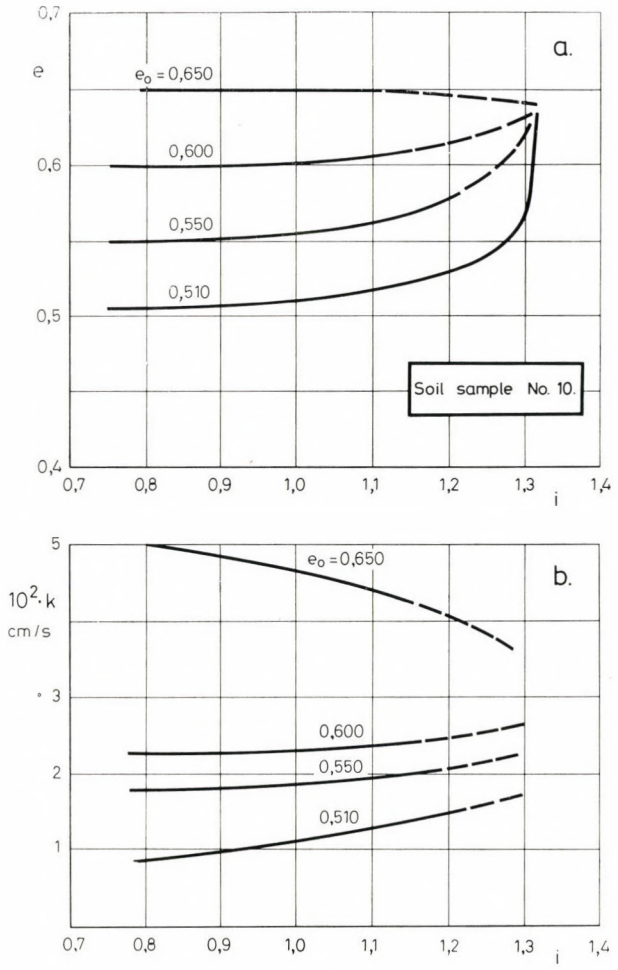

Fig. 5. Development of the void ratio and coefficient of permeability with increasing hydraulic gradient

The grain size distribution curves of the soils investigated are given in Fig. 3. The soil samples were tested at different initial densities. After having saturated the samples by capillarity, Δh was increased stepwise. On reaching the stationary condition the rate of flow of water per minute has been determined and the length of the specimen measured (Fig. 4). Thus the coefficient of permeability and void ratio of the sample could be calculated.

A characteristic result is to be seen in Fig. 5. Here the permeability and void ratio are plotted for samples having different initial density versus the hydraulic gradient. It is an interesting, however, as a matter of course,

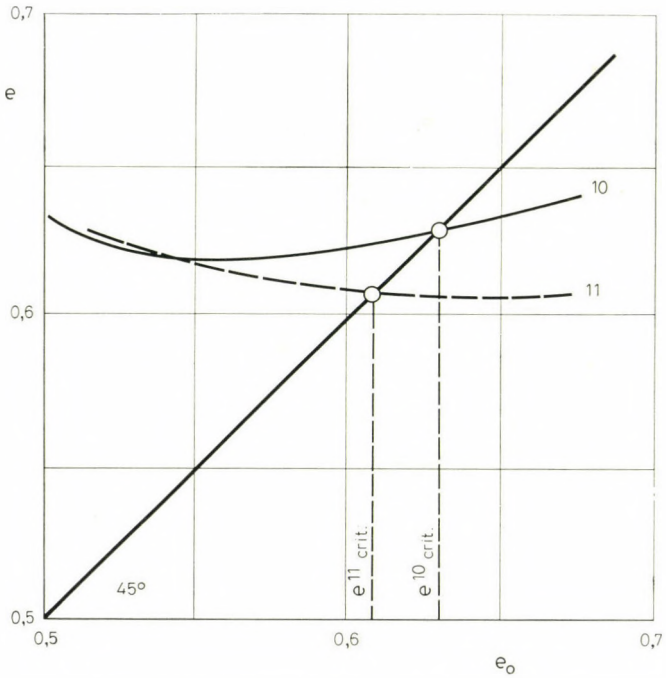

Fig. 6. Determination of the critical void ratio

quite a reasonable phenomenon that in increasing the hydraulic gradient, also here, just as in the case of shear tests, there is a critical void ratio: on increasing the value i, the originally loose sample becomes denser, while the originally dense sample will be looser. Accordingly, the "failure", i.e., the complete liquefaction ("quick condition") of the sand, i.e., the state $\bar{\sigma}_z = 0$ always takes place at a certain void ratio, independently of the initial value.

If one considers, that in the sand mass besides local heterogeneities in the grain size distribution, also during the increase of the hydraulic gradient shear deformations take place which, as a matter of course, also cause volume changes, the phenomenon should be accepted as a logical consequence (KÉZDI, 1963). If we plot the void ratio developed *vs.* the initial void ratio, the critical value can immediately be read off (Fig. 6). These void ratios are also given in Fig. 7 where the grain size distribution curves of the soils are in the system of coordinates ($\log d_{max}$, $\log U$) characterized by one-one point each. From the experiments conducted so far it seems that the smaller the value of U, the greater that of the critical void ratio is which develops at quick condition.

As is familiar, the critical void ratio which occurs in the shear tests and which can be measured, is the function of the normal stress; it decreases

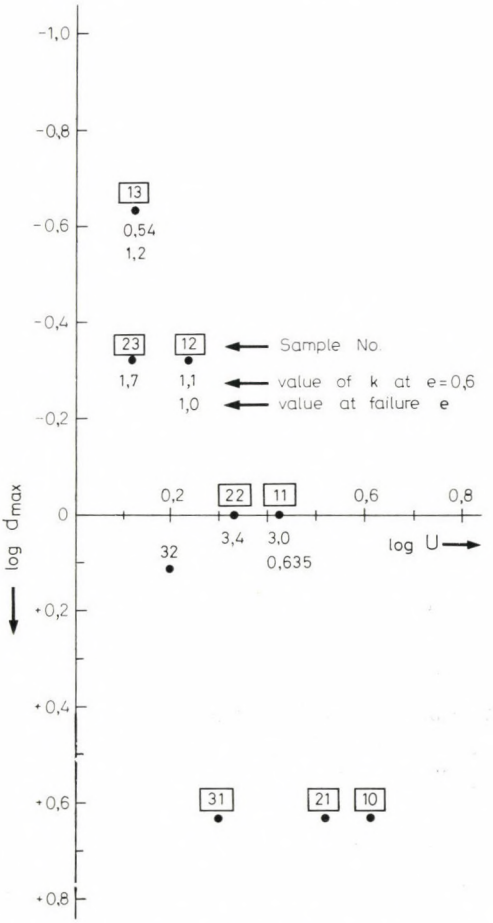

Fig. 7. Critical void ratio of the soils tested in the system of coordinates ($\log d_{max}$, $\log U$) characterizing grain size distribution

with the increase of the latter. The critical void ratio associated with the quick condition may be considered as coordinated to the stress $\bar{\sigma} = 0$, and thus, it represents the maximum value.

As to the coefficient of permeability, its value approaching the quick condition, somewhat increases in that case where it has been started from the dense state, i.e., when the volume change was a loosening. However, the increase is not so significant that it would ensue from the degree of loosening. If the value of the void ratio was high at starting ($e > e_{crit}$) and thus near failure densification took place then, as a matter of course the permeability is reduced. However, this reduction was much greater than would have been assumed. Both experiences showed that the water flow became more and more *turbulent* near the failure and thus, in this region

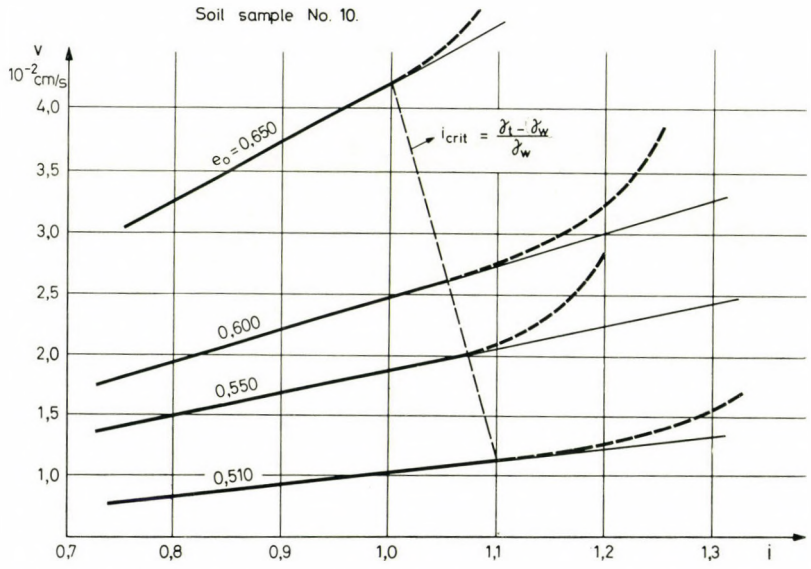

Fig. 8. Behaviour of the seepage velocity with increasing hydraulic gradient

Darcy's law does not hold any longer. This effect is clearly demonstrated in Fig. 8, where the seepage velocity calculated on the basis of the amount of water flown through at different initial void ratios is plotted versus the hydraulic gradient. The relationship is at values $i \leq (\gamma_t - \gamma_w)/\gamma_w$ linear but, by surpassing this value, one obtains a diagram which, anyhow, is characteristic of the turbulence. Thus, the "critical" hydraulic gradient calculated with Eq. (2), indicates the state where the flow of the water, laminar so far, turned into a turbulent one, however, the quick condition did not developed fully. This only occurs if i further increases during this process.

It is also worthwhile to note that in case of coarse grained soils, (for example, at that No. 31) major volume changes could not be observed as a result of the increase of i. It is possible that the water flow here even at small values of i is turbulent owing to the comparatively small specific surface; the effect of the flow on the structure is not too significant. One observes only loosening in the case of the soil No. 23, that is, a sample looser than e_{crit} here could not be produced (Fig. 9).

Contrary to the test results it may be observed in nature, that in three-phase soils at lower values of i, than those given by Eq. (2) a phenomenon takes place which might be called hydraulic failure. Here, two circumstances may interfere: either the effective path of seepage is shorter than that assumed because internal erosion developed or, in the three-phase soil the enclosed air bubbles get compressed under the process and thus, positive neutral air-stresses come into being, thereby reducing the shear strength.

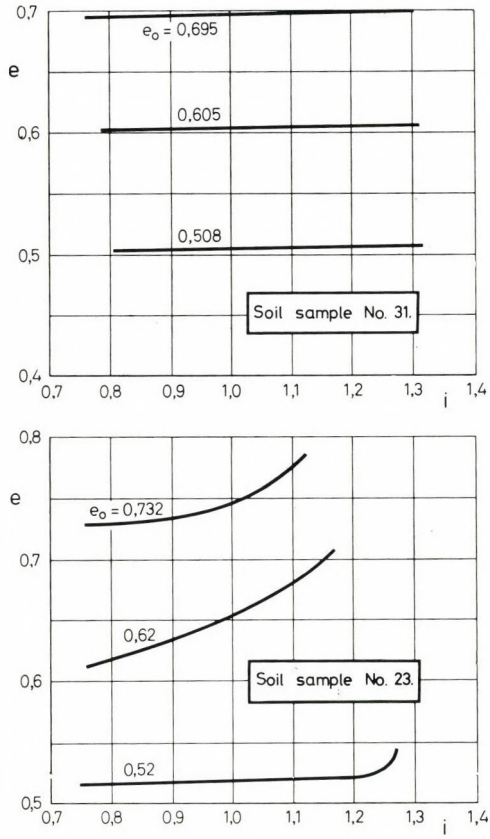

Fig. 9. Development of the void ratio with increasing hydraulic gradient in a coarse grained soil (No. 31) and in a soil of uniform (No. 23) size distribution

REFERENCES

1. KÉZDI Á.: Schwerverformungen von Sand. *Scientific Publications of the Technical University Budapest.* Vol. IX (1963), No. 5
2. KÉZDI Á.: Handbook of Soil Mechanics. Vol. I., p. 155. Elsevier Scientific Publishing Co., Amsterdam 1974

Vorgang des hydraulischen Grundbruchs. Die Bedingung des unter der Einwirkung der in einer Sandmasse aufwärts gerichteten Wasserströmung eintreffenden Grundbruchs wird, im allgemeinen, unter der Voraussetzung ermittelt, daß das Skelett keine Bewegung und keine Volumenänderung vollführt. Es wurde durch Laborversuche nachgewiesen, daß infolge der Erhöhung der hydraulischen Druckgefälle teils Auswaschung, teils Auflockerung oder Verdichtung auftritt, demgemäß, daß der Anfangszustand dicht oder locker war. Der vollständige Bruch, ebenso wie bei einem durch Schubbeanspruchung hervorgerufenen Bruch, ist mit der Entwicklung einer kritischen Porenzahl verbunden. Die Erzielung der kritischen hydraulischen Druckgefälle, die aufgrund des vorausgesetzten steifen Skeletts ermittelt werden kann, ruft einen Übergang von der laminaren in die turbulente Strömung hervor. Unter dem Vorgang der Entwicklung des hydraulischen Bruchs ändert sich die Permeabilität auf eine andere Art, als es aus der Änderung der Dichte voraussichtlich war; diese Erscheinung kann auch durch den Auftritt der Turbulenz erklärt werden.

Процесс гидравлического разрушения грунта. Условия гидравлического разрушения основания, происходящего под воздействием движения воды снизу вверх в песчаных массивах, обычно принято рассчитывать на той основе, что скелетная структура не претерпевает движения. Лабораторные опыты показали, что в процессе повышения гидравлического градиента возникают, с одной стороны, размыв, а с другой стороны, разрыхление или же уплотнение, а именно в зависимости от того, что начальное состояние было ли плотным или же рыхлым. Само полное разрушение, аналогично разрушению сдвига, сопровождается формированием критического коэффициента пористости. Достижение критического гидравлического градиента, определенного на основе упомянутого выше предположения (жесткий скелет), означает переход ламинарного движения потока воды в трубулентное. В процессе формирования гидравлического разрушения проницаемость изменяется иначе, чем это должно было происходить на основе изменения плотности; это явление можно объяснить также возникновением турбулентного движения потока.

Acta Technica Academiae Scientiarum Hungaricae, Tomus 82 (3—4), pp. 255—279 (1976)

INTRODUCTION À QUELQUES PROBLÈMES DE TURBULENCE

I. MATHIEU*

[Manuscrit reçu le 1er Septembre 1974]

Cet exposé qui ne se veut qu'introductif a uniquement pour but de mettre en place une ligne de pensée et un langage commun susceptible de faciliter les discussions que nous serons amenés à conduire dans la présentation des recherches sur les couches limites perturbées ou les couches limites déstabilisées par chauffage. A travers lui, on pressent également quels pourraient être, dans ce domaine, les développements futurs; l'étude des phénomènes thermiques, celle des couches limites tridimensionnelles et des écoulements confinés s'imposent à bien des égards.

Notations

x	vecteur position du point M
x'	vecteur position du point M′
$x_i\ x\ y\ z$	composantes du vecteur position
τ	vecteur position relative M M′
ξ	vecteur position relative
$L\ l$	longueur caractéristique
R	rayon de la conduite
δ	épaisseur de la couche limite
$\overline{U}$	vecteur vitesse
$\overline{U}_i;\ U\ V\ W$	composantes de ce vecteur
$\overline{U}_i;\ \overline{U}\ \overline{V}\ \overline{W}$	composantes de la vitesse moyenne
u	vecteur vitesse fluctante
$u_i;\ u, v, w$	composantes de la vitesse fluctuante
$\overline{q}^2 = \overline{u}^2 + \overline{v}^2 + \overline{w}^2$	
$\tau/q\ \overline{q}^2 = a_1$	
$\overline{P}$	pression moyenne
p	pression fluctuante
$\overline{\varepsilon}$	dissipation moyenne
$s = \partial\overline{U}/\partial y$	$\lambda_{12} = \partial\overline{U}_1/\partial x_2$
t	temps
t_s	temps de structuration
t_e	temps d'extinction
Θ	température
$\overline{\Theta}$	température moyenne
θ	température fluctuante
Γ	concentration
$\vec{k}\ \ \vec{p}\ \ \vec{q}$	vecteurs nombres d'onde
E	fonction spectrale
G	noyau
$\lambda_{lm} = \partial\overline{U}_l/\partial x_m$	$\partial\overline{U}_l/\partial x_m$
$\gamma_l\ \ = \partial\Theta/\partial x_i$	$\partial\theta/\partial x_l$
$R_{ij}\ T_{ij}\ S_{ij}$	tenseurs dans le plan physique
$\Phi_{ij}\ \Psi_{ij}\ \Omega_{ij}$	tenseurs dans le plan spectral
$\varphi_i\ \tau_{ij}\ \eta$	tenseurs spectraux intervenant lors
Γ_i	d'un processus thermomécanique

* J. MATHIEU, École Centrale de Lyon, Université de Lyon

δ_{ij}	symbole de Kronecker
γ_T	viscosité turbulente
τ	contrainte
γ	viscosité cinématique
$\alpha = \lambda/\varrho C_p$	diffusivité thermique
$\mathfrak{P}$	nombre de Prandtl
ϱ	masse volumique
$\mathfrak{R}_1$	nombre de Reynolds turbulent

Il nous a semblé utile, avant d'aborder quelques objectifs de recherche plus spécifiques, d'examiner quelles peuvent être actuellement sur un plan très général les lignes directives suivies au Laboratoire, et comment elles se rattachent aux développements mondiaux sur le thème de la turbulence.

C'est pour nous un sujet de préoccupation ancien que celui d'une liaison université industrie. Si la réalisation d'un tel programme s'avère, dans tous les cas, difficile, cela tient sans aucun doute à ce que pour être mise en place, cette formule doit ménager bon nombre de relais intermédiaires, à travers lesquels chemine l'information. Par le panorama assez étendu des recherches présentées, on peut voir que bon nombre ont pu être ainsi mis en place. Il serait bien évidemment difficile d'intéresser tel ou tel constructeur à quelque structure de «noyau» dans la théorie de KRAICHMAN. Plus tangible lui paraît la fourniture d'un programme de calcul qui, tenant compte au mieux des mécanismes turbulents, fournit des informations dans un très grand nombre de cas. Nous essaierons de montrer dans ce qui suit comment, ouverts aux différentes voies de recherches, nous tentons plus spécialement d'en faire progresser certaines, nous efforçant de toute façon de dégager de ces investigations théoriques ou expérimentales quelques idées utiles à la mise en place de moyens calcul. La formule reste, bien entendu, souple dans son application, c'est-à-dire que le programme défini est, dans bien des cas, une tendance plus qu'un aboutissement. Cependant, ce type d'arbitrage est toujours implicitement recherché.

Nous n'aborderons pas, dans ce qui suit, les travaux conduits dans le domaine de l'aéroacoustique, lesquels bénéficient d'une attention plus spéciale de notre collègue le Professeur G. COMTE-BELLOT; il serait du reste difficile de le faire dans un temps aussi court. Nous préférons donc borner notre exposé aux problèmes des écoulements dans leur relation avec la turbulence.

Qu'il s'agisse d'aérodynamique interne ou d'aéroacoustique, et si l'on met à part les problèmes concernant l'étude des fluides non visqueux lesquels sont à l'heure actuelle assez bien traités, on est dans tous les cas confrontés au problème de la turbulence. Nous ne reviendrons pas sur la description globale de ce phénomène dont l'essentiel avait été déjà bien saisi à la fin du siècle dernier par BOUSSINESQ et REYNOLDS. On peut dire, sans s'inscrire en faux par rapport aux idées actuelles, qu'il s'agit de la manifestation tangible d'une instabilité essentielle propre à la structure des équations de

NAVIER. Des travaux mathématiques récents concernant l'équation de NAVIER elle-même, ou celle qui lui fut très souvent associée du fait qu'elle présente une structure mathématique analogue, nous voulons parler de l'équation de BURGERS, confirment tout à fait ce point de vue. Le caractère non linéaire de ce type d'équation, dû à la présence des termes d'accélération convective, est à coup sûr déterminant. Sur le plan physique, il donne au problème son visage essentiel tandis que, sur le plan mathématique, il le complique à tel point que l'on ne peut montrer que les équations:

$$\frac{\partial \vec{U}(\vec{x}, t)}{\partial t} + \vec{U}(\vec{x}, t) \nabla \vec{U}(\vec{x}, t) = - \Delta p(\vec{x}, t) + \nu \nabla' \, U(\vec{x}, t)$$

$$\nabla \vec{U} = 0$$

jointes à un jeu de conditions aux limites et initiales constituent un problème bien posé. Pour être bref, disons qu'en tridimensionnel, l'unicité est assurée pour des temps très courts si ν est petit et qu'elle est établie pour n'importe quel temps si ν est grand.* Les difficultés rencontrées en tridimensionnel sont évitées en bidimensionnel et en axisymétrique et ceci est en accord avec le fait bien connu que la régularité mathématique des solutions d'une équation aux dérivées partielles croît lorsque décroît le nombre de dimensions de l'espace dans lequel est recherchée une solution. Tout comme sera essentielle l'influence de la viscosité dans le processus turbulent, sera crucial le rôle joué par les termes d'ordre le plus élevé des équations de Navier; la présence de termes biharmoniques assurera par exemple l'unicité de même que l'introduction d'une liaison adéquate entre le coefficient de viscosité et le taux de déformation.

Du point de vue qui nous occupe, la non-linéarité fondamentale des équations de départ traduira une interaction entre modèles et s'il nous est possible de décomposer fictivement l'écoulement en champ moyen et en champ fluctuant, il ne nous est pas permis de considérer ces deux modèles évoluant séparément. Leur cohabitation ne va pas sans une action de l'un sur l'autre; en bref, le champ moyen sur lequel l'ingénieur voudrait porter son attention est profondément remanié par le phénomène turbulent. Les termes d'inertie liés aux fluctuations du champ turbulent sont alors interprétés comme une contrainte supplémentaire dite contrainte de Reynolds que l'on ne sait pas a priori exprimer. Le problème ainsi posé est dit ouvert, et il en va de même de tout problème non linéaire de nature statistique, la théorie quantique des champs en fournissant d'autres exemples. Sous des aspects différents mais rigoureusement identiques quant au fond, le chercheur et l'ingénieur se trouveront ainsi confrontés à une même difficulté centrale.

* Les expressions « temps petits » et « temps grands » sont précisées en tant qu'environnement temporel et aussi spatial en faisant jouer la viscosité.

Pour mieux la réduire, le premier recourra d'emblée à des modèles turbulents simples: tel celui fourni par la turbulence homogène et isotrope, le second confronté à une réalité précise ne pourra pas chercher sur ce plan d'échappatoire, en revanche, il prendra certaines libertés en adoptant le plus souvent des fermetures grossières dont certaines bien connues de tous seront succinctement rappelées. On sent en fait à partir de quel stade du raisonnement les deux cheminements divergent.

Nous tenterons maintenant un très bref tour d'horizon pour essayer de dégager quelles peuvent être les difficultés centrales du problème et comment on y est de toute façon confrontés. Nous avons déjà laissé entendre, pour n'y plus revenir, à quels types de difficultés mathématiques l'on se heurtait. C'est davantage d'un point de vue physique que nous nous placerons désormais. Comme nous le verrons plus en détail, par la suite, la nécessité de classer les structures turbulentes suivant leur taille afin de leur découvrir une certaine spécificité fait que les analyses seront conduites, explicitement ou implicitement, dans l'espace des nombres d'ondes. Aux grosses structures sont attachés de petits nombres d'ondes et aux fines structures de grands nombres d'ondes. La transformée de Fourier jette un pont entre l'espace physique et l'espace spectral, toute propriété établie dans l'un des espaces ayant son corollaire dans l'autre; pour un fluide incompressible l'équation de continuité introduira une liaison dans le plan spectral: les perturbations devront être polarisées dans des plans normaux à la direction de propagation de la perturbation; la nécessité de définir une énergie cinétique d'agitation positive se traduira dans l'espace spectral par la condition de KRAMMER, c'est-à-dire par une contrainte sur la forme du tenseur spectral. Cette transformation intégrale peut être appliquée aux fonctions de corrélations $\overline{u_i u_j}(\vec{\tau})$ qui sont des fonctions régulières et aussi moyennant quelques précautions* aux équations de Navier elles-mêmes. C'est ainsi que pour la fluctuation u_i on obtiendrait:

$$\left(\frac{d}{dt} + \nu k^2\right) u_i(\vec{k}, t) = M_{ijm}(\vec{k})\, \hat{\Sigma} u_j(\vec{p}, t)\, u_m(\vec{q}, t)\,,$$

$$M_{ijm}(\vec{k}) = -\frac{1}{2} i \left\{k_m P_{ij}(\vec{k}) + k_j P_{im}(\vec{k})\right\}\,.$$

$$P_{ij}(\vec{k}) = \delta_{ij} - \frac{k_i k_j}{k^2}\,.$$

Le terme de gauche de cette équation correspond à la partie linéaire du problème de départ, on reconnaît l'opérateur convection diffusion. Ainsi, en tout point $\vec{k}_0$ de l'espace spectral l'évolution convection diffusion de

* Ces précautions viennent du fait que les vitesses u_i ne sont pas des fonctions régulières; on surmonte alors la difficulté en utilisant la théorie des distributions.

$u_i(\vec{k}_0, t)$ est contrôlée par la viscosité intervenant linéairement du fait de l'hypothèse de départ (fluide Newtonien) tandis que les termes d'inertie responsables de la non-linéarité du problème et rejetés au second membre peuvent y être interprétés, pour des raisons de commodité, comme des termes source. On voit ainsi que, si le problème était linéaire, une perturbation d'ordre $\vec{k}_0$ n'évoluerait pas dans l'espace spectral mais seulement dans le temps; il est ici clair que deux perturbations de vecteurs d'ondes différents

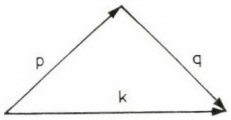

Fig. 1

$\vec{p}$ et $\vec{q}$ peuvent se recombiner pour créer une fluctuation de nombre d'onde $\vec{k}$ à condition toutefois que soit respectée la forme tryadique ici indiquée. On peut donc en principe voir des tourbillons de dimensions très diverses intervenir sur un certain mode $\vec{k}$ étant toutefois entendu que la composition qui vient d'être rappelée engendre certaines contraintes, précisément celles qui résultent de la possibilité de former un triangle. D'une certaine manière, nous ne faisons ici que réaffirmer la possibilité offerte par tout système non linéaire complexe de générer harmoniques et sous harmoniques*. Après l'introduction avec TAYLOR du point de vue statistisque, on peut dire que Kolmogorov formula dès 1941 des idées qui sont encore considérées comme essentielles et que l'on retrouve sous-jacentes dans les théories actuelles.

1. Les transferts inertiels, sont un phénomène local dans l'espace des nombres d'ondes, c'est-à-dire que la probabilité de transfert sur un large domaine reste faible et ceci limite grandement les possibilités offertes dans la construction des triades précédentes.

* En fait, le processus doit bien être retenu: il pourrait sans doute servir de base à une critique des modèles où, développant un mode de transmission par trop local dans l'espace des nombres d'ondes, on arrive, pour une turbulence isotrope, à des difficultés, en particulier dans certaines régions dissipatives du spectre; l'idée d'HEISENBERG qui consiste à prendre en compte les actions dynamiques à un certain nombre k_0 en considérant toutes les structures turbulentes telles que $k > k_0$. Les hypothèses précédentes ne sont donc en fait vérifiées que si le spectre est dit « d'équilibre ». Dans ce cas l'énergie traverse la zone inerte, elle sans altération en moment. Une seule échelle peut alors caractériser le champ turbulent comme associée pour donner une viscosité fictive:

$$\nu_\tau(k_0, t) = \nu_\tau \simeq \int_{k_0}^{\infty} \frac{E(k, t)}{k^3}\, \mathrm{d}k$$

donne pour les grandes valeurs de $|\vec{k}|$ des formes spectrales en puissance 1/7 en contradiction avec l'existence de moments de tous ordres. Une certaine indigence du modèle dans cette région du spectre est peut-être à rapprocher de cette remarque. En effet, l'introduction d'une forme tryadique devrait y précipiter la décroissance de $E(k, t)$. Une discussion approfondie des modèles type diffusion dans l'espace des k, modèles que nous retrouverons sous une autre forme avec KRAICHMAN, serait éclairante.

2. Si le phénomène répond à ce schéma, il est alors possible de distinguer différents domaines dans le spectre, l'énergie cheminant en moyenne de façon bien définie (des grosses vers les petites structures)*

a) le domaine des faibles $|\vec{k}|$ fortement marqués par le champ moyen échappe à une analyse générale, c'est la partie contingente du spectre.

b) le domaine inertiel où s'effectue l'émiettement des structures turbulentes,

c) le domaine dissipatif.

Le comportement des systèmes mécaniques non linéaires à nombre fini de paramètres est assez bien connu et l'on sait que des systèmes non dissipatifs, tel le suivant:

$$\frac{dx_i}{dt} = x_{i+1}\,x_{i+2} + x_{i-1}\,x_{i-2} - 2\,x_{i+1}\,x_{i-1}$$

où

$$x_{i+5} = x_i$$

qui retient un certain nombre de caractères des équations de Navier et en particulier des interactions quadratiques, vérifient au bout d'un certain temps un principe d'équipartition, c'est-à-dire que les $\vec{x}_i^2$ tendent à prendre une valeur identique. Ceci dut encourager KOLMOGOROV à postuler que pour des $|\vec{k}|$ suffisamment grands la turbulence était isotrope, quelle que soit la géométrie des structures primaires qui ont servi à extraire l'énergie de l'écoulement moyen.

Ces idées ont pu servir de guide et doivent être retenues jusqu'à plus ample informé.

Que dire, par contre, des hypothèses de fermeture elles-mêmes? Pour ne parler que de celles de PROUDMAN et REID et de KRAICHNAN, nous en saisirons vite les lacunes ou pour le moins les difficultés. La première qui tentait une démarche au niveau des corrélations quadruples lesquelles étaient supposées reliées aux doubles suivant un schéma de loi normal** a abouti

* Il est bien clair que telle que les interactions ont été précédemment représentées, le cheminement ici indiqué ne peut être considéré comme une contrainte absolue. Une perturbation brutale très localisée caractérisée par un nombre d'onde $|\vec{k}_0|$ affectera dans un premier temps les deux régions voisines du spectre, celle correspondant à $|\vec{k}| < |\vec{k}_0|$ et celle correspondant à $|\vec{k}| < |\vec{k}_c|$.

** Dans une distribution normale les corrélations entre les variables centrées $V_1\,V_2\,V_3\,V_4$ doivent vérifier

$$\langle \overline{V_1\,V_2\,V_3\,V_4} \rangle = \langle \overline{V_1\,V_2} \rangle \langle \overline{V_3\,V_4} \rangle + \langle \overline{V_1\,V_3} \rangle \langle \overline{V_2\,V_4} \rangle + \langle \overline{V_1\,V_4} \rangle \langle \overline{V_2\,V_3} \rangle$$

les corrélations triples étant évidemment nulles. On sait par ailleurs que certaines corrélations triples jouent un rôle essentiel et ceci est flagrant dans l'équation relative au tourbillon. Il faut ici bien remarquer que la condition imposée par PROUDMAN et REID est une condition nécessaire que doit vérifier toute réalisation suivant la loi normale, mais cette condition n'est pas suffisante. L'hypothèse introduite n'était donc pas a priori très restrictive, du moins, elle ne contenait pas — croyait-on un peu naïvement — de contradiction évidente avec le mécanisme connu de la turbulence. Elle conduisait à l'écriture symbolique suivante:

$$\frac{d}{dt}\,\overline{uuu} = \overline{uuuu} = \overline{uu}\;\;\overline{uu}$$

à un échec, certaines régions du spectre fournissant une énergie cinétique turbulente négative, ce qui est évidemment absurde. On comprend assez mal comment une telle hypothèse a pu conduire à un échec aussi net bien ques raisons plausibles aient été avancées par KRAICHNAN et EDWARDS. A coup sûr, les termes d'inertie sont mal pris en compte et dans cette formulation rien ne vient tempérer une erreur possible; le terme que l'on peut considérer comme « terme source » dans l'expression des corrélations quadruples ne faisant intervenir que des corrélations d'ordre deux, aucun autocontrôle de l'équation n'est à espérer. Certaines régions de l'espace spectral peuvent en quelque sorte se vider de leur contenu et provoquer la contradiction mentionnée.*

KRAICHNAN tente de cerner le problème en introduisant une fonction de Green G_{in} caractéristique de la réponse du champ turbulent sollicité de façon infinitésimale par une force δf_n

$$\delta u_i(\vec{k}, t) = \int_{-\infty}^{t} G_{in}(\vec{k}, t, t')\, \delta f_n(\vec{k}, t')\, dt'$$

encore faudrait-il savoir quelle forme donner au noyau G_{in}, lequel vérifie une équation fort complexe. Pour les grands nombres d'ondes si seule intervient la viscosité ν une forme asymptotique peut être aisément donnée

$$G_{in}(\vec{k}, t - t') = G_{in}\ (\text{moyen}) = H(t - t')\ P_{in}(\vec{k})\, e^{-\nu k^2 (t-t')}$$

la forme de P_{in} assurant que l'équation de continuité est remplie. EDWARDS par exemple élargit cette formulation en adoptant pour le noyau une forme diffusion susceptible de prendre en compte les interactions locales, c'est-à-dire celles situées dans la frange $d\vec{k}$ relative à $\vec{k}$.

$$\bar{G}_{in}(\vec{k}, t - t') = H(t - t') P_{in}(\vec{k})\, e^{-\eta(k)(t-t')}$$

avec

$$\eta(k) = \nu k^2 \quad \text{si } k \text{ est grand}$$

et

$$\eta(k) = D\varepsilon^{1/3} k^{2/3}$$

dans le domaine inertiel du spectre. On retrouve là l'introduction sous-jacente d'un coefficient agissant dans l'espace spectral à la manière d'un coefficient de diffusion turbulente; ce coefficient est ici construit sur une vitesse liée à l'énergie cinétique localisée dans la bande dk et une longueur $1/k$. Des calculs complexes sont ensuite conduits mais l'on voit combien sur la plan fonda-

* Certains termes régulateurs introduits très récemment sous la forme d'opérateurs linéaires par certains auteurs pourraient bien être appelés à jouer ce rôle. Toujours symboliquement on écrirait alors

$$\frac{d}{dt}\ \overline{uuu} = \overline{uu}\ \overline{uu} = u'\overline{uuu}$$

mental, la construction de la fonction reste à bien des égards incertaine, les multiples retouches apportées aux différents modèles traduisant un évident embarras*.

Cette ligne de recherche toujours en cours de développement, si elle nous éclaire sur bon nombre de mécanismes turbulents et peut nous servir de guide, est loin de tirer au clair le problème, même dans le cas apparemment simple d'une turbulence homogène et isotrope. On conçoit que d'autres voies dans ces conditions aient été ouvertes. Comme nous l'avons dit, elles abordent des problèmes aux géométries compliquées, mais, dans la plupart des cas, bornent quelque peu leurs ambitions quant à la perception du phénomène. Si nous rappelons très brièvement ici les plus anciennes, bien qu'elles soient actuellement très connues, c'est surtout pour en analyser les causes de succès apparent et montrer que seul un optimisme coupable né d'un irréalisme évident pourrait nous les faire considérer comme définitives. Elles sont, tout au plus, un refuge, ô combien utile, mais ô combien temporaire. L'une introduite par BOUSSINESQ lui-même est une transposition au cas turbulent du formalisme rencontré dans le cas laminaire. L'autre proposée, bien plus tard par PRANDTL, tente d'utiliser un schéma dont on connaît le succès en théorie cinétique des gaz. Retenons que, dans les deux cas, la liaison cherchée entre champ moyen et champ turbulent est locale. Aussi, ces représentations, à vrai dire sans grand fondement, ne seront-elles capables de simuler des phénomènes turbulents, que lorsque s'instaure une situation d'équilibre, c'est-à-dire pour laquelle l'énergie d'agitation produite en tout point est consommée sur place. Les termes convectifs liés à l'action du champ moyen et ceux prenant en charge l'action de la turbulence sur elle-même, c'est-à-dire en fin de compte le processus non linéaire, doivent de toute façon être nuls ou du moins très petits.

Ces deux modèles, malgré leur âge, rendent encore d'importants services, le plus ancien: celui de BOUSSINNESQ n'étant pas le plus démodé. Cette généralisation au cas turbulent des modèles à gradient, dont on connaît les succès en physique classique où un total découplage existe entre l'aspect macroscopique d'un phénomène et le micro-mécanisme qui le contrôle, nous inciterait à discuter précisément le champ d'application des modèles à gradient. Ceci a été fait de façon très suggestive par CORRSIN qui s'appuie sur un modèle unidimensionnel discrétisé prenant en charge la promenade aléatoire d'une particule. La validité de théories dites du «premier gradient» implique que soient vérifiées certaines conditions portant d'une part, sur les dérivées spatiales (définies dans l'étude précitée parr apport à l'unique variable x) de quantités statistiquement définies telle que la concentration $\bar{\Gamma}$, d'autre

* Il est impossible de donner, dans un exposé qui ne veut que situer le problème, un aperçu de cette évolution aux contours multiples.

part sur la valeur du libre parcours moyen 1. On devrait avoir, par exemple:

$$\frac{\bar{\Gamma}_{xxx}}{\bar{\Gamma}_x}\,\frac{l^2}{24} \ll 1\,, \quad \frac{\bar{\Gamma}_{xt}}{\bar{\Gamma}_x} \ll 1\,. \tag{*}$$

En prenant en compte, de façon, il est vrai, quelque peu arbitraire l'histoire de la viscosité turbulente ν_T, KOVÁSZNAY tente d'élargir le champ d'application des modèles à gradient. Cette fois, ν_T est sensé vérifier une équation du même type que celle qui fixe, par exemple, l'évolution de l'énergie cinétique d'agitation; c'est dire que la viscosité turbulente est non seulement produite et dissipée, mais encore convectée et diffusée. Il est intéressant de noter que ν_T règle, dans ce cas, son propre mécanisme de diffusion et ainsi, 'aspect non linéaire du problème, qui résulte de l'action de la turbulence taine sur elle-même, est pris en compte d'une certaine manière:

$$U\frac{\partial \nu_T}{\partial x} + V\frac{\partial \nu_T}{\partial y} = \frac{\partial}{\partial y}\left(\nu_T\frac{\partial \nu_T}{\partial y}\right) + \text{Prod} + \text{Dissip.}$$

Si cette formulation élargit considérablement le cadre d'application des modèles à gradient, puisqu'elle permet d'aborder le cas d'écoulements hors d'équilibre, elle prête assez largement flanc aux critiques. Les conditions brièvement rappelées pour qu'un tel modèle demeure valable n'étant pas ici remplies, JEANDEL prend en charge, de quelque autre façon, le rôle des grosses structures turbulentes par un terme dont le rôle est quelque peu hybride, du fait, qu'il ne vérifie pas les conditions imposées à tout transport.** Les contrôles expérimentaux sont alors satisfaisants. Resterait bien entendu à discuter ainsi que le font JEANDEL et MATHIEU, la validité d'une expression de départ du type

$$\tau(\vec{x}, t) = \nu_T(\vec{x} + \vec{\tau}, t + t')\frac{\partial \bar{U}}{\partial y}(\vec{x}, t)\,.$$

Cette écriture précise clairement que la mémoire des structures turbulentes est ici uniquement prise en compte par ν_T à travers un double voisinage spatial $\vec{\tau}$ et temporel t'; en revanche, contrainte τ et gradient $\partial\bar{U}/\partial y$ sont pris au même point $\vec{x}$ et au même instant.

* Ce modèle a été repris et amélioré par LUMLEY (communication personnelle); les conclusions précédentes demeurent.

** La modification apportée corrige convenablement le modèle, ainsi que le confirme LUMLEY (communication personnelle), si l'on tient compte du caractère hybride du terme ajouté qui altérerait aussi quelque peu les autres.

L'étude des champs turbulents homogènes*, ouverte entre autre par CRAYA, montre que, si la classe des tourbillons qui créent les contraintes échappe à l'emprise directe de la viscosité, ce qui suppose le nombre de Reynolds suffisamment élevé, alors

$$\frac{\tau(\vec{x}, t)}{\varrho \bar{q}^2} = \mathfrak{Z}(st) \quad \text{ou} \quad s = \frac{\partial \bar{U}}{\partial y} .$$

La contrainte devient dépendante de l'action cumulée du gradient de vitesse moyenne supposée ici constante et égale à « s ». La même conclusion peut être tirée de considérations très générales qui prolongent dans ce cas une étude de LUMLEY, récemment publiée. La nécessité d'opérer à grand nombre de Reynolds dans des régions suffisamment éloignées des parois** pour qu'une hypothèse de quasi-homogénéité demeure valide est également ici sous-jacente.

A vrai dire, l'équation proposée par NEE et KOVÁSZNAY résulte surtout d'une intéressante intuition à laquelle certains développements de PHILIPPS pourraient servir de support. La mise en place d'une méthode de calcul opérationnelle fondée sur les équations classiques de continuité et de quantité de mouvement d'une part, et sur l'équation de l'énergie cinétique turbulente d'autre part, revient à BRADSHAW. C'est en fait par l'équation des corrélations en un point que s'introduit l'effet du mouvement d'agitation dans l'équation de quantité de mouvement relative au champ moyen. On pourrait donc s'étonner de l'approche de BRADSHAW qui, travaillant sur l'équation d'énergie cinétique, s'éloigne du problème et ne le rejoint en fait que grâce à une nouvelle hypothèse: en tout point contrainte τ et énergie cinétique turbulente $\varrho \bar{q}^2$ sont dans un rapport constant. C'est dire que le temps de structuration de la turbulence par le champ moyen est considéré comme petit devant celui qui contrôle la vie des structures turbulentes caractérisé par le rapport $q^2/\bar{\varepsilon}$. Bien sûr, ceci s'inscrit en faux par rapport à la relation $\tau/\varrho \bar{q}^2 = \mathfrak{Z}(st)$ mais elle permet à BRADSHAW de travailler sur une équation scalaire qui ne comporte qu'un nombre limité de termes, du fait des contractions qui interviennent lors du passage de l'équation en $\overline{u_i u_j}$ à l'équation en $\bar{q}^2$. Dans ces

* Entendons par là un champ turbulent dans lequel toute propriété statistique définie en deux points M et M′ ne dépendrait que de la position relative de M par rapport à M′, c'est-à-dire de $\overrightarrow{MM'}$ mais pas des vecteurs position absolue $\overrightarrow{OM}$, $\overrightarrow{OM'}$.

** Pour fixer les idées, disons que, dans le cas d'une couche limite d'épaisseur δ, la validité des modèles proposés ne peut de toute façon être considérée comme acceptable que si $y/\delta > 0{,}1$. Des ajustements sont nécessaires près de la paroi lesquels ont fait l'objet d'une étude détaillée conduite par KAM HONG NG à l'Imperial Collège sous la direction du Docteur LAUNDER.

conditions, BRADSHAW considère le problème défini par les équations:

$$\bar{U}\frac{\partial \bar{U}}{\partial x}+\bar{V}\frac{\partial \bar{U}}{\partial y}=-\frac{1}{\varrho}\frac{\partial \bar{P}}{\partial x}+\frac{\partial \tau}{\partial y},$$

$$\bar{U}\frac{\partial \bar{q}^2/2}{\partial x}+\bar{V}\frac{\partial \bar{q}^2/2}{\partial y}=-\overline{uv}\frac{\partial \bar{U}}{\partial y}+\frac{\partial}{\partial y}\left(\overline{vp}+\frac{\overline{vq}^2}{2}\right)+\bar{\varepsilon},$$

$$\frac{\partial \bar{U}}{\partial x}+\frac{\partial \bar{V}}{\partial y}=0, \quad \frac{\tau}{\varrho \bar{q}^2}=Cste.$$

L'hypothèse au demeurant fort restrictive

$$\tau/\varrho\bar{q}^2=\varrho t,$$

élimine du domaine d'application de cette méthode les écoulements confinés encore que même dans le cas des écoulements du type couche limite (entendons par là écoulements à direction privilégiée), bien des restrictions soient à apporter. Dans le cas d'un jet symétrique, une modulation sera nécessaire sur l'axe où la contrainte est nulle sans que, pour autant, l'énergie cinétique d'agitation le soit. Dans le cas d'écoulements dissymétriques: jets pariétaux, sillages asymétriques . . . , l'échec sera encore plus sensible. Indépendamment de ces limitations, deux difficultés demeurent encore: il reste en effet à évaluer, dans l'équation d'énergie, les termes diffusion et dissipation. On sait que l'évaluation des termes diffusion est une des difficultés centrales du problème à laquelle nous ne cessons d'être confrontés, l'introduction d'une fonction ajustée expérimentalement et spécifique à chaque cas; couches limites, jets . . . palliera cette première difficulté

$$\overline{vp}+\frac{\overline{vq}^2}{2}=\frac{\tau_{\max}}{U_1}\tau_R f_1(y/\delta)$$

où $\tau_{\max}$ est la contrainte maximum dans cet écoulement du type couche limite et

$$\tau_R=L^2\left(\frac{\partial U}{\partial y}\right)^2.$$

La dissipation sera prise de la forme

$$\bar{\varepsilon}\cong\bar{u}^3/L,$$

L étant une longueur caractéristique de l'écoulement définie au moyen d'ajustements expérimentaux spécifiques à chaque type d'écoulement et pris sous la forme $L_1/\delta=f_1[y/\delta]$.

HANJALIC et LAUNDER travailleront dans une direction quelque peu similaire, mais leur approche à nombre d'égards beaucoup plus élaborée permettra d'atteindre certains types d'écoulements confinés. A l'équation de quantité de mouvement relative à l'écoulement moyen sera adjointe cette fois l'équation d'évolution des corrélations $\overline{u_i u_j}$ et une équation contrôlant de la dissipation.

$$\frac{D\overline{u_i u_j}}{Dt} = -\left\{\overline{u_j u_k}\frac{\partial \bar{U}_i}{\partial x_k} + \overline{u_i u_k}\frac{\partial \bar{U}_j}{\partial x_k}\right\} - \left\{2\nu\left(\overline{\frac{\partial u_i}{\partial x_k}}\right)\left(\overline{\frac{\partial u_j}{\partial x_k}}\right)\right\} + \\ + \left\{\overline{\frac{p}{\varrho}\left(\frac{\partial u_i}{\partial x_j} + \frac{\partial u_j}{\partial x_i}\right)}\right\} - \left\{\frac{\partial}{\partial x_k}\left(\overline{u_i u_j u_k} - \gamma\frac{\partial \overline{u_i u_j}}{\partial x_k} + \overline{\frac{p}{\varrho}(\delta_{jk}u_i + \delta_{ik}u_j)}\right)\right\},$$

$$\frac{D\bar{\varepsilon}}{Dt} = -2\nu\frac{\partial \bar{U}_i}{\partial x_k}\left(\overline{\frac{\partial u_i}{\partial x_l}\cdot\frac{\partial u_k}{\partial x_l}} + \overline{\frac{\partial u_l}{\partial x_i}\cdot\frac{\partial u_l}{\partial x_k}}\right) - 2\nu\overline{\frac{\partial u_i}{\partial x_k}\cdot\frac{\partial u_i}{\partial x_l}\cdot\frac{\partial u_k}{\partial x_l}} - \\ - 2\overline{\left(\nu\frac{\partial^2 u_i}{\partial x_k \partial x_l}\right)^2} - \frac{\partial}{\partial x_k}\overline{u_k\varepsilon} - \frac{\nu}{\varrho}\frac{\partial}{\partial x_i}\left(\overline{\frac{\partial p}{\partial x_l}\cdot\frac{\partial u_i}{\partial x_l}}\right)*$$

Les nombreux termes figurant dans ces équations seront évalués localement, l'approche-adoptée étant à bien des égards intuitive, mais la démarche plus rigoureuse de LUMLEY qui confirme dans l'ensemble les évaluations de LAUNDER procède un peu du même mode de pensée. Il ne nous est guère possible de rentrer ici dans le détail de cette méthode que l'on désigne souvent par méthode de fermeture en un point (one point closure method), cette appellation pouvant du reste appeler discussion*. Les résultats obtenus par cette voie sont très prometteurs bien que l'on puisse formuler, en ce qui concerne l'approche de LAUNDER, au moins deux remarques. Notons tout d'abord que la fermeture introduite au niveau des corrélations de vitesse fait intervenir une hypothèse de quasi-normalité et l'on sait les ennuis auxquels elle conduit dans le cadre d'une analyse (espace spectral) plus fine telle celle menée par PROUDMAN et REID. Ici, ces difficultés sont aplanies du fait que travaillant dans l'espace physique, on ne retient que l'aspect intégral du problème, c'est-à-dire celui qui prend en compte l'action de toutes les structures turbulentes quelle que soit leur taille. Une autre hypothèse fondée sur l'idée que les pressions jouent dans ces équations un rôle répartiteur, reprend la formu-

* Dans l'approche de LUMLEY (communication personnelle), on ne travaille apparemment que dans l'espace physique (non dans celui des transformées de Fourier). Le fait de se placer à de grands nombres de Reynolds permet bien entendu de traiter spécifiquement la région dissipative du spectre. Les structures turbulentes responsables de la dissipation d'énergie mécanique ont, du fait de leur petite taille, un comportement dynamique qui peut être pris en compte ponctuellement (ce qui revient à dire en langage spectral que l'on travaille dans la région des grands nombres d'onde). Lorsqu'il s'agira d'évaluer des corrélations du type $\overline{pu_i}$, l'introduction de temps de relaxation permettra d'échapper implicitement à une telle localisation.

lation de ROTTA. Il est certain qu'on se trouve ici en présence d'une double fermeture alors que pour un champ turbulent homogène, une seule suffit. La compatibilité de ces deux hypothèses resterait évidemment à montrer. En fait, ces difficultés ne conduisent pas dans le plan physique à des incompatibilités de calcul pour les raisons que nous avons dites et de nombreuses extensions de la méthode ont été faites dans le cas des écoulements confinés, des écoulements siège d'influence thermique, . . .

Les recherches conduites au Laboratoire par JEANDEL essaient d'exploiter au maximum un certain nombre d'informations tirées des modèles turbulents homogènes et d'en appliquer certaines conclusions aux écoulements du type couche limite, des extensions aux écoulements confinés demeurant de toute évidence possibles. La méthode utilise, dans son stade actuel, l'équation de continuité, l'équation de quantité de mouvement, l'équation relative à l'évolution de l'énergie cinétique turbulente et une équation fixant le comportement de la longueur de corrélation*. En outre, le rapport $\tau/\varrho\bar{q}^2$ n'est plus comme dans la méthode proposée par BRADSHAW, supposé constant; c'est ainsi que l'on tient compte de l'effet cumulé des déformations imposées par le champ moyen pour fixer la valeur de ce rapport. L'idée d'une telle liaison donnée par J. MATHIEU a pu être précisée soit par voie théorique, soit par voie expérimentale. Il vient alors:

$$0 = \frac{\bar{U}_1}{2}\frac{\partial}{\partial x_2}(\bar{q}^2\mathfrak{L}) + \frac{\bar{U}_2}{2}\frac{\partial}{\partial x_2}(\bar{q}^2\mathfrak{L}) + \frac{3}{16}\left\{\frac{\partial \bar{U}_1}{\partial x_2}\int_{-\infty}^{+\infty}\overline{u_1 u_2} + dr\right.$$

$$\left. + \int_{-\infty}^{+\infty}\frac{\partial \bar{U}_1}{\partial x_2}\bigg|_{x_2'+r}\overline{u_1 u_2'}dr\right\} - \frac{3}{16}\int_{-\infty}^{+\infty}\frac{\partial}{\partial x_1}(\overline{u_j u_2 u_j'} - \overline{u_j u_2' u_j'})\ dr$$

$$\xrightarrow[\text{principal}]{\text{écoulement}} r \begin{cases} \longrightarrow u_1' \\ \longrightarrow u_1 \end{cases} + \frac{3}{16}\frac{\partial}{\partial x_2}\left\{\int_{-\infty}^{+\infty}(\overline{u_j u_2 u_j'} + \overline{p u_2'} + \overline{p' u_2})\,dr\right\}.$$

On peut lui préférer avec raison l'équation d'évolution de la dissipation dont nous reparlerons ultérieurement.

Avant de voir la méthode plus en détail, il convient de dire ce qui dans cette approche, sépare le champ turbulent réel du modèle homogène faisant référence. Remarquons tout d'abord que les recherches conduites sur les champs turbulents homogènes à travers l'équation donnée par CRAYA portent sur une analyse des corrélations en deux points. En effet, il est, dans ce cas, possible d'évaluer les corrélations pression vitesse en deux points au moyen des seules corrélations doubles et triples de vitesse prises également en deux points et ceci d'autant plus facilement que le problème est d'emblée posé dans l'espace spectral où les opérateurs différentiels deviennent des

* L'équation d'évolution des échelles turbulentes se déduit de l'équation des corrélations en deux points par intégration dans le plan physique.

opérateurs algébriques.* Ceci dit, reprenons dans l'espace physique la comparaison entre champ réel et champ homogène. L'équation complète s'écrit:

$$\frac{\partial}{\partial t}\overline{u_i u_j'} + \underline{\bar{U}_l \frac{\partial \overline{u_i u_j'}}{\partial x_l}} + \{\bar{U}_l' - \bar{U}_l\}\frac{\partial \overline{u_i u_l'}}{\partial r_l} +$$

$$+ \frac{\partial \bar{U}_i}{\partial x_l}\overline{u_l u_j'} + \frac{\partial \bar{U}_j'}{\partial x_l}\overline{u_l' u_i} + \underline{\frac{\partial}{\partial x_l}\{\overline{u_l u_i u_j'}\}} -$$

$$- \frac{\partial}{\partial r_l}\{\overline{u_l u_i u_j'}\} + \frac{\partial}{\partial r_l}\{\overline{u_l' u_j u_i}\} + \frac{1}{\varrho}\left[\underline{\frac{\partial}{\partial x_i}\{\overline{p u_j'}\}} +\right.$$

$$\left. - \frac{\partial}{\partial r_i}\{\overline{p u_j'}\} + \frac{\partial}{\partial r_j}\{\overline{p' u_i}\}\right] - \nu\left[\underline{\frac{\partial^2 \overline{u_i u_j'}}{\partial x_l^2}} + 2\frac{\partial^2 \overline{u_i u_j'}}{\partial r_l^2} - \underline{2\frac{\partial^2 \overline{u_i u_j'}}{\partial x_l \partial r_l}}\right] = 0.$$

Nous avons souligné les termes qui s'effacent dans le cas du modèle homogène. On voit que les termes convectifs liés au mouvement moyen et au mouvement d'agitation sont de ce nombre, ainsi qu'un terme portant sur les corrélations pression vitesse et deux autres contrôlant en partie le processus dissipatif. Tous les termes négligés font nécessairement apparaître des dérivées de position du point M; on peut, de ce fait, penser que leur rôle restera modéré, sauf, bien entendu, celui des deux termes convectifs. Lorsqu'il conviendra d'évaluer la restructuration du champ turbulent, mesuré par le rapport $\tau/\varrho\bar{q}^2$, par le champ moyen, on tiendra compte de la convection par le champ moyen et de quelque façon, des retouches seront apportées pour évaluer l'influence du mouvement d'agitation. L'équation des corrélations en deux points s'écrit, en posant:

$$\lambda_{lm} = \frac{\partial \bar{U}_l}{\partial x_m} = \frac{\bar{U}_l' - \bar{U}_l}{x_m' - x_m} = \frac{\bar{U}' - \bar{U}_l}{\xi_m},$$

$$T_{ij}(+\vec{r}) = \frac{\partial}{\partial \xi_l} Q_{liij}(+\vec{r}),$$

$$S_{ij}(+\vec{r}) = \frac{\partial}{\partial \xi_i} P_j(+\vec{r}),$$

$$\frac{\partial}{\partial t} R_{ij} + \lambda_{lm}\,\xi_m \frac{\partial R_{ij}}{\partial \xi_l} + \{\lambda_{il} R_{lj} + \lambda_{jl} R_{il}\} -$$

$$- \{T_{ij} + T_{ji}'\} - \{S_{ij} + S_{ji}'\} - 2\nu \Delta R_{ij} = 0$$

* Les corrélations pression vitesse en un point sont liées dans le plan physique au champ de vitesse par une intégrale de Poisson étendue à tout l'espace où plus précisément à un domaine avoisinant le point et dans lequel les corrélations ne sont pas négligeables. Le choix d'une équation portant au départ sur les corrélations en deux points se comprend de lui-même. On voit aussi comment les corrélations pression vitesse mettent en jeu à la fois des termes linéaires (corrélations doubles de vitesse) et non linéaires (corrélations triples).

et dans l'espace spectral

$$\frac{\partial}{\partial t}\Phi_{ij} + \Psi_{ij} = \Omega_{ij} - 2\nu k^2 \Phi_{ij}.$$

Le tenseur Φ_{ij} est la transformée de Fourier de R_{ij} . Le tenseur Ψ_{ij} se fait ici l'écho du gradient de vitesse moyenne tandis que Ω_{ij} prend en charge les aspects non linéaires. Le problème de fermeture, sans être bien entendu résolu, est ici bien posé car Ω_{ij} prend également en charge les corrélations pression vitesse qui ont été dans cette approche exprimées en fonction du seul champ de vitesse. Parmi les résultats qui ont pu être aussi obtenus, nous retiendrons ceux donnés par COURSEAU et LOISEAU. Ils concernent entre autre l'évolution du coefficient de corrélation $\overline{u_1 u_2}/(u_1' u_2')$ lequel est obtenu, dans un premier temps, en négligeant les corrélations triples. Un champ turbulent isotrope pour lequel donc $\overline{u_1 u_2} = 0$, introduit en tant que condition initiale dans un champ à gradient constant du type CRAYA, se restructure au cours du temps. Deux quantités règlent en fait ce mécanisme: $\lambda_{12} t = st$ et $\nu k^2 t$, mais l'on peut penser que la classe des tourbillons sur lesquels agit la viscosité est découplée de celle qui crée les contraintes; il suffit, pour cela, que le nombre de Reynolds de la turbulence soit suffisamment grand. On a pu constater que, pour des variations raisonnables du rapport ν/s, $\overline{u_1 u_2}/(u_1' u_2')$ n'était fonction que de st.

Les travaux expérimentaux de CHAMPAGNE, HARRIS et CORRSIN apportent un heureux complément d'informations à ces considérations. Elles ne révèlent en tout cas aucune contradiction. Les valeurs expérimentales du coefficient de corrélation sont plus faibles que celles calculées à partir de l'équation de CRAYA en négligeant les corrélations triples et ceci paraît conforme à l'idée que l'on peut se faire, a priori, du rôle joué par la non-linéarité du mécanisme.

Nous reviendrons ultérieurement sur les problèmes de fermeture, nous attachant pour l'instant à donner un aperçu des résultats que l'on peut obtenir au moyen d'une telle méthode.

Si l'on emprunte à l'expérience des données relatives au temps de vie des structures turbulentes, on s'aperçoit que, dans la plupart des cas, la valeur calculée de l'intégrale des déformations permet d'atteindre l'état que nous avons appelé «d'équilibre turbulent» lequel correspond à la valeur de «a_1» adoptée par BRADSHAW et à celle non moins classique de 0,4 pour le coefficient de corrélation. Dans certains cas: jet pariétal, couches limites se développant dans un écoulement extérieur perturbé . . . des régions d'écoulement échappent à cette analyse et l'on est amené à tenir compte d'un processus de restructuration, contrôlé dans le temps par le gradient de vitesse moyenne $s = \lambda_{12}$. Dans le cas d'un jet pariétal, on sait que l'ordonnée à laquelle s' annulle la contrainte tangentielle ne correspond pas au point où la vitesse

est maximum. L'explication basée sur les réflexions précédentes avait donnée été par J. MATHIEU, dès 1971. La mise en place d'une méthode de calcul rend compte de ce résultat du reste décrit par HANJALIC et LAUNDER mais par une autre voie. Même dans un tel cas du type couche-limite, on constate que, non seulement le rapport $a_1 = \tau/\varrho\overline{q}^2$ n'est pas constant, mais qu'il change de signe dans une section droite du jet. Une situation qui peut paraître paradoxale si l'on s'en tient à une compréhension par trop sommaire du phénomène est celle recontrée sur l'axe d'un jet où la contrainte est nulle, bien que l'énergie cinétique turbulente y soit très importante.

Le problème n'a de commun avec le précédent que l'existence de deux centres producteurs, mais alors que, dans le jet pariétal, le transport convectif jouait un rôle essentiel, c'est ici la combinasion de structures turbulentes émanant des deux centres et algébriquement marqués du point de vue de leur état de structuration qui conduit sur l'axe pour les contraintes à un bilan statisquement nul. Une discrimination des informations a pu être faite dans un tuyau à partir du signe de v par SABOT et COMTE-BELLOT qui ont pu confirmer cette partition des corrélations en $uv < 0$ pour $v > 0$ et $uv > 0$ pour $v < 0$ certaines structures informelles venant se placer dans les alternances.

Si l'on devait en peu de mots caractériser les méthodes du type BRADSHAW où $\tau/\varrho q^2 = a_1$ et celle qui vient d'être ici proposée, on pourrait dire que, dans le premier cas, le temps de structuration de la turbulence est supposé négligeable devant celui qui fixe son déclin, alors que, dans le deuxième cas, on serait au moins, dans un premier stade appelé à les confondre. On pense actuellement que celui-ci est plus grand que celui-là mais, de toute façon, ils sont du même ordre de grandeur, ainsi que le montre le tableau suivant qui permet, à partir des essais de SABOT et CHARNAY, des comparaisons dans le cas d'un écoulement en conduite et d'une couche-limite.

On serait amené à comparer un certain temps d'extinction τ_e au temps mis par exemple par une turbulence isotrope pour atteindre un état que nous appellerons pour faire bref, «d'équilibre» $\tau_s \cong 1/s$ et qui correspond à la valeur adoptée par Bradshaw.

x_2/R	$\frac{\partial \bar{U}_1}{\partial x_2} = s$	$t_s \sim \frac{1}{s}$	$t_e = \frac{\overline{q}^2}{\varepsilon}$	x_2/δ	$\frac{\partial U_1}{\partial x_2} s$	t_s	t_e
0,1	4,15 s^{-1}	0,012	0,08		sec^{-1}		
0,2	208 s^{-1}	0,024	0,12	0,2	93,5	0,153	0,063
0,5	95 s^{-1}	0,053	0,15	0,4	48,3	0,103	0,083
0,7	60 s^{-1}	0,083	0,20	0,6	32,1	0,156	0,095
1	sec^{-1}		0,20	0,8	22,0	0,227	0,11
	conduite				couche-limite		

Nous avons parlé du problème de « fermeture » dans l'équation de CRAYA et signalé que ce type d'approche qui fait intervenir deux points de l'espace physique permettait de le bien poser. C'est donc ici seulement une expression du tenseur qui joue le rôle de terme source Ω_{ij} qu'il faudra postuler. Une toute première tentative a été faite dont on peut saisir très brièvement le cheminement. Pour tout point $\vec{k}$ de l'espace spectral, les composantes du tenseur Φ_{ij} sont du fait de l'incompressibilité localisées dans un plan normal à $\vec{k}$, autrement dit l'espace tensoriel dans lequel est défini Φ_{ij} est construit à partir de ce plan. Si l'on choisit Ω_{ij} dans le même espace, on pourra alors supposer ce terme-source proportionnel à Φ_{ij}. La fonction de transfert empruntée au cas isotrope (exp. de COMTE-BELLOT et CORRSIN par exemple) aura le rôle décisif: celui d'assurer le transfert dans l'espace spectral. On ne pourra parler de fermeture au sens mécanique du terme, puisque dans Ω_{ij} on a introduit une donnée expérimentale: la fonction de transfert de la turbulence isotrope seulement pondérée par Φ_{ij}. Le modèle est exploité par COURSEAU qui s'intéresse pour l'instant au cas de la déformation pure. Si les conditions de CRAMER sont vérifiées de par la forme choisie pour Ω_{ij}, on décèle déjà certaines faiblesses de l'hypothèse dues tout d'abord à sa connexion par trop étroite avec le cas isotrope, par exemple les corrélations pression vitesse provenant des termes non linéaires sont nulles, toutefois, la modification apportée au modèle linéaire par les termes en Ω_{ij} ainsi introduits va bien dans le sens souhaité.

Pour le domaine thermique,* disons seulement qu'il est possible d'introduire des développements analogues, chacune des hypothèses précédentes ayant en quelque sorte son corollaire. On pourra, par exemple, admettre que les corrélations vitesse-température ont une valeur donnée, et travailler, non sur l'équation vectorielle qui fixe l'évolution de $\overline{u_i\Theta}$ mais sur l'équation scalaire plus simple, contrôlant l'évolution de $\overline{\Theta^2}$. Un traitement analogue à celui donné par CRAYA conduit MATHIEU et al au système suivant dans le plan physique:

Si l'on pose $\lambda_{lm} = \partial \overline{U}_l/\partial x_m$ et $\gamma_l\ \partial\overline{\Theta}/\partial x_l$

$$\frac{\partial \overline{u_i\Theta'}}{\partial t} + \lambda_{lm}\xi_m \frac{\partial \overline{u_i\Theta'}}{\partial \xi_l} + \lambda_{il}\overline{u_l\Theta'} + \gamma_l \overline{u_i u_l'} - \frac{\partial}{\partial \xi_l}(\overline{u_i u_l \Theta'} - \overline{u_i u_l'\,\Theta'}) -$$

$$- \frac{1}{\varrho}\frac{\partial \overline{p\Theta'}}{\partial \xi_i} - \nu\left(1 + \frac{1}{\mathcal{P}}\right)\frac{\partial^2 \overline{u_i\Theta'}}{\partial \xi_l^2} = 0\,,$$

$$\frac{\partial\,\overline{\Theta\Theta'}}{\partial t} + \lambda_{lm}\xi_m \frac{\partial\,\overline{\Theta\Theta'}}{\partial \xi_l} + \gamma_l(\overline{u_l\Theta'} + \overline{u'\Theta}) - \frac{\partial}{\partial \xi_l}(\overline{u_l\Theta\Theta'} - \overline{u_l'\Theta\Theta'}) + 2\varkappa \frac{\partial^2\,\overline{\Theta\Theta'}}{\partial \xi_l^2}$$

(λ_{lm} et γ_l étant des constantes),

* La totalité des réflexions qui suivent n'est valable que dans le cas où il n'existe pas interférence entre phénomènes mécaniques et thermiques.

tandis que les tenseurs spectraux étant définis comme suit:

$$\begin{aligned}
\varphi_i(\vec{k}, t) &\rightarrow \overline{u_i \Theta'}(\vec{r}, t) \\
\Phi_{il} &\rightarrow \overline{u_i u_l'}(\vec{r}, t) \\
-i\tau_{il} &\rightarrow \overline{u_i u_l \Theta'} \\
-i\tau_{il}' &\rightarrow \overline{u_i u_l' \Theta'} \\
\eta &\rightarrow \overline{\Theta\Theta'} \\
-i\Gamma_l &\rightarrow \overline{u_l \Theta\Theta'} \\
-i\Gamma_l' &\rightarrow \overline{u_l' \Theta\Theta'}
\end{aligned}$$

on a dans l'espace transformé les équations:

$$\frac{\partial \varphi_i}{\partial t} - \lambda_{lm} \underbrace{\left\{ \frac{\partial}{\partial k_m}(k_l \varphi_i) - \delta_{il}\varphi_m + 2\frac{k_i k_l}{k^2}\varphi_m \right\}}_{\Psi_i \leftarrow} + \gamma_l \Phi_{il} +$$

$$+ \nu\left(1 + \frac{1}{\mathfrak{P}}\right) k^2 \varphi_i = \underbrace{k_l(\Delta_{im}\tau_{ml} - \tau_{il}')}_{\rightarrow \Omega_i},$$

$$\frac{\partial \eta}{\partial t} - \lambda_{lm} \underbrace{\frac{\partial}{\partial k_m}(k_l \eta)}_{\Psi \leftarrow} + \gamma_l(\varphi_l + \varphi_l^*) + 2\alpha k^2 \eta = \underbrace{k_l(\Gamma_l - \Gamma_l')}_{l \rightarrow \Omega}$$

Dans ces conditions, le problème à résoudre se met sous la forme matricielle

$$\frac{\partial}{\partial t}\begin{bmatrix} \Phi_{ij} \\ \varphi_i \\ \eta \end{bmatrix} + \begin{bmatrix} \Psi_{ij} \\ \Psi_i \\ \Psi \end{bmatrix} + \gamma_l \begin{bmatrix} 0 \\ \Phi_l \\ \varphi_l + \varphi_l^* \end{bmatrix} + k^2 \begin{bmatrix} 2\nu\Phi_{ij} \\ (\nu+\alpha)\varphi_i \\ 2\alpha\eta \end{bmatrix} = \begin{bmatrix} \Omega_{ij} \\ \Omega_i \\ \Omega \end{bmatrix}.$$

Pour des laps de temps très courts, GENCE a pu traiter le problème et montrer entre autre qu'il fallait se défier des généralisations trop hâtives, par exemple, en ce qui concerne la restructuration du champ thermique.

En particulier les niveaux et les temps de restructuration dépendent essentiellement du rapport entre le gradient thermique et le gradient cinématique, dans le cas d'un écoulement de cisaillement tout au moins.

φ_l^* conjugué de φ_l.

Annexe I.

Limitation des modèles de transport aléatoire à gradient

Dans ce qui suit, nous mettons en évidence avec CORRSIN l'ensemble des hypothèses qui conduisent au modèle de transport à gradients et nous appliquons ces considérations à un exemple simple à une dimension.

Si l'on s'intéresse au transport spatial d'un champ scalaire, dont la concentration moyenne est $\overline{\Gamma}(z,t)$, nous pouvons écrire que le flux moyen $F(z,t)$ en z de $\overline{\Gamma}$ venant de tous les points de coordonnée inférieure à z s'écrit:

$$\overline{F}(z,t) = \frac{\partial}{\partial t} \int_{-\infty}^{z} \overline{\Gamma}(z',t)\, dz' \,. \tag{1}$$

L'équation différentielle de conservation qui s'en déduit étant:

$$\frac{\partial \overline{\Gamma}}{\partial t} = -\frac{\partial \overline{F}}{\partial z} \,. \tag{2}$$

Dans le cas général, $\overline{F}$ peut être considéré comme une fonctionnelle de $\overline{\Gamma}$ et des propriétés statistiques des fluctuations de vitesse et de concentration, toutefois, pour un mécanisme de transport à caractère local dans l'espace et dans le temps, on peut supposer que $\overline{F}(z,t)$ s'exprime comme une fonction de la concentration $\overline{\Gamma}(z,t)$ et de ses dérivées partielles, soit:

$$\overline{F}(z,t) = f(\overline{\Gamma}, \overline{\Gamma}_z, \overline{\Gamma}_t, \overline{\Gamma}_{zz}, \overline{\Gamma}_{zt}, \overline{\Gamma}t_{tt}, \ldots, z, t) \,. \tag{3}$$

Si, de plus, on suppose le processus homogène, stationnaire, indépendant de $\overline{\Gamma}$ et fonction linéaire des dérivées de $\overline{\Gamma}$ (nous en verrons plus loin un exemple) la relation (3) devient:

$$\overline{\Gamma}(z,t) = k_1 \overline{\Gamma}z + k_2 \overline{\Gamma}_t + k_3 \overline{\Gamma}_{zz} + k_4 \overline{\Gamma}_{zt} + k_5 \overline{\Gamma}_{tt} + \ldots \tag{4}$$

les constantes K_i dépendant du mécanisme (c'est-à-dire des propriétés statistiques du champ des fluctuations de vitesse et de concentration).

Supposons encore le phénomène symétrique dans l'espace et la convection aléatoire s'effectuer à des vitesses suffisamment élevées pour que les dérivées par rapport au temps soient négligeables par rapport aux dérivées spatiales. Il vient alors

$$\overline{F}(z,t) = k^{(1)} \overline{\Gamma}_z + k^{(2)} \overline{\Gamma}_{zzz} + \ldots \tag{5}$$

(les dérivées d'ordre pair en $\dot{z}$ ainsi que les dérivées par rapport au temps ayant disparu).

Enfin si les dérivées d'ordre supérieur sont négligées:

$$\bar{F}(z,t) = -\mathcal{D}\bar{\Gamma}_z \tag{6}$$

et l'on retrouve la loi de Fick qui conduit, en reprenant l'équation (2) à une classique équation de diffusion:

$$\bar{\Gamma}_t = -\mathcal{D}\bar{\Gamma}_{zz}\,. \tag{7}$$

Appliquons ces raisonnements à un phénomène dans lequel le transport de $\bar{\Gamma}$ est effectué par un mouvement aléatoire stationnaire de particules ayant un libre parcours moyen l et étant animées d'une vitesse quadratique moyenne V suffisamment élevée pour que, sur la dilatance l, $\bar{\Gamma}$ ne varie pas sensiblement.

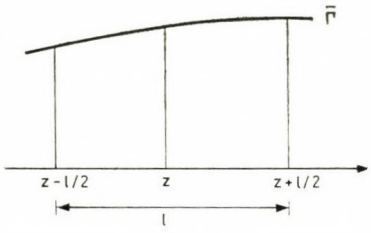

Fig. 2

Si le plan z est tel que:
et si l'on suppose que $n/2$ particules traversent par unité de temps une unité d'aire du plan z dans chaque direction, le flux moyen de $\bar{\Gamma}$ s'écrit:

$$\bar{F} = \frac{1}{2} nV \left\{ \bar{\Gamma}\left(z - \frac{l}{2}\right) - \bar{\Gamma}\left(z + \frac{l}{2}\right) \right\}. \tag{8}$$

Puisque l est petit devant les distances sur lesquelles $\bar{\Gamma}$ varie, on peut développer le deuxième membre en série de Taylor et cela fournit:

$$\bar{F}(z,t) = -nV \left\{ \frac{l}{2}\bar{\Gamma}_z + \frac{1}{3!}\left(\frac{l}{2}\right)^3 \bar{\Gamma}_{zzz} + \cdots \right\}. \tag{9}$$

L'équation différentielle (2) implique alors:

$$\bar{\Gamma}_t(z,t) = nV \left\{ \frac{l}{2}\bar{\Gamma}_{zz} + \frac{1}{3!}\left(\frac{l}{2}\right)^3 \bar{\Gamma}_{zzzz} + \cdots \right\}.$$

L'approximation du l^{er} gradient est alors applicable lorsque les termes d'ordre

supérieur ou égal à deux sont négligeables par rapport à ceux du l^er ordre, ce qui se traduit par:

$$\left|\frac{\bar{\Gamma}_{zzz}}{\bar{\Gamma}_z}\right|\frac{l^2}{24} \ll 1 \text{ pour } \bar{F} \text{ et par } \left|\frac{\bar{\Gamma}_{zzzz}}{\bar{\Gamma}_{zz}}\right|\frac{l^2}{24} \ll 1 \text{ pour } \frac{\partial \bar{\Gamma}}{\partial z}\,.$$

Il vient alors:

$$\bar{F}(z,t) = -nV\frac{l}{2}\cdot\bar{\Gamma}_z.$$

Si, par contre, on ne considère plus que $\bar{\Gamma}(z,t)$ varie de façon négligeable pendant le temps libre moyen $\tau = l/V$, le flux au temps t dépend du champ de concentration qui existait au temps $t-\tau$ et le développement de Taylor doit s'effectuer aussi bien dans l'espace que dans le temps, et ainsi:

$$\bar{F}(z,t) = -nV\frac{l}{2}\{\bar{\Gamma}_z + \bar{\Gamma}_{rt}\,\tau + \ldots\}.$$

Pour retrouver, dans ce cas, l'approximation du premier gradient, il faut

$$\left|\frac{\bar{\Gamma}_{zt}}{\bar{\Gamma}_z}\right| \ll 1 \quad \text{ou} \quad \left|\frac{\bar{\Gamma}_{zzt}}{\bar{\Gamma}_{zz}}\right| \ll 1\,.$$

Annexe II.

Exemple de modélisation d'après LUMLEY

Aux grands nombres de Reynolds (en toute rigueur lorsque $\Re$ tend vers l'infini), la dissipation que l'on peut écrire, dans ce cas

$$\bar{\varepsilon} = \nu\cdot\overline{u_{i,k}\cdot u_{i,k}}$$

est gouvernée par l'équation:

$$\begin{aligned}\dot{\bar{\varepsilon}} + \bar{U}_j\bar{\varepsilon}_{,j} + 2\cdot\nu\cdot\overline{u_{i,k}u_{i,j}}\;\bar{U}_{j,k} + \bar{U}_{i,kj}\cdot 2\cdot\nu\cdot\overline{u_j u_{i,k}} + \\ + \bar{U}_{i,j}\,2\nu\overline{u_{j,k}u_{i,k}} + (\overline{\varepsilon u_j})_{,j} + 2\cdot\nu\cdot\overline{u_{i,k}u_{i,j}u_{i,k}} = \\ = -2\nu\overline{u_{i,k}P_{,ik}}/\varrho + \nu\overline{\varepsilon_{jj}} - 2\cdot\nu^2\cdot\overline{u_{i,kj}u_{i,kj}}\,.\end{aligned}$$

Il est évident que son exploitation nécessite un certain nombre d'approximations dans lesquelles nous ne retiendrons que les termes de l'ordre de $\dot{\bar{\varepsilon}}$ et $\bar{U}_j\cdot\bar{\varepsilon}_{,j}$. Toutefois, une telle évaluation reste complexe et nous donnons un

exemple de la démarche proposée par J. LUMLEY en l'appliquant au terme souligné:

$$2\nu \cdot \overline{u_{i,k}\, u_{i,j}} \cdot \overline{U}_{j,k}$$

qui, comme nous le verrons, est négligeable.

Manifestement $\overline{u_{i,k}\, u_{i,j}}$ est de l'ordre de ε/ν et lui est exactement égal pour $j = k$. D'autre part, ce terme, qui souligne l'influence des petites structures, doit dépendre, si l'on accepte l'hypothèse de Kolmogonov, de $\bar{\varepsilon}$ et ν et de l'anisotropie de grosses structures qui fixent l'énergie à dissiper et qui est caractérisée par les gradients moyens $\overline{U_{i,j}}$. J. LUMLEY propose une relation fonctionnelle du type:

$$\overline{u_{i,k} u_{i,j}} = \frac{\bar{\varepsilon}}{\nu} \mathcal{F}_{kj}\{\overline{U}_{i,j}, \bar{\varepsilon}, \nu\}.$$

Si l'on se place dans le cas d'une turbulence homogène associée à un champ de gradients constants $\overline{U_{i,j}}$, pour les structures considérées, l'histoire de la turbulence rentre peu en ligne de compte, les temps de restructuration étant petits par rapport aux temps caractéristiques de ces structures, et par suite $\mathcal{F}_{kj}$ devient une simple fonction. De plus, nous ne conserverons que la partie taux de déformation S_{ij} du tenseur $\overline{U_{i,j}}$, la partie rotation en bloc n'affectant pas les petites échelles. Il vient ainsi:

$$\overline{u_{i,k}\, u_{i,j}} = \frac{\bar{\varepsilon}}{\nu} \mathcal{F}_{kj}\{S_{ij}, \bar{\varepsilon}, \nu\}.$$

L'analyse dimensionnelle montre qu'avec les trois quantités S_{ij} ε, ν et les deux grandeurs fondamentales intervenant (longueur et temps), on peut former:

$$\tilde{S}_{ij} = \sqrt{\frac{\nu}{\bar{\varepsilon}}}\, S_{ij},$$

d'où

$$g_{kj} = \overline{u_{i,k}\, u_{i,j}} = \frac{\bar{\varepsilon}}{\nu} \cdot \mathcal{F}_{kj}(\tilde{S}_{ij}).$$

Ainsi, le tenseur symétrique $g_{kj} = \mathcal{F}_{kj}(\tilde{S}_{ij})$ est fonction d'un autre tenseur symétrique $\tilde{S}_{ij}$ · . Or, la théorie des invariants montre que la dépendance ne peut être quelconque et en particulier que, si A_k et B_k sont deux vecteurs arbitraires, l'invariant bilinéaire:

$$g_{kj} A_k B_j = q(A, B, \tilde{\mathbf{S}})$$

doit être fonction des invariants que l'on peut former à partir de A, B, $\tilde{\mathbf{S}}$.

En ce qui concerne $\tilde{\mathbf{S}}$ seul, on peut former

$$I = \tilde{S}_{ii} = 0 \text{ (continuité)}; \; II = \tilde{S}_{ij}\,\tilde{S}_{ji}\,; \; III = \tilde{S}_{ij}\,\tilde{S}_{jk}\,\tilde{S}_{ki}$$

les autres étant fonctions des trois premiers d'après le théorème de CAYLEIH HAMILTON.

On aura aussi:

$$\begin{array}{lll} A_i\,A_i & A_i\,B_i & B_i\,B_i \\ A_i\,\tilde{S}_{ij}\,A_j & A_i\,\tilde{S}_{ij}\,B_j & B_i\,\tilde{S}_{ij}\,B_j \\ A_i\,\tilde{S}_{ij}\,\tilde{S}_{jk}\,A_k & A_i\,\tilde{S}_{ij}\,\tilde{S}_{jk}\,B_k & B_i\,\tilde{S}_{ij}\,\tilde{S}_{jk}\,B_k \\ A_i\,\tilde{S}_{ij}\,\tilde{S}_{jk}\,\tilde{S}_{kl}\,A_l & \ldots\ldots & \ldots\ldots \end{array}$$

etc. . . .

Ceux d'ordre supérieur étant fonction des précédents.

Comme, de plus, φ doit être bilinéaire en A et B, nous aurons

$$g_{kj}\,A_k\,B_j = \varphi_1(\mathrm{II},\mathrm{III})\,\delta_{kj}A_j\,B_j + \varphi_2(\mathrm{II},\mathrm{III})_k A_k\,\tilde{S}_{kj}\,B_j + \\ + \varphi_3(\mathrm{II},\mathrm{III})A_k\,\tilde{S}_{kl}\,\tilde{S}_{lj}\,B_j + \varphi_4(\mathrm{II},\mathrm{III})A_k\,\tilde{S}_{kl}\,\tilde{S}_{lm}\,\tilde{S}_{mj}\,B_j$$

ce qui fournit par identification:

$$g_{kj} = \varphi_1(\mathrm{II},\mathrm{III})\delta_{kj} + \varphi_2(\mathrm{II},\mathrm{III})\,\tilde{S}_{kj} + \varphi_3(\mathrm{II},\mathrm{III})\tilde{S}_{kl}\,\tilde{S}_{lj} + \\ + \varphi_4(\mathrm{II},\mathrm{III})\,\tilde{S}_{kl}\,\tilde{S}_{lm}\,\tilde{S}_{mj}$$

Or $\tilde{S}$ est un tenseur assez petit au sens des normes de matrices traditionnelles, comme:

$$\sqrt{\mathrm{II}} = \| \tilde{\mathbf{S}} \| \ll 1$$

On pourra développer chaque φ_l selon:

$$\varphi_l\,(\mathrm{II},\mathrm{III}) \approx a_l + b_l\,\mathrm{II} + c_l\,\mathrm{III}\,.$$

En se limitant au deuxième ordre et en regroupant les constantes, il vient:

$$g_{kj} \approx a\delta_{kj} + b\,\tilde{S}_{kj}\,.$$

Ainsi, nous pouvons écrire

$$\overline{u_{i,k}\,u_{i,j}} = \frac{\bar{\varepsilon}}{\nu}\left(a\,\delta_{kj} + b\sqrt{\frac{\nu}{\bar{\varepsilon}}}\,S_{kj} + \ldots\right)$$

les termes supérieurs plus petits étant négligés.

En sommant sur k et j il vient

$$\frac{\bar{\varepsilon}}{\nu} = \frac{\bar{\varepsilon}}{\nu}(3a + 0 + \ldots).$$

D'où:

$$\overline{u_{i,k}u_{i.j}} = \frac{\bar{\varepsilon}}{\nu}\left(\frac{\delta_{kj}}{3} + b\sqrt{\frac{\nu}{\bar{\varepsilon}}}\,S_{kJ} + \ldots\right).$$

Le terme complet donnera

$$2\nu\overline{u_{i,k}\,u_{i,j}}\;\bar{U}_{j,k}\,2\,\bar{\varepsilon}\left(\underbrace{\frac{1}{3}\bar{U}_{j,j}}_{=0} + b\cdot\bar{U}_{j,k}\,S_{kj}\sqrt{\frac{\nu}{\bar{\varepsilon}}} + \ldots\right)$$

soit enfin:

$$2\nu\overline{u_{i,k}u_{i,j}}\;\bar{U}_{j,k} \approx 2b\sqrt{\nu\,\bar{\varepsilon}}\;\bar{U}_{j,k}\,S_{kj}\,.$$

Si alors 1 est une échelle intégrale et u' la moyenne quadratique des fluctuations de vitesse, on aura:

$$\dot{\varepsilon} \approx \frac{\bar{\varepsilon}}{l/u'} \approx \frac{\bar{\varepsilon}\cdot u'}{l}\,,$$

$$S_{kj} \approx \bar{U}_{j,k} \approx \frac{u'}{l}\,,$$

et enfin

$$\sqrt{\frac{\bar{\varepsilon}}{\nu}} \approx \frac{u'}{\lambda}\,.$$

D'où

$$2\nu\overline{u_{i,k}\,u_{i,j}}\;\bar{U}_{j,k} \approx \bar{\varepsilon}\,\frac{\lambda}{u'}\cdot\frac{u'}{l}\cdot\frac{u'}{l} \approx \bar{\varepsilon}\,\frac{u'}{l}\cdot\frac{\lambda}{l}$$

négligeable devant $\dot{\bar{\varepsilon}}$ qui est lui, conservé.

Introduction in Some Problems of Turbulence. The paper intended to be an introduction for purpose to show the train of thoughts which is the guiding principle of the experiments conducted in the hydrodynamic laboratory of the École Centrale de Lyon in connection with the turbulence. With this the development of a common language is wanted which makes easier the description and discussion of the research work performed on the subject of the boundary layers disturbed and those, instabilized by heating. Through this also the future directions of development of this discipline might be estimated; a number of viewpoints justify the expediency of studying the thermic phenomena, three-dimensional boundary layers and flows bounded by walls.

Einleitung in einige Aufgaben der Turbulenz. Die nur für Einleitung beabsichtigte Abhandlung hat den Zweck eine Gedankenfolge darzulegen, die als Richtlinie zu den im hydrodynamischen Laboratorium der École Central de Lyon im Zusammenhang mit der Turbulenz

angestellten Versuchen dient. Damit soll eine gemeinsame Sprache erschafft werden, die die Beschreibung und Diskussion der im Problemenbereich der gestörten Grenzschichten sowie der durch die Heizung instabilisierten Grenzschichten durchgeführten Forschungsarbeit erleichtert. Dadurch können die zukünftigen Entwicklungsrichtungen auf diesem Fachbereich abgeschätzt werden; die Untersuchung der thermischen Erscheinungen, die dreidimensionalen Grenzschichten und durch Wände begrenzten Strömungen scheint aus mehreren Gesichtspunkten erforderlich und zweckmässig zu sein.

Acta Technica Academiae Scientiarum Hungaricae, Tomus 82 (3—4), pp. 281—301 (1976)

UNTERSUCHUNGEN ÜBER DAS VERHÄLTNIS ZWISCHEN MEMBRAN- UND BIEGESCHNITTKRÄFTN IN KREISZYLINDERSCHALEN UNTER WINDBELASTUNG

L. JANKÓ*

[Eingegangen am 7. Februar 1973]

Mit Hilfe einer vereinfachten Biegetheorie wird das statische Verhalten der Kreiszylindeschale mit Membranabstützung unter Windlast analysiert. In diesem Rahmen wird eine Antwort auf die Frage gesucht, ob im Falle, wenn das Gleichgewicht zwar durch das Membrankräftespiel gewährleistet ist, infolge der auftretenden großen Formänderungen nicht etwa größere Biegespannungen als die Membranspannungen in der Schale auftreten werden. Verfasser stellt fest, daß das Arbeiten als reine Membrane nur bei kleinen Harmonischen und im Falle dünnwandiger, niedriger Schalen möglich ist: daraus folgt, daß sich bei höheren Harmonischen oder für hohe, dickwandige Schalen die Membrantheorie nicht als Partikulärlösung anwenden läßt.

1. Einleitung

Einen wesentlichen Teil der Beanspruchungen der Ingenieurbauten von turmförmigen Kreiszylindern (Fernsehtürme, Fabrikschornsteine, Silos usw., Abb. 1.) bildet die Windlast. Für die Berechnung dieser Beanspruchungen sind mehrere gut brauchbare Verfahren bekannt, z. B. [1], [2], [3], nach denen je nach der erforderlichen Genauigkeit die inneren Kräfte ermittelt werden können. Aus den Untersuchungen geht auch hervor, daß die Windlastkomponenten im Abb. 2 — die entlang der Erzeugenden der Schale gleich verteilt sind — auch allein durch Membrankräfte im Gleichgewicht gehalten werden können.

Sowohl theoretisch als auch praktisch ist jedoch die folgende Frage gerechtfertigt: obzwar es richtig ist, daß die Schale diese Lasten auch durch Membrankräfte tragen kann, wie steht es jedoch dann mit der Kompatibilität der Formänderungen bzw. mit der Wirkung der Querschnittsformänderung auf die in der Konstruktion auftretenden Spannungen? Es ist also in Abhängigkeit von den geometrischen Parametern der Schale (Abb. 1 L, R, h) zu prüfen, wann die Ergebnisse der Membrantheorie infolge der entstehenden Formänderungen und der damit verbundenen Biegebeanspruchungen unannehmbar werden.

In der vorliegenden Arbeit soll diese Frage beantwortet werden. Dazu

* L. Jankó, Lajos u. 142. H-1036 Budapest, Ungarn.

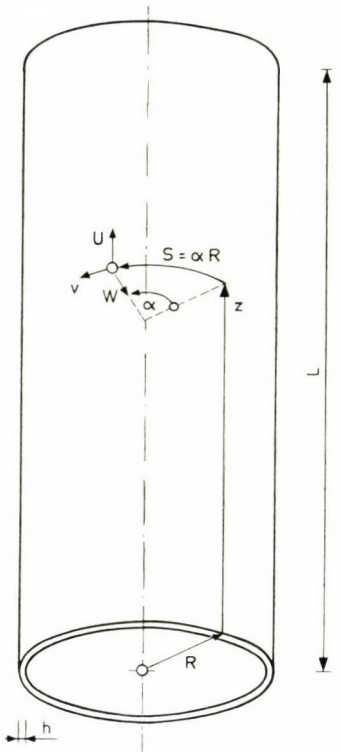

Abb. 1 Geometrie der Kreiszylinderschale

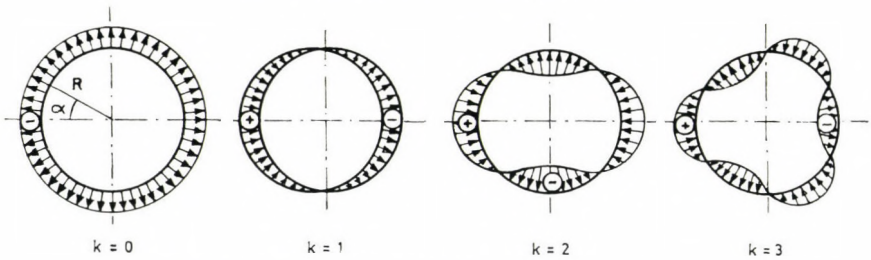

Abb. 2 Verteilung der Windlastkomponenten im Querschnitt

werden die mit Hilfe der Membrantheorie ermittelten inneren Kräfte mit den Ergebnissen einer handlichen annähernden Biegetheorie verglichen.

Das Problem der Randstörungen wird hier nicht behandelt (sie werden als unabhängige Wirkung betrachtet, die z. B. nach [1] leicht zu berechnen sind) und so werden die Berechnungen an einer Kreiszylinderschale mit Membranabstützung durchgeführt. Die Membranabstützung wird mit den Bezeichnungen der Abbildungen 1 und 3, wie folgt, definiert:

$$N_z(L) = N_{zs}(L) = u\,(0) = v(0) = 0\,. \tag{1.1}$$

2. Lastfunktion, statisches Modell

Die längs der Koordinate z als unveränderlich betrachtete, am Umfang verteilte und in jedem Punkt in Normalrichtung wirkende Windlast p wird im allgemeinen in Form eines Polynoms angesetzt:

$$p = \sum_{k=0}^{r} p_k \cos k\alpha \,, \tag{2.1}$$

wo die einzelnen p_k Werte als Produkte der in den Baunormen vorgeschriebenen Formfaktoren c_k und des Staudrucks q erhalten werden. Eine derartig mögliche Lastfunktion lautet nach dem Ungarischen Standard MSZ 15021—57 wie folgt:

$$p = q\,(-0{,}3 + 0{,}5 \cos \alpha + 0{,}8 \cos 2\alpha) + \text{Druck}, \; - \text{Zug}\,.$$

Nach Einführung der Symbole

$$\frac{\partial(\;)}{\partial z} = (\;)' \qquad \frac{\partial(\;)}{\partial \alpha} = (\;)\cdot \tag{2.2}$$

wird die Vorzeichenregel der Schnittkräfte nach Abb. 3. festgelegt.

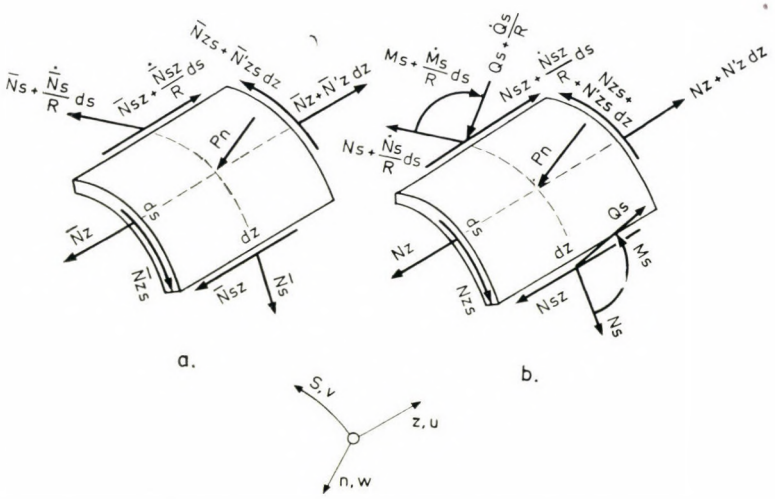

Abb. 3 Membran- und Biegekräfte der Schale

Im weiteren sollen die Grundansätze des von WLASSOW [6] eingeführten, vereinfachten Rechenmodells kurz zusammengefaßt werden:

1. Die Biegungs- und Torsionsmomente in Längsrichtung dürfen vernachlässigt werden, da sich ihre Wirkung auf die unmittelbare Umgebung der an der Formänderung durch die Ränder gehinderten Querschnitte beschränkt. Dementsprechend ist auch die Querkraft in Richtung der Erzeugenden gleich Null, während die übrigen inneren Kräfte auf Abb. 3b veranschaulicht sind.

Es sei bemerkt, daß die daraus folgenden Gleichgewichtsgleichungen den Ergebnissen der im deutschen Fachschrifttum allgemein bekannten »unvollständigen Biegetheorie« bzw. der in der angelsächsischen Literatur als Schorersche Biegetheorie bezeichneten Methode entsprechen.

2. Als Ergänzung dieser statischen Ansätze wird die Dehnung der Schalenkonstruktion in Ringrichtung als gleich Null betrachtet ($\varepsilon_s = 0$) und auch die Formänderung durch Schubbeanspruchung auf der Mittelfläche vernachlässigt ($\gamma_{zs} = 0$).

Die eingehende Analyse der genannten Bedingungen betrachten wir nicht als unsere Aufgabe, es sei nur bemerkt, daß die obigen Vereinfachungen nach [4] aus einer einzigen Vereinfachung abgeleitet werden können: es wird angenommen, daß alle Verschiebungs- und Spannungänderungen in Richtung z glatter ablaufen als in Umfangsrichtung.

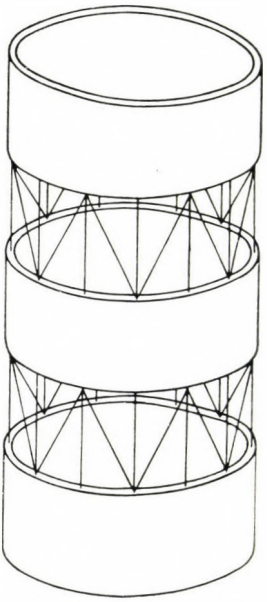

Abb. 4. Statisches Modell der Konstruktion

Von RAMASWAMY [7] werden die von verschiedenen Verfassern für auf Biegung beanspruchte Kreiszylinderschalen aufgestellten Theorien ausführlich erörtert und es wird auch auf die Grenzen der Anwendbarkeit der Schorerschen Theorie eingegangen.

Nach dem Besagten gelten also

$$\begin{aligned} \varepsilon_s &= 0, \\ \gamma_{zs} &= 0. \end{aligned} \tag{2.3}$$

Nach Einführen der genannten Ansätze, läßt sich die behandelte Kreiszylinderschale durch eine dünnwandige Konstruktion nach Abb. 4 ersetzen. Diese besteht aus einer Reihe durch ein Fachwerk verbundener Ringe und die Verbindung zwischen den als Biegeringe arbeitenden, dünnwandigen Schalenringen wird durch das die Membrankräfte aufnehmende Fachwerk gewährleistet.

3. Nach der Membrantheorie wirkende Schnittkräfte

Wird die Gesamtlast lediglich durch Membrankräfte ausgeglichen, so erhält man die Ausdrücke der Schnittkräfte in sehr einfacher Weise, z. B. aus den Gleichgewichtsgleichungen auf S. 86 in [5] unter den Randbedingungen

$$\begin{aligned} \bar{N}_{zs}(L) &= 0, \\ \bar{N}_{z}(L) &= 0. \end{aligned} \tag{3.1}$$

Die drei Schnittkräfte ergeben sich dann zu:

$$\bar{N}_{s\vartheta k} = -\, p_k R \cos k\alpha, \tag{3.2}$$

$$\bar{N}_{zs\vartheta k} = p_k (L - z)\, k \sin k\alpha, \tag{3.3}$$

$$\bar{N}_{z\vartheta k} = p_k \frac{(L - z)^2}{2R} k^2 \cos k\alpha, \tag{3.4}$$

wo $k = 0, 1, 2 \ldots r.$ bedeutet.

Prüft man die Membran-Formänderungen der Schale, so stellt sich heraus, daß die Nullpunkte der Funktion der Verschiebung in normaler Richtung (Abb. 1 w) dort liegen, wo die Nullpunkte der Lastfunktion ([1], im allgemeinen $w = W \cdot \cos k\alpha$). Durch die Inflexionspunkte wird der Umfang in $2k$ Bogen aufgeteilt; analysiert man die Spannungsverhältnisse je eines Bogenabschnitts, so läßt sich feststellen, daß man eigentlich $2k$ Kragbalken ähnlich arbeitende Träger mit bogenförmigem Querschnitt (mit dem Mittelpunktswinkel π/k) erhält, von denen k nach innen und k nach außen gebogen

sind, und die Verbindung zwischen ihnen durch die längs der Anschlußflächen auftretenden Schubspannungen gewährleistet wird. Auf diese Analogie werden wir noch in den Punkten 7 bzw. 8 zurückkommen.

4. Die vereinfachte Biegetheorie

Werden neben den Membrankräften auch die Biegeschnittkräfte zum Tragen der Lasten herangezogen, so erhält man mit den früheren Vereinfachungen folgende Zusammenhänge:

4.1. *Die Differentialgleichung der Aufgabe*

Die Gleichgewichtsbedingung des Schalenelements in Abb. 3b entspricht der Befriedigung der folgenden Gleichungen:

$$N_z' + \frac{\dot{N}_{sz}}{R} = 0\,, \tag{4.1}$$

$$\frac{\dot{N}_s}{R} + N_{zs}' - \frac{Q_s}{R} = 0\,, \tag{4.2}$$

$$N_s + \dot{Q}_s + pR = 0\,, \tag{4.3}$$

$$\frac{\dot{M}_s}{R} - Q_s = 0\,, \tag{4.4}$$

$$N_{zs} = N_{sz}\,. \tag{4.5}$$

Für die weitere Behandlung werden diese Gleichungen zu einer einzigen partiellen Differentialgleichung höherer Ordnung zusammengezogen. Wird (4.1) nach z und (4.2) nach α differenziert, und werden dann die beiden Gleichungen unter Anwendung von (4.5) zusammengezogen, so erhält man

$$R^2 N_z'' - \ddot{N}_s + \dot{Q}_s = 0\,.$$

Sodann wird die aus (4.3) durch zweifache Differenzierung nach α erhaltene Beziehung

$$\ddot{N}_s + \dddot{Q}_s + R\ddot{p} = 0$$

mit Hilfe von (4.4) mit der vorigen zusammengezogen, und man erhält die gewünschte partielle Differentialgleichung vierter Ordnung in der Form

$$N_z'' + \frac{1}{R^3}(\ddot{M}_s + \ddddot{M}_s) = -\frac{\ddot{p}}{R}\,. \tag{4.6}$$

Diese wird im weiteren in die Form mit einer Veränderlichen gebracht.

Die Komponenten in Tangential- (u), Umfangs- (v) und Normalrichtung (w) der Verschiebungsvektoren sämtlicher Punkte in der Mittelfläche können mit den Deformationselementen in der Mittelfläche ε_z, ε_s und γ_{zs} bzw. mit der Krümmungsänderung in Ringrichtung x_s ausgedrückt werden:

$$\varepsilon_z = u', \tag{4.7}$$

$$\varepsilon_s = \frac{1}{R}(\dot{v} - w), \tag{4.8}$$

$$\gamma_{zs} = \frac{1}{R}\dot{u} + v', \tag{4.9}$$

$$x_s = \frac{1}{R^2}(\dot{v} + \ddot{w}). \tag{4.10}$$

Bei der Auflösung wird die Querkontraktion außer acht gelassen ($\mu = 0$) und die physikalischen Gleichungen werden in der folgenden vereinfachten Form aufgeschrieben:

$$\varepsilon_z = \frac{N_z}{D}, \tag{4.11}$$

$$x_s = -\frac{M_s}{K}, \tag{4.12}$$

wo

$$D = Eh, \tag{4.13}$$

und

$$K = \frac{Eh^3}{12}. \tag{4.14}$$

Nach Einführung der Formänderungshilfsfunktion $\varphi = \varphi_{(z,s)}$ entsprechen — unter Berücksichtigung von (4,7 — 4,10) — den Grundsätzen (2.3) über die Formänderungen folgende Zusammenhänge:

$$u = -\varphi', \tag{4.15}$$

$$v = \frac{1}{R}\dot{\varphi}, \tag{4.16}$$

$$w = \frac{1}{R}\ddot{\varphi}, \tag{4.17}$$

$$x_s = \frac{1}{R^3}(\ddot{\varphi} + \ddot{\varphi}''). \tag{4.18}$$

In Kenntnis derselben können die Kraft N_z in Richtung der Erzeugenden und das Biegemoment M_s in Ringrichtung mit Hilfe von φ direkt ausgedrückt werden:

$$N_z = -Eh\,\varphi'', \tag{4.19}$$

$$M_s = -\frac{K}{R^3}(\varphi'' + \varphi''''). \tag{4.20}$$

Wegen der Bedingung (2.3) ($\gamma_{zs} = 0$) läßt sich die Schubkraft N_{zs} nur mit Hilfe einer Gleichgewichtsgleichung mit anderen Größen in Beziehung setzen, u. zw. zweckmäßigerweise mit Hilfe der Gleichung (4.1)

$$\dot{N}_{zs} = -RN_z'. \tag{4.21-a}$$

Infolge der Vernachlässigung der ringförmigen Dehnung ($\varepsilon_s = 0$) wird die Ringkraft N_s aus der Gleichgewichtsgleichung (4.2) bestimmt:

$$N_s = R\int\left(\frac{\dot{M}_s}{R^2} - N_{zs}'\right)d\alpha. \tag{4.21-b}$$

Für eine geschlossene Zylinderschale läßt sich die Hilfsfunktion $\varphi = \varphi(z,s)$ in Form der Reihe (4.22) aufschreiben:

$$\varphi(z, s) = \sum_{k=1}^{r} F_k(z)\cos k\alpha. \tag{4.22}$$

Nach Einsetzen von (4.22) in die Gleichungen (4.19), (4.20) und (4.6) — wobei von den weiteren, ausschließlich mathematischen Erörterungen Abstand genommen wird — erhält man für die Koeffizienten $F_k(z)$ ein unendliches lineares Differentialgleichungssystem mit konstanten Koeffizienten, das durch die Ausdrücke (4.23—24) veranschaulicht wird:

$$aF_1'''' = f_1, \tag{4.23}$$

$$aF_k'''' + b_k F_k = f_k, \tag{4.24}$$

$$k = 2, 3, \ldots r,$$

wo

$$a = h\,R, \tag{4.25}$$

$$b_k = k^4(k^2 - 1)^2\frac{h^3}{12\,R^5}, \tag{4.26}$$

und

$$f_k = -\frac{k^2}{E}p_k, \tag{4.27}$$

$$k = 1, 2 \ldots r.$$

4.2 *Lösung des Differentialgleichungssystems*

Um die Differentialgleichungssysteme (4.23) und (4.24) mit konstanten Koeffizienten zu lösen, wird der Parameter μ_k eingeführt:

$$k = \sqrt[4]{\frac{b_k}{4a}}. \tag{4.28}$$

Die Randbedingungen der Schale mit Membranabstützung werden mit Hilfe von

$$N_z(L) = N_{zs}(L) = u(0) = v(0) = 0 \tag{4.29}$$

wie folgt aufgeschrieben:

$$\begin{aligned} F_1''(L) = F_1'''(L) = F_1'(0) = \dot{F}_1(0) = 0\,, \\ F_k''(L) = F_k'''(L) = F_k'(0) = \dot{F}_k(0) = 0\,. \end{aligned} \tag{4.30}$$

Die Lösung der Gl. (4.23) mit der aus der Theorie des Navierschen Biegebalkens wohlbekannten Form wird durch das Polynom

$$F_1(z) = \frac{f_1}{24a}(z^4 + 6L^2 z^2 - 4Lz^3) \tag{4.31}$$

geliefert.

Sucht man eine Partikulärlösung einer zu den Indizes $k = 2, 3 \ldots r$ gehörenden homogenen Gleichung des Differentialgleichungssystems (4.24) nach Euler in der Form $F_k^\circ = e^{pz}$, so erhält die allgemeine Lösung der homogenen Gleichung mit Hilfe der Wurzeln $p_{1,2,3,4} = (\pm 1 \pm i)\,\mu_k$ der betreffenden charakteristischen Gleichung

$$p^4 + 4\,\mu_k = 0 \tag{4.32}$$

folgende Form:

$$F_k^\circ = C_{k1}\,\Phi_{k1} + C_{k2}\,\Phi_{k2} + C_{k3}\,\Phi_{k3} + C_{k4}\,\Phi_{k4}. \tag{4.33}$$

In diesem Ausdruck sind

$$\begin{aligned} \Phi_{k1}(z) &= \cosh \mu_k z \sin \mu_k z, \\ \Phi_{k2}(z) &= \cosh \mu_k z \cos \mu_k z, \\ \Phi_{k3}(z) &= \sinh \mu_k z \cos \mu_k z\,, \\ \Phi_{k4}(z) &= \sinh \mu_k z \sin \mu_k z\,, \\ k &= 2, 3 \ldots r. \end{aligned} \tag{4.34a–d}$$

Mit Hilfe der Hilfsveränderlichen

$$G_k = \frac{f_k}{b_k} = -\frac{k^2}{Eb_k}\,p_k, \tag{4.35}$$

die eigentlich das Glied $F_k^p = G_k$ der Lösung $F_k = F_k^\circ + F_k^p$ des Differentialgleichungssystems (4.24), also eine Partikulärlösung der inhomogenen Gleichung ist, nimmt die Lösungsfunktion F_k, die die Randbedingungen (4.30) befriedigt, die Form

$$F_k(z) = [C_{k3}(\Phi_{k3} - \Phi_{k1}) + C_{k4}\,\Phi_{k4} + (1 - \Phi_{k2})]\; G_k \qquad (4.36)$$

$$k = 2, 3, \ldots r$$

an.

Die Integranden C_k werden durch Auswertung der folgenden Ausdrücke gewonnen:

$$\begin{aligned} C_{k1} &= -\frac{1}{2}\frac{\sin 2\mu_k L + \sinh 2\mu_k L}{\cosh^2 \mu_k L + \cos^2 \mu_k L}, \\ C_{k2} &= -G_k = \frac{k^2}{Eb_k} p_k, \\ C_{k3} &= -C_{k1}, \\ C_{k4} &= \frac{\sinh^2 \mu_k L + \cos^2 \mu_k L}{\cosh^2 \mu_k L + \sin^2 \mu_k L}. \end{aligned} \qquad (4.37)$$

$$k = 2, 3 \ldots r.$$

5. Die Ausdrücke der inneren Kräfte

5.1 *Schnittkräfte im Falle* $k = 1$

Die Zusammenhänge (4.19), (4.22) und (4.31) ergeben in Form

$$N_{z1} = \frac{p_1}{2R}(L - z)^2 \cos \alpha \qquad (5.1)$$

die aus dem antimetrischen Teil der Windlast stammende Kraft in Richtung der Erzeugenden.

Man kann sich leicht davon überzeugen, daß es sich im vorliegenden Falle um die Lösung einer als Navierscher Balken aufgefaßten Kreiszylinderschale handelt, d. h. daß unter Einwirkung der antimetrischen Lastkomponenten der Querschnitt nicht deformiert wird und auch weiterhin senkrecht zur verformten Längsachse des Stabes stehen wird.

Die Resultierende der Windkräfte in einem beliebigen Querschnitt ist

$$p_1 \int_0^{2\pi} \cos^2 \alpha \, d\alpha = p_1 \pi,$$

damit ist das auf einen Schnitt mit der Koordinate z wirkende äußere Biegemoment

$$M_z(z) = \frac{1}{2} p_1 \pi (L - z)^2 ;$$

daraus erhält man mit Hilfe von $I_0 \approx \pi h R^3$

$$N_{z_{\max(0)}} = \pm \frac{M_z}{I_0} Rh = \pm p_1 \frac{(L - z)^2}{2R}$$

eine Beziehung, die sowohl mit (5.1), als auch mit der Membrankraft (3.4) übereinstimmt, da ja in den Querschnitten kein Ringmoment entsteht, das einen Teil der Last aufnehmen würde.

5.2 *Schnittkräfte im Falle* $k = 2, 3 \ldots r$

In Kenntnis der Ergebnisse in Punkt 4 lassen sich die inneren Kräfte anhand der Biegetheorie leicht ermitteln; die für die Berechnung günstige Form lautet:

$$N_{z,k} = -C_{k3}(\Phi_{k1} + \Phi_{k3}) + C_{k4}\Phi_{k2} + \Phi_{k4} \cdot \cdot \frac{2\sqrt{3}\,R^2}{(k^2 - 1)\,h} p_k \cos k\alpha , \tag{5.2}$$

$$N_{sz,k} = [2 C_{k3}\Phi_{k2} - (C_{k4} + 1)\Phi_{k3} + (C_{k4} - 1)\Phi_{k1}] \cdot \cdot \frac{k}{2\mu_k} p_k \sin k\alpha , \tag{5.3}$$

$$N_{s,k} = \left\{ [C_{k3}(\Phi_{k3} - \Phi_{k1}) + C_{k4}\Phi_{k4} - \Phi_{k2} + 1] \cdot \cdot \frac{k^2}{k^2 - 1} - 1 \right\} R p_k \cos k\alpha , \tag{5.4}$$

$$M_{s,k} = [C_{k3}(\Phi_{k3} - \Phi_{k1}) + C_{k4}\Phi_{k4} - \Phi_{k2} + 1] \cdot \cdot \frac{R^2}{k^2 - 1} p_k \cos k\alpha . \tag{5.5}$$

5.3 *Ein Zahlenbeispiel*

Die bisherigen Ergebnisse sollen durch ein Zahlenbeispiel veranschaulicht werden. Die Abb. 5 bis 8 zeigen die Gestaltung der Beanspruchungen längs der Erzeugenden einer Kreiszylinderschale, die durch die geometrischen

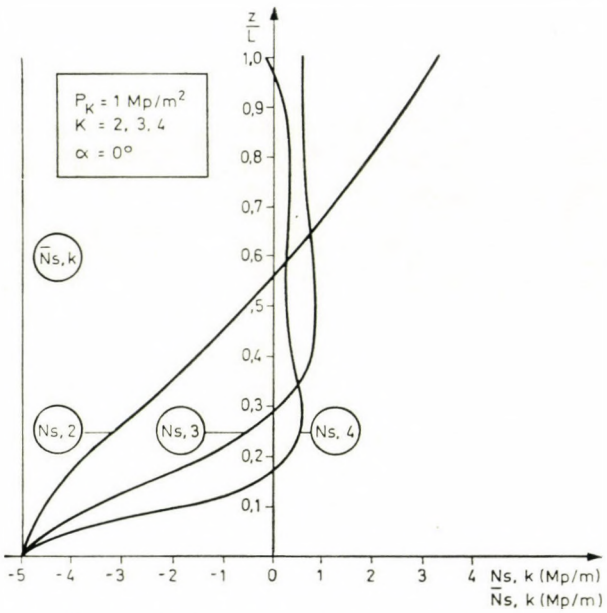

Abb. 5 Verteilung der Ringkräfte längs der Erzeugenden ($L = 50$ m, $R = 5$ m, $h = 0{,}2$ m)

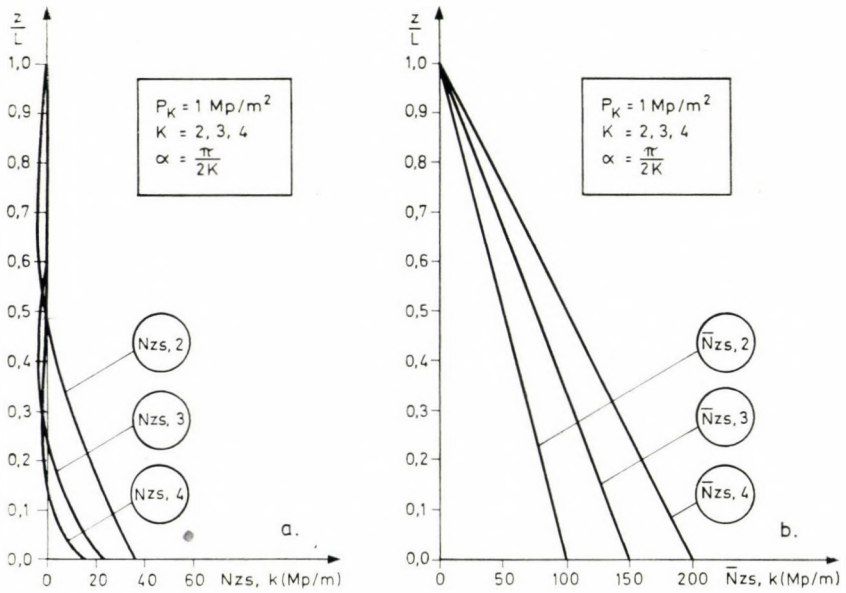

Abb. 6 Verteilung der Mittelflächen-Schubkräfte längs der Erzeugenden ($L = 50$ m, $R = 5$ m $h = 0{,}2$ m)

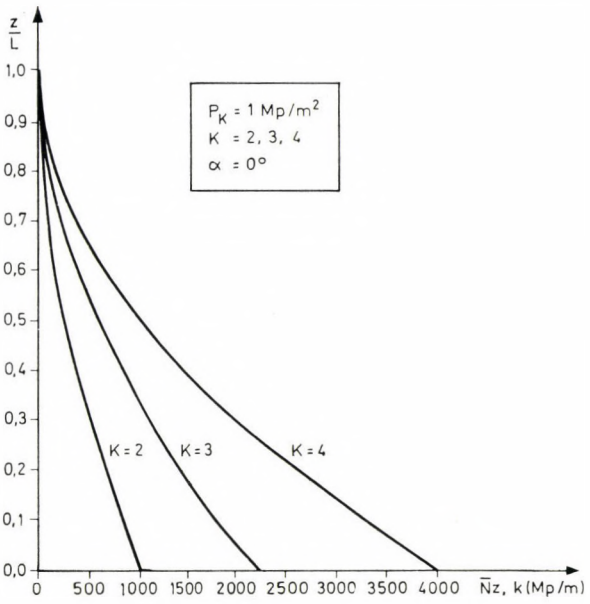

Abb. 7a Verteilung der in Richtung der Erzeugenden wirkenden Membrankräfte längs der Erzeugenden ($L = 50$ m, $R = 5$ m, $h = 0{,}2$ m)

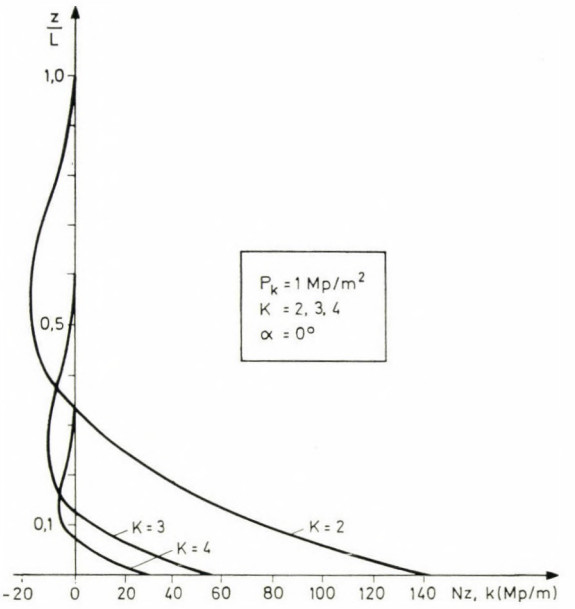

Abb. 7b Verteilung längs der Erzeugenden der nach der Biegetheorie erhaltenen, in Richtung der Erzeugenden wirkenden Kräfte ($L = 50$ m, $R = 5$ m, $h = 0{,}2$ m)

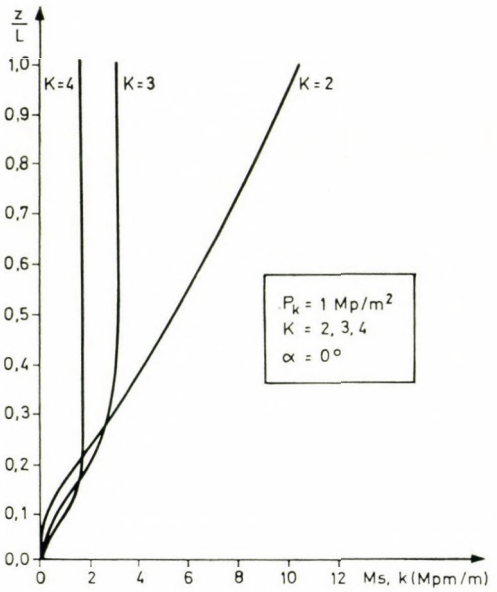

Abb. 8 Ringmomentverteilung längs der Erzeugenden ($L = 50$ m, $R = 5$ m, $h = 0{,}2$ m

Daten $L = 50$ m, $R = 5$ m, $h = 0{,}2$ m gekennzeichnet und durch eine Windlast mit der Amplitude $p_k = 1$ Mp/m² und von der Verteilung $p = p_k \cos k\alpha$ belastet ist, im Falle von $k = 2, 3, 4$. In diesen Abbildungen — und auch im weiteren — werden die nach der Membrantheorie bestimmten Beanspruchungen von den aus der Biegetheorie gewonnenen Beanspruchungen durch einen Hochstrich unterschieden.

Die Berechnungen wurden auf der elektronischen Rechenmaschine TPA des Unternehmens ÉM. SZÁMGÉP von Dénes WILDNER durchgeführt.

6. Die Aufteilung der Gesamtwindlast ($p = p_k \cos k\alpha$) auf durch Ringbiegekräfte (p_k^B) und auf durch Mittelflächenkräfte (p_k^M) aufgenommene Lastanteile

Dem eingeführten statischen Modell entsprechend setzt sich das durch (5.2) bis (5.5) bestimmte Kräftesystem aus zwei Teilen zusammen (Abb. 9):

Die eine Kräftegruppe (Abb. 9a) ist das innere Kräftesystem eines gewöhnlichen Biegeringes ($N^B_{s,k}$, $M^B_{s,k}$, $Q^B_{s,k}$), das die Lastkomponente p^B_k trägt, die andere Kräftegruppe ($N^M_{s,k}$, $N^M_{z,k}$, $N^M_{zs,k}$) nimmt den ihr entsprechenden Lastanteil p^M_k membranartig auf (Abb. 9b). Daher können folgende

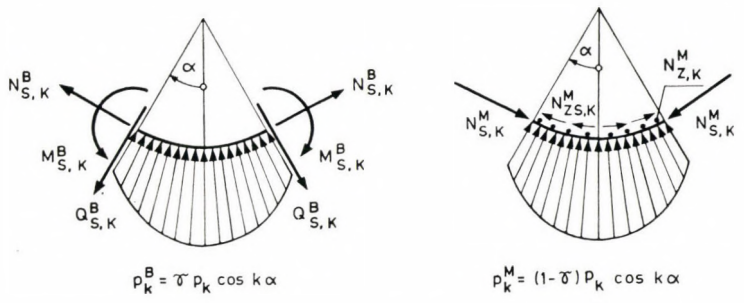

Abb. 9 Verteilung der Gesamtwindlast (p_k) auf durch Ringbiegekräfte (p^B) und Mittelflächenkräfte (p^M) getragene Lastanteile

Beziehungen aufgeschrieben werden:

$$N_{z,k} = N^M_{z,k}\,, \tag{6.1}$$

$$N_{zs,k} = N^M_{zs,k}\,, \tag{6.2}$$

$$N_{s,k} = N^B_{s,k} + N^M_{s,k}\,, \tag{6.3}$$

$$M_{s,k} = M^B_{s,k}\,, \tag{6.4}$$

$$Q_{s,k} = Q^B_{s,k}\,, \tag{6.6}$$

und

$$p_k = p^B_k + p^M_k = \gamma p_k + (1-\gamma)\, p_k\,. \tag{6.6}$$

Danach erhält man unter Anwendung der allgemein bekannten — bzw. aus den Gleichgewichtsgleichungen (4.2) bis (4.5) leicht ableitbaren — Grundformel der Ringbiegung

$$M^B_{s,k} = \frac{p^B_k R^2}{k^2 - 1} \cos k\alpha \tag{6.7}$$

den Zusammenhang zwischen der Amplitude (p_k) der Gesamtlast und der Amplitude (p^B_k) des durch die Ringkräfte aufgenommenen Lastenteils in der Form

$$p^B_k = [C_{k3}(\Phi_{k3} - \Phi_{k1}) + C_{k4}\,\Phi_{k4} - \Phi_{k2} + 1]\, p_k\,. \tag{6.8}$$

Nach dem Besagten beträgt der Prozentanteil der durch die Ringkräfte getragenen Last

$$\gamma = 100\,[C_{k3}\,(\Phi_{k3} - \Phi_{k1}) + C_{k4}\,\Phi_{k4} - \Phi_{k2} + 1] \tag{6.9}$$

und

$$p^B_k = \gamma p_k\,. \tag{6.10}$$

7. Analyse des Verhältnisses der nach der Biegetheorie erhaltenen $(N_{z,k}, N_{zs,k}, N_{s,k})$ zu den nach der reinen Membrantheorie erhaltenen $(\bar{N}_{z,k}, \bar{N}_{zs,k}, \bar{N}_{s,k})$ Mittelflächenkräften

Aus der eingehenden Analyse der Ausdrücke (5.2) bis (5.4) bzw. (3.2) bis (3.4) für die mit Hilfe der Schorerschen Biegetheorie erhaltenen Mittelflächenkräfte $N_{z,k}$, $N_{zs,k}$ und $N_{s,k}$ bzw. für die durch die reine Membrantheorie gelieferten Mittelflächenkräfte $\bar{N}_{z,k}$, $\bar{N}_{zs,k}$ und $\bar{N}_{s,k}$ lassen sich folgende Schlüsse ziehen:

1. Bei konstanten Parametern R/h und L/R wachsen die nach der Membrantheorie erhaltenen inneren Kräfte $(\bar{N}_{zs,k}, \bar{N}_{z,k})$ mit dem zunehmenden Multiplikator k des Arguments, während die nach der Biegetheorie erhaltenen Schnittkräfte $(N_{zs,k}, N_{z,k})$ abnehmen. Das läßt sich dadurch erklären, daß mit der Zunahme von k die Pfeilhöhen der Bogenabschnitte zwischen den Inflexionspunkten des Ringes fortwährend abnehmen, d. h. die Steifigkeit in Erzeugendenrichtung der Kragträger mit den diesen Bogenabschnitten entsprechenden Querschnitten (vgl. Punkt 3) immer geringer wird; mit abnehmender Bogenlänge werden hingegen die Trägerabschnitte im Vergleich zur Membransteifigkeit in Ringrichtung immer steifer. Das bedeutet, daß dann die Kräfte $N_{zs,k}$, $N_{z,k}$ und $N_{s,k}$ (bei $z \neq 0$ vermindert sich auch $N_{s,k}$; vgl. Abb. 5) von der Gesamtlast immer weniger aufnehmen müssen.

Wird von der Biegungssteifigkeit der Schale abgesehen ($K = 0$), also lediglich mit Membrankräften gearbeitet, dann nehmen (bei konstantem $\bar{N}_{s,k}$) die Kräfte $\bar{N}_{zs,k}$ und $\bar{N}_{s,k}$ mit k zu.

2. Bei gleichem k und konstantem L/R werden die Quotienten $N_{z,k}/\bar{N}_{z,k}$ und $N_{zs,k}/\bar{N}_{zs,k}$ mit zunehmendem R/h (d. h. mit abnehmender Biegungssteifigkeit) immer größer, da ja in diesem Falle die Ring-Biegekräfte ($M_{s,k}$, $Q_{s,k}$) einen geringeren Anteil der Gesamtlast tragen werden und sich das Kräftespiel dem reinen Membranzustand nähert.

3. Bei konstanten L/R und R/h machen die bei $k = 4$ auftretenden Kräfte $N_{zs,k}$ und $N_{z,k}$ nur einen Bruchteil der bei $k = 2$ entstehenden entsprechenden Kräfte aus. Diese Tatsache wird auch in den Baunormen berücksichtigt; z. B. die Vorschriften der Norm MSz 15021—57 enthalten von der allgemeinen Lastfunktion

$$p = \sum_{k=0}^{r} p_k \cos k\alpha$$

nur die Glieder $k = 0, 1, 2$.

8. Das Verhältnis der durch die nach der Biegetheorie erhaltenen Ring-Biegekräfte ($M^B_{s,k}, Q^B_{s,k}, N^B_{s,k}$) zu den durch die Schnittkräfte ($N^M_{z,k}, N^M_{zs,k}, N^M_{s,k}$) getragenen Lastenteilen

In den Abbildungen 1 – 12 ist die Änderung längs der Erzeugenden der durch die beiden Kräftegruppen getragenen Lastanteile ($p^B_k = p_k\gamma$ bzw. $p^M_k = p_k(1-\gamma)$ in Abhängigkeit von den Parametern R/h und L/R der Kreiszylinderschale dargestellt.

Eine Analyse der Diagramme führt zu folgenden Schlüssen:

1. Bei konstanten R/h und L/R und zunehmendem k nimmt auch γ zu. Das zeigt wiederum, daß die Zunahme von k durch eine zunehmende Ringsteifigkeit der Schale begleitet wird, d. h. die wie halbe Kragbalken arbeitenden Träger mit durch die Inflexionspunkte getrennten Querschnitten (s. Punkt 3) einen immer kleineren Teil der Gesamtlast tragen können.

2. Hohe dickwandige Türme nehmen den überwiegenden Teil der Lasten durch Biegekräfte auf, während bei niedrigen dünnwandigen Kreiszylinderschalen die Schnittkräfte eine entscheidende Rolle spielen.

3. Eine sehr wichtige Schlußfolgerung ist, daß sich bei höheren Harmonischen und hohen dickwandigen Zylinderschalen die Membrantheorie nicht als Partikulärlösung anwenden läßt. Das betrifft vor allem die Umgebung des oberen Randes. Als reine Membrane kann nämlich nur eine niedrige dünnwandige Zylinderschale bei kleinem k arbeiten.

4. In den Abbildungen 10 bis 12 fällt auf, daß γ stellenweise über 100% ansteigt. Der besseren Verständlichkeit halber betrachten wir Abb. 9. Solang $\gamma < 100\%$, entspricht das Vorzeichen der inneren Kräfte dem Abb. 9. Durch jeden Wert der entstehenden Biegemomente $M^B_{s,k}$ wird je ein Lastanteil bestimmt, der im Falle gewisser geometrischer Verhältnisse auf einem Teil des Zylinders 100% überschreiten wird. In diesem Falle muß $N^M_{s,k}$ das Vorzeichen wechseln und daher wird auch p^M_k das umgekehrte Vorzeichen erhalten. Diese Erscheinung wird nach der Balkenanalogie im Punkt 3 erklärt, d. h. es verschieben sich die Membrankragträger, die als auf den »Ringträgern« elastisch gelagerte Balken arbeiten, im oberen Schalenbereich in einer der Lastrichtung entgegengesetzten Richtung und damit belasten sie die Ringträger. Anstatt an der Lastübernahme teilzunehmen, bedeuten in diesem Falle die Schnittkräfte noch eine Mehrbelastung zu den Ring-Biegekräften. Deshalb erfüllt sich in diesem Falle die Gleichheit

$$p_k = p^B_k + p^M_k \,.$$

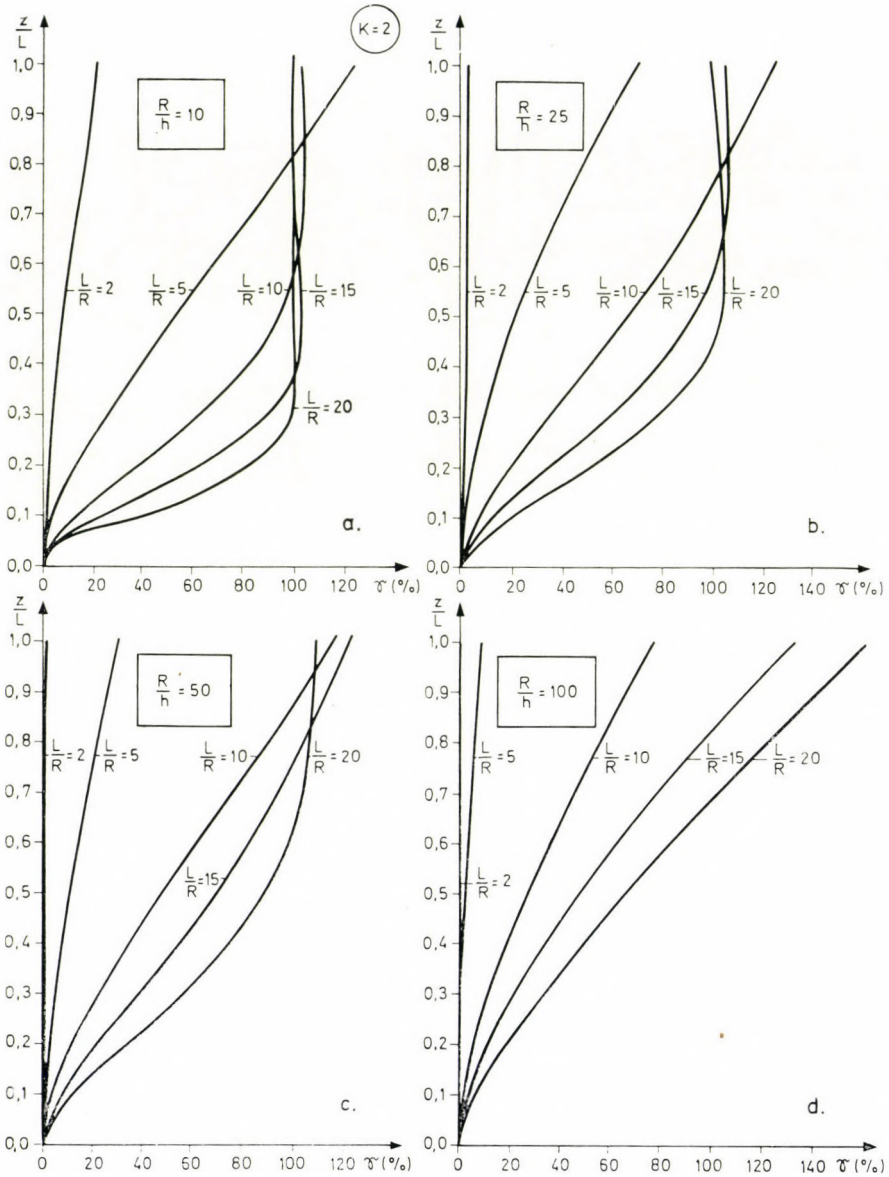

Abb. 10 Änderung der durch Ring-Biegekräfte und der durch Mittelflächenkräfte aufgenommenen Lastanteile ($\gamma\%$ bzw. 100-$\gamma\%$) längs der Erzeugenden, in Abhängigkeit von den Parametern R/h und L/R, bei $k = 2$

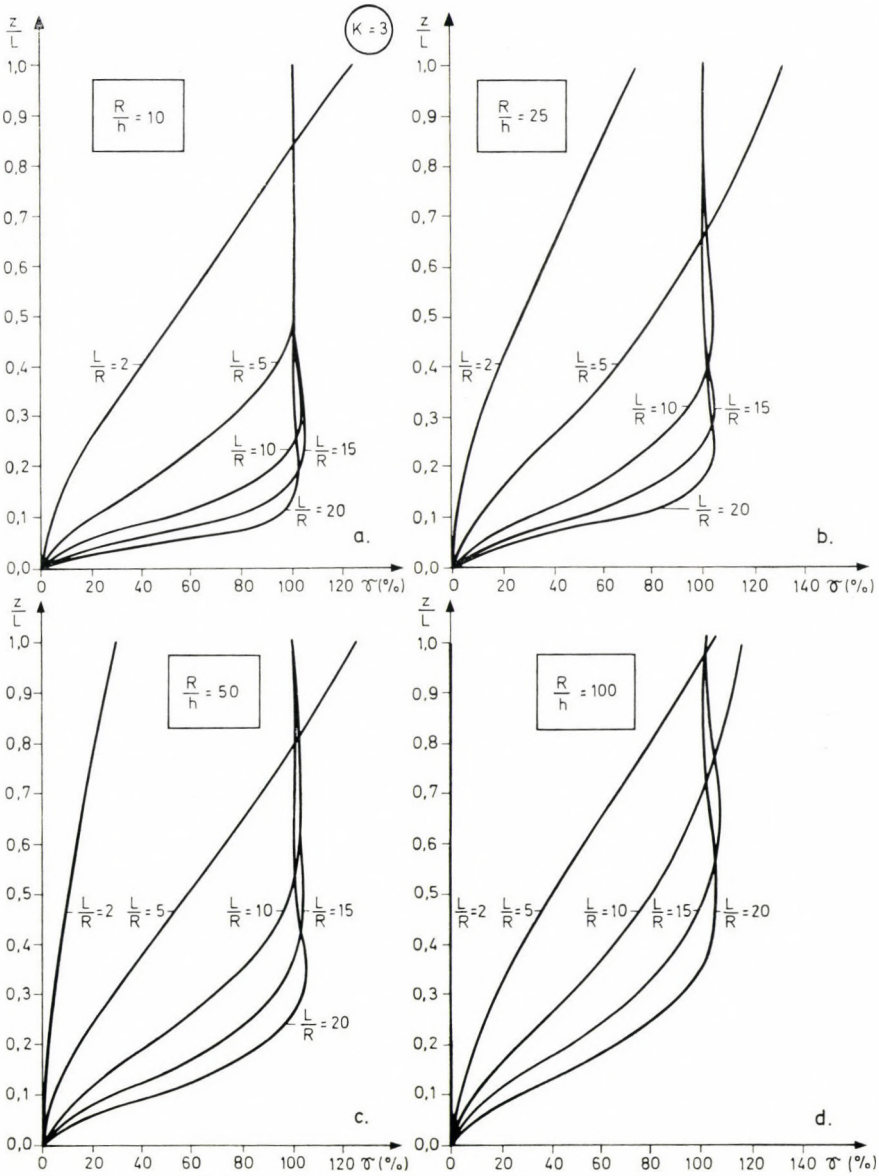

Abb. 11 Änderung der durch Ringbiegekräfte und der durch Mittelflächenkräfte aufgenommenen Lastanteile (γ% bzw. 100-γ%) längs der Erzeugenden, in Abhängigkeit von den Parametern R/h und L/R bei $k = 3$

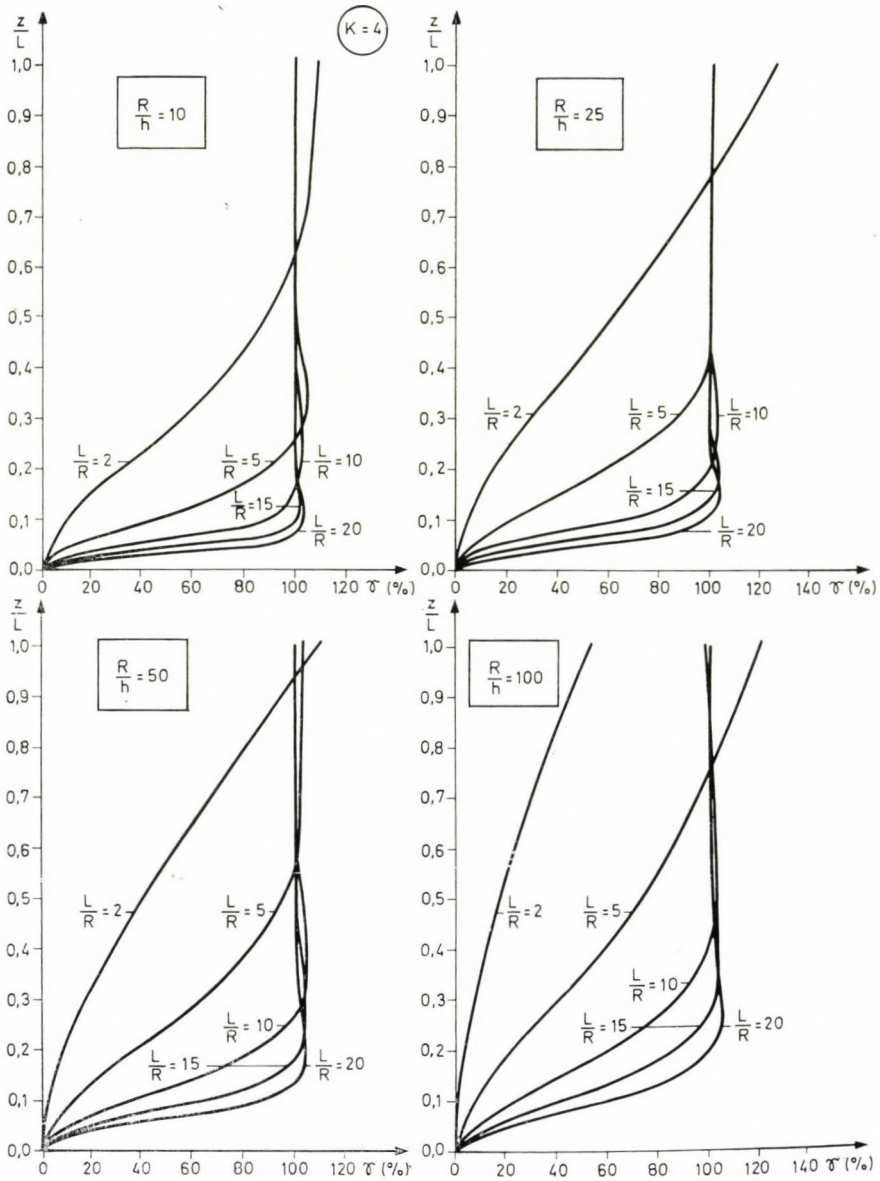

Abb. 12 Änderung der durch Ringbiegekräfte und der durch Mittelflächenkräfte aufgenommenen Lastanteile ($\gamma\%$ bzw. 100-$\gamma\%$) längs der Erzeugenden. in Abhängigkeit von den Parametern R/h und L/R bei $k = 4$

SCHRIFTTUM

1. Beton-Taschenbuch. Band V. VEB Verlag für Bauweisen, Berlin, 1970
2. RABICH, R.: Der Einfluß der Querschnittsverformung auf die Spannungen in Stahlbetonschornsteinen infolge Windlast *Bauplanung — Bautechnik* (1959), Heft 8
3. GIRKMANN, K.: *Flächentragwerke.* Fünfte Auflage. Springer-Verlag, Wien, 1959
4. KRAJCINOVIC, D.: Semimembrane Analyses of Cylindrical Shells Subjected to Wind Loading. *Journal of Applied Mechanics,* December, 1970
5. FLÜGGE, W.: Statik und Dynamik der Schalen. 3. Aufl. Springer, Berlin-Göttingen-Heidelberg 1962
6. WLASSOW, W. S.: Allgemeine Schalentheorie und ihre Anwendung in der Technik. Akademie-Verlag, Berlin 1958
7. RAMASWAMY, G. S.: Design and Construction of Concrete Shell Roofs. McGraw-Hill Book Company, New York—San Francisco—Toronto—London—Sidney 1968

Analysis of the Ratio of the Membrane and Bending Forces of a Cylindrical Shell Subjected to Wind Load. The static behaviour of the membrane supported cylindrical shell-subjected to wind load is analysed with the aid of the simple theory of bending. In this connection answer is given to the question that if the membrane stress pattern realizes the equilibrium, so the large deformations do induce or not bending stresses in the shell wall greater than membrane stresses. It is stated that pure membrane behaviour is only possible in case of small, low, and thin-walled cylindrical shells, therefore, in case of higher harmonics or high, thick-walled cylindrical shells the membrane theory cannot be applied as particular solution.

Анализ отношений мембранных и изгибающих усилий цилиндрических оболочек, работающих при ветровой нагрузке. Автор при использовании упрощенной теории изгиба дает анализ статического поведения работающей при ветровой нагрузке цилиндрической оболочки, имеющей мембранную опору. В рамках чего автор ставит своей целью дать ответ на вопрос, что в том случае, когда работа мембраны обеспечивает разновесие, тогда возникающие большие деформации не создают ли напряжения изгиба в мембране, как мембранные напряжения. Установлено, что чистая мембранная работа возможна лишь в случае небольших гармоник и низких тонкостенных цилиндрических оболочек: вследствие чего в случае более высоких гармоник или высоких толстостенных оболочек мембранная теория не может быть использована в качестве партикулярного решения.

Acta Technica Academiae Scientiarum Hungaricae, Tomus 82 (3—4), pp. 303—332 (1976)

EXPERIMENTAL INVESTIGATIONS OF THE LIFE OF SEMICONDUCTOR DEVICES, IV

THE ROLE OF THE PEAK TEMPERATURE CAUSED BY THE SWITCHING TRANSIENTS IN THE SPATIAL BREAKDOWN OF SWITCHING TRANSISTORS AND DIGITAL INTEGRATED CIRCUITS

P. Á. KEMÉNY

[Manuscript received: 15 Oct. 1973]

The transient temperature rise due to the switching power transients can be made responsible for some characteristic spatial breakdowns in high-level switching operation, such as C—E "pinning" and C—B short-circuit. Calculating the "thermal penetration depth" on both sides of the collector junction, and also the thermal capacity and the thermal resistance of the heated space part until a given moment after the start of the switching transient, a suitable unidimensional thermal model is obtained for estimating the junction temperature rise: in possession of the transient switching power vs. time and the design data of the given bipolar transistor the transient junction temperature can be calculated as a function of time. On numerical examples for some transistor types with characteristic technology (from the large, robust Ge and Si power transistors until the monolithic miniature integrated circuits), assuming faultless structure and uniform current distribution, it is shown that the switching temperature peaks are completely inoffensive.

1. Introduction

Collector-emitter punch-through and collector-base breakdowns are frequently occurring — as typical bulk failures — at high-power-level switching operation of transistors especially if a transistor exhibits uneven structure and so a current concentration takes place preferently at the loci of irregularities which latter leads, by a thermo-electrical feed-back process (runaway), to the occurrence of hot spots and is terminated by such a short [3, 4]. For these failure types the energy of the turnover transient can be blamed, as the author had pointed out earlier [3, 4], the temperature increase caused by these transients are of paramount importance but so far reckoning of these temperature jumps has been too sophisticated in the lack of an appropriate thermal model, due to the intricate nature of thermodynamical behaviour in a rather complicated device as a transistor. An attempt is made here to elucidate the questions on a good-working model.

* Parts I, II and III appeared in this periodical, cf. references [1, 2, 3].

2. Exponential approximation of turning- on and -off voltages, currents and powers

Huge power peaks appear during switching-on and -off transitions being several times higher than the quasy-stationary power losses in saturated (turned-on) or cut-off (turned-off) states of a switching transistor. Recapitulating the findings of the literature [3, 4], the relationships of these quantities are given here briefly.

Collector voltage V_{CB} and collector current I_C, both as a function of time at turnover of a transistor inverter, can be fairly approximated by exponential functions as is depicted in Fig. 1, e.g. at switching-on:

$$V_{CB}(t) = V_{CC} \exp\ (-t/\tau_i) \tag{1a}$$

and

$$I_C(t) = I_{Cp}[1-\exp\ (-t/\tau_i)] \tag{1b}$$

where V_{CC} is the collector supply voltage and $I_{Cp} = V_{CC}/R_C$ is the turned-on saturated) collector current of an inverter whereas τ_i is the switching-on time constant ($\tau_i \cong t_{on}/2$ at a usual inverter where t_{on} is the switching-on or rise time). At turning-off, the above equation pair holds valid symmetrically but currents should be substituted by voltages and vice versa and $\tau_0 = t_{off}/2$ switching-off time constant should be considered:

$$I_C(t) = I_{Cp} \exp\ (-t/\tau_0)\,, \tag{1c}$$

and

$$V_{CB}(t) = V_{CC}\ [1-\exp\ (-t/\tau_0)]. \tag{1d}$$

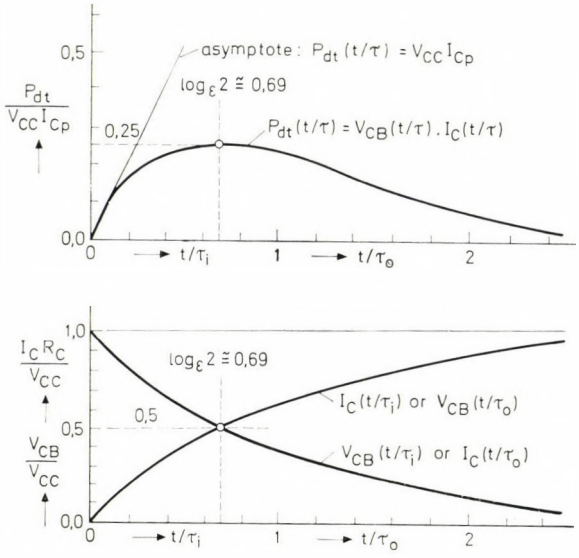

Fig. 1. Exponential approximation of voltages and currents (below) and power (top) of a transistor during commutation

In Eq. (1) it is assumed that $V_{CC} \gg V_{CE}$ sat and also that $I_{Cp} \gg I_{CBO}$ (or I_{CEO}, depending on inverter circuitry), which are true at least at high-voltage, high-power-level transistor switches.

The instantaneous power during the transition from cut-off to saturation (turning-on) can be expressed [3, 4] as the product $V_{CB}(t) \cdot I_C(t)$, i.e. multiplying Eqs (1.a) and (1.b) which gives

$$P_{dt\,i}(t) = V_{CC}\, I_{Cp}\, [\exp(-t/\tau_i) - \exp(-2t/\tau_i)] \tag{2}$$

and substituting τ_0 one gets $P_{dt\,0}(t)$ in the same way, which function is depicted at the top of Fig. 1. Forming $dP_{td\,i}(t)/dt = 0$ by differentiating Eq. (2), the maximum of the transient power-time function comes about [3, 4]:

$$P_{dt\,i\,\max} = P_{dt\,0\,\max} = P_{dt\,\max} = V_{CC}\, I_{Cp}/4 \tag{3}$$

in the instant $t/\tau_i = \log_\epsilon 2 \cong 0{,}69$ (or $z/\tau_0 \cong 0{,}69$ at switching-off as well) just when both I_C and V_{CB} are exactly at the half of their quasi-stationary maximum values I_{Cp} and V_{CC}, resp. which power is rather large, at least compared to the quasi-stationary power losses dealt with in Refs. [3, 4] and later in Eqs (23) and (24).

Finally, the time function of transient turnover energy is of importance which may be presented [3, 4] as the time integral of Eq. (2) multiplied in the same time by τ_i or τ_0:

$$L_{on}(t) = \tau_i \int_0^t P_{dt\,i}(t)dt = (\tau_i\, V_{CC}\, I_{Cp}/2)\,[1 - 2\exp(-t/\tau_i) + \exp(-2t/\tau_i)], \tag{4}$$

standing for the turning-on energy function and being symmetrical for $L_{off}(t)$ turning-off energy by the substitution of τ_0 instead of τ_i. For the whole energy of the transient, i.e. for $t = \infty$ or more practically, $t \gg \tau_i$ or $t \gg \tau_0$, Eq. (4) yields [3, 4]

$$L_{on} = \tau_i\, V_{CC}\, I_{Cp}/2 = 2\,\tau_i\, P_{di\,\max} \cong t_{on}\, P_{dt\,\max} \tag{5a}$$

and

$$L_{off} = \tau_0 V_{CC}\, I_{Cp}/2 = 2\,\tau_0\, P_{dt\,\max} \cong t_{off}\, P_{dt\,\max} \tag{5b}$$

which in turn is a rather high amount of energy if $P_{dt\,\max}$ is high too and, at one also needs the same time, the turnover process is rather long.

For further calculation one also needs the relationship between the reverse voltage V_{CB} and the width of the collector depletion layer, the latter denoted by X, which is [3, 4]

$$X(V_{CB}) = \left(\frac{2\varepsilon_r\,\varepsilon_0}{qN_1}\,V_{CB}\right)^{1/2} = \sqrt{2\,\varepsilon_r\,\varepsilon_0\,\mu_n\,\varrho_n\,V_{CB}} \tag{6}$$

where ε_r is the relative dielectric constant of the semiconductor (12 for silicon and 16,5 for germanium), $\varepsilon_0 = 8{,}86 \times 10^{-14}$ Asec/Vcm the dielectric permittivity of the free space; μ_n denotes the electron mobility (1260 cm^3/Vsec for silicon and 3600 cm^2/Vsec for germanium); q is the electron charge (1.6×10^{-19} Asec); further N_I is the net impurity concentration (cm^{-3}) and ϱ_n the resistivity (ohm. cm), both latter referring to the lighter doped junction side, which in turn is the collector layer at npn planar or mesa structures, whilst it is the base at pnp alloyed devices. Since only these technologies are dealt with here in the numerical examples, the afore mentioned data could be reached for in the calculations.

3. Thermal penetration depth and the heated-up volume section during the turnover transient

Cooling-down after a heating by electrical power in a transistor is a pure heat-conductive process and consequently, a diffusion-like stochastic problem which can generally be described as a special form of a Kolmogorov-equation by the three-dimensional differential equation as a function of time (t) and the space coordinates x, y, z [5...8] as

$$\frac{\partial T}{\partial t} = \Theta \left(\frac{\partial^2}{\partial x^2} + \frac{\partial^2}{\partial y^2} + \frac{s^2}{\partial z^2} \right) \Delta T \tag{7}$$

where Θ is the thermal diffusivity [cm^2 sec^{-1}) obtained as $\Theta = \lambda_\vartheta / \gamma c_\vartheta$ and where λ_ϑ stands for the thermal conductivity [W cm^{-1} °C^{-1}]; γ is the specific density [g cm^{-3}] and c_ϑ denotes the specific heat [W sec g^{-1} °C^{-1}] of the semiconductor material in question. These material constants (valid at approx. 25 °C) are given [9] in Table I.

In the case of a practical transistor the problem can be reduced to a one-dimensional form since the heat source — actually the collector depletion

Table I

Thermal and electrical material constants of semiconductors

Material \ Unit*	Specific density γ g/cm^3	Specific heat c_ϑ Wsec/g °K	cal/g °K	Thermal conductivity λ_ϑ W/cm °K	cal/cm sec °K	Thermal diffusivity $\Theta = \lambda_\vartheta/\gamma c_\vartheta$ cm^2/sec	Relative dielectric constant ε_r	Electron mobility μ_n cm^2/V sec
Germanium	5,3	0,31	0,074	0,64	0,155	0,384	16,5	3600
Silicon	2,3	0,755	0,18	0,84	0,20	0,438	12,0	1260

*at 25 °C.

layer embedded in its own-material — may be regarded as a laminar (plain) layer with a very thin thickness X of some μm as compared to the thickness dimension of the semiconductor wafer (in practice some hundred μm) let alone the diameter of the junction which latter amounts to some 100 $\div$ some 1000 μm. Hence, the differential equation describing the heat conduction can be written as a function of time t and distance x perpendicular to the heat-source surface area A, in a one-dimensional form as

$$dT/dt = \Theta(d^2T/dx^2). \tag{7a}$$

Let us assume $X \ll x$ (that is, a very thin heat source with a minute volume of $V_{\vartheta X}$) submitted to a heat pulse of $\Delta L_{\vartheta 0} = \gamma c_\vartheta V_{\vartheta R} \Delta T_0$ energy taking place in an infinitesimally brief duration, i.e. in a form of Dirac-delta step function where ΔT_0 is the temperature jump above the mean temperature of the wafer. In this case the solution of (7.a) differential equation [5 $\div$ 8] is a normal distribution in the form

$$\Delta T(x, t) = \frac{1}{\sqrt{4\pi\Theta t}} \exp\left[-\frac{x^2}{4\Theta t}\right] \tag{8}$$

having a standard deviation $\sqrt{2\Theta t}$ defined as *thermal penetration depth:*

$$r_\vartheta(t) = \sqrt{2\Theta t}\,. \tag{9}$$

The thermal relations in the case of a brief Dirac-delta heat transfer are depicted in Fig. 2. The heat generated in the depletion layer of X/ξ equivalent thickness (ξ will be elucidated later) spreads on both sides of the

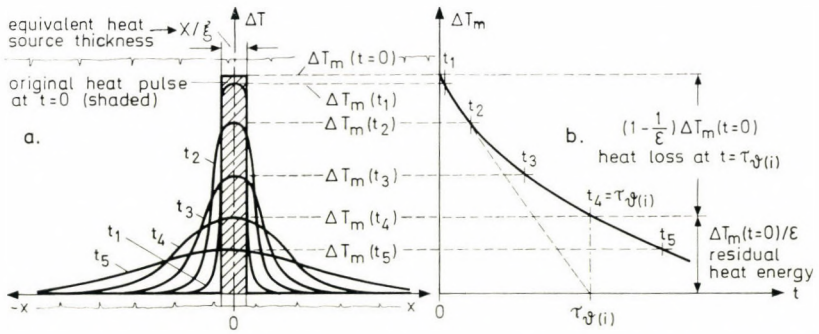

Fig. 2. Temperature distribution in the vicinity of collector depletion layer (a), and time dependence of peak temperature ΔT_m within the depletion-layer heat-source (b), after an infinitely short Dirac-delta heat pulse. Temperature shows a normal distribution perpendicular to the thin laminar heat source, spreading ever wider with advancing time in the same proportion as peak temperature ΔT_m decreases. Thus, the areas (thermal energies) below the bell-shaped distribution frequency curves at various times $t_1 \ldots t_5$ are equal to the original one (the shaded rectangle) at $t = 0$

junction symmetrically and rather quickly in time, further and further — with ever increasing r_ϑ standard deviation in distance — while simultaneously with ever decreasing mean value ΔT_m (at $x = 0$) of the maximal temperature in time, albeit this decreasing time function is not an exponential one — only similar to it — since both terms in the denominator of the coefficient and of the exponent are time-depending. However, the solution (8) holds valid only for a Dirac-delta heat-transfer pulse infinitely short in duration and, consequently, representing an infinitely high thermal energy independent of the value of ΔT_0, hence yielding $\Delta T = \infty$ if $t = 0$. For practical boundary conditions of a finite heat transfer duration incomparably shorter than $(1/\Theta)\,(X/\xi)^2$, the solution differs from Eq. (8) — although this condition also cannot be realized in practice, while switching times are many times longer — but yields finite a result at both $t = 0$ and $x = 0$, with a rectangular short step-function of the L_0 electrical energy

$$\Delta T(x, t) \cong \Delta T_m \exp\left[- \frac{x^2}{4\Theta t + (X/2\xi)^2} \right] = \\ = \frac{L_0}{2\gamma c_\vartheta A[(X/2\xi) + \sqrt{4\pi\Theta t}]} \cdot \exp\left[- \frac{x^2}{4\Theta t + (X/2\xi)^2} \right] \tag{8a}$$

which result will be explained later. However, the spreading of the heat energy in distance x, perpendicular to the heat-source surface in advancing time — in the bell-shaped form of a normal distribution frequency function — is characteristic for this particular one-dimensional heat-conducting process in a transistor, disregarding the initial duration of the heat-dissipating electrical turnover transient. The conditions are qualitatively depicted in Fig. 2(a) as $\Delta T(x)$ function of distance, utilizing time as a parameter, where the normal frequency function is split into two equal and symmetrical parts along the $x = 0$ mean value and jointed symmetrically to both boundaries of the heat source of X/ξ equivalent thickness in which latter the temperature is assumed as being uniformly ΔT_m. In Fig. 2(b) the time dependence of ΔT_m maximal (mean) value of the heat source is shown.

The *thermal penetration depth* r_ϑ, *depending on the square root of time*, can be defined as the distance until the elevated temperature due to a step-wise increase of dissipated electrical power reaches in a given time, that is, where the inflexion point of the bell-shaped $\Delta T(x)$ function lies. Differentiating the $r_\vartheta(t)$ time function, Eq. (9) yields the propagation end-velocity of heat conduction as

$$v_\vartheta(t) = \frac{d}{dt} r_\vartheta(t) = \frac{d}{dt} \sqrt{2\,\Theta t} = \sqrt{\frac{\Theta}{2t}}, \tag{10}$$

whilst the *average* thermal propagation velocity during a given t time is

$$\bar{v}_\vartheta(t) = r_\vartheta(t)/t = \sqrt{2\Theta/t} = 2\,v(t)\,. \tag{10a}$$

Utilizing Eqs (9) and (10), the thermal penetration depth and propagation end velocity are given in Table II depending on time for germanium and

Table II

Thermal propagation end velocity (v_ϑ) and the related thermal penetration depth (r_ϑ) as functions of time

	t (μ sec)	0,01	0,03	0,1	0,3	1	3	10	30	100	Unit
v_ϑ	Ge	44	25,4	14	8,10	4,40	2,54	1,40	0,81	0,44	m/sec
	Si	49	28	15,5	8,95	4,90	2,80	1,55	0,895	0,49	m/sec
r_ϑ	Ge	0,78	1,43	2,5	4,53	7,8	14,3	25	45,3	78	μm
	Si	0,98	1,79	3,1	5,66	9,8	17,9	31	56,6	98	μm

silicon, in a time range covering the swithcing times of most practical transistors. For comparison, the depletion layer width in the dependence of V_{CB} collector reverse voltage and of ϱ_n resistivity of the lightly doped junction side are given both for germanium alloyed pnp and silicon planar npn transistors in Table III. (By these types the lightly doped side is n-type material.)

Table III

Width of collector depletion layer vs. reverse voltage V_{CB} and depending on the ϱ resistivity of the lightly doped junction side

	$\varrho\Omega \cdot$ cm / V_{uu} [V]	1	2	5	10	20	50	100	200	Unit
Germanium p^+-np-^+ alloyed	0,5	0,428	0,604	0,95	1,35	1,90	3,00	theoretical beyond the avalanche breakdown		μm
	1	0,604	0,855	1,35	1,90	2,70	4,28			
	2	0,855	1,20	1,90	2,70	3,82	6,04	8,55		
	5	1,35	1,90	3,00	4,28	6,04	10	13,5	19	
	10	1,90	2,70	4,28	6,04	8,55	13,5	19	27	
Silicon n^+-p-n planar & mesa	0,5	0,365	0,515	0,81	1,15	1,62	2,58	beyond the theoretical avalanche breakdown		μm
	1	0,515	0,73	1,15	1,62	2,30	3,65			
	2	0,73	1,03	1,62	2,30	3,26	5,15	7,30		
	5	1,15	1,62	2,58	3,65	5,15	8,15	11,5	16,2	
	10	1,62	2,30	3,65	5,15	7,30	11,5	16,2	23	

The ranges of V_{CB} and ϱ_n here also cover the practical values of transistors and the depletion layer width is calculated on the basis of Eq. (6).

Comparing the r_ϑ thermal penetration depth occurring at a switching time characterizing a given transistor type, to the depletion layer width taking place at a usual V_{CB} voltage on the same transistor, one can conclude that r_ϑ and X fall in the same order of magnitude. A detailed analysis from this point of view will be dealt with later in the course of practical numerical examples. Presenting here too extreme examples, let us consider a bulky high-voltage, low-speed germanium pnp power transistor with $\varrho_n = 10$ ohm · · cm base resistivity and at $V_{CB} = -50$ V which gives $X = 13.5$ μm while at $t_{off} = 30$ μsec switching-off time $r_\vartheta = 45.3$ μm. The other extreme siatiation is a low-voltage, low-power, silicon planar npn high-speed switching transistor with $\varrho_n = 0.5$ Ohm · cm collector epitaxial layer and $t_{off} = 30$ nanosec switch-off time, at $V_{CB} = 5$ V which yields $X = 0{,}81$ μm and $r_\vartheta = 1{,}79$ μm. Thus the conclusion can be drawn that during the switchover time of practical transistors the ratio of the maximum thermal penetration depth to the maximum depletion layer width hardly exceeds 3.

In the next step the "equivalent" thermal penetration depth should be defined, since expression (9) only gives the r_ϑ standard deviation and ΔT_m mean (i.e., maximum) values of the bell-shaped $\Delta T(x)$ distribution function. The bell-shaped frequency function should be substituted by a rectangle of uniform $\Delta T_m(t)$ height and a base width $r_{\vartheta eff}(t)$ corresponding to a value where the area $\Delta T_m(t) \cdot r_{\vartheta eff}(t)$ is exactly equal to the half area (i.e., half heat energy) below the bell-shaped normal $\Delta T(x)$ distribution frequency function, as is shown in Fig. 3. [It is obvious from Fig. 2(a) that

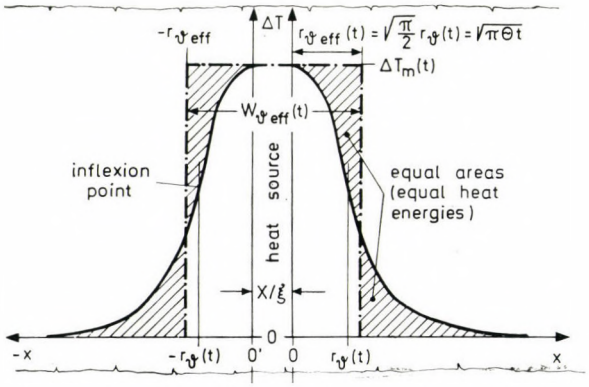

Fig. 3. Definition of equivalent thermal penetration depth $r_{\vartheta eff}$ and the equivalent thickness of heated-up volume section $W_{\vartheta(i)}$. The heat source has an equivalent thickness X/ξ and along both sides the temperature distribution is normal, showing the halved bell-shaped frequency distribution curves with the standard deviation r_ϑ at both inflexion points. The heated-up volume section can be substituted by a layer of $W_{\vartheta eff}$ width or $(X/2\xi) + r_{\vartheta eff}$ half-width, in which the temperature distribution is constant and temperature amounts to ΔT_m maximal value

the amount of original thermal energy remains unaltered in the function of time and only the spread r_ϑ along distance x increases and the mean value ΔT_m decreases in the same proportion, leaving the area under the distribution frequency function unaltered.] Since the normal distribution written in general form is

$$\frac{1}{\sigma\sqrt{2\pi}} \exp\left(-\frac{x^2}{2\sigma}\right) \text{ gives at } x = 0 \text{ the value } 1/(\sigma\sqrt{2\pi}),$$

consequently the standard deviation σ must be multiplied by $(\sqrt{2\pi/2}) = \sqrt{\pi/2}$ to gain a rectangle of $1/(\sigma\sqrt{2\pi})$ height and having the same area as the half area under the bell-shaped original normal distribution frequency function. Thus, $r_\vartheta(t)$ of expression (9) must be multiplied by $\sqrt{\pi/2}$ too, yielding

$$r_{\vartheta\, eff}(t) = (\sqrt{\pi/2}) r_\vartheta(t) = \sqrt{\pi\Theta t}. \tag{9a}$$

4. The equivalent volume of the heat source

The temperature distribution along the width of the collector depletion layer (as the heat source) is actually not constant. At a step junction (i.e., in the case of an alloyed transistor) the field strength E decreases linearly from the maximum value E_M at the metallurgical junction (that is, $x = 0$ in Fig. 4) along the distance x within the lighter doped junction side till $E = 0$ at $x = X$ boundary of the depletion layer. At the same time the potential V as the integral of E, decreases with the square of x from the maximum value V_{CB} at $x = 0$, till $V = 0$ at $x = X$, cf. Fig. 4. Since the heat generation in the depletion layer originates from the inelastic collisions between phonons (i.e. the atomic binding forces of the crystal lattice) and the charge carriers — in our case electrons — that is, heat generation is proportional to the kinetic energy of electrons accelerated by the electrical field, it is obvious that heat generation will be maximal along the metallurgical junction where potential is the maximal $V = V_{CB}$ and its gradient also being the maximal $E = E_M$, and will be zero at the boundary $x = X$. Since the impact heat energy of a colliding electron equals the product of V potential runned through till the collision and the electron charge q, and on the other hand, on the basis of Eq. (6) the dependence of potential on distance may be expressed as $V(x) = (x/X)^2 V_{CB}$, thus the impact energy of charge carriers can be written as $qV(x) = (x/X)^2 qV_{CB}$, which yields, after integration from $x = 0$ till $x = X$

$$\frac{qV_{CB}}{X^2}\int_0^X x^2\,dx = \frac{qV_{CB}}{3X^2}\left[x^3\right]_0^X = \frac{X}{3}qV_{CB} = \frac{X}{\xi}qV_{CB} \tag{11}$$

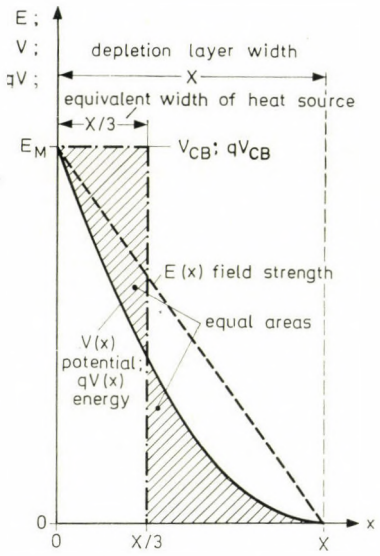

Fig. 4. Explanation of the equivalent heat source thickness X/ξ at a step junction. O and X are the bounds of the depletion layer width, along which field strength E decreases linearly whilst potential V_{CB} and carrier-phonon impact energy qV_{CB} decrease with the square of distance to the metallurgical junction. The equivalent width is $X/3$ within which the impact energy and so temperature may be assumed as constant and maximal

which in fact gives the width $X/3$ of such an equivalent heat source where the impact energy of carriers is assumed to be a constant qV_{CB} value, or in other words, the depletion layer having nonuniform thermal energy distribution may be substituted by an equivalent heat source of uniform maximal thermal energy in a form of a rectangle having $X/3$ base width and the same area as the $qV(x) = (x/X)^2 qV_{CB}$ function, cf. Fig. 4. If the junction is linearly graded (as it is nearly so by planar or mesa transistors), the $E(x)$ field strength function decreases quadratically along the distance x instead of being linear and, consequently, the $V(x)$ potential function decreases with the third power of x. Hence, the equivalent thickness of the heat source will be $X/4$ in this case. Thus, $1/\xi$ denotes the multiplying factor of the equivalent heat source thickness, substituting $\xi = 3$ at a step junction and $\xi = 4$ at a linearly graded junction. The equivalent volume of the heat source is then AX/ξ where A is the collector junction area.

5. The general time dependence of the "inner" thermal resistance and "inner" thermal capacity

The equivalent thickness of the warmed-up volume section till a given time t, along both sides of the junction will be the sum of the equivalent heat source thickness and the doublefold value of the equivalent therma

penetration depth, the latter as expressed in Eq. (9a), since the heat energy spreads symmetrically into both sides of the laminar heat source. Thus, denoting this overall thickness of the warmed-up volume section by $W_{\vartheta eff}$:

$$W_{\vartheta eff}(t) = (X/\xi) + 2\, r_{\vartheta eff}(t) = (X/\xi) + \sqrt{4\pi\Theta t}\,, \tag{12}$$

and in the same way, the equivalent volume of the head-up section will be Eq. (12) multiplied by the junction area A. Multiplying the volume by the specific density and specific heat, one gets the "inner" heat capacity of the warmed-up volume section:

$$C_{\vartheta(i)}(t) = \gamma c_\vartheta A\, [(X/\xi) + \sqrt{4\pi\Theta t}]\,. \tag{13}$$

The "inner" thermal resistance $R_{\vartheta(i)}$, that is, the connection between the warmed-up volume section of A area and $W_{\vartheta eff}$ thickness and the surrounding own-material of the wafer (the latter incomparably larger in volume), is obviously proportional to the half thickness $W_{\vartheta eff}(t)/2 = (X/2\xi) + r_{\vartheta eff}$ of the heated-up "inner" volume, further it is inversely proportional to area A and the specific thermal conductivity λ_ϑ, in full analogy with the electrical conduction. The expression must be divided by 2 since the thermal conduction is symmetrical on both sides of the laminar heat source. Furthermore, a constant β is introduced which is related to the heat transfer and junction geometry: β approaches unity only if the collector layer lies deep in the wafer and $r_{\vartheta eff}$ falls short of the collector junction depth at a mesa or planar structure, but approximates 2 if there is a shallow collector junction, $r_{\vartheta eff}$ exceeding considerably the junction depth. At an alloyed structure, the indium button collector contact lies in the proximity of the metallurgical junction and indium has a bit worser heat-conductive properties than germanium*, thus the constant β should be assumed to be a bit higher than unity, say $1{,}2 \div 1{,}5$. Hence:

$$R_{\vartheta(i)}(t) = \beta\, \frac{r_{\vartheta\,\mathrm{eff}}(t) + (X/2\xi)}{2\lambda_\vartheta A} = \beta\, \frac{\sqrt{\pi\Theta t} + (X/2\xi)}{2\lambda_\vartheta A}\,. \tag{14}$$

The above results are valid only if the thermal penetration depth $r_{\vartheta eff}$ falls well short of the minimum geometrical dimension of the wafer, i.e. the thickness of it. If the penetration depth exceeds the boundary of wafer thickness well, after the passing off of the turnover transient, the thermal resistance of the wafer contacting or soldering-on should also be taken into consideration. The fact that the wafer is soldered-on onto a header or not, can radically influence the thermal conditions in this case. Furthermore, the existing or

* Thermal material constants for indium [9] are at 25 °C: $\gamma = 7{,}3$ g · cm^{-3}; $c_\vartheta = 0{,}24$ Wsec g^{-1} °C^{-1}; $\lambda_\vartheta = 0{,}25$ W cm^{-1} °C^{-1} and consequently, $\Theta = 0{,}137$ cm^2 sec^{-1}.

lacking external heat sink alters substantially the thermal relations in such a case if the wafer is soldered-on onto a header or base plate. In the latter case, Eqs (13) and (14) should be rewritten as

$$C_{\vartheta(i)}(t) = \gamma_{sc}\, c_{sc}\, A_{sc}\, [d_{CB} + X/\xi) + \sqrt{\pi\Theta_{sc}\, t_{sc}}] + \gamma_m\, c_m\, A_m \sqrt{\pi\Theta_m\, t_m} + \ldots \quad (13a)$$

and

$$R_{\vartheta(i)}(t) = \frac{\sqrt{\pi\Theta_{sc}\, t_{sc}} + (X/\xi)\, d_{CB}}{\lambda_{\vartheta sc}\, A_{sc}} + \frac{\sqrt{\pi\Theta_m\, t_m}}{\lambda_{\vartheta m}\, A_m} + \ldots \quad (14a)$$

where the indices "*sc*" denote the material constants of the semiconductor wafer, A_{sc} the collector junction area and t_{sc} the time in which the heat penetration reaches the semiconductor-soldering metal boundary; whilst indices "*m*" denote the material constants of the solder- or header metal, A_m the soldering-on area of the wafer involved in actual heat conduction, and, finally, t_m the duration of heat conduction in the header metal. Naturally, $t = t_{sc} + t_m + \ldots$. The collector junction depth is marked by d_{CB}.

In the case of a usual silicon planar transistor, the depth of the collector junction is relatively shallow: it lies $2 \div 10$ μm below the emitter contact surface (or the SiO_2-Si interface). This depth falls in the magnitude order, or exceeds it but insignificantly, the thermal penetration depth taking place during the usual $10 \div 300$ nanosec switching times of such transistors. Since the thermal conductivity of the alumizized or gilded emitter and base contact areas as well as the thin gold bonding wires may be neglected, the thermal wave front arriving from the collector junction is reflected. Consequently, a factor β near to 2 should be utilized and the first terms of expressions (13a) and (14a) should be used if $r_{\vartheta eff} > d_{CB}$ but $r_{\vartheta eff}$ falls considerably short of the wafer thickness. The same also holds for an alloyed Ge transistor with $d_{CB} = 0$; $A_{sc} = A_m$; $t_{sc} = t_m = t$ and the index m denoting the material constants of indium. In this latter case, a third additive term in the same form as the second one follows in both expressions (13a) and (14a) if the heat penetration depth exceeds the boundary of indium button-base plate metal joint, substituting in the third term the material constants of the base plate metal, the area of joint and the time in which the thermal wafer front spreads in the base plate metal.

6. The "inner" thermal cooling-down time constant

Since the time function of cooling-down [e. g. after a Dirac-delta heat transfer, cf. Eq. (8)], is not an exponential one but a normal distribution, there is no physical reason to for considering the "inner" thermal time constant as the product RC in the electrical analogy, all the more because both the "inner" thermal capacity $C_{\vartheta(i)}$ and "inner" thermal resistance $R_{\vartheta(i)}$ are time-dependent. Hence, the definition of "inner" thermal time constant is more or

less arbitrary: it will be the time $\tau_{\vartheta(i)}$ after which the initial $\Delta T_m(t = 0)$ maximal temperature diminishes to the relative value $1/\epsilon \cong 1/2{,}72 \cong 0{,}368$, as is shown in Fig. 2b. — Since the initial heat energy remains constant but spreads only in the volume along both sides of the collector junction, the "inner" thermal time constant $\tau_{\vartheta(i)}$ will be the time in which the heat energy occurring in the thin laminar heat source of X/ξ equivalent thickness, spreads in a volume $\epsilon = 2{,}72$-times larger as the heat source volume, i. e. 2,72-times larger in thickness as the original X/ξ value. Thus, utilizing Eq. (12):

$$\epsilon \cong 2{,}72 = \frac{(X/\xi) + \sqrt{4\pi\Theta\tau_{\vartheta(i)}}}{(X/\xi)},$$

which yields

$$\tau_{\vartheta(i)} = \frac{(\epsilon - 1)^2}{4\pi\Theta}\left(\frac{X}{\xi}\right)^2 \cong \frac{2{,}36}{\Theta}\left(\frac{X}{\xi}\right)^2, \tag{15}$$

hence the inner thermal time constant depends only on the square of the collector depletion layer thickness*, besides the material constant Θ and type of the junction ($\xi = 3$ or 4), as is shown in Fig. 5. The value of $\tau_{\vartheta(i)}$ is surprisingly low, at least as compared to the switching times of a given transistor. Considering again two extreme cases of

(a) a bulky, low-speed alloyed Ge pnp power transistor ASZ 18 operating in a c. e. inverter circuit of Fig. 8 with the ratings of $V_{CC} = -30$ V; $I_{Cp} = -6$ A; $I_{BX} = -0{,}6$ A

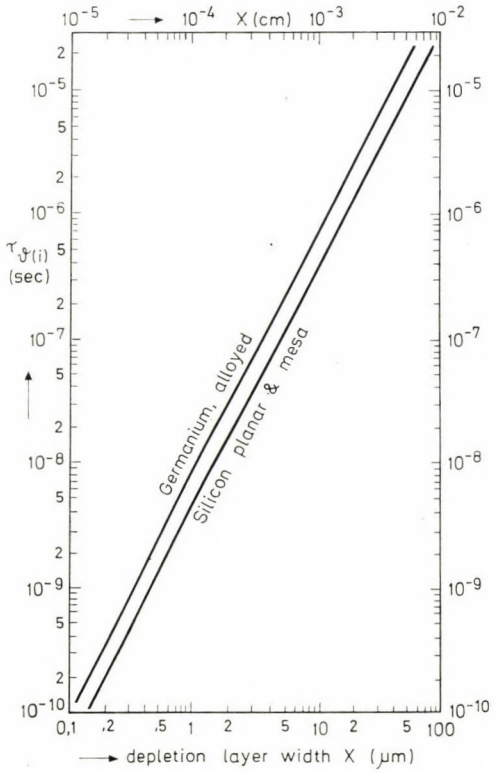

Fig. 5. The "inner" cooling-down thermal time constant $\tau_{\vartheta(i)}$ in dependence of the depletion layer thickness X, by alloyed Ge($\xi = 3$) and planar or mesa Si($\xi = 4$) transistor structures

* However, X depends on the square root of V_{CB} voltage, thus $\tau_{\vartheta(i)}$ is linearly proportional to V_{CB}.

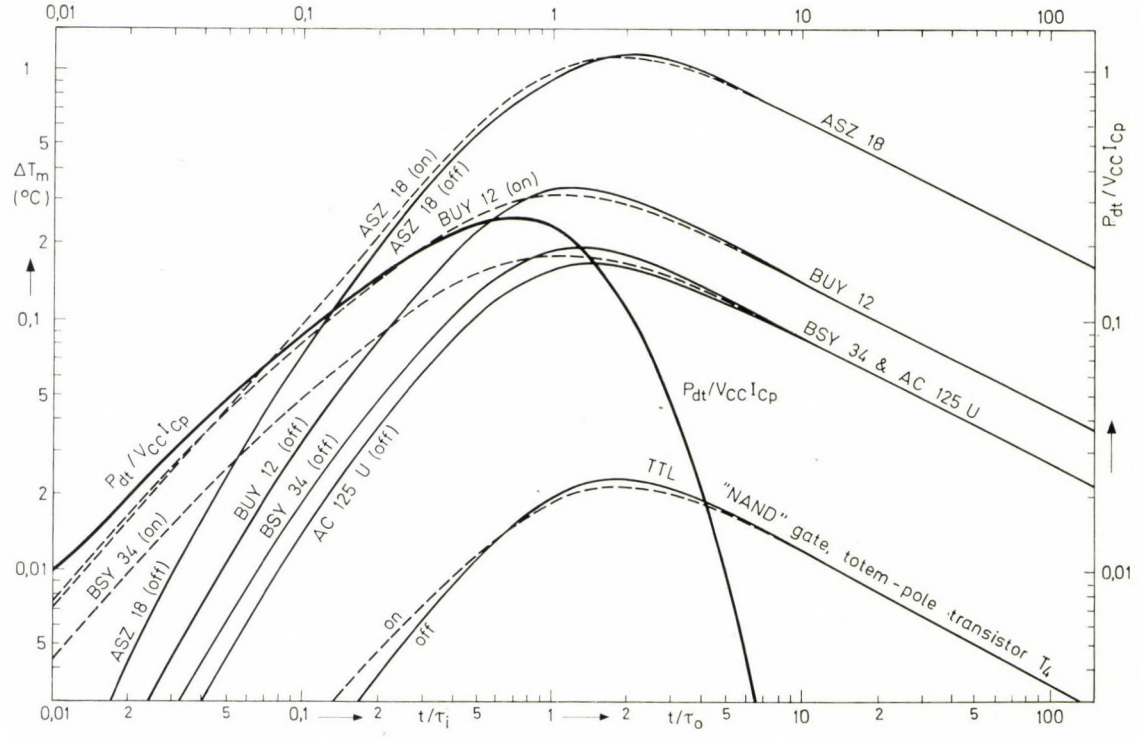

Fig. 6a. Transient temperature jump ΔT_m of the collector junction during switchover of various transistor types vs. normalized time t/τ_i at turning-on (dashed lines) and t/τ_0 at turning-off (solid lines). Also the time function of transient turnover power P_{dt} is shown in $P_{dt}/V_{CC}I_{Cp}$ normalized term (thick line). The falling sections have a slope of $-1/2$ in the doubly logarithmic plot since temperature decreases with the square root of time. ASZ 18 and BUY 12 are power transistors while AC 125 U and BSY 34 are medium-power types

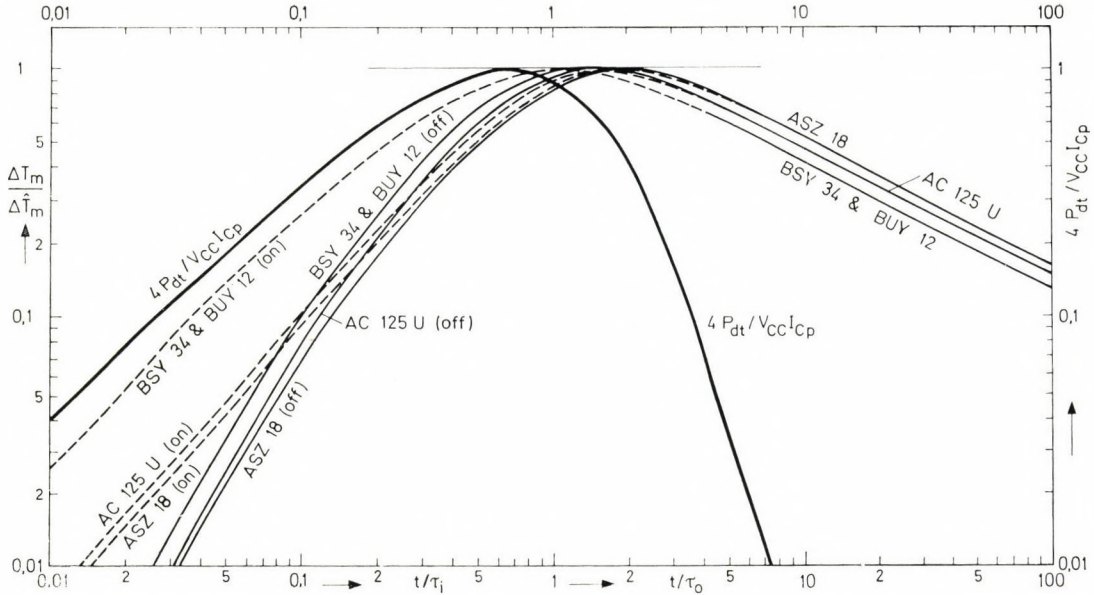

Fig. 6b. The temperature vs. time curves of Fig. 6a. normalized as $\Delta T_m/\Delta \hat{T}_m$, referred to their peak values. The time difference between the maxima of the temperature curve $\Delta T_m/\Delta \hat{T}_m$ and the power function $P_{dt}/P_{dt\,\max}$ fairly approximate the "inner" thermal time constant $\tau_{\vartheta(i)}$ of the various transistors save the ASZ 18. Note that the curves of both silicon (planar and mesa) types coincide and there is also an insignificant difference between the Ge alloyed types

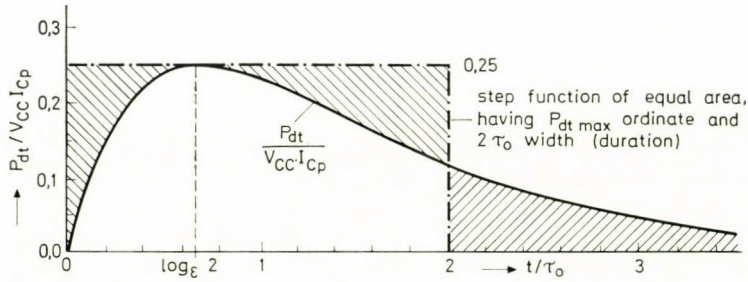

Fi;. 7. Equivalent duration of the turnover transient power vs. time function. The equivalent step function of power has an uniform height of $P_{dt\,max} = V_{CC}I_{Cp}/4$ and a duration of $t = 2\tau_0$ at switching-off or $t = 2\tau_i$ at switching-on, since the shaded areas lying left and right from the abscissa $t/\tau = 2$ have equal areas (thus, representing equal energies)

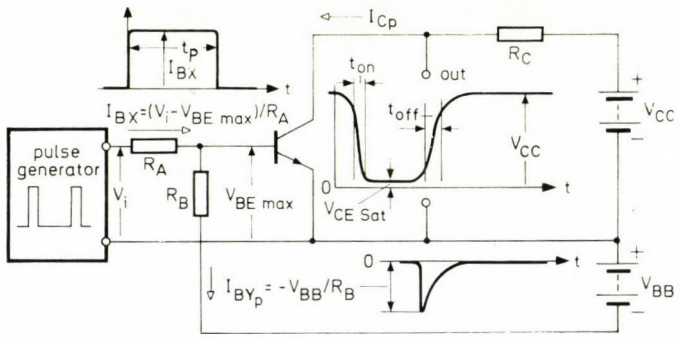

Fig. 8. Common-emitter inverter circuit and its characteristic parameters and wave forms corresponding to the numerical examples of Table IV and Figs 6a and b

forward base current and $I_{BY} = 0{,}6$ A peak drawing-out base current for fast removal of stored charges in the base, in which operating point $t_{off} = 35\ \mu$ sec max. The base resistivity is $\varrho_n = 5$ ohm · cm and $\xi = 3$ in the step junction. The depletion layer width is $X = 5{,}15\ \mu$m at $V_{CC}/2 = -15$ V where the peak transient power occurs, calculated from Eq. (6). On the basis of expression (15), $\tau_{\vartheta(i)} \cong 0{,}2\ \mu$ sec $\gg t_{off} = 35\ \mu$sec.

(b) The minute epitaxial planar transistor (T_4) in the totem-pole output stage of a TTL "NAND" gate integrated circuit, e. g. the SN 7400 N. Operating data during turnover, just at the instant of peak transient turnover power (cf. Fig. 9): $V_{CE} \cong 1{,}3$ V; $V_{CB} \cong 0{,}7$ V; $I_{Cp} \cong 15$ mA. The switching-off time is for this transistor $t_{off} \cong 5$ nanosec, and the collector depletion layer penetrates into the epitaxy of 0,1 ohm · cm resistivity. Thus, with $V_{CB} = 0{,}7$ V eq. (6) gives $X = 0{,}137\ \mu$m. Calculating with $\xi = 4$, Eq. (15) yields $\tau_{\vartheta(i)} \cong 10^{-10}$ sec $= 0{,}1$ *nanosec* $\ll t_{off} = 5$ nanosec.

Thus, it is proved that

$$t_{on} \gg \tau_{\vartheta(i)} \ll t_{off} \quad \text{or} \quad \tau_i \gg \tau_{\vartheta(i)} \ll \tau_0. \tag{16}$$

7. Calculation of the temperature vs. time function and the estimate of the peak temperature during switch-over

The exact calculus of the $\Delta T_m(t)$ function is rather sophisticated. However, the general method is presented here and numerical examples are given

as well, to let one make comparison to the results of a more simple estimation, the latter yielding the peak temperature jump $\Delta\hat{T}_m$ directly.

Eq. (2) gives the time dependence of transient turnover power P_{dt}. Multiplying this instantaneous power by the thermal resistance between the heat source of (X/ξ) equivalent thickness and the surrounding bulk, i.e. by $R_{\vartheta(i)}(t=0) = R_{\vartheta(hs)}$ at a given instant, one gets the $\Delta T_m(t=0)$ temperature jump due to the instantaneous dissipated power P_{dt} at the given instant. However, both P_{dt} and X are time-depending. As it may be seen in Eq. (2), the $P_{dt}(t)$ function is symmetrical for switching-on (by substituting τ_i) and switching-off (substituting τ_0). Contrary to this, the $X(t)$ function may be derived from the voltage dependence of the depletion layer width, utilizing Eq. (6), and V_{CB} voltage there depends on time exponentially (see lower diagram in Fig. 1), the latter showing up only complementary symmetry for switching-on and - off: $V_{CB} = V_{CC} \cdot \exp -(t/\tau_i)$ for switching-on and $V_{CB} = V_{CC}\,[1\text{-}\exp(-t/\tau_0)]$ for switching-off, cf. Eqs (1a) and (1d). Thus, the resulting $\Delta T_m(t)$ function is not symmetrical for switching-on and -off. Consequently, the "inner" thermal resistance of the *heat source* will be from Eq. (14), substituting there $r_{\vartheta eff}(t=0) = 0$, thus $\sqrt{\pi\Theta t} = 0$, also utilizing Eqs (6) and (1.a):

$$R_{\vartheta(hs)on}(t) = \frac{\beta X(V_{CB})}{4\xi\lambda_\vartheta A} = \frac{\beta}{4\xi\lambda_\vartheta A}\sqrt{2\,\varepsilon_r\,\varepsilon_0\,\mu_n\,\varrho_n\,V_{CB}\cdot\exp\left(\frac{t}{\tau_i}\right)} \qquad (17a)$$

for switching-on and using the afore mentioned equations but Eq. (1d):

$$R_{\vartheta(hs)off}(t) = \frac{\beta}{4\xi\lambda_\vartheta A}\sqrt{2\,\varepsilon_r\,\varepsilon_0\,\mu_n\,\varrho_n V_{CC}\left[1-\exp\left(-\frac{t}{\tau_o}\right)\right]} \qquad (17b)$$

for switching-off.

Multiplying this expression by the time function of instantaneous transient turnover power, i.e. by Eq. (2), one gets the instantaneous temrature increment in the junction at a given instant t. However, this temrature increment $P_{dt}(t)$. $R_{\vartheta(hs)}(t)$ builds up over a similar temperature increment preceding this one by the infinitesimal time difference *dt* and diminishing during the time interval *dt* by heat conduction. In other words, the temperature integrates up during the turnover transient and will be much higher than $P_{dt}(t) \cdot R_{\vartheta(hs)}(t)$.

To attack this problem, the electrical circuit analogy of this thermodynamical process is made use of. In the electrical equivalent, voltage V corresponds to temperature difference, current I to thermal power, further electrical resistance R to thermal resistance, capacitance C to thermal capacity. This particular thermal problem is in analogy with a resistor-

capacitor network, the capacitor C being uncharged and series-connected to a charging resistor R and the whole network connected to a voltage source V, to simulate the switching-on thermal process; and, on the other hand, the capacitor charged-up to voltage V is discharged across the resistor, to simulate the switching-off thermal process. For the switching-on process the voltage vs. time differential equation for the electrical equivalent will be

$$V(t) = R \cdot I(t) + \frac{1}{C} \int_0^t I(t)\, dt\,.$$

Of course, the well-known exponential solution of this equation cannot be used for solving the thermodynamical problem since $R_{\vartheta(i)}$ and $C_{\vartheta(i)}$ thermal quantities are both not constants but time-dependent and, on the other hand, the power vs. time function substantially differs here from the exponential $R \cdot I(t)$ one in the electrical analogy. Thus, the differential equation is employed directly, leading with the thermal problem at switching-on to

$$\Delta T_m(t) = P_{dt}(t) \cdot R_{\vartheta(hs)}(t) + \frac{1}{C_{\vartheta(i)}(t)} \int_0^t P_{dt}(t)\, dt \tag{18}$$

where the first term on the right-hand side corresponds to the instantaneous temperature jump due to the instantaneous power $P_{dt}(t)$ while the second term refers to the integrating-up tendency of the temperature and is in fact the thermal energy divided by the heat capacity of the warmed-up volume section, from the beginning of the turnover transient till the instant t.

Thus, utilizing Eq. (2) for $P_{dt}(t)$, further Eq. (4) for the expression of switching-on energy time function and, further, making use of Eq. (17a) for the expression of $R_{\vartheta(hs)on}(t)$ heat source-to-wafer thermal resistance and, finally, employing relationship (13) for $C_{\vartheta(i)}(t)$, one gets the end result for switching-on as:

$$\Delta T_{m(on)}(t) = \frac{V_{CC}\, I_{Cp}}{A} \left\{ \left[\exp\left(-\frac{t}{\tau_i}\right) - \exp\left(-\frac{2t}{\tau_i}\right) \right] \cdot \right.$$
$$\cdot \frac{\beta}{4\xi\lambda_\vartheta} \sqrt{2\,\varepsilon_r\,\varepsilon_0\,\mu_n \varrho_n V_{CC} \cdot \exp\left(-\frac{t}{\tau_i}\right)} + \frac{\tau_i}{2\gamma c_\vartheta} \cdot$$
$$\left. \cdot \frac{1 - 2\exp\left(-\frac{t}{\tau_i}\right) + \exp\left(-\frac{2t}{\tau_i}\right)}{\sqrt{4\pi\Theta t} + \frac{1}{\xi}\sqrt{2\,\varepsilon_r\,\varepsilon_0\,\mu_n\,\varrho_n V_{CC} \cdot \exp\left(-\frac{t}{\tau_i}\right)}} \right\}, \tag{19a}$$

and similarly for switching-off but applying Eq. (17b) for $R_{\vartheta(hs)off}(t)$:

$$\Delta T_{m(off)}(t) = \frac{V_{CC} I_{Cp}}{A} \left\{ \left[\exp\left(-\frac{t}{\tau_0}\right) - \exp\left(-\frac{2t}{\tau_0}\right) \right] \cdot \right.$$

$$\cdot \frac{\beta}{4\xi\lambda_\vartheta} \sqrt{2\,\varepsilon_r\,\varepsilon_0\,\mu_n\,\varrho_n V_{CC}\left[1 - \exp\left(-\frac{t}{\tau_0}\right)\right]} + \frac{\tau_0}{2\gamma c_\vartheta} \cdot$$

$$\left. \cdot \frac{1 - 2\exp\left(-\frac{t}{\tau_0}\right) + \exp\left(-\frac{2t}{\tau_0}\right)}{\sqrt{4\pi\Theta t} + \frac{1}{\xi}\sqrt{2\varepsilon_r\varepsilon_0\mu_n\varrho_n \cdot V_{CC}\left[1 - \exp\left(-\frac{t}{\tau_0}\right)\right]}} \right\} . \quad (19b)$$

Of course these relationships are valid only if $V_{CC} \gg V_{CE\mathrm{sat}}$; $I_{Cp} \gg I_{CB0}$; further $\sqrt{4\pi\Theta t} < d_{CB}$ collector diffusion depth and $\sqrt{4\pi\Theta t}$ remains well within the boundaries of the semiconductor wafer.

Fig. 6/a shows the $\Delta T_m(t)$ functions both for switching-on (broken lines) and switching-off (solid lines) with the time function normalized as t/τ_i or t/τ_0 for five characteristic transistor types of: (a) ASZ 18, a low-speed, alloyed Ge pnp power transistor; (b) AC 125 U, a medium-speed, medium-power, alloyed Ge pnp transistor; (c) BUY 12, a medium-speed, Si npn epitaxial mesa, high-power transistor; (d) BSY 34, a high-speed, medium-power, Si npn epitaxial planare transistor and finally, (e) the minute totem-pole output transistor between the output and ground terminals of a typical TTL-series NAND gate, e.g. SN 7400 N (see Fig. 9), the same as given earlier in example (b) of Section 6. All transistors, except the TTL IC output stage, operate in a common-emitter inverter of Fig. 8 at an operating point given in Table IV as well as in the numerical examples of the last section. In Fig. 6(a) the normalized $P_{dt}(t)$ function is also depicted as $P_{dt}/V_{CC}I_{Cp}$ vs. (t/τ), for comparison. In Table IV are also presented the maximal values of the function as $\Delta\hat{T}_m$ both at turning-on and -off, as well as the loci of the maximums in normalized terms t/τ_i and t/τ_0. As it can be seen, the maximal values $\Delta\hat{T}_m$ are surprisingly low contrary to the fact that the collector current levels in the inverter service are identical to the data-sheet limit-values and V_{CC} voltages also approximate the allowed limit level, leading e.g. to 100 W swithcing power surge at the BUY 12 type. The maximal temperature jump is only 1,2 °C at the alloyed Ge power transistor type ASZ 18 and only 0,34 °C at the Si mesa BUY 12 power type, while it lies between 0,165 ÷ 0,2 °C both at the alloyed Ge and planar Si medium-power types. Negligibly low is the peak temperature jump at the TTL IC transistor contrary to the minute geometrical dimensions, obviously because the very low voltage and current switching levels: approx. 0,023 °C.

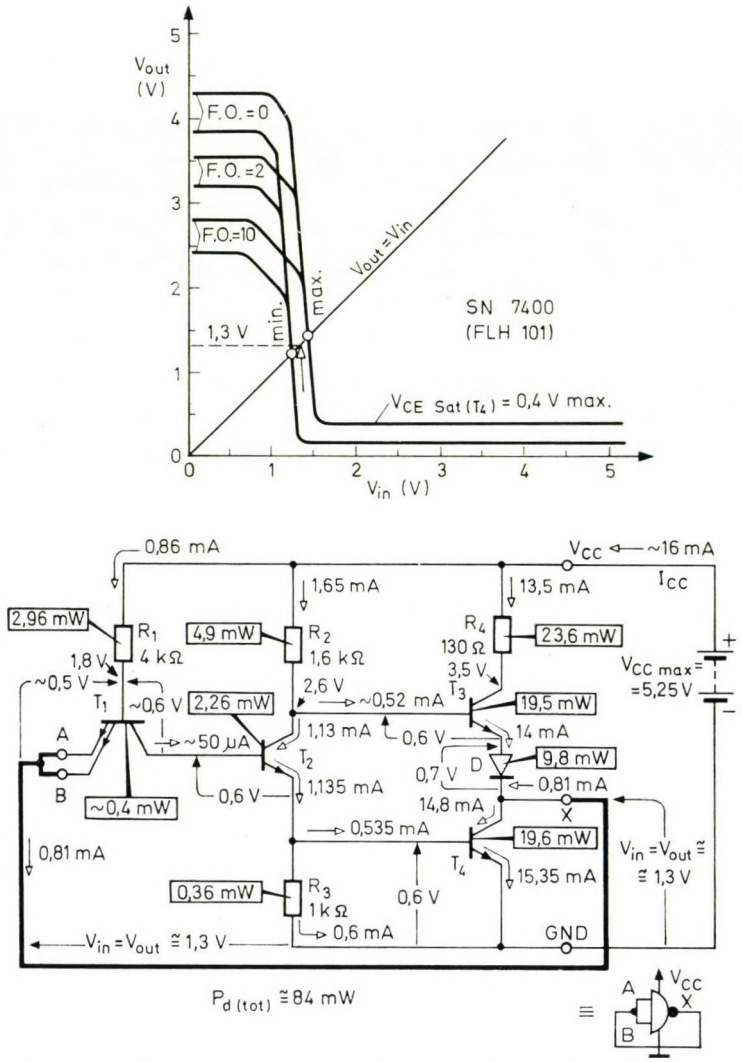

Fig. 9. Circuit diagram (below) and $V_{out}(V_{in})$ transfer characteristics (top) of a typical TTL IC "NAND" gate. Voltages, currents (arrows) and dissipated powers (in rectangles) are shown at the instant of maximum power during commutation. Maximal power dissipation of active elements occurs when $V_{out} = V_{in}$ (simulated by the direct connection of inputs to the output), all transistors being in the active region. The lower transistor T_4 in the totem-pole output stage has in this condition the highest power dissipation of nearly 20 mW

Of course, the afore mentioned peak temperature jumps are related to an even current distribution along the collector (or emitter) junction without any appreciable current concentration, referring to a fair structure: the junction area A equals to the nominal area A_{nom}. This way, the $\Delta\hat{T}_m$ *maximal temperature jumps are completely harmless from degradation point of view, if the structure is fair, because the usual* $\Delta\hat{T}_m$ *peak values ranging*

Table IV

Thermal and electrical relations during switching-off at some characteristic transistor types

Technology / Type	Alloyed germanium		Mesa or planar silicon		TTL IC „NAND" gate, totem pole transistor T_4 (e. g. SN 7400 N)
	ASZ 18 power	AC 125 U medium power	BUY 12 power	BSY 34 medium power	
V_{CC}, supply voltage (V)	−30	−40	40	40	∼ 1,3 V=V
I_{Cp}, peak collector current (A)	− 6	−0,25	10	0,5	$\sim 1{,}55\times10^{-2}$
I_{BX}, driving base current (A)	0,6	−0,025	1	0,05	see Fig. 9
I_{BY}, charge-drawout base current (A)	0,6	0,025	−1	−0,025	
$t_{off\,\max}$, switching-off time (μsec)	35	1	0,5	0,095	$\sim 5\times10^{-3}$
$P_{dt\,\max}$, turnover power (W)	45	2,5	100	5	$\sim 2\times10^{-2}$
X_Φ, depletion layer with (μm) (at $V_{CB} = V_{CC}/2$)	5,15	3,82	6,2	3,26	0,137 (at V_{CE} = = 1,3 V)
$W_{\vartheta eff}$ (at $t = t_{off}$) S (μm)	132	23,3	18,2	8,07	1,69
A_{nom} nominal junction area (mm^2)	5	0,385	5,45	0,25	$\sim 1{,}2\times10^{-3}$
i_{Cnom}, nominal current density (A/mm^2)	1,2	0,65	1,84	2	∼ 1,3
$V_{\vartheta d} = A_{nom}\, X_\Phi/\xi$ heat source volume (mm^3)	$8{,}6\times10^{-3}$	$4{,}9\times10^{-4}$	$8{,}4\times10^{-3}$	2×10^{-4}	$\sim 4{,}1\times10^{-8}$
$P_{dt\,\max}/V_{\vartheta d}$ (W/mm^3) specific turnover power density	$5{,}25\times10^{3}$	$5{,}1\times10^{3}$	$1{,}2\times10^{4}$	$2{,}45\times10^{4}$	$\sim 4{,}9\times10^{5}$
$L_{off}=2\tau_0 P_{dt\,\max}$ (μWsec) switching-off energy	1670	2,5	50	0,475	$\sim 1\times10^{-4}$
$V_{(\vartheta i)}=A_{nom}W_{\vartheta eff}$ ‡ (mm^3) (at $t = t_{off}$)	0,66	$8{,}9\times10^{-3}$	0,1	2×10^{-3}	$\sim 2\times10^{-6}$
$L_{off}/V_{\vartheta(i)}$ (μWsec/mm^3) specific switch-off energy density	2530	280	500	238	∼50

Table IV
(cont.)

Technology / Type	Alloyed germanium ASZ 18 power	Alloyed germanium AC 125 U medium power	Mes or planan silicon BUY 12 power	Mes or planan silicon BSY 34 medium power	TTL IC "NAND" gate, totem pole transistor T_4 (e. g. SN 7400 N)
ΔT_m, peak temperature jump estimated by Eq. (26) $\neq$ (°C)	1,46	0,17	0,29	0,135	~0,029
ΔT_S, at turn-on calculated by Eq. (19a)‡ (°C)	1,15	0,165	0,304	0,180	~0,0213
appearing at $t/\tau_i \cong$	1,8	1,25	1	1	1,6
ΔT_m, at turn-off calculated by Eq. (19b)‡ (°C)	1,20	0,170	0,338	0,197	~0,0236
appearing at $t/\tau_0 =$	2,1	1,4	1,15	1,2	1,75
$\tau_{\vartheta(i)}$, "inner" thermal time constant for cooling-down (μsec) (for a Dirac-delta heat pulse)*	0,2	0,12	0,175	0,045	$\sim 1 \times 10^{-19}$ sec
$\tau_{\vartheta(cd)}$, cooling-down (μsec) time at natural turning-off, for $\Delta T_m/\Delta T_m = 0{,}368$	350 ($t/\tau_0 \simeq 20$)	8,75 ($t/\tau_0 \simeq 17{,}5$)	2,7 ($t/\tau_0 \simeq 10{,}7$)	0,63 ($t/\tau_0 \simeq 14$)	$\sim 4{,}2 \times 10^{-8}$ sec ($t/\tau_0 \simeq 17$)

§ Equivalent thickness of the volume section enclosing the heat source i. e. the collector junction and heated by the turnover transient, in which the transient thermal.

The volume of the above (*s*) standing volume section heated up by the turnover transient energy.

‡ Assuming $A_{eff} = A_{nom}$, i. e. a perfect structure without considerable current concentration.

* At $V_{CB} = V_{CC}/2$.

between some tenth and some °C, fall short by $1 \div 2$ *orders of magnitude of the quasi-stationary temperature increment* $\overline{P}_{dtot}$ averaged at the period time. *Volumetric degradation might be significant only if a considerable current concentration takes place in the form of hot spots where the relative actual junction area* A/A_{nom} *may be decreased to* $10^{-2} \div 10^{-3}$, *since the peak temperature jump is inversely proportional to the actual junction area*, cf. Eqs (19). However, such excessively and originally bad structures can hardly get into a controlled and saled lot because such bad specimens fall out at the static (d. c.) or dynamical parameter measurements. A highly uneven structure can lead only to such a degree of current concentration in prolonged switching service at high current- and voltage-levels by thermal-electrical feedback (runaway), the mathematical model of which being beyond the scope of this work and being rather sophisticated as well.

Some interesting features of the $\Delta T_m(t)$ functions may be observed if they are normalized on their vertical scale as $\Delta T_m/\Delta T_m$ hence, all maxima then lie on the ordinate 1, as is shown in Fig. 6b for the afore mentioned 4 discrete transistor types. The transient turnover-power vs. time function is also normalized in such a manner as $4\,P_{dt}/V_{CC}I_{Cp}$. First of all, the switching-on and -off curves are different but only on their rising and peak section. An insignificant difference arises in the absolute maxima, cf. Fig. 6a, since switching-off maxima are a bit higher and the loci of maxima are shifted but inconsiderably toward higher t/τ_0 values at turn-off as compared to the turn-on t/τ_i maxima (see also in Table IV). The maxima of the $\Delta T_m(t)$ functions are markedly shifted in comparison with the maximum of $P_{dt\,\max}$ peak transient turnover power at $t/\tau_i = t/\tau_0 = \log_\epsilon 2$; i. e. the maxima of silicon planar or mesa transistors lie very near to $t/\tau_i \cong 1$ or $t/\tau_0 \cong 1{,}2$; whilst at the slower alloyed Ge types the maxima are between $t/\tau_i \cong 1{,}25 \div 2{,}1$, depending on type. At both silicon types, the time lag of the maximum of $\Delta T_m(t)$ function as related to the $t/\tau_i = t/\tau_0 = \log_\epsilon 2 \cong 0{,}69$ maximum of the $P_{\vartheta(i)}(t)$ function, is fairly around the $\tau_{\vartheta(i)}$ "inner" thermal time constant value given in Eq. (15) if $V_{CB} = V_{CC}/2$ is considered there [that is, at the maximal value of $P_{dt\,\max} = V_{CC}\,I_{Cp}/4$ at the instant $t/\tau_i = t/\tau_0 = \log_\epsilon 2 \cong 0{,}69$ the collector reverse voltage is just $V_{CC}/2$]. The time lag of maximal transient temperature jump in respect to maximal P_{dt} is, however, a bit higher by the alloyed Ge types, e. g. it is about 3-times the $\tau_{\vartheta(i)}$ thermal time constant by the medium-power alloyed AC 125 U and a greater difference arises only at the ASZ 18 alloyed Ge power type. Thus, $\tau_{\vartheta(i)}$ has also some physical meaning at the relatively slow turnover power transient, yielding roughly the time lag between the power- and temperature-maxima. — At the rising section of the $\Delta T_m(t)$ function, the time lag between the power- and temperature-time functions becomes continually more and more if time is increased, but the time lag is markedly less at switching-on than at switching-off. The cause of this lies — as can be observed comparing Eqs (19a) and (19b) — in the fact that at switching-off the depletion layer width increases from zero to its maximum value at $V_{CB} = V_{CC}$ and consequently the thermal resistance $R_{\vartheta(hs)}$ of the heat source also increases from zero toward its maximum and thus, the first term in the function (19b) gives lower values at a given instant t than the first term in Eq. (19a) but the rise is steeper. Contrary to this, at the beginning of switching-on, the depletion layer width (at $V_{CB} = V_{CC}$) as well as the thermal resistance $R_{\vartheta\,(hs)}$ have their maximal value and both diminish with t. This is the reason too, for the small difference in maximal values $\Delta T_{m(on)}$ and $\Delta \hat{T}_{m(off)}$, as well as in their maximum loci. However, if τ_i and τ_0 are equal, the areas below both functions $\Delta T_{m(on)}(t)$ and $\Delta T_{m(off)}(t)$ are exactly equal, i. e. both heat energies are of course equal, in spite of the differing rising sections and maxima.

If is remarkable that the $\Delta T_m(t/\tau)$ curves of both silicon types dealt with here coincide with each other exactly, while there is only an insignificant difference between the curves of alloyed Ge types. Thus, one may suggest that *a given function normalized in t/τ_i or t/τ_0 terms and as well as in $\Delta T_m/\Delta \hat{T}_m$ terms is characteristic for a given technology and it is sufficient to calculate only some points around the maximum*, to construct the whole function in this way.

Finally, let us consider the falling section of the $\Delta T_m(t)$ functions. There is no perceptible difference between the switching-on and switching-off functions if $t/\tau_i > 4 < t/\tau_0$, since, on the one hand, the first, "thermal resistance" term in Eqs (19) becomes negligible as compared to the second, "thermal capacity" term there. On the other hand, in the numerator of the second ("thermal capacity") term the exponential terms become negligible compared to 1, and finally, in the denominator, the term $\sqrt{4\pi\Theta t}$ becomes incomparably larger than the other additive term under the square root sign. Thus, both Eqs (19a) and (19b) can be reduced to the simple form

$$\Delta T_m(t \geq 4\tau_0) \cong \frac{\tau_0 V_{CC} I_{Cp}}{4\gamma c_\vartheta A \sqrt{\pi\Theta t}} \tag{20}$$

for turning-off process, while the same holds valid with τ_i for turning-on.

Thus, *cooling-down after the rolling-off of the turnover power transient is a relatively slow process since the heat conduction toward the bulk* — i.e. the decrease in temperature — *goes ahead by the square root of time* resulting in a straight falling section in the doubly logarithmic plots of Figs 6(a) and 6(b) with a slope of $-1/2$. In Table IV the cooling-down times $\tau_{\vartheta(c)}$ are given in the last row and defined as the time elapsing between the peak value $\Delta\hat{T}_m$ and the value $\Delta\hat{T}_m/\epsilon = 0{,}368\,\Delta\hat{T}_m$, also expressed in normalized terms t/τ_0. These cooling-down times, however, are relatively brief: between some tenth and some μsec at the various transistors, except the bulky alloyed Ge power transistor.

8. Time function of the absolute junction temperature

If the repetition frequency of switch-over is high, i. e. the switching time t_{on} and t_{off} become comparable to the switch-over period time, the *average* temperature rise due to the switchover transient peaks should also be taken into consideration. The average value will be the sum of both turn-on and turn-off energies of Eqs (5a) and (5b), the sum multiplied by the repetition frequency f_r, the way in which one gets the turnover power averaged for the $1/f_r$ period time:

$$\overline{P_{dt(on+off)}} = (\tau_i + \tau_0)\, f_r\, V_{CC}\, I_{Cp}/2 \cong (t_{on} + t_{off}) f_r\, V_{CC}\, I_{Cp}, \tag{21}$$

and consequently

$$\overline{\Delta T_{j(to)}} = R_T\, \overline{P_{dt(on+off)}} = (\tau_i + \tau_0) f_r V_{CC} I_{Cp} R_T/2 \cong (t_{on} + t_{off}) f_r V_{CC} I_{Cp} R_T \tag{22}$$

will be the average temperature rise caused by the turnover energy peaks. This value must be subtracted from the $\Delta\hat{T}_m$ peak temperature to gain the real maximum temperature jump above the average since the instantaneous temperature fluctuates around the $\overline{\Delta T_{j(to)}}$ average value, having identical areas (thermal energies) above and below the average. Taking the other quasi-stationary power dissipations also into consideration [3, 4] as the turned-on (saturated) average power on the one hand as

$$\overline{P_{on}} = t_p f_r\, (V_{CB\,sat} + V_{EBp}) I_{Cp} \tag{23}$$

and the same for the turned-off (cutoff) state, on the other, as

$$\overline{P_{off}} = (1 - t_p f_r)\, V_{CC} I_{CBo} \tag{24}$$

(t_p denoting the duration of "on" state of inverter $V_{CB\,sat}$ and V_{BEp} the collector and emitter residual voltages in saturation at current I_{Cp} and I_{CBo} the collector reverse current), one obtain by summing up Eqs (23) and (24):

$$T_j(t) = \Delta T_m(t) + R_T(\overline{P_{on}} + \overline{P_{off}}) + T_a \tag{25}$$

which means the $T_m(t)$ function superimposed on the $R_T(\overline{P_{on}} + \overline{P_{off}}) + T_a$ average temperature, the $\Delta T_m(t)$ "rippling" being negligible as compared to the rest of both the last right-hand additive terms, so far as there is no appreciable current concentration or, in other words, occurrence of hot spots. In Eq. (25) T_a stands for the ambient temperature and R_T is naturally the stationary (d. c.) thermal resistance of the transistor between junction and ambient (still air environment).

9. A simplified estimate of turnover-transient temperature jump

The Eqs (19a) and (19b) are too sophisticated for practical quick reckoning of a peak temperature jump. A more simple estimate, however, gives fair results as follows. For starting, the Eq. (19) may be used, neglecting first of all the "thermal resistance" additive term since it shares quite little in $\Delta\hat{T}_m$ peak value and is important only at t/τ_i or t/τ_0 normalized times, less than 0,5. On the other hand, let one substitute the $P_{dt}(t)$ function, as it stands into Eq. (2), by a rectangle step function which has the same area below it as the resulting

$$\int_0^\infty P_{dt}(t)dt = L(t)$$

total turnover energy, i.e. with a constant height $P_{dt\,\max} = V_{CC}I_{Cp}/4$, as is shown in Fig. 7, which has naturally the width (duration) $2\tau_i$ or $2\tau_0$, because Eq. (5b) gives $L_{off} = \tau_0 V_{CC} I_{Cp}/2 = 2\tau_0\ P_{dt\,\max} \cong t_{off}\ P_{dt\,\max}$, since the duration $2\tau_0$ is after all fairly equal to the switching-off time t_{off} (as well as $2\tau_i \cong t_{on}$) if the switching current level is high (comparable to maximum rating) and $I_{Cp}/I_{Bp} \cong 10$ (according to the usual standard of $V_{CE\,Sat}$ and switching-time measurements) and moreover, the switching-on base current I_{BXp} and the reverse-direction "drawing-out" base current peak amplitude $-I_{BY}$ c (for quick carrier charge removal from the base) fall into the same order of magnitude (cf. Fig. 8).

The estimation of peak-temperature jump makes use of the concept $\Delta\hat{T}_m = L_{off}(t = \infty)/C_{\vartheta(i)}(t = 2\tau_0)$ on the basis of the afore mentioned assumptions where the equivalent energy function has a constant ordinate of $V_{CC}I_{Cp}/4$ and equivalent duration of $2\tau_0 \cong t_{off}$ (at switching-off). Thus, the inner thermal capacity $C_{\vartheta(i)}(t = 2\tau_0)$ should be considered in Eq. (13), yielding

$$\Delta\hat{T}_{m(\mathrm{off})} \cong \frac{L_{\mathrm{off}}}{C_{\vartheta(i)}(t = 2\tau_0)} = \frac{\tau_0 V_{CC} I_{Cp}}{1\gamma c_\vartheta A\ [(X_\Phi/\xi) + \sqrt{8\pi\Theta\tau_0}]}\,, \tag{26}$$

here X_Φ means the depletion layer width at $V_{CB} = V_{CC}/2$, where the maximum of the $P_{dt}(t)$ function occurs and which is $\sqrt{2}$-times less than the maximal X at $V_{CB} = V_{CC}$. The resulting Eq. (26) is after all identical to the accurate result of Eq. (19.b) if the first "thermal resistance" additive term within the figure brackets is omitted, further the exponential terms in the numerator of the second "thermal capacity" additive term are neglected as compared to 1 (which is rightful since the whole turnover energy is considered); moreover, the second square root term in the denominator, $\sqrt{2\varepsilon_r \varepsilon_0 \ldots}$ is substituted by X_Φ, i.e. in the last exponential term $t/\tau_0 = \log_\epsilon 2 \cong 0{,}69$ is introduced, which coincides with the instant of the turnover transient power peak,

giving at the same time the average of depletion layer width; and finally, $t = 2\tau_0$ is substituted in the first term under square root sign in the denominator of the "thermal capacity" term.

As is presented in Table IV and in the following numerical examples, expression (26) gives a fair estimate in good agreement with the results based on Eqs (19a) and (19b). — For $\Delta\hat{T}_{m(on)}$, L_{on} and τ_i should be substituted in Eq. (26) instead of L_{off} and τ_0.

10. Numerical examples of some characteristic transistor types

(a) *ASZ* 18, an alloyed Ge pnp, low-speed power transistor, similar to the "test vehicle" used in experiments (c) and (d) in refs [3, 4].

Maximum ratings:

$$V_{CBo} = -80\ \text{V};\ I_{C\,\max} = -6\ \text{A};\ T_{j\,\max} = 90\ ^\circ\text{C};\ R_{Tj-c} = 1{,}5\ ^\circ\text{C/W}.$$

C. E. inverter operation of Fig. 8 at:

$$V_{CC} = -30\ \text{V};\ I_{Cp} = -6\ \text{A};\ I_{BXp} = -0{,}6\ \text{A};\ I_{BYp} = 0{,}6\ \text{A};$$

in which case

$$2\tau_i \cong t_{on\,\max} = 30\ \mu\text{sec and } 2\tau_0 \cong t_{off\,\max} = 35\ \mu\text{sec } (P_{dt\,\max} = 45\ \text{W}).$$

Construction data: $\varrho_n = 5$ ohm · cm base resistivity; $A_{nom} = 5 \times 10^{-2}$ cm². With $A = A_{nom}$: $X_\Phi = 5{,}15\ \mu$m and $\xi = 3$ (step junction); $\Delta\hat{T}_{m(off)} \cong 1{,}46\ ^\circ$C which in fact inconsiderably exceeds the value 1,20 °C gained by Eq. (19b). With $A = 0{,}01\ A_{nom}$, $\Delta\hat{T}_{m(off)}$ will be 146 °C where the occurrence of hot spots and destruction takes place rapidly. Thus, this type is particularly sensitive to volumetric degradation at high switching power levels.

(b) *AC* 125 *U*, medium-power, medium-speed, alloyed Ge pnp transistor, similar to the types used in experiments (a) and (b) in refs [3, 4].

Maximum ratings: $V_{CBo} = -60$ V; $I_{C\,\max} = -0{,}25$ A; $T_{j\,\max} = 70\ ^\circ$C; $R_{T\,\max} = 0{,}4\ ^\circ$C/mW without any radiator in resting air environment. C. E. inverter operation of Fig. 8 at: $V_{CC} = -40$ V; $I_{Cp} = -0{,}25$ A; ($P_{dt\,\max} = 2{,}5$ W); $I_{BXp} = -0{,}025\ A = -I_{BYp}$; in which case $2\tau_0 \cong 2\tau_i \cong t_{off} \cong t_{on} = 1\ \mu$sec max. Construction data: $\varrho_n = 2$ ohm · cm. thus $X_\Phi = 3{,}82\ \mu$m; $A_{nom} = 3{,}85 \times 10^{-3}$ cm². With $A = A_{nom}$ and $\xi = 3$, Eq. (26) yields $\Delta\hat{T}_{m(off)} \cong 0{,}17\ ^\circ$C, exactly the same as gained from Eq. (19b). Having $A = 0{,}01\ A_{nom}$, the peak temperature jump increases to 17 °C which in turn is still harmless from a degradation point of view. Thus, this type is less prone to collector-emitter punch-through.

(c) *BUY* 12, a doubly diffused, silicon mesa npn high-power, high-voltage transistor of medium switching speed and with epitaxial collector layer.

Maximum ratings: $V_{CBo} = 210\ V$; $V_{CEo} = 80\ V$; $I_{C\,\max} = 10\ A$; $T_{j\,\max} = 150\ ^\circ$C; $R_{Tj-c} \leq 1{,}5\ ^\circ$C/W between junction and case (base plate). C. E. inverter operation of Fig. 8. at: $V_{CC} = 40\ V$; $I_{Cp} = 10\ A$; ($P_{dt\,\max} = 100$ W!); $I_{BXp} = 1{,}4\ A = -I_{BYp}$; in which operating point $2\tau_i \cong t_{on} = 0{,}5\ \mu$sec max $= t_{off} \cong 2\tau_0$.

Construction data: ϱ_n 7,5 ohm·cm collector epitaxy resistivity; $A_{nom} = 5{,}45 \times 10^{-2}$ cm² $\xi = 4$ (linearly graded junction). With $A = A_{nom}$, Eq. (26) results in $\Delta\hat{T}_{m(off)} \cong 0{,}29\ ^\circ$C, a bit less than the more accurate result 0,338 °C gained by Eq. (19b). There is no serious harm for deterioration until a current concentration rate of $A_{nom}/A = 10^3$ since a temperature reaching or exceeding 1000 °C is necessary at silicon for the rapid advancement of diffusion profils.

(d) *BSY* 34, a medium-power, high-speed, epitaxial planar npn silicon transistor. Maximum ratings: $V_{CBo} = 60\ V$; $I_{C\,\max} = 0{,}6\ A$; $T_{j\,\max} = 200\ ^\circ$C; $R_{T\,\max} = 0{,}22\ ^\circ$C/mW in resting air without any radiator; $R_{Tj-c} \leq 0{,}06\ ^\circ$C/mW. C. E. inverter operation of Fig. 8 at: $V_{CC} = 40\ V$; $I_{Cp} = 0{,}5\ A$; ($P_{dt\,\max} = 5$ W); $I_{BXp} = 0{,}05\ A$; $I_{BYp} = -0{,}025\ A$; when $2\tau_i \cong t_{on} = 90$ nanosec max., and $2\tau_0 \cong t_{off} = 95$ nanosec max.

Construction data: $\varrho_n = 2$ ohm · cm epitaxy, hence $X_\Phi = 3{,}26\ \mu$m; $A_{non} = 2{,}5 \times \times 10^{-3}$ cm². Substituting $A = A_{nom}$ and $\xi = 4$ into Eq. (26): $\Delta\hat{T}_{m(off)} \cong 0{,}135\ ^\circ$C, sensibly

less than the accurate result 0,197 °C of Eq. (19b). Thus, the type is insensitive for volumetric deterioration still assuming an excessive current concentration ratio of $A_{nom}/A = 10^3$ which in turn can hardly occur, since peak temperature jump approximates in this unbelievable case only 135 (or 197) °C which latter still falls short of $T_{j\,max}$. Finally,

(e) *Totem-pole output transistor* (between output and gnd.) *of a TTL-series NAND gate integrated circuit* (e. g. SN 7400 N). The operation data correspond to those given in section 6 as well as in Table IV and in Fig. 9, at the instant of maximal turnover power during commutation as: $V_{CE} \cong 1{,}3$ V; $I_{Cp} \cong 15$ mA, thus $P_{dt\,max} \cong 20$ mW; $2\tau_0 \cong t_{off} \cong 5$ nanosec fall time for this particular stage. Construction data are $\varrho_n = 0{,}1$ ohm · cm collector epitaxy, so $X_\Phi = 0{,}137\ \mu$m at the appearing $V_{CB} = 0{,}7$ V; $A_{nom} = 1{,}2 \times 10^{-5}$ cm².

Substituting $A = A_{nom}$, $\xi = 4$ and, instead of $V_{CC}I_{Cp}/2$, the power $2\,P_{dt\,max} = 0{,}04$ W into Eq. (26), it yields the very low temperature increment $\Delta\hat{T}_{m(off)} \cong 0{,}028$ °C in good accordance with 0,0236 °C computed on the basis of the accurate Eq. (19b), which results suggest that the harm of a volumetric degradation may still be completely neglected in the improbable case of a current concentration ratio of 10^3 (in which case the peak temperature jump is raised to approx. 24 ÷ 28 °C).

As may be seen in Fig. 9, the maximal transient power during switchover occurs just at this lower totem-pole transistor T_4. A similar transient power peak arises at the upper totem pole transistor T_3, whilst the power peaks by the other transistors can be fully neglected. The peak temperature jumps at transistors T_4 and T_3, however, is only 1/10 ÷ 1/30 of the $\Delta\hat{T}_m$ increments found in the examples of usual discrete bipolar transistors despite the minute geometrical dimensions of transistors in a monolythic *IC*, cf. examples (d) and (e).

11. Refinements of the thermal model if turnover transients are rather elongated

Finally, let us deal with the estimate of $\Delta\hat{T}_m$ in the cases if the turnover transients are rather elongated (as compared to the usually brief t_{on} and t_{off} switching times) and so the bounds of the heated-up volume, or more precisely, the thermal penetration depth, exceed well the distance of the collector-junction-to-the-wafer bounds in either perpendicular direction from the collector junction plane. This is the situation, in general, at shallow-collector-junction planar devices as well as at alloyed devices where the metallurgical junction between indium collector zone and germanium base zone lies very near to the real p-n electrical junction. This problem, however, becomes serious especially at the pulsed service life tests of Refs [3] and [4] where an effective screening technique for latent structural inhomogeneity and as a consequence of the former, for an imminent hot-spot's formation and short, makes use of the artificial elongation principle of turnover transients. Such kinds of screening results have been reported in the experiments (a), (c), (e) and (f) as well as in the corresponding Tables I—IV of Refs [3] and [4] and the $\Delta\hat{T}_m$ values given there are computed on the basis given in this section, as refinements of Eq. (26), and on the construction data (ϱ_n, A_{nom}) presented in these Tables for the case of a perfect-structure transistor. In experiments (e) and (f) and Tables III and IV, resp., of Ref. [4] two medium-power planar transistors (BFY 33 and BSY 56) are dealt with, both types having equal nominal collector junction areas A_{nom}, as well as equal voltage and current ratings, consequently both experiments were conducted at identical operating conditions corresponding to identical V_{CC}, I_{Cp}, t_{on}, t_{off}, t_p, f_r and so L_{on}, L_{off}, $P_{dt\,max}$ conditions were also equal. Thus, $\Delta\hat{T}_{m\,off}$ values there are also identical and were presented only in Table III for the BFY 33 type. The sole difference between both types is that the resistivity of the epitaxial collector layer is $\varrho_n = 4$ ohm · cm at the BSY 56 type while it is 2 ohm · cm at the BFY 33. This difference is, however, still unimportant since in Eq. (26), the term $\sqrt{8\pi\Theta t} \gg (X_\Phi/\xi)$ due to the rather elongated transient switch-over times and the equivalent heat source thickness X_Φ/ξ which is only influenced by ϱ_n, can be totally neglected in comparison with the thermal penetration depth. — Contrary to this, both planar types in experiments (e) and (f), as the most usual planar devices, exhibit relatively shallow collector junction depths d_{CB} of 2,5 μm (BSY 56) and 3 μm (BFY 33) which must be considered in the calculation of thermal capacity $C_{\vartheta(i)}$ here because at the badly elongated switching times $\tau_{\vartheta eff}$ certainly exceeds d_{CB}. As a consequence, the results at the end of Section 5, i. e., expression (13a) fit here naturally utilizing the first term only by substituting it into Eq. (26), leading to

$$\Delta\hat{T}_{m(off)} \cong \frac{\tau_0\, V_{CC} I_{Cp}}{2\gamma c_\vartheta A\,[d_{CB} + (X_\Phi/\xi) + \sqrt{\pi\Theta t_{off}}} \cong \frac{\tau_0 V_{CC}\, I_{Cp}}{2\gamma c_\vartheta A \sqrt{\pi\Theta t_{off}}} \tag{27}$$

where the more complicated first form of the right-hand side is generally valid for shallow-junction planar transistors while the simpler, extreme-right form can be applied at rather elongated turnover times.

Similarly, for the alloyed germanium types where the electrical p-n junction is in the closest to the indium (collector button zone) and germanium (base wafer zone) boundaries, the thermal energy penetrates an one side into the indium and on the other into germanium. In this case also the Eq. (13a) is considered but utilizing both right-hand additive terms, in the first one using indices Ge standing for the germanium wafer (base zone), and in the second one substituting indices In for the indium collector-button metal:

$$\Delta\hat{T}_{m(off)} \cong \frac{\tau_0 V_{CC} I_{Cp}}{2A\left\{\gamma_{Ge} c_{\vartheta Ge}\left[(X_\Phi/\xi) + \sqrt{\pi\Theta_{Ge} t_{off}}\right] + \gamma_{In} c_{\vartheta In}\sqrt{\pi\Theta_{In} t_{off}}\right\}}, \tag{28}$$

where the term X_Φ/ξ may be neglected if t_{off} is rather long. For the turning-on transient naturally $\Delta\hat{T}_{m(on)}$, τ_i and t_{on} should be substituted in Eqs (27) and (28). For the switching-on and -off times, also here $t_{on} \cong 2\tau_i$ and $t_{off} \cong 2\tau_0$ can be substituted in the common-base circuitry with $I_{BV} = 0$ reported in Refs. [3] and [4]. All $\Delta\hat{T}_{m(off)}$ results of the alloyed Ge experiments (a) and (c), i. e. in Tables I and II of Refs [3] and [4] are computed on the basis of Eq. (28).

12. Conclusions

A simple thermal model was constructed for the reckoning of a peak temperature jump and the calculating of the actual junction temperature increment vs. time of a transistor during switch-over, making use of the one-dimensional solution of diffusion-like thermal conductivity differential equation in a solid. Boundary conditions were selected in this manner, e.g. assuming a plane junction with even current concentration to make possible a one-dimensional treatment and utilizing an exponential approximation for the $P_{dt}(t)$ heating switch-over power vs. time function. Thermal behaviour was analyzed first of all by utilizing a delta function heat transfer to the laminar heat source, namely, the collector depletion layer having an effective width less than the electrical, within which the temperature was assumed to be constant and the heat energy as spreading in time toward both junction sides in the form of an ever extending normal distribution and with a mean ΔT_m value diminishing in the same proportion as the standard deviation of the normal distribution (defined as thermal penetration depth) increases, the latter as the square root of elapsed times. This way, the "inner" thermal capacity and the "inner" thermal resistance of the ever increasing heated-up volume can be calculated in the function of time. Multiplying the instantaneous turnover power with the "inner" thermal resistance and, further, superimposing this product onto the ratio of electrical turnover energy to the "inner" thermal capacity, one gets the temperature rise vs. time function.

The model was extended to uneven current flow pattern, i.e. into a three-dimensional case in the most simple way, actually assuming that collector current and so heating power is concentrated in junction areas several times smaller than the nominal, i.e., in "hot spots" and considering

the current flow in the remaining area as zero. This approach, although not exact, gives a fair picture about real bulk degradation conditions and causes, since *with the presumption of a perfectly even current flow pattern*, i.e. calculating with the *nominal* collector junction area, *actual peak temperature jumps due to the turnover transient power spikes at maximum allowed data-sheet switching power levels, and still well beyond them, mount up only to some split °C at medium--power transistors and are well below* $1 \div 2$ *°C at high-power ones let alone the minute transistors of a digital IC chip where jump hardly exceeds some hundredth of a °C and so they are completely harmless from bulk degradation point of view* so far structure (current flow) exhibits no serious unevenness. *A ratio of nominal to actual* (conducting) *junction area of* $10^2 \ldots 10^3$, *that is, extremely bad structure can initiate only a thermal runaway process leading to hot spots in the bulk and finally, to deterioration by short.* A lot of numerical examples of various up-to-date transistor constructions (ranging from the minute monolythic IC transistor to bulky, 100 W alloyed Ge power types) suggests the following conclusions:

(i) The temperature jump due to the turnover is, in general, higher at alloyed Ge types than at planar or mesa silicon devices. This is a consequence of differing technologies since many times thinner base widths and so many times faster transistors can be made by the planar or mesa diffusion techniques with accuracy and ease. This picture is aggravated by the fact that in germanium the diffusion velocity of dopants into the lighter doped junction side is raised to a dangerous degree still at about $450 \div 550$ °C while the same in silicon takes place only at $900 \div 1100$ °C. This drawback of alloyed Ge transistors is compensated somehow by the more robust construction (e.g. thick soldered-on joints instead of the sensitive and thin gold wires bonded by thermocompression) and the thicker base layer.

(ii) The temperature jump during switch-over is especially high and dangerous at power transistors since the $L_{off}/V_{\vartheta(i)} = \tau_0 V_{CC} I_{Cp}/2AW_{\vartheta(i)}$ at specific turnover energy density (see Table IV) it is markedly higher than the usual low- and medium-power types.

(iii) In monolithic (digital) integrated circuits the sole of volumetric degradation processes is unimportant as compared to other (surface- and contact-plague-originated) degradation mechanisms because operating voltages and turnover transient power peaks are both very low. Hence, it is not reasonable to making such expensive kinds of switching-mode life tests on monolithic IC-s.

Acknowledgements

The author is indebted to Mr. J. Szécsei and Dr. F. Kovács of HIKI for the valuable help and co-operation in theoretical problems, as well as to Prof. I. P. Valkó, Ph. D. for encouraging and criticizing this work, finally to Mr. A. Komporday, Dr. J. Katona, Ph. D. and Mr. F. Bráda of the management of the Institute HIKI for the approval of this paper for publication.

REFERENCES

1. KEMÉNY, A. P.: Experimental Investigation on the Life of Semiconductor Devices, I. Accelerated Life Tests of Transistors under Static Electrical Load and at High Temperature Storage, *Acta Techn. Hung.* **74** (1973), 85—144
2. KEMÉNY, A. P.: Experimental Investigation on the Life of Semiconductor Devices, II. Long-Term Life Test of Semiconductor Power Rectifiers with Energy-Sparing Synthetic Circuits — Testing Methods and Some Results; *Acta Techn. Hung.* **74** (3—4), (1973), 275—327
3. KEMÉNY, A. P.: Experimental Investigation on the Life of Semiconductor Devices, III. Volumetric Failure Mechanisms and the Life Testing of Transistors in Switching Operation Mode, *Acta Techn. Hung.*
4. KEMÉNY, A. P.: Experiments Concerning the Life Testing of Semiconductor Devices, II. Life Testing of Transistors in Switching Operation Mode, *Microelectronics and Reliability*, **10** (1971), 75—93
5. KITTEL, C.: Introduction to Solid State Physics; J. Wiley, New York (1961), see Chapter 6
6. PEARS, J. H.: Chemical Engineer's Handbook (4th Ed.); McGraw-Hill, New York, see Chapter "Thermal Conductivitu"
7. DOOB, J. L.: Stochastic Processes; J. Wiley, New York and Chapman and Hall, London 1954
8. RÉNYI, A.: Probability Mathematics (in Hungarian); Textbook Publ. House, Budapest (1954), see Chapter XVI, Section 8 (pp. 636—641)
9. *Rare Metals Handbook* (2nd ed.); Reinhold Publ. Co., Chapman and Hall, London 1954

Experimentelle Untersuchung der Lebensdauer von Halbleiter-Bauelementen. Die Rolle der durch umschalttransienten verursachten Temperaturerhöhung beim räumlichen Zugrundegehen von schalttransistoren und digitalen integrierten Stromkreisen. — Die zufolge der Umschalt-Leistungstransienten zustandekommende transiente Temperaturerhöhung kann beim Schaltbetrieb auf hohem Niveau für einzelne charakteristische räumliche Defekte verantwortlich gemacht werden, wie den C—E "Durchstich" und den C—B Durchschlag. Nach Berechnung der "thermischen Eindringtiefe" auf beiden Seiten der Kollektorübergangs- und Wärmekapazität des sich erwärmenden Raumteiles und seines thermischen Widerstands erhält man ein geeignetes eindimensionales thermisches Modell für die Schätzung des Übergangstemperaturanstiegs. Im Besitz der Zeitabhängigkeit der transienten Umschaltleistung und der Konstruktionsdaten des gegebenen bipolaren Transistors kann die Zeitabhängigkeit der transienten Übergangstemperatur berechnet werden. An Hand von Zahlenbeispielen für einige Transistortypen mit charakteristischer Technologie (von den robusten, großen Ge- und Si-Leistungstransistoren bis zu den integrierten Monolith-Miniaturstromkreisen) wird nachgewiesen, daß — fehlerlose Struktur und gleichförmige Stromverteilung vollkommen gefahrlos sind.

Экспериментальное исследование срока службы полупроводниковых приборов, IV. Роль пиковой температуры, вызванной переходыми процессами переключения, в объемной порче переключательных (импульсных) транзисторов и дигитальных интегральных схем. Переходной рост температуры, возникающий вследствие переключательных переходных процессов мощности, является ответственным за отдельные характерные объемные повреждения, возникающие в переключательном режиме высокого уровня, как, например,»прокол« С—Е и пробой С—Р. При расчете с обоих сторон коллекторного перехода »глубину термического проникновения«, далее теплоемкость и термическое сопротивление нагревающейся части пространства до заданного момента после начала переходного процесса перемены получается подходящая одномерная термодинамическая модель для оценки роста температуры перехода: располагая данными временной функции мощности переходного процесса переключения и конструкционными данными данного биполярного транзистора, можно вычислить временную функцию переходной температуры перехода. На основе числовых примеров нескольких типов транзисторов с характерной технологией (начиная от крупных германиевых и кремниевых транзисторов мощности и вплоть до миниатюрных приборов монолитных интегральных схем), при предположении бездефектной структуры и равномерного распределения тока, автор доказывает, что возникающие скачки никовых температур при переключении являются совершенно безопасными.

Acta Technica Academiae Scientiarum Hungaricae, Tomus 82 (3—4), pp. 333—352 (1976)

CaO AND MgO COMPOUND FORMATION IN PROCESSING CALCITE-DOLOMITE BEARING BAUXITES BY THE BAYER METHOD

ZÁMBÓ, J.* and Mrs. ORBÁN-KELEMEN, M.**

[Manuscript received 8 January, 1974]

The operational problems in the course of processing the Halimba type calcite and dolomite bearing bauxites necessitated the examination of the Na_2O-Al_2O_3-CaO-MgO-TiO_2-SiO_2-H_2O-CO_2 system under the conditions of the Bayer technology parameters. It was observed that the quality and quantitative ratio of the Ca and Mg containing phases produced during the recovery of dolomite bauxites are governed, primarily, by the components dissolved in the alumina liquor, although they are also affected by the solid phases capable of reacting with the individual components of the solution.

1. Theoretical

In certain parts of the Halimba bauxite field the CaO and MgO content of the bauxites exceeds the usual 0,4 and 0,1 per cent values, respectively, to a considerable degree, since this field contains, on the average, 2,7 per cent CaO and 0,7 per cent MgO. Calcium and magnesium appear in the bauxite mainly as calcite and dolomite. In the practice of alumina production the decaustification effect of the carbonate minerals is a well-known phenomenon. However, when processing increasingly contaminated bauxites also some other problems will emerge along the washing line during sludge separation. In the overspill of the Dorr washers the red mud content will greatly increase, and a considerable amount of high solids contaning foam will float over the surface which, when accumulated in the system, may cause a breakdown in the most serious cases preventing the operation of the entire washer line. Since these difficulties are correlated to the calcium and magnesium containing compounds, a detailed study of this problem appeared to be simply indispensable.

In the Na_2O-Al_2O_3-CaO-MgO-CO_2-H_2O system the determination of the solid phases in equilibrium with the solution is an extremely difficult task at the $5 \div 250$ g/lit Na_2O_k concentration usual with the Bayer technology, involving a 1,6 to 3,5 Na_2O_k per Al_2O_3 mole ratio and a 70 to 240 °C temperature

* Dr. ZÁMBÓ, J., Fehérvári út 14, H–1116 Budapest, Hungary
** ORBÁNNÉ dr. KELEMEN M., Lajos u. 11—15, H–1023 Budapest, Hungary

range. The given case is further complicated by the fact that in bauxite digestion part of the SiO_2 and TiO_2 content will also be dissolved, whereby an 8-component system is obtained. In addition, the solid phases thus produced may transform with the changes of temperature and concentration.

In such a complicated system the determination of the solid compounds of equilibrium is simply impossible by increasing the number of components, i.e. in the usual way, because of the great number of investigations required for the purpose. There are, however, an infinite number of data already available on the details of the system rather important from the aspects of alumina industry, on which basis further laboratory investigations clarify, without the determination of the equilibrium phases of the entire system, the conditions of producing calcium and magnesium containing compounds under the circumstances of bauxite digestion and red mud washout.

From the Na_2O-Al_2O_3-SiO_2-H_2O system, according to the temperature and concentration conditions conforming to the alumina industry practices, different sodium-aluminium-silicates will be separated. At temperatures below 100 °C the so-called "Linde-Zeolite A" will be formed, with foreign atoms built in the silicate lattice and its vacant positions. Up to 180 °C there will be sodalites produced, the chemical composition of which has been given by VÖRÖS [1] in the form of $3(Na_2O \cdot Al_2O_3 \cdot 2SiO_2)\, Na_2X \cdot nH_2O$, where where $X = CO_3^{2-}\ SO_4^{2-}, 2Cl^-, 2AlO_2^-, 2OH^-$. Sodalite is, essentially, a mixed crystal which means that the quality and quantity of the X anion depends on the momentary solution concentration, composition, and temperature. The carbonate-sodalite quantity will increase or decrease with the variation of the soda content of the aluminate liquor while the aluminate-sodalite amount will vary with a change in the mole ratio.

According to the investigations by BARRER and WHITE [2], at 210 °C or over, either sodalite and cancrinite, or only the latter will be produced, depending on the mole ratio. Cancrinite is defined by the formula $3(Na_2O \cdot Al_2O_3 \cdot 2SiO_2)Na_2CO_3$ or by $3(Na_2O \cdot Al_2O_3 \cdot 2SiO_2)2\ NaOH$ which are identical to the composition of carbonate-sodalite and hydroxi-sodalite, respectively, although their crystal structures differ. In sodalite the anion changes enable the replacement of part (appr. 10 per cent) of the Na_2O losses by inexpensive NaCl or Na_2SO_3 [3]. SEIMIYA [4] similarly identified sodalite type mixed crystals and cancrinite type compounds in red mud.

Examination of the equilibrium conditions in the Na_2O-Al_2O_3-CaO-CO_2-H_2O system was carried out by a number of Soviet research workers in the 'fifties. Their efforts were aiming at the elaboration of the so-called soda-lime technique which caustifies by lime the soda used to replace the caustic soda losses, simultaneously to the bauxite digestion.

Simple carbonates like calcite, dolomite, or siderite will interact with the liquor during the wet grinding and digestion of the bauxite, and trans-

forming it into soda. At 25 °C the equilibrium constant of the

$$CaCO_3 + 2NaOH \rightleftharpoons Ca(OH)_2 + Na_2CO_3$$

reaction will be $2{,}82 \times 10^{-3}$ [5].

Upon heating, the equilibrium constant of the reaction will increase, since in equation

$$K_a = \frac{a_{CO_3^{2-}}}{a^2_{OH^-}} = \frac{L_{CaCO_3}}{L_{Ca(OH)_2}}$$

where $a_{CO_3^{2-}}$ and a_{OH^-} represent the activity of the ions, the solubility product of $CaCO_3$, that is, (L_{CaCO_3}) will increase while $L_{Ca(OH)2}$ decreases. At 200 °C we obtain $K_a \approx 1$.

It follows that, upon heating, the calcite will react better with the liquor, and an increasing liquor concentration will further promote calcite decomposition.

At 25 °C the magnesite reaction [6] will be

$$K_a = \frac{L_{MgCO_3}}{L_{Mg(OH)_2}} = \frac{1{,}7 \times 10^{-6}}{5 \times 10^{-12}} = 3{,}4 \times 10^5$$

Upon heating, the equilibrium constant will increase, the reaction is irreversible and takes place, in practice, in low concentration liquors as well [7].

In a hot aluminate liquor the calcite will decompose while soda and calcium-hydroaluminate are being produced, the dissolution of which will be lower than that of the lime:

$$3CaCO_3 + 2NaAl(OH)_4 + 4NaOH \rightleftharpoons 3CaO \cdot Al_2O_3 \cdot 6H_2O + 3Na_2CO_3$$

Fig. 1 illustrates the equilibrium curve of soda caustification in aluminate liquor at 95 °C and $\alpha_k = 1{,}65$ as shown by LEITEYSEN and POTAPOVA, while Fig. 2 represents at different temperatures the $CaCO_3$ production range in the CaO-Al_2O_3-Na_2O-CO_2-H_2O [8]. In the domain delineated by the curves, tht solid phase of $CaO \cdot nAl_2O_3 \cdot mH_2O$ composition, while above it the $CaCO_3 \cdot aNa_2CO_3 \cdot bH_2O$ double-carbonate will be separated from the solution.

Tricalcium-hydroaluminate will not stay stable with an increasing temperature, but will react with the liquor according to the equation

$$3CaO \cdot Al_2O_3 \cdot 6H_2O + 2NaOH \rightleftharpoons 2NaAl(OH)_4 + 3Ca(OH)_2$$

The isotherms of the reaction are shown in Fig. 3, according to LEITEYSEN and POTAPOVA [10].

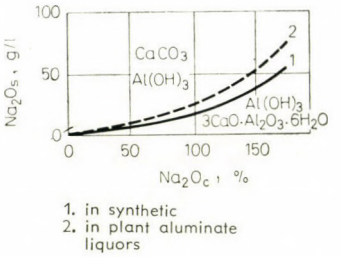

Fig. 1. Caustification curves in the Na_2O-CaO-Al_2O_3-CO_2-H_2O system at 95 °C

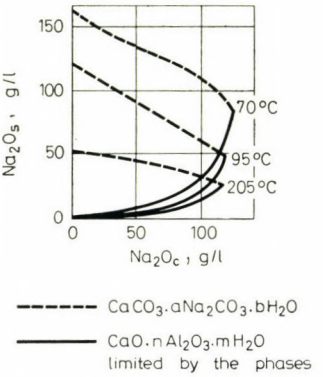

Fig. 2. $CaCO_3$ formation area

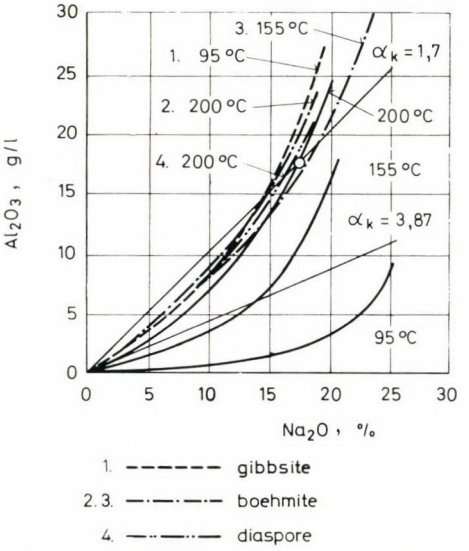

Fig. 3. Isotherms of the reaction according to LEITYSEN [10]

For the sake of comparison the same figure presents the solubility of gibbsite (95 °C), boehmite (155 and 200 °C), and diaspore (200 °C), respectively. At the temperatures of Fig. 3 the Al_2O_3 concentration in equilibrium with tricalcium-hydroaluminate is lower than the solubility of gibbsite or boehmite, while at 200 °C it approximates that of the diaspore, so no calcium-aluminate will be produced when digesting diaspore bauxites. On the other hand, the preconditions of $3CaO \cdot Al_2O_3 \cdot 6H_2O$ formation are very favourable during the cooling and dilution of the sludge.

In the presence of SiO_2 hydrogarnets will be produced. Regularities of the formation of hydrogarnets crystallized from the Na_2O-Al_2O_4-CaO-SiO_2-H_2O system have been thoroughly studied by many authors [10, 11, 12, 13]. It was found that there would be

$$3CaO \cdot Al_2O_3 \cdot kSiO_2 \cdot (6\text{-}2k)H_2O$$

produced, that is, the solid phase of

$$3CaO \cdot Al_2O_3 \cdot 6H_2O = C_3AH_6(*)$$

and

$$3CaO \cdot Al_2O_3 \cdot 3SiO_2 = C_3AS_3(*)$$

According to the examinations [14, 15], the size of the elementary cell in the cubic lattice of hydrogarnets will vary linearly, depending on the $SiO_2 : Al_2O_3$ molecular ratio. In the case of C_3AH_6 we have $a = 12{,}55$ Å which, however, will decrease to 11,86 Å if C_3AS_3 is involved. This change can be readily measured on X-ray diffractograms, but it can be similarly quite clearly followed in well-crystallized phases by the determination of the optical refractivity, since the latter would vary between 1,640 and 1,670 instead of in the 1,590 to 1,600 range.

The k value of hydrogarnets is governed by the $Al_2SO_3 : SiO_2$ mole ratio of the solution which, in turn, is limited by the solubility of SiO_2. In connection with the stable and metastable solubility of SiO_2 and that of the sodium-hydroaluminium-silicates, the relevant data are summarized within a wide concentration and temperature range by [16] and [17]. These reveal that the Al_2O_3 quantity in the aluminate liquors is generally about two orders of magnitude greater than the SiO_2 content whereby under certain concentration conditions, rather interesting from practical aspects, it is easy to understand that the k value of hydrogarnets is less than 1, and a $k \geq 2$ composition phase can be synthetized only under very special circumstances. ARAKELYAN [15] achieved the best results when treating a mixture of $Na_2O \cdot Al_2O_3 \cdot SiO_2 \cdot nH_2O$ and $Ca(OH)_2$ in the 10 to 20 per cent solution of NaOH, at 220 °C for a few days, and obtained $k = 1{,}8$ to 2.

(*) Arbitrary abbreviations.

The Na_2O content of the solid phase is bonded in the NAS, simultaneously precipitating with the hydrogarnets.

On the behaviour of MgO the alumina industry literature has so far hardly published any information. In NAS synthesis at 100 °C, ARAKELYAN [15] discovered needle-prism crystal formation on the effect of MgO additives, with a refractivity between 1,570 and 1,492; so assuming the formation of $Mg(OH)_2$ and such a solid solution where in the sodium-hydroaluminium-silicate a certain part of Na^+ is replaced by Mg^{2+} ions (sodalite and/or cancrinite = NAS).

Many studies have been made of the TiO_2 behaviour in aluminate, liquors, but the opinions on the compounds thus produced greatly differ due, most likely, to the different technological parameters of the experiments and also on the different test methods. The compounds described by these authors have been summarized in a paper by SOLYMÁR and Mrs. HAZAI [18]. Experiments by these authors revealed that 24 per cent of the anatase would not react with the aluminate liquor at 180 °C, and that the titanium content would assume an amorphous sodium-titanate form. In bauxite digestion the reaction of aluminum and titanium minerals with the liquor will parallelly take place but at different rates. Other authors [19, 20] found that the amorphous TiO_2 and anatase would react with the base at a relatively high speed, and at a temperature of 200 to 220 °C the $Na_2O \cdot 3TiO_2 \cdot 2{,}5H_2O$ production would be completed within 30 min. Under similar conditions the rutile would react at a much slower rate, and the titanate formation might not be completed even in 2 hours. In the case of a liquor concentration exceeding 400 g/lit Na_2O_k we shall have $3Na_2O \cdot 5TiO_2 \cdot 3H_2O$ formed. With anatase, this reaction takes place rather rapidly, even at a temperature as low as 110 °C. Aluminate liquor solutions react with TiO_2 at a rate almost identical to that at which its reaction with other bases.

WEFERS measured in detail [21] the equilibrium conditions of the Na_2O-Al_2O_3-TiO_2-H_2O system. The titanium compounds had been determined, and their equilibrium domains are presented in Fig. 4. The existence of these compounds in the equilibrium area is confirmed by the test results obtained in the Hungarian Research Institute for Non-Ferrous Metals [13].

When washing with water, the titanates will hydrolize and the composition of compound thus obtained will depend on the washing time and temperature, although the hydrolysis will not be completed during an extended washing time, either, presumably because of the formation of a continuous protective layer.

In the presence of SiO_2, on the interaction of TiO_2 and alkali solution, we shall have $Na_2O \cdot 2TiO_2 \cdot 2SiO_2$ produced [22] which cannot be observed in the case of aluminate liquor.

With aluminate liquor, when testing the depositions in expansion

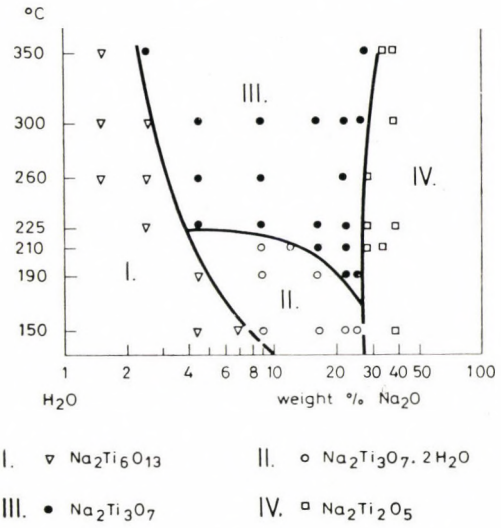

Fig. 4. Equilibrium diagram of $Na_2O = Al_2O_3 = TiO_2 = H_2O$

vessels, a compound of $Na_2TiSi_4O_{11}$ composition was found in $NaAlO_2$ enriched red mud [23].

In these of CaO, independently of any other eventual component of the aluminate liquor, its interaction with TiO_2 will produce perovskite ($CaTiO_3$) or Ca(Mg,Al)-titanate [23].

When caustifying sodium-titanates with CaO, the reaction will lead, via $Na_2O \cdot 5TiO_2$, to the production of $CaO \cdot 5TiO_2$ and $CaTi_2O_4(OH)_2$ phases [13].

Accordingly, calcite and dolomite decomposition in aluminum liquor would start when heating the sludge, while CaO, MgO, and CO_2 are being produced. CO_2 will create soda with caustic soda, while CaO and MgO will either be transformed into hydroxides, or react directly with one of the solution's components. It is well known that in Hungarian bauxites most of the SiO_2 can be found in kaolinite form which would produce NAS as early as at 100 °C. Owing to the equilibrium between the aluminate liquor and the NAS products, there will be a considerable quantity of SiO_2 in the solution which, in turn, satisfies the preconditions of hydrogarnet formation. The intensive dissolution of anatase starts at 180 °C, so the production of various titanates from titanium entering the solution must also be reckoned with.

Smirnov [24] proved that in the Na_2O-Al_2O_3-CO_2-H_2O system, when $CO_2 : Na_2O > 1$, the solid phase of the equilibrium would be represented by sodium-hydroaluminium carbonate wherefrom the compounds

$$Na_2O \cdot Al_2O_3 \cdot 2CO_2 \cdot 2H_2O$$

and

$$Na_2O \cdot Al_2O_3 \cdot 2CO_2 \cdot 5H_2O$$

could be identified, although this should not exclude the presence of other sodium-hydroaluminium carbonates as well. Investigations confirmed that at a suitable temperature these hydroaluminium carbonates might also be produced by the interaction of aluminium hydroxides and bicarbonate solutions.

In the case of a high CO_2 content, the formation of hydroaluminium carbonates is still not excluded. Thus, from calcite or dolomite the production of the following phases might be expected under the conditions of the Bayer technique:

1. $Ca(OH)_2$	ASTM 4—0733
2. $3CaO \cdot Al_2O_3 \cdot 6H_2O$ = CA*	ASTM 3—0125
3. $3CaO \cdot Al_2O_3 \cdot kSiO_2(6-2k)H_2O$ = CAS**	ASTM 3—0125
4. $CaTiO_3$	ASTM 9— 365
5. $Ca_3Al_2O_6(8-12)H_2O$	ASTM 2—0083
6. $CaAl_2O_4$	ASTM 1—0688
7. $Mg(OH)_2$	ASTM 7— 239
8. $Mg_6Al_2CO_3(OH)_{16} \cdot 4H_2O$	ASTM 14— 91
9. $Mg_4Al_2(Al_2Si_2)O_{10}(OH)_8$ = MAS***	ASTM 11— 157
10. $MgAl_2O_4$	ASTM 10— 62
11. Ca(Mg, Al)-titanate	ASTM 13— 552
12. $CaCO_3$	ASTM 5—0586
13. $MgCO_3$, $MgCO_3 \cdot 3H_2O$	ASTM 8— 479, 1—0130
14. $Ca(Mg)CO_3$	ASTM 5—0586
15. $3(Na_2O \cdot Al_2O_3 \cdot 2SiO_2)Na_2X \cdot aq$	ASTM 3—0338
16. TiO_2	ASTM 4—0477
17. $Na_2 \cdot O\ 3TiO_2 \cdot nH_2O$	ASTM 11— 290
18. $NaCa_2Mg_5Si_7AlO_{22}F_2$	ASTM 10— 431
19. $Na_2O \cdot 8CaO \cdot 3Al_2O_3 \cdot 5SiO_2$	ASTM 8— 186
20. $MgTiO_3$	ASTM 6—0494
21. $Mg_2Al_4Si_5O_{18}$	ASTM 12— 244

* CA,
** CAS and
*** MAS are arbitrary abbreviations.

The aim of our investigations was the determination of which possible phases and in what proportion would, during the digestion of calcite-dolomite bauxites be produced, and what transformation the phases thus produced would undergo under the conditions represented by the operational parameters of red mud washing.

2. Experimental

The experiments involved CaO, MgO, amorphous SiO_2, bauxite, calcite, and dolomite all of analytical purity. The chemical and phase compositions of calcite-dolomite bauxite (KDT-3) and of the calcite as well as dolomite obtained directly from the bauxite field (KDT-10 and KDT-9, respectively) are represented in Table I. The experimental parameters were 1,5 h heating

Table I

Chemical composition %	Material (symbol)		
	Calcite= = (KDT-10)	Dolomite = = (KDT-9)	Bauxite = = (KDT-3)
Al_2O_3	1,6	1,5	43,0
SiO_2	0,6	0,2	4,2
Fe_2O_3	0,8	0,5	19,3
TiO_2	0,2	0,2	2,1
CaO	53,0	31,3	6,1
MgO	0,6	20,3	3,8
Izz. v.	43,0	45,9	19,4
CO_2	42,2	46,7	8,9
Mineral composition			
Component per phase			
Al_2O_3 in gibbsite	0,2	0,3	traces
boehmite	0,8	1,1	37,5
diaspore	0,6	—	1,0
goethite	—	—	0,5
hematite	—	—	0,5
kaolinite	traces	0,2	3,2
Fe_2O_3 hematite	0,8	0,5	13,6
goethite	—	—	5,7
SiO_2 kaolinite	traces	—	3,7
quartz	0,6	0,2	0,5
TiO_2 rutile	—	—	0,6
anatase	0,2	0,2	1,5
CaO calcite	52,4	2,5	0,8
dolomite	1,0	28,5	5,3

and 1 h digestion at 210 °C. The ratio of bauxite to digestion base was determined on the basis of the reactions expected in such a way as to make the post-digestion mole ratio of the aluminate liquor equal 1,68, whereafter the reaction of the additive and the 1,6 and 3,5 mole ratio aluminate liquor, respectively, of a concentration as tabulated was studied with respect to the operational conditions of digestion and sludge washing. The experimental results are presented in Tables II –V.

Since the phases obtained from calcite are essentially identical to those produced by the reaction of $CaO + SiO_2 +$ aluminate liquor, these results of the measurements have not been presented separately.

Table II

Compounds produced in the presence of SiO_2 and TiO_2 at 210 °C on the interaction of CaO, MgO and dolomite on one hand, and aluminate solution on the other

		3,5 mole ratio aluminate liquor + additive				1,6 mole aluminate + ratio + additive				
		CaO	CaO SiO_2	MgO	MgO Sio_2	CaO SiO_2	MgO	MgO SiO_2	KDT-9 SiO_2	KDT-9 Sio_2 TiO_2
1.	2.	3.	4.	5.	6.	7.	8.	9.	10.	11.
	Solid phase composition, %									
1.	$Ca(OH)_2$	14	8							
2.	$3CaO \cdot Al_2O_3 \cdot 6H_2O$	45		2						
3.	$3CaO \cdot Al_2O_3 \cdot kSiO_2 \cdot (6\text{-}2k).H_2O$		92			100			29	5
4.	$CaTiO_3$									
5.	$Ca_3Al_2O_6(8-12)H_2O$	41								
6.	$CaAl_2O_4$									
7.	$Mg(OH)_2$			88	54		50	14	9	
8.	$Mg_6Al_2CO_3(OH)_{16} \cdot 4H_2O$			8	2		48	3		
9.	$Mg_4Al_2(Al_2Si_2)O_{10}(OH)_8$							23	7	16
10.	$MgAl_2O_4$			2	4		2			
11.	Ca(Mg, Al)-titanate									11
12.	$CaCO_3$								5	5
13.	$MgCO_3$, $MgCO_3 \cdot 3H_2O$				7			10		
14.	$(Mg, Ca)CO_3$								17	15
15.	$3(Na_2O \cdot Al_2O_3 \cdot 2SiO_2).NaX.aq$				33			50	33	24
16.	TiO_2 anatase									10
17.	$Na_2O \cdot 3TiO_2 \cdot nH_2O$									7
18.	$NaCa_2Mg_5Si_7AlO_{22}F_2$									6
	Combined water									1

Digestion by industrial grade aluminate liquor. Determination of the combined water and amorphous phase by a derivatograph.

The phase analysis data of the sludge obtained by the digestion of KDT-3 bauxite are shown in Table VI as resolved by components.

In order to determine the reaction sequence, Kossuth Mine bauxite was digested at 210 and 240 °C, with the addition of an increasing dolomite quantity. The chemical and phase compositions of bauxite are presented in Table VII, while the X-ray diffraction phase analysis data of the red mud in Figures 5 and 6.

Table III

Phase transformations of the compounds produced under the conditions of in-plant red mud washing

$Na_2O_k = 85$ g/l $\alpha_k = 2{,}1$ T = 85 °C t = 24 hours solids content = 200 g/l

1.	2.	3.	4.	5.	6.	7.	8.	9.	10.	11.
	Solid phase composition, %									
1.	$Ca(OH)_2$	25	10							
2.	$3CaO \cdot Al_2O_3 \cdot 6H_2O$	73		2						
3.	$3CaO.Al_2O_3.kSiO_2.(6-2k)H_2O$		90			100			30	6
4.	$CaTiO_3$									
5.	$Ca_3Al_2O_6 \cdot (8-12)H_2O$									
6.	$CaAl_2O_4$									
7.	$Mg(OH)_2$			81	42			14	8	
8.	$Mg_6Al_2CO_3(OH)_{16} \cdot 4H_2O$			13	14			4	2	
9.	$Mg_4Al_2(Al_2Si_2)O_{10}(OH)_8$				4			23	7	16
10.	$MgAl_2O_4$				2					
11.	Ca(Mg, Al)-titanate									11
12.	$CaCO_3$									
13.	$MgCO_3$, $MgCO_3 \cdot 3H_2O$			2	7			10		
14.	$(Mg, Ca)CO_3$								17	12
15.	$3(Na_2O \cdot Al_2O_3.2SiO_2) \cdot Na_2Xaq$				33			49	31	26
16.	TiO_2 anatase									10
17.	$Na_2O \cdot 3TiO_2 \cdot nH_2O$									7
18.	$NaCa_2Mg_5Si_7AlO_{22}F_2$									6
	Combined water									1

3. Evaluation of the results

The quality and the quantitative proportions of the CaO and MgO containing phases produced when digesting dolomite bearing bauxites are primarily determined by the components dissolved in the alimunate liquor at the time of formation, although they are influenced by the solid phases capable of reacting with the individual components of the solution. From this aspect it is rather important that SiO_2 is present in the form of a readily soluble kaolinite or a quartz rather difficult to digest, whereas TiO_2 as a ready to react anatase or a much less soluble rutile. Calcite and dolomite

Table IV

Phase transformations of the compounds produced under the conditions of in-plant red mud washing

Na_2O_k = 40 g/l α_k = 2,25 T = 80 °C t = 24 hours solids content = 200 g/l

1.	2.	3.	4.	5.	6.	7.	8.	9.	10.	11.
		Solid phase composition, %								
1.	$Ca(OH)_2$	16	14							
2.	$3CaO \cdot Al_2O_3 \cdot 6H_2O$	71		2						
3.	$3CaO.Al_2O_3.kSiO_2.(6-2k)H_2O$		86			97			34	7
4.	$CaTiO_3$									
5.	$Ca_3Al_2O_6 \cdot (8-12)H_2O$									
6.	$CaAl_2O_4$									
7.	$Mg(OH)_2$			73	34			13	6	
8.	$Mg_6Al_2CO_3(OH)_{16} \cdot 4H_2O$			20	19			5	3	
9.	$Mg_4Al_2(Al_2Si_2)O_{10}(OH)_8$				5			23	7	16
10.	$MgAl_2O_4$			2						
11.	Ca(Mg, Al)-titanate									11
12.	$CaCO_3$	10				3			6	5
13.	$MgCO_3, MgCO_3 \cdot 3H_2O$			3	10			11		
14.	$(Mg, Ca)CO_3$								17	13
15.	$3(Na_2O.Al_2O_3.2SiO_2).Na_2X.aq$				32			48	26	24
16.	TiO_2 anatase									10
17.	$Na_2O \cdot 3TiO_2 \cdot nH_2O$									7
18.	$NaCa_2Mg_5Si_7AlO_{22}F_2$									6
	Combined water	1							1	1
	Amorphous $CaCO_3$	2								

will be transformed, depending on the degree of crystallization, only at temperatures above 180 °C into reacting CaO and MgO, whereas kaolinite into sodalite as early as at 100 °C, while quartz and rutile will react with the base only partially, even at a temperature of as much as 240 °C. As a consequence, the mineral phases will precisely determine the feasibly reactions. Based on the experimental data the following conclusions may be drawn:

— on the effect of CaO, calcium-aluminate will always be formed [2] from the aluminate liquor, but in the case of an excessive lime surplus or high mole ratio base $Ca(OH)_2$ [1] will also be found;

Table V

Phase transformations of the compounds produced under the conditions of in-plant red mud washing

Na_2O_k = 5 g/l α_k = 2,70 T = 85 °C t = 24 hours solids content = 200 g/l

1.	2.	3.	4.	5.	6.	7.	8.		10.	11.
		Solid phase composition, %								
1.	$Ca(OH)_2$	15	8							
2.	$3CaO \cdot Al_2O_3 \cdot 6H_2O$	68		1						
3.	$3CaO \cdot Al_2O_3 \cdot kSiO_2 \cdot (6-2k)H_2O$		85			93			36	7
4.	$CaTiO_3$									
5.	$Ca_4Al_2O_6 \cdot (8-12)H_2O$									
6.	$CaAl_2O_4$									
7.	$Mg(OH)_2$			67	25			10	6	
8.	$Mg_6Al_2CO_3(OH)_{16} \cdot 4H_2O$			25	28			8	3	
9.	$Mg_4Al_2(Al_2Si_2)O_{10}(OH)_8$				5			23	7	16
10.	$MgAl_2O_4$			2						
11.	Ca(Mg, Al)-titanate									11
12.	$CaCO_3$	16	7			7			7	5
13.	$MgCO_3$, $MgCO_3 \cdot 3H_2O$			4	10			1		
14.	$(Mg, Ca)CO_3$								18	13
15.	$3(Na_2O \cdot Al_2O_3 2 \cdot SiO_2) \cdot Na_2Xaq$				32			48	23	23
16.	TiO_2-atanase									10
17.	$Na_2O \cdot 3TiO_2 \cdot nH_2O$									7
18.	$NaCa_2Mg_5Si_7AlO_{22}F_2$									7
	Combined water	1		1						1

— the SiO_2 content of the kaolinite will form sodalite [15] or cancrinite [15] with the aluminate liquor;

— in the simultaneous presence of CaO and SiO_2, in practice there will only be a hydrogarnet type [3] calcium-aluminium silicate, that is, CAS [3] separated from the aluminate liquor;

— when MgO is added, there will mainly be $Mg(OH)_2$ [7] produced in the aluminate liquor, magnesium-aluminate $MgAl_2O_4$ [10] will be found only in a small amount, while for the production of basic magnesium-aluminium carbonate $Mg_6Al_2CO_3(OH)_{16} \cdot 4H_2O$ [8] the CO_2 content of an operational grade base will suffice, and in the presence of SiO_2 the basic magnesium-

Table VI

Phase composition of the red mud of KDT-3 bauxite

Components in %

Al_2O_3	in hematite	0,7	Fe_2O_3	in goethite	6,0
	in goethite	0,1		in hematite	30,6
	in CAS	4,0			36,6
	in MAS	2.3			
	in sodalite	1,5	SiO_2	in quartz	0,5
$NaO \cdot 8CaO \cdot 3Al_2O_3 \cdot 10SiO_2$		1,0		in sodalite	1,6
	in diaspore	0,5		in cancrinite	1,9
	in Mg—Al-carbonate	1,5		in MAS	1,3
		13,5		in CAS	0,4
				Na—Ca—Al-silicate	2,0
MgO	in MAS	1,8			7,7
	in dolomite	0,7			
	Mg—Al-carbonate	3,3			
	in titanate	1,1	CaO	in CAS	6,3
		7,2		NaCa—Al-silicate	1,5
				in calcite	0,5
				in dolomite	1,0
				in Ca-titanate	1,5
					10,8

-aluminium silicate (MAS) phase [9] will also appear in addition to $Mg(OH)_2$ [7];

— in the simultaneous presence of CaO and MgO, there will mainly be CAS [3] separated on the effect of SiO_2;

— following the dissolution in the aluminate liquor, TiO_2 will readily react with MgO or CaO, producing Ca(Mg,Al)-titanate (11), Ca [4], or $MgTiO_4$ [20], depending on the ratios involved. The formation of these compounds will precede the production of the usual sodium-titanates. In the case of a sufficient amount of TiO_2 there will be no $Mg(OH)_2$ [7] produced and, interestingly, if SiO, is added to the system, then a $Mg_2Al_3Si_5O_{18}$ composition compound [21], rather different from those referred to above will be formed;

— a reduced mole ratio of the base (increase its Al content) will decrease the crystallization degree and grain size of the solids while phases of a higher Al content will be formed, while the surface articulation of the phases is increasing;

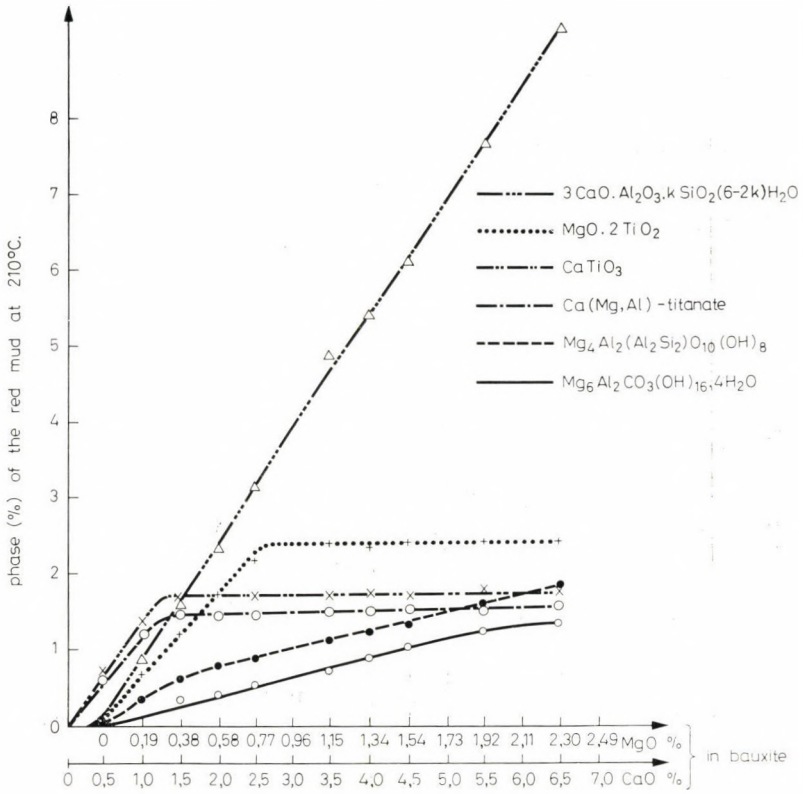

Fig. 5. Production of the Ca, Mg containing phases

— when digesting calcite-dolomite bearing bauxites, the SiO_2 content of the kaolinite will be transformed into sodalite [15] prior to the production of active CaO-MgO, part of which will then be caustified or transformed into CAS [3] and MAS [9];

— the phase formation sequence in the case of Hungarian bauxites is as follows:

In the case of minor calcite and dolomite contaminations first the Ca,Mg-titanates will be produced, parallel to the CAS [3] formation; with an increasing calcite and dolomite content the titanate formation will be completed and MAS [9], too, can be discovered in addition to CAS [3]; in the absence of free SiO_2, there will be CA [2], low k-value CAS [3], $Ca(OH)_2$ [1], and mainly $Mg(OH)_2$ [7] or Mg-Al-carbonate [8] produced from the entire CaO and MgO quantity;

— under the conditions of sludge washing the Ca and Mg-titanates [11], MAS [9], and the Mg-Al-carbonate [8] will not undergo any changes, CA [2], $Ca(OH)_2$ [1], and CAS [3] will caustify the soda content of the base or the

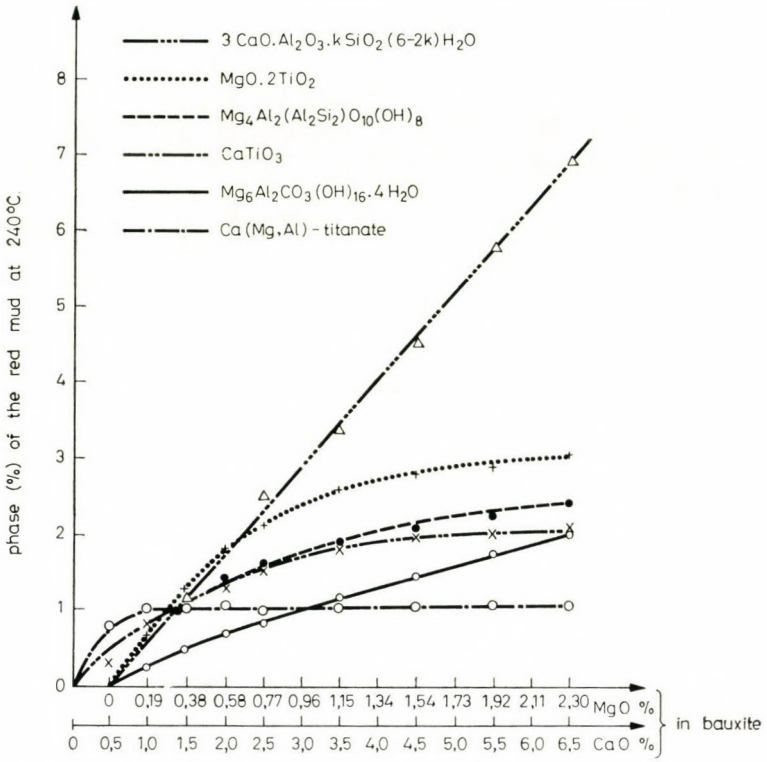

Fig. 6. **Production of the Ca, Mg content phases of red mud at 240 °C**

sodalite [15], while $Mg(OH)_2$ [7] will be transformed into a Mg-Al-carbonate [8].

The qualitative and quantitative ratio, respectively, of the compounds thus produced will significantly modify the NaO_2 and Al_2O_3 losses which can usually be observed. The soda quantity obtained will be proportional to the calcite and/or dolomite quantities introduced into the cycle. The dissolution efficiency and the final result of the Dorr-series recaustification referred to may be calculated on the basis of the $CaCO_3$ and $MgCO_3$ content of the red mud, being in practice usually about 70 to 75 per cent.

The magnitude of Al_2O_3 and Na_2O losses in red mud is related to the sodalite [15], where the ratio of the Na_2O/SiO_2 molecules is 1,67 while SiO_2/Al_2O_3 is 2. In CAS [3], if the k factor is 2, the Al_2O_3 loss will decrease, otherwise it will increase; the latter is more frequent.

The bonded Na_2O loss will decrease proportionally to the SiO_2 in CAS [3]. Mg-Al-silicate formation [9], too, will reduce Na_2O losses but the Al loss in this compound, if related to SiO_2, will be double.

Ca(Mg)-titanate formation is associated with a slight decrease of the

Table VII

Chemical composition of the bauxite, %

Fe_2O_3	23,3
Al_2O_3	47,3
SiO_2	7,43
lose	18,6
TiO_2	2,3
CaO	0,5
MgO	<0,1

Phase composition of the bauxite, %

Al_2O_3	in kaolinite	5,0
Al_2O_3	in gibbsite	23,3
Al_2O_3	in diaspore	1,7
Al_2O_3	in boehmite	16,1
Al_2O_3	in goethite	0,5
Al_2O_3	in maghemite	0,2
Al_2O_3	in hematite	0,5
Fe_2O_3	in goethite	6,0
Fe_2O_3	in hematite	14,8
Fe_2O_3	in maghemite	2,5
SiO_2	in kaolinite	5,9
SiO_2	in quartz	1,5
TiO_2	in anatase	1,6
TiO_2	in rutile	0,8
CaO	in calcite	0,4
CaO	in dolomite	<0,2
MgO	in dolomite	<0,15

soda loss. From a practical viewpoint, the $Mg(OH)_2$ [7] or Mg-Al-carbonate [8] produced on increased Mg contamination will lead to a significant base loss excess, and a considerably reduced Al recovery.

The quantity and quality of the phases produced, as well as the development of the fixed Na_2O and Al_2O_3 losses in the function of increasing dolomite content are shown, in the case of a Halimba bauxite, in Figures 5, 6, 7, and 8. Figures 5 and 6 also illustrate the formation sequence of the individual phases.

In addition to the chemical losses, the new phases thus produced will cause the operational problems mentioned above. In the supernatant material formed at red mud washing, the enrichment of MAS [9] and that of the basic Mg-Al-carbonate [8] could always be observed together with undigested boehmite and the Dorr-series hydrolysis product: gibbsite. However, this

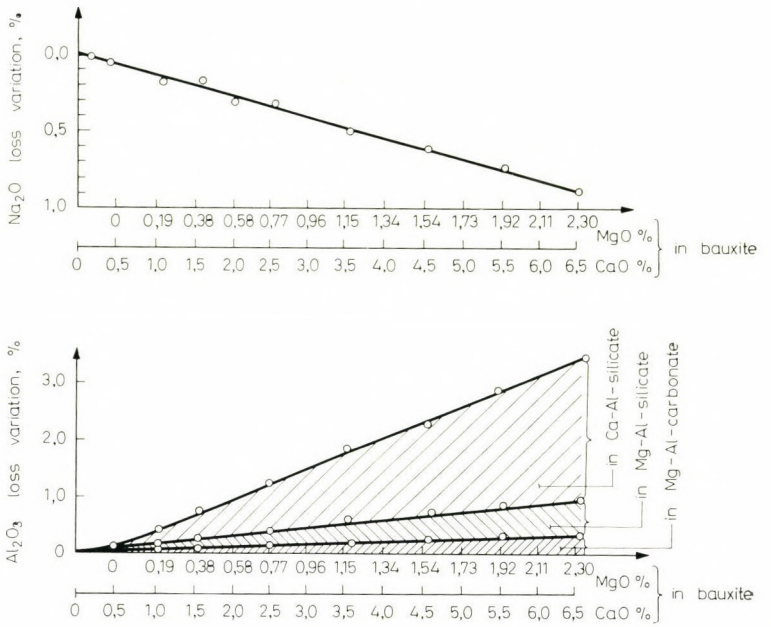

Fig. 7. Development of the Na_2O– and Al_2O_3–losses in the function of the CaO, MgO content at 210°C

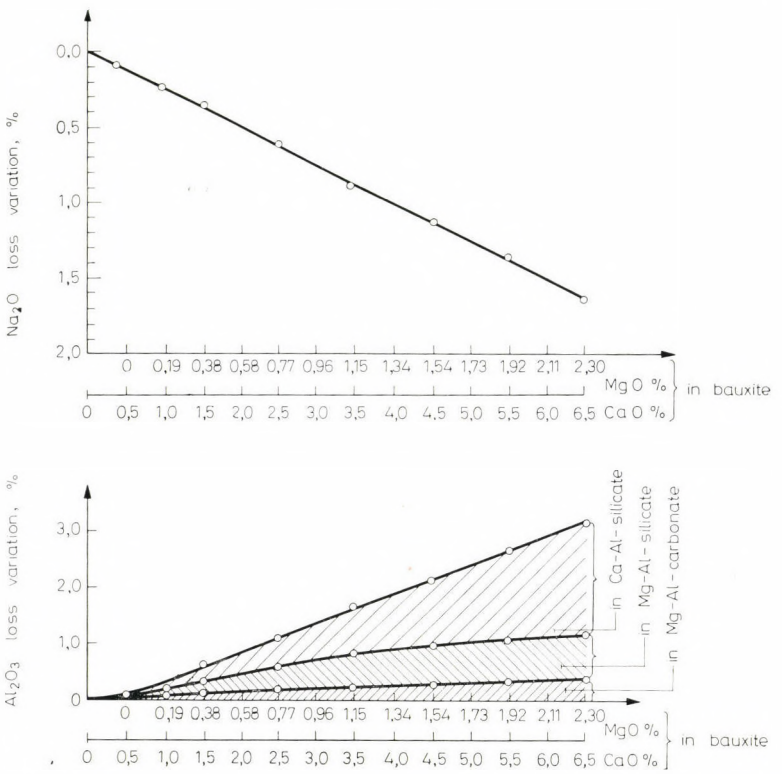

Fig. 8. Development of theNa_2O– and Al_2O_3– losses in the function of the CaO, MgO content at 240°C

phenomenon may be regarded as a usual flotation process since these Mg-containing phases are of a lamellar structure, having small grains but a large surface, and under Dorr-series conditions, in spite of the high soda concentration and temperature, they are excessively connected to the air bubbles always present in the sludge. Characteristically, while the specific surface of a red mud made of normal bauxite is 12 to 15 m^2/g, that of MAS [9] is 35 to 40 m^2/g, and that of $Mg(OH)_2$ [7] or the Mg-Al-carbonate [8] is as much as 45—50 m^2/g. The different physico-chemical properties of the phases produced, including

— hydration heat,
— surface adsorption,
— foaming capacity

have revealed that the behaviour and characteristics of the Mg-containing phases, in an aluminate liquor conforming to the Dorr-series conditions, will be entirely different from those of the other red mud components where the adhesion of the solid phase and air is excessive and, in certain cases, the red mud content of the foam phase may exceed that of the settled sludge. This, however, would make the operation of the washing line quite impossible.

REFERENCES

1. Vörös, I.: *Fémipari Kutató Intézet Közleményei* (9), 105—124, in Hungarian
2. Barrer, R. and White, E.: *I. Chem. Soc.* (1962), 1561—1571
3. A method to reduce and replace the caustic lye of soda losses in the Bayer process — Hungarian Patent Application No. Fe-856, 30 Dec. 1971, in Hungarian
4. Seimiya, S.: Some Properties of Sodalite in Red Mud — *Extractive Metallurgy of Aluminium* **1**, Alumina, 115—132, Interscience Publishers
5. Серебреникова, О. В.: О взаимодействии карбоната кальция с водными растворами и едкого натрия. Труды У. П. И. им. С. М. Кирова Металлургиздат 1957. № 58 стр. 57—67.
6. Бесков, С. Д.—Слизковская, О. А.: Аналитическая химия Учпедиз. 1958. стр. 560.
7. Бернштейн, В. А.—Маценок, Е. А.: О взаимодействии Fe_2CO_3 и $MgCO_3$ со щелочно-алюминатным раствором при выщелачивании боксита по Байеру. *Труды ВАМИ. Металлургиздат* (1957) № 39, стр. 72—73.
8. Мазель, В. А.: Определение границ поля $CaCO_3$ в системе $CaO—Al_2O_3—Na_2O—CO_2—H_2O$ статистическим методам. *Труды ВАМИ Металлургиздат* (1957) № 39, стр. 19—23.
9. Кузнецов, С. М.—Деревянкин, В. А.: Физическая химия производства глинозема по способу Байера. *Металлургиздат* (1964), стр. 206.
10. Лейтейзен, М. Г.—Белецкий, М. С.: »*Цветные металлы*« (1963), № 9.
11. Juhász, A.—Orbán, *M.* Mrs—Matula, M.: *BKL Kohászati Lapok* (1965), 513—521, in Hungarian
12. Vörös, I.: Caustification of the Sodium-aluminum-silicates and Red Mud — *Periodical Report of the „Fémipari Kutató Intézet"* Budapest 1967, in Hungarian
13. Vörös, I.—Bujdosó, E.—Orbán, M.—Tóth, L.: Caustification of Red Mud — Paper presented at the ICSOBA Colloquium, Banska Bystrica 6—10 June, 1972
14. Бергер, А. С.: Об образовании гидрогранатов при атмосферном давлении. Химия и технология глинозема. Изд-во Наука. Сибирское отделение Новосибирск (1971), стр. 270—280.
15. Аракелян, О. М.: К вопросу о причинах различия фазового состава белых шламов. Химия и технология глинозена. Изд-во Наука. Сибирское отделение Новосибирск (1971), стр. 188—195.

16. Горячев, А. А.—Игнатев, О. С.: О формах нахождения кремнезема в метастабильных Алюминатных растворах. Химия и технология глинозема. Изд-во Наука. Сибирское отделение. Новосибирск 1971, стр. 173—181.
17. Ни, Л. П.: О поведении кремнезена в алюминатных растворах. Химия и технология линозема. Изд-во Наука. Сибирское отделение. Новосибирск 1971. стр. 143—150.
18. H. Borsiczky, V.—Solymár, K.: *BKL Kohászati Lapok*, **101** (1968), 187—192, in Hungarian
19. Миронов, М. В.—Пазухин, В. А.: О повидении двуокиси титана в щелочных и алюминатных растворах. Изв. вузов. Цветная металлургия (1959), № 1, стр. 83—90.
20. Миронов, М. В.—Пазухин, В. А.: О поведении двуокиси титана в щелочных и алюминатных растворах в присутствии извести и кремнезема. Изв. вузов. Цветная металлургия (1959), № 2, стр. 89—95.
21. Wefers, K.: *Metall.* **25** (1971), 239—250
22. Белов лН. В.: Структура ионных кристаллов и металлургических фаз. Изд-4о АН СССР 1947, стр. 108.
23. Zámbó, J.—Orbán, *M.* Mrs.—Solymár, K.: Examination of Alumina Plant Depositions—*Periodical Report of the "Fémipari Kutató Intézet"* Budapest 1970, in Hungarian
24. Смирнов, М. Н.: Образование гидроалюмакарбонатов натрия при взаимодействии гидрокисей алюминия с содобикарбонатным растворами. Химия и технология глинозема. Новосибирск, 1971. Изд-во Наука. Сибирское отделение, стр. 381—387

Bildung von CaO- und MgO-Verbindungen bei der Verarbeitung der kalzitisch-dolomitschen Bauxite nach dem Bayer-Verfahren. Die bei der Verarbeitung der kalzitisch-dolomitischen Bauxite von Halimba auftretenden Betriebsprobleme machten es notwendig das $Na_2O-Al_2O_3-CaO-MgO-TiO_2-SiO_2-H_2O-CO_2$-System unter den Bedingungen der Bayer-Technologie zu untersuchen. Es wurde festgestellt, daß die quantitativen und qualitativen Verhältnisse der bei der Aufschließung sich bildenden Ca- und Mg-hältigen Phasen vor allem von den in der Aluminatlauge gelösten Komponenten bestimmt, aber auch von den, mit einzelnen Komponenten der Lösung reaktionsfähigen, festen Phasen beeinflußt werden.

Образование соединений CaO и MgO в процессе переработки кальцитно-доломитных бокситов методом Байера. Возникающие во время переработки кальцитно-доломитных бокситов месторождения Халимба проблемы по ведению технологического процесса потребовали проведения анализа системы $Na_2O-Al_2O_3-CaO-MgO-TiO_2-SiO_2-H_2O-CO_3$ при параметрах технологии Байера. Установлено, что пропорции качества и количества фаз с содержанием Ca и Mg, образующихся при разложении доломитовых бокситов, определяются первую очередь растворенными в алюминатной щелочи компонентами, но на указанные выше пропорции воздействуют также твердые фазы, способные вступать в реакцию с отдельными компонентами раствора.

Acta Technica Academiae Scientiarum Hungaricae, Tomus 82 (3—4), pp. 353—375 (1976)

SOLUTION OF ELASTIC CONTACT PROBLEMS BY THE FINITE ELEMENT DISPLACEMENT METHOD

I. PÁCZELT*

CAND. TECHN. SCI.

[Manuscript received June 26, 1974]

Contact problem of elastic continua subject to arbitrary load and of arbitrary surface is a rather intricate one, contact domains not being known a priori. Here, the continuum is replaced by a bulk of elements of finite degrees of freedom, the obtained elastic system serving as basis for the solution of the problem based on the principle of potential energy minimum. Because of the unilateral relations between the bodies, the mathematical programming can be discussed as a quadratic programming problem. Use of the Khun-Tucker conditions yields a solution for the dual of this primal problem, much easier to establish and solve than the original one. Friction and adherence between the bodies are considered as negligible, and displacements, deformations to be small.

Introduction

With the advent and generalization of computers, elasticity and mathematical methods easy to computerize have been developed, such as the method of finite elements and various methods of mathematical programming.

In spite of the approximation involved in the combined application of both methods, its practical significance must not be underestimated, since the complexity of mechanical or architectural structures, of various types of load practically prevents any exact solution.

A practical satisfactory solution of the contact problem is possible by discretizing the finite elements according to size and kind, and applying the so-called condition of the contact/separation discussed in item 1.2.2.2.

According to the Author's knowledge, the first publications on the mathematical programming of contact problems date back to 1967. An interesting, universal, efficient method has been suggested by FRIEDMANN, V. M. and TSCHERNINA, V. S. [1], [2], i. e. cyclic iteration based on the gradient method, to approximate the first-kind integral equation-inequality describing the contact-separation phenomenon; and that with a universal formulation, suitable for examining a wide range of structures. As an example, solution of contact problems of coaxial cylinders and rings, as well as of a circular plate under symmetric load and a Winkler type foundation is described in [2].

Theoretical bases and a concrete solution method for the calculation of

* Dr. I. PÁCZELT, Győri Kapu u. 37, H-3531 Miskolc, Hungary.

elastically an bedded structures — involving the method of quadratic programming — has been considered in the significant, pioneering work by DUPUIS, G. and PROBST, A. [3]; potential energy of the system is minimalized under the constraint expressing the conditions of the contact/separation at a finite number of points. The elastic strain energy of the foundation and the beam contacting is approximated by the method of differences.

For the sake of completeness, let us mention references [4] to [7] concerning the theoretical and practical problems of unilateral relations occurring at structure supports — although these do not strictly belong to the scope of this study.

Thesis [8] suggests developping ideas in [2] permitting the consideration, in addition to rigid-body displacements, also of angular rotation between solids, what is more, a subsequent paper [9] accepts — in addition to contact forces, — internal forces developing at structural joints (e. g. of shells, plates) as unknowns.

[10] and [11] are concerned with the contact problem of advancing bodies by means of the method of quadratic programming assuming that within the proposed zone of the contact, the system of (other than contact) forces acting on the bodies causes no displacement, and that the relative rigid body translation between the bodies can only be positive, i. e. an approach. Solutions in [1] and [9] are exempt from these restrictions.

The problem of contact between the beam or plate and a Winkler-type foundation is solved in [12] and [13], so as to minimize the potential energy by the constants involved in the series expansion of the deflection functions, keeping in mind the conditions of the contact separation; the solution is obtained by quadratic programming.

A similar concept is encountered in [14] for the solution of the contact between a symmetrically loaded circular plate and the elastic semi-space.

Several works by CONWAY, H. D. and ENGEL, P. A. have been concerned with contact problems in cold rolling. Among them, [15] analyses the contact between the stiff cylinder and the elastic layer; the contact separation condition is checked at a finite number of points; step-wise load increments are determined by involving ever more points in the contact. The algebraic equation-inequality system expressing the contact separation is essentially the same as that for the approximate solution of the Fredholm integral equation inequality encountered on setting up this problem. In this relation it is affine to that by FRIEDMANN, V. M., TSCHERNINA, V. S., while solution steps of the algebraic equation inequality system are quite different. Another paper by them [16] also reckons with the effect of friction.

Along with the popularization of the finite element method, several papers were published on the calculation of various elastic supports ([17], [18], [19]), *considering the connection between the bodies as bilateral.*

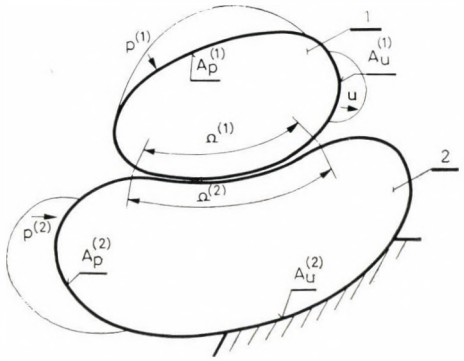

Fig. 1. The problem is to find the real contact domain Ω_p between bodies 1 and 2, displacement vector field and stress state of the bodies

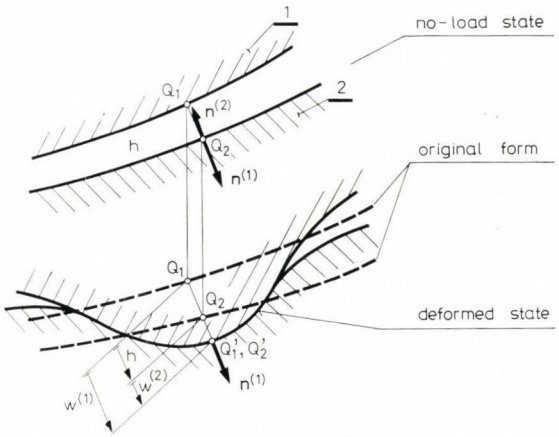

Fig. 2. Geometry conditions of contact separation:

for $w^{(2)} - w^{(1)} + h = 0$ contact,
for $w^{(2)} - w^{(2)} + h > 0$ separation (gap)

A quite different approach is encountered in [27], also taking the Coulomb friction between the bodies into account; separation and contact domains can be determined by gradually increasing the load and solving the problem step-wise. Convergency of the method is, however, questionable.

[20] presents a contact problem between a rigid sphere and an ideally plastic semi-space.

Slide ways of tool machines are analysed by the finite element method in [21], making use of the empirical relationship between deflection and pressure, depending on the design, to determine the contact pressure. The method suggested in this study eliminates the empirical relationship.

After this short survey of literature — with no claim to completeness — let us consider the contact problem itself.

For the sake of simplicity, let us assume that the elastic system consists of two bodies, with no restriction for the generality of the problem, at the same time facilitating to expose, set out and simply treat peculiar problems of contact.

Let the bodies in Fig. 1 be denoted by $t = 1, 2$; assignment of any magnitude will be indicated by the superscript in parentheses. Body surfaces will be separated into three domains:

$A_p^{(t)}$ — body surface part bearing a given surface load;

$A_u^{(t)}$ — body surface part with given displacements (kinematic boundary conditions);

$\Omega^{(t)}$ — proposed zone of contact;

$A^{(t)} = A_p^{(t)} + A_u^{(t)} + \Omega^{(t)}$ — body surface.

Coupling each two points of body surfaces into domain $\Omega^{(t)}$ their displacements or a component in some direction e. g. normally will be represented in course of the deformation[1] (Fig. 2.).

Correlation between points in domains $\Omega^{(1)}$ and $\Omega^{(2)}$ being settled, in the following the superscript will be omitted, writing Ω alone.

Unilateral relations between bodies implies that for a difference

$$n^{(1)r}(u_r^{(2)} - u_r^{(1)} + h_r) = w^{(1)} - w^{(2)} + h \equiv y > 0, \tag{1}$$

between the projections of the displacement vectors[2] $u_r^{(t)}$ of points in domain Ω in a given direction (e. g. the outer normal of body 1 at point Q_1) *separation* occurs, that is, the contact force is zero, $p = 0$, and for

$$n^{(1)r}(u_r^{(2)} - u_r^{(1)} + h_r) = w^{(2)} - w^{(1)} + h \equiv y = 0, \tag{2}$$

the body point couples contact each other, hence $p \geq 0$. Let the separation gap domain be denoted by $x \in \Omega_0$, the contact domain by $x \in \Omega_p$, and be $\Omega = \Omega_0 + \Omega_p$, where x is a tridimensional co-ordinate in spatial problems, a two-dimensional one for planar problems, and a linear one for single-variable problems; $n^{(1)r}$ — is the outer normal of body 1; $u_r^{(t)}$ the displacement vector of body t; and h_r the vector of the initial gap. By definition, $w^{(t)}$ is the projection of the displacement of a point in domain Ω in the indicated direction, furthermore, domains Ω_0 and Ω_p are unknown.

Because of the unilateral connections, for points in domain Ω:

$$yp = 0, \quad x \in \Omega\,. \tag{3}$$

[1] The same hypothesis is encountered in classic solutions of rigid-punch semi-space semi-plane contact problems assuming small displacements (see e. g. in [22]).

[2] Vectors and tensors with covariant or contravariant components are denoted by subscripts and superscripts, as is usual. Latin letters may assume values of 1,2,3 [22].

1. Solution of contact problems according to the principle of potential energy minimum

1.1 *Setting the problem*

To solve the contact problem, the displacement vector field of bodies belonging to the elastic system will be approximated by the finite element method, also taking the interaction of bodies due to unilateral connections (contact effect) into consideration, in determining the unknown parameters. This approximation is especially advantageous for bodies complex in form, difficult to clamp, and subject to combined loads; inconvenient, practically impossible to solve.

Let us assume a priori a bilateral connection between the bodies in the indicated direction $n_r^{(1)}$, that is:

$$w^{(2)} - w^{(1)} + h = 0, \; x \in \Omega. \tag{4}$$

The displacement field $u_r^{(t)}$ to be approximated is required to meet kinematic boundary conditions on surface $A_u^{(t)}$. Then the potential energy of body t (for zero initial deformation and stress):

$$\pi^{(t)} = \frac{1}{2} \int_{(V^{(t)})} C^{klrs} a_{kl} a_{rs} dV - \int_{(V^{(t)})} q^s u_s dV - \int_{(A_p^{(t)})} p_o^s u_s dA, \quad t = 1,2 \tag{5}$$

where $V^{(t)}$ — volume of body t; $A_p^{(t)}$ — its surface under prescribed surface traction p^s; C^{klrs} — matrix of material constants; a_{rs} — strain tensor; q^s — volumetric force intensity vector, $\sigma^{rs} = C^{rskl} a_{kl}$ — stress tensor according to Hooke's law.

Introducing functional

$$L_1 = L_1(u_r^{(1)}, u_r^{(2)}, p) = \pi^{(1)} + \pi^{(2)} + \int_{(\Omega)} p(w^{(1)} - w^{(2)} - h) dA \tag{6}$$

in view of $a_{rs} = [(u_r \nabla_s) + (\nabla_r u_s)]/2$, for small displacements, involving the Hamilton differential operator ∇_s; and $C^{klrs} = C^{rskl}$, displacement field i. e. stress $n_r^{(t)} \sigma^{(t)\,rs}$ in points of domain Ω can be separated into components in a given direction $n^{(1)r}$ and normally to it, then, from Hooke's law and the Gauss—Ostrogradsky integral transformation theorem, the following conclusions of the Euler equations belonging to the stationary value of the functional ($\delta L_1 = 0$) are obvious, *assuming the relation to be bilateral:*

1. the Lamé equilibrium equation in terms of the displacement vector:

$$\nabla_k \sigma^{(t)kl}(u_s^{(t)}) + q^{(t)l} = 0, \; x \in V^{(t)};$$

2. fulfilment of the dynamic boundary condition:

$$n_r^{(t)} \sigma^{(t)rs} = p_0^s, \; x \in A_p^{(t)};$$

3. fulfilment of the supplementary kinematic boundary condition (4) related to both bodies, arising from their bilateral relation;

4. relationship for the contact force as an internal force:

$$p = - n_r^{(1)} \sigma^{(1)rs} n_s^{(1)}, \qquad p = n_r^{(1)} \sigma^{(2)rs} n_s^{(2)};$$

5. zero tangential stresses from neglecting the friction and adherence

$$\tau^{(1)} = | n_r^{(1)} \sigma^{(1)rs} n^{(1)p} \varepsilon_{spv} | = 0,$$
$$\tau^{(2)} = | n_r^{(2)} \sigma^{(2)rs} n^{(1)p} \varepsilon_{spv} | = 0,$$

where ε_{rst} is the Levi-Civita tensor [22].

Change of functional (6):

$$\Delta L_1 = \delta L_1 + \delta^2 L_1 = \delta^2 \pi + \int_{(\Omega)} \delta_p (\delta w^{(1)} - \delta w^{(2)}) \, \mathrm{d}A \,,$$

since $\delta L_1 = 0$, while according to $\delta^2 \pi > 0$, $\pi = \pi^{(1)} + \pi^{(2)}$ is a potential energy with a minimum.

Taking note that, because of (4), in case of an exact solution

$$L_1 = \pi^{(1)} + \pi^{(2)} \,. \tag{7}$$

This relationship is also valid in case of a unilateral relation between the bodies, hence, where equality (4) is replaced by inequality-equality (1), (2) and expression (3). Since the unilateral relation leads to $p \geq 0$, $y \geq 0$, $y \cdot p = 0$, the problem has to be developed so as to permit application of mathematical programming methods.

1.2. *Treatment of the contact problem by quadratic programming*

From the mentioned aspect, the problem has to be discretized; partly, the displacement vector field of the bodies will be approximated by a kinematically admissible displacement field, and partly, the integral value from the constraint over the domain Ω involved in the functional L_1 (see in (6)) will be so approximated that it appears as a finite sum.

1.2.1 *Assumption of the displacement field to be approximated*

Kinematically possible displacement fields are required to meet the kinematical boundary conditions on the surface $A_u^{(t)}$ and to deliver the strain tensor. The displacement vector field could also be approximated in series form according to the Ritz method, but because of the important change of the stress tenzor field adjacent to the contact domains, as well as the complicated form and load of the bodies constituting the elastic system, it seems more expedient to apply the so-called compatible displacement model of the finite element method[3] or of any other model expressing the potential energy of the system obtained by transforming the functional, to be minimized in terms of the generalized nodal displacement vector, such as models of hybrid displacement, by P. TONG [24] and by T. H. H. PIAN [25] of hybrid stress and mixed fields.

In the compatible displacement model of the finite elements method, the kinematically admissible displacement field is approximated by the entity of functions assumed to be element-wise [26]. Let the displacement field be[4] inside element e obtained by seperating the body denoted by $\mathbf{u}^e(x)$, and its (generalized) nodal displacements by $\mathbf{u}^e$. In terms of the assumed approximation matrix $\mathbf{A}^e(x)$, the displacement field inside the element is:

$$\mathbf{u}^e(x) = \mathbf{A}^e(x)\,\mathbf{u}^e. \tag{8}$$

Denoting vectors formed of members of the strain and stress tensor by $\boldsymbol{\epsilon}^e(x)$ and $\boldsymbol{\sigma}^e(x)$ resp., and in knowledge of the displacement field:

$$\boldsymbol{\epsilon}^e(x) = \mathbf{D}\,\mathbf{u}^e(x) = \mathbf{B}^e(x)\,\mathbf{u}^e \tag{9}$$

where $\mathbf{D}$ — differential operator matrix, while making use of Hooke's law and assuming initial deformations and stresses to be zero,

$$\boldsymbol{\sigma}^e(x) = \mathbf{C}^e\,\boldsymbol{\epsilon}^e(x) = \mathbf{C}^e\,\mathbf{B}^e(x)\,\mathbf{u}^e \tag{10}$$

where $\mathbf{C}^e$ — is the matrix of material constants.

Applying the compatible displacement model, the assumed approximation matrix $\mathbf{A}^e(x)$ must yield strain $\boldsymbol{\epsilon}^e(x) \equiv 0$ if the element performs a rigid body motion, further, the transition from one element to the other has to respect the displacement continuity [26].

Introducing the above magnitudes in (5) yields the potential energy for element e:

$$\pi_e = \frac{1}{2}\,\mathbf{u}^{e,T}\,\mathbf{K}^e\,\mathbf{u}^e - \mathbf{q}_*^{e,T}\,\mathbf{u}^e, \tag{11}$$

[3] Bases of the finite element method are assumed to be known.

[4] Multidimensional vectors and matrices are marked by bold letters, and their transposition by the right superscripts T.

where

$$\mathbf{K}^e = \int_{(V^e)} \mathbf{B}^{e,T}(x)\, \mathbf{C}^e\, \mathbf{B}^e(x)\, \mathrm{d}V \quad \text{— the stiffness matrix of the element;}$$

and

$$\left.\begin{aligned} \tilde{\mathbf{q}}^e &= \int_{(V^e)} \mathbf{A}^{e,T}(x)\, \mathbf{q}^e(x)\, \mathrm{d}V \\ \tilde{\mathbf{p}}^e &= \int_{(A_p^e)} \mathbf{A}^{e,T}(x) \mathbf{p}^e(x)\, \mathrm{d}A \end{aligned}\right| \begin{array}{l} \text{generalized nodal force values from volumetric and} \\ \text{surface loads } \mathbf{q}^e(x) \text{ and } \mathbf{p}^e(x), \text{ resp., and:} \end{array}$$

$$\mathbf{q}_*^e = \tilde{\mathbf{q}}^e + \tilde{\mathbf{p}}^e.$$

Making use of the identity of the generalized displacement vector at identically marked nodes of adjacent elements, permitting the production of potential energy for the tested body:

$$\pi^{(t)} = \frac{1}{2}\, \tilde{\mathbf{u}}^{(t),T}\, \widetilde{\mathbf{K}}^{(t)}\, \tilde{\mathbf{u}}^{(t)} - \tilde{\mathbf{u}}^{(t),T}\, \tilde{\mathbf{q}}_*^{(t)}, \quad t = 1,2 \tag{12a}$$

where:

$\tilde{\mathbf{u}}^{(t)}$ — generalized nodal displacement vector for body t;
$\widetilde{\mathbf{K}}^{(t)}$ — stiffness matrix ($\widetilde{\mathbf{K}}^{(t)} = \widetilde{\mathbf{K}}^{(t),T}$);
$\tilde{\mathbf{q}}_*^{(t)}$ — generalized nodal load vector from external loads.

The value of the displacement vector field at nodes on the body surface $x \in A_u^{(t)}$ being known, $\tilde{\mathbf{u}}^{(t)}$ can be separated into two parts, i. e. vectors with unknown and with known components: $\dot{\mathbf{u}}^{(t),T} = [\mathbf{u}^{(t),T} \;\vdots\; \mathring{\mathbf{u}}^{(t),T}]$; and so can be $\tilde{\mathbf{q}}_*^{(t)}$: $\dot{\mathbf{q}}_*^{(t),T} = [\bar{\mathbf{q}}^{(t),T} \;\vdots\; \mathring{\mathbf{q}}^{(t),T}]$. Then:

$$\pi^{(t)} = \frac{1}{2}\, [\mathbf{u}^{(t),T} \;\vdots\; \mathring{\mathbf{u}}^{(t),T}] \begin{bmatrix} \mathbf{K}^{(t)} & \widetilde{\mathbf{K}}_{12}^{(t)} \\ \widetilde{\mathbf{K}}_{1}^{(t)} & \widetilde{\mathbf{K}}_{22}^{(t)} \end{bmatrix} \begin{bmatrix} \mathbf{u}^{(t)} \\ \mathring{\mathbf{u}}^{(t)} \end{bmatrix} - [\mathbf{u}^{(t),T} \;\vdots\; \mathring{\mathbf{u}}^{(t),T}] \begin{bmatrix} \bar{\mathbf{q}}^{(t)} \\ \mathring{\mathbf{q}}^{(t)} \end{bmatrix}$$

and after performing the operations, and taking into consideration that in $\dot{\mathbf{u}}^{(t)}$ the only unknown is $\mathbf{u}^{(t)}$, for the functional to be constructed, $\pi^{(t)}$ may be simply understood as:

$$\pi_*^{(t)} = \frac{1}{2}\, \mathbf{u}^{(t),T}\, \mathbf{K}^{(t)}\, \mathbf{u}^{(t)} - \mathbf{u}^{(t),T}\, \mathbf{q}^{(t)} = \pi^{(t)} - \text{const} \tag{12b}$$

where

$\mathbf{q}^{(t)} = \bar{\mathbf{q}}^{(t)} - \widetilde{\mathbf{K}}_{12}^{(t)}\, \mathring{\mathbf{u}}^{(t)}$ — generalized nodal load vector from the known external load system and the displacement vector $\mathring{\mathbf{u}}^{(t)}$.

1.2.2 *Discretization of the constraint*

Let us approximate the integral value in functional L_1:

1.2.2.1 Checking contact/separation in discrete points:

$$\int_{(\Omega)} p(w^{(1)} - w^{(2)} - h)\, dA = \int_{(\Omega)} p(x)\big(w^{(1)}(x) - w^{(2)}(x) - h(x)\big)\, dA \cong$$

$$\cong \sum_{i=1}^{k} \big[p(x_i)\, \Delta A_i\big]\big(w^{(1)}(x_i) - w^{(2)}(x_i) - h(x_i)\big) =$$

$$= \sum_{i=1}^{k} P_i\big(w_i^{(1)} - w_i^{(2)} - h_i\big) = -\sum_{i=1}^{k} P_i y_i\,, \tag{13}$$

introducing notations

$$P_i = p(x_i)\, \Delta A_i \geq 0\,, \quad w^{(t)}(x_i) = w_i^{(t)}, \quad t = 1,2\,,$$
$$y_i = w_i^{(2)} - w_i^{(1)} + h_i \geq 0\,;$$

non-negativity of P_i and y_i follows from the unilateral relations (see in (1) through (3)).

Integral approximation can be mechanically interpreted as follows: domain Ω is separated into k finite small parts ΔA_i, the contact force distributed over them is replaced by its "resultant" P_i realized at an inner point (e. g. center) of the given domain part ΔA_i, and other terms of the integrand are calculated at these inner points.

Thereby the contact separation condition is checked at k points. Increase of k and a more exact calculation of integral (13) means the increase in accuracy by solving the contact problem.

Introducing the resultant vector of the contact surface stress

$$\bar{\mathbf{p}}^T = [\mathbf{P}_1, P_2 \ldots, P_k] \geq \mathbf{0} \tag{14}$$

and vectors of size $(1xk)$

$$\mathbf{w}^{(t),T} = [w_1^{(t)}, w_2^{(t)}, \ \ldots, w_k^{(t)}], \ t = 1,2 \tag{15}$$

$$\bar{\mathbf{h}}^T = [h_1, h_2, \ldots, h_k]\,, \tag{16}$$

$$\bar{\mathbf{y}}^T = [y_1, y_2, \ldots, y_k] \geq \mathbf{0} \tag{17}$$

construction of a corresponding permuting matrix may yield:

$$\mathbf{w}^{(t)} = \mathbf{G}^{(t)}\, \mathbf{u}^{(t)}, \quad t = 1,2 \tag{18}$$

hence, in view of (3), the constraint (13) may be written more concisely:

$$\int_{(\Omega)} p(w^{(1)} - w^{(2)} - \mathrm{h})\, \mathrm{d}A = \bar{\mathbf{p}}^T[\mathbf{G}^{(1)}\, \mathbf{u}^{(1)} - \mathbf{G}^{(2)}\, \mathbf{u}^{(2)} - \bar{\mathbf{h}}]\,, \tag{19a}$$

$$\bar{\mathbf{p}}^T\, \bar{\mathbf{y}} = \mathbf{0};\ \bar{\mathbf{p}} \geq \mathbf{0};\ \bar{\mathbf{y}} \geq \mathbf{0}. \tag{19b, c, d}$$

1.2.2.2 Checking contact/separation in small finite sections

The previous approximation is valid for a displacement field inside the element, considered as varying, according to a linear law. Now, the stress state of the element is constant (in a spatial case it is a tetrahedron of 12 degress of freedom, in plane problems triangles of 6 degrees of freedom), i. e., the generalized nodal force due to contact force p considered as constant becomes a concentrated force (resultant) of direction $w^{(t)}$.

In cases where the selected element type approximates the displacement field inside the element by polynomials higher than of first degree, the generalized nodal force due to the contact force developed on the element surface in domain Ω can only be calculated from the relationship

$$\widetilde{\mathbf{p}}^e = \int_{(A_\Omega^e)} \mathbf{A}^{eT}(x)\, \mathbf{p}^e(x)\, \mathrm{d}A\,.$$

The initially unknown contact force $p^e(x)$ cannot be approximated by a polynomial of higher degree than the selected element type is able to yield. If this fact is respested, our calculation will comply with the relationship for "the contact force as internal force" belonging to the stationary value of the functional L_1.

Three points of view support the use of element types delivering a non-constant stress field inside the element, viz.:

1. according to computational experience, applying the element type of more degrees of freedom for approximating the stress state at the same accuracy leads to far less unknowns in the final set of equations than for the simpler elements;

2. stress state approximation is improved, a major requirement especially near domain Ω;

3. not too small elements have to be handled near the domain Ω, either.

Assuming the approximation matrices $\widetilde{\mathbf{A}}^{(t)}(x)$ (row vectors) to be produced by using matrices $\mathbf{A}^e(x)$ for approximating displacements $w^{(t)}(x)$ $(t = 1,2)$ along the indicated direction in domain Ω. If the generalized displacement vector $\tilde{\mathbf{u}}^{(t)}$ is known:

$$w^{(t)}(x) = \widetilde{\mathbf{A}}^{(t)}(x)\, \tilde{\mathbf{u}}^{(t)} = \mathbf{A}^{(t)}(x)\, \mathbf{u}^{(t)} + \mathring{\mathbf{A}}^{(t)}(x)\, \mathring{\mathbf{u}}^{(t)}, \quad x \in \Omega\,. \tag{20}$$

The initial gap can be written by means of vector h composed of approximation matrix $\mathbf{L}(x)$ (row vector) and its $\mathbf{h}$ values at discrete points:

$$h(x) = \mathbf{L}(x)\, \mathbf{h}. \tag{21}$$

Accordingly, the contact force is approximated in the form:

$$p(x) = \mathbf{P}^T(x)\, \mathbf{p}, \quad x \in \Omega \tag{22}$$

where

$\mathbf{P}^T(x)$ — approximation matrix (row vector) depending on the element type;

$\mathbf{p}$ — a vector produced from the contact surface stresses developing at a finite number of points but not absolutely element nodes [N/cm^2].

Now:

$$\int_{(\Omega)} p[w^{(1)} - w^{(2)} - h]\, \mathrm{d}A \cong \mathbf{p}^T[\mathbf{A}^{(1)}\mathbf{u}^{(1)} - \mathbf{A}^{(2)}\,\mathbf{u}^{(2)} - \mathbf{b}]\,, \tag{23a}$$

where

$$\mathbf{A}^{(t)} = \int_{(\Omega)} \mathbf{P}(x)\, \mathbf{A}^{(t)}(x)\, \mathrm{d}A, \quad t = 1,2 \tag{23b}$$

$$\underset{(k\times 1)}{\mathbf{b}} = \int_{(\Omega)} \mathbf{P}(x)\, \mathbf{L}(x)\, \mathrm{d}A\, \mathbf{h} + \int_{(\Omega)} \mathbf{P}(x)\, \mathring{\mathbf{A}}^{(2)}(x)\, \mathrm{d}A\, \mathring{\mathbf{u}}^{(2)} - \int_{(\Omega)} \mathbf{P}(x)\, \mathring{\mathbf{A}}^{(1)}(x)\, \mathrm{d}A\, \mathring{\mathbf{u}}^{(1)}\,. \tag{23c}$$

Introducing magnitudes

$$\underset{k\times(m+n)}{\mathbf{A}} = [\underset{(k\times m)}{\mathbf{A}^{(1)}} \;\vdots\; \underset{(k\times n)}{\mathbf{A}^{(2)}}]\,, \tag{24a}$$

$$\underset{(m+n)\times 1}{\mathbf{u}} = \begin{bmatrix} \underset{(m\times 1)}{\mathbf{u}^{(1)}} \\ \underset{(n\times 1)}{\mathbf{u}^{(2)}} \end{bmatrix}, \tag{24b}$$

$$-\underset{(k\times 1)}{\mathbf{y}^{(0)}} \equiv \mathbf{A}\,\mathbf{u} - \mathbf{b} \leq \mathbf{0} \tag{24c}$$

permits the production of the constraint in the form:

$$\int_{(\Omega)} p[w^{(1)} - w^{(2)} - h]\, \mathrm{d}A \cong \mathbf{p}^T\,[\mathbf{A}\,\mathbf{u} - \mathbf{b}] \tag{25a}$$

$$\mathbf{p} \geq \mathbf{0},\ \mathbf{y}^{(0)} \geq \mathbf{0},\ \mathbf{p}^T\,\mathbf{y}^{(0)} = \mathbf{0}\,. \tag{25b, c, d}$$

1.2.3 *Formulation of the quadratic programming problem*

1.2.3.1 Primal problem

Constraints obtained by transformations described in items 1.2.2.1 and 1.2.2.2 were seen to be formally identical but physically, qualitatively

different. Further computations will be based on constraint expressed by relationships (25a—d) in item 1.2.2.2 but statements are also valid for constraint in 1.2.2.1.

Solution of the examined contact problem was proved in item 1.1 to be provided for by the stationary position of functional L_1, provided bodies are bilaterally related. Because of the constraint (25a—d) resulting from unilateral relations, and of the kinematically possible displacement field approximated by the finite element method, the functional is modified, that is, applying (12b), (24a, b) and (25a), the initial L_1 is replaced by L_2:

$$L_1 = L_1(u_r^{(1)}, u_r^{(2)}, p) \to L_2 = L_2(\mathbf{u}^{(1)}, \mathbf{u}^{(2)}, \mathbf{p}),$$

that is

$$L_2 = \frac{1}{2}[\mathbf{u}^{(1),T} \mid \mathbf{u}^{(2),T}] \begin{bmatrix} \mathbf{K}^{(1)} & \mathbf{0} \\ \mathbf{0} & \mathbf{K}^{(2)} \end{bmatrix} \begin{bmatrix} \mathbf{u}^{(1)} \\ \mathbf{u}^{(2)} \end{bmatrix} - [\mathbf{u}^{(1),T} \mid \mathbf{u}^{(2),T}] \begin{bmatrix} \mathbf{q}^{(1)} \\ \mathbf{q}^{(2)} \end{bmatrix} + \\ + \mathbf{p}^T \left([\mathbf{A}^{(1)} \mid -\mathbf{A}^{(2)}] \begin{bmatrix} \mathbf{u}^{(1)} \\ \mathbf{u}^{(2)} \end{bmatrix} - \mathbf{b} \right) \tag{26}$$

or, more concisely:

$$L_2 = L_2(\mathbf{u}, \mathbf{p}) = \frac{1}{2}\mathbf{u}^T \mathbf{K}\,\mathbf{u} - \mathbf{u}^T \mathbf{q} + \mathbf{p}^T(\mathbf{A}\,\mathbf{u} - \mathbf{b}) = \pi(\mathbf{u}) + \mathbf{p}^T \mathbf{y}^{(0)}, \tag{27}$$

where

$$\mathbf{K} = \begin{bmatrix} \mathbf{K}^{(1)} & \mathbf{0} \\ \mathbf{0} & \mathbf{K}^{(2)} \end{bmatrix}, \mathbf{q} = \begin{bmatrix} \mathbf{q}^{(1)} \\ \mathbf{q}^{(2)} \end{bmatrix}, \tag{28a, b}$$

$$\mathbf{p} \geq \mathbf{0}, \quad \mathbf{y}^{(0)} \geq \mathbf{0}, \quad \mathbf{p}^T \mathbf{y}^{(0)} = 0. \tag{29a, b, c}$$

Assuming a rigid-body-like relative displacement between solids to be possible, matrix $\mathbf{K}$ is positive semidefinite ($\mathbf{x}^T \mathbf{K}\,\mathbf{x} \geq 0$, for $\mathbf{x} \neq \mathbf{0}$), that is, potential energy $\pi(\mathbf{u})$ of the system is a strictly quasi-convex quadratic function of the generalized displacement vector $\mathbf{u}$.

Thereby, the contact problem could be reduced to the following quadratic programming problem:

$$\min \left\{ \frac{1}{2}\mathbf{u}^T \mathbf{K}\,\mathbf{u} - \mathbf{u}^T \mathbf{q} \mid \mathbf{A}\,\mathbf{u} - \mathbf{b} \leq \mathbf{0} \right\} \tag{30}$$

(27) can be considered as a Lagrange function of programming problem (30).

1.2.3.2 Dual problem

Theory of mathematical programming has demonstrated that the primal problem can be assigned a dual problem, and that the existence of solution

for one involves that for the other. Often — in actual computations — solution of the dual problem, followed by the determination of unknowns in the original problem, seems more practical than finding a direct solution for the primal problem.

In this case, the dual problem belonging to (30) can be produced by making use of the Khun—Tucker theorems of non-linear programming (see in the Appendix).

The theorem leads to relationships

$$\frac{\partial L_2}{\partial \mathbf{u}^{(1)}} = \mathbf{K}^{(1)}\,\mathbf{u}^{(1)} - \mathbf{q}^{(1)} + \mathbf{A}^{(1),T}\,\mathbf{p} = \mathbf{0}\,, \tag{31a}$$

(according to (A.8) where $\mathbf{x} = \mathbf{u}^{(t)}$, $t = 1,2$)

$$\frac{\partial L_2}{\partial \mathbf{u}^{(2)}} = \mathbf{K}^{(2)}\,\mathbf{u}^{(2)} - \mathbf{q}^{(2)} - \mathbf{A}^{(2),T}\,\mathbf{p} = \mathbf{0}\,, \tag{31b}$$

further:

$$\frac{\partial L_2}{\partial \mathbf{p}} = \mathbf{A}^{(1)}\,\mathbf{u}^{(1)} - \mathbf{A}^{(2)}\,\mathbf{u}^{(2)} - \mathbf{b} = -\,\mathbf{y}^{(0)} \leq \mathbf{0} \tag{32a}$$

$$\mathbf{p}^T\,\frac{\partial L_2}{\partial \mathbf{p}} = \mathbf{p}^T\,\mathbf{y}^{(0)} = 0 \tag{32b}$$

(according to (A.7) where $\mathbf{u} = \mathbf{p}$).

Assuming body 2 not performing rigid-body motion, $\det \mathbf{K}^{(2)} \neq 0$, thus, from (31b):

$$\mathbf{u}^{(2)} = [\mathbf{K}^{(2)}]^{-1}\,\mathbf{q}^{(2)} + [\mathbf{K}^{(2)}]^{-1}\,\mathbf{A}^{(2),T}\,\mathbf{p}\,. \tag{33}$$

Body 1 can perform rigid-body motion, hence, its stiffness matrix is a singular one, but a non-singular quadratic matrix of the size of the original matrix lessened by the degrees of freedom of the rigid-body motion can always be designated to it. Assuming matrix $\mathbf{K}_{22}^{(1)}$ in the lower right corner of matrix $\mathbf{K}^{(1)}$ not to be singular. (This is always possible by duly rearranging rows and columns.) Partitioning Eq. (31a) yields:

$$\begin{bmatrix} \mathbf{K}_{11}^{(1)} & \mathbf{K}_{12}^{(1)} \\ \mathbf{K}_{21}^{(1)} & \mathbf{K}_{22}^{(1)} \end{bmatrix} \begin{bmatrix} \mathbf{u}_{\mathrm{I}}^{(1)} \\ \mathbf{u}_{\mathrm{II}}^{(1)} \end{bmatrix} - \begin{bmatrix} \mathbf{q}_{\mathrm{I}}^{(1)} \\ \mathbf{q}_{\mathrm{II}}^{(1)} \end{bmatrix} + \begin{bmatrix} \mathbf{A}_{\mathrm{I}}^{(1),T} \\ \mathbf{A}_{\mathrm{II}}^{(1),T} \end{bmatrix} \mathbf{p} = \mathbf{0} \tag{34}$$

thus, partly

$$\mathbf{u}_{\mathrm{II}}^{(1)} = [\mathbf{K}_{22}^{(1)}]^{-1}\,\mathbf{q}_{\mathrm{II}}^{(1)} - [\mathbf{K}_{22}^{(1)}]^{-1}\,\mathbf{A}_{\mathrm{II}}^{(1),T}\,\mathbf{p} - [\mathbf{K}_{22}^{(1)}]^{-1}\,\mathbf{K}_{21}^{(1)}\,\mathbf{u}_{\mathrm{I}}^{(1)} \tag{35}$$

and partly, by introducing magnitudes:

$$\mathbf{D} = \mathbf{K}_{11}^{(1)} - \mathbf{K}_{12}^{(1)}[\mathbf{K}_{22}^{(1)}]^{-1}\,\mathbf{K}_{21}^{(1)}, \tag{36a}$$

$$\mathbf{G}^T = \mathbf{A}^{(1),T} - \mathbf{K}_{12}^{(1)}[\mathbf{K}_{22}^{(1)}]^{-1}\mathbf{A}_{II}^{(1),T}, \tag{36b}$$

$$\mathbf{q} = \mathbf{q}_I^{(1)} - \mathbf{K}_{12}^{(1)}\,[\mathbf{K}_{22}^{(1)}]^{-1}\mathbf{q}_{II}^{(1)} \tag{36c}$$

yields:

$$\mathbf{D}\,\mathbf{u}_I^{(1)} - \mathbf{q} + \mathbf{G}^T\,\mathbf{p} = \mathbf{0}\,, \tag{37}$$

equilibrium equation of nodes belonging to vector $\mathbf{u}_I^{(1)}$; $\mathbf{D}\,\mathbf{u}_I^{(1)}$, $-\mathbf{q}$ and $\mathbf{G}^T\,\mathbf{p}$ being generalized force values transmitted from the internal forces, from the known external load, and from contact forces, respectively, to the node, $\mathbf{D}$ being a positive semidefinite matrix[5].

$$\text{Since} \quad \underset{(1\times m)}{\mathbf{u}^{(1),T}} = \left[\underset{l}{\mathbf{u}_I^{(1),T}} \;\middle|\; \underset{m-l}{\mathbf{u}_{II}^{(1),T}}\right],$$

applying (35) yields

$$\mathbf{u}^{(1)} = \left[\begin{array}{c} \mathbf{E}^{(1)} \\ \hline -[\mathbf{K}_{22}^{(1)}]\;\;\mathbf{K}_{21}^{(1)} \end{array}\right]\mathbf{u}_I^{(1)} + \left[\begin{array}{c|c} \mathbf{0} & \mathbf{0} \\ \cdots & \cdots\cdots \\ \mathbf{0} & [\mathbf{K}_{22}^{(1)}]^{-1} \end{array}\right]\left[\begin{array}{c} \mathbf{q}_I^{(1)} \\ \\ \mathbf{q}_{II}^{(1)} \end{array}\right] - \left[\begin{array}{c} \mathbf{0} \\ \hline [\mathbf{K}_{22}^{(1)}]\;\;\mathbf{A}_{II}^{(1),T} \end{array}\right]\mathbf{p}, \tag{38}$$

($\mathbf{E}^{(1)}$ — is a unit matrix of size $(l\times l)$) and from (32a) taking (38) and (33) into consideration:

$$\begin{aligned} &\underset{(k\times l)}{\left[\mathbf{A}_I^{(1)} - \mathbf{A}_{II}^{(1)}\,[\mathbf{K}_{22}^{(1)}]^{-1}\,\mathbf{K}_{21}^{(1)}\right]}\mathbf{u}_I^{(1)} + \left[\mathbf{0} \;\middle|\; \mathbf{A}_{II}^{(1)}\,[\mathbf{K}_{22}^{(1)}]^{-1}\right]\mathbf{q}^{(1)} - \\ &- \left[\mathbf{A}_{II}^{(1)}\,[\mathbf{K}_{22}^{(1)-1}]\,\mathbf{A}_{II}^{(1),T}\right]\mathbf{p} - \\ &- \mathbf{A}^{(2)}\,[\mathbf{K}^{(2)}]^{-1}\,\mathbf{q}^{(2)} - \mathbf{A}^{(2)}\,[\mathbf{K}^{(2)}]^{-1}\,\mathbf{A}^{(2),T}\,\mathbf{p} - \mathbf{b} = -\,\mathbf{y}^{(0)} \end{aligned} \tag{39}$$

Since $\mathbf{K}_{21}^{(1)} = \mathbf{K}_{12}^{(1),T}$ taking (36b) as well as matrices and vectors

$$\underset{(k\times m)}{\mathbf{F}^{(1)}} = \left[\underset{(k\times l)}{\mathbf{0}} \;\middle|\; \underset{(k\times(m-l))}{\mathbf{A}_{II}^{(1)}\,[\mathbf{K}_{22}^{(1)}]^{-1}}\right], \quad \underset{(k\times 1)}{\mathbf{f}^{(1)}} = \underset{(k\times m)}{\mathbf{F}^{(1)}}\;\underset{(m\times 1)}{\mathbf{q}^{(1)}}, \tag{40a, b}$$

[5] It can easily be demonstrated. $\mathbf{K}^{(1)}$ being a positive semidefinite symmetric matrix, the inequality

$$0 \leq \mathbf{u}^{(1),T}\,\mathbf{K}^{(1)}\,\mathbf{u}^{(1)} = \mathbf{u}_I^{(1),T}\,\mathbf{K}_{11}^{(1)}\,\mathbf{u}_I^{(1)} + 2\mathbf{u}_I^{(1),T}\,\mathbf{K}_{12}^{(1)}\,\mathbf{u}_{II}^{(1)} + \mathbf{u}_{II}^{(1)}\,\mathbf{K}_{22}^{(1)}\,\mathbf{u}_{II}^{(1)}$$

holds. Be

$$\mathbf{u}_{II}^{(1)} = -\,[\mathbf{K}_{22}^{(1)}]^{-1}\,\mathbf{K}_{21}^{(1)}\,\mathbf{u}_I^{(1)},$$

then for symmetric $\mathbf{K}^{(1)}$, for any $\mathbf{u}^{(1)}$:

$$0 \leq \mathbf{u}_I^{(1),T}\,[\mathbf{K}_{11}^{(1)} - \mathbf{K}_{12}^{(1)}\,[\mathbf{K}_{22}^{(1)}]^{-1}\,\mathbf{K}_{21}^{(1)}]\,\mathbf{u}_I^{(1)} = \mathbf{u}_I^{(1),T}\,\mathbf{D}\,\mathbf{u}_I^{(1)}\,.$$

Q.e.d.

$$\underset{(k\times n)}{\mathbf{F}^{(2)}} = \underset{(k\times n)}{\mathbf{A}^{(2)}}\,\underset{(n\times n)}{[\mathbf{K}^{(2)}]^{-1}} \quad , \quad \underset{(k\times 1)}{\mathbf{f}^{(2)}} = \underset{(k\times n)}{\mathbf{F}^{(2)}}\,\underset{(n\times 1)}{\mathbf{q}^{(2)}}\,, \tag{40c, d}$$

$$\underset{(k\times 1)}{\mathbf{t}} = \mathbf{f}^{(1)} - \mathbf{f}^{(2)} - \mathbf{b} \quad , \tag{40e}$$

$$\underset{(k\times k)}{\mathbf{H}^{(1)}} = \underset{[k\times(m-l)]}{\mathbf{A}_{11}^{(1)}}\;\underset{[(m-l)\times(m-l)]}{[\mathbf{K}_{22}^{(1)}]^{-1}}\;\underset{[(m-l)\times k]}{\mathbf{A}_{11}^{(1),T}} \quad , \tag{41a}$$

$$\underset{(k\times k)}{\mathbf{H}^{(2)}} = \underset{(k\times n)}{\mathbf{A}^{(2)}}\;\underset{(n\times n)}{[\mathbf{K}^{(2)}]^{-1}}\;\underset{(n\times k)}{\mathbf{A}^{(2),T}}\,, \tag{41b}$$

$$\mathbf{H} = \mathbf{H}^{(1)} + \mathbf{H}^{(2)}, \tag{41c}$$

into consideration, geometrical equation inequality (39) expressing contact separation can be replaced by

$$\mathbf{H}\,\mathbf{p} - \mathbf{G}\,\mathbf{u}_1^{(1)} - \mathbf{t} = \mathbf{y}^{(0)} \geq \mathbf{0} \tag{42a}$$

and from (29c)

$$\mathbf{p}^T\,\mathbf{y}^{(0)} = 0 \tag{42b}$$

H being the resultant "influence coefficient matrix", **t** the displacement from known loads and the initial gap, and **G** a matrix also involving the structure geometry.

Equations of equilibrium (37) and of geometry (42a) yield a hypermatrix equation

$$\underbrace{\begin{bmatrix} \mathbf{D} & \mathbf{G}^T \\ -\mathbf{G} & \mathbf{H} \end{bmatrix}}_{\mathbf{M}^0} \begin{bmatrix} \mathbf{c} \\ \mathbf{p} \end{bmatrix} - \begin{bmatrix} \mathbf{q} \\ \mathbf{t} \end{bmatrix} - \begin{bmatrix} \mathbf{0} \\ \mathbf{y}^{(0)} \end{bmatrix} = \mathbf{0}\,, \tag{43}$$

where

$$\mathbf{c} = \mathbf{u}_1^{(1)} \tag{44}$$

denoting the unknown beyond the contact forces. Matrix $\mathbf{M}^0$ of the obtained equation is positive semidefinite.[6] To have positive quantities for unknowns, vector **c** is produced as the difference of two positive vectors, i. e.

$$\begin{aligned} &\mathbf{c} = \mathbf{c}^+ - \mathbf{c}^-\,, \\ &\mathbf{c}^+ \geq \mathbf{0}\,, \quad \mathbf{c}^- \geq \mathbf{0} \end{aligned} \tag{45}$$

[6] This statement is easy to prove. Since

$$(\mathbf{z}^T\,\mathbf{M}^0\,\mathbf{z})^T = \mathbf{z}^T\,\mathbf{M}^{0,T}\,\mathbf{z}\,,$$

it is:

$$\mathbf{z}^T\,(\mathbf{M}^0 + \mathbf{M}^{0,T})\,\mathbf{z} = 2\mathbf{z}^T\,\mathbf{M}^0\,\mathbf{z}\,,$$

and

$$\mathbf{M}^0 + \mathbf{M}^{0,T} = 2\begin{bmatrix} \mathbf{D} & \mathbf{0} \\ \mathbf{0} & \mathbf{H} \end{bmatrix},$$

a positive semidefinite matrix because of **D** and **H**.

and the first matrix equation in (43) is replaced by two matrix inequalities, resulting in

$$\underbrace{\begin{bmatrix} \mathbf{D} & -\mathbf{D} & \mathbf{G}^T \\ -\mathbf{D} & \mathbf{D} & -\mathbf{G}^T \\ -\mathbf{G} & \mathbf{G} & \mathbf{H} \end{bmatrix}}_{\mathbf{M}} \underbrace{\begin{bmatrix} \mathbf{c}^+ \\ \mathbf{c}^- \\ \mathbf{p} \end{bmatrix}}_{\mathbf{x}} - \underbrace{\begin{bmatrix} \mathbf{q} \\ -\mathbf{q} \\ \mathbf{t} \end{bmatrix}}_{\mathbf{d}} - \underbrace{\begin{bmatrix} \mathbf{y}^{(1)} \\ \mathbf{y}^{(2)} \\ \mathbf{y}^{(0)} \end{bmatrix}}_{\mathbf{y}} = \mathbf{0} \tag{46a}$$

or, more concisely:

$$\mathbf{M}\,\mathbf{x} - \mathbf{d} - \mathbf{y} = \mathbf{0}, \quad \mathbf{x}^T\mathbf{y} = \mathbf{0}, \quad \mathbf{x} \geq \mathbf{0}, \quad \mathbf{y} \geq \mathbf{0} \tag{46b—e}$$

where the positive semi-definiteness of $\mathbf{M}^0$ involves that of matrix $\mathbf{M}$.

From the Khun—Tucker theorems it is obvious that the programming problem belonging to (46) is:

$$\min \{\psi(\mathbf{x}) = \mathbf{x}^T\,\mathbf{M}\,\mathbf{x} - \mathbf{x}^T\,\mathbf{d} \mid \mathbf{x} \geq \mathbf{0}, \quad -\mathbf{M}\,\mathbf{x} + \mathbf{d} \leq \mathbf{0}\} \tag{47}$$

easy to solve by the standard methods of quadratic programming [23]. Problem (47) can be considered as dual of (30).

In knowledge of $\mathbf{x}$ and $\mathbf{y}$ obtained by solving (47) and making use of (45), (44) yields $\mathbf{u}_{\mathrm{I}}^{(1)}$, (35) yields $\mathbf{u}_{\mathrm{II}}^{(1)}$, hence the generalized nodal displacement vector of body 1, and from (33) that of body 2, all these permitting the determination of deformation and stress states of the bodies.

1.2.4 *Formulation of the quadratic programming problem where one body is rigid*

Quite often, structures are encountered where one body can be considered as rigid compared to the other one.

1.2.4.1 Rigid body acted upon by a known system of forces

Assuming body 1 to be rigid and able to perform rigid-body motion. Let the vector be composed from the couple of vectors $(F_s^{(1)}, M_s^{(1)})$ reduced to the origin of the reference system of the known force system acting on this body denoted by

$$[\mathbf{f}_0^{(1),T} \mid \mathbf{m}_0^{(1),T}] = \mathbf{q}^{(1),T}, \tag{48}$$

where

$F_s^{(1)} \to \mathbf{f}_0^{(1)}$ being the resultant force, and

$M_s^{(1)} \to \mathbf{m}_0^{(1)}$ the resultant moment. Applying (12b), potential energy of the system is:

$$\pi = \frac{1}{2}\,\mathbf{u}^{(2),T}\,\mathbf{K}^{(2)}\,\mathbf{u}^{(2)} - \mathbf{c}^{(T)}\,\mathbf{q}^{(1)} - \mathbf{u}^{(2),T}\,\mathbf{q}^{(2)}, \tag{49}$$

where

$\mathbf{c}$ is the vector of the rigid-body motion of body 1 composed of its displacement along, and rotation about, the co-ordinate axes.

Lagrange function belonging to the contact problem can be written as:

$$L_3 = \pi + \int_{(\Omega)} p(w^{(1)} - w^{(2)} - h)\, dA\,. \tag{50}$$

Body 1 being rigid,

$$w^{(1)}(x) = \mathbf{A}_R^{(1)}(x)\,\mathbf{c} \tag{51}$$

$\mathbf{A}_R^{(1)}(x)$ being a matrix (row vector) depending on the body geometry, on the direction of unilateral relations.

Approximating the integral from the constraint in L_3 according to 1.2.2.2 and applying (20) to (22) and (51), we get:

$$\int_{(\Omega)} p(w^{(1)} - w^{(2)} - h)\, dA \cong \mathbf{p}^T[\mathbf{G}_R\,\mathbf{c} - \mathbf{A}^{(2)}\,\mathbf{u}^{(2)} - \mathbf{b}_R]\,, \tag{52}$$

where $\mathbf{A}^{(2)}$, $\mathbf{G}_R$ and $\mathbf{b}_R$ are quantities obtained from (23b) and by omitting the last terms in (23c).

Repeating statements in item 1.2.3 yields functional belonging to the quadratic programming problem of the form:

$$\begin{aligned} L_4 = L_4(\mathbf{c}, \mathbf{u}^{(2)}, \mathbf{p}) = \frac{1}{2}\,[\mathbf{c}^T \mid \mathbf{u}^{2,T}] \begin{bmatrix} \mathbf{0} & \mathbf{0} \\ \mathbf{0} & \mathbf{K}^{(2)} \end{bmatrix} \begin{bmatrix} \mathbf{c} \\ \mathbf{u}^{(2)} \end{bmatrix} - \\ - [\mathbf{c}^T \mid \mathbf{u}^{(2),T}] \begin{bmatrix} \mathbf{q}^{(1)} \\ \mathbf{q}^{(2)} \end{bmatrix} + \mathbf{p}^T \Big([\mathbf{G}_R \mid -\mathbf{A}^{(2)}] \begin{bmatrix} \mathbf{c} \\ \mathbf{u}^{(2)} \end{bmatrix} - \mathbf{b}_R \Big) \end{aligned} \tag{53}$$

or, more concisely:

$$L_4 = \frac{1}{2}\,\mathbf{u}_R^T\,\mathbf{K}_R\,\mathbf{u}_R - \mathbf{u}_R^T\,\mathbf{q}_R + \mathbf{p}^T(\mathbf{A}_R\,\mathbf{u}_R - \mathbf{b}_R)\,, \tag{54}$$

all quantities in (54) being obvious from a comparison with (53), and from the unilateral relation,

$$\mathbf{p} \geq \mathbf{0},\ -\mathbf{y}_R \equiv \mathbf{A}_R\,\mathbf{u}_R - \mathbf{b}_R \leq \mathbf{0},\ \mathbf{p}^T\,\mathbf{y}_R = 0\,.$$

The programming problem:

$$\min \left\{ \frac{1}{2}\,\mathbf{u}_R^T\,\mathbf{K}_R\,\mathbf{u}_R - \mathbf{u}_R^T\,\mathbf{q}_R \mid \mathbf{A}_R\,\mathbf{u}_R - \mathbf{b}_R \leq \mathbf{0} \right\}. \tag{55}$$

Dual of problem (55) is obtained by applying the Khun—Tucker theorems. Repeating statements in item 1.2.3.2 into the same sense, in conformity

with the Khun—Tucker theorem:

$$\frac{\partial L_4}{\partial \mathbf{c}} = -\mathbf{q}^{(1)} + \mathbf{G}_R^T \mathbf{p} = \mathbf{0}, \tag{56a}$$

$$\frac{\partial L_4}{\partial \mathbf{u}^{(2)}} = \mathbf{K}^{(2)} \mathbf{u}^{(2)} - \mathbf{q}^{(2)} - \mathbf{A}^{(2),T} \mathbf{p} = \mathbf{0} \tag{56b}$$

further

$$\frac{\partial L_4}{\partial \mathbf{p}} = \mathbf{G}_R \mathbf{c} - \mathbf{A}^{(2)} \mathbf{u}^{(2)} - \mathbf{b}_R \equiv -\mathbf{y}_R \leq \mathbf{0}, \tag{56c}$$

$$\mathbf{p}^T \frac{\partial L_4}{\partial \mathbf{p}} = \mathbf{p}^T \mathbf{y}_R = 0. \tag{56d}$$

Again assuming body 2 not performing any rigid-body motion, $\mathbf{u}^{(2)}$ can be expressed from (56b) and substituted into (56c):

$$-\mathbf{G}_R \mathbf{c} + \mathbf{H}^{(2)} \mathbf{p} - \mathbf{t}_R = \mathbf{y}_R \geq \mathbf{0}, \tag{57}$$

where

$$\mathbf{H}^{(2)} = \mathbf{A}^{(2)} [\mathbf{K}^{(2)}]^{-1} \mathbf{A}^{(2),T},$$

$$\mathbf{t}_R = -\mathbf{A}^{(2)} [\mathbf{K}^{(2)}]^{-1} \mathbf{q}^{(2)} - \mathbf{b}_R = -\mathbf{f}^{(2)} - \mathbf{b}_R.$$

Hypermatrix equation from (56a) and (57):

$$\begin{bmatrix} \mathbf{0} & \mathbf{G}_R^T \\ -\mathbf{G}_R & \mathbf{H}^{(2)} \end{bmatrix} \begin{bmatrix} \mathbf{c} \\ \mathbf{p} \end{bmatrix} - \begin{bmatrix} \mathbf{q}^{(1)} \\ \mathbf{t}_R \end{bmatrix} - \begin{bmatrix} \mathbf{0} \\ \mathbf{y}_R \end{bmatrix} = \mathbf{0}. \tag{58}$$

Again, producing vector $\mathbf{c}$ as a difference of two positive vectors:

$$\underbrace{\left[\begin{array}{c|c|c} \mathbf{0} & \mathbf{0} & \mathbf{G}_R^T \\ \hline \mathbf{0} & \mathbf{0} & -\mathbf{G}_R^T \\ \hline -\mathbf{G}^{(1)} & \mathbf{G}_R^{(1)} & \mathbf{H}^{(2)} \end{array}\right]}_{\mathbf{M}_R} \underbrace{\left[\begin{array}{c} \mathbf{c}^+ \\ \hline \mathbf{c}^- \\ \hline \mathbf{p} \end{array}\right]}_{\mathbf{x}} - \underbrace{\left[\begin{array}{c} \mathbf{q}^{(1)} \\ \hline -\mathbf{q}^{(1)} \\ \hline \mathbf{t}_R \end{array}\right]}_{\mathbf{d}_R} - \underbrace{\left[\begin{array}{c} \mathbf{y}^{(1)} \\ \hline \mathbf{y}^{(2)} \\ \hline \mathbf{y}_R \end{array}\right]}_{\mathbf{y}} = \mathbf{0}$$

or, concisely:

$$\mathbf{M}_R \mathbf{x} - \mathbf{d}_R - \mathbf{y} = \mathbf{0}, \quad \mathbf{x} \geq \mathbf{0}, \ \mathbf{x}^T \mathbf{y} = 0. \tag{59}$$

The relevant programming problem:

$$\min \left\{ \varkappa(\mathbf{x}) = \mathbf{x}^T \mathbf{M}_R \mathbf{x} - \mathbf{x}^T \mathbf{d}_R \mid \mathbf{x} \geq \mathbf{0}, \quad -\mathbf{M}_R \mathbf{x} + \mathbf{d}_R \leq \mathbf{0} \right\}. \tag{60}$$

Obviously, the final programming problem is the same, either both contacting bodies are elastic or one of them is rigid. Of course, equilibrium equations (58) and (43) are essentially different by physical purport: one referring to the body as a whole, the other to given nodes for the support of the "primary structure" (det $\mathbf{K}_{22}^{(1)} \neq 0$).

1.2.4.2 Known displacement of a rigid body

In the case where rigid-body displacement $\mathbf{c}$ of body 1 is a given value, no equilibrium equations need be written for body 1, the contact problem can be set up by means of the geometry equation/inequality expressing the contact separation.

Omitting deduction:

$$\mathbf{H}^{(2)}\,\mathbf{p} - (\mathbf{G}_R\,\mathbf{c} + \mathbf{t}_R) \equiv \mathbf{y}_R \geq \mathbf{0}\,, \quad \mathbf{p}^T\,\mathbf{y}_R = 0\,, \tag{61a}$$

where

$$\mathbf{t}_R = -\,\mathbf{A}^{(2)}[\mathbf{K}^{(2)}]^{-1}\,\mathbf{q}^{(2)} - \left\{ \int_{(\Omega)} \mathbf{P}(x)\,\mathbf{L}(x)\,dA\,\mathbf{h} + \right. \\ \left. + \int_{(\Omega)} \mathbf{P}(x)\,\mathring{\mathbf{A}}^{(2)}(x)\,dA\,\mathring{\mathbf{u}}^{(2)} \right\} \tag{61b}$$

$\mathbf{H}^{(2)}$ being a positive definite matrix, the programming problem is:

$$\min \left\{ \Lambda(\mathbf{p}) = \frac{1}{2}\,\mathbf{p}^T\,\mathbf{H}^{(2)}\,\mathbf{p} - \mathbf{p}^T(\mathbf{G}_R\,\mathbf{c} + \mathbf{t}_R) \mid \mathbf{p} \geq \mathbf{0} \right\}. \tag{62}$$

1.2.5 *Another possibility for solving the contact problem*

Let us remark that if both bodies are elastic, one construction of the problem may be similar to (58), except for $\mathbf{H}^{(2)}$ being replaced by the sum of the influence function matrix $\mathbf{H}^{(1)}$ based on the "primary structure" 1 and of $\mathbf{H}^{(2)}$, $\mathbf{t}_R$ is modified to the same sense, replaced by

$$\mathbf{t} = \mathbf{f}^{(1)} - \mathbf{f}^{(2)} - \mathbf{b}$$

terms delivered by (40), (41) and (23). Interpretation of vector $\mathbf{c}$ for a plane structure is to be seen in Fig. 3.

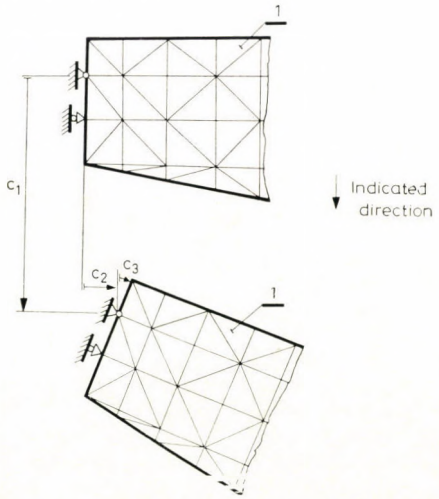

Fig. 3. Body 1 of the plane structure may perform rigid-body motion. Interpretation of vector $\mathbf{c}$: $\mathbf{c}^T = [c_1, c_2, c_3]$

Such a setup of the problem is considered in [1], [2] and [9], the solution being obtained by a cyclic iteration according to the method of gradients.

Obviously, such a setup of the problem cannot be considered as the strict dual of programming problem (30), (47) being the dual of problem (30).

1.3 *Comments on practical computations*

In actual applications of the described method, setup of influence matrices (41a, b) involves the inversion of matrices $\mathbf{K}^{(t)}$. Complicated body designs often call for a high number of elements to be assumed, preventing the $\mathbf{K}^{(t)}$ for the entire structure to be kept in the active storage unit of the computer. In this case, influence matrices $\mathbf{H}^{(t)}$ are advisably produced as follows:

1. In case of body 1 performing rigid-body motion, a "primary structure" with a kind of support has to be assumed, so that the relevant $\mathbf{K}_{22}^{(1)}$ will not degenerate any longer, and supports have to be located in a domain where matrix $\mathbf{A}_1^{(1)}$ is absolutely zero (see in (23), (34); see e. g. Fig. 4).

2. Respective J-th columns of matrices $\mathbf{H}^{(t)}$, $t = 1,2$, will be delivered by vectors obtained by multiplying from the left the displacement vectors

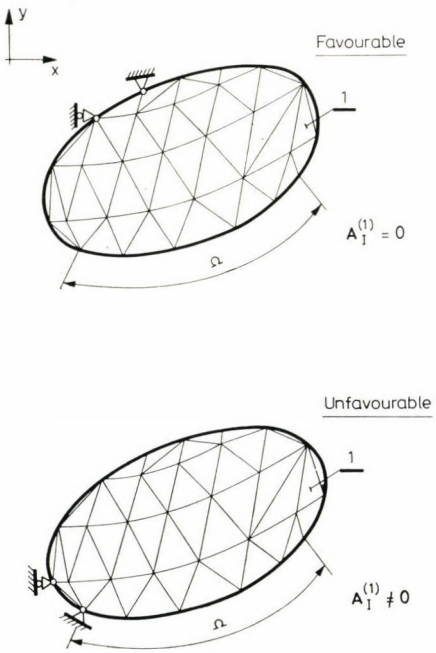

Fig. 4. Assumption of basic structure for a plane structure if co-ordinates of the generalized nodal displacement vector are displacements

at nodes $\mathbf{u}_J^{(1)}$ and $\mathbf{u}_J^{(2)}$, arrived at by solving algebraic equations

$$\mathbf{K}_{22}^{(1)}\,\mathbf{u}_J^{(1)} = \mathbf{A}_{11}^{(1),T}\,\mathbf{p}\,,$$
$$\mathbf{K}^{(2)}\,\mathbf{u}_J^{(2)} = \mathbf{A}^{(2),T}\,\mathbf{p}$$

related to loads for unit values of vector $\mathbf{p}$ in (22) at different points J.

3. Knowing $\mathbf{K}_{11}^{(1)}$, $\mathbf{K}_{12}^{(1)} = \mathbf{K}_{21}^{(1),T}$ obtained in producing the "primary structure" of structure 1, matrices $\mathbf{D}$ and $\mathbf{G}$ can easily be calculated.

4. Nodes in domain Ω are advisably consecutively numbered; thereby matrix $\mathbf{A}^{(t)}$ will become quasidiagonal, greatly simplifying calculations.

Conclusions

The contact problem was seen to be constructed on the Lagrange variation principle, and treated as a quadratic programming problem owing to unilateral relations. The kinematically possible displacement field is approximated by the finite element method, and the condition of contact/separation is checked in a predetermined (indicated) direction at a finite discrete number of points according to item 1.2.2.1 and by comparing integral values for small finite sections according to item 1.2.2.2 (see (23) to (25)).

This latter procedure is justified anyway in case of a field of displacement vectors approximated by a higher than linear polynomial element-wise, and it is especially adequate for thin shells and plates. Use of elements of higher degrees of freedom leads to a decrease in the size of the final algebraic equation system, permitting an important time saving, and besides, yielding a true picture of the stress state prevailing on the contact domain.

Appendix

Essentials of the theory of quadratic programming.

A quadratic programming problem I is understood as minimizing the strictly quasi-convex quadratic function[7]:

$$l(\mathbf{x}) = \mathbf{x}^T\,\mathbf{C}\,\mathbf{x} - \mathbf{c}^T\,\mathbf{x} + \gamma, \quad \mathbf{x} \geq \mathbf{0},\ \mathbf{x}^T\,\mathbf{C}\,\mathbf{x} \geq 0, \tag{A. 1}$$

subject to the constraints of equation-inequality

$$\mathbf{A}\,\mathbf{x} \leq \mathbf{b}, \quad \mathbf{x} \geq \mathbf{0} \tag{A. 2}$$

$$\text{I. min } \{\mathbf{x}^T\,\mathbf{C}\,\mathbf{x} - \mathbf{c}^T\,\mathbf{x} + \gamma \mid \mathbf{x} \geq \mathbf{0},\ \mathbf{A}\,\mathbf{x} \leq \mathbf{b}\} \tag{A. 3a}$$

[7] A function $l(x)$ is quasi-convex if for any $0 < \lambda < 1$ of the convex domain $\mathbf{x} \in \mathrm{D}$ and for conditions $\mathbf{x}^1$ and $\mathbf{x}^2 \in \mathrm{D}$ the inequality

$$l\big(\lambda\,\mathbf{x}^1 + (1-\lambda)\,\mathbf{x}^2\big) \leq \lambda\,l(\mathbf{x}^1) + (1-\lambda)\,l(\mathbf{x}^2)$$

holds; this is invariably the case if $\mathbf{C}$ is a positive semidefinite matrix.

Besides, depending on the constraints, also problems II and III are spoken about, namely:

$$\text{II. min } \{\mathbf{x}^T \mathbf{C}\,\mathbf{x} - \mathbf{c}^T\mathbf{x} + \gamma \mid \mathbf{A}\,\mathbf{x} = \mathbf{b},\ \mathbf{x} \geq \mathbf{0}\} \tag{A. 3b}$$

and

$$\text{III. min } \{\mathbf{x}^T \mathbf{C}\,\mathbf{x} - \mathbf{c}^T\mathbf{x} + \gamma \mid \mathbf{A}\,\mathbf{x} \leq \mathbf{b}\} \tag{A. 3c}$$

Problems II and III can be transformed to problem I; II by means of inequalities $\mathbf{A}\,\mathbf{x} \leq \mathbf{b}$ and $-\mathbf{A}\,\mathbf{x} \leq -\mathbf{b}$; III requiring a variable transformation $\mathbf{x} = \mathbf{x}^+ - \mathbf{x}^-$, $\mathbf{x}^+ \geq \mathbf{0}$, $\mathbf{x}^- \geq \mathbf{0}$, $\tilde{\mathbf{x}}^T = [\mathbf{x}^{+,T}\,\mathbf{x}^{-,T}] \geq \mathbf{0}$.

The conditional extreme value calculation is generalized by the Khun–Tucker theorem for the case where the constraints not only contain equations but also inequalities. According to this theorem, the Lagrange function belonging to (A. 3a):

$$L = \mathbf{x}^T \mathbf{C}\,\mathbf{x} - \mathbf{c}^T\mathbf{x} + \gamma + \mathbf{u}^T(\mathbf{A}\,\mathbf{x} - \mathbf{b}) \tag{A. 4}$$

has a saddle point for the optimum solution for $\mathbf{x}^0$ of the minimization problem (A. 3a), hence there is vector $\mathbf{u}^0$ with an inequality relationship

$$L(\mathbf{x}, \mathbf{u}^0) \geq L(\mathbf{x}^0, \mathbf{u}^0) \geq L(\mathbf{x}^0, \mathbf{u}) \tag{A. 5}$$

for any $\mathbf{x} \geq \mathbf{0}$ and $\mathbf{u} \geq \mathbf{0}$. This fulfils of so-called local conditions

$$\mathbf{v} = \frac{\partial L}{\partial \mathbf{x}}\bigg|_{(\mathbf{x}^0, \mathbf{u}^0)} \geq \mathbf{0}\,,\ \mathbf{x}^{0,T}\frac{\partial L}{\partial \mathbf{x}}\bigg|_{(\mathbf{x}^0, \mathbf{u}^0)} = 0\,, \tag{A. 6a, b}$$

$$\mathbf{y} = -\frac{\partial L}{\partial \mathbf{u}}\bigg|_{(\mathbf{x}^0, \mathbf{u}^0)} \geq \mathbf{0},\ \mathbf{u}^{0,T}\frac{\partial L}{\partial \mathbf{u}}\bigg|_{(\mathbf{x}^0, \mathbf{u}^0)} = 0 \tag{A. 7a. b}$$

as necessary and sufficient conditions. $\partial L/\partial \mathbf{x}$ being a column vector with components obtained by taking the partial derivative of function $L(\mathbf{x}, \mathbf{u})$ with respect to components of $\mathbf{x}$; $\partial L/\partial \mathbf{u}$ being a similarly interpreted vector. Lacking a non-negativity requirement for $\mathbf{x}$, (A. 6a) is replaced by relationship [23]:

$$\frac{\partial L}{\partial \mathbf{x}} = \mathbf{0}\,. \tag{A. 8}$$

REFERENCES

1. Фридман, В. М.—Чернина, В. С.: Итерационный процесс для решения конечномерной контактной задачи, Ж. ВМиМФ, Т. **7,** № 1 (1967), 160—163.
2. Фридман, В. М.—Чернина, В. С.: Решение задачи о контакте упругих тел итерационным методом, *МТТ*, АН СССР, № 1 (1967), 116—120.
3. Dupuis, G.—Probst, A.: Étude d'une structure élastique soumise à des conditions unilatérales, *J. méc.* **1** (1967), 3—41
4. Гордеев, В. Н.—Перелмутер, А. З.: Расчет упругих систем односторонними связями как задача квадратического программирования. *Сб. Исследования по теории сооружений*, вып. **15** Строиздат М., (1967), 208—212.
5. Кузненова, Р. Е.: Применение нелинейного программирования к расчету неопределемых систем, имеющих в числе лишних односторонние связи. *Тр. Томский инж.—строит. ин-та*, **14** (1968), 40—46.
6. Рабинович, И. М.: Энергетические свойства и особенности расчета статически неопределимых стержневых систем с односторонними лишними связями, *Исследование по теории сооружений*. М., XVII. (1969), 141—153.
7. Портаев, Л. П.—Яцура, В. Г.: Применение линейного программирования для расчета стержневых систем с односторонними связями, *Строительная механика и расчет сооружений*, М., № 3 (1972), 12—15.
8. Пацельт, И.: Деформация торообразной оболочки на упругом винклеровском основании, Автореферат диссертации на соискание ученой степени кандидата технических наук. Ленинград, ЛПИ, (1969).
9. Пацельт, И.: Итерационный метод для решения контактной задачи упрулих систем с односторонними связями, Acta Tech. Hung. **76** (1—2), (1974), 217—241.
10. Conry, T. F.—Seireg, A.: A Mathematical Programming Method for Design of Elastic Bodies in Contact, *Journal of Applied Mechanics*, Vol. **38,** Trans. ASME, Series E, June (1971), 387—392
11. Kalker, J. J.—van Randen, Y.: Non-Hertzian Frictionless Problems, *ZAMM*, **51** (1971), 116—117

12. Чистякова, И. П.: Численный метод рещения задач изгиба балок на упругом основании с односторонними связями, *Сб. тр. Моск. инж.-строит. ин-та*, № 84 (1970), 244—248.
13. Хименко, В. В.: К расчету балок на упругом основании с учетом отрыва, *Сб. исслед. по строит. мех. и расчету конструкций*, Томск, (1969), 81—83.
14. Кузнецова, Р. Е.: Расчет круглой плиты на упругом основании с учетом отрыва на действие симметрической нагрузки, *Сб. Материалы Научн.* конференции, посвящ. 100-летию со дня рождения В. И. Ленина. Томский инж.-строит. ин-т Секция Сопротивл. Материалов и строит. механика, Томск (1970), 43—44.
15. Conway, H. D.—Engel, P. A.: Contact Stresses in Slabs due to Round Rough Indenters, *Int. J. Mech. Sci*, **11** (1969), 709—722
16. Engel, P. A.—Conway, H. D.: Contact Stress Analysis for an Elastic Cylinder Indetending a Slab in the Presence of Friction, *Int. J. mech. Sci.*, **13** (1971), 391—402
17. Cheung, Y. K.—Zienkiewicz, O. C.: Plates and Tanks on Elastic Foundation. An Application of the Finite Element Method, *Int. J. Solids Struct.*, **1** (1965), 451—456
18. Carpenter, W. C.: Analysis of Plates on elastic Foundations, *Int. J. num. Meth. Engng.* **7** (1973), 408—410
19. Svec, O. J.—Gladwell, G. M. L.: A Triangular Plate Bending Element for Contact Problems, *Int. J. Solids Structures*, **9** (1973), 435—446
20. Hardy, C.—Baronet, C. N.—Tordion, G. V.: The Elastic-plastic Indentation of a Half-space by a Rigid Sphere, *Int. J. for Num. Methods in Engineering*, **3** (1971), 451—462
21. Back, N.—Burdekin, M.—Cowley, A.: Pressure Distribution and Deformations of Machined Components in Contact, *Int. J. mech. Sci.*, **15** (1973), 993—1010
22. Лурье, А. И.: *Теория упругости*, Наука, М., (1970).
23. Künzi, H. P.—Krelle, W.: *Nichtlineare Programmierung*, Springer-Verlag, Berlin—Göttinge—Heidelberg (1962)
24. Tong, P.: New Displacement Hybrid Finite Element for Solid Continua, *Int. J. Num. Meth. Engng*, **2** (1870), 73—83
25. Pian, T. H. H.—Tong, P.: Basis of Finite Element Methods for Solid Continua, *Int. J. Numer. Meth. Engng*, **1** (1969), 3—28.
26. Zienkiewicz, O.: *The Finite Element Method in Engineering Science*, McGraw-Hill, London 1971
27. Chan, S. K.—Tuba, I. S.: A Finite Element Method for Contact Problems of Solid Bodies, Part I., Part II., *Int. J. Mech. Sci.* **13** (1971), 615—625, 627—639

Anwendung der Verschiebungsmethode der finiten Elemente zur Lösung von Problemen der elastischen Berührung. Die Klärung des Berührungsproblems elastischer Kontinua bei beliebiger Belastung und Fläche ist sehr umständlich, da die Berührungsbereiche im vorherein nicht bekannt sind. Im Beitrag wird das Kontinuum durch eine Menge von Elementen mit endlichen Freiheitsgraden ersetzt und auf das so erhaltene elastische System wird nach dem Prinzip des Minimums der Potentialenergie die Lösung der Aufgabe aufgebaut, die sich wegen der einseitigen Verbindungen zwischen den Körpern (die Kontaktkraft kann nur gegen das Innere des Körpers gerichtet sein und wird dann als positiv betrachtet) als quadratische Programmierungsaufgabe der mathematischen Programmierung behandeln läßt. Unter Anwendung der Khun—Tuckerschen Bedingungen ist auch die zu dem obigen Primalproblem gehörende Dualaufgabe geklärt, die es bei konkreten Berechnungen vorteilhafter aufzustellen und zu lösen ist, als die ursprüngliche Aufgabe. Es wird vorausgesetzt, daß die Reibung und Haftung zwischen den Körpern vernachlässigt werden können und daß die Verschiebungen, Formänderungen gering sind.

Применение метода конечных элементов для решения контактных задач. Решение контактных задач для сплошных сред при произвольных нагрузках и конфигурациях является очень сложным, так как заранее неизвестны области контакта. В данной работе сплошная среда замещается множеством элементов с конечной степенью свободы. На полученную таким образом упругую систему базируется — на основе минимума потенциальной энергии — решение задачи, которая вследствие односторонней связи между телами (контактное давление может бытьнаправлено только в тело, и в этом случае оно считается положительным) в конечном счете сведена к решению задачи квадратического программирования. При использовании условий Куна-Таккера выяснена дуальная задача, относящаяся к вышеу помянутой примальной задаче. Постановка и решение дуальной задачи при конкретных вычислениях кажется более выгодной, чем решение примальной задачи. Предполагается, что трением и сцеплением между телами можно пренебречь, далее перемещение и деформация являются мальими.

Acta Technica Academiae Scientiarum Hungaricae, Tomus 82 (3—4), pp. 377—390 (1976)

INFLUENCE OF EXPERIMENTAL ERROR ON EFFECTIVENESS OF CERTAIN BULK MATERIAL INSPECTION SCHEMES*

V. HORÁLEK**

DOCTOR OF TECHN. SCI.

[Manuscript received 25 January, 1974]

A theoretical analysis of three sampling inspection schemes, used when inspecting bulk materials, (liquids, powder and the like) is given. The influence of the experimental error on the operating-characteristic is investigated. In order to describe more accurately the effectiveness of the inspection scheme the graphs of the errors of the first and of the second kind, from the point of view of the experimental error, are introduced besides the operating-characteristics. In order to facilitate the calculation of the points of these graphs nomographs have been constructed.

1. Introduction

This paper describes the mathematic statistical analysis of three standardized inspection schemes currently used for the inspection of bulk materials (solid and powder materials, liquids, etc.) which are dispatched in bags, barrels, casks, etc. An extension and generalisation of results of [1] and [2] are given.

The decision about the quality of the inspected lot with regard to the characteristic under consideration, is arrived at by one of these methods:

A:) on the basis of the analysis of one sample chosen at random from the lot;

B:) on the basis of the result of the analysis of one average sample, which was obtained by thoroughly mixing a sample (of identical weight, volume etc.), which was picked at random from the lot. At the same time we assume, that the so-formed average sample will yield the average value of the checked quality characteristic of all the chosen samples;

C:) on the basis of the value of the mean sample the results of the analysis of n random samples, each sample being analysed separately.

In inspection schemes B and C, one sample at the most is taken from every primary unit (bag, barrel, etc.).

If we denote the number of samples taken m and the number of analyses performed n, then instead of speaking of inspection schemes A), B), C),

* A part of this work was presented at the 10th EOQC Conference, Section C, Stockholm 1966.

** V. Horálek, DrSc., National Research Institute for Machine Design, Běchovice, ČSSR

we can denote them uniformly $(m|n)$ and therefore

$$A = (1 \mid 1); \quad B = (m \mid 1); \quad C = (n \mid n).$$

In all further discussions we shall therefore speak of inspection scheme $(m|n)$.

We assume, that the specification limits U (the upper limit) eventually L (the lower limit) of the checked quality characteristic of the raw material are given by a standard, a technical requirement and the like. We identify the concept of the accuracy of the analysis with the term "total analysis error", into which we include errors arising during the preparation and the proper analysis of the inspection samples such as, for example, the influence of the duration and quality of the mixing of the samples, the ambient temperature, the errors of the chemical analysis etc.

In this paper the influence of the total analysis error on the operating-characteristic for the inspection scheme $(m|n)$ is investigated. It assumes, that the magnitude of the total analysis error is independent of the real value of the checked quality characteristic and further, that the total analysis error has a normal distribution $N(O,\sigma_y^2)$ resp. $N(O,\sigma_z^2)$, with known variances σ_y^2 and σ_z^2.

In order to describe more accurately the effectiveness of the inspection scheme the graphs of the errors of the first and of the second kind, from the point of view of the experimental error are introduced, besides the operating characteristics. Nomographs have been constructed in order to facilitate the calculation of the points of these graphs.

The results of the solution have been applied for working out the draft of an inspection scheme for certain raw materials for the manufacture of cables (chalk, tar, oil R 40 etc.) and certain raw materials for the chemical industry.

2. Fundamental consideration

Let us consider a random variable η having the probability density

$$h(y) = \frac{1}{\sqrt{2\pi}\sigma_y} \exp\left\{-\frac{1}{2}\left(\frac{y-\mu}{\sigma_y}\right)^2\right\}, \quad -\infty < y < \infty \tag{1}$$

with unknown parameter μ, but with a known σ_y. Let L and $p_1 (-\infty < L < \infty; 0 < p_1 < 1)$ be given constants. On the basis of a random sample of the size m we have to test the hypothesis H_0 against the hypothesis H_1, where

$$H_0: \int_L^\infty h(y)dy = p_1 \quad \text{and} \quad H_1: \int_L^\infty h(y)dy > p_1 . \tag{2}$$

This test is equivalent with the test of the hypothesis

$$H_0: \mu = L - K_{p_1}\sigma_y \quad \text{against} \quad H_1: \mu > L - K_{p_1}\sigma_y, \tag{3}$$

where

$$\frac{1}{\sqrt{2\pi}} \int_{K_p}^{\infty} e^{-\frac{t^2}{2}} \, dt = p \, . \tag{4}$$

For the test we use the sample characteristic

$$\eta_m = \frac{1}{m} \sum_{i=1}^{m} \eta^{(i)}, \tag{5}$$

where the mutually independent random variables $\eta^{(i)}$ $(i = 1, 2, \ldots m)$ are equally distributed with the probability density (1). The sample space, i.e. the set of all points $\boldsymbol{\eta} = (\eta^{(1)}, \ldots, \eta^{(m)})$ is identical with the m-dimensional Euclidean space $\mathbf{E}_m$. The critical region $\mathbf{U}_m^{\eta} = \mathbf{E}_m$ of the given size α consists of these element of $\mathbf{E}_m$, for which $\eta_m > c$, where

$$c = L + \frac{K_{p_1} \sqrt{m} - K_{\alpha}}{\sqrt{m}} \sigma_y \, . \tag{6}$$

Equation (6) follows from the expression for the α-per cent critical point of the distribution of the random variable η_m, defined in (5), and from (3).

It is evident, that the described test also includes that case, when the hypothesis H_0 has the form H_0: $\mu \leq L - K_{p_1} \sigma_y$, since for every $p \leq p_1$ is $P(\boldsymbol{\eta} \in \mathbf{U}_m^{\eta} | p) \leq \alpha$, so that the probability of an error of the first kind is at best α.

The operating characteristic of this test, which we shall denote $L(p|p_1)$, is evidently given by

$$L(p \mid p_1) = P(\boldsymbol{\eta} \in \mathbf{E}_m - \mathbf{U}_m^{\eta} \mid p) = \Phi[R(p \mid p_1)] \, , \tag{7}$$

where

$$R[p \mid p_1] = \sqrt{m} \, (K_p - K_{p_1} + K_{\alpha}/\sqrt{m}) \tag{8}$$

and

$$\Phi(u) = \frac{1}{\sqrt{2\pi}} \int_{-\infty}^{u} e^{-\frac{t^2}{2}} \, dt \, . \tag{9}$$

Let us now assume, that an experimental error exists and let us consider the random variable ζ, which takes on the values of this error and has the probability density

$$\varphi(z) = \frac{1}{\sqrt{2\pi} \, \sigma_z} \exp \left\{ -\frac{1}{2} \left(\frac{z}{\sigma_z} \right)^2 \right\}, \quad -\infty < z < \infty \tag{10}$$

where the parameter σ_z is known.

In that case for the test of the hypothesis (2) its equivalent test (3) against the corresponding alternative hypothesis, we have to use the sample characteristic

$$\xi_n = \eta_m + \zeta_n$$

where

$$\zeta_n = \frac{1}{n} \sum_{i=1}^{n} \zeta^{(i)}, \tag{12}$$

while $\zeta^{(i)}$, $i = 1, 2, \ldots, n$, are mutually independent random variables equally distributed with a probability density (10). According to the assumption $\eta^{(i)}$ and $\zeta^{(i)}$ they are mutually independent.

The sample space, i.e. the set of all points $\xi = (\xi^{(1)}, \ldots, \xi^{(n)})$ corresponding to the given test is, therefore, identical with the n-dimensional Euclidian space $\mathbf{E}_n$. The critical region $\mathbf{U}_n^{\xi} \subset \mathbf{E}_n$ of the same size α as $\mathbf{U}_m^{\eta}$ consists of these elements of $\mathbf{E}_n$, for which $\xi_n > c^*$. We have determined the value of c^* from the expression for the α — per cent critical point of the distribuion of the random variable ξ_n and from (3).

With respect to the mutual independence of $\eta^{(i)}$ and $\zeta^{(i)}$, ζ_n has again evidently a normal distribution with the parameters μ and $\sigma_x^2 = \sigma_y^2/m + \sigma_z^2/n$ again. If we put

$$b = \sigma_z/\sigma_y \, c^*, \tag{13}$$

we find, that c^* is the solution of the equation

$$\frac{\sqrt{m \cdot n}}{\sqrt{2\pi(n + m\delta^2)}\sigma_y} \int_{c^*}^{\infty} e^{-\frac{m \cdot n}{2(n+m\delta^2)} \left(\frac{x-\mu}{\sigma_y}\right)^2} dx = \alpha, \tag{14}$$

so that according to (3) and (4)

$$b^* = L + \sigma_y \left(K_{p_1} - K_{\alpha} \sqrt{\frac{n + m\delta^2}{m \cdot n}} \right). \tag{15}$$

From (6) it follows, that always $c < c^*$.

The operating characteristic of this test is

$$L^*(p \mid p_1) = P(\xi \in \mathbf{E}_n - \mathbf{U}_n^{\xi} \mid p) = \Phi[R^*(p \mid p_1)], \tag{16}$$

where

$$R^*(p \mid p_1) = \sqrt{\frac{m \cdot n}{n + mb^2}} \left[K_p - K_{p_1} + K_{\alpha} \sqrt{\frac{n + mb^2}{m \cdot n}} \right]. \tag{17}$$

Due to the presence of an experimental error in the sample characteristic (11) the following events may occur:

a) ($\xi \in \mathbf{U}_n^{\xi}$; $\eta \in \mathbf{E}_m - \mathbf{U}_m^{\eta}$) that means, that on the basis of an observed value, containing an experimental error, we reject hypothesis H_0 despite the fact, that if the experimental error would have a zero value, we might accept it. This, therefore, causes a sort of error of the first kind;

b) ($\xi \in \mathbf{E}_n - \mathbf{U}_n^{\xi}$; $\eta \in \mathbf{U}_n^{\eta}$) that means, that on the basis of an observed value, including an experimental error, we accept hypothesis H_0, despite the fact, that if the experimental error were zero, we would reject it. This, therefore, causes a sort of error of the second kind.

The probability of the above described events is a function of the true value of parameter p.

Let $\mathbf{N}$ be a set of all natural numbers and $\mathbf{E}_1$ a set of all finite real numbers.

Definition 1 : Probabilities

$$P(\xi \in \mathbf{U}_n^{\xi}\,;\, \eta \in \mathbf{E}_m - \mathbf{U}_m^{\eta}) = Q_1(p \mid p_1)\,, \tag{18}$$

and

$$P(\xi \in \mathbf{E}_n - \mathbf{U}_n^{\xi}\,;\, \eta \in \mathbf{U}_m^{\eta}) = Q_2(p \mid p_1) \tag{19}$$

will be called the functions of the errors of the first, resp. of the second kind from the point of view of the experimental error, if the true value of the parameter be p.

Definition 2 : The trio of numbers (m, n, c), where $m \in \mathbf{N}$, $n \in \mathbf{N}$, $c \in \mathbf{E}_1$, we call the acceptance plan of inspection scheme $(m|n)$, when no experimental error exists.

Definition 3: The trio of numbers (m, n, c^*), where $m \in \mathbf{N}$, $n \in \mathbf{N}$, $c^* \in \mathbf{E}_1$, we call the acceptance plan of inspection scheme $(m|n)$, due to experimental error.

The effectiveness of every acceptance plan (m, n, c) is fully described by the operating characteristic $L(p|p_1)$. The effectiveness of every acceptance plan (m, n, c^*) is fully described by the functions L^* $(p|p_1)$, $Q_1(p|p_1)$ and $Q_2(p|p_1)$.

3. Relations between functions L, L^*, Q_1 and Q_2

The acceptance plans (m, n, c) and (m, n, c^*) have already been given. Then from relations (7) and (16) if we realize, that according to their definition the quantities m, n, and b are positive and that K_p is the decreasing function of p, we obtain

$$\begin{aligned} L(p \mid p_1) - L^*(p \mid p_1) &> 0 \quad \text{for} \quad p \in (0, p_1)\,, \\ &= 0 \quad \text{for} \quad p = 0, p_1, 1\,, \\ &< 0 \quad \text{for} \quad p \in (p_1, 1)\,. \end{aligned} \tag{20}$$

Further, due to the assumptions about the random variables $\eta^{(i)}$ and $\zeta\mathbf{J}^{(i)}$, for the joint probability density $g(x_n, y_m)$ of random variables ζ_n and η_m holds

$$g(x_n, y_m) = \frac{\sqrt{m \cdot n}}{2\pi\sigma_y\sigma_z} \exp\left\{-\frac{1}{2}\left[m\left(\frac{y_m - \mu}{\sigma_y}\right)^2 + n\left(\frac{x_n - y_m}{\sigma_z}\right)^2\right]\right\}, \quad (21)$$

so that with respect to (18) and (19)

$$Q_1(p \mid p_1) = \iint_{\substack{c^* < x_n < \infty \\ -\infty < y_m \leqq c}} g(x_n, y_m) dx_n\, dy_m\,, \quad (22)$$

$$Q_2(p \mid p_1) = \iint_{\substack{-\infty < x_n \leqq c^* \\ c < y_m < \infty}} g(x_n, y_m) dx_n\, dy_m\,. \quad (23)$$

Applying the transformation

$$y_m = \frac{t\sigma_y}{\sqrt{m}} + \mu \quad \text{and} \quad x_n = \frac{s\sigma_z}{b}\sqrt{\frac{n + mb^2}{m \cdot n}} + \mu \quad (24)$$

in (22), we obtain the probability density of a bivariate normal distribution $f(s, t, \varrho)$ with a coefficient of correlation

$$\varrho = \sqrt{\frac{n}{n + mb^2}}\,, \quad (25)$$

where b is defined in (13). According to (8) and (17) the expressions (22) and (23) become

$$Q_1(p \mid p_1) = \iint_{\substack{R^*(p|p_1) < s < \infty \\ -\infty < t \leqq R(p|p_1)}} f(s, t, \varrho) ds\, dt \quad (26)$$

and

$$Q_2(p \mid p_1) = \iint_{\substack{-\infty < s \leqq R^*(p|p_1) \\ R(p|p_1) < t < \infty}} f(s, t, \varrho) ds\, dt. \quad (27)$$

Now let

$$M(\mu, k, \varrho) = \iint_{\substack{u < s < \infty \\ k < t < \infty}} f(s, t, \varrho) ds\, dt \quad (28)$$

where $u,\ k \geqq 0$. If we use (28) and (9) and write $Q_i(p|p_1;\ R,\ R^*)$ instead of $Q_1\ (p|p_1)$, $i = 1, 2$, in order to express the dependence on integration limits of integrals in (26) and (27), we obtain

$$Q_1(p \mid p_1;\ R, R^*) = Q_2(p \mid p_1;\ -R;\ -R^*) = 1 - \Phi(R^*) - M(R^*, R, \varrho)\,, \quad (29)$$

$$Q_2(p \mid p_1;\ R, R^*) = Q_1(p \mid p_1;\ -R;\ -R^*) = 1 - \Phi(R) - M(R^*, R, \varrho)\,; \quad (30)$$

$$Q_1(p \mid p_1;\ R, -R^*) = Q_2(p \mid p_1;\ -R, R^*) = \Phi(R^*) + \Phi(R) + M(R^*; R; -\varrho) - 1\,, \quad (31)$$

$$Q_2(p \mid p_1;\ R, -R^*) = Q_1(p \mid p_1;\ -R, R^*) = M(R^*, R, -\varrho) \quad (32)$$

where R and R^* are non-negative numbers.

From (29) and (30) eventually from (31) and (32) we obtain with respect to (7) and (16)

$$L(p \mid p_1) - L^*(p \mid p_1) = Q_1(p \mid p_1) - Q_2(p \mid p_1) \tag{33}$$

for every $p \in \langle 0, 1 \rangle$.

From (20) and (33) it follows that

$$\begin{aligned} Q_1(p \mid p_1) - Q_2(p \mid p_1) &> 0 \quad \text{for} \quad p \in (0, p_1), \\ &= 0 \quad \text{for} \quad p = 0; p_1; 1, \\ &< 0 \quad \text{for} \quad p \in (p_1, 1). \end{aligned} \tag{34}$$

Further it may be shown that

$$\sup_{p \in \langle 0,1 \rangle} Q_1(p \mid p_1) = Q_1(p^{(1)} \mid p_1), \tag{35}$$

$$\sup_{p \in \langle 0,1 \rangle} Q_2(p \mid p_1) = Q_2(p^{(2)} \mid p_1), \tag{36}$$

where $p^{(1)}$ is the unique solution of equation

$$\left[1 - \Phi\left(\frac{K_\alpha \sqrt{1-\varrho^2}}{1+\varrho}\right)\right] \exp\left\{-\frac{1}{2} R^2(p)\right\} -$$

$$- \varrho \Phi\left[(K_p - K_{p_1})\sqrt{m(1-\varrho^2)} + K_\alpha \frac{\sqrt{1-\varrho^2}}{1+\varrho}\right] \exp\left\{-\frac{1}{2}[R^*(p)]^2\right\} = 0, \tag{37}$$

and $p^{(2)}$ is the unique solution of equation

$$\Phi\left[\frac{K_\alpha \sqrt{1-\varrho^2}}{1+\varrho}\right] \exp\left\{-\frac{1}{2} R^2(p)\right\} -$$

$$- \varrho\left\{1 - \Phi\left[(K_p - K_{p_1})\sqrt{m(1-\varrho^2)} + K_\alpha \frac{\sqrt{1-\varrho^2}}{1+\varrho}\right]\right\}$$

$$\exp\left\{-\frac{1}{2}[R^*(p)]^2\right\} = 0. \tag{38}$$

Proof of equations (35) and (26) is given, in the Appendix.

4. Modification of the model in the case of the selection of the value p_2

So far the considerations assumed the case, that the supplier desires a guarantee, that lots with a fraction p_1 of sub-standard quality raw material will be rejected with a probability α (usually $\alpha = 0{,}05$). The results derived for this case can, after a simple modification, be also applied to the case, when the customer desires a guarantee, that the lots with a fraction $p_2 > p_1$ of sub-

standard quality raw material will be rejected with a probability $1-\beta$ (usually $\beta = 0{,}05$ or $0{,}1$). All we have to do is to replace the values K_α and K_{p_1} by values $K_{1-\beta}$ resp. K_{p_2}. All the expressions determined under the condition, that p_1 be given, are thus transformed into expressions dependent on the given value p_2. Thus we obtain expressions for $L(p|p_2)$, $L^*(p|p_2)$, $R(p|p_2)$, $R^*(p|p_2)$, $Q_1(p|p_2)$ and $Q_2(p|p_2)$. We introduce only one change, in the designation of c c^*. In the case of unacceptable fraction p_2 we shall use the symbols d and d^*. The corresponding acceptance plans will have the form (m, n, d) resp. (m, n, d^*), where always $d > d^*$. This designation will also be used in the numerical example described in paragraph 6.

5. Graphs for the calculation of the function Q_j

The functions $Q_j(p)$ — $j = 1{,}2$ — can be advantageously plotted with the aid of 9 points, of which 7 we shall determine from graphs I to IV (Fig. 1 to 4) and the remaining two from the relations $Q_j(0) = Q_j(1) = 0$, $j = 1, 2$.

For the fixed values $R(p)$ and $j (j = 1, 2)$ the graphs represent the relation (following from the annulled equation (26) resp. (27)) between the three variables $Q_j(p)$, $R^*(p)$ and $b_{m,n}$, where

$$b_{m,n} = \sqrt{\frac{mb^2}{n}}, \tag{39}$$

b being given by (13). For the construction of the graphs we put $L(p) = \gamma$ for $\gamma = 0{,}95$; $0{,}90$; $0{,}70$; $0{,}50$; $0{,}30$; $0{,}10$ and $0{,}05$.

In the construction of the graphs we started out from equations (29) to (32), using the tables [5] of distribution function $\Phi(u)$ and further

a) for $b_{m,n} \geq 0{,}3286$ the tables [4] of distribution function $M(u, k, \varrho)$ defined in (28) and tabulated for $u \geq 0$, $k \geq 0$ and $0 < \varrho < 1$ (by steps of 0,05) and

b) for $0 \leq b_{m,n} < 0{,}3286$ the tables [3] of function

$$T(u, a) = \frac{1}{2\pi} \int_0^a \frac{1}{1 + x^2} e^{-\frac{1}{2}u^2(1+x^2)}\, dx,$$

in which $0 \leq u \leq 4{,}75$ and $0 \leq a \leq 1{,}0$.

Each of the graphs permits the calculation of both values $Q_j(p_\gamma^*)$ — $j = 1, 2$ — with the aid of the given values $b_{m,n}$ and $R^*(p_\gamma^*)$, where p_γ^* is a root of the equation

$$L(p) = \gamma\,, \quad \text{for} \quad 0 \leq \gamma \leq 1 \text{ fixed.} \tag{40}$$

We determine the value $b_{m,n}$ from equation (39), the value $R^*(p_\gamma^*)$ from equation

$$R^*(p_\gamma^* \mid p_1) = K_{1-\gamma} \sqrt{\frac{n}{n + m\delta^2}} + K_\alpha \left[1 - \sqrt{\frac{n}{n + m\delta^2}}\right]. \tag{41}$$

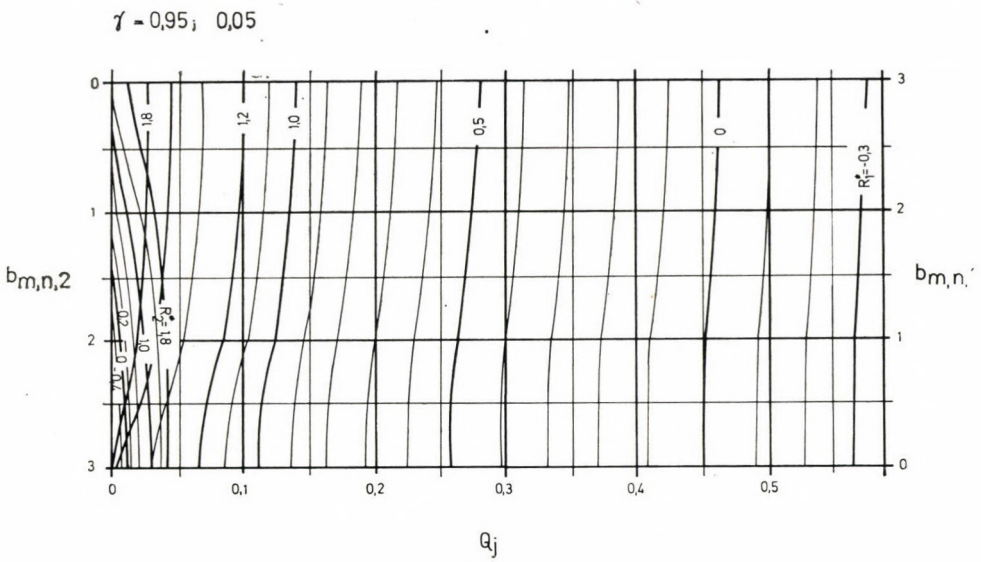

Fig. 1

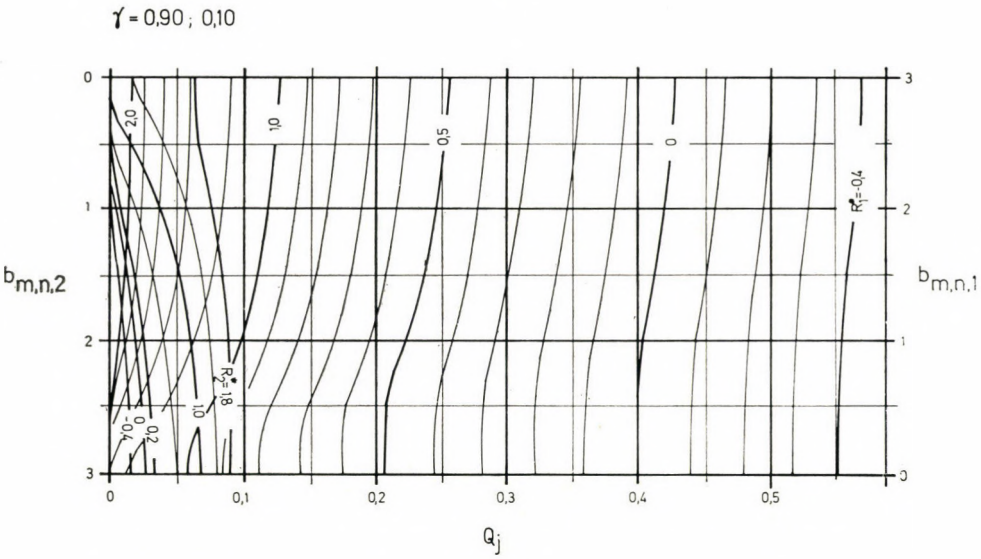

Fig. 2

We can obtain this equation as follows: According to the assumption (40) is valid. Then, due to (7) p_γ^* is the root of equation

$$\Phi[R(p)] = \gamma\,. \tag{42}$$

The existence of a solution of (42) and its uniqueness are evident. For a given

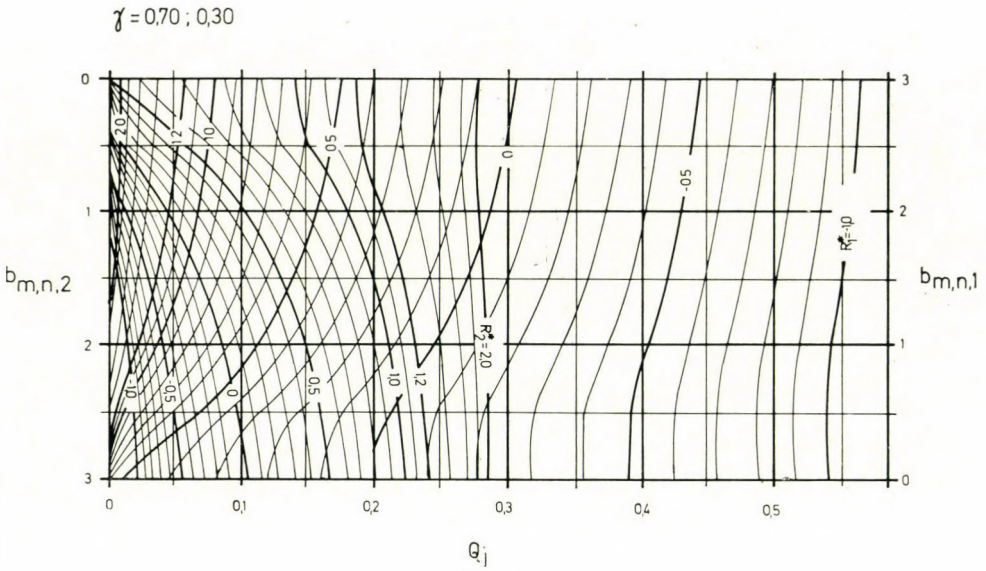

Fig. 3

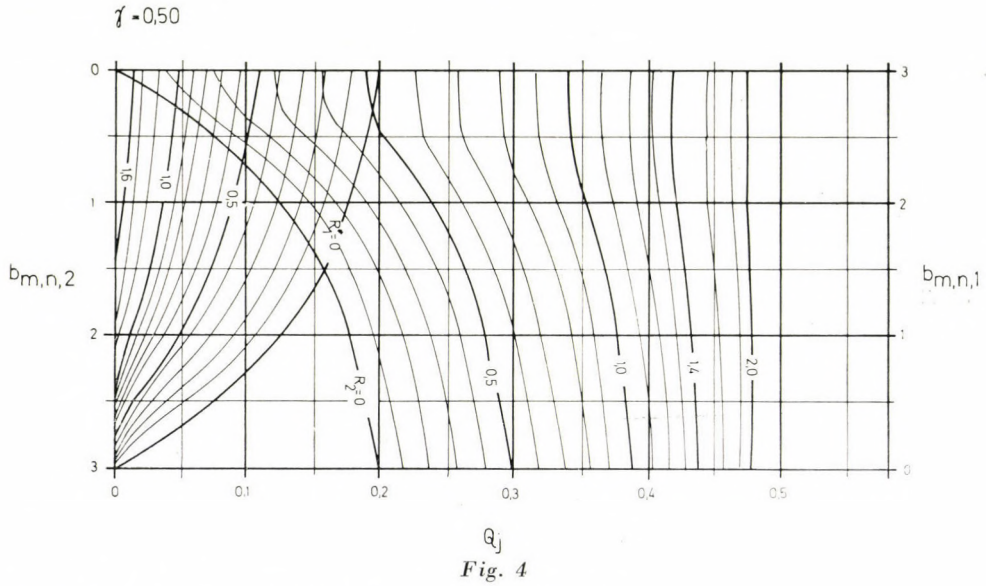

Fig. 4

m, n, p_1 and α then it follows from (8) due to (4)

$$K^*_{p\,\gamma} = \frac{1}{\sqrt{m}} [K_{1-\gamma} - K_\alpha] + K_{p_1}. \tag{43}$$

After the substitution of this expression into (7) we obtain (41). Equation (43) further permits a determination of the values p^*_γ from the tables [5] of the normal distribution.

On the graphs the scale Q_j is common for both considered cases ($j = 1, 2,$). To determine the values $Q_1(p_\gamma^*)$ we use the values R_1^* and $b_{m,n,1}$ and analogously in the case $Q_2(p_\gamma^*)$ the values R_2^* and $b_{m,n\ 2}$. The mutual relations between the values $Q_1(p)$ and $Q_2(p)$ are expressed by equations (29) to (32). As is evident from these equations, all values $Q_1(p)$ and $Q_2(p)$ can be mutually expressed as functions of the non-negative values of the argument R.

Therefore it is sufficient as a consequence of the validity of the relation

$$\Phi[R(p_\gamma^*)] = \Phi[-R(p_{1-\gamma}^*)] = \gamma;\ R \geq 0;\ 0 \leq \gamma \leq 1\,, \tag{44}$$

to construct graphs only for the levels $0{,}5 \leq \gamma < 1$ since this also includes the complementary levels $1 - \gamma$.

Graph I permits the calculation of values $Q_1(p_\gamma^*)$ and $Q_2(p_\gamma^*)$ for the levels $\gamma = 0{,}95$ and $0{,}05$, corresonding to values $R^*(p_{0,95}^*) = 1{,}6449$ and $R(p_{0,05}^*) = -1{,}6449$; graph II for levels $\gamma = 0{,}90$ and $0{,}10$, corresponding to values $R(p_{0,90}^*) = 1{,}2816$ resp. $R(p_{0,10}^*) = -1{,}2816$; graph III for the levels $\gamma = 0{,}70$ and $0{,}30$, corresponding to values $R(p_{0,70}^*) = 0{,}5244$ resp. $R(p_{0,30}^*) = -0{,}5244$, and finally graph IV for the level $\gamma = 0{,}50$ corresponding to the value $R(p_{0,5}^*) = 0$.

6. Effectiveness of acceptance tests of asphalt consistency

The consisitency of asphalt is determined by a penetration test which is performed on a treated average sample tempered to a temperature of 25°C. There is a requirement, that asphalt for the production of cables have a maximum penetration of 50 penetrating units (p. u.). Currently inspection scheme B is used, where the number of tested barrels m is 3.

Let us suppose that $\sigma_z^2 = 4{,}6.$, $\sigma_y^2 = 3{,}2$, $p_2 = 0{,}02$ and $\beta = 0{,}05$. The corresponding acceptance plan is ($m = 3$; $n = 1$; $d^* = 42{,}4$ p.u.), while in the case of a zero experimental error ($m = 3$; $n = 1$; $d = 44{,}6$ p.u.). We determine the operating characteristics $L(p|p_2)$ resp. $L^*(p|p_2)$ from the modified equations (7) resp. (16), which in the case of inspection scheme B and the selection of value p_2 have the form:

$$L(p \mid p_2) = \Phi\{\sqrt{m}(K_p - K_{p_2} + K_{1-\beta}/\sqrt{m})\}\,, \tag{45}$$

and

$$L^*(p \mid p_2) = \Phi\left\{\frac{\sqrt{m}}{\sqrt{1+mb^2}}\left(K_p - K_{p_2} + K_{1-\beta}\sqrt{\frac{1+mb^2}{m}}\right)\right\}. \tag{45'}$$

We can perform the calculation of the points of the operating characteristics either by the current method, selecting several values p in the interval $\langle 0, p_2\rangle$ and determining for them the values $L(p_2)$ resp. $L^*(p|p_2)$ or in such

a manner, that for selected values of $L(p|p_2)$ we calculate back the values of p and then the values $L^*(p|p_2)$. This second method is more suitable in case that besides the operating characteristics we also wish to determine the functions $Q_1(p|p_2)$ resp. $Q_2(p|p_2)$. The values of $L(p|p_2)$ and $L^*(p|p_2)$ determined by the first method for the given acceptance plan are listed in Table I. For their calculation equations (45) and (45') have been used.

Table I

p	$L(p/p_2)$	$L^*(p/p_2)$
0,0005	0,6904	0,2369
0,005	0,2295	0,1052
0,010	0,1204	0,0759
0,015	0,0745	0,0597
0,020	0,05	0,05

When applying the second method, we first determine the values p' for which

$$L(p \mid p_2) = \gamma\,, \quad 0 \leq \gamma \leq 1\,, \tag{46}$$

where we choose γ equal to 0,95; 0,90; 0,70; 0,50; 0,30; 0,10; 0,05. We determine the values of p^*_γ, which satisfy equation (46) by means of equation (43) and the normal distribution tables [5]. The values $Kp^*{}_\gamma$ and p^*_γ for the given levels γ are listed in Table 2 in columns (2) resp. (3). Column (4) of Table 2 lists the value $R^*(p^*_\gamma)$, determined by means of (41), and column (5) the values $L^*(p^*_\gamma|p_2)$, determined by means of (45'). The corresponding values $Q_1(p^*_\gamma|p_2)$ and $Q_2(p^*_\gamma|p_2)$ in columns (6), resp. (7) of Table 2. can be determined by means of graphs I to IV. One of the input quantities, $R^*(p^*_\gamma)$, is already known (column (4) of Table 2), the second $b_{m,n}$ can be determined from (39). For $m = 3$, $n = 1$, $b = 1, 2$ is $b_{m,n}$ equal to 2,07.

Let us, for example, determine the values $Q_1(p^*_{0,70})$ and $Q_2(p^*_{0,70})$. From graph III we can read off for $b_{m,n,1} = 2{,}07$ and from $R^*_1 = -0{,}702$ (cf. Table II) on scale Q_j

$$Q_1(p^*_{0,7}) = Q_1(p; R, R^*) = Q_1(p; 0{,}5244; -0{,}702) = 0{,}49$$

and for $b_{m,n,2} = 2{,}07$ and $R^*_2 = -0{,}702$ on scale Q_j

$$Q_2(p^*_{0,7}) = Q_2(p; 0{,}5244; -0{,}702) = 0{,}03\,.$$

On the same graph we can also read off the values $Q_1(p^*_{0,3})$ and $Q_2(p^*_{0,3})$. In this case $R^*(p^*_{0,3}) = -1{,}158$ (cf. Table II) and $R(p^*_{0,3}) = -0{,}5244$. But according to (30)

$$Q_1 \mid p; -0{,}5244; -1{,}158) = Q_2(p; 0{,}5244; 1{,}158)\,.$$

Table II

γ	Kp^*_γ	$100p^*_\gamma$	$R^*(p^*_\gamma)$	$L^*(p^*_\gamma)$	$Q_1(p^*_\gamma)$	$Q_2(p^*_\gamma)$
0,95	3,9532	0,0039	−0,215	0,415	0,540	0,005
0,90	3,7434	0,0091	−0,372	0,356	0,555	0,011
0,70	3,3063	0,0473	−0,702	0,240	0,490	0,030
0,50	3,0035	0,1335	−0,930	0,176	0,367	0,043
0,30	2,7007	0,3460	−1,158	0,123	0,229	0,052
0,10	2,2636	1,1800	−1,487	0,069	0,079	0,048
0,05	2,0538	2,0000	−1,645	0,050	0,041	0,041

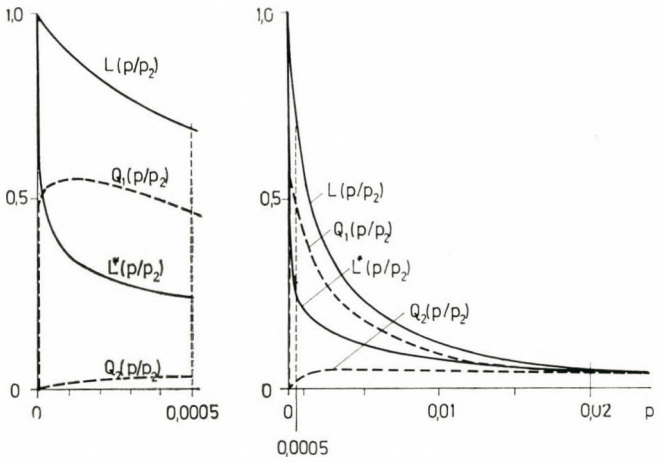

Fig. 5

From graph III for $b_{m,n,2} = 2{,}07$ and $R_2^* = 1{,}158$ we can read off on scale Q_j the value Q_2 $(p;\ 0{,}5244;\ 1{,}158) = 0{,}229$ and therefore $Q_1(p^*_{0,3}) = 0{,}229$. We obtain the value $Q_2(p^*_{0,3})$ by means of equation (29). According to this equation

$$Q_2(p;\ -\ 0{,}5244;\ -\ 1{,}158) = Q_1(p;\ 0{,}5244;\ 1{,}158)\,.$$

On scale Q_j of graph III we find, that to the values $b_{m,n,1} = 2{,}07$ and $R_2^* = 1{,}158$ correspond the value $Q_1(p;\ 0{,}5244;\ 1{,}158) = 0{,}052$ and therefore $Q_2(p^*_{0,3}) = 0{,}052$.

We proceed in the same way when using the other graphs. The calculated values $Q_1(p^*_\gamma)$ and $Q_2(p^*_\gamma)$ are listed in columns (6) and (7) of Table II.

The operating characteristics $L(p|p_2)$ and $L^*(p|p_2)$ and graphs $Q_1(p|p_2)$ resp. $Q_2(p|p_2)$ are on Fig. 5.

Let us look mose closely at the shape of curves $Q_1(p)$ and $Q_2(p)$. While the curve $Q_2(p)$ attains the maximum values of 0,053 at the value $p = 0{,}0048$, the curve $Q_1(p)$ attains the maximum value of 0,556 at the point $p = 0{,}0001$ (the values of p are found by solving the modified equation (37) resp. (38). The presence of an experimental error makes itself unfavourably felt, mainly for the supplier, not only by increasing of the steepness of the operating characteristic $L^*(p)$ in comparison with the steepness of $L(p)$ but also by the fact, that even lots, containing a very small fraction of low-grade raw material will be incorrectly assesed (approximately in 50% of all cases) as being of sub-standard quality, due to the influence of a large experimental error.

REFERENCES

1. HORÁLEK, V.: On Certain Inspection Schemes of Raw Materials. *Aplikace matematiky* **2** (1957) 370—389 (in Czech)
2. HORÁLEK, V.: Some Special Sampling Inspection Procedures for Bulk Materials. *Proc. 10th EOQC Conference*, Stockholm (1966)
3. OWEN, D. B.: The Bivariate Normal Probability Distribution. Res. Rep. SC-3831-Sandia Corporation (1957).
4. PEARSON, K.: Tables for Statistician and Biometricians, Part II. Cambridge University Press, London 1931
5. JANKO, J.: Statistical Tables. Prague 1958 (in Czech)

Einfluß des Versuchsfehlers auf die Wirksamkeit von gewissen Verfahren für die Prüfung von Massengütern. Die Arbeit befasst sich mit der theoretischen Untersuchung von drei Kontrollmethoden mit Stichprobenentnahme für die Prüfung von Massengütern (Flüssigkeiten, Pulver u. dgl.). Der Einfluß des Versuchsfehlers auf die Operations-Charakteristik wird untersucht. Um die Wirksamkeit des Kontrollverfahrens genauer beschreiben zu können werden außer den Operations-Charakteristiken noch die Kurven der Fehler erster und zweiter Art eingeführt. Um die Berechnung der Punkte dieser Kurven zu erleichtern wurden Nomogramme konstruiert.

Воздействие опытной ошибки на эффективность системы контроля определенных бесформенных материалов. Автор в своей статье рассматривает теорию трех систем контроля отбора проб, которые используют для контрля бесформенных материалов (жидкости, порошки и схожие материалы). Анализируется воздействие опытной ошибки на оперативную характеристику. Чтобы можно было бы точнее описать эффективность системы контроля, кроме оперативной характеристики вводятся кривые диаграммы опытной ошибки первого вида и второго вида. Для облегчения вычисления точек этих кривых автором построены соответствующие номограммы.

Acta Technica Academiae Scientiarum Hungaricae, Tomus 82 (3—4), pp. 391—399 (1976)

BEWEGUNG VON KÖRNER IN FLÜSSIGEN ODER GASFÖRMIGEN MEDIEN IM BEREICH $\mathrm{Re} = 0{,}6 \div 800$

S. PETHŐ*
KANDIDAT DER TECHN. WISS.

[Eingegangen am 3 Januar 1974]

Im Aufsatz sind die Bewegungsgleichungen für Teilchen abgeleitet, die sich in flüssigem oder gasförmigem Medium absetzen, wenn weder die Gesetze der laminaren, noch der turbulenten Strömung gültig sind. Die Bewegungsgesetze der laminaren und turbulenten Strömung wurden von J. FINKEY in seinem vor 50 Jahren erschienenen Buche »Die wissenschaftlichen Grundlagen der nassen Erzaufbereitung« hergeleitet.

Es ist bekannt, daß im Stokesschen Bereich, d. h. bei Reynolds-Zahlen 0,6 zwischen dem Widerstandskoeffizienten des Mediums und der Reynolds-Zahl die Beziehung

$$c = \frac{24}{\mathrm{Re}}, \tag{1}$$

für Reynolds-Zahlen 30 bis 300 nach ALLEN

$$c = \frac{10}{\mathrm{Re}^{1/2}}, \tag{2}$$

und für $\mathrm{Re} > 800$ die Beziehung

$$c = \frac{0{,}43}{\mathrm{Re}^{0}} \tag{3}$$

bestehen.

Sucht man die auf die Endfallgeschwindigkeit eines Kornes bezogenen Bewegungsgesetze für den Bereich $\mathrm{Re} = 0{,}6 \div 800$, so wird es zweckmäßig sein, den Zusammenhang zwischen Widerstandskoeffizient und Reynolds-Zahl auch im Bereich $\mathrm{Re} = 0{,}6 \div 30$ bzw. $\mathrm{Re} = 300 \div 800$ ähnlich den vorstehenden Formeln zu definieren, nämlich als Quotienten aus einer Konstanten und der Reynolds-Zahl mit einem bestimmten Exponenten:

$$c = \frac{A}{\mathrm{Re}^{2/3}}, \tag{4}$$

bzw.

$$c = \frac{C}{\mathrm{Re}^{1/3}}, \tag{5}$$

* Prof. DR. S. PETHŐ, Csabai Kapu 36, 3529 Miskolc, Hungary.

A und C sind Konstanten, die durch Versuche [2] und mit Hilfe der Methode der kleinsten Quadrate bestimmt wurden. Tafel I zeigt die Konstanten mit den zugehörigen Wertepaaren Re und c. Die Werte der Konstanten sind: $A = 23{,}06$; $B = 11{,}06$ und $C = 4{,}49$. Die Konstante B gilt für den Bereich $30 \leq \mathrm{R}_e \leq 300$, die damit etwas größer ist als der von ALLEN vorgeschlagene Wert. Weiterhin enthält die Tafel die Gegenüberstellung der versuchsweise ermittelten und der berechneten c-Werte, die praktisch voneinander nicht abweichen.

Im Bild 1 sind Funktionen $\lg c = f(\lg \mathrm{Re})$ mit den angeführten Konstanten für die entsprechenden Re-Bereiche eingezeichnet. Weil die Widerstandskraft F_k der mit der Geschwindigkeit v im Medium mit der Dichte γ absinkenden Kugel des Durchmessers d

$$F_k = c\,\gamma \frac{v^2}{2g} \cdot \frac{d^2\,\pi}{4} \tag{6}$$

ist, werden die speziellen Werte in den Re-Bereichen $0{,}6 \div 30$; $30 \div 300$ und $300 \div 800$ nach folgenden Formeln errechnet:

$$F_{0{,}6\,\ldots\,30} = \frac{A\pi}{8g^{1/3}}\,\gamma^{1/3}\,\mu^{2/3}\,(dv)^{4/3}, \tag{7}$$

$$F_{30\,\ldots\,300} = \frac{B\pi}{8g^{1/2}}\,\gamma^{1/2}\,\mu^{1/2}\,(dv)^{3/2}, \tag{8}$$

$$F_{300\,\ldots\,800} = \frac{C\pi}{8g^{2/3}}\,\gamma^{2/3}\,\mu^{1/3}\,(dv)^{5/3}. \tag{9}$$

Die Endfallgeschwindigkeiten v_0 sind entsprechend den Widerstandskräften und dem Auftrieb

$$F_A = \frac{d^3\pi}{6}(\delta - \gamma) \tag{10}$$

folgende:

$$v_{0,\,0{,}6\,\ldots\,30} = \left(\frac{4}{3A}\right)^{3/4}\left(\frac{g}{\gamma}\right)^{1/4}\frac{d^{5/4}}{\mu^{1/2}}(\delta - \gamma)^{3/4}, \tag{11}$$

$$v_{0,\,30\,\ldots\,300} = \left(\frac{4}{3B}\right)^{2/3}\left(\frac{g}{\gamma}\right)^{1/3}\frac{d}{\mu^{1/3}}(\delta - \gamma)^{2/3}, \tag{12}$$

$$v_{0,\,300\,\ldots\,800} = \left(\frac{4}{3C}\right)^{3/5}\left(\frac{g}{\gamma}\right)^{2/5}\frac{d^{4/5}}{\mu^{1/5}}(\delta - \gamma)^{3/5}. \tag{13}$$

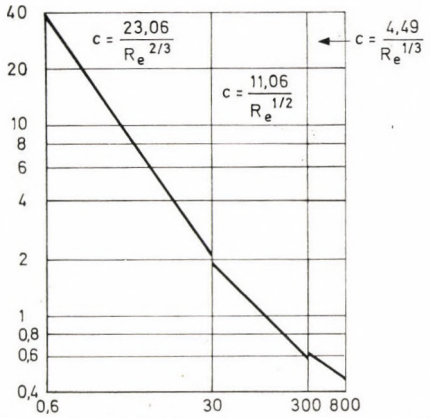

Bild 1. $\lg c = f(\lg \mathrm{Re})$ für die verschiedenen Re-Bereiche

Tafel I

Re-Zahlen und Widerstandskoeffizienten für verschiedene Re-Bereiche

$0{,}6 \leqq R_e \leqq 30$			$30 \leqq R_e \leqq 300$			$300 \leqq R_e \leqq 800$		
Re	c	$\frac{23{,}06}{R_e^{2/3}}$	Re	c	$\frac{11{,}06}{Re^{1/2}}$	Re	c	$\frac{4{,}49}{Re^{1/3}}$
1	2	3	4	5	6	7	8	9
			30	2,045	(2,018)			
0,8	33,8	26,8	40	1,735	1,749	300	0,684	(0,671)
1,0	27,6	23,1	50	1,540	1,564	400	0,612	0,609
2,0	14,9	14,5	60	1,398	1,428	500	0,563	0,566
4,0	8,32	9,15	70	1,295	1,322	600	0,526	0,532
6,0	6,05	6,98	80	1,213	1,237	700	0,498	0,506
8,0	4,89	5,77	90	1,148	1,166	800	0,488	0,484
10,0	4,15	4,97	100	1,092	1,106			
20,0	2,62	3,13	200	0,806	0,764			
30,0	2,045	2,388	300	0,684	0,639			

Zur Bestimmung der Sinkgeschwindigkeit während der Beschleunigungsperiode muß die Differentialgleichung

$$m\frac{dv}{dt} = mg_0 - F_k \tag{14}$$

gelöst werden. In der Gleichung ist g_0 die Erdbeschleunigung in dem gegebenen Medium:

$$g_0 = g\frac{\delta - \gamma}{\delta}\,. \tag{15}$$

Unter Berücksichtigung der beschriebenen Strömungswiderstände gilt in allen drei Re-Bereichen

$$\frac{dv}{dt} = g_0\left[1 - \left(\frac{v}{v_0}\right)^n\right], \tag{16}$$

bzw.

$$\int \frac{dv}{1-(v/v_0)^n} = g_0 \int dt\,. \tag{17}$$

v_0 sind die durch die Gleichungen (11), (12) und (13) gegebenen Endfallgeschwindigkeiten. Der Exponent beträgt für die Re-Zahlen:

$$\text{Re} = \quad 0{,}6 \div \quad 30 : n = 4/3,$$

$$\text{Re} = \quad 30 \quad \div 300 : n = 3/2,$$

$$\text{Re} = 300 \quad \div 800 : n = 5/3.$$

Die Lösung der Differentialgleichung für $n = 4/3$ lautet:

$$3v_0\left[\frac{1}{4}\ln\frac{1+\left(\frac{v}{v_0}\right)^{1/3}}{1-\left(\frac{v}{v_0}\right)^{1/3}} - \frac{1}{2}\arctan\left(\frac{v}{v_0}\right)^{1/3}\right] = g_0\, t_{0,6\,\ldots\,30} + C\,. \tag{18}$$

Für $t = 0$ und $v = 0$ ist die Integrationskonstante $C = 0$ und somit ergibt sich:

$$t_{0,6\,\ldots\,30} = 3\,\frac{v_0}{g_0}\left[\frac{1}{4}\ln\frac{1+\left(\frac{v}{v_0}\right)^{1/3}}{1-\left(\frac{v}{v_0}\right)^{1/3}} - \frac{1}{2}\arctan\left(\frac{v}{v_0}\right)^{1/3}\right]. \tag{19}$$

Für $n = 3/2$ lautet die Lösung:

$$2v_0\left\{-\frac{1}{9}\ln\frac{\left[1-\left(\frac{v}{v_0}\right)^{1/2}\right]^2}{1+\left(\frac{v}{v_0}\right)^{1/2}+\frac{v}{v_0}} - \frac{1}{3}\arctan\frac{2\left(\frac{v}{v_0}\right)^{1/2}+1}{\sqrt{3}}\right\} = \tag{20}$$

$$= g_0\, t_{30\,\ldots,\,300} + C\,.$$

Die Integrationskonstante ist dann für die Bedingungen $t = 0$ und $v = 0$:

$$C = \frac{v_0 \pi}{3\sqrt{3}} \tag{21}$$

und es ergibt sich:

$$t_{30\,\ldots\,300} = 3\,\frac{v_0}{g_0}\left\{\frac{\pi}{9\sqrt{3}} - \frac{1}{9}\ln\frac{\left[1-\left(\frac{v}{v_0}\right)^{1/2}\right]^2}{1+\left(\frac{v}{v_0}\right)^{1/2}+\frac{v}{v_0}} - \right.$$
$$\left. - \frac{2}{3\sqrt{3}}\arctan\frac{2\left(\frac{v}{v_0}\right)^{1/2}+1}{\sqrt{3}}\right\}. \tag{22}$$

Bei $n = 5/3$ gilt:

$$3v_0\left\{\left\{-\frac{1}{5}\ln\left[1-\left(\frac{v}{v_0}\right)^{1/3}\right]+\frac{1}{5}\left\{\left(\cos\frac{3\pi}{5}\right)\ln\left[1-2\left(\frac{v}{v_0}\right)^{1/3}\cos\frac{\pi}{5}+\right.\right.\right.$$
$$\left.+\left(\frac{v}{v_0}\right)^{2/3}\right]+\left(\cos\frac{9\pi}{5}\right)\ln\left[1+2\left(\frac{v}{v_0}\right)^{1/3}\cos\frac{3\pi}{5}+\left(\frac{v}{v_0}\right)^{2/3}\right]\right\}+$$
$$+\frac{2}{5}\left[\left(\sin\frac{3\pi}{5}\right)\arctan\frac{\left(\frac{v}{v_0}\right)^{1/3}+\cos\frac{3\pi}{5}}{\sin\frac{\pi}{5}}+\right. \tag{23}$$
$$\left.\left.\left.+\left(\sin\frac{9\pi}{5}\right)\arctan\frac{\left(\frac{v}{v_0}\right)^{1/8}+\cos\frac{3\pi}{5}}{\sin\frac{3\pi}{5}}\right]\right\}\right\} = g_0\,t_{300\,\ldots\,800} + C\,.$$

Die Integrationskonstante ist:

$$C = 3v_0\left\{\frac{2}{5}\left[\left(\sin\frac{3\pi}{5}\right)\arctan\left(\cot\frac{\pi}{5}\right)+\right.\right.$$
$$\left.\left.+\left(\sin\frac{9\pi}{5}\right)\arctan\left(\cot\frac{3\pi}{5}\right)\right]\right\} = 3v_0\,\frac{2\pi}{25}\,0{,}5878 \tag{24}$$

und

$$t_{300\ldots800} = \frac{3v_0}{g_0}\left\{\left[-\frac{2\pi}{25}0{,}5878 - \frac{1}{5}\ln\left[1-\left(\frac{v}{v_0}\right)^{1/3}\right]+\right.\right.$$

$$+\frac{1}{5}\left\{0{,}3090\ln\left[1-1{,}6180\left(\frac{v}{v_0}\right)^{1/3}+\left(\frac{v}{v_0}\right)^{2/3}\right]+\right.$$

$$\left.+0{,}3090\ln\left[1+0{,}6180\left(\frac{v}{v_0}\right)^{1/3}+\left(\frac{v}{v_0}\right)^{2/3}\right]\right\}+ \qquad (25)$$

$$+\frac{2}{5}\left[0{,}9511\ \text{arc tan}\frac{\left(\frac{v}{v_0}\right)^{1/3}+0{,}8090}{0{,}5878}-\right.$$

$$\left.\left.-0{,}5878\ \text{arc tan}\frac{\left(\frac{v}{v_0}\right)^{1/3}+0{,}3090}{0{,}9511}\right]\right.$$

Die Gleichungen (19), (22) und (25) ergeben die Funktionen $t = f(v)$ für die entsprechenden Re-Bereiche. Die Funktionen $v = f(t)$ lassen sich aus denselben Gleichungen nicht explizite darstellen, da zwischen ln- und arc tan-Funktionen keine mathematische Beziehung besteht. Im Falle einer Reihenentwicklung werden wegen der erforderlichen Genauigkeit auch die Glieder höherer Ordnung benötigt. Aus diesem Grunde lassen sich mit den auf diese Weise zu entwickelnden Gleichungen die Geschwindigkeiten nicht ausdrücken. Deshalb können auch die Beschleunigungen dv/dt als Funktion der Zeit in geschlossener Form nicht dargestellt werden.

Zu Werten, die der Beschleunigung dv/dt verhältnisgleich sind, gelangt man mit Hilfe einer numerischen Lösung. Zu den Verhältnissen $w = v/v_0$ lassen sich aus Gl. (16) die Beschleunigungsverhältnisse

$$\frac{dv}{dt}\cdot\frac{1}{g_0} = 1 - \left(\frac{v}{v_0}\right)^n \qquad (26)$$

bzw. aus den Gln. (19), (22) und (25) die der seit Beginn der Bewegung verstrichenen Zeit $T = g_0\ (t/v_0)$ verhältnisgleiche Werte bestimmen. Damit ist das Beschleunigungsverhältnis gemäß Gleichung (26) als Funktion des Zeitverhältnis gemäß T bekannt.

Zu Werten, die dem zurückgelegten Weg

$$s = \int_0^t v\,dt \qquad (27)$$

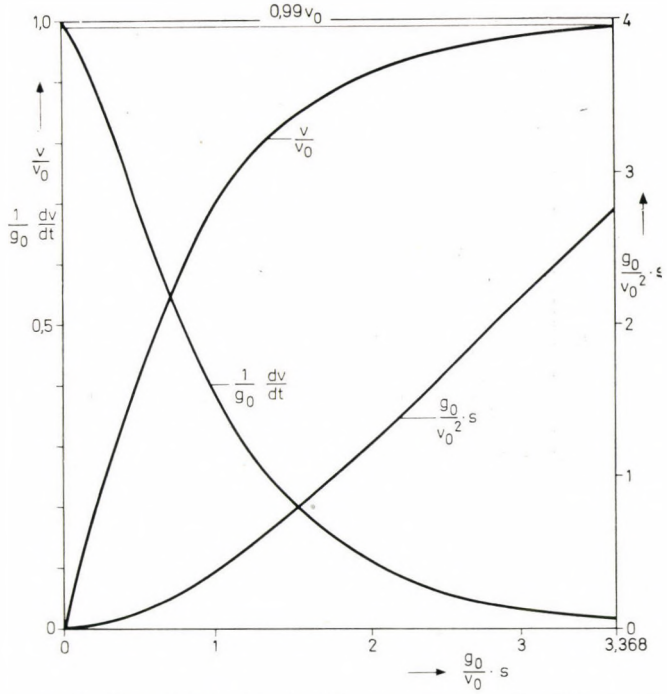

Bild 2, 3, 4. Graphische Darstellung der der Geschwindigkeit, der Zeit der Beschleunigung und dem zurückgelegten Weg verhältnisgleichen Werte als Funktion des Zeitverhältnisses $T = g_0 t/v_0$

Bild 2. Re = 0,6 ÷ 30

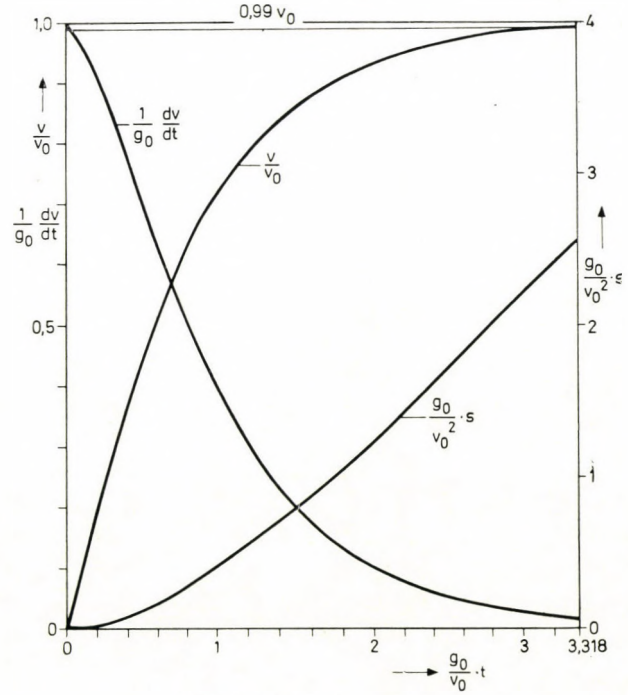

Bild 3. Re = 30 ÷3

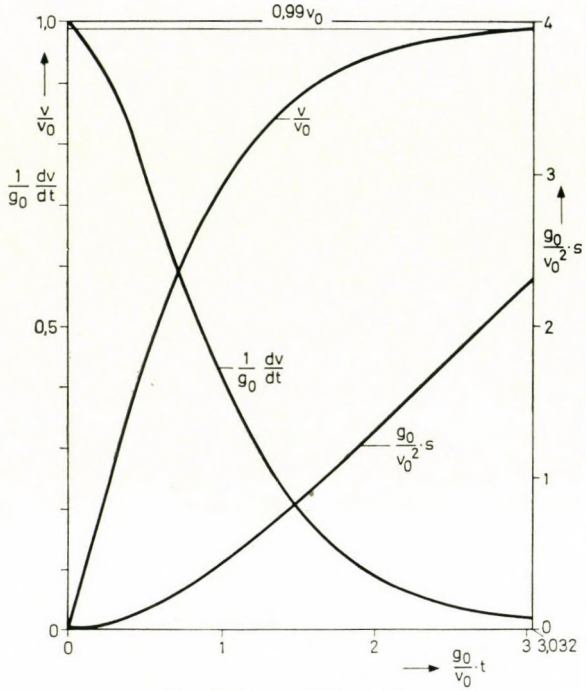

Bild 4. Re = 300 ÷ 800

verhältnisgleich sind, gelangt man durch folgende Überlegung. Fixiert man die Geschwindigkeit

$$v = v_0 \frac{v}{v_0} = v_0 w \tag{28}$$

und die Zeit

$$t = \frac{v_0 T}{g_0}, \tag{29}$$

so wird s:

$$s = \int_0^{v_0 T/g_0} v_0 w \frac{v_0}{g_0} dT = \frac{v_0^2}{g_0}\left[w\left(\frac{v_0 T}{g_0}\right) - w(0)\right] = \frac{v_0^2}{g_0} f\left(\frac{v}{v_0}, T\right). \tag{30}$$

Aus (30) ergibt sich der dem zurückgelegten Weg verhältnisgleiche Wert:

$$s = \frac{g_0}{v_0^2} = f\left(\frac{v}{v_0}, T\right). \tag{31}$$

Tafel II zeigt die der Geschwindigkeit, der Zeit, der Beschleunigung und dem zurückgelegten Weg verhältnisgleichen Werte für vorgegebene Verhältnisse v/v_0.

Auf den Bildern 2, 3 und 4 sind die Daten der Tafeln in Abhängigkeit vom Zeitverhältnis $T = g_0\, t/v_0$ dargestellt.

Tafel II

Die der Zeit, der Beschleunigung und dem Weg verhältnisgleichen Werte für verschiedene Re-Bereiche

Re	0,6 — 30			30—300			300—800		
$\frac{v}{v_0}$	$\frac{g_0 t}{v_0}$	$\frac{1}{g_0}\frac{dv}{dt}$	$\frac{g_0}{v_0} s$	$\frac{g_0}{v_0} t$	$\frac{1}{g_0}\frac{dv}{dt}$	$\frac{g_0}{v^2} s$	$\frac{g_0}{v_0} t$	$\frac{1}{g_0}\frac{dv}{dt}$	$\frac{g_0}{v^2} s$
1	2	3	4	5	6	7	8	9	10
0	Ø	1,0000	Ø	Ø	1,0000	Ø	Ø	1,0000	Ø
0,1	0,1020	0,9536	0,0051	0,1013	0,9684	0,0051	0,1008	0,9785	0,0050
0,2	0,2109	0,8830	0,0215	0,2075	0,9106	0,0210	0,2054	0,9316	0,0207
0,3	0,3297	0,7992	0,0512	0,3222	0,8257	0,0497	0,3165	0,8656	0,0485
0,4	0,4627	0,7053	0,0978	0,4482	0,7460	0,0938	0,4378	0,7829	0,0910
0,5	0,6158	0,6031	0,1666	0,5918	0,6465	0,1584	0,5742	0,6850	0,1523
0,6	0,7983	0,4939	0,2667	0,7617	0,5352	0,2518	0,7330	0,5732	0,2397
0,7	1,0288	0,3785	0,4169	0,9728	0,4143	0,3890	0,9295	0,4481	0,3674
0,8	1,3468	0,2573	0,6554	1,2618	0,2845	0,6058	1,1952	0,3106	0,5874
0,9	1,8797	0,1311	1,1084	1,7418	0,1462	1,0138	1,6325	0,1611	0,9591
0,95	2,4061	0,0661	1,5950	2,2129	0,0741	1,4496	2,0587	0,0819	1,3533
0,97	2,7916	0,0398	1,9655	2,5564	0,0447	1,7793	2,3693	0,0494	1,6515
0,99	3,6183	0,0133	2,7750	3,3682	0,0150	2,5749	3,0324	0,0166	2,3014

Danksagung

Für die seitens des Herrn Doz. I. Raisz bei der Lösung der im Aufsatz behandelten Differentialgleichungen geleistete Hilfe möchte der Verfasser an dieser Stelle seinen Dank aussprechen.

SCHRIFTTUM

1. Finkey, J.: Die wissenschaftlichen Grundlagen der nassen Erzaufbereitung
2. Tarján, G.: Ércelőkészítéstan, Tankönyvkiadó, Budapest 1974
3. Schubert, H.: Aufbereitung fester mineralischer Rohstoffe, Bd. I. 2. Aufl. Verlag für Grundstoffindustrie, Leipzig 1968

The Laws of Motion of a Solid Body for Reynolds Numbers between 0,6 and 800. — The paper presents the laws of motion of a body descending in a gaseous or liquid medium if in the laws of motion, neither of laminar nor of turbulent flow can be applied. These laws have been deduced by Josef Finkey in his basic work "Die wissenschaftlichen Grundlagen der nassen Erzaufbereitung", published 50 years ago. In the solving of the differential equations contained in the paper and in carrying out the calculation, the author has been aided by Mr. Iván Raisz, assistant professor, to whom he wishes to express his sincere thanks.

Законы движения твердого тела при значениях числа Рейнольдса в пределах между 0,6 и 800. В статье приведены уравнения движения твердого тела, погружающегося в газообразную или жидкую среду, когда не действительны ни законы турбулентного движения потока, ни законы ламинарного движения потока. Уравнения движения ламинарного и турбулентного потоков выведены Йожефом ФИНКЕИ в фундаментальном труде »Ди Виссеншафтлихен Грундлаген дер нассен Эрцафбереитунг« (Научные основы мокрой рудоподготовки), опубликованном 50 лет тому назад.

Acta Technica Academiae Scientiarum Hungaricae, Tomus 82 (3—4), pp. 401—415 (1976)

KINEMATISCHE UNTERSUCHUNG DER AN DEN SICH BERÜHRENDEN FLÄCHENPAAREN VERWIRKLICHTEN ZWANGSSYSTEME

B. KIRÁLY*

KANDIDAT DER TECHN. WISSENSCHAFTEN

[Eingegangen am 15. Dezember 1974]

Bei einem der in technischer Hinsicht wichtigsten Typen der holonomen Systeme verwirklichen sich die Zwänge durch sich berührende Flächenpaare, die an den starr zu betrachtenden Körpern ausgestaltet sind. Die Arbeit beschäftigt sich mit der kinematischen Untersuchung solcher Zwangssysteme. Zuerst führt sie den Begriff des auf einem einzigen Flächenpaar verwirklichten, sogenannten oberflächlichen Zwanges und des zum einzigen Berührungspunkt gehörenden Elementarzwanges ein, dann ersetzt sie das Zwangssystem durch ein solches System der Elementarzwänge, in dem die einzelnen oberflächlichen Zwänge den voneinander linear unabhängigen Elementarzwängen entsprechen. So kann man das auf den Geschwindigkeitszustand des holonomen Systems bezügliche Zwangsgleichungssystem — auch in allgemeinen räumlichen Fällen — in gedrängter, für die weiteren Untersuchungen geeigneter Matrizenform aufschreiben.

Bezeichnungen

$\mathbf{a}$	Richtungsvektor aufgenommen auf der Wirkungslinie a des Elementarzwanges
$\mathbf{b}$	Moment des zur Wirkungslinie a des Elementarzwanges gebundenen Vektors $\mathbf{a}$, auf den willkürlich gewählten Bezugspunkt A
$\mathbf{g}_a$, $\mathbf{g}_i$	Plücker-Vektor des Elementarzwanges, mit 6 Dimensionen (mit *: als Zeilenvektor aufgeschrieben)
$\mathbf{G}$	Matrix des oberflächlichen Zwanges
$\mathbf{H}$	geometrische Kennzeichnung des Zwangssystems
N	Anzahl der zum System gehörenden starren Körper mit unbekannten Geschwindigkeitszustand
$\mathbf{p}_j$	Geschwindigkeitszustand-Vektor des j-ten starren Körpers
T_j	Zeichen des j-ten starren Körpers
$\mathbf{u}$	kinematische Kennzeichnung des Zwangssystems
$\mathbf{v}_j$	Geschwindigkeit des zu T_j gebundenen Punktes A
V_{aj}	Projektionsgeschwindigkeit des j-ten starren Körpers, gehörig zur (gerichteten) Wirkungslinie des Elementarzwanges a
$\mathbf{w}$	Geschwindigkeitszustand-Vektor der starren Körper, deren Geschwindigkeitszustand unbekannt ist
Γ	Matrix, konstruiert aus den Plücker-Vektoren der zum oberflächlichen Zwang gehörigen Elementarzwänge
ϱ	Rang von Matrix Γ, bzw. $\mathbf{G}$
ω_j	Winkelgeschwindigkeitsvektor des j-ten starren Körpers

1. Einleitung

Zahlreiche technische Konstruktionen sind bekannt, in denen feste Körper mit verschiedenen Funktionen durch Berührung der daran ausgebildeten Oberflächen miteinander in Zwangsverbindung sind. Je eine solche

* Dr. B. KIRÁLY, Csabai kapu 34, H-3529 Miskolc, Ungarn

Verbindung — abhängig von der Ausgestaltung der Oberflächen — kann die unterschiedlichste Beschränkung für die relative Bewegung der Körper bedeuten. Diese Verbindungen haben eine sehr wichtige Rolle, besonders in der Ausbildung und in der Funktion der sich bewegenden Konstruktionen (Mechanismen), sie sind jedoch bedeutungsvoll auch im Aufbau vieler ruhender Konstruktionen.

Bei kinematischer Untersuchung solcher Zwangsverbindungen soll man zuerst die beschränkende Wirkung der einzelnen sich berührenden Flächenpaare, ausgeübt auf die relative Bewegung der entsprechenden zwei Körper, klarstellen, sodann kann die Untersuchung des ganzen Zwangssystems folgen. Auf dem Gebiet der technischen Anwendungen werden die Zwänge oft durch solche speziell ausgebildete Flächenpaare (Ebenen, Kreiszylinder, Kugeln, Schraubenflächen) verwirklicht, bei denen man auf die relative Bewegung der vorliegenden zwei Körper, beziehungsweise auf die beschränkende Wirkung des Zwanges auch auf Grund der unmittelbaren Anschauung folgern kann. Wahrscheinlich ist gerade dies ein Grund dafür, daß die ein solches Thema behandelnden Arbeiten (z. B. [1—5]) die Zwangssysteme überwiegend aus solchen speziellen Verbindungen (speziellen kinematischen Paaren) aufbauen und die Möglichkeit für deren weitere Zerlegung nicht untersuchen. Um die zusammengesetzten, räumlichen Probleme leichter behandeln zu können, ist es doch zweckmäßig, die Gesetzmäßigkeiten des zwischen den zwei Körpern auftretenden Zwanges etwas eingehender, auch von anderer Seite zu untersuchen.

Die Arbeit führt den Begriff des Elementarzwanges ein, dann macht sie eine solche Methode bekannt, die das Zwangssystem aus Elementarzwängen aufbaut, und mit ihrer Hilfe kann man die Zwangsgleichungen auf den Geschwindigkeitszustand bezüglich so schreiben, daß man aus diesen sowohl auf die Äquivalenz der Zwangssysteme, als auf die Verhältnisse der kinematischen Bestimmtheit des Systems (beziehungsweise auf seinen Freiheitsgrad) — auch in allgemeinen, räumlichen Fällen — eindeutig folgern kann [6].

Bei den Untersuchungen gehen wir von den nachfolgenden Voraussetzungen aus:

a) die zu untersuchende Konstruktion ersetzen wir mit einem aus endlich vielen vollkommen starren Körpern bestehenden Modell;

b) zwischen den Elementen des aus starren Körpern bestehenden Systems ist eine solche holonome Zwangsverbindung, die mittels der auf diesen Körpern ausgestalteten, sich berührenden Flächenpaare verwirklicht wird;

c) zu jedem einzelnen Berührungspunkt der sich berührenden Flächenpaare gehört nur eine gemeinsame oberflächliche Normale;

d) die auf das Zwangssystem bezüglichen kinematischen Untersuchungen verrichten wir in einer möglichen Lage des Systems, in bezug auf den momentanen Geschwindigkeitszustand;

e) die Zwänge sind zweiseitig, oder sie sind in der betreffenden Lage (im betreffenden Augenblick) in Betracht zu ziehende einseitige Zwänge.

Den auf dem einzigen Flächenpaar verwirklichten (die Voraussetzungen b) und c) befriedigenden) Zwang nennen wir *oberflächlichen Zwang*.

Zum Schluß ist es zweckmäßig zu erwähnen, daß man die folgenden kinematischen Untersuchungen auch auf die hinsichtlich der Geschwindigkeitskoordinaten linearen anholonomen Zwangsverbindungen erweitern kann.

2. Der zwischen zwei starren Körpern verwirklichte oberflächliche Zwang

Das an zwei starren Körpern ausgestaltete Flächenpaar kann sich miteinander in einem einzigen Punkt, oder in mehr als einem — aber in endlich vielen — Punkten, oder in unendlich vielen Punkten, z. B. entlang einem Linien-, oder Flächenstück berühren.

2.1 Im einfachsten Falle kommt die Berührung in einem einzigen Punkt (auf dem Bild 1 P) vor. Einen solchen oberflächlichen Zwang nennen wir *Elementarzwang*. Die über den Berührungspunkt P durchgehende, gemeinsame oberflächliche Normale ist die *Wirkungslinie des Elementarzwanges* (a). Diese kann mit Hilfe des aus zugehörigen Plücker-Koordinaten aufgebauten sechsdimensionalen Zeilenvektors

$$\mathbf{g}_a^* = [\mathbf{a}^* ; \quad \mathbf{b}^*] = [a_x, a_y, a_z, b_x, b_y, b_z] \tag{1}$$

($\mathbf{g}_a^*$ ist der Transponierte des Spaltenvektors $\mathbf{g}_a$) in irgendeinem orthogonalen Koordinatensystem x, y, z mit Einheitsvektoren gegeben werden,

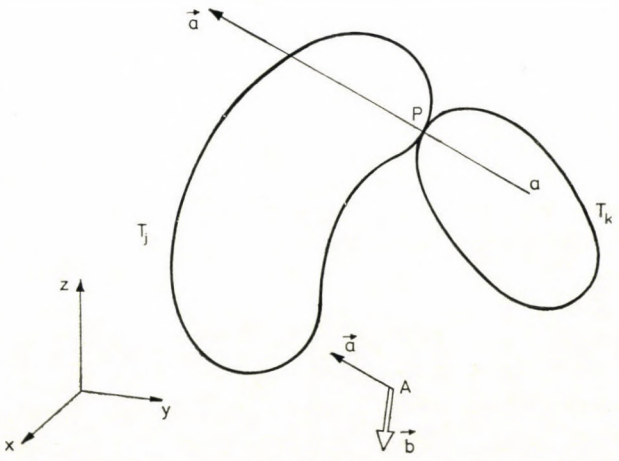

Bild 1

wo $\mathbf{a} = a_x\mathbf{i} + a_y\mathbf{j} + a_z\mathbf{k}$ der Richtungsvektor der Wirkungslinie a ist (im allgemeinen ist es zweckmäßig, wenn $|\mathbf{a}| = 1$); $\mathbf{i}, \mathbf{j}, \mathbf{k}$ bedeuten die Einheitsvektoren des Koordinatensystems x, y, z;

$\mathbf{b} = b_x\mathbf{i} + b_y\mathbf{j} + b_z\mathbf{k}$, das Moment des zur Wirkungslinie a gebundenen Vektors $\mathbf{a}$, gerechnet auf einen willkürlich gewählten Punkt A, ist (man kann dieses auch in der Form $\mathbf{r}_{AP} \times \mathbf{a}$ schreiben, wenn $\mathbf{r}_{AP}$ der von Punkt A zu Punkt P gerichtete Ortsvektor ist).

Bei einem solchen Elementarzwang drückt die auf den Geschwindigkeitszustand bezügliche Zwangsgleichung (die sogenannte Elementarzwangsgleichung) das aus, daß die auf die Wirkungslinie a des Elementarzwanges bezogenen Projektionsgeschwindigkeiten V_{aj} und V_{ak} des Berührungspunktes der Körper T_j und T_k (und zugleich jedes auf der Wirkungslinie des Elementarzwanges liegenden Punktes) gleich sind, das heißt

$$V_{aj} = V_{ak}. \tag{2}$$

Vorausgesetzt, daß $|\mathbf{a}| = 1$,

$$V_{aj} = \mathbf{a}\,\mathbf{v}_{Pj} = \mathbf{a}(\mathbf{v}_{Aj} + \boldsymbol{\omega}_j \times \mathbf{r}_{AP}) = \mathbf{a}\,\mathbf{v}_{Aj} + \mathbf{b}\,\boldsymbol{\omega}_j,$$

wo $\mathbf{v}_{Pj}$ die momentane Geschwindigkeit des Berührungspunktes P des Körpers T_j ist;

$\mathbf{v}_{Aj} = \mathbf{v}_j$ die momentane Geschwindigkeit des mit Punkt A zusammenfallenden Punktes des Körpers T_j ist;

$\boldsymbol{\omega}_j$ die momentane Winkelgeschwindigkeit des Körpers T_j ist.

Mit Hilfe der letzteren Quantitäten führen wir jetzt den in Form eines sechsdimensionalen Spaltenvektors aufgeschriebenen Geschwindigkeitszustand-Vektor

$$\mathbf{p}_j = \begin{bmatrix} \mathbf{v}_j \\ \boldsymbol{\omega}_j \end{bmatrix} = \begin{bmatrix} v_{jx} \\ v_{jy} \\ \cdot \\ \cdot \\ \cdot \\ \omega_{jz} \end{bmatrix} \tag{4}$$

des Körpers T_j ein, dann auf ähnliche Weise den Vektor $\mathbf{p}_k$ auf den Körper T_k. So läßt sich die Gleichung (2) mit Benützung der Gln. (1), (3) und (4) in die Form

$$\mathbf{g}_a^*\,\mathbf{p}_j = \mathbf{g}_a^*\,\mathbf{p}_k, \tag{5}$$

oder in die auf eine Seite geordnete Form

$$\mathbf{g}_{aj}^*\,\mathbf{p}_j + \mathbf{g}_{ak}^*\,\mathbf{p}_k = 0 \quad (\mathbf{g}_{aj}^* = -\mathbf{g}_{ak}^* = \mathbf{g}_a^*) \tag{6}$$

schreiben.

$\mathbf{p}_j$, $\mathbf{p}_k$ und $\mathbf{g}_a^*$ sind auf denselben, sonst willkürlich wählbaren Punkt A bezogen, d. h., sie bedeuten in denselben Punkt A reduzierte Vektorzweier.

Diejenigen Elementarzwänge, die gemeinsame Wirkungslinie haben, bedeuten ebensolche Beschränkung hinsichtlich des Geschwindigkeitszustandes

(gleichviel, wo der Berührungspunkt P sich daran befindet). Deshalb ist der sechsdimensionale Zeilenvektor $\mathbf{g}_a^*$ nicht nur zur Kennzeichnung der Wirkungslinie des Elementarzwanges, sondern auch zur Kennzeichnung des Elementarzwanges selbst geeignet. Im weiteren nennen wir $\mathbf{g}_a^*$ den *Plücker-Vektor des Elementarzwanges.*

Im Interesse des Weiteren ist es schon hier zweckmäßig, auch solche fiktive Elementarzwänge einzuführen, deren Wirkungslinie irgendeine unendlich ferne Gerade des Raumes ist. In ihren Plücker-Vektoren

$$\mathbf{g}_a^* = [\mathbf{a}^*; \mathbf{b}^*]$$

ist $\mathbf{a} = 0$ (und zweckmäßig $|\mathbf{b}| = 1$). Solche fiktive Elementarzwänge nennen wir *Drehung behindernde Zwänge*, weil die entsprechenden Zwangsgleichungen nur auf die Winkelgeschwindigkeitskoordinaten der sich berührenden Körper T_j und T_k Beschränkungen bedeuten. Den Vektor $\mathbf{b}$ im Plücker-Vektor des Drehung behindernden Zwanges nennen wir den *Richtungsvektor des Drehung behindernden Zwanges.* Dieser ist der Normalvektor jener Ebenen, deren unendlich ferne Gerade die Wirkungslinie des vorliegenden Elementarzwanges ist.

2.2 Untersuchen wir jetzt den Fall, wenn zwei Elemente des Flächenpaares sich in endlich vielen (mehr als einem) Punkten (auf dem Bild 2 $P_1, P_2, \ldots, P_M$) berühren. Da sollen die zu Körpern T_j und T_k gehörigen Projektionsgeschwindigkeiten auf die Wirkungslinie a_i bezüglich in jedem einzelnen Berührungspunkt P_i ($i = 1, 2, \ldots, M$) gleich sein, d. h., man kann je eine Elementarzwangsgleichung auf jeden von den Punkten P_i schreiben. So läßt sich ein solcher oberflächlicher Zwang als ein aus M Stücken bestehendes System betrachten. Das den Zwang ausdrückende Gleichungssystem hat auf Grund der Gln. (5), bzw. (6) die Form

$$\mathbf{g}_i^* \mathbf{p}_j = \mathbf{g}_i^* \mathbf{p}_k, \text{ bzw. } \mathbf{g}_{ij}^* \mathbf{p}_j + \mathbf{g}_{ik}^* \mathbf{p}_k = 0 \quad (i = 1, \ldots, M), \tag{7}$$

die sich auch in einer einzigen Matrixgleichung

$$\mathbf{\Gamma} \mathbf{p}_j = \mathbf{\Gamma} \mathbf{p}_k, \text{ bzw. } \mathbf{\Gamma} \mathbf{p}_j + (-\mathbf{\Gamma}) \mathbf{p}_k = 0 \tag{8}$$

zusammenfassan läßt. Die Matrix

$$\mathbf{\Gamma} = \begin{bmatrix} \mathbf{g}_1^* \\ \mathbf{g}_2^* \\ \cdot \\ \cdot \\ \cdot \\ \mathbf{g}_M^* \end{bmatrix}$$

in den Gln. (8) hat einen Typ $M \times 6$, d. h., sie hat M Zeilen und 6 Spalten. Wie es bekannt ist, bedeutet der Rang einer Matrix die maximale Anzahl ihrer voneinander linear unabhängigen Zeilen (bzw. Spalten). Aus dem Aufbau

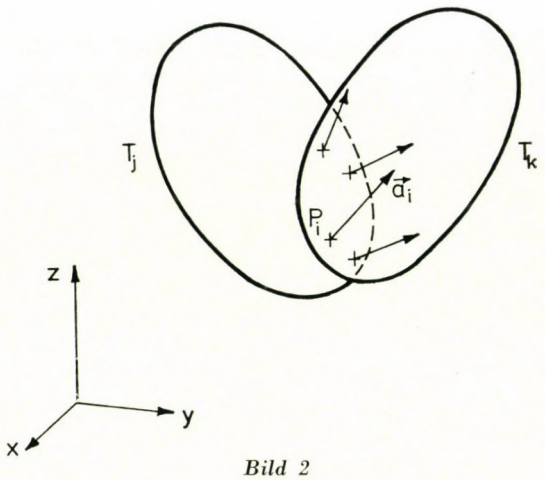

Bild 2

der Matrix $\mathbf{\Gamma}$ folgt, daß ihr Rang $\varrho = \varrho(\mathbf{\Gamma})$ zugleich auch die maximale Anzahl jener zum betreffenden oberflächlichen Zwang gehörenden Elementarzwänge angibt, deren Wirkungslinien voneinander linear unabhängige Geraden sind. Solche Elementarzwänge selbst nennen wir auch *voneinander linear unabhängig*. Offensichtlich kann ϱ weder größer als M, noch als 6 sein. So soll man zwei Fälle voneinander unterscheiden:

a) wenn $\varrho = M$ $(M \leq 6)$, dann sind die zum oberflächlichen Zwang gehörenden Elementarzwänge voneinander linear unabhängig;

b) wenn $\varrho < M$, dann sind die zum oberflächlichen Zwang gehörenden Elementarzwänge voneinander linear nicht unabhängig, d. h. sie sind linear zusammenhängend.

In diesem letzteren Fall ist die Folge der Erfüllung der voneinander linear unabhängigen ϱ Gleichungen auch die Erfüllung der restlichen $M - \varrho$ Gleichungen wegen der Linearität der Gln. (7). Deshalb ändert sich in solchen Fällen die beschränkende Wirkung des auf den Geschwindigkeitszustand bezogenen Zwanges mit Weglassen der erwähnten $M - \varrho$ Gleichungen nicht, auch dann nicht, wenn wir die entsprechende Elementarzwänge weglassen. So brauchen wir im Falle b) zur Kennzeichnung des originalen oberflächlichen Zwanges statt der Matrix $\mathbf{\Gamma}$ im weiteren die Matrix

$$\mathbf{G} = \begin{bmatrix} \mathbf{g}_1^* \\ \vdots \\ \mathbf{g}_\varrho^* \end{bmatrix}, \tag{9}$$

die die Plücker-Vektoren der — voneinander linear unabhängigen — Elementarzwänge mit maximaler Anzahl in ihren Zeilen enthält. Da von den zu einem oberflächlichen Zwang gehörenden Elementarzwängen höchstens sechs von-

einander linear unabhängig sein können, so kann auch die Matrix **G** nicht mehr als sechs Zeilen haben. (Natürlich ist im Falle a) $\mathbf{G} = \mathbf{\Gamma}$.) Die Matrix **G** nennen wir die *Matrix des oberflächlichen Zwanges.*

2.3 Im dritten Falle berührt sich das an zwei starren Körpern ausgestaltete Flächenpaar in unendlich vielen Punkten — meistens entlang eines Linien-, oder Flächenstückes (Bild 3) — miteinander. Auch in solchen Fällen gehört zu jedem Berührungspunkt ein Elementarzwang, dessen Wirkungslinie mit der oberflächlichen Normalen zusammenfällt. So kann man den vorliegenden oberflächlichen Zwang als System der unendlich vielen Elementarzwänge betrachten. Diese Elementarzwänge sind immer linear zusammenhängend. Auf ähnliche Weise, wie im Falle b) des Punktes 2.2 ist es auch hier genügend, von den unendlich vielen Elementarzwängen eine solche Gruppe der Elementarzwänge auszuwählen, die die — voneinander linear unabhängigen — Elementarzwänge mit größtmöglichster Anzahl ϱ enthält. Dies bedeutet zugleich, daß sämtliche weitere Elementarzwänge von den zur ausgewählten Gruppe gehörenden Elementarzwängen schon linear abhängen. Aus den Plücker-Vektoren dieser ϱ Elementarzwänge kann die auf die Kennzeichung des vorliegenden oberflächlichen Zwanges geeignete Matrix **G** von Form (9) geschrieben werden, die wir auch hier die Matrix des oberflächlichen Zwanges nennen.

3. Die Äquivalenz der oberflächlichen Zwänge

Die oberflächlichen Zwänge — von der Ausgestaltung der sich berührenden Oberflächen abhängig — können sehr vielfältig sein. Im Interesse eines leichteren Überblickes und leichterer Manipulation lassen sich diese auch von mehreren Gesichtspunkten vergleichen. Im folgenden möchten wir die verschiedenen oberflächlichen Zwänge von jenem Gesichtspunkt aus vergleichen, welche auf den relativen Geschwindigkeitszustand der anschließenden zwei starren Körper gleiche Beschränkung bedeuten. Die Einführung der Elementarzwänge erleichtert diesen Vergleich und macht sie wesentlich übersichtlicher.

Auf dieselben zwei starren Körper bezogene zwei verschiedene oberflächliche Zwänge nennen wir dann miteinander äquivalent, wenn diese gleiche Beschränkung auf den relativen Geschwindigkeitszustand der zwei Körper bedeuten, d. h., wenn die entsprechenden (auf den Geschwindigkeitszustand bezogenen) Zwangsgleichungssysteme äquivalent sind. Dies besteht dann, wenn sämtliche Lösungen des einem oberflächlichen Zwang entsprechenden Gleichungssystems — gegenseitig — auch das zum anderen gehörende Zwangsgleichungssystem befriedigen.

Im Punkt 2 haben wir schon gesehen, daß die oberflächlichen Zwänge sich durch den Plücker-Vektor eines einzigen Elementarzwanges, oder durch

eine aus Plücker-Vektoren mehrerer (aber höchstens sechs) Elementarzwänge aufgebaute Matrix (durch die Matrix des oberflächlichen Zwanges) charakterisieren läßt, abhängig davon, ob die Berührung in einem Punkt, oder in mehreren Punkten verwirklicht wird. Auf Grund der obigen Definition läßt sich folglich auch das ausdrücken, daß jeder oberflächliche Zwang mit höchstens sechs — voneinander linear unabhängigen — Elementarzwängen äquivalent ist.

Wenn wir von zwei verschiedenen oberflächlichen Zwängen bestimmen wollen, ob sie äquivalent sind, oder nicht, dann ist es zweckmäßig diese Untersuchung in den folgenden Schritten durchzuführen. Zuerst ersetzen wir die originalen oberflächlichen Zwänge durch das System der zugehörigen Elementarzwänge, dann lassen wir von diesem alle Elementarzwänge weg, die von den restlichen schon linear abhängen. Damit ersetzen wir die einzelnen oberflächlichen Zwänge durch voneinander linear unabhängige Elementarzwänge. Im folgenden Schritt soll man die so erhaltenen zwei Systeme der Elementarzwänge vergleichen. Zwei auf dieselben zwei starren Körper bezogene oberflächliche Zwänge sind dann und nur dann miteinander äquivalent, wenn gegenseitig jeder zu einem oberflächlichen Zwang gehörige Elementarzwang von den zum anderen oberflächlichen Zwang gehörigen Elementarzwängen linear abhängig ist. Damit haben wir die Untersuchung der Äquivalenz der oberflächlichen Zwänge zum Problem der linear zusammenhängenden Geraden reduziert, was schon leichter zu überblicken ist. Dies bedeutet eine gute Hilfe auch beim Schreiben der Zwangsgleichung, und so können wir auch darüber einen Überblick bekommen, welche weitere Matrizen statt der für die Kennzeichnung der einzelnen oberflächlichen Zwänge eingeführten Matrix **G** brauchbar sind, bzw., wie wir zu den einfachsten Ausdrücken gelangen.

Im nachfolgenden werden einige Spezialfälle als Beispiel — die einfache Beweisführung weglassend — für Äquivalenz der aus Elementarzwängen bestehenden Systeme, bzw. der oberflächlichen Zwänge angeführt.

a) Zwei verschiedene Elementarzwänge (a_1, a_2) mit sich in einem gemeinsamen Punkt P schneidenden (und in einer gemeinsamen Ebene S liegenden) Wirkungslinien sind äquivalent

— mit zwei, oder mehr, beliebigen, verschiedenen Elementarzwängen, deren Wirkungslinien (z. B. a_1', a_2', a_3') sich an den Punkt P und an die Ebene S fügen (Bild 4);

— mit einem oberflächlichen Zwang mit einem entlang einer Kreislinie sich berührenden — aus einem Kreiszylinder und einer Kugel bestehenden — Flächenpaar, wenn der Mittelpunkt der Kreislinie P, und ihre Ebene S ist (Bild 5).

b) Drei Elementarzwänge (auf Bild 6 a_1, a_2, a_3) mit sich in einem gemeinsamen Punkt P schneidenden, nicht in einer gemeinsamen Ebene liegenden Wirkungslinien sind äquivalent

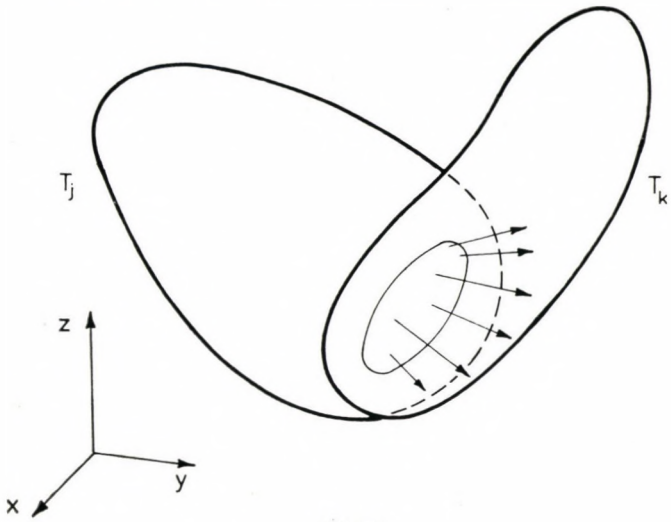

Bild 3

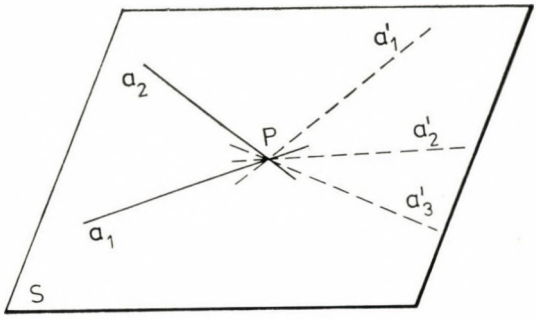

Bild 4

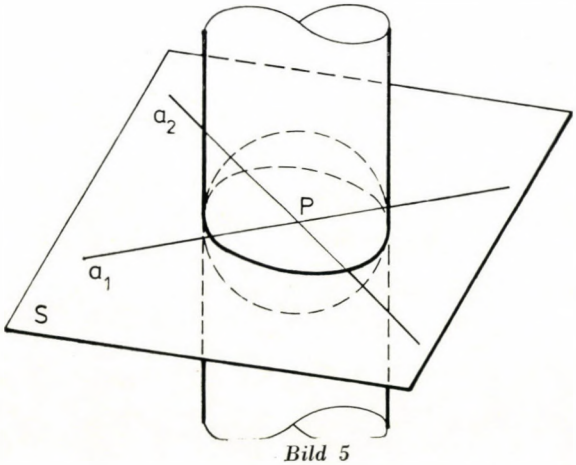

Bild 5

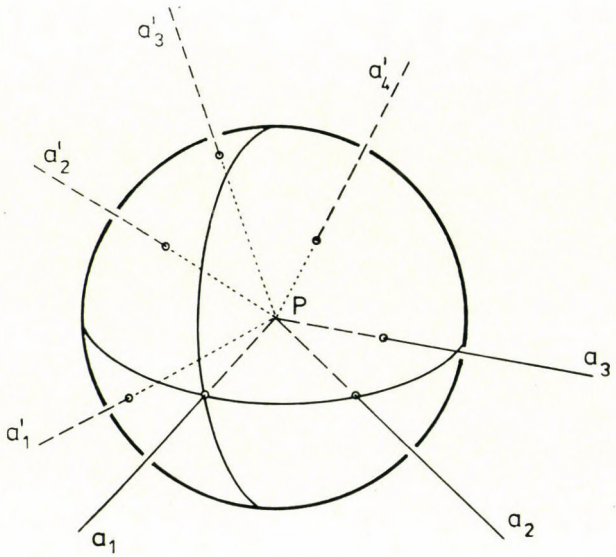

Bild 6

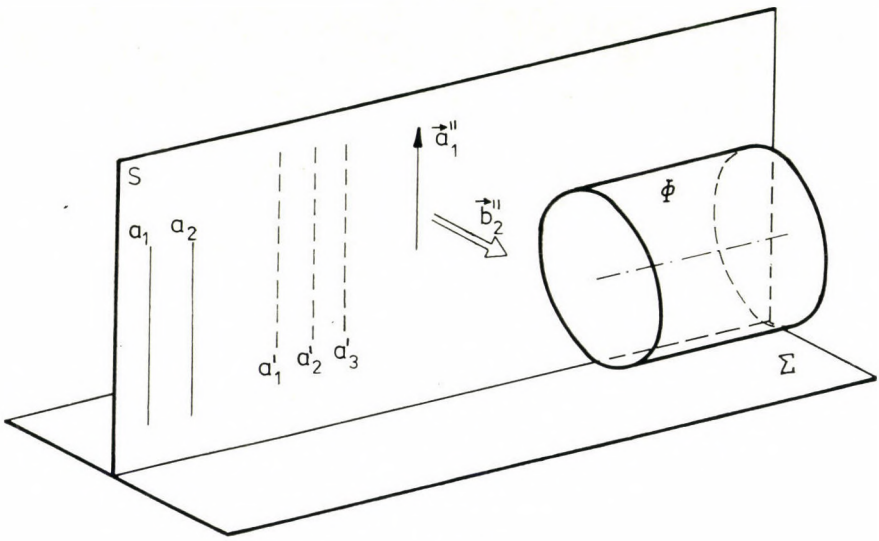

Bild 7

— mit drei, oder mehr, beliebigen Elementarzwängen, deren Wirkungslinien (z. B. a_1', a_2', a_3', a_4') sich an den Punkt P fügen und die nicht komplanar sind;

— mit oberflächlichem Zwang eines Kugelgelenkes, wenn der Mittelpunkt der Kugel P ist.

c) Zwei die Ebene S bestimmende Elementarzwänge mit parallelen Wirkungslinien (auf Bild 7 a_1, a_2) sind äquivalent

— mit zwei, oder mehr, beliebigen, verschiedenen Elementarzwängen,

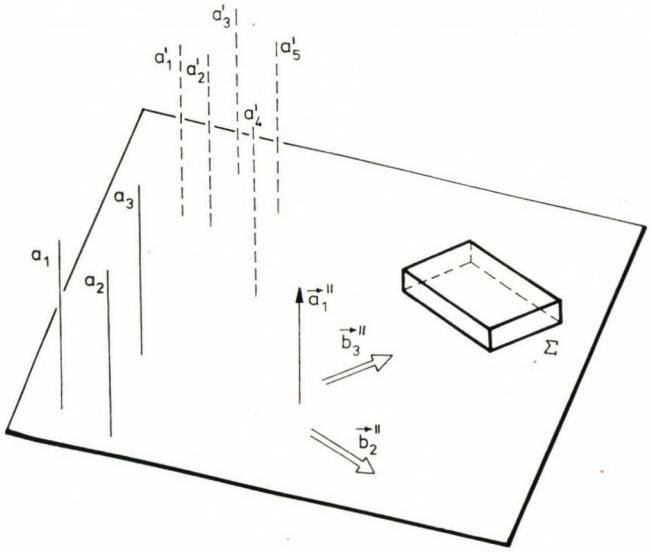

Bild 8

deren Wirkungslinien (z. B. a'_1, a'_2, a'_3) sich an die Ebene S fügen und die mit den Wirkungslinien der zwei originalen Elementarzwänge parallel sind;

— mit einem Elementarzwang ($\mathbf{a}''_1$) und einem Drehung behindernden Zwang ($\mathbf{b}''_2$), vorausgesetzt, daß die Wirkungslinie des Elementarzwanges sich an die Ebene S fügt und die mit den Wirkungslinien der originalen Elementarzwänge parallel ist, doch der Richtungsvektor des Drehung behindernden Zwanges auf die Ebene S normal ist:

— mit einem oberflächlichen Zwang mit einem entlang einem geraden Linienstück sich berührenden — aus einer Ebene Σ und einem Kreiszylinder Φ (oder aus einem Kegel) bestehenden — Flächenpaar, wenn das gerade Linienstück sich an die Ebene S fügt, und die Ebene Σ auf die Wirkungslinien der originalen Elementarzwänge normal ist.

d) Drei Elementarzwänge (auf Bild 8 a_1, a_2, a_3) mit parallelen, nicht in gemeinsamer Ebene liegenden Wirkungslinien sind äquivalent

— mit drei, oder mehr, beliebigen Elementarzwängen, deren Wirkungslinien (z. B. a'_1, a'_2, a'_3, a'_4, a'_5) mit den Wirkungslinien der originalen Elementarzwänge parallel und nicht komplanar sind;

— mit einem Elementarzwang ($\mathbf{a}''_1$) und mit zwei Drehung behindernden Zwängen ($\mathbf{b}''_2$, $\mathbf{b}''_3$), wenn die Wirkungslinie des Elementarzwanges mit den Wirkungslinien der originalen Elementarzwänge parallel ist, doch die zwei verschiedenen Richtungsvektoren der Drehung behindernden Zwänge darauf normal sind;

— mit einem oberflächlichen Zwang mit einem entlang einem ebenen Flächenstück (Σ) sich berührenden Flächenpaar, wenn die ebene Fläche auf die Wirkungslinien der originalen Elementarzwänge normal ist.

4. Die Kennzeichnungen des an den sich berührenden Flächenpaaren verwirklichten Zwangssystems, die Matrixgleichung des Zwangssystems

Jedes solche — aus starren Körpern bestehende — holonome System läßt sich als System oberflächlicher Zwänge untersuchen, wo die Zwänge infolge der Berührung der an den starren Körpern ausgebildeten Oberflächen sich verwirklichen. Die Kennzeichnung und die mathematische Beschreibung eines solchen Zwangssystems kann sich durch Zusammenfassung der Matrizen mit Aufbau (9) der einzelnen oberflächlichen Zwänge (Punkt 2.2) in eine einzige Matrix ereignen. Von dieser Matrix erfordern wir aber auch, daß mit ihrer Hilfe die Matrixgleichung des Zwangssystems unmittelbar aufschreibbar sei.

Im Falle der mit aus starren Körpern bestehendem System modellierten, sich bewegenden Konstruktionen (Mechanismen) ist es zweckmäßig, zum Aufschreiben der auf den Geschwindigkeitszustand bezogenen Zwangsgleichungen im allgemeinen die Körper in zwei Gruppen aufzuteilen, je nachdem, ob deren Geschwindigkeitszustand unbekannt (gesucht), oder bekannt (vorgeschrieben) ist. Von den vorgeschriebenen Geschwindigkeitszuständen soll man natürlich voraussetzen, daß diese mit den unter ihnen vorhandenen oberflächlichen Zwängen nicht in Widerspruch sind (dies läßt sich erforderlichenfalls auch kontrollieren). Bei Untersuchung — gerichtet in erster Reihe auf die Klarstellung der Frage der kinematischen Bestimmtheit — der ruhenden Konstruktionen kann meistens nur der Geschwindigkeitszustand jenes einzigen in Ruhe stehenden Körpers als bekannt angenommen werden, woran das Koordinatensystem gebunden ist, aber die übrigen Geschwindigkeitszustände sind unbekannt.

Bezeichnen wir die Anzahl der zum System gehörenden starren Körper mit unbekannten Geschwindigkeitszuständen mit N. Der Geschwindigkeitszustand dieser Körper läßt sich in irgendeinem Koordinatensystem x, y, z insgesamt mit $6N$ Geschwindigkeits-, bzw. Winkelgeschwindigkeitskoordinaten angeben, was auch in der Form eines einzigen, $6N$-dimensionalen Spaltenvektors schreibbar ist. Diesen unbekannten Geschwindigkeitszustand-Vektor bezeichnen wir mit

$$\mathbf{w} = \begin{bmatrix} \mathbf{p}_1 \\ \mathbf{p}_2 \\ \cdot \\ \cdot \\ \cdot \\ \mathbf{p}_N \end{bmatrix},$$

wo $\mathbf{p}_j$ der Geschwindigkeitszustand-Vektor des j-ten Körpers nach (4) ist ($j = 1, 2, \ldots, N$). Schließlich kann die auf $\mathbf{w}$ bezogene Zwangsgleichung immer in die Matrixgleichung

$$\mathbf{H}\mathbf{w} = \mathbf{u} \tag{10}$$

geschrieben werden, wo die Matrix **H** das geometrische Kennzeichen und **u** das kinematische Kennzeichen des Zwangssystems ist.

Aus obenstehendem folgt, daß in Matrix **H** die geometrischen Matrizen aller solchen oberflächlichen Zwänge auftreten sollen, welche mit einem Körper mit unbekanntem Geschwindigkeitszustand in Verbindung stehen. Es ist zweckmäßig, die Matrix **H** auf solche Art aufgeteilt zu schreiben, daß jede einzelne Blockzeile je einem oberflächlichen Zwang, aber jede einzelne Blockspalte je einem Körper mit unbekanntem Geschwindigkeitszustand entsprechen soll (Bild 9). So haben sämtliche (N Stücke) Blöcke in der i-ten Blockzeile einen Typ $\varrho_i \times 6$, wenn ϱ_i die größte Anzahl der voneinander linear unabhän-

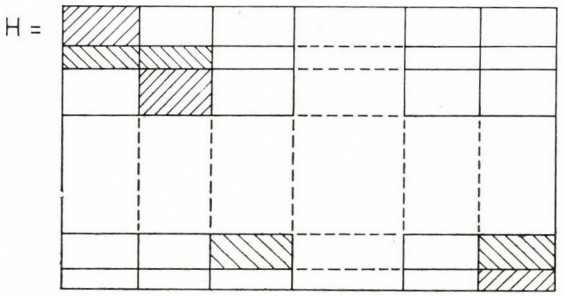

Bild 9

gigen Elementarzwänge ist (dies kann niemals größer als sechs sein). Da ein oberflächlicher Zwang immer zu zwei Körpern gehört, stehen zwei von Null abweichende Blöcke in jeder solchen Blockzeile der Matrix **H**, die einem zwischen zwei Körpern mit unbekanntem Geschwindigkeitszustand auftretenden oberflächlichen Zwang entspricht (die anderen sind Nullblöcke). Dagegen steht nur ein von Null abweichender Block in der Blockzeile des oberflächlichen Zwanges zwischen einem Körper mit bekanntem und einem mit unbekanntem Geschwindigkeitszustand. Die von Null abweichenden Blöcke stimmen mit den Matrizen der entsprechenden oberflächlichen Zwänge überein. Wenn in einer Zeile zwei solche stehen, sind diese voneinander — gemäß (8) — nur im Vorzeichen verschieden.

Danach kommen wir auf die Bedeutung des Vektors **u**, auf die Bestimmung der kinematischen Kennzeichnung des Zwangssystems. Ähnlich wie beim Geschwindigkeitszustand-Vektor **w**, fassen wir den Geschwindigkeitszustand-Vektor jener Körper mit bekannten (vorgeschriebenen) Geschwindigkeitszuständen in den Spaltenvektor $\mathbf{w}_0$ zusammen, die eine unmittelbar in Form oberflächlichen Zwanges verwirklichte Verbindung mit den Körpern mit unbekanntem Geschwindigkeitszustand haben. Mit Hilfe des so definierten Vektors $\mathbf{w}_0$ läßt sich das kinematische Kennzeichen **u** des Zwangssystems aus der Matrixgleichung

$$\mathbf{u} = \mathbf{H}_0\mathbf{w}_0$$

berechnen, wo $\mathbf{H}_0$ im Aufbau der Matrix $\mathbf{H}$ ähnlich ist; die Blockzeilen von $\mathbf{H}_0$ nacheinander zu denselben oberflächlichen Zwängen gehören, wie die entsprechenden Blockzeilen der Matrix $\mathbf{H}$, aber die Blockspalten von $\mathbf{H}_0$ den Körpern mit bekannten Geschwindigkeitszuständen entsprechen. $\mathbf{H}_0$ enthält in jeder solchen Blockzeile auch nur einen Block, wo $\mathbf{H}$ nur einen von Null abweichenden Block enthält, und zwar einen mit vorstehendem übereinstimmenden. Dagegen enthält $\mathbf{H}_0$ keinen einzigen in jenen Blockzeilen (d. h. nur Nullblöcke), wo $\mathbf{H}$ je zwei von Null abweichende Blöcke enthält. So bedeuten die im Spaltenvektor $\mathbf{u}$ zusammengefaßten Quantitäten — nach und nach — die zum entsprechenden oberflächlichen Zwang gehörenden, auf die Wirkungslinien der voneinander linear unabhängigen Elementarzwänge bezogenen Projektionsgeschwindigkeiten der Körper mit bekannten Geschwindigkeitszuständen.

Die kinematische Untersuchung jedes an den sich berührenden Flächenpaaren verwirklichten Zwangssystems läßt sich zufolge des Obenstehenden immer auf die Untersuchung eines solchen Systems der Elementarzwänge zurückführen, bei dem zu einzelnen oberflächlichen Zwängen voneinander linear unabhängige Elementarzwänge gehören. Auf Grund weiterer — auf die Theorie der linearen Gleichungssysteme sich stützenden — Untersuchung der Matrix gleichung von Form (10) eines solchen Zwangssystems kann man eindeutige Bedingungen für die Existenz und auch für die Eindeutigkeit der Lösung gewinnen.

SCHRIFTTUM

1. Autorenkollektiv: Getriebetechnik, VEB Verlag Technik, Berlin, 1968
2. Kolcsin, N. I.: Mechanika mašin 1. Izd. Mašinostroenie, Leningrad 1971
3. Koźevnikov, S. N.: Teorija mechanizmov i mašin. Izd. Mašinostroenie, Moskva 1973
4. Prentis, J. M.: Dynamics of Mechanical Systems, Longman Group Ltd., London 1970
5. Waldron, K. J.: A Study of Overconstrained linkage Geometry by Solution of Closure Equations. Part 1. Method of Study. *Mechanism and Machine Theory*, **8** (1973), No. 1, 95 —104
6. Király, B.: Merev testekből álló holonom rendszer sebességállapota, kényszerrendszere és kinematikai határozottsága (Der Geschwindigkeitszustand, das Zwangssystem und die kinematische Bestimmtheit des aus starren Körpern bestehenden, holonomen Systems). Kandidaturarbeit, 1972

Kinematic Examination of Constraint Systems Realized on Pairs of Surfaces in Contact. From the technical point of view at one of the most important types of holonomic systems the constraints are realized on pairs of surfaces in contact which are formed on rigid bodies. This paper deals with the kinematic examination of such constraint systems. Firstly it initiates the idea of surface constraint which is realized on a single pair of surfaces and the idea of elementary constraint belonging to one contact point, and then it replaces the constraint system by a system of elementary constraints in which each surface constraint corresponds to elementary constraints linearly independent of each other. In this way the set of constraint equations concerning the speed state of a holonomic system — also in general space cases — can be expressed in a concise matrix form which is suitable for further examinations.

Кинематическое исследование систем связей, осуществленных по парам контактных друг с другом поверхностей. Из технической точки зрения у одного из важнейших тип голономных систем связи осуществляются по парам контактных поверхностей жёстких тел. Эта работа занимается кинематическим исследованием таких систем связей. Сперва вводится идея поверхностной связи, осуществленной при единственной паре поверхностей и идея элементарной связи, принадлежащей к одному пункту касания. Далее система связей заменяется такой системой элементарных связей, у которой в отдельной поверхностной связи элементарные связи линейно независимы друг от друга. Таким образом систему уравнений связей, относящуюся к скоростному состоянию голономной системы — и в общих пространственных случаях — можно выразить в сжатой, подходящей к дальнейшим исследованиям матричной форме.

Acta Technica Academiae Scientiarum Hungaricae, Tomus 82 (3–4), pp. 417–434 (1976)

THE NEAR FIELD OF FLAT ACOUSTIC RADIATORS*

D. GAÁL**

[Manuscript received April 13, 1975]

The paper investigates the near field of plane radiators in an infinite wall, using a new mathematical approach. The method consists of a hitherto unknown series expansion of the Sommerfeld-King integral and of a coordinate transformation of the Green's function. Using the new method the author solves mathematically also the problem of the sound field of the plane radiators working in a finite circular baffle.

1. Introduction

Numerous papers on acoustics deal with the sound field generated by plane radiators. But the mathematically formulated results presented in the papers are not suitable for immediate numerical calculation near the radiator, not even in the most simple cases. Even in the most commonly known case and at the same time the most simple one (the radiating piston in the infinite rigid wall) the sound field can be calculated (with the aid of tables of functions) only in the axis of symmetry and in the plane of the radiator. Already the sound pressure at a general point of the field is given by an improper integral to be evaluated by a computer. Let us remember here that STENZEL [1] has numerically determined the acoustic field in the proximity of the piston (by double infinite series) but that he did not deduce relations for the sound pressure in an arbitrary point of the field with predetermined accuracy. This was probably prevented just by the mathematical apparatus chosen by Stenzel.

For the acoustic pressure of the plane radiator working in a finite rigid wall no mathematical formulation whatsoever is known, even for the most simple velocity distribution (rigid piston). Let us mention that PACHNER's paper [2] which from the outset excludes the near field, is based on an incorrectly evaluated improper integral. The limit case (piston radiating without baffle) is treated with strong neglections by SOMMERFELD [3], while SILBIGER [4], investigating the radiation of the ellipsoid of rotation — and then

* Detailed report on the lectures delivered at the 8th International Conference on Acoustics (ICA), London and at the 5th Hungarian Conference on Acoustics.

** GAÁL D., Dolgozó u. 2, H-1184 Budapest, Hungary.

reducing the big axis to zero — obtains a correct result for the sound field of the freely radiating piston.

The first aim of the present paper is to deduce for the plane radiator in an infinite rigid baffle with rotationally symmetrical velocity distribution, relations permitting directly computing (with the aid of tables of functions) and with predetermined accuracy the acoustic pressure at an arbitrarily small distance from the radiator and in any direction from the axis of symmetry. The need for deducing these relations for the near field is justified by the fact that they permit quasi to dimension the sound field also in cases where the observation — measuring — point is not in the far field. (In decentralized sound-systems the ear of the hearer is often very near to the sound source.) A further aim of the paper is to give in some kind of mathematical form the acoustic pressure, also for the finite baffles which provide much better approximations for practical purposes, even if the deduced relation can be evaluated only by a computerized method.

2. Some mathematical theorems

For deducing the results mentioned in the introduction the following mathematical theorems will be used; but, their detailed proof will be omitted.

2.1. *The solution of the Dirichlet problem for the half-space limited by the infinite plane*

If the pressure on the surface S is given — while the time ratio of change of the pressure is determined by the factor $e^{j\omega t}$ — the solution of the Dirichlet problem for the part of the space $|z| > 0$ can be given as follows [5] (with the notations of Fig. 1):

$$p(r_1, \gamma) = \int_0^{2\pi} \int_0^{\infty} p_0(r) \left[\frac{\partial G'(R_1, R_2)}{\partial z_0} \right]_{z_0=0} \cdot r \cdot dr \cdot d\varphi \qquad (2.1.1)$$

where

$p(r_1, \gamma)$	is the sound pressure in the space part $\|z\| > 0$
$p_0(r)$	is the sound pressure in the plane of the source
$G(R_1, R_2)$	is the Green's function for the half-space, complying with the boundary conditions
r_0	is the radius of the plane radiator.

Naturally, expression (2.1.1) is valid only if we succeed in determining the Green's function $G'(R_1,R_2)$ in such a way that its value is zero in the plane $S(z_0 = 0)$. Considering that the Green's function is also proportional to the sound field complying with the boundary conditions created by the point source (point radiator) or point sources, $G'(R_1,R_2)$ can be assumed as

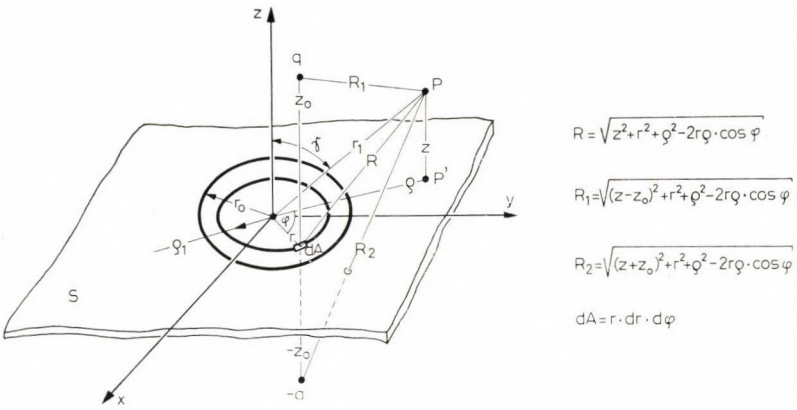

Fig. 1. System of coordinates for deducing the Green's function in the space part $|z| > 0$

being:

$$G'(R_1, R_2) = \frac{e^{-jkR_1}}{4\pi R_1} - \frac{e^{-jkR_2}}{4\pi R_2} \tag{2.1.2}$$

where

$k = \omega/c = 2\pi/\lambda$ is the wave number
ω is the angular frequency
c is the velocity of the propagation of sound
λ is the wavelength.

The Green's function according to (2.1.2) has been obtained, by taking into consideration Fig. 1, and placing point radiators of intensity q and $-q$, respectively, on both sides of the plane S at identical distances z_0. If, now, in Eq. (2.1.2) $|z_0| \to 0$, then $R_1 \to R$ as well as $R_2 \to R$, and $G'(R_1,R_2) \to 0$. But it easy to recognize from the character of the plane problem that

$$\left[\frac{\partial G'}{\partial z_0}\right]_{z_0=0} = \left[\frac{\partial}{\partial z_0}\left(\frac{e^{-jkR_1}}{4\pi R_1} - \frac{e^{-jkR_2}}{4\pi R_2}\right)\right]_{z_0=0} = -\frac{\partial}{\partial z}\cdot\frac{e^{-jkR}}{2\pi R} = -\frac{\partial G}{\partial z}.$$

Taking this into consideration, (2.1.1) can be written as follows:

$$p(r_1, \gamma) = \int_0^{2\pi}\int_0^{\infty} p_0(r)\,\frac{\partial G(R)}{\partial z}\cdot r\cdot dr\cdot d\varphi. \tag{2.1.3}$$

Eq. (2.1.3) was originally established by RAYLEIGH, but in deducing it he, of course, followed another train of thought. Subsequently it will be assumed that owing to the properties of $p_0(r)$ and G the order of the differentiation with respect to z and of the surface integration in (2.1.3) can be interchanged, i.e.

$$p(r_1, \gamma) = \frac{\partial}{\partial z}\int_0^{2\pi}\int_0^{\infty} p_0(r)\cdot G(R)\cdot r\cdot dr\cdot d\varphi. \tag{2.1.4}$$

In the calculations relation (2.1.4) shall always be used.

2.2 *Shifting the origin of the coordinate system of the Green's function*

If, in Eq. (2.1.4) $p_0(r)$ is continuous along the whole range $0 \leq r \leq \infty$, or if it is a function with a finite number of discontinuities or distribution (Heaviside function, Dirac delta, etc.) defined by an integral transformation which is univocally characterized by the integral transformation itself — also for the range $0 \leq r \leq \infty$ — then according to Figs 1 and 2, (2.1.4) can also be written as:

$$p(r, \gamma) = \frac{\partial}{\partial z} \int_0^{2\pi} \int_0^{\infty} p_0(r) \cdot G(R) \cdot r \cdot dr \cdot d\varphi \equiv \frac{\partial}{\partial z} \int_0^{2\pi} \int_0^{\infty} p_0(\varrho_1) \cdot G(R') \cdot r_2 \cdot dr_2 \cdot d\varphi,$$

or else

$$p(r, \gamma) = \frac{\partial}{\partial z} \int_0^{2\pi} \int_0^{\infty} p_0\left(\sqrt{\varrho^2 + r_2^2 - \varrho r_2 \cdot \cos\alpha}\right) \cdot \cdot \frac{\exp\left(-jk\sqrt{r_2^2 + z^2}\right)}{2\pi\sqrt{r_2^2 + z^2}} \cdot r_2 \cdot dr_2 \cdot d\varphi \,. \tag{2.2.1}$$

Thus, in Eq. (2.2.1), p_0 and G are given in co-ordinate systems with different origins, as opposed to (2.1.4). It will appear that using (2.2.1) considerably simplifies the calculations.

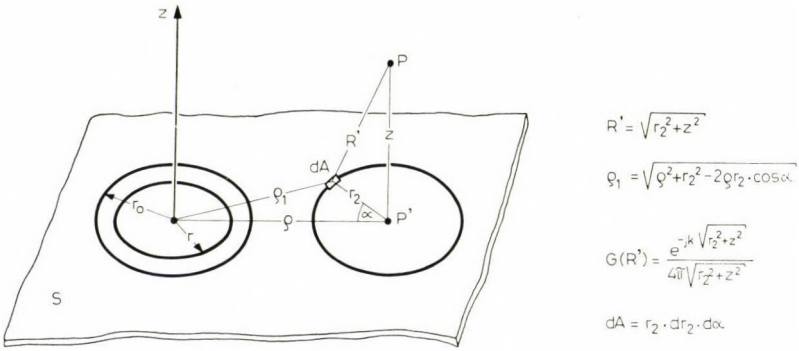

Fig. 2. System of coordinates for the transformation of coordinates of the Green's function

2.3 *Series expansion of the Sommerfeld—King integral for* $z = 0$

SOMMERFELD and KING [6] have deduced for the surface integral of the free-field of Green's function the following integral formula:

$$\int_0^{r_0} \int_0^{2\pi} \frac{e^{-jkR}}{4\pi R} \cdot r \cdot dr \cdot d\varphi = \frac{r_0}{2} \int_0^{\infty} \frac{\exp\left(-z\sqrt{\eta^2 - k^2}\right)}{\sqrt{\eta^2 - k^2}} \cdot J_0(\eta\varrho) \cdot J_1(\eta r_0) \cdot d\eta \,.$$

Let us separate in the right-hand side of this equation the real and the imaginary parts in case $z = 0$. Then

$$I = \frac{r_0}{2} \int_0^\infty J_0(\eta\varrho) \cdot J_1(\eta r_0) \frac{d\eta}{\sqrt{\eta^2 - k^2}} = I_{re} + jI_{im},$$

or

$$I_{im} = -\frac{r_0}{2} \int_0^{\pi/2} J_0(k\varrho \cdot \sin\vartheta) \cdot J_1(kr_0 \cdot \sin\vartheta) \cdot d\vartheta ; \tag{2.3.1}$$

$$I_{re} = \frac{r_0}{2} \int_0^\infty J_0(k\varrho \cdot \cosh u) \cdot J_1(kr_0 \cdot \cosh u) \cdot du \tag{2.3.2}$$

where J_0 is the zeroth-order Bessel function, J_1 the first-order Bessel function. In the above two expressions the transformation $\eta/k = \sin\vartheta$ and $\eta/k = \cosh u$ have been introduced.

For the imaginary part let us apply the expansion [7]

$$J_0(k\varrho \cdot \sin\vartheta) = \sum_{n-0}^{\infty} \varepsilon_n J_n^2\left(\frac{k\varrho}{2}\right) \cdot \cos(2n\vartheta)$$

where $\varepsilon_n = 1$ if $n = 0$ and $\varepsilon_n = 2$ if $n > 0$; and using furthermore the integral [8]

$$\int_0^{\pi/2} J_1(kr_0 \cdot \sin\vartheta) \cdot \cos(2n\vartheta) \cdot d\vartheta = \frac{\pi}{2} (-1)^n J_{n+\frac{1}{2}}\left(\frac{kr_0}{2}\right) \cdot J_{-(n-\frac{1}{2})}\left(\frac{kr_0}{2}\right),$$

one gets

$$\begin{aligned} I_{im} &= -\frac{r_0}{2} \int_0^{\pi/2} \sum_{n=0}^{\infty} \varepsilon_n (-1)^n J_1(kr_0 \cdot \sin\vartheta) \cdot J_n^2\left(\frac{k\varrho}{2}\right) \cdot \cos(2n\vartheta) \cdot d\vartheta = \\ &= -\frac{r_0 \pi}{4} \sum_{n=0}^{\infty} \varepsilon_n (-1)^n J_n^2\left(\frac{k\varrho}{2}\right) \cdot J_{n+\frac{1}{2}}\left(\frac{kr_0}{2}\right) \cdot J_{-(n-\frac{1}{2})}\left(\frac{kr_0}{2}\right) \cdot \end{aligned} \tag{2.3.3}$$

Because in Eq. (2.3.3) the series under the integral sign uniformly converges with respect to ϑ, the term-wise integration was justified.

For the real part the integral representation of J_0 and J_1 is considered [9]:

$$J_0(k\varrho \cdot \cosh u) = \frac{2}{\pi} \int_0^{\pi/2} \cos(k\varrho \cdot \cosh u \cdot \sin\gamma) \cdot d\gamma ;$$

$$J_1(kr_0 \cdot \cosh u) = \frac{2}{\pi} \int_0^{\pi/2} \sin(kr_0 \cdot \cosh u \cdot \sin\delta) \cdot \sin\delta \cdot d\delta .$$

Inserting them into (2.3.2,)

$$I_{re} = \frac{r_0}{2}\int_0^{\infty}\left[\frac{2}{\pi}\int_0^{\pi/2}\cos(k\varrho\cdot\cos hu\cdot\sin\gamma)\cdot d\gamma\right]\cdot$$
$$\cdot\left[\frac{2}{\pi}\int_0^{\pi/2}\sin(kr_0\cdot\cos hu\cdot\sin\delta)\cdot\sin\delta\cdot d\delta\right]\cdot du\,.$$

In the above expressions the integrals with respect to γ and δ uniformly converge for $0 \leqq u \leqq \infty$, therefore, the order of integrations can be interchanged, hence,

$$I_{re} = \frac{r_0}{\pi^2}\int_0^{\pi/2} d\gamma\int_0^{\pi/2} d\delta\int_0^{\infty}\cdot\left\{\sin\left[(k\varrho\cdot\sin\gamma + kr_0\cdot\sin\delta)\cdot\cos hu\right] -\right.$$
$$\left. - \sin\left[(k\varrho\cdot\sin\gamma - kr_0\cdot\sin\delta)\cdot\cos hu\right]\right\}\cdot\sin\delta\cdot du\,.$$

Now let us consider here another integral representation of J_0 [10],

$$J_0(x) = \frac{2}{\pi}\int_0^{\infty}\sin(x\cdot\cos hu)\cdot du\,.$$

With this, the real part takes the following form:

$$I_{re} = \frac{r_0}{2\pi}\int_0^{\pi/2}\int_0^{\pi/2}\left[J_0(k\varrho\cdot\sin\gamma + kr_0\cdot\sin\delta) -\right.$$
$$\left. - J_0(k\varrho\cdot\sin\gamma - kr_0\cdot\sin\delta)\right]\cdot\sin\delta\cdot d\delta\cdot d\gamma\,.$$

Applying the following addition at theorem [11],

$$J(x \pm y) = \sum_{n=0}^{\infty}\varepsilon_n(\mp 1)^n\cdot J_n(x)\cdot J_n(y)$$

we get

$$I_{re} = \frac{r_0}{\pi}\int_0^{\pi/2}\int_0^{\pi/2}\sum_{n-0}^{\infty}\varepsilon_n J_{2n}(k\varrho\cdot\sin\gamma)\cdot J_{2n}(kr_0\cdot\sin\delta)\cdot\sin\delta\cdot d\delta\cdot d\gamma\,.$$

Because of the uniform convergence of the above series, with the aid of the integrals [12], [13]

$$\int_0^{\pi/2} J_{2n}(k\varrho\cdot\sin\gamma)\cdot d\gamma = \frac{\pi}{2}J_n^2\left(\frac{k\varrho}{2}\right);$$

$$\int_0^{\pi/2} J_{2n}(kr_0\cdot\sin\delta)\cdot\sin\delta\cdot d\delta = \frac{\pi}{2}J_{n+\frac{1}{2}}\left(\frac{kr_0}{2}\right)\cdot J_{n-\frac{1}{2}}\left(\frac{kr_0}{2}\right)$$

the series can be integrated termwise and finally

$$I_{re} = \frac{r_0 \pi}{4} \sum_{n=0}^{\infty} \varepsilon_n J_n^2 \left(\frac{k\varrho}{2} \right) \cdot J_{n+\frac{1}{2}} \left(\frac{kr_0}{2} \right) J_{n-\frac{1}{2}} \left(\frac{kr_0}{2} \right). \tag{2.3.4}$$

Also considering that [14]

$$(-1)^n J_{-(n-\frac{1}{2})}(x) = N_{(n-1)+\frac{1}{2}}(x); \; H^{(1)}_{(n-1)+\frac{1}{2}}(x) = J_{(n-1)+\frac{1}{2}}(x) + jN_{(n-1)+\frac{1}{2}}(x)$$

then from (2.3.3) and (2.3.4)

$$I = I_{re} + j \cdot I_{im} = \frac{r_0 \pi}{4} \sum_{n=0}^{\infty} \varepsilon_n \cdot J_n^2 \left(\frac{k\varrho}{2} \right) \cdot J_{n+\frac{1}{2}} \left(\frac{kr_0}{2} \right) \cdot H^{(1)}_{(n-1)+\frac{1}{2}} \left(\frac{kr_0}{2} \right) \tag{2.3.5}$$

is obtained.

Thus, (2.3.5) provides the series expansion of the Sommerfeld—King integral for $z = 0$. Hence,

$$\begin{aligned} I &= \frac{r_0}{2} \int_0^{\infty} J_0(\eta\varrho) \cdot J_1(\eta r_0) \cdot \frac{d\eta}{\sqrt{\eta^2 - k^2}} = \\ &= \frac{r_0 \pi}{4} \sum_{n=0}^{\infty} \varepsilon_n \cdot J_n^2 \left(\frac{k\varrho}{2} \right) \cdot J_{n+\frac{1}{2}} \left(\frac{kr_0}{2} \right) \cdot H^{(1)}_{(n-1)+\frac{1}{2}} \left(\frac{kr_0}{2} \right) \end{aligned} \tag{2.3.6}$$

where $H_\nu^{(1)}$ is the Hankel function of the first kind.

The series (2.3.6) is uniformly convergent in the range $0 \leq k\varrho \leq \infty$ for the values $0 \leq kr_0 \leq \infty$. Furthermore, every member of the series disappears in the infinite as the function $1/k\varrho$. These properties make it possible to deduce, with the aid of the series (2.3.6), a relatively simple and easily surveyed formulae for the near field of the plane radiator in an infinite rigid wall.

In the further calculations the derivative with respect to r_0 of the series (2.3.6) is needed, this is as follows:

$$\begin{aligned} \frac{dI}{dr_0} &= \frac{d}{dr_0} \left[\frac{r_0}{2} \int_0^{\infty} J_0(\eta\varrho) \cdot J_1(\eta r_0) \frac{d\eta}{\sqrt{\eta^2 - k^2}} \right] = \\ &= \frac{r_0}{2} \int_0^{\infty} J_0(\eta\varrho) \cdot J_0(\eta r_0) \frac{\eta \cdot d\eta}{\sqrt{\eta^2 - k^2}} = \frac{kr_0 \pi}{8} \sum_{n=0}^{\infty} \varepsilon_n \cdot J_n^2 \left(\frac{k\varrho}{2} \right) \times \\ &\times \left[J_{(n-1)} \left(\frac{kr_0}{2} \right) \cdot H^{(1)}_{(n-1)+\frac{1}{2}} \left(\frac{kr_0}{2} \right) - J_{n+\frac{1}{2}} \left(\frac{kr_0}{2} \right) \cdot H^{(1)}_{n+\frac{1}{2}} \left(\frac{kr_0}{2} \right) \right]. \end{aligned} \tag{2.3.7}$$

3. The sound field of the circular line radiator

In order to determine the sound field of a plane radiator with some rotationally symmetrical velocity distribution, as a first step let us calculate the sound field of the circular line radiator. For the sake of uniform treatment the mathematical theorems of Chapter 2 will be used, as now.

Inasmuch as each point of the circular line radiates at the same phase and with the same source intensity, the velocity distribution function can be characterized by the Dirac delta $v(\varrho_1) = v_0 \cdot \delta(\varrho_1 - r_0)$, where r_0 is now the radius of the circular line. The velocity function $v(\varrho_1)$ is represented with the aid of the Bessel—Fourier integral [20]:

$$v(\varrho_1) = v_0 \cdot \delta(\varrho_1 - r_0) = \int_0^\infty \left[\int_0^\infty J_0(\eta u) \cdot v_0 \cdot \delta(u - r_0) \cdot u \cdot du \right] \cdot \\ \cdot J_0(\eta \varrho_1) \cdot \eta \cdot d\eta = v_0 r_0 \int_0^\infty J_0(\eta \varrho_1) \cdot J_0(\eta r_0) \cdot \eta \cdot d\eta \tag{3.1}$$

where $[v] = \mathrm{m/sec^{-1}\,m^{-1}}$.

The integral representation of $v(\varrho_1)$ according to 3.1 produces the velocity function for the whole range $0 \leqq \varrho_1 \leqq \infty$, hence, according to Huyghens' principle, for determining the sound field the shifting of the origin of the co-ordinate system according to (2.2), and (3.1) can be used, and then

$$p_c = \frac{jk\varrho_a c \cdot v_0}{2\pi} \int_0^{2\pi} \int_0^\infty \left[\int_0^\infty J_0(\eta r_0) \cdot J_0\left(\eta \sqrt{\varrho^2 + r_2^2 - 2\varrho r_2 \cdot \cos\alpha}\right) \cdot \eta \cdot d\eta \right] \times \\ \times \frac{\exp\left(-jk\sqrt{r_2^2 + z^2}\right)}{\sqrt{r_2^2 + z^2}} \cdot r_2 \cdot dr_2 \cdot d\alpha$$

where $\varrho_a \cdot c$ is the specific acoustic resistance of the air. Using also the additional theorem [15]

$$J_0\left(\eta \sqrt{\varrho^2 + r_2^2 - 2\varrho r_2 \cdot \cos\alpha}\right) = \sum_{n=0}^{\infty} \varepsilon_n \cdot J_n(\eta\varrho) \cdot J_n(\eta r_2) \cdot \cos(n\alpha),$$

after integrating with respect to α

$$p_c = jkr_0 \varrho_a \cdot cv_0 \int_0^\infty \left[\int_0^\infty J_0(\eta r_0) \cdot J_0(\eta\varrho) \cdot J_0(\eta r_2) \cdot \eta \cdot d\eta \right] \cdot \\ \cdot \frac{\exp\left(-jk\sqrt{r_2^2 + z^2}\right)}{\sqrt{r_2^2 + z^2}} \cdot r_2 \cdot dr .$$

Let us now apply the integral [16]

$$\int_0^\infty J_0(\eta r_2)\,\frac{\exp\left(-jk\sqrt{r_2^2+z^2}\right)}{\sqrt{r_2^2+z^2}}\cdot r_2\cdot dr_2=\frac{\exp\left(-z\sqrt{\eta^2-k^2}\right)}{\sqrt{\eta^2-k^2}},$$

then the well-known Sommerfeld—King result is obtained, which had been deduced by these authors by another train of thoughts:

$$p_c=jkr_0\varrho_a c\cdot v_0\int_0^\infty\frac{\exp\left(-z\sqrt{\eta^2-k^2}\right)}{\sqrt{\eta^2-k^2}}\cdot J_0(\eta\varrho)\cdot J_0(\eta r_2)\cdot\eta\cdot d\eta. \tag{3.2}$$

If now into (3.2) $z=0$ is inserted and (2.3.7) is taken into account, the sound field of the circular line radiator in the plane of the radiator is obtained in the form of an infinite series

$$p_{c0}=j\,\frac{k^2 r_0\pi\varrho_a c\cdot v_0}{4}\sum_{n=0}^{\infty}\varepsilon_n\cdot J_n^2\left(\frac{k\varrho}{2}\right)\cdot F_n'(r_0) \tag{3.3}$$

where the abbreviation

$$F_n'(r_0)=J_{(n-1)+\frac{1}{2}}\left(\frac{(kr_0)}{2}\right)\cdot H^{(1)}_{(n-1)+\frac{1}{2}}\left(\frac{kr_0}{2}\right)-J_{n+\frac{1}{2}}\left(\frac{kr_0}{2}\right)\cdot H^{(1)}_{n+\frac{1}{2}}\left(\frac{kr_0}{2}\right)$$

has been introduced. If now (2.2.1) is applied, from (3.3) the sound pressure of the circular line radiator is obtained for an arbitrary point of the field. Thus,

$$p_c=j\,\frac{k^2 r_0\pi p_0}{4\cdot 2\pi}\,\frac{d}{dz}\int_0^{2\pi}\int_0^\infty\frac{\exp\left(-jk\sqrt{r_2^2+z^2}\right)}{\sqrt{r_2^2+z^2}}\times$$
$$\times\sum_{n=0}^{\infty}\varepsilon_n\cdot J_n^2\left(\frac{k}{2}\sqrt{\varrho^2+r_2^2-2\varrho r_2\cdot\cos\alpha}\right)\cdot F_n'(r_0)\cdot r_2\cdot dr_2\cdot d\alpha$$

where, as a further abbreviation, the notation $p_0=\varrho_a\cdot v_0$ has been used.

With the integral [17]

$$J_n^2(x)=\frac{1}{\pi}\int_0^\pi J_0(2x\cdot\sin\beta)\cdot\cos(2n\beta)\cdot d\beta$$

and the additional theorem used in (3.2), one can write

$$p_c=j\,\frac{k^2 r_0 p_0}{8\pi}\,\frac{d}{dz}\int_0^{2\pi}\int_0^\infty\frac{\exp\left(-jk\sqrt{r_2^2+z^2}\right)}{\sqrt{r_2^2+z^2}}\times$$
$$\times\sum_{n=0}^{\infty}\varepsilon_n\cdot\int_0^\pi\sum_{m=0}^{\infty}\varepsilon_m\cdot J_m(k\varrho\cdot\sin\beta)\cdot J_m(kr_2\cdot\sin\beta)\cdot F_n'(r_0)\cdot$$
$$\cdot\cos(2m\alpha)\cdot\cos(2n\beta))\cdot r_2\cdot dr_2\cdot d\alpha\cdot d\beta\ .$$

The series and the integrals uniformly converging, the order of the additions and the integration can be interchanged and after integrating with respect to α,

$$p_c = j\frac{k^2 r_0 p_0}{4} \cdot \frac{d}{dz}\int_0^{\infty}\int_0^{\pi} \frac{\exp(-jk\sqrt{r_2^2+z^2})}{\sqrt{r_2^2+z^2}} \sum_{n=0}^{\infty} \varepsilon_n J_0(k\varrho \cdot \sin\beta) \cdot$$
$$\cdot J_0(kr_2 \cdot \sin\beta) \cdot F_n'(r_0) \cdot \cos(2n\beta) \cdot r_2 \cdot dr_2 \cdot d\beta .$$

Now integration with respect to r_2 is carried out as in the deduction of (3.2):

$$p_c = j\frac{k^2 r_2 p_0}{4} \cdot \frac{d}{dz}\int_0^{\pi} \sum_{n=0}^{\infty} \varepsilon_n \frac{\exp(jz\sqrt{k^2 - k^2\cdot\sin^2\beta})}{\sqrt{k^2 - k^2\cdot\sin^2\beta}} \cdot$$
$$\cdot J_0(k\varrho \cdot \sin\beta) \cdot \cos(2n\beta) \cdot F_n'(r_0) \cdot d\beta .$$

Carrying out the differentiation with respect to z as well,

$$p_c = j\frac{k^2 r_0^2 p_0}{4}\int_0^{\pi} \sum_{n=0}^{\infty} \varepsilon_n \exp(jkz\cdot\cos\beta)\cdot J_0(k\varrho\cdot\sin\beta)\cdot\cos(2n\beta)\cdot F_n'(r_0)\cdot d\beta .$$

Obviously

$$\int_0^{\pi} \sin(kz\cdot\cos\beta)\cdot J_0(k\varrho\cdot\sin\beta)\cdot\cos(2n\beta)\cdot d\beta = 0 ,$$

hence, finally

$$p_c = j\frac{k^2 r_0 p_0}{4}\int_0^{\pi} \sum_{n=0}^{\infty} \varepsilon_n \cdot J_0(k\varrho\cdot\sin\beta)\cdot\cos(kz\cdot\cos\beta)\cdot\cos(2n\beta)\cdot F_n'(r_0)\cdot d\beta . \quad (3.4)$$

The zeroth member of (3.4) can be determined by taking into account the integral [18]

$$\int_0^{\pi} J_0(y\cdot\sin\beta)\cdot\cos(x\cdot\cos\beta)\cdot d\beta = \pi\cdot J_0\left(\frac{\sqrt{x^2+y^2}+x}{2}\right)\cdot J_0\left(\frac{\sqrt{x^2+y^2}-x}{2}\right).$$

Finally

$$p_c^{(0)} = j\frac{k^2 r_0 \pi p_0}{4} F_0'(r_0)\cdot J_0\left(k\frac{\sqrt{z^2+\varrho^2}+z)}{2}\right)\cdot J_0\left(k\frac{\sqrt{z^2+\varrho^2}-z}{2}\right).0 \quad (3.5)$$

The first member of the series (3.4) can be determined considering that

$$\cos(x\cdot\cos\beta)\cdot\cos(2\beta) = -\left[\cos(x\cdot\cos\beta) + 2\frac{d^2}{dx^2}\cdot\cos(x\cdot\cos\beta)\right].$$

So from the zeroth member and from its second derivative

$$p_c^{(1)} = -2\frac{F_1'(r_0)}{F_0'(r_0)}\left[p_c^{(0)} + 2k^2\frac{d^2}{d(kz)^2}\cdot p_c^{(0)}\right],$$

$$p_c^{(0+1)} = p_c^{(0)} - 2\frac{F_1'(r_0)}{F_0'(r_0)}\left[p_c^{(0)} + 2k^2\frac{d^2}{d(kz)^2}\cdot p_c^{(0)}\right].$$

By this method every member of the series (3.4) can be determined. But from the series (3.4) other approximate formulae also can be deduced. If e.g. kr_0 is sufficiently small, then it is enough to consider a few members of the series (3.4); and if simultaneously kz or $k\varrho$ has a predetermined value too, so the functions $\cos(kz\cdot\cos\beta)$ or $J_0(k\varrho\cdot\sin\beta)$ can be approximated with suitable accuracy by power functions, and then the integration with respect to β can be performed. If e.g. the members of the series are only considered until $n=1$, furthermore, if

$$\cos(kz\cdot\cos\beta)\approx 1-\frac{(kz)^2}{2}\cdot\cos^2\beta = 1-\frac{(kz)^2}{4}[1+\cos(2\beta)],$$

then

$$p_c \approx j\frac{k^2 r_0 p_0}{4}\int_0^{\pi}\sum_{n=0}^{\infty}\varepsilon_n\left[1-\frac{(kz)^2}{4}(1+\cos 2\beta)\right]\cdot J_0(k\varrho\cdot\sin\beta)\cdot$$

$$\cdot\cos(2n\beta)\cdot F_n'(r_0)\cdot d\beta = j\frac{k^2 r_0\pi p_0}{8}\sum_{n=0}^{\infty}\varepsilon_n F_n'(r_0)(-1)^n\times \qquad (3.7)$$

$$\times\left\{\left[1-\frac{k^2z^2}{4}\right)\cdot J_n^2\left(\frac{k\varrho}{2}\right)-\frac{k^2z^2}{8}\left[J_{n+1}^2\left(\frac{k\varrho}{2}\right)+J_{n-1}^2\left(\frac{k\varrho}{2}\right)\right]\right\}.$$

Thus carrying out the summation until $n=1$:

$$p_c^{(0+1)}\approx j\frac{k^2 r_0\pi p_0}{8}\left\{F_0'(r_0)\left[\left(1-\frac{k^2z^2}{4}\right)\cdot J_0^2\left(\frac{k\varrho}{4}\right)-\right.\right.$$

$$-\frac{k^2z^2}{4}\cdot J_1^2\left(\frac{k\varrho}{2}\right)\Big]-2F_1'(r_0)\left[\left(1-\frac{k^2z^2}{2}\right)\cdot\right. \qquad (3.8)$$

$$\left.\left.\cdot J_1^2\left(\frac{k\varrho}{2}\right)-\frac{k^2z^2}{4}\left(J_2^2\left(\frac{k\varrho}{2}\right)+J_0^2\left(\frac{k\varrho}{2}\right)\right)\right]\right\}.$$

Now let us approximate (3.4) in the following way:

$$J_0(k\varrho\cdot\sin\beta)\approx 1-\frac{k^2\varrho^2}{4}\cdot\sin^2\beta = 1-\frac{k^2\varrho^2}{8}(1-\cos 2\beta)$$

and then it is possible to write

$$p_c \approx j \frac{k^2 r_0 p_0}{4} \int_0^{\pi} \sum_{n=0}^{\infty} \varepsilon_n \cdot \cos(kz \cdot \cos\beta) \cdot F_n'(r_0) \times \\ \times \left[1 - \frac{k^2 \varrho^2}{8}(1 - \cos 2\beta)\right] \cdot \cos(2n\beta) \cdot d\beta .$$

Given that [19]

$$(-1)^n \cdot J_{2n}(x) = \frac{2}{\pi} \int_0^{\pi/2} \cos(x \cdot \cos\varphi) \cdot \cos(2n\varphi) \cdot d\varphi ,$$

the following is obtained:

$$p_c \approx j \frac{k^2 r_0 \pi p_0}{8} \sum_{n=0}^{\infty} \varepsilon_n \cdot F_n'(r_0)(-1)^n \times \\ \times \left\{\left(1 - \frac{k^2 \varrho^2}{8}\right) \cdot J_{2n}(kz) - \frac{k^2 \varrho^2}{16}[J_{2(n-1)}(kz) + J_{2(n+1)}(kz)]\right\}. \tag{3.9}$$

And now carrying out the summation only for $n = 1$,

$$p_c^{(0+1)} \approx j \frac{k^2 r_0 \pi p_0}{8} \left\{F_0'(r_0)\left[\left(1 - \frac{k^2 \varrho^2}{8}\right) \cdot J_0(kz) - \frac{k^2 \varrho^2}{8} J_2(kz)\right] - \right. \\ \left. - 2 F_1'(r_0)\left[\left(1 - \frac{k^2 \varrho^2}{8}\right) \cdot J_2(kz) - \frac{k^2 \varrho^2}{8}(J_0(kz) + J_4(kz))\right]\right\}. \tag{3.10}$$

4. The sound field of the plane radiator with rotationally symmetrical velocity distribution

Let the rotationally symmetrical velocity distribution function on the surface of the plane radiator of radius r_0 be $v(r)$, then on the base of (3.4) the sound field of the radiator operating in the infinite wall, will be there

$$p_v = j \frac{k^2 p_0}{4} \int_0^{\pi} \int_0^{r_0} \sum_{n=0}^{\infty} \varepsilon_n \cdot \cos(kz \cdot \cos\beta) \cdot \\ \cdot J_0(k\varrho \cdot \sin\beta) \cdot \cos(2n\beta) \cdot F_n'(r) \cdot v(r) \cdot r \cdot dr \cdot d\beta . \tag{4.1}$$

If now in Eq. (4.1) $v(r) = 1$ (case of the rigid piston),

$$p_p = j \frac{k r_0 p_0}{2} \int_0^{\pi} \sum_{n=0}^{\infty} \varepsilon_n \cdot \cos(kz \cdot \cos\beta) \cdot J_0(k\varrho \cdot \sin\beta) \cdot \cos(2n\beta) \cdot F_n(r_0) \cdot d\beta \tag{4.2}$$

where

$$\int_0^{r_0} F_n'(r)\cdot r\cdot dr = \frac{2r_0}{k} F_n(r_0) = \frac{2r_0}{k} J_{n+\frac{1}{2}}\left(\frac{kr_0}{2}\right)\cdot H^{(1)}_{(n-1)+\frac{1}{2}}\left(\frac{kr_0}{2}\right) \tag{4.3}$$

has been taken into account. Applying here, too, the approximations (3.7) and (3.8), it is possible to write

$$\begin{aligned} p_p \approx j\frac{kr_0\pi p_0}{4}\Bigg\{F_0(r_0)\left[\left(1-\frac{k^2z^2}{4}\right)\cdot J_0^2\left(\frac{k\varrho}{2}\right)-\frac{k^2z^2}{4}J_1^2\left(\frac{k\varrho}{2}\right)\right]- \\ -2F_1(r_0)\left[\left(1-\frac{k^2z^2}{4}\right)\cdot J_1^2\left(\frac{k\varrho}{2}\right)-\frac{k^2z^2}{4}\left(J_2^2\left(\frac{k\varrho}{2}\right)+J_0^2\left(\frac{k\varrho}{8}\right)\right)\right]\Bigg\}, \end{aligned} \tag{4.4}$$

or

$$\begin{aligned} p_p \approx j\frac{kr_0\pi p_0}{4}\Bigg\{F_0(r_0)\left[\left(1-\frac{k^2\varrho^2}{8}\right)J_0(kz)-\frac{k^2z^2}{8}\cdot J_2(kz)\right]- \\ -2F_1(r_0)\left[\left(1-\frac{k^2\varrho^2}{8}\right)J_2(kz)-\frac{k^2\varrho^2}{8}\left(J_0(kz)+J_4(kz)\right)\right]\Bigg\}. \end{aligned} \tag{4.5}$$

As a further example let us assume that $v(r) = 1 - (r^2/r_0^2)$ and that kr_0 is sufficiently small, then on ground of (4.1)

$$\int_0^{r_0}\left(1-\frac{r^2}{r_0^2}\right)F_0'(r)\cdot r\cdot dr = j\frac{-4}{k^4 r_0^2\pi}\times$$

$$\times\left[e^{jkr_0}\cdot(kr_0+2j)kr_0-(1-e^{jkr_0})(k^2r_0^2+2)\right] = j\frac{-4}{k^4 r_0^2\pi}\cdot f_0(r_0),$$

$$\int_0^{r_0}\left(1-\frac{r^2}{r_0^2}\right)F_1'(r)\cdot r\cdot dr = j\frac{-4}{k^4 r_0^2\pi}\times$$

$$\times\left[6(1-e^{jkr_0})+kr_0(2je^{jkr_0}+4j-kr_0)\right] = j\frac{-4}{k^4 r_0^2\pi}\cdot f_1(r_0).$$

From the above the near field of the radiator with parabolic velocity distribution is

$$\begin{aligned} p_{pa}\approx\frac{p_0}{2r_0^2k^2}\Bigg\{f_0(r_0)\left[\left(1-\frac{k^2z^2}{4}\right)\cdot J_0^2\left(\frac{k\varrho}{2}\right)-\frac{k^2z^2}{4}J_1^2\left(\frac{k\varrho}{2}\right)\right]+ \\ +f_1(r_0)\left[\left(1-\frac{k^2\varrho^2}{8}\right)J_1^2\left(\frac{k\varrho}{2}\right)-\frac{k^2\varrho^2}{8}\left(J_2^2\left(\frac{k\varrho}{2}\right)+J_0^2\left(\frac{k\varrho}{2}\right)\right)\right]\cdot 2\Bigg\}, \end{aligned}$$

or else

$$\begin{aligned} p_{pa}\approx\frac{p_0}{2r_0^2k^2}\Bigg\{f_0(r_0)\left[\left(1-\frac{k^2\varrho^2}{8}\right)J_0(kz)-\frac{k^2\varrho^2}{8}J_2(kz)\right]+ \\ +2f_1(r_0)\left[\left(1-\frac{k^2\varrho^2}{8}\right)J_2(kz)-\frac{k^2\varrho^2}{8}\left(J_0(kz)+J_4(kz)\right)\right]\Bigg\}. \end{aligned}$$

Investigating the speed of convergency of the deduced series, let us limit ourselves to the investigation of the axial pressure of the piston radiator $|\ \varrho = 0\ |$. From (4.2)

$$p_p(\varrho = 0) = j\frac{kr_0 p_0}{2}\int_0^{\pi}\sum_{n=0}^{\infty}\varepsilon_n \cdot \cos(kz \cdot \cos\beta)\cdot\cos(2n\beta)\cdot F_n(r_0)\cdot d\beta = \\ = j\frac{kr_0\pi p_0}{4}\sum_{n=0}^{\infty}\varepsilon_n(-1)^n \cdot F_n(r_0)\cdot J_{2n}(kz). \tag{4.6}$$

Instead of detailed mathematical investigations let us consider the absolute values of some members of the series (4.6) for the values $kr_0 = 1$ and $kz = 2$ which already take into account practical points of view. From the tables of functions:

Table 1

Absolute value of the first four members determining the axial near field of the piston membrane working in an infinite wall

n	$\left\lvert \frac{\pi}{2} J_{n+\frac{1}{2}}\left(\frac{1}{2}\right)\cdot H^{(1)}_{(n-1)+\frac{1}{2}}\left(\frac{1}{2}\right)\right\rvert$	$\left\lvert J_{2n}^{(2)}\right\rvert$	$\varepsilon_n \cdot \left\lvert \frac{\pi}{2} J_{n+\frac{1}{2}}\left(\frac{1}{2}\right) H^{(1)}_{(n-1)+\frac{1}{2}}\left(\frac{1}{2}\right)\right\rvert \cdot \left\lvert J_{2n}^{(2)}\right\rvert$
0	0,83	0,22	$1{,}82 \cdot 10^{-1}$
1	0,29	0,35	$2 \cdot 10^{-1}$
2	$0{,}87 \cdot 10^{-1}$	$0{,}39 \cdot 10^{-3}$	$6{,}8 \cdot 10^{-5}$
3	$0{,}32 \cdot 10^{-1}$	$0{,}12 \cdot 10^{-4}$	$2{,}4 \cdot 10^{-7}$

From the above table it is clear that for (4.4) and (4.5) it was sufficient to consider only the zeroth and the first member (if $kr_0 = 1$; $kz = 2$ or $k\varrho = 2$), the member belonging to $n = 2$ is already smaller by more than three orders of magnitude than the member belonging to $n = 1$.

5. The radiator in the finite baffle

Let us start out again from the sound field of the circular line radiator. The investigations are limited to the case when the circular radiator baffle and the circular line radiator are concentric. If it is assumed that each point of the circular line radiates with the same source intensity and at the same phase, then on the base of Fig. 3 the velocity distribution function in the plane S is given by

$$v(\varrho_1) = \begin{cases} v_0 \cdot \delta(\varrho_1 - r) & \text{if} \quad 0 \leqq \varrho_1 \leqq R_0\,, \\ v_{R_0}(\varrho_1) & \text{if} \quad R_0 < \varrho_1 \leqq \infty \end{cases} \tag{5.1}$$

where $v_{R_0}(\varrho_1)$ is a function unknown for the time being.

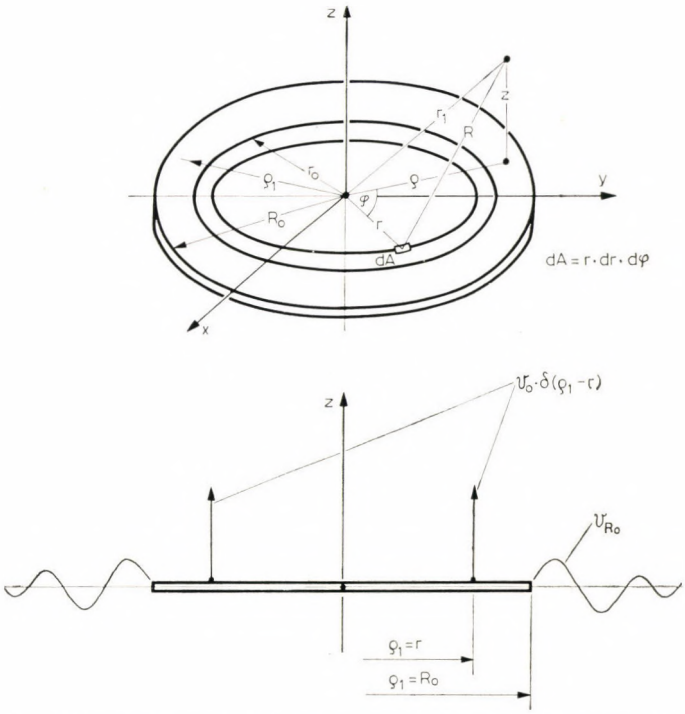

Fig. 3. System of coordinates and velocity distribution function for calculating the sound field in the case of a finite baffle

Let to representate now (5.1) similarly to (3.1) with the aid of the Fourier—Bessel integral:

$$v(\varrho_1) = v_0 r \int_0^\infty J_0(\eta r) \cdot J_0(\eta \varrho_1) \cdot \eta \cdot d\eta + \int_0^\infty \left[\int_{R_0}^\infty v_{R_0}(\varrho_0) \cdot J_0(\eta \varrho_0) \cdot \varrho_0 \cdot d\varrho_0 \right] \cdot$$

$$\cdot J_0(\eta \varrho_1) \cdot \eta \cdot d\eta .$$

Applying again the Huyghens principle and the shifting of the origin of coordinate system of the Green's function, the sound pressure can be calculated:

$$p_{cR_0} = jk\varrho_a cr \left[v_0 \int_0^\infty \frac{\exp(-z\sqrt{\eta^2 - k^2})}{\sqrt{\eta^2 - k^2}} J_0(\eta\varrho) \cdot J_0(\eta r) \cdot \eta \cdot d\eta + \right.$$

$$\left. + \frac{1}{r} \int_0^\infty \int_{R_0}^\infty v_{R_0}(\varrho_0) \frac{\exp(-z\sqrt{\eta^2 - k^2})}{\sqrt{\eta^2 - k^2}} J_0(\eta\varrho) J_0(\eta\varrho_0) \varrho_0 \cdot \eta \cdot d\varrho_0 \cdot d\eta . \right] \tag{5.2}$$

If now the fact is taken into account that the circular line generates by its back-and-forth movement — in the z direction — a sound field where the

sound pressure in the plane of the radiator $|\, z = 0 \,|$, in the range $\varrho > R_0$ is zero (dipole effect), so inserting $z = 0$ into (5.2) and applying (3.3)

$$0 = v_0 r \sum_{n=0}^{\infty} \varepsilon_n F'_n(r) \cdot J_n^2\left(\frac{k\varrho}{2}\right) + \\ + \int_0^{\infty} J_0(\eta\varrho)\left[\int_{R_0}^{\infty} v_{R_0}(\varrho_0) \cdot J_0(\eta\varrho_0) \frac{\varrho_0 \cdot d\varrho_0}{\sqrt{\eta^2 - k^2}}\right] \cdot \eta \cdot d\eta \,. \tag{5.3}$$

The relation (5.3), valid only for the range $\varrho > R_0$, is an integral equation of the first kind for the unknown function $v_{R_0}(\varrho_0)$ and is solved by using the Fourier—Bessel transformation and the inverse Fourier—Bessel one.

From these

$$v_{R_0}(\varrho_0) = - v_0 r \sum_{n=0}^{\infty} \varepsilon_n F'_n(r) \int_0^{\infty} J_0(\eta\varrho_0) \times \\ \times \left[\int_{R_0}^{\infty} J_0(\eta\varrho) \cdot J_n^2\left(\frac{k\varrho}{2}\right) \cdot \varrho \cdot d\varrho\right] \sqrt{\eta^2 - k^2} \cdot \eta \cdot d\eta \,. \tag{5.4}$$

Basically, the problem of radiation from a finite, circular baffle has been mathematically solved by the determination of function (5.4).

Inasmuch as on the surface of the baffle some radiator operates with an arbitrary velocity distribution $v(r)$, the velocity distribution in the $z = 0$ plane within the range $\varrho_0 > R_0$ is

$$v_{R_0 v}(\varrho_0) = \int_0^{r_0} v_{R_0}(\varrho_0, r) \cdot v(r) \cdot dr \,. \tag{5.5}$$

If now, as a special case

$$v(r) = v_p(r) = \begin{cases} 1 & \text{if } 0 \leq r \leq r_0 \,, \\ 0 & \text{if } r_0 < r \leq R_0 \,, \end{cases}$$

(case of the rigid piston)

so considering (5.5), (5.3) and (5.4)

$$v_{R_0 v_p}(\varrho_0) = - \frac{2 v_0 r_0}{k} \sum_{n=0}^{\infty} \varepsilon_n F_n(r_0) \int_0^{\infty} J_0(\eta\varrho_0) \times \\ \times \left[\int_{R_0}^{\infty} J_0(\eta\varrho_0) J_n^2\left(\frac{k\varrho}{2}\right) \cdot \varrho \cdot d\varrho\right] \sqrt{\eta^2 - k^2} \cdot \eta \cdot d\eta \,. \tag{5.6}$$

Re-inserting (5.4) and (5.6) into Eq. (5.2), respectively, the sound field of the circular line and of the rigid piston operating in a finite wall can be calculated.

6. Summary

The formula (3.4) deduced in the paper, giving in the form of an infinite function series the sound field of the circular line radiator in an infinite baffle permits calculating, by using function tables, the near field of plane radiators with an arbitrary, rotationally symmetrical velocity distribution. Hence, Eq. (3.4) is a basic formula, which can be multiplied by the dimensionless velocity distribution function and integrated termwise, being a uniformly convergent series.

The relation (5.6) for finite baffles is a basic formula too, and provides the velocity of the particle excited by the circular line radiator in the plane of the baffle, but outside its range. This series uniformly converges and, therefore, it can be integrated termwise after multiplication by the arbitrary, rotationally symmetrical velocity distribution. Using the relation (5.2) and with computerized calculation, the practically very important radiation impedance can be determined, too.

The author, thanks in advance all those who will let him know, in any form, their professional critical remarks.

REFERENCES

1. Stenzel, H.: Leitfaden zur Berechnung von Schallvorgängen, Springer 1939, p. 61—103
2. Pachner, J.: On the Acoustical Radiation of an Emitter Vibrating Freely or in a Wall of Finite Dimensions, *J.A.S.A.*, **23** (1951), 198—208
3. Sommerfeld, A.: Die frei schwingende Kolbenmembran, *Annalen der Physik*, **42** (1942), 389—420
4. Silbiger, Radiation from Circular Piston of Elliptical Profile, *J.A.S.A.* **33** (1961), 1515—1522
5. Morse—Ingard, Theoretical Acoustics, McGraw-Hill, New York 1968, pp. 306—394
6. King, L. V.: On the Acoustic Radiation Field of the Piezo-electric Oscillator and the Effect of Viscosity on Transmission, *Canadian Journal of Research*, **11** (1934), 135—155
7. Gradsteyn—Ryzhik: Table of Integral, Series and Products, Academic Press, New York 1965, p. 979, 8531
8. Cf. 7., p. 739, 6681
9. Cf. 7., p. 952, 8411
10. Cf. 7., p. 953, 8411
11. Cf. 7., p. 980, 8538
12. Cf. 7., p. 671, 6519
13. Cf. 7., p. 671, 6681
14. Cf. 7., p. 739, 8465
15. Cf. 7., p. 979, 8531
16. Cf. 7., p. 710, 6616
17. Cf. 7., p. 738, 6681
18. Cf. 7., p. 742, 6688
19. Cf. 7., p. 402, 3715
20. Cf. 5., p. 32. 1.3.27
21. Erdélyi, A. —Magnus, W.—Oberhettinger, — W. Tricomi, F. G.: Tables of Integral Transforms, MacGraw-Hill, New York 1954, pp. 5—92 and 33—389
22. Gaál, D.: A New Mathematical Theory of the Sound Radiator's Near Field, *The* 8. *ICA*, Contributed Papers, Vol. **2** (1974), p. 493

Das Nahfeld von ebenen Schallstrahlern. Die in der Arbeit abgeleitete Formel gibt das Schallfeld eines Kreislinienstrahlers in einer unendlichen Schallwand in Form einer unendlichen Funktionenreihe an. Sie ermöglicht, mit Hilfe von Funktionentafeln, auch die Berechnung des Nahfeldes von Strahlern mit beliebiger rotationssymmetrischer Geschwindigkeitsverteilung. Diese Formel ist daher ein grundlegender Zusammenhang, der als gleichförmig konvergierende Reihe, multipliziert mit der dimensionslosen Geschwindigkeitsverteilungsfunktion, gliedweise integriert werden kann. Die Beziehung für die endliche Schallwand ist ebenfalls eine grundlegende Formel, welche in der Ebene der Schallwand aber im Bereich außerhalb derselben die vom kreislinienförmigen Strahler erregte Teilchengeschwindigkeit angibt. Zufolge ihrer gleichförmigen Konvergenz kann auch diese Reihe nach Multiplikation mit einer rotationssymmetrischen Geschwindigkeitsfunktion gliedweise integriert werden.

Ближнее поле плоскостных звуковых излучателей. В данной работе рассматривается ближнее поле плоскостных излучателей, работающих в бесконечных стенах, при использовании нового метаматического метода. Новый математический метод основывается, с одной стороны, на неизвестном до сих пор разложении в ряд интеграла Зоммерфельда — Кинга, а с другой стороны, на преобразовании координат функций Грина. При помощи нового метода автор математически решает также проблемы звукового поля плоскостных излучателей, работающих в круглых звуковых перегородках конечных размеров.

Acta Technica Academiae Scientiarum Hungaricae, Tomus 82 (3—4), pp. 435—441 (1976)

PENNY-SHAPED CRACK IN AN INFINITE VISCOELASTIC MEDIUM

SATYANARAYAN MANDAL*

[Manuscript received 20 September 1975]

In this paper the stress field is obtained in the neighbourhood of a penny-shaped crack in the interior of a special type of linear viscoelastic medium by employing Laplace and Hankel transforms. The general solution is illustrated in three specific cases.

1. Introduction

In recent years the problem of interest in fracture and structural mechanics is the calculation of the elastic stress field in the neighbourhood of Griffith or penny-shaped cracks in the interior of an elastic body. Knowledge of the elastic stress field is potentially useful for the estimation of the material strength based upon brittle fracture theory. Solutions for axisymmetric stress distribution in the neighbourhood of a penny-shaped crack have been given by SNEDDON [1], OLESIAK and SNEDDON [2]. In this analysis it is assumed that the two faces of the crack are loaded exactly the same way.

Using the system of cylindrical polar coordinates and employing the method of Hankel transforms, developed by HARDING and SNEDDON [3], OLESIAK and SNEDDON [2], the problem of distribution of stress in the neighbourhood of a penny-shaped crack is reduced to that in a semi-infinite elastic medium. It leads to calculation of the solutions of a pair of dual integral equations obtained by the application of the boundary conditions of the mixed type.

In this paper cylindrical polar coordinates and methods of Laplace and Hankel transforms are employed. The axis of symmetry is the Z-axis normal to the boundary plane $z = 0$ of the solid. The solid considered here is a special type of linear viscoelastic medium. When the uniformly distributed normal pressure, which is a function of γ at a particular instant of time, is taken as constant, the shape of the crack is found to be elliptical.

* Satyanarayan Mandal, Hatuganj M.N.K. High School, P. O. Hatuganj, Dist. 24-Parganas, West Bengal, India.

The general solution is illustrated in three specific cases. The expression, at a particular instant of time, for the normal component of stress in viscoelastic medium considered above agrees with that in elastic medium [1]. The stress intensity factor has been calculated in the general case. In this paper the author's treatment involving the standard linear solid is a special case of the problem considered by GRAHAM [5]. In this special case the time and space dependence are clearly separated because of the proportional loading.

2. Formulation and method of solution

The stress-strain relation for a special type of linear viscoelastic medium is given by

$$\left(1 + a_1 \frac{\partial}{\partial t}\right) \sigma_{ij} = 2\, k_1 \left(1 + b_1 \frac{\partial}{\partial t}\right) e_{ij} \tag{1}$$

where σ_{ij} is the stress tensor and e_{ij} is the strain tensor, a_1, b_1, k_1 being material constants.

The cylindrical co-ordinate system (r, Θ, z) is used with origin at the centre of the penny-shaped crack of radius unity and z-axis, the axis of symmetry, is taken into the medium.

If we assume deflection to be symmetrical with respect to z-axis, then a typical point of the solid may be taken to have coordinates (u, o, w) in this co-ordinate system and the vanishing components of the stress tensor will be $\sigma_{\Theta z}$ and $\sigma_{r\Theta}$.

Hence the equations of equilibrium are

$$\begin{aligned} &\frac{\partial \sigma_{rr}}{\partial r} + \frac{\partial \sigma_{rz}}{\partial z} + \frac{\sigma_{rr} - \sigma_{\Theta\Theta}}{r} = 0\,, \\ &\frac{\partial \sigma_{rz}}{\partial r} + \frac{\partial \sigma_{zz}}{\sigma_z} - \frac{\partial_{rz}}{r} = 0\,. \end{aligned} \tag{2}$$

On $z = 0$, the boundary conditions are given by

$$\begin{aligned} &\sigma_{rz} = 0 && \text{for all } r \\ &\sigma_{zz} = -p(r) f(t), && 0 < r << 1 \\ &w = 0 && r > 1 \end{aligned} \tag{3}$$

From Eqs (1) we obtain

$$\begin{aligned}
&\left(1 + a_1 \frac{\partial}{\partial t}\right) \sigma_{rr} = 2k_1 \left(1 + b_1 \frac{\partial}{\partial t}\right) e_{rr} = 2k_1 \left(1 + b_1 \frac{\partial}{\partial t}\right) \frac{\partial u}{\partial r}, \\
&\left(1 + a_1 \frac{\partial}{\partial t}\right) \sigma_{\Theta\Theta} = 2k_1 \left(1 + b_1 \frac{\partial}{\partial t}\right) e_{\Theta\Theta} = 2k_1 \left(1 + b_2 \frac{\partial}{\partial t}\right) \frac{u}{r}, \\
&\left(1 + a_1 \frac{\partial}{\partial t}\right) \sigma_{zz} = 2k_1 \left(1 + b_1 \frac{\partial}{\partial t}\right) e_{zz} = 2k_1 \left(1 + b_1 \frac{\partial}{\partial t}\right) \frac{\partial w}{\partial t}, \\
&\left(1 + a_1 \frac{\partial}{\partial t}\right) \sigma_{\gamma z} = 2k_1 \left(1 + b_1 \frac{\partial}{\partial t}\right) e_{rz} = \\
&\qquad = k_1 \left(1 + b_1 \frac{\partial}{\partial t}\right) \left(\frac{\partial \omega}{\partial r} + \frac{\partial u}{\partial z}\right).
\end{aligned} \tag{4}$$

Now substituting Eqs (2) into Eqs (4) we have

$$\begin{aligned}
&2k_1 \left(1 + b_1 \frac{\partial}{\partial t}\right) \left(\frac{\partial^2 u}{\partial r^2} + \frac{1}{2} \frac{\partial^2 \omega}{\partial r \partial z} + \frac{1}{2} \frac{\partial^2 u}{\partial z^2} + \frac{1}{r} \frac{\partial u}{\partial r} - \frac{u}{r^2}\right) = 0, \\
&2k_1 \left(1 + b_1 \frac{\partial}{\partial t}\right) \left(\frac{1}{2} \frac{\partial^2 \omega}{\partial r^2} + \frac{1}{2} \frac{\partial^2 u}{\partial r \partial z} + \frac{\partial^2 w}{\partial z^2} + \frac{1}{2r} \frac{\partial \omega}{\partial r} + \frac{1}{2r} \frac{\partial u}{\partial z}\right) = 0.
\end{aligned} \tag{5}$$

Laplace transform of a function $F(r, z, t)$ is defined by

$$\bar{F}(r, z, s) = \int_0^\infty F(r, z, t) e^{-st} \, dt. \tag{6}$$

Applying transform (6) to Eqs (5) gives

$$2\left(\frac{\partial^2 \bar{u}}{\partial r^2} + \frac{1}{r} \frac{\partial \bar{u}}{\partial r} - \frac{\bar{u}}{r^2}\right) + \frac{\partial^2 \bar{u}}{\partial z^2} + \frac{\partial^2 \bar{\omega}}{\partial \gamma \partial z} = 0, \tag{7}$$

$$\left(\frac{\partial^2 \bar{\omega}}{\partial \gamma^2} + \frac{1}{2} \frac{\partial \bar{\omega}}{\partial r}\right) + 2 \frac{\partial^2 \bar{\omega}}{\partial z^2} + \frac{\partial}{\partial z}\left(\frac{\partial \bar{u}}{\partial r} + \frac{\bar{u}}{r}\right) = 0, \tag{8}$$

Introducing

$$\bar{\bar{u}}(\xi, z, s) = \int_0^\infty r \bar{u}(r, z, s) J_1(\xi\gamma) \, dr, \tag{9}$$

and

$$\bar{\bar{w}}(\xi, z, s) = \int_0^\infty r \bar{\omega}(r, z, s) J_0(\xi r) \, dr, \tag{10}$$

we obtain [2] from Eqs (7) and (8)

$$(D^2 - 2\xi^2) \bar{\bar{u}} - \xi D \bar{\bar{\omega}} = 0 \tag{11}$$

and

$$(2D^2 - \xi^2)\bar{\bar{\omega}} + \xi D\bar{\bar{u}} = 0 \tag{12}$$

where

$$D = \frac{d}{dz}.$$

Now eliminating $\bar{\bar{u}}$ and $\bar{\bar{\omega}}$ in turn from Eqs (11) and (12) we obtain

$$(D^2 - \xi^2)^2\,\bar{\bar{u}} = 0\,, \tag{13}$$

$$(D^2 - \xi^2)\,\bar{\bar{\omega}} = 0\,. \tag{14}$$

For a semi-infinite solid $z \geqslant 0$, the solution of Eq. (14) is given by

$$\bar{\bar{\omega}} = [A(\xi,s) + B(\xi,s)z]e^{-\xi z}. \tag{15}$$

Introducing Eq. (15) into Eq. (12) gives

$$D\bar{\bar{u}} = -e^{-\xi z}\,[\xi(A + BZ) - 4B]\,. \tag{16}$$

Applying transform (6) to last equation of Eqs (4) gives

$$\bar{\sigma}_{rz} = \frac{k_1(1 + b_1 s)}{(1 + a_1 s)}\left(\frac{\partial\bar{\omega}}{\partial\gamma} + \frac{\partial\bar{u}}{\partial\gamma}\right). \tag{17}$$

Hence

$$\bar{\bar{\sigma}}_{rz} = \int_0^\infty r\bar{\sigma}_{rz}J_1(\xi r)\,dr = \frac{k_1(1+b_1 s)}{(1 + a_1 s)}(D\bar{\bar{u}} - \xi\bar{\bar{\omega}})\,. \tag{18}$$

Now the boundary condition

$$[\sigma_{rz}]_{z=0} = 0$$

gives

$$2\,B = \xi\,A\,. \tag{19}$$

Applying transform (6) to last but one equation in Eqs (4), substituting inversion of Hankel transform of Eq. (15) into it, we have

$$\bar{\sigma}_{zz} = \frac{2\,k_1(1+b_1 s)}{(1 + a_1 s)}\int_0^\infty \xi J_0(\xi r)\left[B - \xi\left\{A + Bz\right\}\right]e^{-\xi z}\,d\xi\,. \tag{20}$$

Introducing the relation (19) and the other two boundary conditions into Eqs (15) and (20)

$$\int_0^\infty \psi(\xi, s)\,J_0(\xi r)\,d\xi = 0 \qquad , \qquad r > 1$$

$$\int_0^\infty \xi\psi(\xi, s)\,J_0(\xi r)\,d\xi = \frac{(1 + a_1 s)\,\bar{f}(s)\,p(r)}{k_1(1 + b_1 s)}\,, 0 < r < 1 \tag{21}$$

where

$$\xi A(\xi, s) = \psi(\xi, s) . \tag{22}$$

The solution of Eq. (21) is known to be [2]

$$\psi(\xi, s) = \frac{2(1 + a_1 s)\bar{f}(s)}{k_1 \pi (1 + b_1 s)} \int_0^1 \sin(\xi s_1)\, ds_1 \int_0^{s_1} \frac{x_1 p(x_1)\, dx_1}{\sqrt{s_1^2 - x_1^2}} . \tag{23}$$

Taking inversion of Hankel transform of Eq. (15), substituting Eqs (22) and (23) into it, we have on $z = 0$

$$\begin{aligned} \bar{\omega} &= \frac{2(1 + a_1 s)\bar{f}(s)}{k_1 \pi (1 + b_1 s)} \int_0^1 \int_0^{s_1} \frac{x_1 p(x_1)}{\sqrt{s_1^2 - x_1^2}} \left[\int_0^\infty J_0(\xi r) \sin(\xi s_1)\, d\xi \right] dx_1\, ds_1 = \\ &= \frac{2(1 + a_1 s)\bar{f}(s)}{k_1 \pi (1 + b_1 s)} \int_r^1 \frac{q(s_1)\, ds_1}{\sqrt{s_1^2 - r^2}} \end{aligned} \tag{24}$$

where

$$q(s_1) + \int_0^{s_1} \frac{x_1 p(x_1)\, dx_1}{\sqrt{s_1^2 - x_1^2}} \tag{25}$$

and [4]

$$\int_0^\infty J_0(\xi \varrho) \sin(\xi t)\, d\xi = \begin{cases} (t^2 - \varrho^2)^{-1/2} , & \varrho < t , \\ 0 , & \varrho > t . \end{cases} \tag{26}$$

Now inverse Laplace transform of Eq. (24) gives

$$\omega(r, 0, t) = \frac{2 a_1}{\pi k_1 b_1} \left[f(t) + \frac{b_1 - a_1}{a_1 b_1} \int_0^t f(\tau) e^{-\frac{(t-\tau)}{b_1}} d\tau \right] \int_r^1 \frac{q(s_1)\, ds_1}{\sqrt{s_1^2 - r^2}} . \tag{27}$$

Substituting the relation (19) into Eq. (20) we have on $z = 0$ by the application of Eqs (22), (23) and (25)

$$\begin{aligned} \bar{\sigma}_{zr} &= -\frac{2\bar{f}(s)}{\pi} \int_0^1 q(s_1) \left[\int_0^\infty \xi J_0(\xi \gamma) \sin(\xi s_1)\, d\xi \right] ds_1 = \\ &= \frac{2\bar{f}(s)}{\pi} \int_0^1 q(s_1) \left[\frac{d}{ds_1} (r^2 - s_1^2)^{-1/2} \right] ds_1 \end{aligned} \tag{28}$$

where [4]

$$\int_0^\infty J_0(\xi \varrho) \cos(\xi t)\, d\xi = \begin{cases} 0 , & 0 < p < t \\ (p^2 - t^2)^{-1/2} , & t < p . \end{cases} \tag{29}$$

Hence inverse Laplace transform of Eq. (28) gives

$$\sigma_{zz}(r, o, t) = \frac{2 f(t)}{\pi} \int_0^1 q(s_1) \left[\frac{d}{ds_1} (\gamma^2 - s_1^2)^{-1/2} \right] ds_1 . \tag{30}$$

Now for the case of a uniform pressure $p(x_1) = p_0$ we have from Eq. (25)

$$q(S_1) = p_0 S_1 . \tag{31}$$

Substituting Eq. (31) into Eq. (27) we obtain the displacement component normal to the crack surface:

$$\omega = \frac{2\,a_1\,p_0}{\pi\,k_1\,b_1}\left[f(t) + \frac{b_1 - a_1}{a_1\,b_1}\int_0^t f(\tau)\,e^{-\frac{(t-\tau)}{b_1}}\,d\tau\right]\sqrt{1-r^2}, \quad 0 < r < 1 . \tag{32}$$

At a particular instant of time, writting

$$b = \frac{2\,a_1\,p_0}{\pi\,k_1\,b_1}\left[f(t) + \frac{b_1 - a_1}{a_1\,b_1}\int_0^t f(\tau)\,e^{-\frac{(t-\tau)}{b_1}}\,d\tau\right]. \tag{33}$$

Eq. (32) may be expressed as

$$\frac{\omega^2}{b^2} + \frac{r^2}{l^2} = 1 \tag{34}$$

which shows that at a particular time the effect of the uniform pressure is to widen the crack into an elliptical one.

Substituting Eq. (31) into Eq. (30)

$$\sigma_{zz}(r, o, t) = \frac{2p_0 f(t)}{\pi}\left[(r^2 - 1)^{-1/2} - \sin^{-1}\frac{1}{r}\right], \quad r < 1 . \tag{35}$$

Hence stress intensity factor

$$N = \lim_{r \to 1+} \sigma_{zz}(r, o, t)\sqrt{r - 1} = \frac{v_2\,p_0 f(t)}{\pi} . \tag{36}$$

The general solution is illustrated in three specific cases, for the displacement.

Case I. Let

$$f(t) = H(t)$$

where $H(x)$ is the Heaviside unit function defined by

$$H(\mathrm{x}) = \begin{cases} 0, & x < 0 , \\ 1, & x > 0 . \end{cases}$$

Hence Eq. (32) changes to

$$\omega(r, o, t) = \frac{2a_1\,p_0}{\pi\,k_1\,b_1}\left[H(t) + \frac{b_1 - a_1}{a_1}\left\{1 - e^{-t/b_1}\right\}\right]\sqrt{1-r^2} , \quad 0 < r < 1 . \tag{37}$$

Case II. Let

$$f(t) = \delta(t)$$

where $\delta(t)$ is Dirac delta function.

Hence

$$\omega(r, o, t) = \frac{2a_1 p_0}{\pi k_1 b_1}\left[\delta(t) + \frac{b_1 - a_1}{a_1 b_1} e^{-t/b_1}\right]\sqrt{1-\gamma^2}\ , \quad 0 < r < 1 \qquad (38)$$

Case III. Let

$$f(t) = e^{-\Omega t}\ .$$

Hence

$$\omega(r, o, t) = \frac{2a_1 p_0}{\pi k_1 b_1}\left[e^{-\Omega t} + \frac{b_1 - a_1}{a_1}\left\{\frac{e^{-\Omega t} - e^{-(t/b_1)}}{1 - b_1 \Omega}\right\}\right]\sqrt{1-r^2}\ , \quad 0 < r < 1 \quad (39)$$

Acknowledgements

The author expresses his sincere thanks to Dr. S. K. SARKAR of Jadavpur University for his guidance in the preparation of this paper.

REFERENCES

1. SNEDDON, I. N.: The Distribution of Stress in the Neighbourhood of a Crack in an Elastic Solid, *Proc. Roy. Soc.* A **187** (1946), 229
2. OLESIAK, Z.—SNEDDON, I. N.: The Distribution of Thermal Stress in an Infinite Elastic Solid Containing a Penny-shaped Crack, *Arch. Rational. Mech. Anal.* **4** (1959—1960), 238
3. HARDING, J. W.—SNEDDON, I. N.: *Proc. Camb. Phil. Soc.* **41** (1945), 16
4. SNEDDON, I. N.—LOWENGRUB, M.: Crack Problems in the Classical Theory of Elasticity, Wiley 1969
5. PRAHAM, G. A. C.: The Correspondence Principle of Linear Viscoelasticity Theory for Mixed Boundary Value Problems Involving Time-dependent Boundary Regions, *Quart. Appl. Maths.* **26** (1968), 167

Pennyförmiger Riß in einem unendlichen viskoelastischen Mittel. Der Spannungszustand in der Umgebung eines pennyförmigen, d. h., Griffithschen Rißes wird in einem Mittel besonderer Art mit linearen viskoelastischen Eigenschaften, durch Anwendung der Laplaceschen und Hankelschen Transformierten, bestimmt. Die allgemeine Lösung ist anhand zweier spezieller Beispiele dargestellt.

Монетообразная трещина в бесконечно вязкой упругой среде. В специальной линеарно вязко-упругой среде вблизи монетообразной трещины напряженное состояние можно определить с помощью преобразований Лапласа и Ганкеля. Общее решение демонстрируется примером, действительным для трех специальных случаев.

Acta Technica Academiae Scientiarum Hungaricae, Tomus 82 (3—4), pp. 443—446 (1976)

CRYOSTAT FOR THE MEASUREMENT OF GALVANOMAGNETIC EFFECTS IN SEMICONDUCTORS

K. SOMOGYI*, B. PŐDÖR**

[Manuscript received 25 August 1975]

A simple but reliable cryostat for galvanomagnetic measurements in semiconductors is described. The cryostat is designated to cover the temperature range of 77—400 K and can be fitted into a small gap magnet.

Electric conductivity, Hall coefficient and carrier mobility are the most frequently measured parameters of semiconducting materials. In most cases these parameters should be measured in function of the temperature. For this purpose different kinds of metal or metal-glass cryostats are used. Most of them are difficult to construct or to work with. In most cases vacuum systems are also needed. The usual glass cryostats are generally bulky, thus they could not be fitted into small gap magnets.

In the present paper a cryostat, which is simple to construct and also to build, but easy to handle, is described. This cryostat was designed to cover the temperature range of 77÷400 K, and can be fitted between the pole pieces of a relatively small magnet. It has proved itself very reliable and useful in the course of many series of measurements in the past six years. The cryostat is basically similar in design to the one first described by URE [1].

Fig. 1 shows the drawing of the cryostat. Basically it is composed of two double-walled silvered Dewars and of a sample holder. Fig. 2 shows an "exploded" picture of the sample holder block. The sample under investigation (double-cross or van der Pauw type for galvanomagnetic measurements, or different diode structures) is housed inside the copper block which can be opened from both sides. The inner chamber is provided with a teflon insulation, and the thermocouple sensor is placed in intimate contact with the sample. The copper block which covers the sample from all sides eliminates the unwanted thermal gradients, and at the same time ensures the stability of the temperatures.

The coolant is liquid nitrogen which is contained in the bigger, lower Dewar. The sample chamber is connected with the nitrogen bath via a copper

* K. SOMOGYI, K.: Paksi J. u, ltp; II/A H—1047 Budapest, Hungary
** B. PŐDÖR, B.: Szendrői u. 152/3, Érd—Parkváros, Hungary

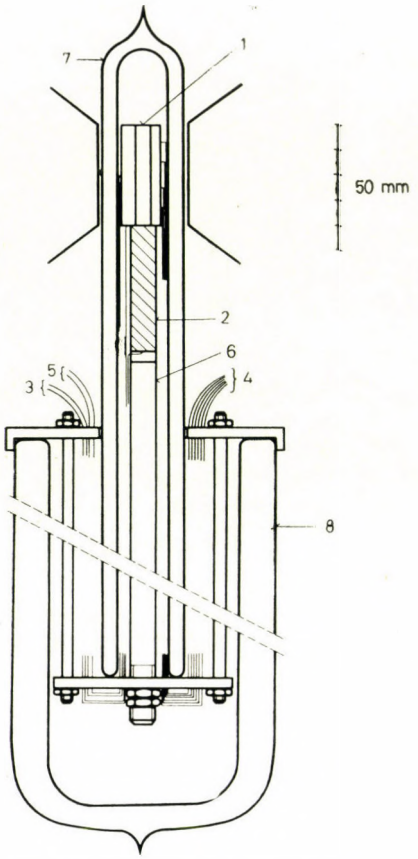

Fig. 1. Drawing of the cryostat and sample holder.
1 — sample block, 2 — brass rod with heater, 3 — lead-through of the heater, 4 — electrical leads, 5 — thermocouple, 6 — copper rod, 7 — upper glass Dewar, 8 — lower glass Dewar

rod of 10 mm diameter, and via a short piece of brass rod, the latter serving as a thermal bridge. The stability and uniformity of temperatures are ensured by the smaller upper Dewar, which is filled with the dry nitrogen vapours, evaporated from the nitrogen bath. The outer diameter of the upper Dewar is 30÷33 mm in our case, so the whole assembly can be fitted into a 35 mm magnet gap. Because of the double Dewar configuration the temperature of the sample block depends very weakly on the level of liquid nitrogen in the lower Dewar. On the short brass rod, just under the sample chamber a heating coil is mounted, with the help of which any temperature above the boiling point of liquid nitrogen can be set in.

The electrical leads (six) and the thermocouple are led through the nitrogen bath as shown in Fig. 1. The thermocouple is chromel-alumel, which has a relatively large thermopower in the temperature range of interest,

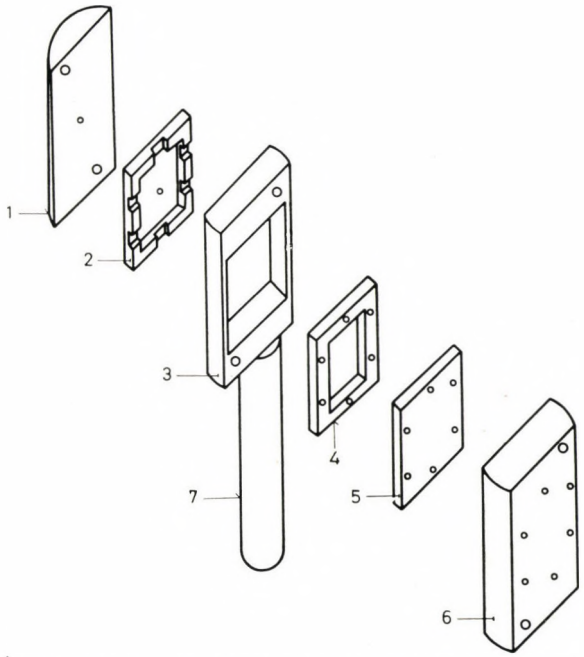

Fig. 2. Sample chamber, "exploded" picture.
1— copper cover, bore in the middle for the thermocouple, 2 — teflon piece, 3 — copper holder, 4— teflon piece with six pins for electrical contacts, 5 — teflon insulator with six holes for electrical leads, 6 — copper cover, 7 —brass rod (thermal bridge)

about 17 μV/K at 77 K and about 40 μV/K at room temperature. The reference point is at 0 °C temperature.

Before starting the measurements, the sample holder is placed upside down into liquid nitrogen, then after about 30 minutes, the upper Dewar is flushed with liquid nitrogen, and the cryostat is assembled. In this way the temperature of the sample chamber is closer to the boiling point of liquid nitrogen than 0,5 K, surpassing the performance of URE's original construction [1]. The higher temperatures are set in with heating, supplying the heater by stabilized voltage. The maximum heating power is less than 20 watts, and ~~the~~ maximum temperature is 400 K or above. The stability of the system is so good, that a stability of 0,1 K can be achieved with mere manual control. The full temperature range can be covered in 6÷8 hours in one cycle.

The construction of the cryostat can be modified to accomodate a sample holder suitable for thermomagnetic measurements, too [2, 3].

The authors operated the above described cryostat for more than 6 years without any difficulties or problems worth mentioning.

REFERENCES

1 URE, R. W.: *Rev. Sci. Instr.* **28** (1957) 836
2. SOMOGYI, K.—SZIDJAKIN, V. G.: *Híradástechnika*, **20** (1969) 262
3. Давиденко, Н И. Факидов И. Г. *Приборы и техника эксперимента* **67** 254 (1967) 254

Kryostat für die Messung von galvanomagnetischen Effekten in Halbleitern. Ein einfacher und zuverlässiger Kyrostat für galvanomagnetische Messungen in Halbleitern wird beschrieben. Der Kryostat ist zu Messungen im Temperaturbereich von 77÷400 K geeignet und kann zu einem Magnet mit schmalem Luftspalt angepasst werden.

Криостат для измерения гальваномагнитных явлений в полупроводниках. Описывается простой и надежный криостат для измерения гальваномагнитных явлений в полупроводниках. Криостат предназначен для измерений в температурном интервале от 77 до 400 К и может быть помещен в узком зазоре магнита.

Acta Technica Academiae Scientiarum Hungaricae, Tomus 82 (3—4), pp. 447—469 (1976)

FERTIGUNG VON FINGERFRÄSERN ZUR HERSTELLUNG VON SCHRÄGVERZAHNTEN STIRNRÄDERN

II. TEIL. BESCHREIBUNG UND EINSTELLUNG DER VORRICHTUNG**

B. SZŐKE*
KANDIDAT DER TECHN. WISSENSCHAFTEN

[Eingegangen am 3. April 1974]

In den Kapiteln 5—7 des zweiten Teiles werden der Aufbau und die Einstellung der Fertigugsvorrichtung behandelt. Mit Rücksicht auf die erforderliche hohe Drehzahl schien es angebracht zu sein, einen im Handel erhältlichen Antrieb zu verwenden. Bezüglich der Ausführung schien es für richtig, zweierlei Aufbauformen bekannt zu geben. Eine dieser Ausführungen bietet eine gute Wirtschaftlichkeit im Falle, wenn nur wenige Größentypen des Fingerfräsers benötigt sind. Die zweite Bauart ist günstig im Falle einer größeren Reihe von verschiedenen Fingerfräsern. Beide Bauarten sind dazu geeignet, auf irgendeine Werkzeugmaschine montiert zu werden.

5. Aufbau der Vorrichtung

Als ein, zur Abwicklung (und zur Rückwicklung) der Berührungsebene des Grundzylinders (mit Halbmesser r_a) dienendes, einfachstes Mittel können, gemäß Bild 6, zwei Paar Stahlbänder verwendet werden. Die Berührungsebene soll als ein steifer Rahmen betrachtet werden, in welchem die (geradwinklige oder schiefe) zahnflächenerzeugende Gerade e als Führungsleiste enthalten ist. Die Enden der gleichlangen Stahlbänder sind derart festgehalten, daß die einzelnen Bänderpaare abwechselnd an der Berührungsebene ($A-B-C-D$) und dann am Grundzylinder ($A_1 - B_1 - C_1 - D_1$) befestigt sind. In dem Bild ist die Berührungsebene durchsichtig dargestellt.

Beim Abwälzen beschreibt jeder einzelne Punkt der Erzeugenden e in der zur Achse rechtwinkligen Ebene eine Kreisevolvente (Bild 7). Die nacheinander folgenden Positionen e_0, e_1, e_2 ... der Zylindererzeugenden bilden zugleich die Erzeugende der Zahnfläche des geraden Zahnes.

NB.: Zum besseren Verständnis wird hier vorerst die Geradverzahnung und danach die Schrägverzahnung besprochen.

In der Herstellung eines Fingerfräsers für eine zylindrische Geradverzahnung kann man die Werkzeugfläche herstellen, indem man die Schar der bereits für das Werkzeug ausgebildeten Zahnflankenerzeugenden e_0, e_1, e_2, ... um die Achse des ruhenden Fingerfräserrohstückes rotieren läßt. Wir wollen die Normaltransversalen zwischen der Fräserachse x und der

* Dr. B. Szőke, Batthyány u. 139, H-1182. Budapest, Ungarn
** I. Teil in *Acta Techn. Hung.* **81** (1975) 411—437

letzterwähnten Erzeugenden als n_0 , n_1 , n_2 ,... bezeichnen. Es ist ersichtlich, daß während der Rotation von den einzelnen (e_0...) Erzeugenden eine Schar von Hüllgeraden gebildet wird, die ihrerseits die Kreise berühren, deren Halbmesser den gegebenen Abschnitten der Normaltransversalen entsprechen.

Die Fläche des Fingerfräsers kann auch derart gebildet werden, daß man das Fingerfräserrohstück um die x-Achse rotieren, und gleichzeitig die alleinige Erzeugende e durch die Punkte E_0 , E_1 , E_2 ,... der Kreisevolvente laufen läßt.

Eine dritte Methode ergibt sich, wenn das Fingerfräserrohstück um die x-Achse rotiert und erfolgt auch eine Rotation der Erzeugenden e um dieselbe Achse, wobei diese Erzeugende zugleich die Punkte, E_0 , E_1 , E_2 ,... der Normaltransversalen durchläuft.

Die technologische Operation besteht aus einem doppelten Arbeitsgang, d. h. die Erzeugende soll zuerst einen Weg vom Grundzylinder zum Zahnkopf, dann aber denselben Weg zurück zum Grundzylinder belaufen. Diese Hin- und Herbewegung wird in folgender Weise verwirklicht: es wird in der Achslinie des ruhenden Grundzylinders eine rotierende Welle z mit einem verstellbaren Kurbelarm k zusammen angebracht: der Zapfen c der Berührungsebene ist durch den Pleuel l mit dem Kurbelarm verbunden (Bild 6).

Wenn nun das oben als drittes bezeichnete Fertigungsverfahren gewählt wird, so wird eine Konstruktion benötigt, um den Grundzylinder samt der Berührungsebene um die x-Achse rotieren zu lassen.

Hierzu wird an der negativen Strecke der x-Achse eine Welle mit dem Kegelrad k_x montiert, welches mit dem Kegelrad k_z der z-Achse des Grundzylinders gekoppelt ist. Infolge der Drehung des Kegelrades k_x wird die Berührungsebene des Grundzylinders durch das Kurbelgetriebe der Achse z in eine hin- und hergerichtete Abrollung gebracht.

Zum weiteren Aufbau unserer Vorrichtung müssen die folgenden, geometrischen Zusammenhänge berücksichtigt werden: vor allem ist der jeweilige Winkel zwischen Berührungsebene und den nacheinander folgenden Normaltransversalen eine veränderliche Größe, u. zw. in dem Sinne, daß dieser Winkel den Winkel zwischen der Berührungsebene und der x-Achse zum Rechtwinkel ergänzt. Daraus folgen diese alternativen Lösungsmöglichkeiten: — die Erzeugende e der Zahnfläche kann in der Vorrichtung entweder als die Achse eines zylindrischen Stabes, um welche die Rotation der Normaltransversale stattfindet, verwirklicht werden, — oder wird die Erzeugende in der Vorrichtung mittels einer prismatischen Stange, die um die e-Achse rotiert, verwirklicht.

Die Beschreibung der Herstellung einer Geradverzahnung war notwendig, um nun auf die Unterschiede verweisen zu können, welche bei der Herstellung einer Schrägverzahnung auftreten. Ein Unterschied ergibt sich

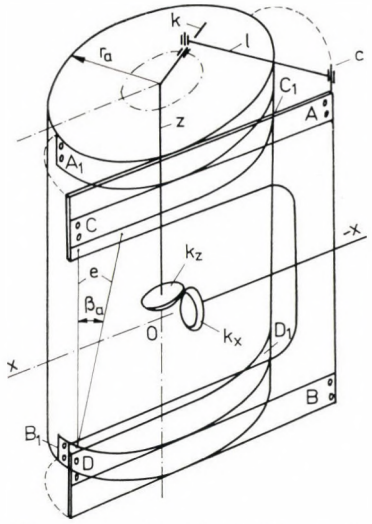

Bild 6. Prinzip der Abwälz-Berührungsebene

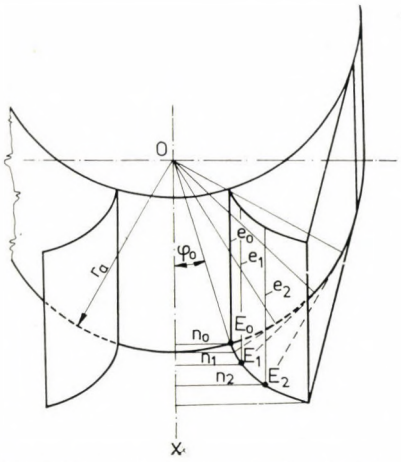

Bild 7. Entstehung der geraden Zahnflanke

in dem Umstand, daß zwischen den Elementen, mittels welcher einerseits die Erzeugende e der Schrägzahnfläche, andererseits die Normaltransversale verwirklicht wird (Bild 8), nicht nur eine Drehbewegung, sondern auch eine Verschiebung in Richtung e zustande kommt.

Dies ist klar ersichtlich aus den Zeichnungen (Daraufsicht und Vorderansicht) im Bild 9a. Hier bedeutet die Punktreihe E_i den Evolventen-Planschnitt der Erzeugenden e, und die gestrichelte Linie (Punktreihe N_i) die Raumkurve der Normaltransversalen. Wir können weiters aus Bild 8 (bei gleichzeitiger Betrachtung des Bildes 12) erkennen, daß Achse x_1 des

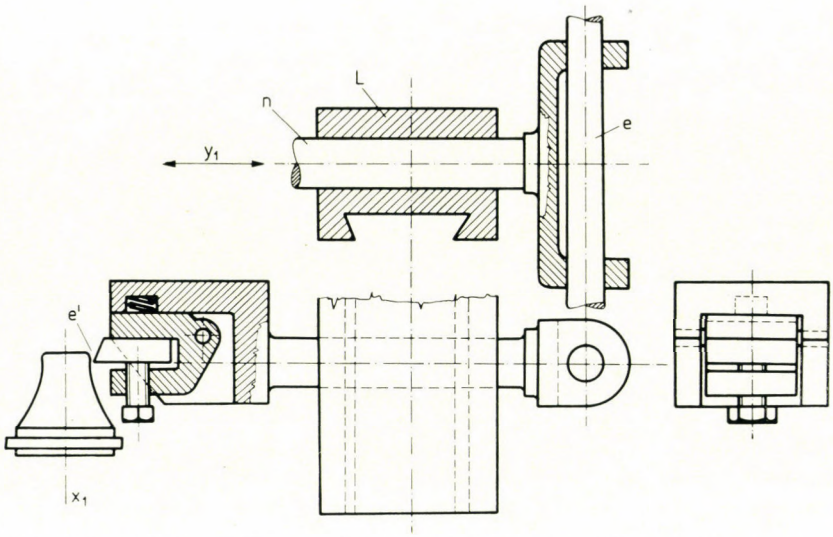

Bild 8. Die gleichzeitig eine Drehung und eine Verschiebung durchführende Normaltransversale als Halter des Stahles mit geradliniger Schneide (Draufsicht, Vorderansicht, Seitenansicht)

Fingerfräsers parallel zur Koordinate x des Zylinders verläuft. Da die Normaltransversale n im Lager L eine zur Grundkoordinate y parallele gleitende Bewegung in Richtung y_1 durchführen kann (Bild 9a), ist es möglich, *bei der Herstellung einer Geradverzahnung* im Lager L (anstelle einer zylindrischen) eine prismatische Bohrung zuzulassen, weil das Werkzeug mit der geradlinigen Schneide e' unverändert in einer, zur Zylinderachse z parallelen Lage verharrt. Es ist aber von großer Wichtigkeit zu wissen, daß der Zapfen n und zugleich auch das Werkzeug e' mit geradliniger Schneide bei der Herstellung einer Schrägverzahnung nicht nur eine gleitende Verschiebung, sondern gleichzeitig eine drehende Bewegung durchführen. Dies soll mit besonderem Nachdruck festgestellt werden, da erfahrungsgemäß Fachleute in der Erkennung der obigen Tatsache ziemlichen Schwierigkeiten begegneten.

Das Lager L (mit zylindrischer Bohrung) soll eine Verschiebung parallel zur Koordinatenachse x mittels einer Schlittenführung durchführen. In der praktischen Ausführung ist es oft richtiger, das Lager nur für Drehung des Zapfens n zu verwenden, und für die Gleitbewegung in Richtung y_1 einen besonderen Schlitten vorzusehen. Im Bild 8 haben wir den Werkzeugkopf als den Schlitten des Hobelstahls dargestellt. Im Arbeitshub wirkt der Anschlag der Rückfläche derart, daß die Schneide e' in der durch die Zahnflächenerzeugende e und die Normaltransversale n gebildeten Ebene eine genaue Lage einnimmt. Hierdurch ist die Genauigkeit des Fingerfräserprofils gesichert. Im Leerlauf wird üblicherweise beim Schwingen um den Zapfen eine Federkraft zum Abheben des Hobelstahls von der Arbeitsfläche angewendet.

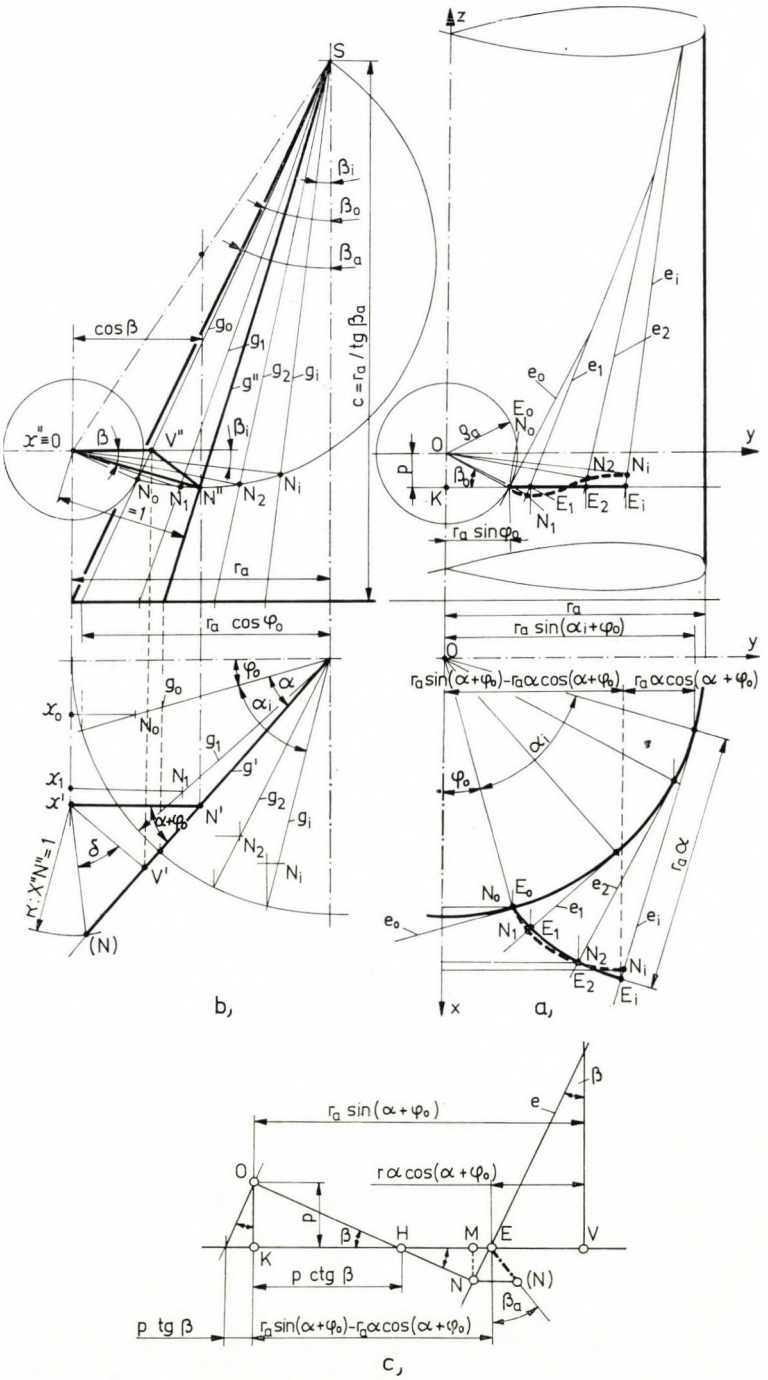

Bild 9a. Entstehung der schrägen Zahnfläche, Draufsicht und Vorderansicht
Bild 9b. Richtungskegel der Grundschraubenlinie (Draufsicht und Vorderansicht). Bestimmung des Neigungswinkels der Normaltransversalen zur Berührungsebene des Grundzylinders
Bild 9c. Die Bestimmung der Normaltransversalen-Verschiebung.

Mit Hilfe der Bilder 9a, 9b und 9c sind wir in der Lage, den Neigungswinkel der Normaltransversalen zur Berührungsebene und auch die Gleitbewegung entlang der Führungsleiste zu bestimmen. In dem bereits erwähnten Bild 9a sehen wird die Zahnfläche schrägverzahnter Stirnräder als Berührende der Grundschraubenlinie in Vorderansicht und Draufsicht. Die Berührungsgerade e_0 (mit dem Neigungswinkel β_0) der Grundschraubenlinie der Zahnfläche schmiegt sich an den Halbmesser ϱ_0 des Fingerfräsers in dem Punkt $N_0 \equiv E_0$. Im Bild 9b ist der Richtungskegel der Grundschraubenlinie dargestellt. Es ist ein geradliniger Kreiskegel mit dem Grundkreishalbmesser r_a; die Kegelerzeugenden bilden einen Winkel β_a mit der Achse. Demnach ist die Höhe des Kegels

$$c = r_a/\tan\ \beta_a\,.$$

Jeder einzelnen Berührungsgeraden e der Schraubenlinie entspricht eine zu ihr parallele Erzeugende g am Richtungskegel. Unter Beibehaltung der Bezeichnungen vom Bild 9b gilt für den durch die zweite Projektion der Geraden g_0 und der z-Achse gebildeten Winkel β_0 die Formel

$$\tan\ \beta_0 = r_a\ \cos\ \varphi_0/c\,,$$

und durch Substituieren des obigen Ausdrucks von c erhält man:

$$\tan\ \beta_0 = \cos\ \varphi_0\ \tan\ \beta_a$$

d. h., in allgemeiner Form

$$\tan\ \beta = \cos\ (\alpha + \varphi_0)\ \beta_a\,. \tag{I}$$

Um den Winkel bestimmen zu können, der am Richtungskegel durch die Normaltransversale und die Berührungsebene des Grundzylinders gebildet ist, wollen wir uns die folgende geometrische Regel vor Augen halten: wenn wir eine Ebene parallel zu sich selbst in Richtung der Normaltransversale verschieben, so bleibt der Neigungswinkel der Normaltransversale mit jeder einzelnen verschobenen Ebene derselbe.

Wir betrachten eine Normaltransversale, welche einer, den Punkt O enthaltenden, zur x-Achse parallel verlaufenden Geraden und irgendeiner Kegelerzeugenden g zugeordnet ist; hierbei sei, gemäß Bild 9b, $X''\,N'' = 1$. Wie bekannt, ist die durch die Kegelerzeugende g und die c-Achse bestimmte Ebene parallel zur die Zahnflächenerzeugende enthaltenden Abwälzebene, u. zw. aufgrund folgender Parallelitäten:

$g \parallel e$, und die Achse des Richtungskegels $c \parallel$ Achse z:

Eine als Normale zu g' und zugleich normal zur ersten Projektionsebene $(g'c')$ gezogene Gerade $X'V'$, ist gleichzeitig (d. h. in der Vorderansicht) in

der zweiten Projektion parallel zur Grundfläche des Kegels, wobei, in der Projektion der Winkel $\beta'' = \sphericalangle V''X''N''$ ist. Die tatsächliche Winkelgröße β kann gefunden werden, wenn wir das Raumdreieck VXN um seine Höhenlinie (in der ersten Projektion) $X'V'$ in die horizontale Lage niederlegen. In dieser Lage wird $X'N' = X'(N) = 1 = X''N''$ in ihrer wirklichen Größe sichtbar. Aus der Vorderansicht des Richtungskegels kann bestätigt werden, daß der Winkel β zwischen einer, durch Punkt O gezogenen Horizontale und der Normaltransversale gleich jenem Winkel ist, welcher von der zweiten Projektion g'' mit der c Achse gebildet ist; auch der Winkel $(\varphi_0 + \alpha)$, welcher von der ersten Projektion g' und der Horizontale gebildet ist, kann erkannt werden.

Bei Beibehaltung der Bezeichnungen gemäß Bild 9b, gilt für die erste Projektion der Einheitsgröße XN die Formel:

$$X'N' = \cos\beta\,, \tag{II}$$

bzw.

$$X'V' = X'N' \sin(\alpha + \varphi_0) = \cos\beta \cdot \sin(\alpha + \varphi_0). \tag{III}$$

Mit Rücksicht auf (III) und das Dreieck $X'V'(N)$ ergibt sich die Gleichung

$$X'V' = X'(N) \cos\delta = \cos\delta = \cos\beta \cdot \sin(\alpha + \varphi_0)\,.$$

Weiters erhält man aus Gl. (I)

$$\tan\beta = \cos(\alpha + \varphi_0) \tan\beta_a$$

und es gilt, nach geometrischen Regeln

$$\cos\beta = 1/\sqrt{1 + \tan^2\beta} = 1/\sqrt{1 + \cos^2(\alpha + \varphi_0)\tan\beta_a}\,,$$

woraus die Gleichung

$$\cos\delta = \frac{\sin(\alpha + \varphi_0)}{\sqrt{1 + \cos^2(\alpha + \varphi_0)\tan^2\beta_a}} \tag{8}$$

folgt.

Um die obige Ableitung zu ergänzen, soll hier zur Bestimmung des Winkels δ, welcher durch die Normale zur Berührungsebene des Grundzylinders und die Normaltransversale gebildet wird, auch der von I. LIPKA abgeleitete, analytische Beweis angeführt werden.

Um die Zahnflankenerzeugende in der Berührungsebene zu bestimmen, greifen wir auf Gl. (1) — im Teil I — zurück, wobei wir darauf achten, daß

die Berührungsebene vom Parameter $(\varphi_0 + \alpha) = \varphi$ abhängt. Hieraus ergibt sich für die genannte Erzeugende das folgende Gleichungssystem:

$$\left.\begin{aligned} x &= r_a \cos\varphi - t\, r_a \sin\varphi\,, \\ y &= r_a \sin\varphi + t\, r_a \cos\varphi\,, \\ z &= c(\varphi - \varphi_0) + c\, t\,. \end{aligned}\right\} \varphi = \alpha + \varphi_0\,.$$

In diesem System gilt für die Richtungskosinuswerte (der Zahnflankenerzeugenden)

$$-\frac{r_a \sin\varphi}{\sqrt{r_a^2 + c^2}}\,;\quad \frac{r_a \cos\varphi}{\sqrt{r_a^2 + c^2}}\,;\quad \frac{c}{\sqrt{r_a^2 + c^2}}\,.$$

Mit anderen Worten, wir haben die Koeffizienten des Parameters t jeweils mit der Quadratwurzel der Quadratsummen der Koeffizienten dividiert.

Um die bezüglichen Richtungswerte der Normaltransversale zu finden, ist folgendes zu überlegen:

Die zur x-Achse in rechtem Winkel stehende Normaltransversale ist relativ zur selben Achse durch den Richtungskosinuswert Null gekenzeichnet. Wenn wir den Winkel zwischen der y-Achse und der Normaltransversale als ψ bezeichnen, so ist der Richtungskosinus zur selben Achse *cos* ψ. Offensichtlich ist der Richtungskosinus zur z-Achse gleich *sin* ψ. Zusammenfassend wird die Lage der beschriebenen Normaltransversale von den folgenden Richtungskosinuswerten bestimmt:

$$0;\ \cos\psi\,;\quad \sin\psi\,.$$

Da die Normaltransversale mit der Erzeugenden gleichfalls einen rechten Winkel bildet, ist der betreffende Richtungskosinuswert gleich Null. So haben wir

$$\frac{r_a \cos\varphi}{\sqrt{r_a^2 + c^2}} \cos\psi + \frac{c}{\sqrt{r_a^2 + c^2}} \sin\psi = 0\,,$$

d. h.

$$r_a \cos\varphi \cdot \cos\psi + c \sin\psi = 0\,,$$

$$\tan\psi = -\frac{r_a \cos\varphi}{c}\,.$$

Mit Rücksicht auf die goniometrische These

$$\cos\psi = \frac{1}{\sqrt{1 + \tan^2\psi}} \text{ und } \sin\psi = \frac{\tan\psi}{\sqrt{1 + \tan^2\psi}}\,,$$

und auf die Zusammenhänge

$$\cos\psi = \frac{c}{\sqrt{c^2 + r_a^2 \cos^2\varphi}}\,; \quad \sin\psi = \frac{-\,r_a \cos\varphi}{\sqrt{c^2 + r_a^2 \cos^2\varphi}}\,,$$

ergeben sich die entwickelten Richtungskosinuswerte

$$0\,; \quad \frac{c}{\sqrt{c^2 + r_2^2 \cos^2\varphi}}\,; - \frac{r_a \cos\varphi}{\sqrt{c^2 + r_a^2 \cos^2 c}}\,.$$

Zur Bestimmung der Normale der vom Parameter wert $\varphi = \varphi_0 + \alpha$ gekennzeichneten Berührungsebene des Grundzylinders dienen die folgenden Richtungskosinuswerte:

$$\cos\varphi, \quad \sin\varphi, \quad 0\,;$$

dieselbe Normale bildet mit der Normaltransversale den Winkel δ. Wenn wir die beiden Richtungskosinuswerte (nämlich diese der oben besprochenen Normale und jene der Normaltransversale) miteinander komponieren so erhalten wir den Kosinuswert des Winkels δ.

$$\cos\delta = \frac{c \sin\varphi}{\sqrt{c^2 + r_a^2 \cos^2\varphi}}\,.$$

Nun ist

$$c = r_a \operatorname{cot\,tg}\beta_a\,,$$

und daher

$$\cos\delta = \frac{r_a \cot\beta_a \sin\varphi}{\sqrt{r_a^2 \cot^2\beta_a + r_a^2 \cos^2\varphi}} = \frac{\cot\beta_a \sin\varphi \tan\beta_a}{\sqrt{1 + \cos^2\varphi \tan^2\beta_a}} = \frac{\sin\varphi}{\sqrt{1 + \cos^2\varphi \tan^2\beta_a}}\,.$$

Hier sei bemerkt, daß bei $\varphi = \alpha + \varphi_0$ der Ausdruck von $\cos\delta$ der oben erwähnten Formel (8) entspricht.

Es ist nicht schwer, die wirkliche Größe der Verschiebung entlang der Führungsleiste am Richtungskegel zu bestimmen. Dies kann geschehen, indem man den Abstand $E_i N_i$ an der Erzeugenden e_i auf eine, durch den Kegelwinkel β_a gekennzeichnete Erzeugende projiziert. Diese Projektion (E_i) (N_i) stellt die tatsächliche Größe der Verschiebung dar.

Dagegen ist die rechnerische Ermittlung umständlicher.

Nach dem Zusammenhang laut Formel (I) und bei Beibehaltung der Bezeichnungen des Bildes 9a, kann man für den Fall $\alpha = 0$ folgende Gleichung aufschreiben:

$$p = r_a \sin\varphi_0 \tan\beta_0 = r_a \sin\varphi_0 \cos\varphi_0 \tan\beta_a = r_a \frac{\tan\beta_a \sin 2\varphi_0}{2}\,.$$

Mit Rücksicht auf Formel (I), und durch Anwendung der Bezeichnungen des Bildes 9c erhält man:

$$KH = p \tan \beta = \frac{r_a \tan \beta_a \sin 2\varphi_0}{2 \cos(\alpha + \varphi_0) \tan \beta_a} = \frac{r_a \sin 2\varphi_0}{2 \cos(\alpha + \varphi_0)},$$

und wir setzen die Ableitung fort:

$$KE = r_a \sin(\alpha + \varphi_0) - r_a \alpha \cos(\alpha + \varphi_0),$$

$$HE = KE - KH = r_a \sin(\alpha + \varphi_0) - r_a \alpha \cos(\alpha + \varphi_0) - r_a \frac{\sin 2\varphi_0}{2 \cos(\alpha + \varphi_0)},$$

$$HN = HE \cos \beta,$$

$$OH = p/\sin \beta,$$

$$p : MN = OH : HN,$$

$$MN = pHN/OH = pHE \cos \beta \cdot \sin \beta / p = HE \cos \beta \cdot \sin \beta,$$

$$\sin \beta \cdot \cos \beta = \frac{\tan \beta}{1 + \tan^2 \beta},$$

$$\tan \beta = \cos(\alpha + \varphi_0) \cdot \tan \beta_a,$$

$$\sin \beta \cos \beta = \frac{\cos(\alpha + \varphi_0) \tan \beta_a}{1 + \cos^2(\alpha + \varphi_0) \tan^2 \beta_a}.$$

daher

$$MN = \frac{\cos(\alpha + \varphi_0) \tan \beta_a}{1 + \cos^2(\alpha + \varphi_0) \tan^2 \beta_a} HE.$$

Die effektive Länge der Verschiebung beträgt:

$$E(N) = MN/\cos \beta_a = \frac{\cos(\alpha + \varphi_0) \cdot \tan \beta_a}{\cos \beta_a [1 + \cos^2(\alpha + \varphi_0) \tan^2 \beta_a]} HE,$$

bzw. nach Einsetzen des Wertes von HE:

$$E(N) = \frac{\cos(\alpha + \varphi_0) \tan \beta_a}{\cos \beta_a [1 + \cos^2(\alpha + \varphi_0) \tan^2 \beta_a]} \times$$

$$\times \left[r_a \sin(\alpha + \varphi_0) - r_a \alpha \cos(\alpha + \varphi_0) - r_a \frac{\sin 2\varphi_0}{2 \cos(\alpha + \varphi_0)} \right].$$

Wir wollen aus dem zweiten Polynom das Glied $r_a/\cos(\alpha + \varphi_0)$ herausheben:

$$\frac{\cos(\alpha+\varphi_0)\tan\beta_a}{\cos\beta_0\left[1+\cos^2(\alpha+\varphi_0)\tan^2\beta_a\right]}\left[\frac{r_a}{\cos(\alpha+\varphi_0)}\right]\times$$

$$\times\left[\frac{\sin(\alpha+\varphi_0)}{1/\cos(\alpha+\varphi_0)}-\frac{\alpha\cos(\alpha+\varphi_0)}{1/\cos(\alpha+\varphi_0)}-\frac{\sin 2\varphi_0}{2}\right]=(EN)$$

bzw.

$$\frac{r_a\tan\beta_a}{\cos\beta_a\left[1+\cos^2(\alpha+\varphi_0)\tan^2\beta_a\right]}\left[\frac{\sin 2(\alpha+\varphi_0)}{2}-\right.$$

$$\left.-\frac{\sin 2\varphi_0}{2}-\cos^2(\alpha+\varphi_0)\right]=E(N),$$

und, in durchgeführter Form erhält man

$$\frac{r_a\tan\beta_a}{\cos\beta_a\left[1+\cos^2(\alpha+\varphi_0)\tan^2\beta_a\right.}\left[\cos(\alpha+2\varphi_0)\sin\alpha-\alpha\cos^2(\alpha+\varphi_0)\right]=E(N). \tag{9}$$

Aus Gl. (9) folgt, daß die Verschiebung $E(N)$ in zwei Fällen zu Null wird: erstens, wenn $\alpha = 0$, da in diesem Fall, innerhalb der Klammern, jedes der beiden Glieder verschwindet. Der zweite Fall ist durch die folgende Gleichheit bestimmt, da die Differenz in den eckigen Klammern verschwindet:

$$\cos(\alpha+2\varphi_0)\cdot\sin\alpha=\alpha\cos^2(\alpha+\varphi_0).$$

Hierzu soll bemerkt werden, daß die Punkte jeder einzelnen Normaltransversalen N_0, N_1, N_2, ... an dem Richtungskegel (Bild 9b) zugleich die Punkte eines Thales-Kreises vom Durchmesser SO bilden. Die Tiefste Lage in diesem Kreis ist durch den vertikalen Halbmesser gekennzeichnet.

Die im Bild 8 dargestellte Vorrichtung ist tatsächlich dazu geschaffen, ein genaues Evolventenprofil herzustellen, da die gerade Werkzeugschneide e' effektiv an der Hüllfläche der entstehenden Hyperboloide tangential entlanggleitet. Diese Bewegung entsteht dadurch, daß die genannte Schneide während der Fortbewegung in der x Richtung auch eine Verdrehung um den Zapfen n durchführt.

Im Bild 10 ist das Profil des Fräsers als Hüllkurve der durch den Meridianschnitt der Hyperboloidenschar entstehenden Hyperbel dargestellt. Wir ersetzen jede einzelne Hyperbel durch den Krümmungskreis am Scheitelpunkt, gekennzeichnet durch den bekannten Scheitelkrümmungsradius $R = p = b^2/a$, wobei b die halbe imaginäre, a die halbe reelle Achse bezeichnet. Die Scheitelpunkte sind als Berührungspunkte bezeichnet. Wenn wir die, vom Zapfen n während der Operation durchgeführte Drehbewegung unbeachtet

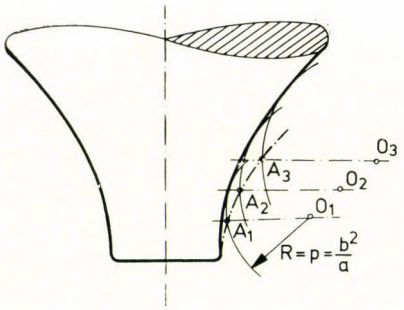

Bild 10. Profil des Fingerfräsers als Hüllkurve der als Meridianschnitte der Hyperboloide entstandenen Hyperbel

lassen, so können wir leicht dem Irrtum verfallen, als ob die Profilkurve des Fingerfräsers durch die Punktreihe A_1, A_2, ... der Normaltransversalen gebildet wäre.

Zum Einspannen der Fräser und Schleifwerkzeuge verwenden wir spezielle Vorrichtungen, die wir an einen im Handel erhältlichen Antrieb anschließen können. Den Turbo-Schleiffräser Type USF-35 (Bild 11a) erhielten wir von der Wiener Firma Groh und Sohn (A-1011 Wien, Lugeck 1); die Anwendungsmöglichkeiten desselben sind auf Bild 11b dargestellt.

Der Apparat ist durch folgende Angaben gekennzeichnet:
Antrieb: patentierter Druckluftmotor.
Betriebsdruck: 2 $\sim$ 4 kp/cm², je nach Drehzahl und Leistung.
Luftverbrauch: 280 liter/min bei 4 kp/cm² Druck
Drehzahl: 25 000 — 40 000 U/min
Leistung: 720 W, bei 40 000 U/min
Lagerung: hochgenau, vorgespannt, spielfrei.
Schmierung: durch Ölnebel, kontinuierlich.
Kühlung: Selbstkühlung, durch Antriebsluft.
Rundlaufgenauigkeit der Spindel: 0,002 mm.
Einspann-Nabe A. D.: 18 mm, auf Wunsch 40 mm.
Werkzeugaufnahme: Spannzange, Verlängerungsdorn.
Werkzeuge: Hartmetallfräser, Diamantwerkzeuge, Schleifstifte, Ringschleifkörper.
Nettogewicht: 3,2 kg.

Laut Mitteilung der Herstellerfirma kann man bei einer Umdrehung von 40 000 U/min auch zylindrische Schleifscheiben keramischer Bindung mit einem Durchmesser von 6 $\approx$ 10 mm in der Vorrichtung verwenden. Die Stabilität der Vorrichtung läßt die Anwendung von Verlängerungsdornen $\varnothing 12 \times 125$ mm, oder $\varnothing 12 \times 130$ mm zu, ohne jedwede nachteilige Wirkung befürchten zu müssen.

Die Zusammenstellung unserer Vorrichtung ist auf 3 Abbildungen dargestellt, u. zw.: Vorderansicht; Bild 12a; Seitenansicht bzw. Querschnitt: Bild 12b; Draufsicht: Bild 12c. Aus diesen Bildern geht klar hervor, daß diese Vorrichtung einfach auf eine Drehbank oder auf eine andere Werkzeugmaschine montiert werden kann, wobei die Antriebswelle x des Abwälzmechanismus in der Rohrwelle X gelagert und das Lager V dieser Welle am Drehbankbett befestigt wird. Ein anderes Lager Z, das entweder mit der Rohrwelle ein Stück bildet, oder daran rechtwinklig befestigt ist, dient zur Aufnahme der Welle z. Am Lager Z sind ferner zwei Grundzylinderscheiben,

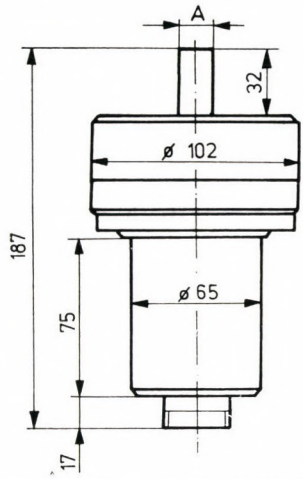

Bild 11a. Umriß eines mit einer Drehzahl von 40 000 U/min wirkenden Turbo-Werkzeuges; zur Verfügung gestellt von der Firma Groh und Sohn

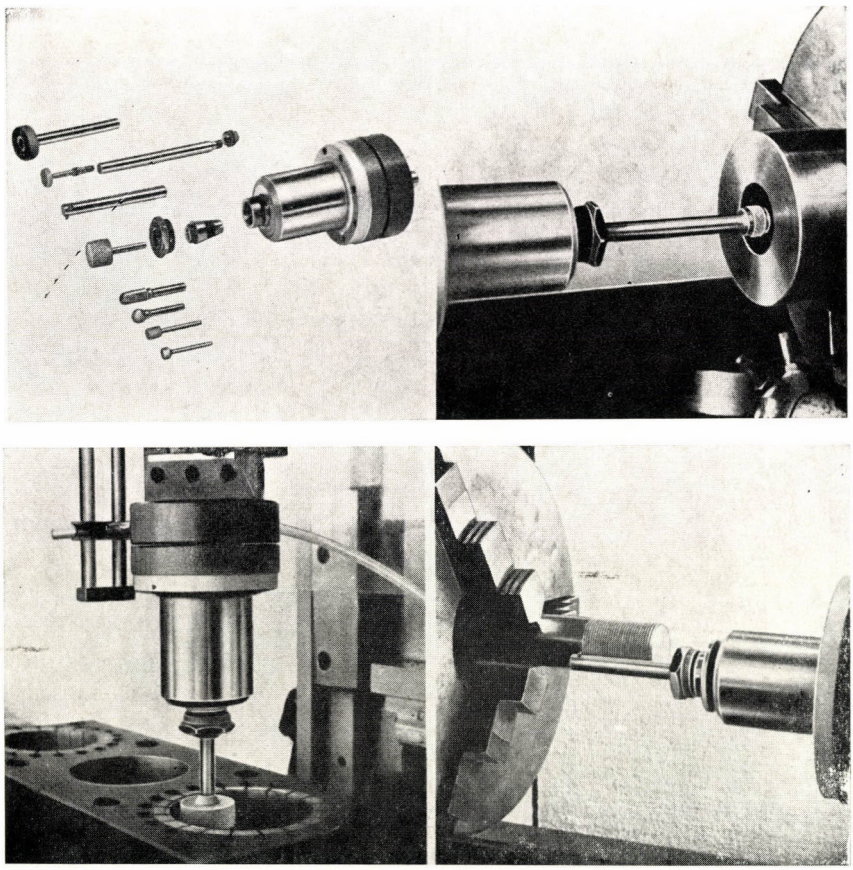

Bild 11b. Montage und Anwendbarkeit des Turbo-Schleiffräsers auf Werkzeugmaschinen

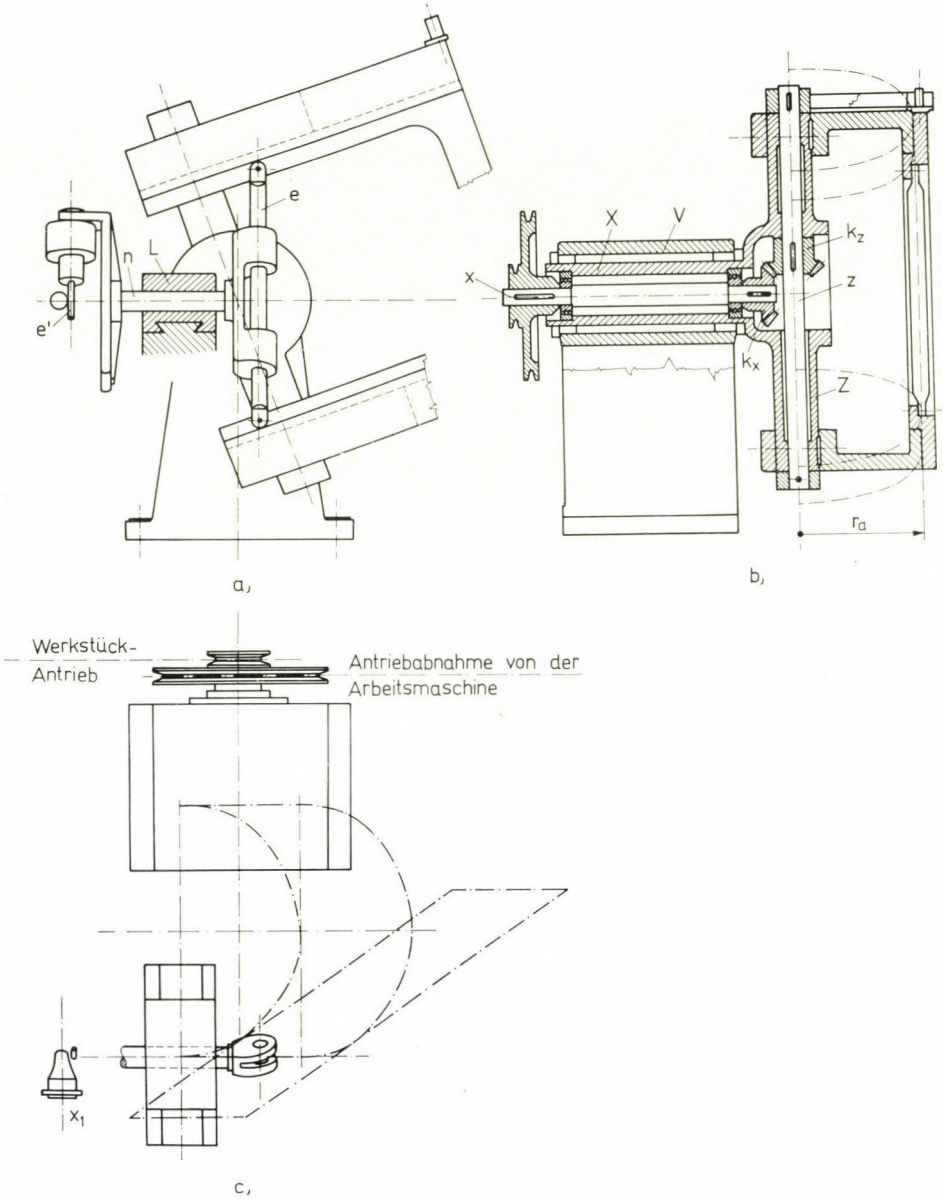

Bild 12a. Zusammenstellung der nach dem Prinzip der Abwälzebene arbeitenden Vorrichtung. Vorderansicht
Bild 12b. Seitenansicht bzw. Querschnitt derselben Vorrichtung
Bild 12c. Draufsicht derselben Vorrichtung

eine obere und eine untere, beide mit dem Halbmesser r_a, angebracht. Zum Zweck der Abwälzbewegung genügt je eine halbe Scheibe. Demzufolge können wir uns mit einem einzigen Gußstück begnügen, welches nach dem Prinzip einer zweiteiligen Riemenscheibe, jedoch in einer Ausführung einer doppelt

langen Radnabe bearbeitet werden kann, um beide Halbscheiben einfach auf die Rohrwelle Z aufspannen können.

Der steuerbare Bearbeitungsmechanismus und die Lagerung des drehbaren Arbeitsstückes kann anstelle des Stahlhalters am Schlitten montiert werden. Am Ende der Welle x befinden sich 2 Keilriemenscheiben. Eine davon, die innere, wird von der Drehbankhauptspindel angetrieben. Die zweite dient zum Antreiben unseres Werkstückes. Natürlich kann der Fingerfräser auch direkt von der Hauptspindel aufgenommen werden. In diesem Falle wird die Abwälzvorrichtung entweder am Schlitten, oder unmittelbar am Bett befestigt.

6. Steuerung nach dem Prinzip der Schraubenbewegung

Im vorigen Kapitel haben wir das Abwälzen der Berührungsebene besprochen und gezeigt, daß die Zahnerzeugende e ihre erwünschten Positionen mit Hilfe der beiden Grundzylinderscheiben nacheinander einnehmen konnte. Jedoch ist ein solches Verfahren nur bei der Herstellung von wenigen Fräsertypen wirtschaftlich. Nun wollen wir die Notwendigkeit, für jede Fräsertype das spezifische Paar von Grundzylinderscheiben herzustellen, umgehen. Dies kann verwirklicht werden, wenn wir an die Wellen z der Steuervorrichtung (Bilder 13a und 13b) eine obere und eine untere Schlittenführung anbringen, die beliebigerweise gegeneinander verdrehbar sind und deren Schlitten in der nach Wunsch verschobenen Lage fixiert werden können. Die Führungsleiste e kann in verschiebbare Gelenke des oberen s_1 und des unteren s_2 Schlittens eingespannt und befestigt werden.

Diese Anordnung bildet mit dem Grundzylinder ein starres System.

Wenn dieses System als Grundzylinder die doppelte Bewegung durchführt, indem es axial verschoben und um die eigene Achse entsprechend rotiert wird, so wird durch die aufeinanderfolgenden geometrischen Stellen der Führungsleiste e die Zahnflanke erzeugt.

Nach Bild 13a dient das durch Kegelrad k_x angetriebene Kegelrad k_z zugleich als Mutter für die Gewindespindel z. Nun ist das Kegelrad k_z in dem um die x-Achse drehbaren Lager X abgestützt und so hat die Drehung dieses Kegelrades zur Folge, daß die Gewindespindel in der axialen Richtung z verschoben wird. Wir erwarten von der Vorrichtung, daß sie zu jeder Kombination der Grundzylinder von verschiedenem Halbmesser r_a und der verschiedenen Zahn-Neigungswinkel β_a verwendbar sei. Dies kann erreicht werden, wenn dafür gesorgt wird, daß die Drehung der Welle und die axiale Verschiebung der Spindel genau jener Schraubenbewegung entsprechen, die entsteht, wenn die Tangente des Grundzylinders ihre eigene Schraubenbewegung dem Neigungswinkel β_a und der Ganghöhe h entsprechend durchführt.

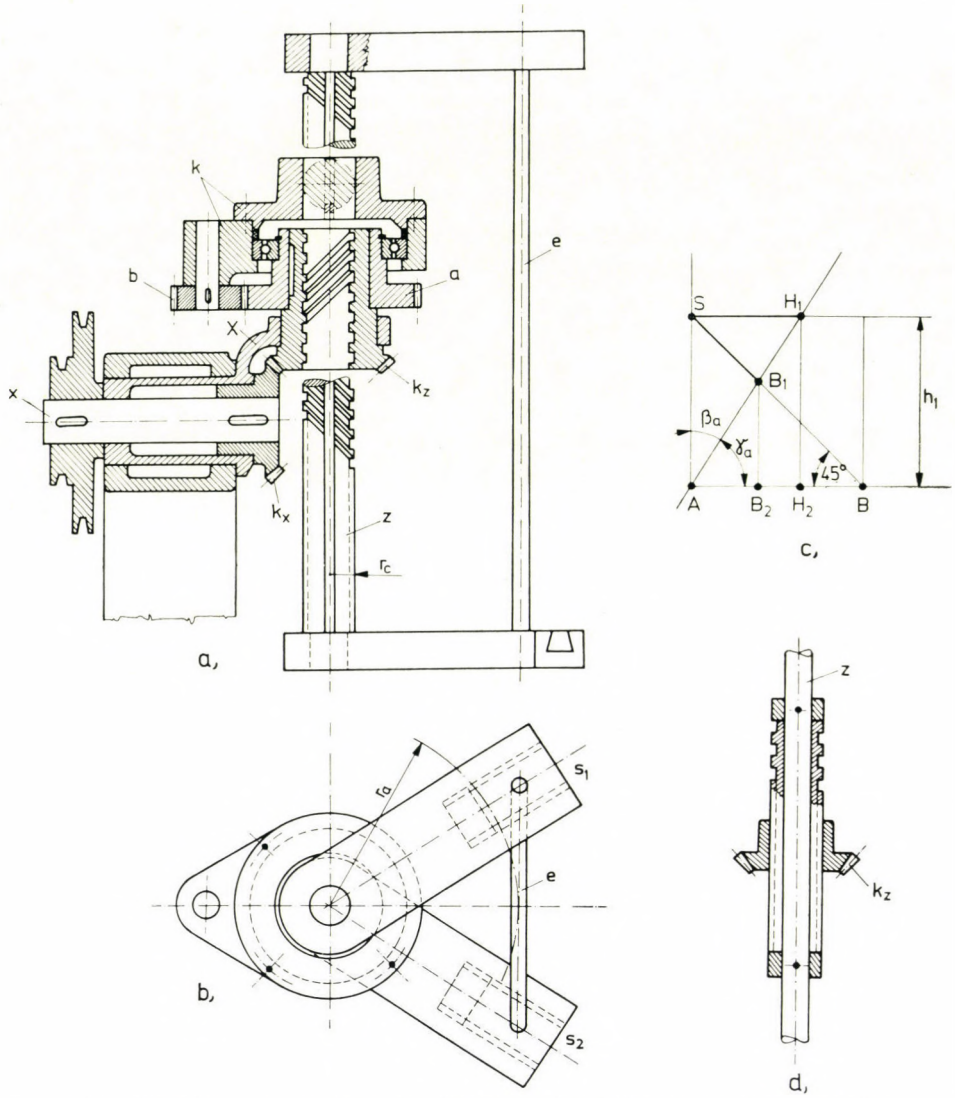

Bild 13a. Zusammenstellung der Gewindespindel-Vorrichtung. Seitenansicht
Bild 13b. Teildraufsicht derselben Vorrichtung
Bild 13c. Fortbewegungsrichtungen am Grundzylindermantel, in einer Ebene ausgebreitet
Bild 13d. Alternative Ausführung als hülsenförmige Gewindespindel mit einer darin rotierenden Welle

Wir haben im Bild 13*c* folgende bewegungs-geometrische Elemente eingezeichnet: die Berührungsgerade der Schraubenlinie mit dem Neigungswinkel β_a, u. zw. an der in eine Ebene entfalteten Grundzylindermantelfläche, ferner die Steigungsrichtung des Gewindes in der Bohrung des Kegelrades k_z, ebenfalls in der entfalteten Ebene. Bekanntlich ist die Gewindespindel, als Maschinenelement, durch den Wirkungsgrad $\eta = \tan \alpha / \tan (\alpha + \varrho)$ gekennzeichnet

mit α als Steigungswinkel und ϱ als Reibungswinkel. In diesem Zusammenhang ist der günstigste Steigungswinkel $\alpha = 45°$; dieser Fall wurde in unsere Zeichnung (Bild 13*c*) aufgenommen. Nun ist das Verhältnis des Verdrehungsbogens und der axialen Verschiebung der Spindel gleich $\tan \beta_a$. Um dies zu verwirklichen, stehen uns zwei verschiedene Konstruktionsmöglichkeiten zur Verfügung.

Im Bild 13*d* ist eine der beiden Lösungen dargestellt.

Diese Lösung läßt sich wie folgt beschreiben:

Die *Gewindespindel* ist als ein *Führungsrohr* ausgebildet. In diesem Rohre befindet sich die Grundzylinderwelle, wobei die hohle Gewindespindel und die darin drehbare Welle eine gemeinsame axiale Verschiebung durchführen. Während einer Umdrehung des Kegelrades k_z legt des Rohr (samt Welle) einen Weg von $AS = h_1$ zurück, und die Welle im Rohr verrichtet eine dem Bogen SH_1 entsprechende Drehung, wobei $SH_1/SA = \tan \beta_a$ sein muß.

Bei der *anderen* konstruktiven *Lösung besitzt die Gewindespindel keine Führungsbohrung*. Durch das Muttergewinde des Kegelrades k_z erhält die Gewindespindel die notwendige Längsverschiebung. Ferner befindet sich an der Gewindespindel eine *axiale Keilbahn* (Bild 13*a*). Die zusätzlich benötigte Drehung der Spindel wird mittels des Dreharmes k bzw. des daran montierten Einsatzkeils erzielt. Da die hierdurch in Drehung gebrachte Gewindespindel gezwungen ist, sich auch in den rotierenden Schraubengängen des Muttergewindes im Kegelrad fortzubewegen, muß eine Drehung entlang des Bogens AB_2 zugleich einer axialen Verschiebung SB_1 entsprechen.

Der Verdrehungsbogen im Dreieck ABB_1 entspricht dem Umfang der Schraubenspindel mit dem Halbmesser r_c und mit Rücksicht auf den Steigungswinkel von 45°, haben wir

$$2r_c \pi = h_1 = AB$$

und

$$AB_2 = AB_1 \sin \beta_a ,$$

bzw.

$$AB_1 : \sin 45° = AB : \sin (45° + \beta_a) .$$

Unter Berücksichtigung der folgenden Zusammenhänge:

$$\sin 45° = \cos 45° \text{ und } AB = h_1 = 2r_c \pi ,$$

erhalten wir

$$AB_2 = 2r_c \pi \tan \beta_a / (1 + \tan \beta_a) .$$

Als Beispiel nehmen wir folgende Werte an:

$$r_c = 50 \text{ mm}; \quad \tan \beta_a = 0{,}532,$$

so ist

$$AB_2 = 314 \cdot 0{,}532/1{,}1532 = 109.$$

$314 : 109 \approx 23/8$, und demgemäß soll der Arm k 8 Umdrehungen vorauseilen, während dessen das Kegelrad 23 Umdrehungen durchführt. Also ist die Umdrehungszahl n_k des Armes k gleich $23 + 8 = 31$.

Im Falle einer rohrförmigen Gewindespindel (Bild 13*d*) soll die Voreilung des Armes k während einer Umdrehung des Schraubenmutterkegelrades SH_1

$$SH_1 = h_1 \tan \beta_a = 314 \cdot 0{,}532 = 167{,}05$$

Umdrehungen betragen.

Da nun $314 : 167{,}05 \approx 20/11$, also ist die Voreilung des Armes k gleich 11, gegenüber der Kegelradumdrehung 20. Die Umdrehung n_k des Armes k ist gleich $20 + 11 = 31$.

Die Konstruktionslösung kann leichter gestaltet werden, wenn wir, im Sinne des Bildes 14*a*, die Umdrehung des Kegelrades k_z als die Umdrehung eines Sonnenrades in einem Zweirad-Planetengetriebe auffassen, und zugleich das Sonnenrad a und das Planetenrad b als Wechselräder betrachten, die dem jeweiligen Neigungswinkel β_a zugeordnet sind. Wir wollen auf die Umdrehungszahlformeln [11], [12] und [15] des außenverzahnten Zweirad-Planetengetriebes zurückgreifen:

$$an_a + bn_b - (a + b)\, n_k = 0\,. \tag{10}$$

In dieser Formel haben die Bezeichnungen folgende Bedeutung:

a — irgendeine passende Angabe des Sonnenrades, d. h. Halbmesser bzw. Durchmesser oder Zähnezahl,

b — eine ähnliche Angabe des Planetenrades,

k — Planetengetriebearm,

n_a, n_b und n_k — Drehzahlen gemäß Fußindex.

Die Formel (10) kann als Gleichung einer Ebene, dargestellt in einem dreidimensonalen System aufgefaßt werden, mit den Zähnezahlen a und b als Konstanten (bzw. gegebene Zähnezahlen) und n_a, n_b, n_c als Variabeln. Wenn also unser Koordinatensystem durch die Koordinatenachsen n_a, n_b und n_k gebildet wird, so läßt sich die erste Bildebene durch die Achsen n_k, n_a, die zweite durch n_k, n_b, die dritte durch n_a, n_b bestimmen (Bild 14*b*).

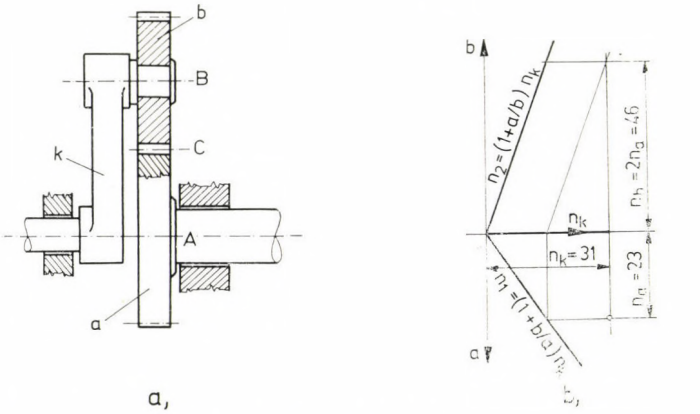

Bild 14a. Prinzip eines außenverzahnten Zweirad-Planetengetriebes
Bild 14b. Darstellung des Rechnungsganges zum Zweirad-Planetengetriebe

Die erste Spurlinie ergibt sich bei $n_b = 0$, die zweite bei der Annahme $n_a = 0$;

$$n_1 = n_a = \left(1 + \frac{b}{a}\right) n_k , \tag{10a}$$

$$n_2 = n_b = \left(1 + \frac{a}{b}\right) n_k . \tag{10b}$$

Hierzu sei bemerkt, daß am Halbmesser a die Richtung AC als positiv, am Halbmesser b die Richtung BC als negativ gilt. Bezeichnenderweise gilt Gl. (10) für ein außenverzahntes Sonnenrad. Für ein innenverzahntes Sonnenrad lautet die Gleichung:

$$an_a - bn_b - (a - b)\, n_k = 0 . \tag{10'}$$

Als Zahlenbeispiel sollen die Angaben der außenverzahnten Wechselräder a und b in Kenntnis der Umdrehungszahl n_a des Sonnenrades a, unter folgender Bedingung bestimmt werden:

$$n_b = q\, n_a \text{ und } n_k = n_a + i,$$

wo q und i beliebig gewählte Zahlenwerte bedeuten.

Im Sinne der Formel (10) kann man schreiben:

$$an_a + bqn_a - (a + b)(n_a + i) = 0,$$
$$an_a + bqn_a - an_a - bn_a - ai - bi = 0,$$
$$ai = b(qn_a - n_a - i),$$

und daraus

$$a/b = \frac{n_a(q - 1) - i}{i} = \frac{n_a(q - 1)}{i} - 1 .$$

Gemäß Bild 13*a* haben wir $n_a = 23$, $q = 2$, $i = 8$.
Deshalb gilt:

$$a/b = 23/8 - 1 = 15/8.$$

In einem anderen Fall mit $n_a = 23$, $q = 3$ und $i = 8$, ergibt sich

$$a/b = 2\, n_a/8 - 1 = 46/8 - 1 = 38/8.$$

Ein weiteres Beispiel sei bestimmt durch $a = 30$, $b = 16$, entsprechend dem Verhältnis $a/b = 15/8$.

Hieraus erhält man nach Bild 14b die Spurlinien der bezüglichen Ebene, wie folgt:

$$n_1 = \frac{23}{15}\, n_k ; \quad n_2 = \frac{23}{8}\, n_k .$$

Wenn einmal die Spurlinien n_1 und n_2 der Ebene bestimmt wurden, so ist es möglich, die dem Wert z. B. $n_a = 23$ zugeordneten Werte $n_b = 46$ und $n_k = 31$ durch geometrische Konstruktion zu finden, wie dies aus Bild 14*b* hervorgeht.

Es sei z. B. ein Punkt gewählt, für welchen der Abstand n_a der ersten Projektion von der n_k-Achse gleich 23 und der Abstand der zweiten Projektion gleich $n_b = 2\, n_a = 46$ ist; so ist der koordinierte Wert $n_k = 31$ in Übereinstimmung mit Gl. (10), wie folgt:

$$15.23 + 8.46 - (15 + 8)\ 31 = 0$$

das heisst

$$15\, n_a + 8\, n_b - 23\, n_k = 0.$$

Im Bild 13*a* ist eine Konstruktionsart dargestellt, in welcher der Einlegeteil zur Übertragung der Drehbewegung an die Gewindespindel, zwecks Erleichterung der Montage, sich im Deckelteil des Armes *k* befindet.

Wenn eine automatische Hin- und Herbewegung der Gewindespindel gewünscht ist, dann muß für einen mechanisierten Richtungswechsel der Drehung der Welle gesorgt werden.

Zur Bestimmung der Verschiebung der Gewindespindel dienen die geometrischen Zusammenhänge der Bilder 9a und 13c. Der Evolventenabwälzbogen am Grundkreis im Stirnprofil ist $r_a\alpha$; die diesem Bogen zugeordnete Bogenlänge der Schraubenlinie ist

$$l = r_a \alpha / \sin \beta_a \,.$$

7. Einstellung der Vorrichtung

Die Führungsleiste *e* soll an der Wälzebene-Vorrichtung in einem Winkel β_a zur *z*-Achse eingestellt werden. Für eine Zähnezahl *z* und mit den Bezeichnungen im Bild 15, ergeben sich:

$$\begin{aligned} \varphi &= 2\pi/4z = \pi/2z \,, \\ r_a \tan \alpha &= r_a \operatorname{arc} (\vartheta + \alpha) \,, \\ \tan \alpha &= \operatorname{arc} \vartheta + \operatorname{arc} \alpha \,. \end{aligned} \tag{11}$$

Mit Hilfe der Evolvententabelle [13] und als Funktion des Eingriffswinkels α kann man schreiben:

$$\operatorname{arc} \vartheta = \operatorname{inv} \alpha = \tan \alpha - \operatorname{arc} \alpha \,,$$

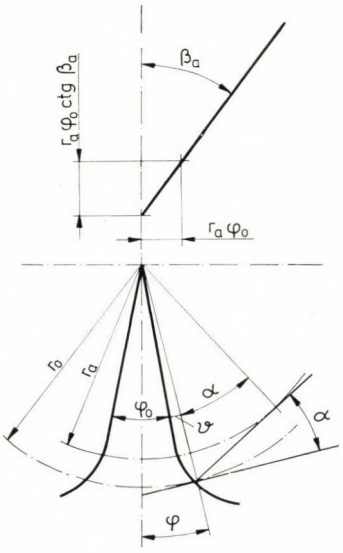

Bild 15. Einstellung der Führungsleiste in der nach dem Prinzip der Abwälzebene arbeitenden Vorrichtung

und im Bogenmaß

$$\varphi_0 = \varphi - \vartheta = \frac{\pi}{2z} - \vartheta \,. \tag{12}$$

Um die Gewindespindel-Vorrichtung gemäß Bild 13*a* einzustellen, müssen wir den Neigungswinkel β_a der Grundzylinderschraubenlinie bestimmen. In Kenntnis des Teilzylinder-Neigungswinkels β_0 läßt sich auch die Formel der Ganghöhe anschreiben:

$$h = 2r_0\,\pi/\tan\beta_0 = 2r_a\,\pi/\tan\beta_a\,,$$

d. h.

$$\tan\beta_a = r_a \tan\beta_0/r_0\,,$$

da

$$r_a = r_0\cos\alpha = mz\cos\alpha/2\,,$$

erhält man für den Winkel β_a die praktischere Formel

$$\tan\beta_a = \tan\beta_0\cos\alpha\,. \tag{13}$$

Wenn nun Winkel $\beta = 0$, dann ist die Führungsleiste e parallel zur Achse z des Grundzylinders und die erzeugte Profilkurve ist eine Evolvente.

Zum Zwecke der Einstellung des Fingerfräsers einer Schrägverzahnung gemäß β_a wollen wir den Zusammenhang zwischen dem Neigungswinkel 2δ der Schlitten s_1 und s_2, und ihrem Abstand p und dem Winkel β_a festlegen.

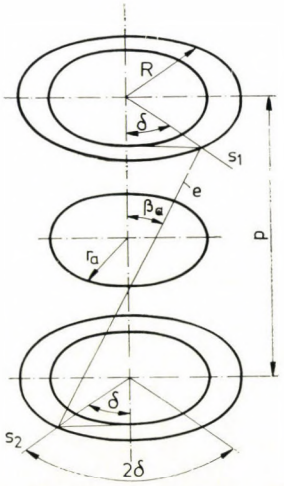

Bild 16. Einstellung der Führungsleiste in der Gewindespindel-Vorrichtung

Wir wollen die Bezeichnungen nach Bild 16 beibehalten:

$$\cos \delta = r_a/R = mz \cos \alpha/2R\,, \tag{14}$$

$$p = 2R \sin \delta/\tan \beta_a\,. \tag{15}$$

Unter Berücksichtigung der Gleichung $m_h z = 2r_0$, erhält man aus den obigen zwei Formeln und nach (13)

$$\begin{aligned} \tan \delta &= p \tan \beta_a\, 2R/2R\, m_h z \cos \alpha = \\ &= p \tan \beta_a/2r_0 \cos \alpha = p \tan \beta_a/2r_0\,. \end{aligned} \tag{16}$$

Aus Gl. (14) ist

$$R = r_0 \cos \alpha/\cos \delta\,.$$

In Kenntnis der Größen R, p und Winkel δ sind wir in der Lage, den Winkel β_a einzustellen.

Es soll hier — im Anschluß an die Berechnung der Wechselräder (a) und (b) des Zweiradplanetengetriebes — auf die bereits angeführten Zusammenhänge Bezug genommen werden:

Mit Rückblick auf das Kapitel 4 kommen wir auf unsere früheren Besprechungen betreffs der Berechnung eines Rades mit Pfeilverzahnung zurück:

Werkzeugmodul $m_n = 27$ mm,
Zähnezahl $z = 26$,
Neigungswinkel am Teilzylinder $= \beta_0 = 30°$,
Stirnmodul $m_h = 31{,}177$ mm,
Teilkreishalbmesser $r_0 = 405{,}299$ mm,
Werkzeugeingriffswinkel $\alpha_n = 20°$,
Eingriffswinkel im Stirnschnitt $\tan\alpha = \tan 20°/\cos 30°$, d. h. $\alpha = 23° 45'$,
Grundkreishalbmesser: $r_a = r_0 \cos \alpha = 405{,}299 \cos 23° 45' = 373{,}64$ mm.
Es beträgt die Ganghöhe am Teilzylinder: $h = 2r_0\pi/\tan 30° = 4410$ mm,
d. h.

$$\tan \beta_a = 2r_a\pi/h = 0{,}532,$$

d. h.

$$\beta_a = 28°.$$

Es diene als Rekapitulation, daß (nach Bild 13*c*) das Drehzahlverhältnis sich folgendermaßen ergibt:

Ausgangswert ist $\tan \beta_a = 0{,}532$: demgemäß erhält man für die Ausführung mit einer Gewindespindelachse nach Bild 13*a* $n_a/n_h = 23/31$. Weiters wurde nach Bildern 14*a* und 14*b* bewiesen, daß man dieses Drehzahlverhältnis bei einem Verhältnis der Wechselräder $a/b = 15/8$, z. B. $z_a/z_b = 30/16$ erhält.

Für eine durchbohrte Ausführung der Gewindespindel (Bild 13*d*) d. h. mit einer Voreilung nach Bild 13*c* $SH_2 = SH_1$ gilt nach vorheriger Berechnung das Verhältnis der Wechselräder $a/b = 29/11$.

SCHRIFTTUM

1. SZŐKE, B.: Schleif- und Abrichtgerät für Formwerkzeuge von Schrägstirnrädern. *Acta Techn. Hung.*, **60** (1968), 21—38
2. LIPKA, I.: Bemerkungen zu dem Aufsatz von J. DRAHOS Jr., L. HORNYIK und M. HOSSZÚ: Die mathematische Lösung eines werkzeuggeometrischen Problems. *Mitteilungen des Mathematischen Forschungsinstitutes der Ung. Akademie der Wissenschaften*, **3** (1958), 219—236

3. LIPKA, I.: Geometrie der Wölbung von Laufflächen an Wälzlagerringen. *Acta Techn. Hung.* **31** (1960), 339—390
4. SZŐKE, B.: Das richtige Profil des Fingerfräsers für Kammwalzen. *Werkstattstechnik* (1924), 417—421
5. SZŐKE, B.: Schleifwerkzeug für Formfingerfräser. *Maschinenbau* (1926), 308—311
6. SZŐKE, B.: A fogaskerék profilmaróinak gépi előállítása (Mechanische Herstellung von Zahnprofilfräsern). *A Magyar Mérnök- és Építészegylet Közlönyének Havi Füzetei* (1927), 124—129
7. DRAHOS, I.—HORNYIK, L.—HOSSZÚ, M.: Modulujjmaró profiljának meghatározása szerkesztéssel és számítással (Konstruktive und rechnerische Bestimmung des Profils eines Modulprofil-Fingerfräsers). *GÉP*, **10** (1958), 306—310
8. DRAHOS, J. junior—HORNYIK, L.—HOSSZÚ, M.: Die mathematische Lösung eines werkzeuggeometrischen Problems. *A Magyar Tudományos Akadémia Kutató Intézetének Közleményei* (1958), 83—95
9. NIEMANN, G.—LOOMAN, J.: Abrichtgeräte für das Profilschleifen von Schrägstirnrädern. *VDI-Zeitschrift*, **102** (1960), 231—238
10. SZŐKE, B.: A térláttató ábrák társszerzője PÁL, I.: A forgácsoló szerszámok geometriája (Geometrie der Zerspanungswerkzeuge). Műszaki Könyvkiadó, Budapest 1966, pp. 166—171
11. SZŐKE, B.: Engranages Planétaires. *Acta Techn. Hung.* **58** (1967), 245—270
12. SZŐKE, B.: Bolygókerekes fogaskerékhajtások (Zahnräder-Planetengetriebe). *Gépgyártás Technológia.* Budapest **8** (1968), 293—302
13. RADVÁNYI, B.: Involut. Az „inv" α függvény nyolcjegyű táblázata (Die Funktion „Involute α"; 8stellige Tabelle). Nehézipari Könyv- és Folyóiratkiadó Vállalat, Budapest 1954
14. LITVIN, F. L.: A fogaskerékkapcsolás elmélete (Theorie des Zahnrädereingriffes). Műszaki Könyvkiadó, Budapest 1972
15. SZŐKE, B.: Cranked Epicyclic Gear Drives. *Nehézipari Műszaki Egyetem Közleményei*, Miskolc, **30** (1970), 141—164

Generating of the End Milling Cutters for Helical Gears II. The Design and the Adjustment of the End Milling Cutter.. — In Chapters 5—7 the arrangement of the production and its adjustment are dealt with. As for the design — considering the high r.p.m. required by the work — it was thought that use of a commercially available gear would be the best solution. Two designs are discussed: one would be economic where only few sizes of end cutters are needed, while the other solution could be used for the production of the most different cutters. Any of them could be mounted one some suitable machine tool.

Изготовление обкаткой концевой фрезы косозубых цилиндрических колес, II Конструкция и установка концевой фрезы. Авторы предлагают применение готовогс привода и описывают два вида решения, а именно: один из них был бы экономичен в таких местах, где требуется небольшое число размеров концевых фрез, а второй — может быть использован для изготовления самых различных видов концевых фрез. Любая из них может быть смонтирована на какой-нибудь подходящий металлорежущий станок.

RECENSIONES

H. Jordan—V. Klima—K. P. Kovács:

ASYNCHRONMASCHINEN

FUNKTION, THEORIE, TECHNISCHES

Akadémiai Kiadó, Budapest und Friedrich Vieweg & Sohn Verlagsgesellschaft mbH, Braunschweig 1975. ISBN 963 05 0092 2, 531 Seiten, 316 Abbildungen und Tabellen.

Asynchronmaschinen, in dem Leistungsbereich von Bruchteilen eines Watt bis zu vielen tausenden Kilowatt, werden heute in der ganzen Welt jährlich zu Hundertmillionen erzeugt. Viele Fachleute beschäftigen sich mit diesen meistverbreiteten Motoren, demzufolge ihre Entwicklung einen hohen technischen Stand erreicht hat.

Trotz des einfachen konstruktiven Aufbaus finden in den Asynchronmotoren komplizierte elektromagnetische Vorgänge statt, andererseits kommt den störenden Nebenerscheinungen, wie Laufruhe, magnetischer Lärm, Zusatzverluste, Drehmomentsättel usw. eine steigende Bedeutung zu. Diese Probleme sind zwar in der Fachliteratur behandelt, aber es ist für den Leser unmöglich, die große Unmenge der Literatur zu verfolgen und erfolgreich zu bearbeiten. Das vorliegende Buch verfolgt das Ziel, die grundlegenden und weiterführenden Kenntnisse der Asynchronmaschinen zusammenzufassen und aufzuarbeiten.

Das Buch ist als Lehrbuch für Studierende und als Nachschlagwerke für Fachleute gedacht und deshalb legen die Verfasser großen Wert darauf, den Asynchronmotor stets als ein physikalisches Gebilde mit elektromagnetischen Erscheinungen zu betrachten. Die netzwerktheoretische Behandlung mit Matrizendarstellung als Hilfsmittel der Lösung transienter Vorgänge wird im zweiten Band des Buches behandelt werden.

Das vorliegende Buch ist der erste Band einer zweibändigen Serie. Es hat außer der Einleitung elf Kapitel, ein Sachverzeichnis und eine Bezeichnungsliste.

Die Einleitung erklärt die Bildung des Drehmoments und zeigt einige typische Beispiele. Das Kapitel I behandelt den Problemkreis Drehfelder, Drehmomentbildung und Spannungserzeugung. Die idealisierte Drehstromasynchronmaschine und die wichtigsten Grundbegriffe werden im Kapitel II beschrieben. Kapitel III beschäftigt sich mit der Theorie der Wicklungen.

Der Grundfeldmotor und dessen klassische Behandlung mit Hilfe der Primärstromortskurve (Kreisdiagramm) wird im Kapitel IV beschrieben. Hier werden auch die Besonderheiten des Käfigläufermotors behandelt. Dieses Kapitel ist durch drei Anhänge ergänzt, die die Problemkreise SI-Maßsystem, die Per-Unit-Schreibweise und die funktionstheoretischen Betrachtungen über Kreisdiagramme erörtern.

Im Kapitel V werden die Fragen des konstruktiven Aufbaus und der technischen Einzelheiten der Drehstromasynchronmaschinen behandelt und im Anfang die wichtigsten VDE und DIN Normen angeführt.

Zu der klassischen Theorie gehört noch das Thema des VI Kapitels, die Theorie der Motoren mit Doppelkäfig- und Stromverdrängungsläufern. Die folgenden Kapitel beschäftigen sich mit Betriebsproblemen, wie Antriebs- und Erwärmungsfragen (Kapitel VII); Anlassen, Bremsen, Umsteuern, Schaltwärme (Kapitel VIII); Drehzahlstellen (Kapitel IX).

In dem Kapitel X werden die Sonderbetriebsarten (Generatorbetrieb, Drehsteller, asynchrone Frequenzumformer, elektrische Welle, Gleichstrombremsung) und im Kapitel XI die unsymmetrischen Schaltungen von Induktionsmaschinen behandelt.

Die kurze Beschreibung des Inhalts des Buches beweist, daß es die klassische Theorie der Drehstromasynchronmotoren umfaßt. Es wird großer Wert auf die einwandfreie physikalische Erklärung der Zusammenhänge und auf eingehende, sorgfältige Diskussionen der Ergebnisse gelegt.

Die einzelnen Kapitel sind mit einem ausführlichen Literaturverzeichnis versehen. Schöne und zweckmäßige Bilder erleichtern dem Leser die Bearbeitung des Stoffes. Für den Text ist klare und zielstrebende Schreibweise charakteristisch. Die schöne Ausführung des Buches ist ein besonderer Verdienst des Verlages.

F. Csáki und *P. Magyar*

Kenneth L. Johnson:

OPERATIONS RESEARCH

VDI-Taschenbücher, T 27, VDI-Verlag Düsseldorf 1973, pp. 193

The subject of the investigation of the scientific trend developed and widely adopted under the name *Operations Research* is the structure and characteristic behaviour of integrated (man-machine) systems organized and controlled with a definite purpose, i. e., the totality of interrelated activities planned or to be expected, necessary for reaching the result required in an actual situation. Just this latter, i. e., the way of activity aiming to perform a definite and perhaps repeatedly occuring task of the man-machine system, is called *operation*. The purpose of the operations research is to be helpful in decision making, to make it more deeply understood; analysis of the operations of the organized system for the most part in a symbolic *model*, by determining its optimum or by (computerized) simulation. However, the "Operations Research" as a key word, does not only countermark the activities of such trends but this expression is used as a collective title for specific mathematical models, methods and disciplines (linear and non-linear programming; integral programming, sequence programming; theory of games; dynamic programming and theory of process control; graph theory, theory of network processes; organization networks; network control systems analysis; theory of stochastic processes; theory of mass attendance; stock piling; and to cover all the mentioned subjects, heuristic methods and systems simulation, etc.) promoting the solution to decision and management problems.

Although the expression "Operations Research" has been adopted all over the world, it may not be considered to be very lucky in any of the languages. Namely, the *operation* (i. e., decision and management strategies) — according to the present common use of the expression — is not so much researched as — by relying on the information based upon *analysis* of the decision and management situation and on the *prevision* of the consequences of interventions — as *planned*. Therefore, also in the English special literature, several synonyms are applied to designate this concept. In the special literature of West Germany (and also in that of the Operations Research Society) for several years the American expression has been used. This is the origin of the title of the VDI-volume.

The book of K. L. JOHNSON was compiled from the material of the seminary lectures held for industrial managers.

In *Chapter* 1, by way of introduction, the interrelation between the operations research and systems theory, or to be more exact, the approach of the *system of operations research* is discussed. It is made clearly understandable that this is not a new discipline of mathematics but the special technics or technico-economic field which is dealt with, partly developing together with the field of automatic data processing and computer technique.

In *Chapter* 2 the *linear optimization* (or, in other words *linear programming*) with the aid of bivariate problems is explained, and the attention is shortly drawn to such further possibilities as the integer valued, parametric, stochastic as well as non-linear optimization, and the own limits of linear programming are pointed out. Then a concise description is given of the significant types of problems as, for example, the distribution, cutting out, transport, planning of roundabout circulation systems and designation problems.

Chapter 3 deals with the questions of *dynamic optimization*. Here the linear (and other mathematical) optimization treated in the foregoing chapter, is supplemented with time data. This is indispensable in situations where decisions relating to given periods, affect those of the following ones. Here the significant concepts are the planning time horizon, state-space which also contains the possible states of the system in the given periods, probability of each systems states, and the optimum politics. Also for the application of the Markov-chain some simple examples are to be seen.

Chapter 4 makes known the most significant elements and viewpoints of the *network technique*.

The subject of *Chapter* 5 is the *digital simulation* and within this the production of random numbers. These means of anylsis and experimentation is shown by a simple mass attendance example, by the analysis of the capacity of one sf the small repair shops.

Chapter 6 gives insight into the *theory of games*, gives a glance into models practicably treatable, however, where a real operations research problem could only rarely be defined.

Chapter 7 deals in a relatively more detailed and very up-to-date way with the *time functions*. These are very useful and often indispensable in the operations research and mainly in the theory of simulation and prognostics, but as a discipline belongs to the statistics, therefore, commonly no stress is laid on it in the curriculum of the operations research.

Chapter 8 reports on the interrelated problems of *stock piling*, i. e., on the amount of stocks, terms of reorders and on the amounts of the material to be ordered.

Chapter 9 presents the simpler types of *sequence planning* to be handled more easily; then in *Chapter* 10 the work is finished by describing the theory of *waiting rows* (in other terms, the theory of mass attendance) and a small example problem to be treated in this way.

The Publisher of the Society of German Engineers (VDI) deserves credit for that in its series of books, so popular in the professional world, draws the attention of engineers to the potentialities of the operations research.

G. Jándy

L. Kollár—E. Dulácska:

SCHALENBEULUNG

THEORIE UND ERGEBNISSE DER STABILITÄT GEKRÜMMTER FLÄCHENTRAGWERKE

Akadémiai Kiadó Budapest — Werner Verlag Stuttgart, 1975. 172 Seiten, 125 Abbildungen, 5 Zahlentafeln, Literaturverzeichnis, Namen- und Sachverzeichnis.

Die verschiedenen Schwingungsprobleme der Stabkonstruktionen wurden bereits in zahlreichen Werken ausführlich behandelt, doch ermangelte es bisher einer die Stabilitätsprobleme der Flächentragwerke erfassenden Monographie. Diesem Mangel soll auf dem Gebiet der Schalenkonstruktionen das Werk der Verfasser Lajos KOLLÁR und Endre DULÁCSKA abhelfen.

L. KOLLÁR, einer der beiden Autoren schrieb das vorzüglich verfaßte einleitende Kapitel, das die Beulung der Zylinder- und Kegelschalen, der kugelförmigen und elliptischen Kuppeln, sowie die Stabilitätsprobleme der hyperbolischen Paraboloidschalen behandelt. Er ist auch der Autor der Kapitel, die sich mit den Stabilitätsproblemen der Schalen mit freien Rändern, sowie mit der Beulung der Rippen und Fachwerkschalen befassen. Die, die Stabilitätsprobleme der orthotropen, der Wellen- und Sandwichschalen betreffenden Kapitel hat E. DULÁCSKA verfaßt. Auch das Schlußkapitel, das die praktische Anwendung der Ergebnisse der Stabilitätstheorie beinhaltet, schrieb E. DULÁCSKA.

Die Beulungsprobleme der Schalen bilden das komplizierteste und in vielen Beziehungen auch heute noch ungeklärte Kapitel der technischen Festigkeitslehre. Hunderte von Forschern suchten diese Probleme theoretisch oder im Versuchswege zu lösen, doch zeitigten ihre Bestrebungen umso weniger eine befriedigende Lösung, da ihre Feststellungen voneinander in vielen Beziehungen wesentlich abweichen. Besonders auffallend ist die vielfach beobachtete Tatsache, daß die kritische Last der Schalen in einem weiten Bereich schwankt, wie dies Versuche und die Erfahrungen der Baupraxis zeigen, und wesentlich kleiner ist als der auf Grund der Berechnungen zu erwartende Wert. Diese Abweichungen finden ihre Begründung einerseits darin, daß im Rahmen der theoretischen Untersuchungen statt der tatsächlichen Materialeigenschaften von diesen mehr oder weniger abweichende, idealisierte Eigenschaften der Baustoffe angenommen werden, andererseits darin, daß in den einzelnen Phasen der mathematischen Berechnung, mit Rücksicht auf die hierbei auftretenden Schwierigkeiten, verschiedene Vernachlässigungen vorgenommen werden. Eine weitere Ursache der Abweichungen besteht darin, daß bei den theoretischen Untersuchungen die Form der Konstruktion und die Unterstützungsart idealisiert und die infolge von Ungenauigkeiten in der Bauausführung auftretenden Beulungen außer acht gelassen, bzw. regelmäßig angeordnete Beulungen regelmäßiger Form angenommen werden. Im allgemeinen lassen die theoretischen Untersuchungen auch die chemischen und physikalischen Wirkungen, wie Wärmedehnung, Schwinden, Kriechen, Korrosion, die während des Bestehens der Konstruktion auftreten, unberücksichtigt. Ein weiterer Fehler ergibt sich ferner daraus, daß die theoretischen Untersuchungen statt der unendlich vielen Arten der Beulungsverformungen nur eine beschränkte Anzahl dieser ins Auge fassen. Diese Umstände, sowie der unbekannte Unterschied, der zwischen der theoretischen und der tatsächlichen Dicke der Schale besteht, verursachen ein ernstes Problem in der praktischen Anwendung der theoretischen Ergebnisse im Zusammenhang mit der zweckdienlichen Bestimmung des Sicherheitsfaktors.

Im vorliegenden Werk sind die Autoren bestrebt, einerseits einen Überblick des zu behandelnden Themas zu geben, andererseits für die Praxis einen gut brauchbaren Behelf zur wirtschaftlichen und zuverlässig sicheren Bemessung von Schalen zu bieten. Diese zweifache Aufgabe löst das Werk — trotz des komplizierten Problems — erfolgreich. Die Berechnung

der kritischen Spannung nach der linearen Theorie wird — unter Verzicht auf lange Ableitungen — nur nach dem von E. DULÁCSKA entwickelten Verfahren erörtert, das in geistreicher Weise auf der Beobachtung beruht, daß sich die Beulungswelle oder die Beulungswellen der Schalen im allgemeinen auf kleine Flächen erstrecken und so die Beulung auf Grund der vereinfachten Beulungstheorie flacher Schalen behandelt werden kann.

Das Werk befaßt sich eingehend mit der Wirkung, die die Abweichung der tatsächlichen Form der Schale von der theoretischen auf den Beulungsvorgang ausübt. Anstatt in Form von Formeln und Ableitungen sind die Untersuchungsergebnisse der verschiedenen Forscher in klaren Diagrammen veranschaulicht und auch die theoretischen Ermittlungen sowie die versuchsmäßigen Beobachtungen des Verhaltens der Schale im überkritischen Bereich dargestellt. Anhand einer ungemein anschaulichen — in der internationalen Literatur bisher unbekannten — Abbildung wird die wahrscheinliche Beulungsform der über einem windschiefen Viereck errichteten Schale und die Möglichkeit der dehnungslosen Formänderung erklärt. Von Interesse ist auch die Zusammenfassung der theoretischen und versuchsmäßigen Ergebnisse, die L. KOLLÁR im Zusammenhang mit der Stabilität der Schalen mit freien Rändern veröffentlicht.

Mit Rücksicht auf die praktische Anwendung des Werkes wurden die Beulung orthotroper Schalen sowie die Stabilitätsprobleme von Schalen besonderer Konstruktion und im Rahmen dieser die selbstständigen Forschungsergebnisse der Autoren eingehend behandelt. Besondere Aufmerksamkeit verdient auch das geistreiche und mit praktischem Sinn verfaßte Schlußkapitel.

Im allgemeinen kann festgestellt werden, daß das Werk — seiner Zielsetzung entsprechend — die ungemein komplizierte Erscheinung der Beulung und deren physikalische Ursachen anschaulich und allgemeinverständlich erläutert. Auch die in der internationalen Fachliteratur veröffentlichten, die Beulung der Schalen betreffenden Forschungsergebnisse, einige wertvolle Abhandlungen der Autoren mitinbegriffen, sind sorgfältig angeführt. Die Hinweise auf die Fachliteratur und der mehr als 200 Posten umfassende Literaturnachweis bieten große Möglichkeiten für weitere Forschungsarbeiten auf diesem Gebiet.

Das Buch der beiden Autoren L. KOLLÁR und E. DULÁCSKA stellt eine nützliche Ergänzung der einschlägigen internationalen Fachliteratur dar und erhebt zweifellos Anspruch auf ausgedehntes Interesse.

P. Csonka

Máté Major:

GESCHICHTE DER ARCHITEKTUR, BAND I.

Akadémiai Kiadó Budapest 1974 (Gemeinschaftsausgabe des Akadémiai Kiadó und des Henschelverlages Kunst und Gesellschaft), pp. 719, 423 figures, annexe: 4 geographical maps.

The book of M. MAJOR, member of the Academy, is the first volume of the trilogy dealing with the universal history of architecture first published in the Hungarian language between 1954 and 1960 (dates of publication of the three volumes are: 1954, 1955 and 1960 respectively) then, between 1957 and 1960 in German (1957, 1958 and 1960). Thus, this book seems to be the beginning of the third edition of the work, however, neither this volume, nor the second and third ones (the former being completed in manuscript and the latter in hand) are the mere reprints of the former volumes because their structure and even their function has undergone a great change since their author first wrote them.

Habent sua fata libelli — this ancient saying, its drift in this regard: this work has its own history and destiny, and as a work dealing with history has a peculiar affinity with the branch of our cultural history reviving after our liberation, one of leading personalities of which was M. MAJOR: this being the revival and development of architecture in Hungary. In the late forties, the author together with several fellow-workers could be seen among those who tried to lay down and solve the enormous problems banking up in front of our building industry. These personalities whose professional and political activities were represented before our liberation was a pledge of a successful evolution. However, the running events caused M. MAJOR's conclusion in playing an immediate part of leading and forming the building industry, and he gave up his job he had held down in the ministry, for the university chair, the practice of science. At the Technical University of Budapest he organized a chair of special scope and herewith became a militant personality not only of the present but also of the immediate future thus having just as great significance: educationalist of architects of a quite new type with a qualification to carry out great tasks. He had already had a definite opinion of the up-to-date architecture of those days knowing that this could be simply replanted into the youth

as it was done at the university earlier where even in the years following the liberation the ancient tradition, deducing, understanding and teaching of architecture on the basis of certain formalistic principles, was in vogue. The aim was laid clearly before his eyes, however, he devoided the methods which would help him in achieving it.

Every kind of revolution has a characteristic, accompanying factor in the intellectual field; sometimes preceeding it, sometimes being concomitant, the revaluation and consequently the revision of the material of knowledge. The character of this revaluation is, in general, twofold, because, on the one hand it takes every motif and information into account in order to prevent the repetition of errors committed, which led the evolution into a tangle; and on the other hand, the revaluation cannot be a purpose in itself but is intended to teach and educate; not only to diffuse information but knowledge. This artistic manner of activity was matured by similar changes of fortune which is called encyclopedia, and is kept in evidence as such by science. Well now, M. MAJOR who, at the very beginning had a definite Marxist ideology, and who by extensive theoretical studies gradually developed the outlines of an up-to-date discipline so far not existing, the outlines of an architectural theory based on the grounds of dialectic materialism. He started out with this kind of activity when the task arose to confront him in bringing his principles into affinity with the tremendous build-up of history, hereby justifying their correctness. He undertook the hardly realizible work with a revolutionist's sense of vocation and a scientist's humility, knowing how it should not be done and how it must be done, beginning his university lectures not in the traditional way which disclosed only one (and therefore necessarily distorted) aspect of architecture, but tried to present its Protean entity. In order to do this, he extended his lectures to the domain of the prehistory up to that time which had bean wholly neglected and is rather significant in understanding the essentials of architecture, and did not stagnate in analysing the building practice of ancient times, Near-East and classic cultures also previously discussed, as he drew the attention of his students to the Far-East architecture which, although hardly influencing European evolution, still constituted an integral part of the general aspect of the history of architecture. Undoubtedly, M. MAJOR had a basis when starting his undertaking: the encyclopedical works written by a community of several scientists of the Soviet architectural academy, however, these only dealt with the architecture of the ancient times and did not discuss a later evolution. Therefore, the task of starting out with the up-to-date interpretation of the mediaeval, modern times and our days' architectural history awaited him. However, all of these would in themselves have been only the mere quantitative extension of the subject, it became ever more significant as he disclosed it saying: the widely drawn social-economic bases, the technical-technological development, and last but not least, the cultural achievements: among them presentation of character, defining the strength of sciences and arts, together with architecture, served to guarantee the dialectical approach to architectural achievements.

All of these first were published in the form of lecture notes and served as sources for the young generation in thirst of knowledge in architects and in getting acquainted with the science of architecture. The authenticity of the foregoing has not only been justified by its inward high scientific level but also by the personality of the professor, because everybody knew that not a stranger in the professional science is speaking from the chair, but a creative architect who left had a successful activity behind, one of the combatants of the avangardist movement of the years prior to the lineration which was not without any danger; the value the theory of the scientist and teacher has been countermarked by the status achieved in the domain of practice. And also inversely: he would not have been so far rigthed in the frantic architectural discussions without historical studies; at this point his scientific entity came to the assistance of the person who had to decide in practical affairs, and preserved him against concessions despite his own convictions, against dogmata, also taking upon himself the grief of confrontation, But this, however, relaxed before long, just because the complex architectural approach of M. MAJOR eventually achieved his historical justification.

With this, the direct educational didactical "experimental" period of the work came to an end, it matured into the form of a book. And not only the form of a university textbook but a scientific manual, as the whole professional society missed the history of architecture written in the period of the dialectical-historical materialism. Criticism of sorts have been made in respect to the trilogy, more exactly, its first volume referring to the related branches of knowledge, on the side of history of art and archeology as, for example, the connections between the foundation and superstructure are not made perceptible with the necessary plasticity: the sources utilized are not up-to-date enough. These assertions notwithstanding, neither the dialectics just acquired, nor the selfconceited, and sometimes sardonic positivism of some reviewers were not able to contest either the pioneering significance of the work, nor the fact that no general synthesis of architectural history had ever been published in Hungary, written by only one author, and representing a uniform and modern view, but the one in question.

Neither could they prevent the book from becoming the competent and authentic guide for the historical information of the Hungarian society of architects. And as it turned out, not only in Hungary was such a work ever published but neither in other socialist countries, thus, its publication in a foreign language was also justified. After three years the publication in Hungarian was followed by the first volume translated into German and the two others will be published in the same year in both languages.

Anyhow, without what was said in the foregoing the review of the first volume of the work would not be complete because the book is the integral continuation of its antecedents, and yet, it is not only such. The basic conception, as a matter of course, remained unchanged, but the structural modifications carried out made a more refined and detailed explanation of the phenomena possible. This was promoted by the fact that the social-economic, annals historical and culture historical part introducing the different eras has been written almost in the same measure as that discussing architecture. These numerical particulars also express in themselves the intention of the work, and the advantageous, rich possibilities implied in its use now becoming quite clear, so much so that the title of the book almost designates less than its contents. Namely, this is not only the way of the strictly described development of architecture keeping an eye on the professional viewpoint, but, the summary of thousands of factors creating, and giving way to architecture. Perhaps, all of these could have been better expressed by such a title as: "History of the architectural culture".

The subject of the first volume of the *Geschichte der Architektur* is the presentation of the architectural culture of a primitive community and slave-holder societies, i. e., the history of architecture beginning in prehistoric times up to the fall of the roman empire. M. MAJOR, taught by experience, partly narrows down the content of the first volume (he only refers to the a«hievement attained in the Far East, partly enlargens on it: in the section finishing the discussion of ancient Rome, exhibiting the prelude to the future, analysis of the remains of early christian architecture of all of the eras, are treated in the same system and order of sequence, however, in a more detailed manner than in the preceeding work. Namely, while in the first Hungarian and German editions the description of the historical stages was treated only in two chapters, one from among them dealing with culture and the other with architecture, in the new edition this subject is divided into four chapters. The chapter on general history is succeeded by the history of culture then, after that chapter the treatment of architecture, is closed by a short summary. Within this framework, the chapter devoted to *general history* starting with the achievements of the material culture, begins with outlining the social economic bases and continues with the annals of history; the *section treating of the culture*, first studies the phenomena and characteristics of religion, then science, and finally the arts, in the following order of succession: literature, representational arts and music. In the *chapter on architecture* after the *rewiev of the architectural subject matter*, demanded by the respective epochs the description of the building materials and building technic follows, with the material and personal conditions of implementing, is succeeded by the largest and most important section: development of history of architecture. All of these are closed by the section with the title: "*Short summary*" which sums up the architectural achievements, and points to those effects which were exerted on the future developments by the respective eras.

The author applies that system which is capable of displaying consequently those direct relationships, together with the demonstration of the areas and epochs, which are comparatively short, independent and the art according to which their architecture might be characterized by strong features. (See the different periods of architecture of Asia Minor, the architectural cultures developed round the eastern basin of the Mediterranean). However, curiously one possibility remained unused: in discussing the architecture of the comparatively long-lasting eras and, therefore, exhibiting a certain but only illusive uniformity (as the ancient community, Egypt, Hellas, Rome) this subdivision into four chapters did not prove convenient because the discussion of the different eras distributed among the different sections of the development is not followed by summaries; the conclusions drawn from the character and significant features of the architecture of the respective areas are summarized only in one place after demonstrating the whole subject. Thus, consciously following up the course of development becomes somewhat difficult and compels the reader to do some re-thinking. Straightforwardly: for example, the history, culture and architecture of the ancient Egyptian Empire and those of the Middle Empire, etc., are treated in different chapters, however, the evaluations, short summaries of each part do not follow up these different sections, only a single one referring to all the sections, although if the changes in history and culture had been exposed according to their stages, also the development of the architecture of that time ought to be recapitulated briefly with marked features. In the development of architecture within the different epochs, embracing in many cases thousands of years, it is all the same whether we mention them as a whole, under the same term, notwithstanding great changes took place. Thus, for example, between the architec-

ture of the Greek Homeric and archaic periods and Hellenism and between that of the Roman kingdom and republic or the imperial period, there was at least such a great difference as between the Sumerian and ancient Babylonian architecture, if not greater, etc. However, the latter have the border mark of their history of evolution, the former have not. As a matter of fact, the answer to this contestable statement might be given by itself: the author does not want unnecessarily to interrupt the course of discussion.

The classic, conservative and elegant appearance of the work with which it was published and the illustrative aids which brings the text near to life, equals the contents of the book. The abundance and variety of the photographic material which is to a great part quite new, is completed by drawings which were made by the co-workers of the author, E. H. SIPOS and dr. Gy. ISTVÁNFI. From among the drawings the schemes of building constructions, the works of dr. Gy. ISTVÁNFI, of new aspect should be emphasized as for example, the scenographic and axonometric cross sections of the Cheops pyramid, the rock-cut tomb of Beni-Hassan, the Consu church in Carnac, the Bouleuterion in Miletos, etc., the demonstration in a new, didactical, but not boring and not stiff manner, as well as the closed-up maps. Use of the book gives enlightment by the annexe of 1. register of figures where the date of origin of the historic monument and the origins of the photographs are also indicated; 2. list of professional literature; 3. index; 4. register of sites; 5. register of subjects.

This review written in a somewhat irregular manner will exceptionally be terminated by a recension of the recension and by the recension of another book. In one number of the English architectural review *Architectura Design* (Volume XLV, April, 1975, page 254) the author Hugh PLOMMER, among others, writes in the first volume of Simpson's *Architectural History*, about the book of the academician M. MAJOR, under the title *Marxist History*. The, to say, the least biased written reports on this books as being a typical work from behind the iron curtain which accumulated from the deposit of the western science according to the dogmata of the Marxist—Leninist philosophy. He justifies this statement by the periodicity also taking the economic and social bases into account, declaring that in contradistinction to the western custom the origins of not all of the ideas, figures, drawings are recorded, and some of the imaginary reconstructions do not take recent researches into account, and lastly, from some of the drawings the indication of the scale has been omitted. He admits that the book of fine workmanship is a well edited, detailed work which, of course, contains also well-founded details, as for example, in connection with Boghazköi and Tiryns estimation of relief-art; however, its use is, owing to several motifs, not recommendable.

In reading this criticism one wonders and would like to know what can be the basic standard of this categoric judgment, this self-confidence. If somebody takes Hugh PLOMMER's book on the same subject (Ancient and Classical Architecture, Simpson's History of architectural Development, vol. I, 1956) and only runs over the table of contents, he immediately observes how a book of history of the ancient architecture is free from dogmata, written in an up-to-date manner. Namely, this book is over-abound in dogmata, surely not as those he thinks of in connection with M. MAJOR's book but in professional ones. PLOMMER is so Greco-centric, as he was as one of the direct students of WINCKELMANN and by that he is adherent to an aspect which through more than a century old has made the history of art, dealing with the ancient architecture, quite one-sided. This is at least demonstrated by the large-scale subdivision into three volumes of his work: *I — Architecture before Greece, II — Greece, III — Architecture after Greece.* He applies the very same peculiar method of "exclusion" in the first part, chapter three, where he deals with architecture, with the styles of Asia Minor, Mediterranean Bronze Age and with other prehellenistic styles, under the title *Architecture outside Egypt:* thus, the reference basis is Egypt, merely because owing to the durable building material and favourable climatic conditions a great number of remains are to be found here, and the events of history, in comparison to others may well be reconstructed. The illustrious author lingers on handling ancient Greece at such a great length that it could even be to Palladio's or Vignola's credit, and besides, he sometimes applies the chronologic and sometimes the typologic method with astonishing elasticity, by that strengthening one's opinion formed on the pure conception of the book. To all of these, as a matter of course, the scrupulously careful details on the sources of the authentic drawings as well as those of recent knowledge of the subject are added. Thus, the "eastern" reader may certainly amuse himself in guessing how that great number of obsolete trivialities could be compatible with the novelties precised by auctorial details.

By the collation of the two books the following lessons may be drawn. The details may be up-to-date even if the building in its integrity is obsolete, and the house may be new and may be the property of the future even then, if not all of its details are the products of recent discoveries. For, in the latter case, only a few bricks should be possibly replaced, while in the former the whole house is to be demolished.

Gy. Hajnóczy

György Sitkei:

HEAT TRANSMISSION AND THERMAL LOAD IN IC ENGINES

Akadémiai Kiadó 1974, 268 Seiten, 231 Abb.

The book considerably enriches the literature on IC piston engines. Specialists concerned with piston engines were awaiting for quite a long the publication of book satisfying also scientific demands which treats the heat transmission phenomena in piston engines and the related thermal load problems strictly in systematical order, from basic facts up to the most recent research results.

The first two chapters of the book present the physical and theoretical bases of heat transmission, heat conduction and heat radiation in IC engines. The author pays special attention to the correct and precise treatment of radiation problems in the combustion process, radiation processes which had not been investigated with sufficient thoroughness during research work undertaken in this direction, so far. The following chapters deal with the possibilities of determining the thermal state and the thermal load of the piston, the cylinder liner, the cylinder head and the valves. Besides giving a comprehensive review of the subject, the author also presents the results of his own research. Especially valuable are his theoretical and experimental results on heat transmission and radiation, and on temperature distribution in the most important parts (piston, liners, precombustion chamber resp. combustion space) mainly concerning the Csepel Diesel engines.

The last chapter deals with the problems of thermal stress arising in the IC engines under the action of thermal load. The varying thermal stress as causing fatigue in the parts of piston engines the author briefly resumes the knowledge on the fatigue of piston engine parts, with special regard to the aluminium alloys which are not yet completely known as to fatigue phenomena, and which are of increasing importance as structural materials for IC engines. For the calculation of thermal stresses the author presents two methods: one is the already classical method based on the solution of differential equations which can be put to good use in special cases, and the other is the modern method of finite elements also suitable for the calculation of arbitrary cases and for asymmetrical shapes. This latter is of special importance with the spreading of the use of electronic computers and basically it is the only method for the calculation of any case with whatever required accuracy. A special merit of the author is that the method of finite elements, which is of general interest, is presented in such detail that it is really possible to carry out the calculations.

In the final part the reader becomes acquainted with the elements of experimental stress analysis. The appendix contains the most important data on the structural materials for IC engines and the tables of functions required for swiftly carrying out some elements of the presented calculations. The work is completed by an ample list of references also containing the most recent literature on the subject.

E. Pásztor

Kázmér Szmodits:

BEHELF ZUR STATISCHEN BEMESSUNG VON WANDPLATTENBAUTEN

Építéstudományi Intézet (Institut für Bauwissenschaft), Budapest 1975, 175 Seiten, 70 Bilder

Das Werk verfolgt den Zweck, den praktisch tätigen Ingenieuren mit einem Behelf zu dienen, der in einer allgemein verständlichen Form, anhand von zahlreichen praktischen Beispielen die zweckdienlichen Methoden für die Lösung der im Laufe der Berechnung von Wandplattenbauten auftretenden verschiedenen Problemen enthält.

Hinsichtlich des Inhaltes setzt sich das Werk aus drei Teilen zusammen. Der erste Teil behandelt die Bemessung auf Windlast von, aus Vollwandplatten erbauten Gebäuden mit unregelmäßigem Grundriß, wobei die Wandelemente als in den Boden eingespannte Konsolen aufgefaßt sind, deren Zusammenwirken die als steif angenommenen Decken gewährleisten. Die Formeln und Phasen der Berechnung der einzelnen Elemente und ihres zusammenwirkenden Systems sind in Punkte gefaßt und ihre Anwendung ist anhand der ausführlichen Berechnung eines konkreten Beispiels erörtert. Die Ableitung und Begründung der zu verwendenden Formeln, enthält der dritte Teil des Buches.

Der zweite Teil des Werkes befaßt sich vorerst mit der Bemessung von mit Öffnungen durchbrochenen Wandelementen auf Windlast und Axialkraft. Die aus vertikalen und horizontalen Wandstreifen bestehenden Umrahmungen der regelmäßigen Öffnungsreihen werden bei stets gleicher Geschoßhöhe als ein biegebeanspruchtes zusammenwirkendes System aufgefaßt. Die vertikalen Wandstreifen sind in axialer Richtung als zusammendrückbar, die balkenförmigen horizontalen Wandstreifen in axialer Richtung als unzusammendrückbar angenommen. Die von den balkenähnlichen Streifen auf die vertikalen Wandstreifen übertragenen Kräfte werden als stetige Kraftwirkung betrachtet. Zur Berechnung des Kräftespiels dieses zusammenwirkenden Systems entwickelt der Autor außer einem komplizierten, genauen Verfahren auch ein verhältnismäßig einfaches Näherungsverfahren und weist an einem praktischen Beispiel nach, daß letzteres den Anforderungen der Praxis vollkommen genügt.

Nach der Bekanntgabe der Berechnung des von Öffnungen durchbrochenen Wandelementes befaßt sich der Autor mit dem Kräftespiel von aus solchen Elementen nach dem Querwandsystem erbauten Gebäuden. Außer dem genauen Berechnungsverfahren teilt er auch ein, praktischen Zwecken dienendes Näherungsverfahren mit, in welchem entsprechend dicke Vollwände die von Öffnungen durchbrochenen Querwände ersetzen. Die Anwendung der genauen Berechnungsmethode und des Näherungsverfahrens sind auch hier anhand eines Zahlenbeispiels erläutert.

Der dritte Teil des Werkes ist zuerst der Torsionstheorie dünnwandiger, prismatischer Stäbe offenen Querschnitts, dann der Biegeverdrehungstheorie gewidmet. In diesem Teil sind die sektorialen Größen der Torsionstheorie, sowie ihre Transformation und Normierung ausführlich behandelt und ihre Anwendung an konkreten Zahlenbeispielen dargestellt. Sodann wird die Theorie der reinen Torsion dünnwandiger Stäbe mit geschlossenem Querschnitt, dann die Biegeverdrehungstheorie dieser erläutert und die Bestimmung der sektorialen Größen anhand von Beispielen erklärt. Abschließend ist die praktische Anwendung der im Buch enthaltenen Ausführungen an zahlreichen Beispielen dargestellt.

Der Anhang des Buches enthält das von Ottó Csuri ausgearbeitete Rechenmaschinen-Programm zur Bemessung von mit Öffnungen durchbrochenen Querwänden.

Dank des nützlichen und wertvollen Inhaltes, sowie der die Gesichtspunkte der Ingenieurpraxis berücksichtigenden Vortragsweise entspricht das Buch allen Anforderungen, die an ein gutes Fachwerk gestellt werden können. Besonders hervorzuheben ist jener Teil des Buches, der sich mit der Bemessung von vollwandigen Wandplattenbauten mit unregelmäßigem Grundriß befaßt und hinsichtlich der Einteilung und der Durchführung der Berechnungen klare und übersichtliche Hinweise enthält. Es wäre zweckmäßig gewesen, auch die Berechnung der von Öffnungen durchbrochenen Wände, sowie die Bemessung von Gebäuden mit von Öffnungen durchbrochenen Querwänden in derselben Weise behandeln. Auch wäre es von Vorteil gewesen, darauf hinzuweisen, daß in vielen Fällen infolge verschiedener Ursachen, vornehmlich infolge von Fehlern in der Bauausführung, die theoretisch als stetig angenommene Verbindung der Elemente lockerer als vorausgesetzt ist, ein Umstand, der sich auf das Kräftespiel der ganzen Konstruktion in bedeutendem Maße auswirken kann.

Die obigen, an sich unbedeutenden Bemerkungen vermindern keinesfalls das mit diesem Werk erworbene Verdienst des Autors. Das Buch enthält ausführliche, seit langem entbehrte Anweisungen zur statischen Berechnung von Hochhäusern und veröffentlicht ein Näherungsverfahren, das die sehr komplizierte rechnerische Arbeit weitgehend vereinfacht. Zahlreiche sorgfältig konstruierte, lehrreiche Bilder und sorgsam ausgearbeitete praktische Beispiele erläutern den Text des Buches.

Zusammenfassend ist festzustellen, daß das vorliegende. Buch ein bedeutendes, in der Fachliteratur lang entbehrtes Werk darstellt, dem seitens der auf dem Gebiet der Bemessung von Hochhäusern tätigen Fachleuten bestimmt großes Interesse entgegengebracht wird.

P. Csonka

Reményi Károly:

THE THEORY OF GRINDABILITY AND THE COMMINUTION OF BINARY MIXTURES

Akadémiai Kiadó, 144 pp. 85 fig.

The concept of grindability seems to be selfevident, yet somehow, it could not be exactly defined so far, still less for developing a commonly adopted method for its investigation. However, even if one accepts certain grindability indices determined by more or less

current procedures, also these are only typical with respect to homogeneous materials. In case of grinding mixed materials, and in practice mostly such are dealt with, the components interacting on each other, sometimes promote, sometimes impede grinding, and — depending on the mixing ratio — changing over from helping to making grinding more difficult.

The author worked out the relatively poor and sometimes contradictional literature of the subject treated, amply completed with his own experimental findings and their thorough analysis. He performed his tests with two well defined materials which can well be seperated by solution in water, with rock salt and limestone. Incitement to this work was given by the coal-grinding problems in the power plants supplied with coals of domestic origin from different mines. The author, starting from simple cases approaches his objective systematically.

Subjects of the main chapters of the monography are as follows: a) analysis of formulas widely accepted, concerning size distribution of ground products; b) applicability of these formulas to mixed ground products; c) energy requirement for grinding; d) thorough critical description, not yet published in the special literature so far, of different devices and methods; e) grinding tests with rock salt and limestone mixes and their evaluation; f) grinding tests with coal mixtures and their estimation.

On the basis of the test results author points out that the size distribution of each component, obeys also in the mixtures the familiar laws, consequently the law loses its validity with respect to the mixtures. Further, he establishes that the mixing ratio differs in each size fracture class. For this statement mathematical analysis and extreme values are given. Finally it was verified that the distribution energy of grinding varies according to the components during grinding.

Everybody being an axpert in grinding technique may profitably read this book, and those being well informed on this subject, will find new ideas and statements in it.

B. Beke

H. Hofman:

DAS ELEKTROMAGNETISCHE FELD

THEORIE UND GRUNDLEGENDE ANWENDUNGEN

Springer-Verlag, Wien, New York, 1974, 518 S., 284 Abb.

»Die Elektrodynamik stellt für alle Elektrotechniker und für einen Großteil der Physiker die Basis für ihre berufliche Fachausbildung dar« schreibt der Verfasser im Vorwort seines Buches. Hiermit kann jedermann einverstanden sein und dies erklärt die Tatsache, daß zum hundertsten Jahrestag der Geburt der klassischen Elektrodynamik immer wieder neue, mit Interesse rechnende Bücher über das klassische elektromagnetische Feld erscheinen. Der Grund hierfür ist meistens, daß die Verfasser ihr Thema in je ein gegebenes Unterrichtssystem — nach gut definierten Vorstudien, also auf gegebenem mathematischem Niveau, mit bestimmter Zielsetzung — einbauen. Eine andere Neuheit kann darin bestehen, daß die klassische Elektrodynamik noch nicht vollständig geklärt ist, und so ihre auch heute noch lebendige Problematik eingehender oder in neuem Lichte vorgestellt bzw. gelöst wird. Ein weiterhin mögliches Mehr ist die Betonung der neuen, durch die elektronische Rechentechnik gegebenen quantitativen Lösungsmöglichkeiten. Eventuell kann auf die Zusammenhänge zwischen der klassischen Feldtheorie und der modernen Quatentheorie hingewiesen werden, da auch hier praktische Beziehungen bestehen. Neues kann daher in bezug auf Niveau und Struktur, also im wesentlichen in pädagogischer Hinsicht, aber auch inhaltlich geboten werden.

Das vorliegende Buch bietet auf beiden Gebieten Neues. Es besteht in einfacher und übersichtlicher Weise aus 4 Teilen: 1. Das elektrostatische Feld. 2. Das stationäre elektrische Strömungsfeld. 3. Das stationäre magnetische Feld. 4. Das nichtstationäre elektromagnetische Feld. Diese vereinfachte Einteilung verbirgt neben den Vorteilen auch Fallen. Das stationäre Strömungsfeld bedeutet im wesentlichen elementare Netztheorie. Sein Umfang beträgt 84 Seiten (bloß das galvanische Element erstreckt sich auf 3 Seiten). Dabei umfaßt aber im 4. Teil der Abschnitt über elektromagnetische Wellen nur 39 Seiten. Auch die Besonderheit und Neuheit der Darstellung der Energie- und Kraftwirkungen wäre in einem gesonderten Teil besser zur Geltung gekommen als in dieser Weise, verstreut.

Als fachliche Neuheit muß — wie dies auch der Verfasser betont — die Besprechung des Einflusses der magnetischen Werkstoffe auf das elektromagnetische Feld erwähnt werden. Der Verfasser untersucht die Erscheinungen sowohl aufgrund des magnetischen Momentes, als anhand des molekularen Elementarströmungsmodells. Die Darlegung der Kraft- und

Momentverhältnisse ist mustergültig. Schade, daß bei den schnell wechselnden Feldern dieser Themenkreis fehlt, obwohl auch das Impulsmoment des elektromagnetischen Feldes sehr schön in diesen Rahmen hätte eingefügt werden können. Sowohl was die Verwendung der mathematischen Mittel anbelangt, als auch vom Standpunkt der Theorie aus betrachtet, überragen diese Teile das allgemeine Niveau des Buches, das dadurch einen etwas heterogenen Charakter bekommt. Es wäre zweckmäßig, diesen Teil in einer neuen Auflage drucktechnisch — durch Petitsatz, oder durch Bezeichnung mit einem Stern — vom laufenden Text zu trennen.

Zusammenfassend kann gesagt werden, daß das Buch durch seine klare Beweisführung, übersichtliche Anordnung, seine vielen gut durchdachten Abbildungen und praktischen Beispiele dazu geeignet ist, den Leser mit den Grundgesetzen des elektromagnetischen Feldes bekannt zu machen, und ihm in einzelnen Teilen auch heutige Probleme vorzuführen.

Imre Botka — *György Erney:*

BEMESSUNG VON ZAHNRADPAAREN

2. SCHRÄGVERZAHNUNG

Akadémiai Kiadó, Budapest 1974, 398 Seiten

Das vorliegende Werk der Verfasser über Schrägverzahnungen ist ein Dreivierteljahr nach ihrem Buch über Fragen der *Geradverzahnungen* erschienen. Sein Aufbau ist dem des 1. Bandes ähnlich, d. h. nach einer Zusammenfassung der Bezeichnungen folgt der Aufbau des Tabellenwerks und danach folgt die Dimensionierung der schrägverzahnten Stirnräderpaare samt einigen Zahlenbeispielen. Dies umfaßt — samt dem Literaturverzeichnis — 38 Seiten. Die übrigen 360 Seiten sind Tabellen, und zwar Haupttafeln für 10°, 20° und 30° Schrägungswinkel, mit den zugehörigen Hilfstabellen und den Zahnformfaktor-Tabellen.

Ähnlich dem 1. Teil enthalten auch die Tabellen dieses Teiles die Angaben der sog. Ganz—Botka-Verzahnung, d. h. jene für die wärmeausgeglichene allgemeine Kreisevolventenverzahnung für den Bezugsprofilwinkel von 20°. Die Verfasser haben die Zähnezahlsummen und Zähnezahlverhältnisse samt den ganzzahligen Eingriffswinkeln so dicht gewählt, daß für Zwischenwerte die Interpolation praktisch überflüssig ist. Nur bei höheren Genauigkeitsansprüchen muß zwischen zwei benachbarten ganzzahligen Eingriffswinkeln interpoliert werden.

Die Bereichsgrenzen der Zahlentafeln liefern der Zahnfußunterschied, das Schwinden des Profilüberdeckungsgrades (frühere Benennung: Stirnüberdeckungsgrad) auf 1 und der Unterschnitt (und manchmal auch die Zuspitzung des Zahnes).

Die Tabellen wurden für die günstigste Bearbeitung mittels Zahnstange ausgearbeitet, so daß bei Fertigung mittels Schneidrad die Bereichsgrenzen durch die Interferenz eingeengt werden.

Bei der Berechnung des Wärmeausgleichs akzeptierten die Verfasser als Bedingung die Niemann-Richtersche Kosinus-Näherung entlang der Eingriffslinie.

Gemäß den Tabellen des Werkes stimmt in den meisten Fällen die wärmeausgeglichene Verzahnung mit der sog. *AE*-Verzahnung überein, wenn also in den Endpunkten *A* und *E* der Eingriffsstrecke nicht nur die Blokschen Temperaturspitzen, sondern auch die aus zwei Faktoren bestehenden Almen-Produkte (die Produkte der *Hertz*-Spannungen und der Gleitgeschwindigkeit) und die relativen Gleitungen ausgeglichen sind (der Fall des sog. dreifachen Ausgleichs). Das Buch behandelt aber auch jene Fälle, in denen im Abschnitt *CE* der Eingriffsstrecke *AE* (C ist die Bezeichnung des Wälzpunktes) die Temperaturspitze in einem im Vergleich zum Punkt *E* weiter innen gelegenen Punkt *P* auftritt (dies ist die sog. *AP*-Verzahnung) und so die wärmeausgeglichene Verzahnung von der *AE*-Verzahnung abweicht.

Die Tabellen beruhen auf der Annahme, daß die Reibungszahl während des Eingriffs konstant ist, wie dies vorläufig auch die Fachliteratur der ganzen Welt als Vereinfachung annimmt.

Unter diesen Bedingungen geben die Haupttabellen die auf die sog. gemeinsame Zahnhöhe bezogenen Verteilungszahlen für die Zähnezahlsummen, die Zähnezahlverhältnisse, die Eingriffswinkel und die Zahnneigungswinkel an, ferner die Profilverschiebungszahlen des Ritzels, die auf den Einheitsmodul bezogene gemeinsame Zahnhöhe, und die vollen Zahnhöhen, wie auch schließlich die Summe der Profilverschiebungsfaktoren.

Die Hilfstabellen enthalten die Profilüberdeckungsgrade; die sog. Wältzpunktfaktoren der Linienpressung für den Fall, daß die Überdeckung (nach der früheren Benennung: der axiale Überdeckungsgrad) eine ganze Zahl ist; die Faktoren der Hertz-Spannung im Punkte A; die zum Halbierungspunkt M der Eingriffsstrecke gehörigen Faktoren der Hertz-Spannung; und die zum Einheitsmodul gehörige Kopfflächenbreite des Ritzels. Den Zahnformfaktor-Tabellen können die in der Fachliteratur auffindbaren verschiedenen Zähneformfaktoren (nach Niemann und nach ISO) entnommen werden.

Ein besonderer Wert des Buches ist das Kapitel »Bemessung von schrägverzahnten Stirnräderpaaren«, welches zur Zeit die in der ungarischen Literatur modernste derartige Zusammenfassung darstellt.

Beide Verfasser des Werkes waren Maschinenbauingenieure der Lokomotiv-, Waggon- und Maschinenfabrik Ganz-MÁVAG (bzw. ihres Rechtsvorgängers der Ganz-Werke). Beide bauten während ihrer täglichen konkreten Aufgaben in der Fabrik (Beantwortung von Berechnungs-, Projektierungs- und Fertigungsproblemen) alles das auf, was sie dann wissenschaftlich verallgemeinern und jetzt jedem Zahnradfachmann zur Verfügung stellen konnten.

Imre BOTKA's größtes Verdienst war die Schaffung der Ganz—Botka-Verzahnung und der Nachweis der Vorteile der allgemeinen Verzahnung auch für schrägverzahnte Stirnräderpaare. György ERNEY untersuchte mit voller Genauigkeit die Verzahnungsbereiche. Es ist von großem Vorteil für die Fachliteratur, daß das Verfasserpaar diese beiden Bände geschrieben hat; daß mit Hilfe des Elektronenrechners der Ganz-MÁVAG-Fabrik die Tabellen angefertigt werden konnten; und daß der Verlag der Ungarischen Akademie der Wissenschaften auf Empfehlung des Ausschusses für Maschinenbaukunde diese beiden Bücher in geschmackvoller Ausführung in erstaunlich kurzer Zeit herausgebracht hat.

Z. Terplán

INDEX

BUCHBESPRECHUNG — BOOK REVIEW

Printed in Hungary

A kiadásért felel az Akadémiai Kiadó igazgatója. Műszaki szerkesztő: Zacsik Annamária

A kézirat nyomdába érkezett: 1976. II. 4. — Terjedelem: 22,4 (A/5) ív, 98 ábra

76.2759 Akadémiai Nyomda, Budapest — Felelős vezető: Bernát György

Acta Techn. Hung. **82** (1976) pp. 233—244

BÖLCSKEI, E.: *Membrane Shells Written in Cylindrical Co-ordinates*

Examples have been presented to showunambiguously that several types of shell structures lend themselves for treatment in cylindrical co-ordinates, rather than for shells of revolution alone. This statement is also valid for shells with intricate cyclic folds, or waves. For shells over sector — or ring sector — shaped ground-plans, also the boundary conditions can be relativity simply to be taken into consideration.

Acta Techn. Hung. **82** (1976) pp. 245—254

KÉZDI, Á.: *Process of Hydraulic Soil Failure*

The quicksand condition which takes place under the influence of the water flow directed upwards within a sand mass, is commonly calculated on the basis that the soil structure forms a rigid skeleton. Laboratory tests showed that by increasing the values of the hydraulic gradient, partly the phenomenon of outwash, partly loosening or densification takes place, depending on whether the initial state was dense or loose, respectively. The full failure itself, just as the shear failure, is associated with the development of a critical void ratio. Attaining a hydraulic gradient determined on the basis of the assumption of a mentioned rigid skeleton, means the transition from the laminar flow of water into the turbulent one. In the course of the development of the quick condition, the permeability changes in another way than had been believed on the basis of the change in density; also this may be explained by the occurrence of turbulent flow.

Acta Techn. Hung. **82** (1976) pp. 255—279

MATTHIEU, I.: *Introduction in Some Problems of Turbulence*

The paper intended to be an introduction for purpose to show the train of thoughts which is the guiding principle of the experiments conducted in the hydrodynamic laboratory of the Ecole Centrale de Lyon in connection with the turbulence. With this the development of a common language is wanted which makes easier the description and discussion of the research work performed on the subject of the boundary layers disturbed and those, instabilized by heating. Throug this also the future directions of development of this discipline might be estimated: a number of viewpoints justify the expediency of studaying the thermic phenomena, three-dimensiona boundary layers andflows bounded by walls.

Acta Techn. Hung. **82** (1976) pp. 281—301

JANKÓ, L.: *Analysis of the Membrane and Bending Forces of a Cylindrical Shell Subjected to Wind Load.*

The static behaviour of the membrane supported cylindrical shellsubjected to wind load is analysed with the aid of the simple theory of bending. In this connection answer is given to the question that if the membrane stress pattern realizes the equilibrium, so the large deformations do induce or not bending stresses in the shell wall greater than membrane stresse. It is stated that pure membrane behaviour is only possible in case of small, low, and thin-walled cylindrical shells, therefore, in case of higher harmonics or high, thick-walled cylindrical shells the membrane theory cannot be applied as particular solution.

Acta Techn. Hung. **82** (1976) pp. 303—332

KEMÉNY, A. P.: *Experimental Investigations of the Life of Semiconductor Devices IV, The Role of the Peak Temperature Caused by theSwithing Transients in the Spatial Breakdown of Switching Transistors and Digital Integrated Circuits*

The transient temperature rise due to the switching power transients can be made responsible for some characteristic spatial breakdowns in high-level switching operation, such as C—E "pinning" and C—B short-circuit. Calculating the "thermal penetration depth" ou both sides of the collector junction, and also the thermal capacity and the thermal resistance of the heated space part until a given moment after the start of the switching transient, a suitable unidimensional thermal model is obtained for estimating the junction temperature rise: in possession of the transient switching power vs. time and the design data of the given bipolar transistor the transient junction temperature can be calculated as a function of time. On numerical examples for some transistor types with characteristic technology (from the large, robust Ge and Si power transistors until the monolitic miniature integrated circuits), assuming faultless structure and uniform current distribution, it is shown that the ewitching temperature peaks are completely inoffensive.

Acta Techn. Hung. **82** (1976) pp. 333—352

ZÁMBÓ, J.—ORBÁN-KELEMEN, M.: *CaO and MgO Compound Formation in Processing Calcite=Dolomite Bearing Bauxites by the Bayer-Method*

The operational problems in the course of processing the Halimba type calcite and dolomite bearing bauxites necessitated the examination of the $Na_2O-Al_2O_3-CaO-MgO-TiO_2-SiO_2-H_2O-CO_2$ system under the conditions of the Bayer technology parameters. It was observed that the quality and quantitative ratio of the Ca and Mg containing phases produced during the recovery of dolomite bauxites ate governed, primarily, by the components dissolved in the alumina liquor, although they are also affected by the solid phases capable of reacting with the individual components of the solution.

Acta Techn. Hung. **82** (1976) pp. 353—375

PÁCZELT, I.: *Solution of Elastic Contact Problems by the Finite Element Displacement Method*

Contact problem of elastic continua subject to arbitrary load and of arbitrary surface is a rather intricate one, contact domains not being known a priori. Here, the continuum is replaced by a bulk of elements of finite degrees of freedom, the obtained elastic system serving as basis for the solution of the problem based on the principle of potential energy minimum. Because of the unilateral relations between the bodies, the mathematical programming can be discussed as a quadratic programming problem. Use of the Khun-Tucker conditions yields a solution for the dual of this primal problem, much easier to establish and solve than the original one. Friction and adherence between the bodies are considered as negligible, and displacements, deformations to be small.

Acta Techn. Hung. **82** (1976) pp. 391—399

PETHŐ, SZ.: *The Laws of Motion of a Solid Body for Reynolds Numbers between* **0,6** *and* **800**

The paper presents the laws of motion of a body descending in a gaseous or liquid medium if in the laws of motion, neither of laminar nor of turbulent flow can be applied. These laws have been deduced by Josef Finkey in his basic work "Die wissenschaftlichen Grundlagen der nassen Erzaufbereitung", published 50 years ago. In the solving of the differential equations contained in the paper and in carrying out the calculation, the author has been aided by Mr. Ivan Raisz, assistent professor, to whom he wishes to express his sinctre thanks.

Acta Techn. Hung. **82** (1976) pp. 401—415

KIRÁLY, B.: *Kinematic Examination of Constraint Systems Realized on Paris of Surfaces in Contact*

From the technical point of view at one of the most important types of holonomic systems the constraints are realized on pairs of surfaces in contact which are formed on rigid bodies. This paper deals with the kinematic examination of such constraint systems. Firstly it initiates the idea of surface constraint which is realized on a single pair of surfaces and the idea of elementary constraint belonging to one contact point, and then it replaces the constraint system by a system of eleementary constraints in which each surface constraint corresponds to elementary constraints lineary independent of each other. In this way the set of constraint equations concerning the speed state of a holomonic system — also in general spare cases — can be expressed in a concise matrix from which is suitable for further examinations.

Acta Techn. Hung. **82** (1976) pp. 417—434

GAÁL, D.: *The Near Field of Flat Acoustic Radiators*

The paper investigates the near field of plane radiators in an infinite wall, using a new mathematical approach. The method consists of a hitherto unknown series expansion of the Sommerfeld-King integral and of a coordinate transformation of the Green's function. Using the new method the author solves mathematically also the problem of the sound field of the plane radiators working in a finite circular baffle.

Acta Techn. Hung. **82** (1976) pp. 435—441

MANDAL, S.: *Penny-Shaped Crack in an Infinite Viscoelactic Medium*

In this paper the strees field is obtained in the neighbourhood of a penny-shaped crack in the interior of a special type of linear vicoelastic medium by employing Laplace and Hankel transforms. The general solution is illustrated in three specific cases.

Acta Techn. Hung. **82** (1976) pp. 443—446

SOMOGYI, K.—PŐDÖR, B.: *Cryostat for the Measurement of Galvanomagnetic Effects in Semiconductors*

A simple but reliable cryostat for galvanomagnetic measurements in semiconductors is described. The cryostat is designated to cover the temperature range of 77—400 K and can be fitted into a small gap magnet.

Acta Techn. Hung. **82** (1976) pp. 447—469

Szőke, B.: *Generating of the End Milling Cutters for Helical Gears II.*

The Design and the Adjustment of the End Milling Cutter. — In Chapters 5—7 the arrangement of the production and its adjustment are dealt with. As for the design — considering the high r. p. m. required by the work — it was thought that use of a commercially avai able gear would be the best solution. Two designs are discussed: one would be economic where only few sizes of end cutters are needed, while the other solution could be used for the production of the most different cutters. Any of them could be mounted one some suitable machine tool.

The *Acta Technica* publish papers on technical subjects in English, French, German and Russian.

The *Acta Technica* appear in parts of varying size, making up one volume.

Manuscripts should be addressed to

Acta Technica
1051 Budapest
Münnich Ferenc u. 7.
Hungary

Correspondence with the editors and publishers should be sent to the same address.

The rate of subscription is $ 32.00 a volume. Orders may be placed with "Kultúra" Foreign Trade Company for Books and Newspapers (1389 Budapest 62, P.O.B. 149 Account No. 218 10990) or with representatives abroad.

Les *Acta Technica* paraissent en français, allemand, anglais et russe et publient des travaux du domaine des sciences techniques.

Les *Acta Technica* sont publiés sous forme de fascicules qui seront réunis en volumes.

On est prié d'envoyer les manuscrits destinés à la rédaction à l'adresse suivante:

Acta Technica
1051 Budapest
Münnich Ferenc u. 7.
Hongrie

Toute correspondance doit être envoyée à cette même adresse.

Le prix de l'abonnement est de $ 32.00 par volume.

On peut s'abonner à l'Entreprise pour le Commerce Extérieur de Livres et Journaux «Kultúra» (1389 Budapest 62, P.O.B. 149 compte courant No. 218 10990) ou à l'étranger chez tous les représentants ou dépositaires.

«*Acta Technica*» публикуют трактаты из области технических наук на русском, немецком, английском и французском языках.

«*Acta Technica*» выходят отдельными выпусками разного объема. Несколько выпусков составляют один том.

Предназначенные для публикации рукописи следует направлять по адресу:

Acta Technica
1051 Budapest
Münnich Ferenc u. 7.
Венгрия

По этому же адресу направлять всякую корреспонденцию для редакции и администрации.

Подписная цена — $ 32.00 за том. Заказы принимает предприятие по внешней торговле книг и газет «Kultúra» (1389 Budapest 62, P.O.B. 149 Текущий счет № 218 10990) или его заграничные представительства и уполномоченные.

Reviews of the Hungarian Academy of Sciences are obtainable at the following addresses:

AUSTRALIA

C. B. D. Library and Subscription Service
Box 4886, G. P. O.
Sydney N. S. W. 2001

Cosmor Bookshop
145 Acland St.
St. Kilda 3182

AUSTRIA

Globus
Höchstädtplatz 3
A—1200 Wien XX

BELGIUM

Office International de Librairie
30, Avenue Marnix
1050-Bruxelles

Du Monde Entier
162 Rue du Midi
1000—Bruxelles

BULGARIA

Hemus
Bulvar Ruszki 6
Sofia

KANADA

Pannonia Books
P. O. Box 1017
Postal Station "B"
Toronto, Ont. M5T 2T8

CHINA

C N P I C O R
Periodical Department
P. O. Box 50
Peking

CZECHOSLOVAKIA

Mad'arská Kultura
Národní třida 22
115 66 Praha

PNS Dovoz tisku
Vinohradská 46
Praha 2

PNS Dovoz tlače
Bratislava 2

DENMARK

Ejnar Munksgaard
Nörregade 6
DK—1165 Copenhagen K

FINLAND

Akateeminen Kirjakauppa
P. O. Box 128
SF—00101 Helsinki

FRANCE

Office International de Documentation et Librairie
48 Rue Gay Lussac
Paris 5

Librairie Lavoisier
11 Rue Lavoisier
Paris 8

Europeriodiques S. A.
31 Avenue de Versailles
78170 La Celle St. Cloud

GERMAN DEMOCRATIC REPUBLIC

Haus der Ungarischen Kultur
Karl-Liebknecht-Strasse 9
DDR—102 Beriin

Deutsche Post
Zeitungsvertriebsamt
Strasse der Pariser Kommüne 3—4
DDR—104 Berlin

GERMAN FEDERAL REPUBLIC

Kunst und Wissen
Erich Bieber
Postfach 46
7 Stuttgart S

GREAT BRITAIN

Blackwell's Periodicals
P. O. Box 40
Hythe Bridge Street
Oxford OX1 2EU

Collet's Holdings Ltd.
Denington Estate
London Road
Wellingborough Northants NN8 2QT

Bumpus Haldane and Maxwell Ltd.
5 Fitzroy Square
London W1P 5AH

Dawson and Sons Ltd.
Cannon House
Park Farm Road
Folkestone, Kent

HOLLAND

Swets and Zeitlinger
Heereweg 347b
Lisse

Martinus Nijhoff
Lange Voorhout 9
The Hague

INDIA

Hind Book House
66 Babar Road
New Delhi 1

India Book House
Subscription Agency
249 Dr. D. N. Road
Bombay 1

ITALY

Santo Vanasia
Via M. Macchi 71
20124 Milano

Libreria Commissionaria Sansoni
Via Lamarmora 45
50121 Firenze

JAPAN

Kinokuniya Book-Store Co. Ltd.
826 Tsunohazu 1-chome
Shinjuku-ku
Tokyo 160—91

Maruzen and Co. Ltd.
P. O. Box 5050
Tokyo International 100—31

Nauka Ltd.—Export Department
2—2 Kanda
Jinbocho
Chiyoda-ku
Tokyo 101

KOREA

Chulpanmul
Phenjan

NORWAY

Tanum-Cammermeyer
Karl Johansgatan 41—43
Oslo 1

POLAND

Węgierski Instytut Kultury
Marszalkowska 80
Warszawa

BKWZ Ruch
ul. Wronia 23
00—840 Warszawa

ROUMANIA

D. E. P.
Bucureşti

Romlibri
Str. Biserica Amzei 7
Bucureşti

SOVIET UNION

Sojuzpechatj — Import
Moscow
and the post offices in each town

Mezhdunarodnaya Kniga
Moscow G—200

SWEDEN

Almqvist and Wiksell
Gamla Brogatan 26
S—101 20 Stockholm

A. B. Nordiska Bokhandeln
Kunstgatan 4
101 10 Stockholm 1 Fack

SWITZERLAND

Karger Libri AG.
Arnold-Böcklin-Str. 25
4000 Basel 11

USA

F. W. Faxon Co. Inc.
15 Southwest Park
Westwood, Mass. 02090
Stechert-Hafner Inc.

Serials Fulfillment
P. O Box 900
Riverside N. J. 08075

Fam Book Service
69 Fifth Avenue
New York N. Y. 10003

Maxwell Scientific International Inc.
Fairview Park
Elmsford N. Y. 10523
Read More Publications Inc.
140 Cedar Street
New York N. Y. 10006

VIETNAM

Xunhasaba
32, Hai Ba Trung
Hanoi

YUGOSLAVIA

Jugoslovenska Knjiga
Terazije 27
Beograd

Forum
Vojvode Mišića 1
21000 Novi Sad

22. XI. 1976

Index: 26.025